中国科学院上海应用物理研究所

年报

2015-2016

(第 27 卷)

《中国科学院上海应用物理研究所年报》
编辑委员会

2015-2016 年报

前　言

2015-2016 年，“十二五”规划已收官，“十三五”规划已开始。全所广大干部职工在所领导班子带领下，按照“三个面向”、“四个率先”的新时期办院方针，深入实施科学院“率先行动”计划，紧跟科学院改革创新的步伐并积极融入上海科创中心建设，调整、优化组织机构和科技布局，着力推进加速器科学技术、光子科学、核能科学技术和核科学技术与前沿交叉科学持续发展，勇攀高峰、砥砺前行，为“十三五”发展奠定了坚实基础。

一、系统谋划“十三五”，不断增强研究所核心竞争力

2016 年，根据“十二五”验收结果及院年度工作会议的精神，我所进一步补充完善了“十三五”规划编制提纲，立足目前形势，梳理了科技布局，编制完成“十三五”规划：在核科学技术领域从事面向世界科技前沿和国家战略需求的基础与应用研究，开展原始创新和集成创新。研发钍基熔盐堆核能系统（TMSR）与相关核心技术，打造 TMSR 全产业链，建成仿真堆和实验堆；与相关研究所联合建设和发展中科院先进核能创新研究院，成为国际上新一代反应堆研发的重要基地。发展加速器光源大科学装置集群，高效运行和开放上海光源并不断产出重大成果；建设 X 射线自由电子激光和上海光源后续线站；发展相关核心技术和实验方法，开展应用研究；建设和发展中科院上海大科学中心，成为世界级光子科学研究基地。在核科技前沿交叉与核技术应用领域做出有特色和重要创新性的基础研究工作，以及有显示度和重要社会效应的应用研究工作。

二、深入推进“率先行动”计划，抓好各类重大任务

2015-2016 年，根据院统一部署，按照院党组“率先行动”计划，以“四类机构”建设为抓手，全力推进上海大科学中心和先进核能创新研究院筹建工作，分解细化目标任务，加强协同配合，形成工作合力，

统筹落实各项改革举措，努力探索新机制，确保取得实效。2016 年，上海大科学中心通过验收，进入正式运行阶段。

2015-2016 年，钍基熔盐堆核能系统（TMSR）在优化发展战略、突破关键技术、打造核心能力、推进实验堆工程前期、促进溢出技术产业化、深化国际合作、探索体制机制等方面取得扎实进展。建立钍铀循环、堆本体工程设计、系列高温熔盐回路、安全与许可等四个原型系统；关键设备研制和关键技术与材料研发取得重大进展；建立技术成果认定体系，探索科研与产业紧密结合的新模式；发展路线图进行动态调整，进一步明确将小型模块钍基熔盐堆作为示范堆的堆型，同时研究确定了“三步走”的钍铀循环技术路线。TMSR 先导专项通过“十二五”验收，“突破钍基核能系统核心技术，建成原型系统”入选了中科院“十二五”重大科技成果及标志性进展。

2015 年，上海光源迎来了开放六周年，光源的主要运行技术指标处于国际先进水平，用户实验取得了一批高水平的研究成果，发挥了支撑科技创新发展的平台作用，“上海光源国家重大科学工程”入选了中科院“十二五”重大科技成果及标志性进展，上海光源团队荣获中国科学院“十二五”突出贡献团队。上海光源后续工程建设稳步推进，取得了实质性进展；上海大科学中心圆满完成筹建期工作目标，通过中科院组织的验收，进入正式运行阶段。2016 年 5 月 16 日，上海光源线站工程（二期工程）工程可行性研究报告获得国家发展改革委批复。10 月 24 日，工程初步设计概算获得国家发展改革委批复。11 月 20 日，工程正式开工建设。X 射线自由电子激光试验装置（SXFEL 试验装置）于 12 月 30 日完成出光调试。上海软 X 射线自由电子激光用户装置（SXFEL 用户装置）于 2016 年 11 月 20 日正式开工建设。

核科学技术与前沿交叉学科研究领域积极瞄准国际科学前沿，在若干研究方向上取得了突破性进展，并积极推进基于大科学装置的 In-house 研究。在中高能重离子碰撞研究和反质子相互作用测量、

DNA 纳米结构相关研究、界面水的微观性质研究等方面取得了骄人的成绩，其中 2 项成果获得了国家自然科学二等奖。首次实现了反物质相互作用的测量，在目前的实验精度下，发现反物质间相互作用和正物质作用相同，该成果被科技部评选为 2015 年度“中国科学十大进展”，入选《科技导报》组织的“2015 年中国重大科学进展”，《上海科技报》的 2015 年上海十大科技事件。

2015-2016 年全所新增各类科研项目 226 项，到位经费总量为 22.74 亿元，年度到位经费首次突破十亿，跻身全院经费总量前十名。发表论文 1200 余篇，其中 SCI 论文 849 篇，以第一作者单位发表影响因子大于 5 的高水平论文 122 篇。共申请专利 200 件，专利授权 80 件。

2015-2016 年，我所获得主要奖项如下：“重离子碰撞中的反物质探测与夸克物质的强子谱学与集体性质研究”（马余刚、陈金辉）获国家自然科学奖二等奖；“生物分子界面作用过程的机制、调控及生物分析应用研究”（樊春海、宋世平、王丽华、李迪）获国家自然科学奖二等奖；樊春海获得 2016 年度上海市青年科技杰出贡献奖。

三、多措并举，凝聚培养造就人才队伍

“十二五”期间，我所以凝聚和造就创新人才队伍为重点，采取多种措施，建设满足本所持续健康发展需求的人才队伍。结合所和院“四类机构”建设实际情况，以重大科技任务为牵引，开展“千人计划”、“百人计划”等高端人才的引进工作。骨干队伍中，新增中央千人计划 1 人、中科院百人计划 9 人、上海领军人才 4 人、中央万人计划青年拔尖人才 2 人；1 人入选“万人计划—中青年科技创新领军人才”、1 人入选科技部“中青年科技创新领军人才”、7 人受聘“中科院特聘研究员”、1 人入选中科院“关键技术人才”。

2015-2016 年度，毕业博士生 93 名、硕士生 96 名，4 人获院长优秀奖、4 人获朱李月华优秀博士生奖，8 人被评为国科大“三好学生

标兵”，17 人被评为“优秀学生干部”，132 人被评为“三好学生”，7 人获国科大“优秀毕业生”称号，12 人获“上海市高校优秀毕业生”称号，4 人获“梦想奖学金”，13 人获博士研究生国家奖学金，8 人获硕士研究生国家奖学金。

四、纵深拓展国际合作

2015-2016 年，上海应物所围绕上海光源大科学装置、钍基熔盐堆核能系统、核技术与前沿交叉三大学科领域持续拓展和深化国际合作，形成了多层次、重实效的对外开放合作格局。我所因公出访近 700 人次，接待外宾来访 670 余人次。举办了第十二届国际计算加速器物理大会、第七届高频低电平国际学术研讨会等国际会议 14 项，新签署国际合作协议 3 项。马余刚研究员荣获 2015 年度国际华人物理与天文学会亚洲成就奖并入选 2015 年美国物理学会会士；樊春海研究员入选 2015 年度全球高引用科学家等。这些国际性人才的出现，极大的提升了我所的国际知名度，为我所发展成为具有国际竞争力的科研机构发挥了重要作用。

在科学院改革创新的前进步伐及上海科创中心建设中，我所进入了历史上最快的发展时期。面对前所未有的历史机遇，按照“三个面向”、“四个率先”的新时期办院方针，我所在向独具特色、不可替代和具有国际竞争力的核科技强所奋进的过程中，实现着跨越式发展。

目 录

大科学装置

钍基熔盐堆核能系统

基础与交叉

附录

大科学
装置

上海光源运行状况（2015–2016）

上海光源加速器运行组

上海光源是第三代中能同步辐射光源，包括一台 3.5 GeV 的电子储存环、一台全能量增强器、一台 150 MeV B 的直线加速器以及 7 条束线站（一期）。

上海光源自从 2004 年破土动工以来，加速器于 2006 年 11 月开始安装，仅用 10 个月的时间即完成全部加速器设备的安装，并在随后几个月的老练和设备调试以后，于 2007 年 12 月 21 日开始上海光源储存环的正式调试，并于当天获得上海光源的第一次束流存储，三天后，在上海光源束线前端获得第一束同步辐射光。2009 年 5 月，上海光源正式对用户开放。

上海光源自从对用户开放以来，根据计划每年都会向用户提供 4 000~5 000 h 的用户机时，2015–2016 年，上海光源共计划向用户提供 9 312 h 的实验机时，图 1 和图 2 分别给出了上海光源 2015 年和 2016 年的机时安排计划

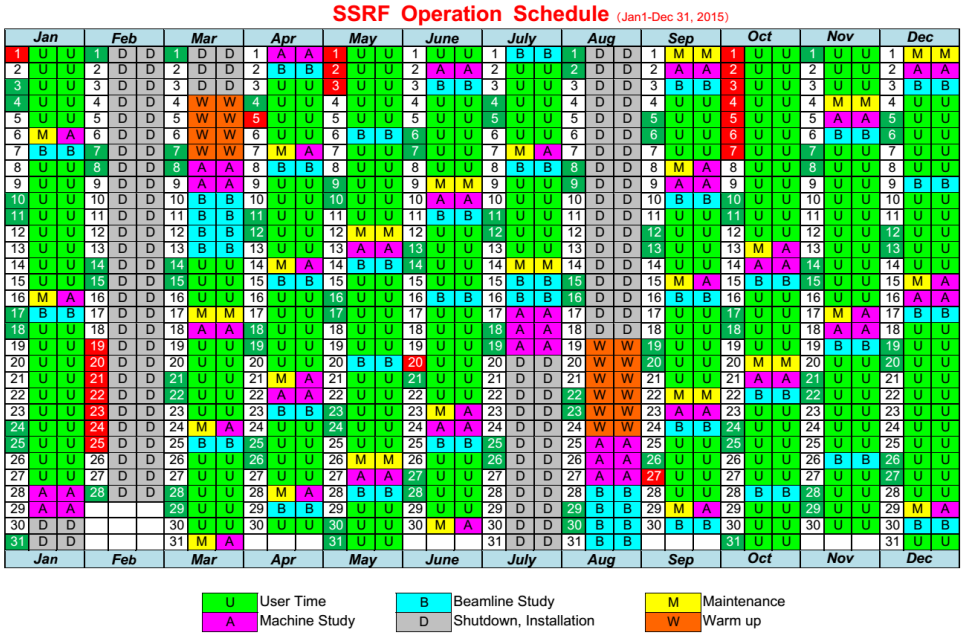

图 1　上海光源 2015 年运行计划

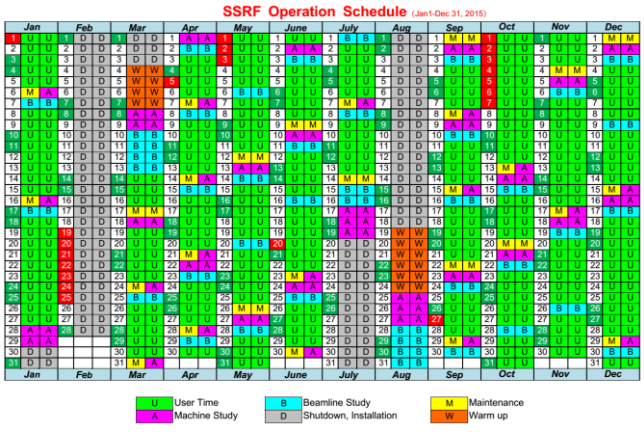

图 2　上海光源 2016 年运行计划

在 2015–2016 年，上海光源实现对用户开放机时为 9 087.02 h，期间共有 151 次因设备故障引起的束流丢失，在此期间上海光源的开机率为 9%，平均无故障时间为 59.78 h，平均故障处理时间为 1.49 h。

参考文献

1. Xu H J, Zhao Z T. Nuclear Science and Techniques, 2008, **19**(1): 1–6.
2. Zhao Z T, Xu H J, Ding H. EPAC2008, Genoa Italy, TUOAM01.
3. Zhang M Z, Hou J, Jiang B C, *et al*. IPAC2011 San Sebastian, Spain, WEPC017.

Operation Status of SSRF in 2015–2016

SSRF Operation Group

The Shanghai Synchrotron Radiation Facility (SSRF), a third generation light source, comprises a 3.5 GeV electron storage ring, a full energy booster, a 150 MeV Linac, and with seven beamlines in Phase I of the project.

Beginning at the end of 2004 with a groundbreaking ceremony, the accelerators were installed in ten months from November 2006, and were successfully tested and commissioned in a couple of months, On December 21 2007, storing electron beams in the storage ring was realized, and the first synchrotron radiations were observed three days later on the front-end of the Beamline. In May 2009 we welcomed our first user, it marked that SSRF opened to the user and turned to the operation period.

After the opening to the user, SSRF planned to provide 4 000~5 000 h to user operation every year, in 2015 and 2016, we planned to deliver 9312 hours to users, the Fig.1 and Fig.2 gave the operation schedule of SSRF in 2015 and 2016.

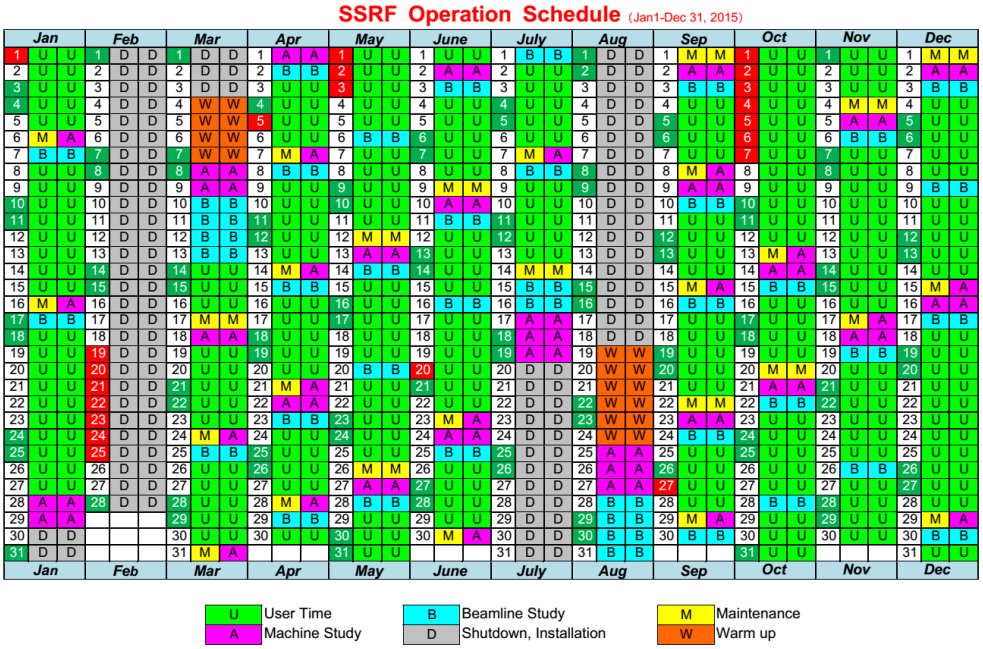

Fig.1 The operation Schedule of SSRF in 2015

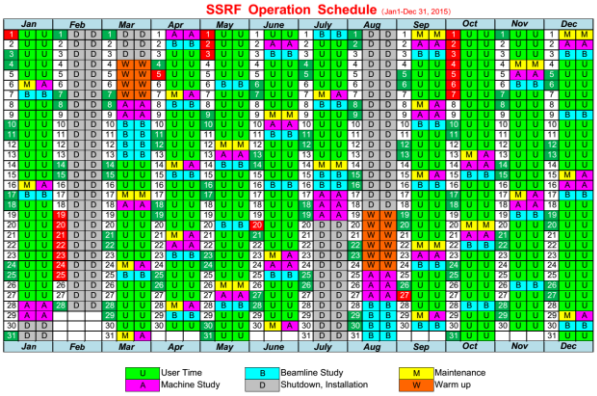

Fig.2 The operation Schedule of SSRF in 2016

In 2015−2016, we achieved to deliver the synchrotron radiation light to user for 9087.02 hours, and there were 151 beam trips during the user operation. The availability of SSRF is 97.6% and the Mean Time Between Failures (MTBF) is 59.78 h, the Mean Down Time (MDT) is 1.49 h.

Reference

1 XU Hongjie, Zhao Zhentang. Nuclear Science and Techniques, 2008, **19**(1):1-6.

2 Zhao Z T, Xu H J, Ding H. EPAC2008, Genoa Italy, TUOAM01.

3 Zhang M Z, Hou J, Jiang B C, *et al.* IPAC2011 San Sebastian, Spain, WEPC017.

上海质子治疗装置加速器的物理设计

加速器物理与射频技术部

上海质子治疗装置加速器部分的物理设计主要集中在质子环和输运线部分，作为定位于商品化为目标的治疗装置，在整个物理设计过程中主要遵循要采用尽量简单可靠和紧凑的结构，采用国际上比较成熟的技术。设计部分包括质子环和输运线两个部分。

质子环的物理设计

质子环的物理设计主要根据对国际上同类型机器的调研以及治疗要求，按照设计目标，lattice 设计，注入引出的设计和模拟，空间电荷效应的模拟，以及对相关系统的要求等方面。

根据治疗需求和治疗对加速器的要求，设置上海质子治疗装置的主环物理设计目标如下：

被加速粒子：质子；注入能量：7 MeV；引出能量范围：70~250 MeV；环周长 24.6 m；引出电荷：6.4 nC（保证最低 4×10^{10}，争取 8×10^{10}）；升能时间：0.7 s；重复频率为 0.67~0.1 Hz；二极铁磁场变化范围 0.27~1.74 T。

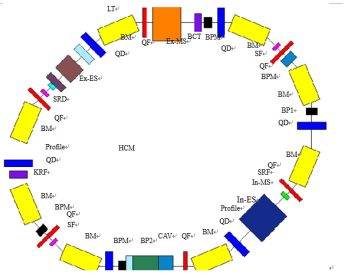

图 1　主环 lattice 结构

主环采用 4 个超周期结构的类 FODO 磁聚焦结构，全环的磁铁排列结构如图 1 所示。全环有 4 个单元组成，周长 24.6 m，谐波数为 1。图 1 中 QF、QD 分别是水平和垂直方向聚焦四极磁铁；BM 为弯转磁铁；SF、SRD、SRF 为六极磁铁。

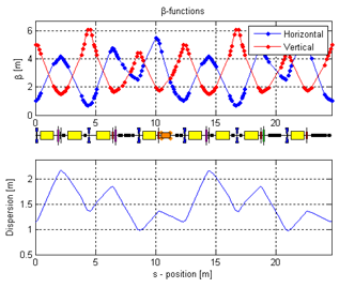

图 2　注入时 twiss 参数

为了结构尽量简单、元件数量尽量少，采用了 QD 和 QF 各 6 块的排列方式。β 函数和色散函数是根据 hardt 条件的要求来进行设计的，这样也决定了 lattice 的排列方式。图 2 给出了全环 β 函数和色散函数，4 个 2 m 直线节用于安放注入、引出、高频和束测元件，其余元件安装在四极铁和弯转磁铁间。

低能输运线的物理设计

低能输运线需要完成从直线加速器到同步环的束流传输匹配，除了根据注入相空间填充的要求进行横向相空间的特殊匹配外，还要完成将直线加速器引出的较大动量分散降低到同步环所希望的 0.15%的水平；同时，考虑到同步环注入点的色散，最好也能进行色散匹配。在设计中采用了尽量简单并且总长度较短的方案，采用一块二极磁铁以便尽量减小注入静电切割板的长度和强度，采用四块四极铁进行相空间的匹配，并且在前两块四极铁中间的空间放置降低束流动量分散的散束器。

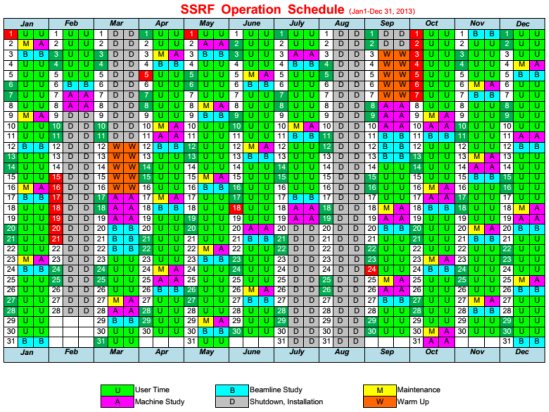

高能输运线的物理设计

高能输运线主要包括从引出点到治疗室的束流分配主线和开关磁铁到治疗室内部的束流传输线。目前第一期主要考虑的治疗室为两个固定治疗头，而两个 gantry 线分别是散射模式和扫描模式各一，目前设计方面只完成了散射模式的初步设计，扫描模式的设计在下一步的设计中完成，该线的设计只完成到了 gantry 入口处。

Physical Design of Shanghai Advanced Proton Therapy Accelerator

Department of Accelerator Physics and Radio Frequency

The physical design of the accelerator of the Shanghai Advanced Proton Therapy (SAPT) is mainly focused on the proton ring and transport lines. As the treatment device targeted at the commercialization, the whole physical design process is mainly followed by the use of a simple, reliable and compact structure and the international mature technology. The design section consists of the proton ring and transport lines.

The physics design of the proton ring

The physical design of the proton ring is mainly based on the investigate and survey of the same type accelerator in the world and treatment requirements. According to the design goal, the physic design include the lattice design, the design and simulation of the injection and extraction, the simulation of the space charge effect and the requirements of related systems.

On the basis of the treatment needs and treatment requirements for the accelerator, the design goals of the proton ring of the SAPT are set as follows: Particle: proton; Injection energy: 7 MeV; Extraction energy: 70~250 MeV; Ring circumference: 24.6 m; Extraction charge: 6.4 nC (4×10^{10} as lowest, 8×10^{10} as target); Time of increase energy: 0.7 s; Repeat frequency: 0.67~0.1 Hz; Bend magnetic field: 0.27~1.74 T.

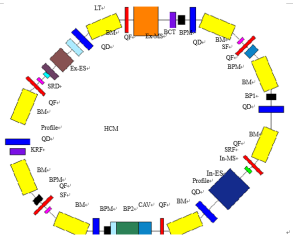

Fig.1 Lattice of the ring

The ring is used by 4 super-periodic structures with the similar FODO magnetic focusing structure. The lattice is shown in Fig.1. The whole ring has 4 units and the circumference is 24.6 meters with the harmonics 1. In Fig.1, QF and QD are horizontal and vertical focus quadrupole magnet and BM is the bending magnet. SF, SRD and SRF are sextupole magnets.

The ring is used by 4 super-periodic structures with the similar FODO magnetic focusing structure. The lattice is shown in Fig.1. The whole ring has 4 units and the circumference is 24.6 meters with the harmonics 1. In Fig.1, QF and QD are horizontal and vertical focus quadrupole magnet and BM is the bending magnet. SF, SRD and SRF are sextupole magnets.

In order to design the structure as simple as possible and the number of components as little as possible, 6 QD and 6 QF are adopted for the arrangement of lattice. The beta function and dispersion function are in the light of the requirements of the Hardt condition which determines the lattice. Fig.2 shows the beta function and the dispersion function of the ring. There are 4 straight sections with the length of 2 m for the placement of the injection, extraction, radio frequency and beam diagnosis elements. The remaining components are installed between quadrupole and bend magnets.

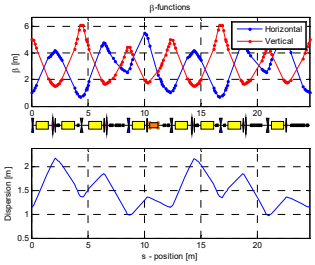

Fig.2 Injection twiss

The physics design of low energy transport line

The low energy transport line needs to complete the beam transfer match from the linear accelerator to the synchrotron. In addition to the special match of the transverse phase space according to the requirements of the injection phase space fill, the large momentum dispersion from the linear accelerator is reduced to the synchrotron at the desired level of 0.15%. At the same time, taking into account the dispersion of the injection point of the synchrotron, it is also possible to perform the dispersion match. In the design, an almost simple program with a short length is used. A bend magnet is used to minimize the length and intensity of the injection electrostatic septum. 4 quadrupoles are used for the phase space match and in the space of the first 2 quadrupoles, a debuncher is used to reduce the beam momentum dispersion.

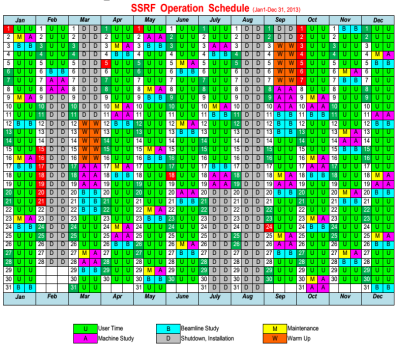

The physics design of high energy transport line

The high energy transport line mainly includes the beam distribution line from the lead-out point to the treatment room and the line from the switch magnet to the treatment room. At present the treatment room on consideration consists 2 fixed treatment head. There are 2 gantry lines with the scattering mode and the scan mode each. The current design is only completed for the preliminary design of the scattering mode. The design of scan mode is in the next step. The design of the line is only to the gantry entrance.

高频组研究进展

高频组

为满足高频运行中对储存环高频故障高效，全面的分析，2015−2016 年高频组对原有的储存环高频快速故障分析系统进行了全面的升级。

原高频快速故障分析系统由两台 LDS 记录仪构成。采样率较低(200 kSPS)，通道数较少(48 CHs)，两台记录仪间同步不精确，数据处理和分析较为繁琐，需导出数据并用第三方软件集中分析。无法全面满足对高频相关故障数据的采集和高效分析。升级后的高频快速故障分析系统主要包含三部分。用于 RF 信号检测的 I/Q 机箱，用于同步采集的 NI-PXIe 系统及用于后期数据处理和分析的高频故障分析服务器。

I/Q 机箱最多可安装 11 个 4 通道 I/Q 板卡，可实现对 44 路 RF 信号的相位和幅度检测。板卡延迟<4 ns，幅度精度优于 ±2%，相位精度优于 ±0.4 °。

NI PXIe 系统针对不同响应速度的信号分别采用高速和中速板卡，中速板卡采样率最高 6 MSPS，高速板卡采样率最高 60 MSPS；总通道数>100 CHs。

故障服务器对故障后产生的数据进行标定。使用 DIADEM 软件对故障数据进行快速和便捷的分析。故障发生后 2 min 内，故障的概略曲线图片就可发往中控，方便中控人员判断故障是否来自高频。

系统在线运行后，高频快速联锁故障分析系统发现并帮助我们快速定位和处理了诸如原三号位低电平 400 kHz 震荡，三号超导腔 pick-up 打火，以及 2 号阳极高压电源电压高速波动等故障。

我们也对所有的 IOC 进行了时间同步，将所有重要 PV 量放入 Archiever 系统记录。方便对慢速响应信号的分析和对所有信号长时间趋势的分析。

经过以上的改进，对于高频故障。我们形成了一套完善的故障分析系统。以联锁系统为初步判断的工具，以高频故障概略图片为初步判断辅助工具。以快速故障分析系统和 Archiever 数据库为事后详细分析手段。从而形成了一套完整的高频故障分析系统。满足了对储存环高频系统故障全面和便捷的分析。极大提高了运行效率。

参考文献

1. Zhao S J, Chang Q, Hou H T, *et al*. DOI: 10.18429/ JACoW-IPAC2016-THPOY036.

Research Development of RF Group

RF Group

To make the storage ring RF trip diagnostics more efficient and precise, RF group upgraded the RF fast trip diagnostics system from 2015 to 2016.

The original diagnostics system consists of two LDS recorders with lower sample rate (maxim 200 kSPS), and fewer signal channels (48 CHs). It's hard to synchronize the acquisition between the two records. The data can't be easily analyzed. The upgraded system consists of three parts, I/Q crate for RF detection. NI-PXIe system for acquisition and RF trip server for data process and analysis.

In I/Q crate there are 11 I/Q boards, each board has 4 channels for RF detection, which delay is less than 4 ns, amplitude precision is less than ±2% and phase precision is less than ±-0.4 °.

Fast acquisition boards (maxim sample rate 60 MSPS) and middle acquisition boards (maxim sample rate 6 MSPS) are installed in NI-PXIe system for signals with different response speed. The total acquisition channel is more than 100 CHs.

The trip data can be scaled in trip server. The DIADEM software is adopted in trip server to analyze the trip data after scaled. After each trip, a trip picture, which includes several most important signals, will be sent to computer in central control room, in 2 min. The trip picture can help the operator to determine if the trip comes from RF system or not.

After this fast trip diagnostics system run online, it help us to find many important RF problems, 400 kHz vibration of original No3 LLRF, pickup arc of No3 cavity and negative voltage pulse of No2 anode high power.

All valuable PVs are filled in achiever sever and the time of all IOCs are synchronized to time server to make the analysis of slow signals and trend of all signals accurate.

After all above, a comprehensive RF trip diagnostics system has been built. Preliminary tool include interlock and trip picture. Fast trip diagnostics system and achiever are post diagnostics tool. This makes the storage ring RF trip diagnostics precise and efficient.

Reference

1. Zhao S J, Chang Q, Hou H T, *et al*. DOI: 10.18429/ JACoW-IPAC2016-THPOY036.

2015–2016 年度电源部脉冲组工程技术研究研制情况

电源部脉冲组

2015–2016 年度，脉冲组所承担的工程研制任务主要包括以下三方面：1) 脉冲调制器相关工程任务及先进技术研究；2) 上海先进质子治疗装置 RFKO 系统研制及注入引出系统电源研制；3) 插入件及段间设备，弯转磁铁控制系统研制。下面分别展开介绍。

高功率脉冲调制器研究研制

2015–2016 年承担了 SXFEL 试验装置、DCLS 装置、巴西 SIRIS 直线加速器的脉冲功率源系统的设计及研制工作。功率源系统主要由脉冲调制器及速调管组成。各个项目中功率源指标参数以及进展如表 1 所示。截至 2016 年底，DCLS 项目微波功率源系统已完成设备安装、调试和验收，性能指标达到设计要求；SXFEL 试验装置项目微波功率源系统除 1 套 X 波段 5 MW 功率源外，其余 11 套功率源已完成设备安装、调试，性能指标满足设计要求；巴西 SIRIS 脉冲调制器已完成调试验收，性能指标满足设计要求。

表 1 各项目功率源指标及进展

项目	参数			
	类型	数量	功率	进展情况
SXFEL 试验装置	S-Band	4	50 MW	调试验收
	C-Band	7	50 MW	调试验收
	X-Band	1	6 MW	工程设计
DCLS 装置	S-Band	2	50 MW	调试验收
	S-Band	2	80 MW	调试验收
巴西 SIRIS	S-Band	2	50 MW	调试验收

图 1 SXFEL 试验装置 C_band 微波功率源系统

随着自由电子激光技术的发展，对脉冲调制器稳定性的要求越来越高。脉冲组在完成工程任务的同时开展了高稳定性脉冲调制器的研究工作。包括高稳定性充电电源的研究，高稳定高精度高压取样及控制技术研究，高功率脉冲变压器技术研究等。这些研究工作为将来高稳定性脉冲调制器的研制打下了坚实的基础。

SAPT RFKO 系统及注入引出电源系统

SAPT RFKO 系统。慢引出 RFKO 的主要功能是根据束流三阶共振的要求，产生一定带宽的扫频信号，在治疗定时作用下，通过对施加在 RF-Kicker 的信号进行幅度调制，进而缓慢而均匀引出束流。图 2 为慢引出 RFKO 控制总体框图。

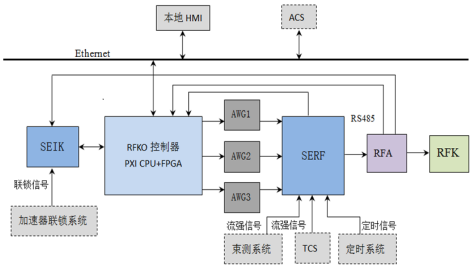

图 2 SAPT RFKO 控制总体框图

在 2015–2016 年度全面展开慢引出系统各项研制工作，包括完善接口卡 SERF、SEIK 及 SEHD 接口电路设计，包括流强接口、RF 信号接口、连锁接口等；完成 SERF、SEIK 及 SEHD 接口的调试以及与 PXI 的集成；完成 RF-KICKER 验收测试，与 RF 电源的集成，并测试了 RF 电极的调频信号；完成 RF 阻抗匹配器优化设计及加工，系统集成测试。如图 3 所示。

图 3 SERF 板卡及 PXI 集成

完成 RFKO 与本地 HMI 的通信程序调试，实现了与 EPICS 通信调试，并给出了慢引出与 ACS

控制接口信号表；完成基于粒子在引出边界呈瑞利分布的 AM 函数模型，并增加了 BM_Enable 信号自动计算 AM 函数，模拟了慢引出定时控制时序；完成了慢引出控制反馈 PID 算法设计以及 RFKO 系统安装前的验收测试。计划在 2017 年初进入现场安装。

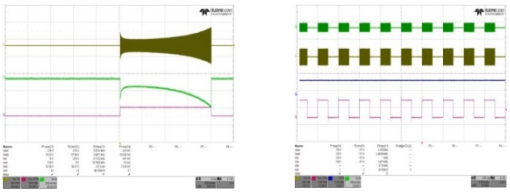

图 4　RF 电源波形及时序波形

SAPT 注入引出励磁电源及控制器

质子注入引出系统由两台静电切割板、两台凸轨磁铁、三台静磁切割磁铁以及它们的激励电源和控制组成。重点关注凸轨磁铁脉冲电源设计与本地控制、静电切割板的长距离抗干扰光纤频率信号传输控制等

注入单元有两块 Bumper,每块需独立配套励磁电源（表 2），且两台励磁电源间一致性要求较高。

表 2　Bump 磁铁脉冲电源的主要工作参数

励磁电流脉冲波形	40 μs 半正弦波
最大工作电流（峰值）	3 723 A
励磁电流时间抖动	＜±25 ns (1 h)
重复频率	0.1~0.2 Hz
励磁电流幅度稳定度	0.1%　(1 h)
波形一致性误差	＜1%
励磁电感	0.47 μH
励磁线圈电阻	0.088 23 mΩ
运行方式	长期连续运行
工作环境温度	18~30 ℃

励磁电源采用 LC 串联谐振方案，充电电源选取 TECHNIX 的 CCR 系列；采用高压大功率快速可控硅作为放电开关，产生脉宽为 40 μs 的半正弦励磁电流。设计有能量回收电路并利用快恢复二极管保护充电电源。通过串联的反向充电电荷二极管器件有效降低脉冲励磁电流反冲比。

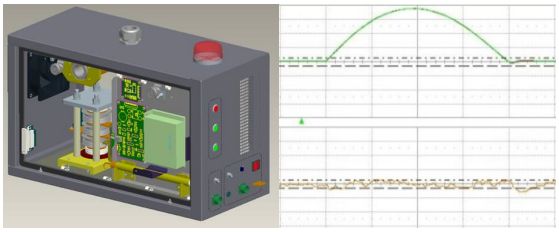

图 5　励磁电源布局和脉冲电流波形

同时设计了凸轨磁铁和静电切割板的本地控制器（图 6，7）用于对上述励磁电源和充电电源（TECHNIX 充电电源和 SPELLMAN 高压电源）进行监测和控制，完成系统内外部的联锁逻辑以及对人身和设备的安全保护，并将处理结果与 SAPT 中控交互。

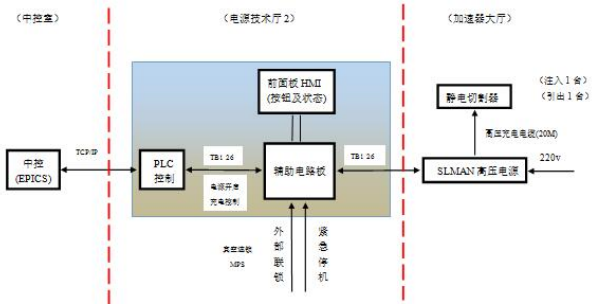

图 6　凸轨磁铁本地控制器框图

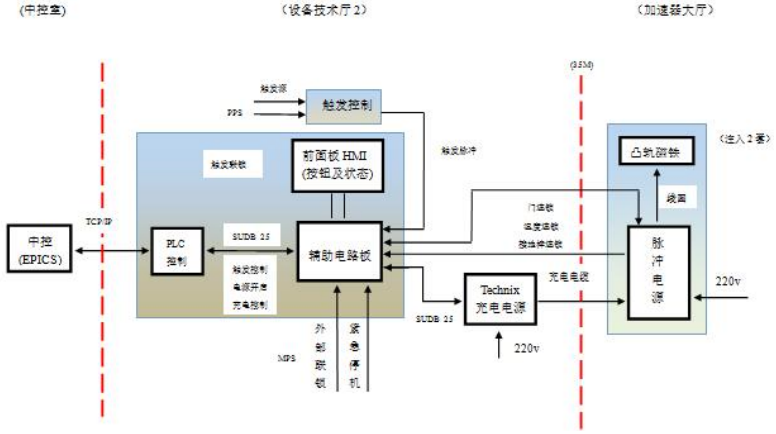

图 7 静电切割板本地控制器框图

为了解决隧道内 SPELLMAN 高压电源与设备技术厅 2 控制器之间的长距离抗干扰通信，设计了 12 路 V/F&F/V 频率信号光纤传输通道，其幅值稳定度 RMS 优于 0.1%。

插入件及弯转磁铁控制

插入件控制。插入件的控制工作主要包括 SSRF、SXFEL、DCLS 插入件及其段间设备运动控制系统的设计、调试及安装。先后分别完成了加拿大波荡器的运动控制工作；完成了低温波荡器内低温探头抗束流干扰实验；完成了首台镨铁鹏低温波荡器的运动控制和温度监测研制；完成了 DCLS 项目 6 台 U30 及 1 台 U50 波荡器的安装调试工作；完成 SXFEL 实验装置的 U23.5、U30、U40、U80 等插入件的运动控制工作及 chincane 的运动控制工作。

同时，完成了基于分布式的 SXFEL 用户装置插入件及其段间运动控制系统的工程设计。在运动控制上，将波荡器及其相邻的 BBA 以及移相器作为一个控制单元（本地控制单元）。这样将数量众多的波荡器及其段间设备划分成若干个小的控制单元，这些小的控制有独立的控制器系统，在将这些独立的控制系统与一个中央控制节点 PLC 联网，就实现了一条波荡器线的整个波荡器及其段间设备互联。一个波荡器控制单元中，波荡器控制采用 4 个伺服电机来控制磁极间隙的运动，BBA 采用两个伺服电机控制，移相器采用一个伺服电机的控制，所有这些设备的控制精度，都是采用直线绝对编码器获取位置信息进行闭环反馈后实现的。同时，控制精度除了取决于电气上传动以及检测设备的精度外，尤为重要的还要取决于机械传动的相关精度，如减速机（减速比）以及丝杠等。

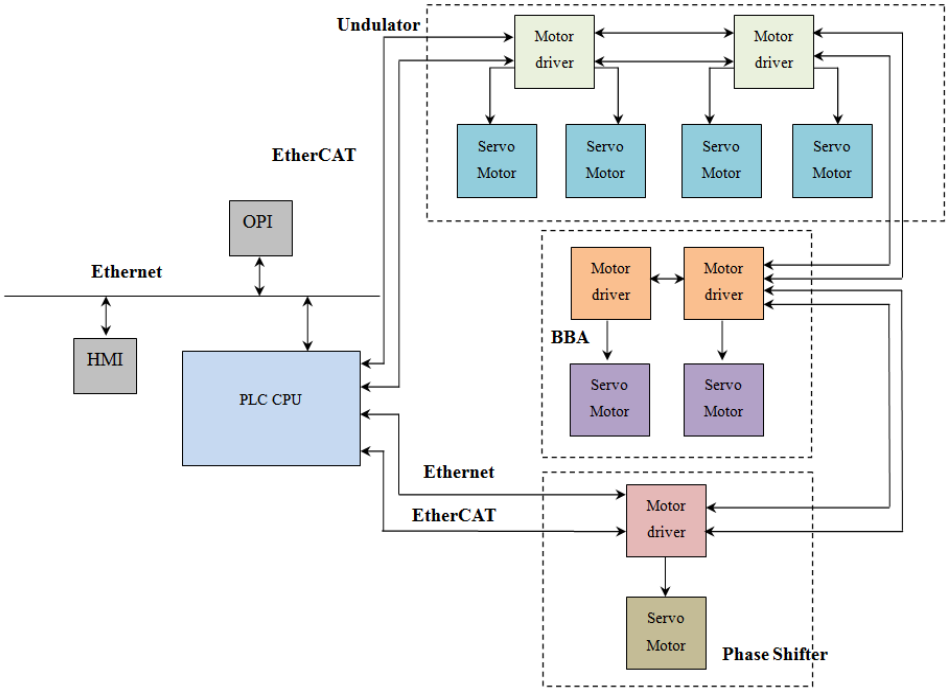

图 8　一个波荡器单元控制的示意框图

参考文献

1. 亚运, 谷鸣, 陈志豪, 等. 质子治疗装置脉冲电源研制[J]. 核技术, 2016, **39**(4): 040401.
2. 童金. 质子注入引出系统凸轨磁铁脉冲电源测试报告[R]. 内部报告, 2016.
3. 童金. 质子注入引出系统本地控制系统设计[R]. 内部报告, 2016.
4. 袁启兵, 等. 一种多路频率信号的产生及合成装置[P]. 中国, 发明专利, 2016.
5. 刘永芳, 等. 一种窄带频率信号发生器[P]. 中国, 实用新型专利, 2016.
6. 刘永芳, 等. 一种用于质子治疗装置慢引出系统的线性扫频信号发生器[R]. 中国, 实用新型专利, 2016.
7. 童金, 等. 一种基于伪随机函数的窄带噪声频率信号发生装置[P]. 中国, 实用新型专利, 2016.

2015−2016 Research & Development Annual Report of Pulse Technique Group

Power Division Pulse Technique Group

During 2015 and 2016, Pulse Technique Group is mainly in charge of 3 aspects of tasks. These tasks include:

1) High-power pulse modulator design in LINAC of SXFEL, DCLS and Brazil SIRIUS. High- power pulse modulator research and development for next generation light source.

2) Engineering design on slow extraction RFKO (RF-Knock out) system and injection& extraction power supply of Shanghai Advanced Proton Therapy Facility (SAPT)；

3) Control system of insertion devices (IDs), intersection devices (BBA, phase shifter), chicane and bending magnet in SXFEL and DCLS.

Partly development contents are presented in the following texts.

High-power pulse modulator systems

Pulsed power supply system parameters and development phase in different projects are as follows:

Table 1　System parameters and development phase

Project	Parameter		
	Type	Quan.	Kly_power
SXFEL Testing facility	S-Band	4	50 MW
	C-Band	7	50 MW
	X-Band	1	6 MW
DCLS	S-Band	2	50 MW
	S-Band	2	80 MW
SIRIS	S-Band	2	50 MW

By the end of 2016, SXFEL testing facility have already finished acceptance test for S-band and C-band modulators. Testing performance can achieve the requirement of SXFEL facility. A set of X-band modulator is under design for SXFEL. Six sets of modulator for DCLS and SIRIS also have finished acceptance test.

Fig.1　Layout of RF power supply system in SXFEL

With the development of FEL, stability requirement of pulse modulator is becoming more and more tight. In this two years, pulse technique group do some R&D work to improve the stability of pulse modulator. Such as high stability capacitor charging power supply research, high voltage high resolution high stability data acquisition system design, high power pulse transformer design and manufacture. All of these works build a strong basis in next generation modulator design.

RFKO System and Injection and Extraction Systems of SAPT

SAPT RFKO System　Main function of RFKO (RF Knock Out) for Slow extraction is to produce a certain width FM (Frequency Modulation) and AM (Amplitude Modulation) signal in accordance with beam three-order resonance requirements, which is applied on the RF Kicker under therapy timing time structure in order to extract particles slowly and uniformly. The overall control diagram of SAPT RFKO is illustrated in Fig.2.

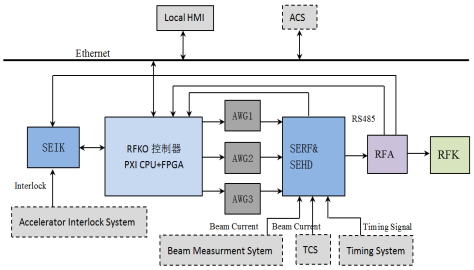

Fig.2　SAPT RFKO Overall Control Diagram

All research tasks of RFKO system are have been carried forward and accomplished successfully. These tasks are consisted of the following content:

Improving and confirming the latest PXI-power- based interface card such as SERF (RF input and output), SEIK(interlock and beam monitor card) and SEHD (SEIK function extending card) (Fig.3);

Fig.3　SERF,SEIK,SEHD card and PXI integration

Finishing FAT (Factory Acceptance Test) of RF-Kicker, and commissioning of RF-Kicker and RF power supply;

Achieving RF impedance matcher (All-Pass- Nets) optimization design and developing and system integration;

Accomplishing communication debugging between RFKO and local HMI(Human Machine Interface), communication debugging between remote EPICS, and providing process variable information table for remote ACS(Accelerator Control System);

Finishing AM function model of RFKO control based on particles Rayleigh distribution on the extraction separatrix, introducing BM_Enable signal for automatic calculation of AM function, and simulating RFKO timing control(Fig.4);

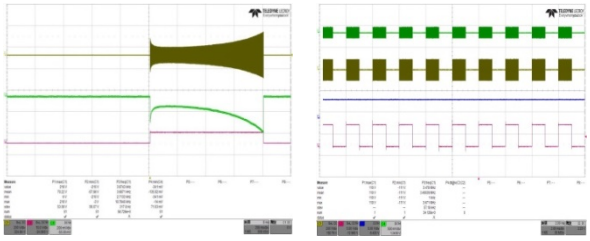

Fig.4 RF Power Waveform and Timing

Finishing PID control algorithm design and RFKO system off-line verification test.

At present, all preparation works for field installation have been ready, and field installation is scheduled to be carried out in early February of 2017.

E. Molina Marinas, J.M. Cela-Ruiz, *et al*., Proceedings of ICALEPCS2011, Grenoble, France.

Injection and Extraction Power Supply

Injection and extraction system is composed of two electric septums (ES), two bumps, three magnetic septums (MS) and their exciting power supplies and control. Focusing on the design of exciting power, anti-interference transmission of frequency signal through optical fiber in long distance and their local controls.

Injection unit has two bumpers, each of which need an independent excitation source (key parameters are shown in Table 2). The demand of consistency between two sources is strict.

Excitation source takes the scheme of LC series resonance and charging power supply selects Technix CCR series. High-voltage fast thyristor is adopted as discharge switch to produce 40 microseconds width half-sine excitation current. Energy recycle circuit is designed and using the fast recovery diode to protectcharging power supply. A series of low reverse charging diodes effectively reduce the recoil ratio of excitation current.

Table 2 Key parameters for BUMPer power supply

Wave form of exciting current	4μs , half-sine
Maximum working current(peak)	3723A
Timing jitter of exciting current	<±25ns (1 hour)
Repetition frequency	0.1-0.2 Hz
Stability of amplitude	0.1% (1 hour)
Consistency error	<1%
Inductance of magnetic	0.47μH
Resistance of magnetic coil	0.08823mΩ
Operation mode	continuous
Working temperature	18-30℃

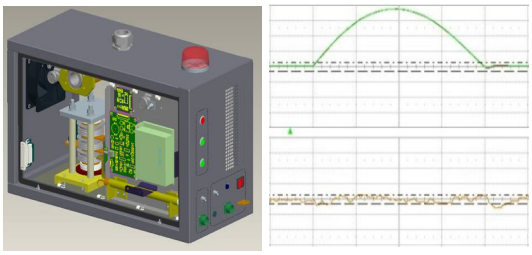

Fig.5 Excitation power supply and pulse waveform

Besides, the local control system (LCS) for the BUMPer and ES also has been designed (as shown in Fig.6,7). The LCS is aimed at monitoring and controlling of Technix charging power supply and Spellman HV power supply, dealing with the interlock logic and safety protection for personal and equipment. At last, the LCS will exchange information with SAPT central.

To solve the problem of long distance anti-interference communication from tunnel to hall 2, twelve V/F & F/V frequency signal transmission channels within optical fiber have been designed. Amplitude stability (RMS) of 12 channels is better than 0.1%.

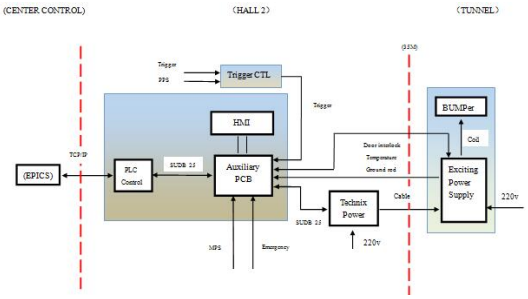

Fig.6 Block diagram for local controller of BUMPer

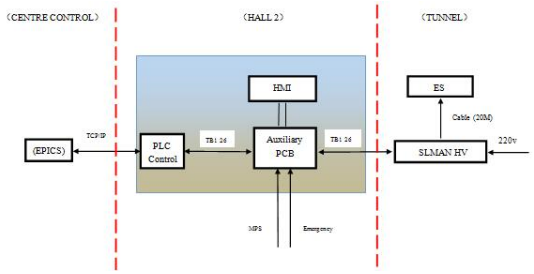

Fig.7 Block diagram for local controller of ES

Control System of IDs and Bending magnets

Motion control tasks are mainly consisted of motion control design, commissioning and field installation for SXFEL and DCLS. The concrete tasks are as follows:

Finishing motion control function and anti-bothering experiment of cryogenic temperature sensors for cryogenic permanent magnet undulator (CPMU, PrFeB); Finishing installation and commissioning of U30s and U50 for DCLS;Finishing installation and commissioning of Chicane, U23.5 , U30, U40, U80 for SXFEL test facility;

In the meantime, another work is to accomplishing innovative motion control design based on BeckHoff (servo motor)substituting Siemens-based and stepper motor-based mo-

tion control solution under investigation of counterpart solution of EXFEL and LCLS-II.

The motion control architecture is demonstrated in Fig.8. For the control aspect, an undulator line (or system) can be divided into many similar constitutional cells (undulator cell). Each undulator cell is composed of one undulator, one quadrupole mover and one phase shifter movers. An undulator consists of two magnet arrays and the gap between which ultimately determines the wavelength of the laser light. Four servo motors equipped with two drivers are adopted to drive respectively relative reducers and screw systems of undulator. For the intersection segment, three servo motors are applied two for a quadrupole mover and one for a phase shifter. All the above moving structure is equipped with LAEs (Linear Absolute Encoder) with high position acquisition resolution (0.1 μm).‘

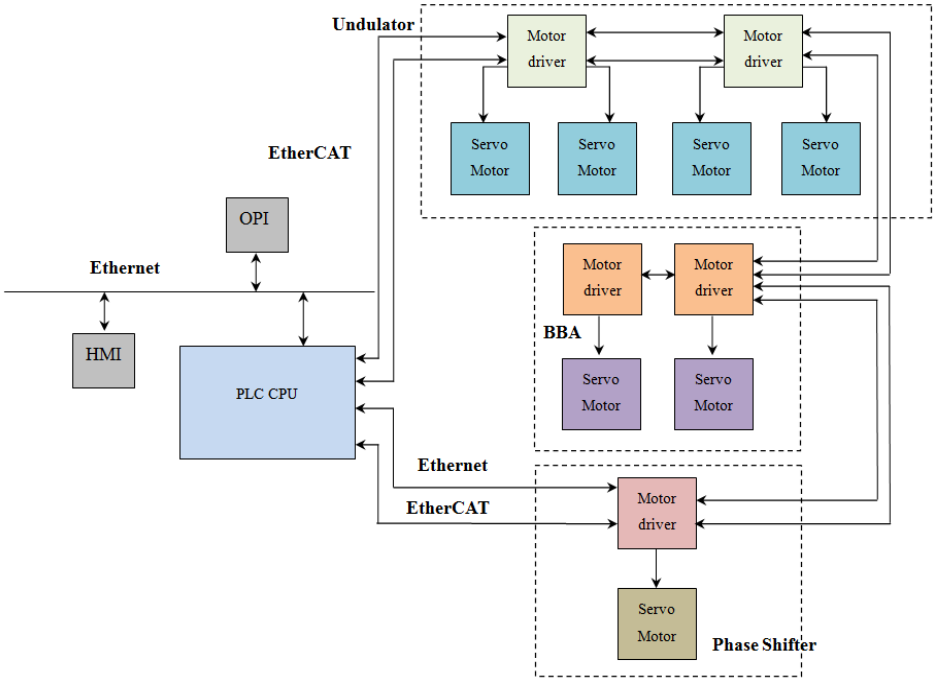

Fig.8 The control architecture of undulator cell

Reference

1. Yayun MIAO, *et al*. Development of pulsed power supply in proton therapy. Nuclear Techniques, 2016, **39**(4): 040401.
2. Tong Jin. Test report of exciting power supply for IE system of SAPT, Internal Report, 2016.
3. Tong Jin. Design of local control system for IE system of SAPT, Internal Report, 2016.
4. Yuan Q B, *et al*. A multi - channel frequency signal generation and synthesis devices, patent of invention, 2016.
5. Liu Yongfang, *et al*. A narrow-band frequency signal generator, patent for utility models, 2016.
6. Liu Yongfang, *et al*. A linear sweep signal generator used in slow extraction system for Proton therapy devices, patent for utility models, 2016.
7. Tong Jin. *et al*. A narrow band noise frequency signal generator based on pseudo - random function, patent for utility models, 2016.

束测控制部束测组研究进展

束测组

束测组承担加速器大科学工程束测系统的设计、开发、调试建造工作及上海光源束测系统的运行维护与束流研究工作。

束测组在保证上海光源一期束测系统良好运行维护外，还完成了上海光源二期束测系统的设计及经费预算等工程工作。在国内率先开展储存环逐束团测量研究工作，包括：逐束团束长测量、逐束团相位测量、逐束团电荷量测量、逐束团截面测量。引领储存环束流研究工作从束流整体行为研究转为逐束团行为研究，在加速器束测领域取得领先的研究成果[1–5]。

束测组群策群力，按时按质完成了自由电子激光大科学工程束测系统的工程建设任务，包括大连相干光源(DCLS)束测系统的设计、开发、调试建造工作，上海软 X 射线自由电子激光试验装置(SXFEL)束测系统的设计、开发、调试建造工作。在自由电子激光装置调束期间，实现对电子束流各项参数的实时测量，测量结果通过控制网发布提供给调束、运行人员，各类诊断设备的测量动态范围满足初始调束的需求；在装置进行验收时，对电子束流关键参数进行精确测量，作为主要验收手段；在装置投入运行之后，实现对电子束流主要运行参数的实时在线监测，为运行人员监测及优化运行状态提供手段，系统具有高可靠性、重复性及稳定性；

为了满足正在建设的大连自由电子激光装置和上海软 X 射线自由电子激光试验装置对束流位置分辨率优于 1 μm 的要求，上海光源束测组开展了 CBPM 系统的工程研制工作[6]。

CBPM 测量系统由探头、RF 前端、DBPM 电子学三部分组成。腔式 BPM 探头采用无氧铜谐振腔结构，包括参考腔和位置腔，位置腔水平和垂直隔离度好于 50 dB，显著降低了水平和垂直测量的耦合度，提高了测量分辨率。CBPM 的 RF 前端电子学采用数字接收机架构，BPM 探头输出的 RF 信号经腔式滤波后由低噪声放大器进行信号放大，混频至中频，带通滤波后的中频信号输入到数字信号处理器。研制完成的 RF 前端电子学经过实验室测试，其噪声水平好于−90 dBc。为实现逐束团的位置测量，采用 FPGA 技术实现全硬件流水线结构 DDC 算法，高速完成信号处理，并对 CBPM 信号处理系统进行了系统的实验室测试，得到的 0.31 μm 位置分辨率测试结果满足设计指标，达到国际同类装置水平。通过 CBPM 系统的工程研制，掌握了探头及 DBPM 电子学设计方法及批量加工工艺，实现 RF 前端关键器件的国产化，以及信号处理算法及数据采集板卡实验室原型研发技术。

图 1　CBPM 探头及 DBPM 工程批量

参考文献

1. Yang Y, Leng Y B, Yan Y B, *et al*. Development of the bunch-by-bunch beam position acquisition system based on BEEcube[J]. Nuclear Science and Techniques, 2016, **27**(2): 47.
2. Yang Y, Leng Y B, Yan Y B, *et al*. Injection performance evaluation for SSRF storage ring[J]. Chinese Phys C, 2015, **39**(9): 108-112.
3. 陈汉骄, 陈杰, 冷用斌, 等. 主成分分析方法在空间干涉仪图像处理中的应用[J]. 强激光与粒子束, 2016, **28**(12): 128-135.
4. 赖龙伟, 阎映炳, 陈之初, 等. 上海光源工作点在线监测系统[J]. 强激光与粒子束, 2015, **27**(4): 27045105.
5. 赖龙伟, 冷用斌, 陈之初, 等. 上海光源全局束流诊断数据仓库开发[J]. 原子能科学技术, 2015(6): 1149-1152.
6. 赖龙伟, 冷用斌, 阎映炳,等. 数字 BPM 信号处理器的研制进展[J]. 原子能科学技术, 2015, 49(zengkan2): 607-610.

Research Development of Beam Instrument Group

Beam Instrument Group

Beam Instrument Group undertakes the design, development, commissioning and construction of the Beam Diagnostics System for Accelerator Scientific Engineering and the research on the operation, maintenance and beam research of the beam diagnostics system of SSRF.

Besides guaranteeing the safety operation of Beam Diagnostics System of SSRF first-phase project, Beam Instrument Group have successfully carried out several major projects including the design of Beam Diagnostics System of SSRF second-phase project and appropriation budget etc. Meanwhile, the research works of bunch measurement at SSRF storage ring such as bunch-by-bunch length measurement, bunch-by-bunch phase measurement, bunch-by- bunch charge measurement, bunch-by-bunch profile measurement have taken the leading position in domestic. The research works not only changes the research idea which focuses on bunch-by-bunch rather than all bunch beam about bunch measurement at SSRF storage ring, but also obtain some breakthrough results in the field of Accelerator Beam Measurement[1–5].

Beam Instrument Group have worked together to accomplish the construction task of beam diagnostics system for the free-electron laser facilities (FELs), including the design, development, commissioning and construction of the beam diagnostics system of Dalian coherent light source (DCLS) and shanghai soft x-ray free electron laser test facility (SXFEL). During the commissioning of the SXFEL, we realized the real-time measurement of different beam parameters and provided the results to the operator through control network. Moreover, the dynamic range of various diagnostics equipment meet the needs of initial beam commissioning. When the facility is checking for acceptance, the accurate measurement of the electron beam main operating parameters has been the key acceptance means. After the facilities have been successfully put into operation, the real-time online measurement system, of electron beam, with high reliability, repeatability and stability, has provided great convenience for operators to monitor and optimize the electron beam status.

Fig.1 The probe of CBPM and DBPM.

In order to meet the requirement of beam position resolution better than 1 μm for DCLS and SXFEL facilities which are under construction, Beam Instrument Group of SSRF carried out the engineering development work of CBPM system[6].

The cavity BPM system consists of a cavity probe, a dedicated RF front-end, and a home-made digital BPM (DBPM) processor. The CBPM probe adopt resonant cavity structure and oxygen-free copper material was used. The cavity probe including a reference cavity and a position cavity, it is worth noting that the isolation of the horizontal and vertical position cavity better than 50 dB which improve the measurement resolution by reduces the coupling between them significantly. The RF front-end electronics adopt RF receiver architecture, an input cavity band-pass filter (BPF) to suppress other harmonics coupling from the cavity or the spatial disturbance into the low-noise amplifier (LNA) that follows, then the pre-amplified RF signal is down-converted to IF using a LO signal, a BPF as an ant-aliasing filter to suppress other amplified harmonics is used before the IF signal digitized by DBPM processor. The noise level of developed RF front-end electronics better than -90 dBc tested in laboratory. In order to achieve bunch-by-bunch position measurement, the FPGA technology was used to achieve DDC algorithm of full hardware pipeline architecture to complete signal processing with a high-speed. The CBPM signal processing system has been tested systematically in the laboratory, the test result of position resolution is 0.31 μm which meet the design specifications and reach the international level of similar devices.

Through the engineering development of the CBPM system, we have mastered the design methods and batch processing technology of the cavity probe and the DBPM electronics, realized the localization of key components for RF front-end, completed the signal processing algorithms and mastered the R&D technology of Data acquisition board prototype.

Reference

1. Yong Y, Leng Y B, *et al*. Development of the bunch-by-bunch beam position acquisition system based on BEEcube[J]. Nuclear Science and Techniques, 2016, **27**(2): 47.
2. Yong Y, Leng Y B, *et al*. Injection performance evaluation for SSRF storage ring[J]. Chinese Phys C, 2015, **39**(9): 108-112.
3. Chen H J, Chen J, Leng Y B, *et al*. Principal component analysis for interferometer image processing in SSRF[J]. High Power Laser and Particle Beams, 2016, **28**(12): 128-135.
4. Lai L W, Leng Y B, Chen Z C, *et al*. Real-time tune monitor system on Shanghai Synchrotron Radiation Facility[J]. High Power Laser and Particle Beams, 2015, **27**(4): 27045105.
5. Lai L W, Leng Y B, Chen Z C, *et al*. Development of Global Data Warehouse fot Beam Diagnostics at SSRF[J]. Atom Energ Sci Technol, 2015, (6): 1149-1152.
6. Lai L W, Leng Y B, Yan Y B, *et al*. Process of Digital BPM Signal Processor[J]. Atom Energ Sci Technol, 2015, **49**(zengkan2): 607-610

控制组

2015−2016 年度，上海光源控制系统在保持稳定可靠运行的同时，专注于系统的维护与优化，并根据新的要求及新技术的发展，开展控制系统升级改造工作，主要包括虚拟服务器系统升级、存储系统升级改造、MPS 系统优化升级、插入件控制等方面工作，同时，在 SXFEL 实验装置、大连相干光源 DCLS、巴西 SIRIUS 光源直线加速器、质子治疗装置等项目控制系统取得了一定的进展。

1 SSRF 虚拟服务器系统升级

上海光源虚拟化服务器系统已经运行 4 年，其中虚拟机系统使用的 Dell 服务器已经运行 7 年，存在设备老化，虚拟化软件版本陈旧等问题，为确保光源控制系统环境的正常运行，在 2015 年度 7 月底高温假期间对现有虚拟化系统及设备进行升级，将系统更新到新的软硬件平台上。

原有系统信息：上海光源虚拟化服务器系统现有用于虚拟化的主机 15 台，VCenter 服务器 1 台，系统均为 VMware ESXI 4.0，共有 25 台虚拟机在运行中。EMC CX3-20 存储 1 台，容量 10 TB。博科光纤交换机 2 台。

升级后系统信息：用于虚拟化的主机 IBM x3650 M4 服务器 4 台，博科光纤交换机 2 台，华为 S5600T 存储 1 台，容量 30 TB，系统为 VMware ESXi 5.5 Update2。

(a) 通过本次虚拟化系统升级、设备更新，提供虚拟化服务的设备由原来的 16 台减至 4 台，但是性能比原服务器高出很多。(b) 虚拟机可分配资源大大增加，虚拟服务器运行的稳定性得到充分的保障。(c) ESXi 主机升级成 VMware ESXi 5.5 后，对于单个磁盘可分配的空间限制从原来的 2 TB 增加至 16 TB。整个存储空间足够满足当前数据存储的需求。(d) vCenter 升级成 VMware vCenter 5.5 后，vSphere HA 变得更加简单易用，设置 vSphere HA 群集之后，群集内的所有虚拟机无需额外配置即可获得故障切换支持。虚拟机可充当应用程序的移动容器，可在主机之间移动。管理员会避免在多台计算机上进行重复配置。(e) 和存储相连的光交换机由来的一台变成两台，双链路结构能带来更高的可靠性，任何一台交换机故障，系统都能平稳运行。(f) 迁移后所有数据都从 EMC 存储上迁到了华为 ST5600 上，原有的 EMC 存储作为备份存储应用到新的系统中，为整个系统的数据安全提供了进一步的保障。

综上所述，本次升级后直接效果是将原有的 16 台服务器整合为 4 台，服务器数量、网络设备、机架、机房空调功率，能耗，其它外设以及 IT 支撑设备会大量减少，机房环境变得更加易于管理，虚拟机性能以及可用性和数据安全方面也有了极大的提升。

2 数据存储系统改造工作

目前光源数据存储采用 Channel Archiver 系统。Channel Archiver 系统为文件存储类型，其驱动 2009 年后停止维护更新。RDB Archiver 是 CSS (control system studio)的数据存储部分，其数据存储为关系型数据库。CSS 为一个工具集，它将数据存储，数据浏览，控制系统诊断工具及操作界面整合为一个整体，使 OPI 端的操作变得简洁高效。考虑到今后驱动的维护更新，数据存储系统需要从 Channel Archiver 系统升级为 RDB Archiver 系统。

2015 年数据存储系统的工作主要集中在对 oracle 数据库数据读取的优化和测试。对数据存储表进行优化，建立了按时间 + hash 分区的 sample_hash 表和按时间分区的 sample 表，并为其建立了 channel_id + sample_time 的索引。对两张表按未加 order by 排序和加入 order by 排序进行 1 个月和 6 个月的单通道和多通道数据查询，比较分析两张表的数据读取速度，得出以下结论：

经过 hash 子分区的 sample_hash 表查询速度明显快于未经过 hash 子分区的 sample 表；单通道查询中，sample_hash 表未进行 order by 的查询速度约为 3.8 万行/秒，有 order by 的查询速度约为 2.5 万行/秒，长时间段查询和短时间段查询速度差别不大；单通道查询中，sample 表查询速度约为 3～4 千行/秒，有 order by 的查询速度略大于没有 order by 的速度，长时间段查询速度略大于短时间段查询速度；双通道查询中，sample_hash 表查询速度波动较大，最快可以达到 2.9 万行/秒，最慢只有 4.6 千行/秒，分析 4.6 千行/秒的结果，发现通道查

询的时间与其他通道的时间相近，但是查询得到的数据远小于其他通道，造成了查询速度远小于其他通道；相连通道的查询速度大于不相连通道的查询速度，在长时间段查询中这种速度差距愈加明显；双通道查询中，sample 表查询速度约 4 千行/秒，相连通道的查询速度与不相连通道的查询速度在短时间段查询中相差不明显，在长时间段查询中相连通道的速度明显快于不相连通道；三通道查询中，sample_hash 表查询速度有很大波动，最快可以达到 2 万行/秒，最慢只有 2 千行/秒，相连通道与不相连通道的速度没有可比性；三通道查询中，sample 表查询速度有很大波动，最快可以达到 1.5 万行/秒，最慢只有 1.8 千行/秒，相连通道与不相连通道的速度没有可比性。考虑的光源数据库的需求，我们需要选择 order by 查询条件，所有的查询实例中，sample_hash 的表结构+order by 查询条件最靠近我们的需求，它的单通道查询速度在 2.5 万行/秒，离我们的目标还有一定距离，还需对数据存储表或者数据读取方式进行优化。

3 MPS 系统优化升级

3.1 增强器真空联锁改造

由于历史原因，增强器的真空联锁在建造过程中采用了两套 PLC：一套用于 MPS 联锁，由控制组负责，具备信号旁路功能；另一套用于真空阀门的开关控制，由真空组负责，不具备信号旁路功能。从实际运行情况来看，大部分故障为真空测量设备故障而非真空度发生变化。测量设备故障发生后，需要对该设备的联锁信号进行旁路，以避免发生丢束、关阀等问题。针对真空组提出的需求，本年度对增强器真空联锁软件进行了修改，增加联锁旁路功能，并将软件界面集成到 MPS 体系之中。

与原程序和功能对比，改造主要涉及以下几个方面：增加了真空报警信号的旁路、锁存及复位功能，现 EDM 界面一个真空点对应 4 个信号(Alarm, Lathed, Bypass, Reset)；在排除旁路信号的情况下，只要有相邻点同时报警，则实施联锁，关闭对应区域阀门；阀门的输出信号以锁存信号作为输入信号进行逻辑计算，也就是说联锁的解除必须进行人为的干预。即使报警消失，但是没有复位锁存信号，则系统仍处于联锁状态，阀门关闭；相邻点无报警的情况下，必须在界面点击手动开，阀门才打开；相邻点有报警，或者相邻点无报警但界面点击手动关阀门，阀门关闭；此外，保留了原程序中的部分逻辑，如下：

PLC01 控制增强器环与高能输运线的真空点和阀门，但是环与高能线的真空报警逻辑分别单独实现。PLC02 控制增强器环与低能输运线的真空点和阀门，环与低能段的真空报警逻辑合在一起实现，只要相邻点报警，环与低能段的所有阀门都放下关闭；只要低能输运线和增强器有相邻点报警，即发生联锁，则低能输运线和增强器的所有阀门全部放下；高能输运线的阀门联锁状态与其独立；保留了原程序与 MPS 和对方 PLC 的接口；真空报警联锁判断，相邻两点的顺序完全按照原真空组原程序进行编写。

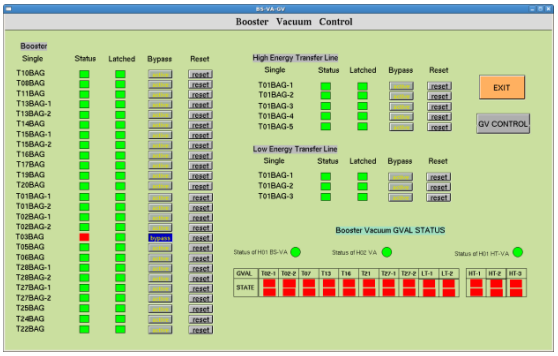

图 3.1 改造后的 OPI 界面

3.2 储存环 MPS 真空预警修改工作

修改原因： 因目前储存环真空预警采用自动复位的方式并且单点预警不联锁束流，因此当发生短暂的单点真空预警时，MPS 只发出声光预警提示，而界面上没有锁存信息，因而难以定位短暂预警信号的来源。

修改方案： 储存环所有单元的真空预警联锁处理修改为锁存方式，涉及单元 MPS 的 PLC 程序修改和 EDM 界面程序修改。

操作说明： 本次修改后，当发生真空单点预警时，单元 MPS 处理中将其锁存，MPS 总界面的“VA Warn Status”区以黄色信号保持显示发生预警的单元，如图 3.2，C01 单元发生了真空单点预警，总界面的显示方式跟修改前是一致的，只不过修改前因为预警信号未采用锁存，所以如果预警信号很快又恢复正常了，则此处的信号很快也恢复了，就看不到显示是哪个单元发生了预警。

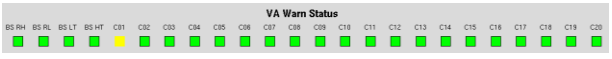

图 3.2 VA Warn Status

知道是哪个单元发生了预警后，然后进入该单

元的 MPS 界面，如图 3.3 为 1 单元 MPS 界面，在此可以看到具体是哪个真空点发生了预警。本次修改在单元 MPS 界面上增加了真空预警信号的锁存信号的显示，在“latched”栏目下的两排锁存信号，左边的为预警锁存信号，右边为报警锁存信号。预警信号的复位与报警信号共用原来的复位按钮。

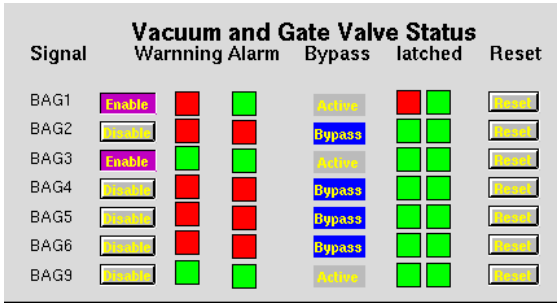

图 3.3 修改后的 1 单元 MPS 界面

4 插入件控制

4.1 CPMU 相关

CPMU 远程控制主要实现以下功能：设计 IOC 程序，对本地控制的西门子 PLC 进行控制；设计 OPI 界面，实现命令输入（如启动、停止、间隙、速度等）与状态显示（如电机状态、限位状态、光栅尺读数等）；提供 EPICS 控制接口给实验站，实现用户对插入件的操作

系统结构基于 EPICS 分布式控制系统架构，输入输出控制器(IOC)选用研华 IPC-100-60SE 工控机，安装 Linux 操作系统，使用 drvs7plc 设备驱动，数据库设计以信号表为基础，并实现相互关联的逻辑控制功能。

4.2 C03 EPU200 远程控制系统

远程控制的任务包括：通过计算机控制方法，实现对 EPU200 的间隙(Gap)及相位(Phase)进行远程调节和控制，并显示其相关设备状态及参数；提供 EPICS 控制接口给试验站，实现用户对插入件的控制；28 台前馈电源的远程控制

系统采用基于 Ethernet 的分布式控制结构，OPI 开发软件为 Edm（可扩展界面显示管理器），控制软件平台为 Epics（实验物理及工业控制系统），输入输出控制器(IOC)选用研华 ARK-2150L-S6A1E 工控机。

4.3 插入件远程控制系统权限开通

本年度进行了 DEPU 控制权限（BL09U）及五线六站(BL18U，BL19U1，BL19U2)的权限开通工作。主要工作包括：控制界面修改；Db 增加权限控制记录；整理需要权限下放信号表；EPICS 网关更新；和线站控制组进行功能测试联调。

5 SXFEL 实验装置及 DCLS 控制系统

2015 年度，全面完成了 DCLS 工程样机研制，同时工程样机研制工作增加了 MPS 控制样机与 LLRF IOC 控制样机。控制样机作为 FEL 工程关键设备研制通过了工程样机评审。

图 5.1 LLRF/EPICS 控制样机

以全开源软件为系统实现目标，制定了软件开发的标准与技术规范；明确了 FEL 控制设备的选型，编制了详细的控制系统设备表，完成了主要控制设备的采购及其研制工作；通过对 IOC 系统软件开发与集成，形成了标准安装软件包；编制了设备控制与各专业系统的接口文件，设备控制电缆表；定时系统，进行了详细设计，包括端口分配与电缆表编制；联锁系统，完成 DCLS 和 SXFEL 控制系统详细设计，开发了 MPS 工作模式控制器，基于 Master / Stations 的结构，建立了主站与各子站的信号表，联锁逻辑表，站点间信号关联表及其各站安装电缆表；控制网络的设计也初步完成。同时设备控制、定时和连锁系统进行了软件设计。

2016 年度，进入全面安装调试阶段，截至 2016 年 9 月，完成了 DCLS 控制系统的现场安装与各子系统联调与优化工作，实现了稳定可靠运行并交付大连化学物理所使用。2016 年 12 月底，对 SXFEL 已安装设备，完成了控制系统控制网络、设备控制、数据采集、定时、联锁系统的设备安装、布线与联调工作，满足了物理调束、调光要求。

图 5.2 SXFEL 设备安装与控制界面示例

6 巴西 SIRIUS 光源直线加速器控制系统

巴西直线加速器完成了注入器的束流调试，达到设计指标，控制系统运行正常，无明显故障并通过巴西方验收。用户手册等技术文档已编写完毕并提交。所有控制系统设备已可以打包。

7 质子治疗装置控制系统

加速器控制系统完成了动态电源控制等关键部件的调试，同时各个系统例如真空、注入引出等各系统控制相关的软硬件都已准备就绪。Gantry 上位控制软件已初步调试，等待设备安装后联调完成即可。

质子治疗装置的加速器安全联锁系统基于以高可靠性的 PLC 控制器为核心的硬件平台，联锁逻辑控制软件全部在 PLC 内部运行，联锁控制功能不依赖于后台服务器和网络环境，可确保 7x24 小时持续稳定可靠运行。安全联锁系统的硬件系统由两部分组成，加速器和注入器相关的联锁信号与联锁逻辑处理任务，由安装在技术厅 2 的联锁机柜内的联锁软硬件子系统完成；高能线、分支线和治疗室相关的联锁信号与联锁逻辑处理任务，由安装在技术厅 1 的联锁机柜内的联锁软硬件子系统完成。两者之间以 PLC 专用光纤通讯连接。

安全联锁系统的软件部分基于 EPICS 控制软件平台开发，由 IOC 和 OPI 组成，IOC 运行在控制系统 IOC 服务器内，OPI 软件为操作人员提供了查询、控制联锁信息和功能的操作接口。联锁事件的记录和历史记录查询功能，统一集成在加速器控制系统的数据存档系统内。

整套安全联锁系统的时间相应特性控制在 10 毫秒内，可满足加速器大部分安全联锁功能需求。超快速的束流联锁功能，由治疗系统通过专用高速接口直接连接到 RF-KO 系统和 Abort 系统实现。

安全联锁系统安装调试结束后，已投入加速器调束运行，运行稳定可靠，操作直观方便，历经数月的调束运行未发生故障和异常，其可靠性和设计的合理性得到验证。

8 质子放射信息系统 PRIS

作为一个使用质子治疗装置的医院，其完整的医院信息系统应包含 HIS、PACS、TPS、OIS 等系统。质子放射信息系统 PRIS 承担着 OIS 的功能，它与医院信息化系统、治疗装置各系统的关系如图 1-1 所示。PRIS 系统根据 HIS、PACS 系统的病人信息和 TPS 系统的病人治疗计划，对病人的治疗过程进行安排，并跟踪记录整个治疗过程，治疗结果储存在数据库中。PRIS 系统是治疗计划系统、治疗控制系统和定位系统进行数据交换的平台。

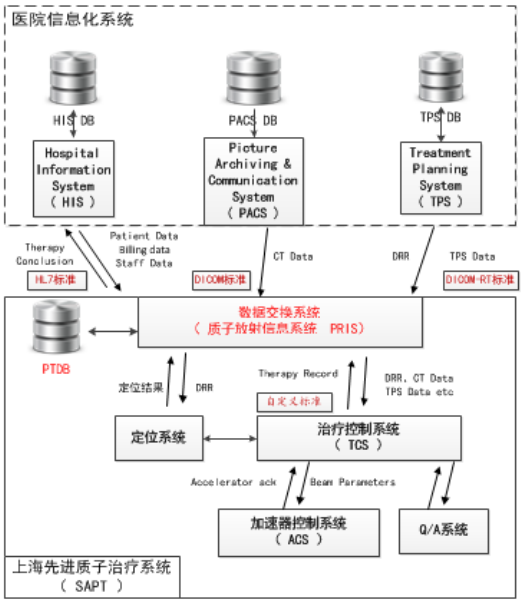

图 8.1 质子放射信息系统与医院信息化系统、治疗装置各系统关系

PRIS 系统功能包括患者管理、诊断分期管理与审核、放疗处方管理与审核、疗程管理、放疗计划管理、三维可视化与审核、排程管理、治疗实时跟踪与验证、报表统计、账户管理、治疗计划解析、定位及治疗控制系统接口、数据库管理。

根据医院的需求和治疗流程完成了系统初步设计、工程设计及评审。PRIS 软件在公开招标后，与大连现代集团签订合同，并完成了 PRIS 软件的方案设计的评审和会签，并进行了软件流程与界面设计。此外还完成医科达肿瘤信息系统 MOSAIQ 招标采购，签订 MOSAIQ 接口模块合同。

Control Group of Beam Instrument and Control Department

Control Group

From the year 2015 to 2016, the control group of Shanghai Light Source keeps the stable and reliable running. Meanwhile, they focus on the system maintenance and optimization and according to the new requirements and the development of new technology, we start the control system upgrade work. The development of the control system mainly including the upgrade of virtual server system, upgrade transformation of storage system, upgrade optimization of MPS system, control of the new insertion device, and so forth. In the meantime, the control group makes progress in SXFEL experimental apparatus, relevant light source DCLS at Dalian, Brazil SIRIUS light source linear accelerator, proton therapeutic system, etc.

1 Upgrade of SSRF virtual server system

Shanghai light source virtualized server system has run for 4 years. Dell server, used in virtual machine system, has run for 7 years, existing the defect of aging equipment, obsolete virtualization software version, and so on. In order to ensure the normal operation of light source control system, we upgrade owned virtualized system and equipment, and update this system to a new software and hardware platform during high-temperature vacation in July, 2015.

Previous system information:

In current, Shanghai light source virtualized server system has 15 hosts and 1 VCenter server with VMware ESXI 4.0 system used in virtualization, totally 25 virtual machines in running. There are 1 EMC CX3-20 storage with 10T capacity and 2 Boke optical fiber switches.

Updated system information:

We have 4 IBM x3650 M4 servers, 2 Boke optical fiber switches, 1 Huawei S5600T storage with 30T capacity and VMware ESXi 5.5 Update2 system used in virtualization.

(a) The devices offering virtualized service decrease from 16 to 4 via upgrade of virtualized system and updating of devices, but the performance is much higher than the previous servers.

(b) The allocated resources increase significantly, the stability of running the virtual servers is fully guaranteed.

(c) The allocated space restriction of single disk increases from 2T to 16T after ESXi host upgrades to VMware ESXi 5.5. The whole storage space adequately meet the current data storage requirement.

(d) vSphere HA becomes more simple and easy to use after vCenter upgrades to VMware vCenter 5.5. After setting vSphere HA cluster, all the virtual machines within the cluster can obtain fault-switching support without additional configuration. Virtual machine can be regarded as movable container of application program, moving among hosts.

(e) Light switches concatenating storage grow from 1 to 2, double link structure harvest higher reliability, the system is able to function smoothly no matter which switch has fault.

(f) All the migrated data migrate from EMC storage to Huawei ST5600, the previous EMC storage is applied to new system as backup storage, providing further protection for the data security of entire system.

In conclusion, the direct effect after upgrade is that we integrate the previous 16 servers into 4 servers. The quantity of server, network device, rack, the power of air-conditioner in machine room, energy dissipation, other peripherals and IT support equipment will reduce drastically. The environment of machine room tend to be more manageable. And there is a dramatic promotion of virtual machine performance and availability as well as data security.

2 Transformation project of data storage system

Recently, light source data takes advantage of Channel Archiver system. It is a file-storage category, its Driver cease maintenance and updating after 2009. RDB Archiver is the data storage part of CSS, its data storage is relational database. CSS, as a toolset, integrates the data storage, data browsing, control system diagnosis tools and operation interface, generating a concise and efficient OPI port operation. Considering the maintenance and updating of Driver in the future, the data storage system requires to upgrade from Channel Archiver system to RDB Archiver system.

The main project of data storage system in 2015 is concentrated on the optimization and testing of oracle database data reading. We optimize the data storage table, establish sample_hash table distinguished by time + hash, coupled with sample table distinguished by time, and set up the index of channel_id + sample_time for them. After one-month single channel data searching and six-month multi-channel data searching to this two tables with ordering of ‘order by’ and without ordering of ‘order by’, and also, compare and analyze the data reading velocity of two different tables, we draw the conclusion as follows:

(1) The searching speed of sample_hash table sub-partitioned by hash is noticeably higher than the one without being sub-partitioned.

(2) In the single-channel searching, the searching speed of sample_hash table without ‘order by’ is 38,000 lines per second, by contrast, the table with ‘order by’, its speed reaches around 25,000 lines per second. There is not much difference between long-time segment searching speed and short-time segment searching speed.

(3) In the single-channel searching, the searching speed of sample table is about 3000-4000 lines per second, the searching speed with ‘order by’ is slightly higher than the one without ‘order by’, long-time segment searching speed is marginally longer than short-time segment searching speed.

(4) In the double-channel searching, the searching speed of sample_hash table fluctuates notably, as the highest rate peaking at 29,000 lines per second, the lowest rate 4,600 lines per second. Analyzing the consequence of 4,600 lines per second, we find the channel-searching time is similar with

other channel time, but the data from searching result is far less than other channel, causing the searching speed being far less than other channel. The searching speed of connected channels higher than the unconnected channels, and there is an obvious distinction for long-time segment searching while comparing the velocity.

(5) In the double-channel searching, the searching speed of sample table is around 4,000 lines per second, there isn't an obvious distinction between connected channels and unconnected channels in short-time segment searching, while the speed of connected channels is significantly faster than unconnected channels.

(6) In triple-channel searching, the searching speed of sample_hash table fluctuates notably, with highest rate of 20,000 lines per second and lowest rate of 2,000 lines per second. And there is no comparability for the speed of connected channels and unconnected channels.

(7) In triple-channel searching, the searching speed of sample table fluctuates notably, with highest rate of 15,000 lines per second and lowest rate of 1,800 lines per second. And there is no comparability for the speed of connected channels and unconnected channels.

Taking into consideration the requirement of light-source database, we need to choose the searching condition of 'order by'. Within all searching example, the structure of sample_hash table plus the searching condition of 'order by' is nearest to our requirement. Its single-channel searching speed reaches 25,000 lines per second, there is still some way to achieve our goal, we also need to optimize data-storage table or data-reading method.

3 Optimization and upgrade of MPS system

3.1 Transformation of Booster vacuum interlock

Due to the historical reason, the vacuum interlock of booster utilizes two sets of PLC in the process of construction: one is used in MPS interlock, in charged by control group, has the function of signal bypass, the other is used in switch controlling of vacuum valve, in charged by vacuum group, doesn't have the function of signal bypass. In the actual operation condition, a majority of faults are vacuum measurement device faults, not the alteration of vacuum degree. After the fault of measurement device occurs, we need to bypass the interlock signal of this device, avoiding the lose of beam, valve shutoff, etc. Aiming to the request raised by vacuum group, the booster vacuum interlock software is revised during this year. Additionally, the function of interlock bypass is added, and we integrate the software interface into MPS system.

Compared with the previous program and function, the transformation primarily involves the following aspects:

(1) Add the function of vacuum alarm signal bypass, lock and reset, in current, one vacuum point of EDM interface corresponds to four signals (Alarm, Lathed, Bypass, Reset).

(2) Under the case of excluding the bypass signal, we should implement interlock, shut down the valve of corresponding area as long as the contiguous points give an alarm simultaneously.

(3) The output signal of valve use latch signal as input signal to conduct logical computing, that is to say, in order to remove interlock, it must be intervened by people. Even if the alarm vanishes, the system is still in interlock state and valve shutoff without reset latch signal.

(4) We must click manually at interface, so that the valve opens under the case of no alarm within contiguous points. Contiguous points has alarm, or contiguous points has no alarm but the valve shutoff by clicking interface manually, the valve shuts down.

what's more, we reserve a portion of logic in previous program, as follows:

(1) PLC01 control booster ring and vacuum points and valve of high-energy transport line, however, the vacuum alarm logic of ring and high-energy line are achieved respectively. PLC02 control booster ring and vacuum points and valve of low-energy transport line. As a whole, ring and the vacuum alarm logic of low-energy segment fulfill together. All the valves of ring and low-energy segment shut off as long as the contiguous points give an alarm. The interlock occurs as long as the contiguous points of low-energy transport line and booster give an alarm, and then, all the valves of low-energy transport line and booster put down. The valve interlock state of high-energy transport line is independent to it.

(2) Reserve the previous program, MPS and interface of PLC.

(3) The judgement of vacuum alarm interlock, writing the sequence of two contiguous points utterly according to the previous program of previous vacuum group.

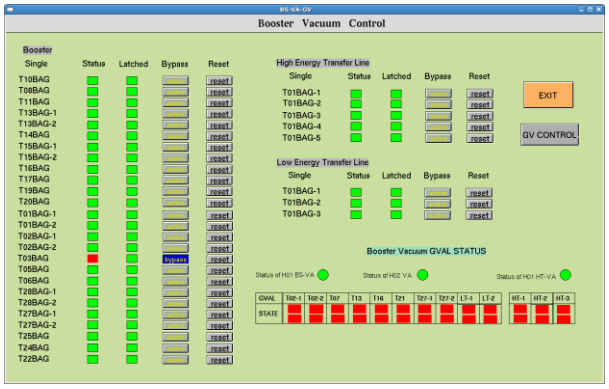

Fig.3.1 OPI interface after transformation

3.2 Storage ring MPS vacuum alarm prediction revision work

The reason for revision:

Because the current storage ring vacuum alarm prediction utilizes the method of automatic reset and the single point alarm prediction doesn't interlock beam, MPS gives out the alarm prediction hint of sound and light with no latch information on interface when ephemeral single point gives an alarm prediction. Therefore, we have a hard time to locate the source of ephemeral alarm prediction signal.

The scheme to revise:

Revise all unit of vacuum alarm prediction interlock disposal in storage ring to latch method, which involves unit MPS's PLC program rectification and EDM interface program's rectification.

Operation specification:

After revision, when vacuum single point gives an alarm prediction, unit MPS disposal larch it. 'VA Warn Status' on MPS interface uses yellow signal to maintain display the unit that gives out alarm prediction. As shown in figure 3.2, C01 unit appears vacuum single point alarm prediction, the display mode of interface is consistent with the previous. Because alarm prediction signal doesn't use latch before revision, if alarm prediction signal recovers to the normal state rapidly and the signal here recovers soon as well, then we cannot see which unit makes alarm prediction.

Fig.3.2 VA Warn Status

Entering the MPS interface of a particular unit when we know which one makes alarm prediction. As shown in figure 3.3, it's a one-unit MPS interface, we can see which vacuum point gives out alarm prediction concretely here. After revision, we add the display of latch signal of vacuum alarm prediction signal on the unit MPS interface. Two rows of latch signal beneath the 'latched' column, alarm prediction latch signal on the left, alarm latch signal on the right. Both reset of alarm prediction signal and alarm signal use previous reset button.

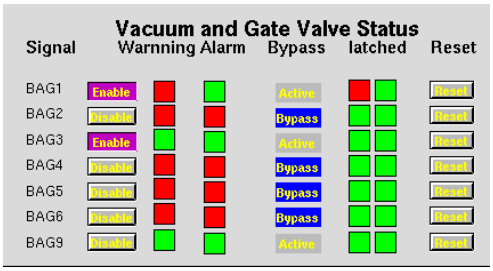

Fig.3.3 One-unit MPS interface after revision

4 Insertion device control

4.1 CPMU relevance

CPMU remote control mainly achieve the following functions:

(1) Design IOC program, control Siemens PLC of local control.(2) Design OPI interface, achieve commands input (such as start, stop, interval, speed) and state display (such as the state of electric machine, limit state, grating scale reading).(3) Offer EPICS control interface to experiment station, achieving that users operate the insertion device.System construction is based on EPICS distributed control system structure. Input and output controller (IOC) is from Yanhua IPC-100-60SE industrial personal computer, installing Linux operation system, using drvs7plc device driver. Based on signal table, the design of database achieve correlated logical control function.

4.2 C03 EPU200 remote control system

Remote control task include:

(1) Achieve the remote regulation and control of EPU200's gap and phase by computer control method, and display related device states as well as parameters.

(2) Offer EPICS control interface to experiment station, achieving that users operate the insertion device.

(3) The remote control of 28 feedforward power supply.

System uses distributed control structure based on Ethernet, OPI development software is Edm (scalable interface display administrator), control software platform is Epics (experimental physics and industrial control system), input and output controller (IOC) uses Yanhua ARK-2150L-S6A1E industrial personal computer.

4.3 Granting permission to insertion device remote control system

In this year we allow access to DEPU (BL09U) and five lines six station (BL18U，BL19U1，BL19U2). The primary work is as follows:

(1) Revision of control interface; (2) Db add permission control record; (3) Make up required permission delegate signal table; (4) Update of EPICS gateway; (5) Union debugging of function testing with line-station control group

5 SXFEL experimental apparatus and DCLS control system

In 2015, we completely finish the research of DCLS project model machine, and at the same time, the research of project model machine add MPS control model machine and LLRF IOC control model machine. Control model machine, as FEL project key device research, passes the review of project model machine.

Fig.5.1 LLRF/EPICS control model machine

We regard utterly open source software as system achievement goal, enact standard and technical specification of software development, specify the exterior of FEL control device, write specific control system device table, finish the collection and research of main control device, form a standard installation software package via the IOC system software development and integration, write the interface document of device control and every specialty system, and device control cable list. As to timing system, we make specific design, including port distribution and cable list standard. As for interlock system, we finish the specific design of DCLS and SXFEL control system, develop MPS work mode controller, based on the structure of 'Master / Stations', set up signal table, interlock logical table, inter-station signal correlation table,installation cable list between main station and each substation. The design of control network is preliminarily finished. Meanwhile, we conduct the software design for device control, timing and interlock system.

In 2016, we are in the stage of comprehensive installation and debugging. By September 2016, we accomplish field installation of DCLS control system and joint debugging together with optimization of each subsystem, achieving stable and reliable functioning and give it to Dalian chemical physics for

use. At the end of December, 2016, we finish control system control network, device control, data collection, timing, device installation of interlock system, wiring and joint debugging for SXFEL installed apparatus, and meet the requirement of phsical adjusting beams and luminance.

Fig.5.2 Example of SXFEL apparatus installation and control interface

6 Brazil SIRIUS light source linear accelerator control system

Brazil linear accelerator finishes beam adjusting of injector, meet the design indicator. The cotrol system functions normally without obvious fault and passes the acceptance of Brazil. Technical files such as user's manual have already been writen down and submitted. All the control system device can be packed.

7 Proton therapy apparatus control system

Accelerator control system finishes debugging of dynamic power supply control and so forth, meanwhile, the relevant software and hardware of each system such as vacuum, injection and extraction, etc. are ready. The upper control software of Gantry has preliminarily debugged, waiting for joint debugging after installation of devices.

Accelerator security interlock system of proton therapy apparatus is based on hardware platform with high reliability PLC controller as its core. All of the interlock logical control software runs in the interior of PLC. Interlock control function doesn't rely on the backend server and network environment, which ensures 7x24 hours running constantly, stably and reliably. The hardware system of security interlock system consists of two parts. Accelerator and interlock signal relevant to injector and interlock logical disposal task, finished by interlock software hardware subsystem put in the interlock cabinet owned by No.2 technology department. High-energy line, branch line and interlock signal relevant to treatment room and interlock logical disposal task, finished by interlock software hardware subsystem put in the interlock cabinet owned by No.1 technology department. They are connected by PLC exclusive fiber-optic communication.

The software of security interlock system is developed by EPICS control software platform, consisting of IOC and OPI. IOC runs in the control system IOC server, while OPI provides operators with operation interface of searching, control interlock information and function. The record of interlock events and the searching function of historical record are uniformly integrated in the data archiving system of accelerator control system.

The time corresponding features of the whole security interlock system is controlled within 10 milliseconds, which satisfies a majority of accelerator's security interlock function requirement. Ultra-fast beam interlock function is achieved by treatment system that concatenates to RF-KO system and Abort system directly via exclusive and high-speed interface.

After installation and debugging of security interlock system, it is applied to the running of accelerator's beam tuning. Its running is stable as well as reliable, and it has a straightforward and convenient manipulation. Its reliability and rationality of design prove to be eligible because it doesn't have any fault or exception throughout several months' debugging and running.

8 Proton radiation information system PRIS

As a hospital using proton therapy apparatus, the complete hospital information system should contain HIS system, PACS system, TPS system, OIS system, etc. Proton radiation information system undertakes the function of OIS, the relationship among proton radiation information system, hospital information system and therapy apparatus system is reflected figure 8.1. the PRIS system arranges the therapy process for patients and keeps track of the entire treatment process according to patient's information of HIS, PACS system and patient's therapy scheme of TPS system. The treatment results are stored in the database. PRIS system is the platform of data exchanging for therapy scheme system, therapy control system and location system.

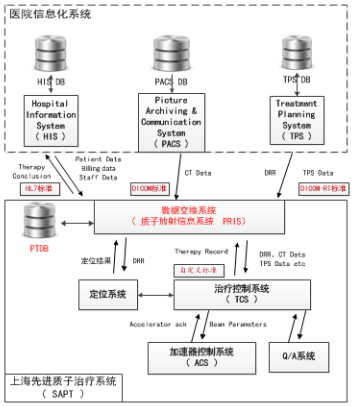

Fig.8.1 The relationship among proton radiation information system, hospital information system and therapy apparatus system

The function of PRIS system includes patient administration, diagnostic phased management and audit, radiation therapy prescription management and audit, management of treatment course, radiation therapy plan administration, three-dimensional visualization and audit, scheduling management, treatment real-time tracking and validation, statistical reports, account management, therapy plan analysis, location and treatment control system interface, database management.

We fulfill system preliminary design, project design and audit in accordance with the requirements and therapy procedures of hospital. After open tendering, PRIS software signs a contract with Dalian Modern corporation, finishes the audit and countersignature of designed plan of PRIS software, designs software procedure and interface. Moreover, it finishes MOSAIQ purchasing by invitation to bid of Yikeda tumor information system, signs a contract of MOSAIQ interface module.

基于同步辐射光束线电子激发的气体解吸实验装置研制

束线机械工程技术部

概述

光电解吸气载是通光条件下，光束线真空系统内的主要气载。材料的种类及表面处理工艺决定了光电解吸气载的气体种类和多少。

电子激发气体解吸实验装置，可以在较为清晰简单的物理过程下，模拟光电子及二次电子对光电解吸气载产生的作用。得到各种材料在各种表面处理工艺下的电子解吸系数。本课题以研制电子激发实验装置为目的，完成整个实验装置的设计、安装及电子枪加速电压、栅极电压和聚焦极等参数的调试。并在有限的条件下实验得到经机械抛光、去离子水超声波水洗后无氧铜材料电子解吸系数。

为今后进行其它材料的解吸实验研制可行的实验装置和有效的实验流程。为整个光束线真空系统在材料选择，表面处理工艺选择提供第一手的实验数据支撑，从而提高整个光束线真空系统的研制水平。

项目成果

装置设计

完成了装置的设计，其中包括：真空排气系统、传输机构、换样机构、排气和激发腔体、三维调节机构和具有冷却、绝缘、加正偏压功能的样品台结构。如图 1~5 所示。

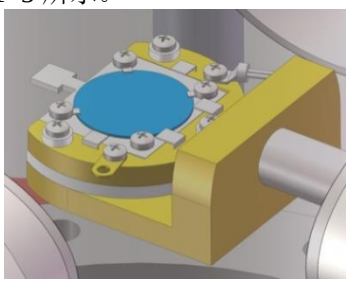

图 1　样品台

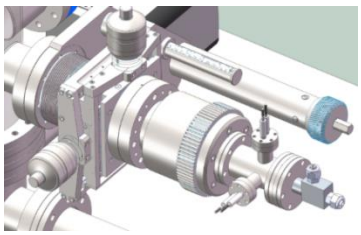

图 2　三维调节机构

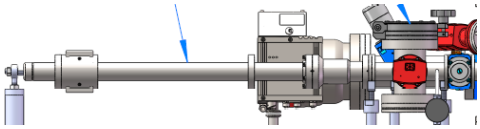

图 3　进样系统

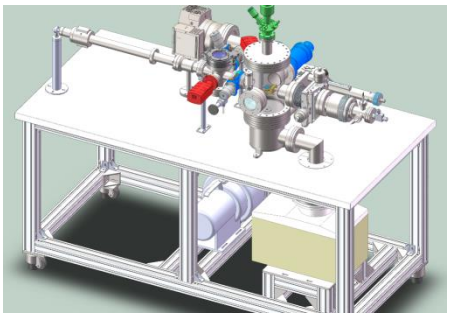

图 4　整体设计

图 5　实体装置调试

初步实验

设计整个实验流程，找到合适的电子枪参数，其中包括阴极灯丝活性操作方法、调制极(Grid)与加速阳极电压施加关系、聚焦极与光斑大小关系等。

经真空调试至本底 2.9~8 Torr 排气腔 7.2~9 Torr。并获得本底气载谱图：

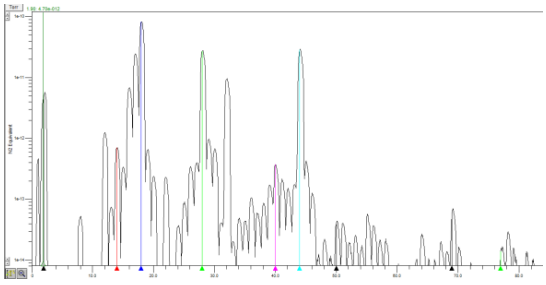

图 6 本底谱图

开启电子枪进行样品轰击 200 eV，经 12 h 后

记录各个气体分子的分压强如下：

表 1 经 12 h 轰击后的分压对比

气体分子质量	本底分压 / Torr	12h 轰击后分压 / Torr
2	4.96×10^{12}	4.91×10^{12}
14	7.06×10^{13}	9.03×10^{13}
18	8.21×10^{11}	5.82×10^{11}
28	2.69×10^{11}	4.08×10^{11}
40	3.74×10^{13}	6.00×10^{13}
44	2.84×10^{13}	7.89×10^{11}
50	3.94×10^{14}	2.97×10^{13}
69	5.88×10^{14}	3.99×10^{13}
77	1.38×10^{14}	1.02×10^{413}

项目总结

本项目对上海光源光束线真空系统的材料选型，表面处理工艺选择有重要的数据支撑作用。

本实验装置可以进行在线升级改造为光子激发气体解吸装置。

该实验装置由于经费问题，缺少各种材料在各种表面处理下的样品，1/8 英寸通气管与转接，一套分子泵抽气组和远端控制用电脑。该装置在满足上述材料及耗材供应的前提下，可以增加磁偏转系统，用于抵消电子直接轰击样品上造成的热解吸，从而得到更准确的电子解吸气体参数。

The Study Of the Electron-Stimulated Desorption Equipment For Synchrotron Radiation

Beam Line Mechanical Engineering Technology Department Beam Line Technology Group

Photo-stimulated-desorption is unique to the synchrotron radiation beam line, which is the main part of the dynamic gas load of beam line vacuum system. In the process of the whole Photo-stimulated-desorption, photoelectron and secondary electron excitation of vacuum material surface adsorption gas plays a main role. By using electron-stimulating desorption equipment (ESD), Some experiments with different materials in different processes can be done. Through theoretical calculation and analysis based on the physical process of electron-stimulating desorption , this paper has developed the equipment for above-mentioned experiments in electron energy range 400~1 000 eV.

Equipment Developed

Com Completed the device design, including: vacuum exhaust system, transmission mechanism, HuanYang institutions, exhaustand stimulate cavity, three-dimensional adjusting mechanism and with functions of coolings, insulation, and positive bias the sample of the structure. See figure1 to 5.

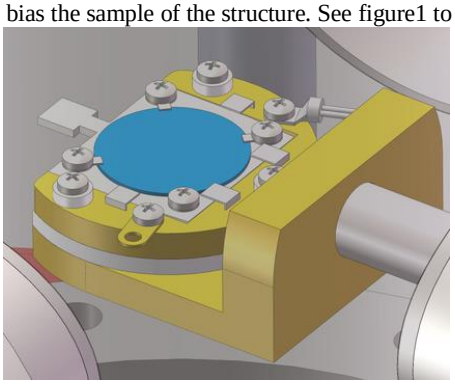

Fig.1 Sample table

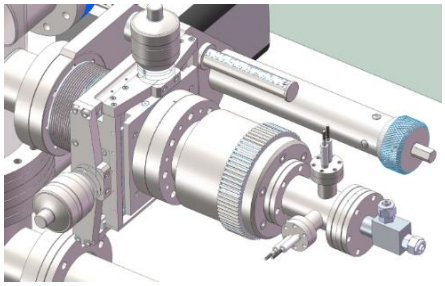

Fig.2 Adjusting mechanism

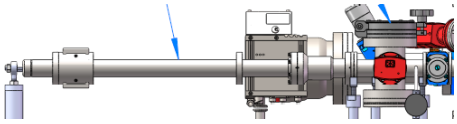

Fig.3 Transmission mechanism

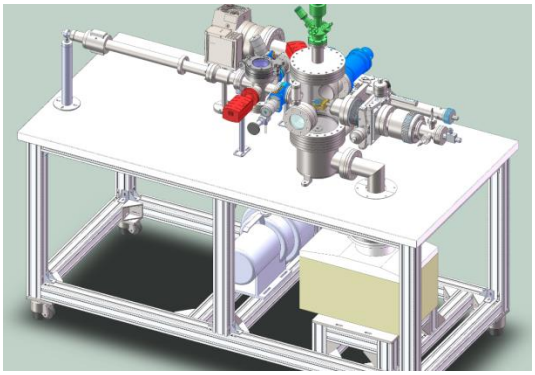

Fig.4 Overrall design

Preliminary Experiment

Design the whole experiment process, to find the right gun parameters, including the cathode filament active operation method, modulation (Grid) and accelerating the anode voltage applied relationship, focus on pole and spot size, etc.

After vacuum debugging, the exhaust cavity of 2.9~8 torr is 7.2~9 torr. And obtain the background gas load spectrum:

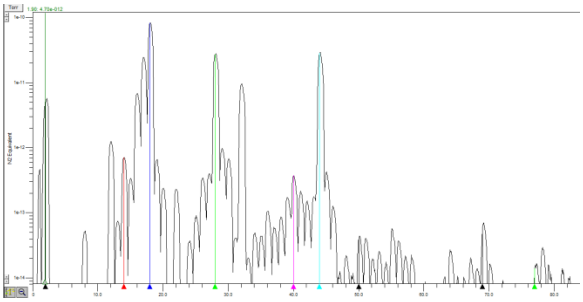

Fig.5 Spectrogram

X 射线自由电子激光试验装置诊断光束线进展

束线机械部

关键进展

2015 年 6 月，完成光束线工程方案设计评审；2015 年 12 月，完成高精度谱仪等主要设备的采购；2016 年 5 月，完成高精度谱仪等设备工程设计评审；2016 年 12 月，完成前端现场安装调整，并探测到光。

总体设计

光束线设计波长范围 5~10 nm，能量分辨率要求 10000@8.8 nm，真空要求小于 1×10^{-7} Torr。光学布局如图 1 所示，二维总图如图 2 所示。

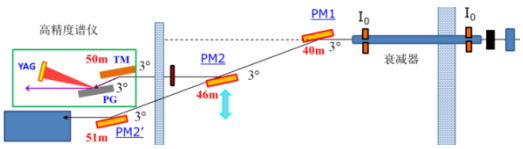

图 1 光束线光学布局图

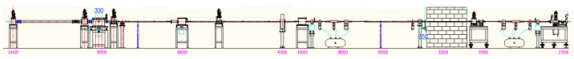

图 2 光束线二维总图

前端

前端主要包括固定光阑、挡光器、气体通量衰减器、安全光闸等。难点在于在紧凑的空间（约 2 m）内实现 7 个量级以上的真空差分，衰减器设计方案如图 3 所示，建成的前端如图 4 所示。

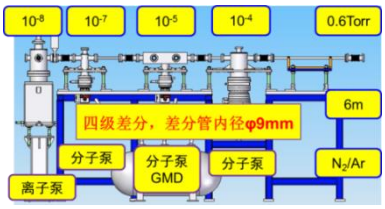

图 3 气体通量衰减器真空差分设计

图 4 光束线前端

束线

束线主要包括高精度谱仪、偏转镜箱、非标加工及束线集成等，其中谱仪是 FEL 脉冲谱学测量的关键设备，包含由超环面镜和光栅组成的光栅单色器、以及 YAG 探测器等，其主要设计参数如表 1 所示，工程总图如图 5 所示。

表 1 高精度谱仪主要参数

参数		调整范围	分辨率	重复精度
超环面镜	Y	±1 mm	0.01 mm	0.02 mm
超环面镜	Z	±1 mm	0.01 mm	0.02 mm
超环面镜	r-Z	±1°	5″	10 ″
平面光栅	Y	±1 mm	0.01 mm	0.02 mm
平面光栅	r-Z	±1°	5″	10 ″
YAG 晶体	平移	±130 mm	1 mm	—

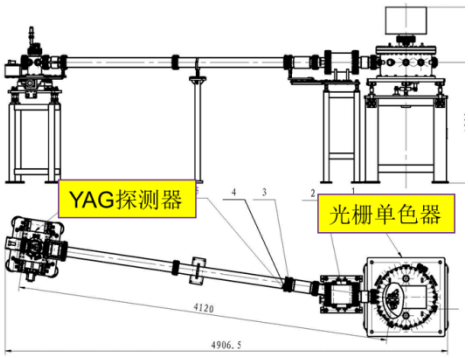

图 5 高精度谱仪工程总图

在线测试

2016 年 12 月 31 日，使用皮安计测量挡光器开闭两种状态下，前端光电二极管引出光电流的变化，首次探测到光进入到前端，如图 6 所示。

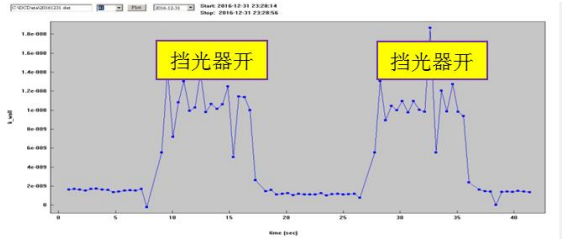

图 6 光电流变化图

Progresses in Diagnostic Beamline at SXFEL

Beamline Mechanical Department

Key progress

2015.06 Design review of beanline project plan; 2015.12 Purchasing of the high-precision Spectrometer etc; 2016.05 Design review of the high-precision Spectrometer etc.;2016.12 Installation of front end, and the light was detected.

Overall design

The designed wavelength range of the beamline is 5~10 nm, the energy resolution demands 10000@8.8 nm, and the vacuum requires less than 1×10^{-7} Torr. The layout of the beamline just like Fig.1, and the general drawing sees Fig.2.

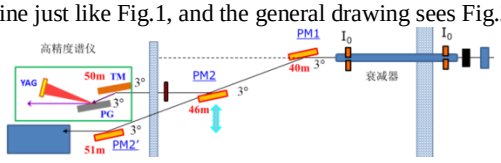

Fig.1 The layout of the beamline

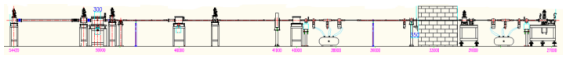

Fig.2 The genera drawing of the beamline

Front end

Front end includes fixed aperture, photon shutter (PS), gas attenuator (GAT), safety shutte(SS)r etc. The difficult point is seven orders of magnitude vacuum differential in the compact space (~2 m). The design of GAT see Fig.3, and the built front end see Fig.4.

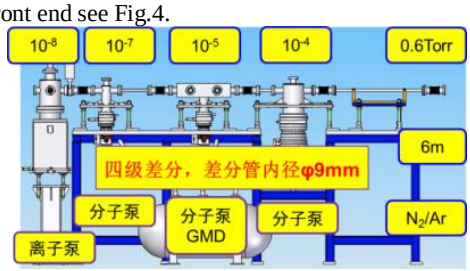

Fig.3 The vacuum differential of GAT

Fig.4 The front end

Beamline

Beamline includes high-precision spectrometer, deflection mirror chambers, non-standard equipments manufacture and integrated, and the spectrometer is the key equipment of FEL pulses spectrometric measurement, including grating monochromator, which consists of toroidal mirror (TM) and plane grating (PG), the main parameters of the spectrometer see table 1, and the general project drawing see Fig.5.

Table 1 The main parameters of the spectrometer

Parameters		Range	Resolution	Repeatable precision
TM	Y	±1 mm	0.01 mm	0.02 mm
TM	Z	±1 mm	0.01 mm	0.02 mm
TM	r-Z	±1°	5″	10″
PG	Y	±1 mm	0.01 mm	0.02 mm
PG	r-Z	±1°	5″	10″
YAG	translation	±130 mm	1 mm	—

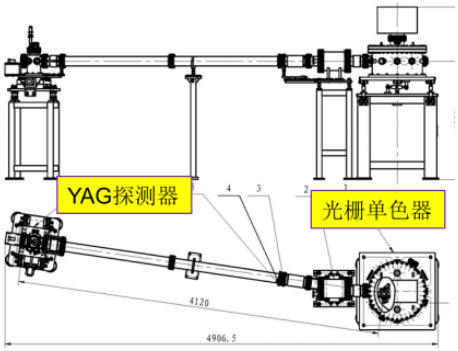

Fig.5 The general project drawing of the spectrometer

Beamline

The light is detected at the front end on the last day of 2016, through the photocurrent variation of the photodiode (Fig.6), using the picoammeter to measure under the two states of PS open or not.

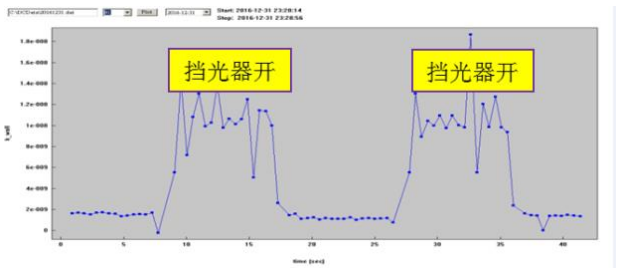

Fig.6 The photocurrent variation

束线工艺组工作进展(2015-2016)

束线机械工程技术部

新建光束线站棚屋系统工程建设

本组根据光源二期线站进度计划，完成了膜蛋白、表面衍射、纳米磁学、P2、超小角（大厅内）、动力学和能源材料等二期首批 8 条线站辐射防护棚屋的工程设计，包括线站棚屋工程设计说明书、线站棚屋总体布局图、线站棚屋结构设计总图等；编制完成二期线站辐射防护棚屋建造 CPM 表；完成首批线站棚屋屏蔽铅版采购的明细表以及材料明细表。

编制完成首批线站棚屋加工与安装招投标文件，完成棚屋加工与安装的招投标工作；完成棚屋加工与安装项目的合同签订，完成首付款；完成膜蛋白、表面衍射、纳米磁学线站辐射防护棚屋结构设计总图和全部部件图设计，完成图纸 176 张，图纸会签后直接发给工厂进行加工图设计。

初步完成 P2、超小角线（大厅内）站辐射防护棚屋结构设计总图和全部部件图设计，完成图纸 116 张；完成通用谱学线站棚屋改造的结构设计总图和全部部件图设计，完成图纸 23 张。

完成 X 光学测试线辐射防护棚屋结构设计、设计评审、加工与安装招投标，签订加工与安装合同，完成标准设备采购；编制设计说明书 1 份，招投标技术文件 1 份，完成部件结构设计图纸 107 张；完成线站辐射防护棚屋现场安装、测试；完成棚屋内 4 套手动吊车的加工、安装与测试以及通光测试的相关配合工作。

上海光源 X 光学测试线站(BL09B)辐射防护棚屋

完成 BL03U 线站辐射防护棚屋、单色器恒温棚屋结构设计、设计评审，签订加工合同； 编制设计说明书 1 份，加工工艺要求 2 份，完成部件设计图纸 58 张； 完成棚屋工厂加工，等待发货、现场安装；完成了单色器棚屋恒温系统方案设计，编制恒温系统设计、加工、测试与验收工艺要求 1 份；完成合同签订，正在进行设备加工与采购。

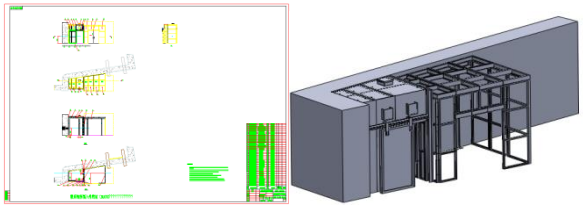

BL03U 线站辐射防护棚屋、单色器恒温棚屋

新建光束线站水电气系统工程建设

完成了微系统所弯铁线站及插入件线站前端区水、电、气公用设施系统设备安装、测试、通光调试；并完成了微系统所弯铁线站及插入件线站棚屋内水、电、气等公用设施系统主要设备安装，完成束线集成阶段的水、电、气系统设备安装（含真空电缆、控制电缆布线、接线及调试）与通光测试。

本组完成 X 光学测试线站(BL09B)前端区水、电、气公用设施系统的设备安装、测试工作，完成测试线站水、电、气公用设施系统工艺设计、设计评审、设备安装招投标，签订设备安装合同，完成标准设备采购以及设备安装； 编制完成设计说明书 1 份，招投标技术文件 1 份，完成工艺设计图纸 12 张；

本组完成了软 X 射线自由电子激光试验装置(SXFEL)束流诊断操作实验区水、电、气系统工艺设计及设计评审，完成水、气系统标准设备采购，完成设备安装。

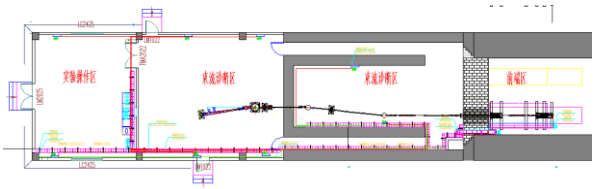

软 X 射线自由电子激光试验装置工艺设计

Work Progress of Beamline Process Group Duration 2015 to 2016

Department of Beamline Mechanical Engineering

Construction of new beamline hutches

Our group has completed the design of the radiation protection hutches of Membrane Protein, Surface Diffraction, Nanometer Magnetism, P2, Ultra-low Angle Scattering (in the hall), Dynamics and Energy Materials, which are the the first 8 beamlines in the second stage of the project. We have completed the design specification of the beamline hutches, the general layout of the beamline hutches, the general plan of the structure design of the beamline hutches. We also have completed the CPM schedule for the construction of radiation protection hutches in the second stage of the project. We have finished the material list of the first 8 beamlines hutches.

Our group has completed the bidding documents for first 8 beamlines hutches, then we have completed bidding of the construction of the first 8 beamlines hutches. We have completed the general layout and structural design of hutches of Membrane Protein, Surface Diffraction, Nano Magnetic beamlines, including 176 drawings. We have send the drawings to the factory after out signatures.

We have completed the general layout and structural design of hutches of P2 and Ultra-low Angle Scattering beamlines(in the hall), including 116 drawings.

We have completed the general layout and structural design of hutch of General Spectroscopy beamline,including 23 drawings.

Radiation protection hutch of X Optical Test Beamline

We have completed the structure design, design review, bidding of the construction, contract signing of the hutch of X Optical Test beamline. We have finished 1 copy of the design specification, 1 copy of the bidding technical documents, and 107 drawings of the structure design.We also have completed the construction of radiation protection hutch, 4 sets of manual crane in the hutch and related work of the light test.

We have completed the structure design, design review, contract signature and construction of radiation protection hutch and monochromator constant temperature hutch of BL03U beamline.

We have finished the design specification, processing process and 58 drawings of design.

We have completed design of the thermostat system of monochromator hutch.

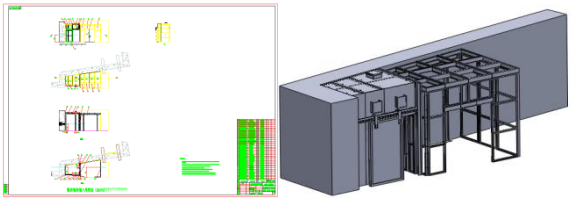

Radiation protection hutch and monochromator constant temperature hutch of BL03U beamline

Construction of process system for new beamlines

Our group has completed the construction of process system at the front end of the two beamline of Institute of Microsystems, and completed equipment installation, test, light debugging.

We have finished the equipment installation and testing of the process system at the front end of the X optical Test beamline (BL09B),and completed process design,design review, equipment installation and bidding of the beamline.We have finished 1 copy of the design specification, 1 copy of bidding documents and 12 drawings.

Our group has completed process design,design view, purchase of standard equipment, equipment installation of soft X-ray free electron laser (SXFEL) beamline. We have finished the Process system design of diagnosis area.

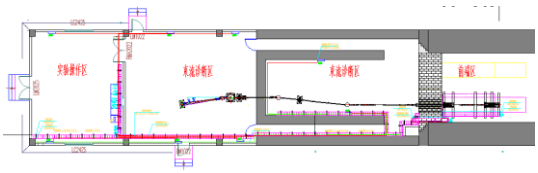

Process system design of soft X-ray free electron laser test device.

束线机械组的研究进展(2015-2016)

束线机械工程技术部

束线机械组主要承担“上海光源”已建线站光束线机械系统的运行维护和新建线站机械系统的工程建设任务。已建线站光束线机械系统运行稳定，设备可靠性不断完善，有力支持了线站总体的稳定运行。工程建设方面，完成了 SiP·ME2 项目建设基于上海光源弯铁(02B)的软 X 射线光束线以及 X 射线自由电子激光试验装置诊断光束线，二期关键技术研制方面，完成了单色光狭缝、亚微弧度压弯机构、色散弯晶单色器以及高能劳厄单色器等关键部件的结构设计。

基于上海光源弯铁(02B)的软 X 射线光束线，为提高弯铁线光通量，椭圆柱面聚焦镜箱(ECM1)尽量靠近光源点，是上海光源首个放置于前端区的光束线镜箱。镜箱采用大尺寸方形腔体，通过优化结构材料以及真空处理工艺，实现超高真空和高的洁净度；设计直通光冷却组件，防止直通光照坏其他部件且保证反射光顺利通过；将垂直驱动组件包铅皮，前面和侧面封铅板以作辐射防护；为方便安装与维护，采用可整体吊入吊出墙设计。该光束线光子通量达到 6×1011 phs/s/0.1%bw，明显高于国际同类线站。

X 射线自由电子激光试验装置诊断光束线光束线设计波长范围 5~10 nm，能量分辨率要求 10000@8.8nm，真空要求小于 1×10^{-7} Torr。主要包括高精度谱仪、偏转镜箱、非标加工及束线集成等，其中谱仪是 FEL 脉冲谱学测量的关键设备，包含由超环面镜和光栅组成的光栅单色器、以及 YAG 探测器等，2016 年 12 月 31 日，使用皮安计测量挡光器开闭两种状态下，前端光电二极管引出光电流的变化，首次探测到光进入到前端。

单色光狭缝是光束线上的重要部件之一，它的作用为：调节样品处光斑尺寸和光通量，定义整个束线的水平和垂直接收角，且可根据需要调整光斑尺寸；阻挡其他不需要的散射光，部分隔离上游光源和光学部件不稳定对样品处光斑位置的影响。完成了不同机械结构（分别为双向、四向）的单色光狭缝的标准化设计，实现二期光束线大部分常规单色光狭缝的批量生产。主要技术指标如表 1 所示。

表 1　单色光狭缝主要技术指标

刀口行程	−5~15 mm
刀口平行度	1 mrad
刀口直线度	2.5 μm/全程
分辨率	0.25 μm
重复精度	1 μm

由于反射镜的掠入射角很小，实际需要的有效镜面长度约 800~1 200 mm，在这样长度的镜子上直接加工子午方向曲率半径为数公里的圆弧或椭圆弧面，很难得到高精度的面形，因此，目前在同步辐射装置上使用的大尺寸反射镜，普遍采用压弯等方式来得到高精度的子午方向面形。通过采用可调节的压弯技术，可以精确地得到所需要的曲率半径，同时还可灵活调节镜子的曲率，以适应不同的聚焦焦距和掠入射角。完成了千斤顶式和拉杆式亚微弧度压弯机构的设计，用以满足上海光源二期束线项目中绝大部分光束线大尺寸压弯反射镜的要求。主要性能指标如表 2 所示。

表 2　压弯机构镜箱系统主要技术指标

最大子午方向半径	≥30 000 m
最小子午方向半径	≤2 000 m
压弯后有效尺寸内子午面型误差(RMS 值)	≤0.8 μrad（有效范围内）
压弯分辨率	30 m (R: 2 500~4 500)
压弯重复精度	±40 m (R: 2 500~4 500)

高能劳厄单色器能够有效的收集水平方向的光束，100 m 的地方可以有效收集水平方向发散 0.5 mrad 的光束。超硬多功能线站的劳厄单色器将采用非对称切割晶体并在弧矢方向压弯。优点是水平聚焦的高能单色光，光斑尺寸可小于 0.5 mm。压弯机构通过一组对称的力矩将晶体在弧矢方向，压弯最小压弯半径约 1 m。另外，为了保证晶体两端夹持机构的平行，在晶体的一端设置了 twist 电机来调节晶体的扭曲。

Research Development of Beamline Mechanics Groups Duration 2015 to 2016

Department of Beamline mechanics Engineering

Our group is responsible for the mechanical system operation and maintenance of constructed beamlines, and mechanical system engineering construction tasks of new beamlines at SSRF. The stable mechanical system operation of constructed beamlines and the continuously improvement of the equipment reliability were the strong support for the stable operation of the whole beamline system. Our group has completed the mechanical systems installation of the SiP·ME^2 beamline and diagnostic beamline at SXFEL. We also completed the structural design of mono-beam slit, sub-microradian mirror bender system, polychromator and high energy laue crystal monochromator (DLM) in key technology pre-research project of SSRF phase two.

SiP·ME2 beamline is a soft X-ray beamline which is originating from the bending magnet source (02B) of SSRF, one Elliptical cylinder mirror system (ECM1) was the first mirror system placed in front-end in order to get close to the light source as much as possible. The vacuum vessel was rectangular and fabricated from dull polished 304L grade stainless steel plates with full penetration welds and cleaned and prepared in accordance with UHV requirements. The stopper was designed to allow the reflected beam pass and protect the downstream component from the direct beam. The vertical jacks and the front and side of vessel were wrapped with sheets of lead as radiation protection. For the convenience of installation and maintenance, the mirror system was designed to be lifted as a whole. The photon flux of this beamline reached to 6×10^{11} phs/s/0.1%bw, which was significantly higher than the international similar beamlines.

The designed wavelength range of the beamline is 5~10 nm, the energy resolution demands 10000@8.8nm, and the vacuum requires less than 1×10^{-7} Torr. Beamline includes high-precision spectrometer, deflection mirror chambers, non-standard equipments manufacture and integrated, and the spectrometer is the key equipment of FEL pulses spectrometric measurement, including YAG monitor and grating monochromator, which consists of toroidal mirror (TM) and plane grating (PG). The light is detected at the front end on the last day of 2016, through the photocurrent variation of the photodiode(Fig.6), using the picoammeter to measure under the two states of PS open or not.

mono-beam slit is one of the important equipment, it is used to adjust the beam size and flux, define the acceptance angle, block the stray light and partially isolate position change of the sample spot from the instability of light source and upstream optical equipments. The mechanical standardized design of mono-beam slit(two direction and four direction structural), most of the conventional mono-beam slit in SSRF phase two can achieve batch production. The main specifications of mono-beam slit see table 1.

Table 1 **M**ain specifications of mono-beam slit

Travel range of blade	-5~15 mm
Parallelism of blades	1 mrad
Straightness of blades	2.5 μm/full range
Resolution	0.25 μm
Repeatability	1 μm

Because the grazing incidence angle of mirror bender system is very small, the active area of mirror should be 800 to 1 200 mm. It is very hard to obtain high accuracy mirror shape according to manufacture a fixed cylinder or Elliptical cylinder with several km radius, usually mirror bender system is used to obtain the high accuracy tangential shape. The mirror bender system could obtain the required tangential radius with high accuracy and adjust the tangential radius conveniently to adapt to different focal distance and incidence Angle. Our group has completed the mechanical design of two sets of sub-microradian mirror bender (Jack type bender and lever type bender) to meet the requirement of most of the large size mirror bender systems in SSRF phase two.The main specifications of mirror bender system see Table 2.

Table 2 Main specifications of mirror bender system

Maximum radius of curvature	≥30 000 m
Minimum radius of curvature	≤2 000 m
Tangential slope error (RMS) (after bending)	≤0.8 μrad over active length
Resolution of radius	30 m (R: 2 500~4 500)
Repeatability of radius	±40 m (R: 2 500~4 500)

The DLM could collect the X-ray in the horizontal direction effectively, when the DLM is located at 100 meter from the light source, it could collect the X-ray that horizontal divergence angle is 0.5 mrad. The DLM for the ultra-hard applications beamline applies a piece of thin asymmetric crystal and a pair of leaf springs which push the crystal to a sagittally bent radius. The advantage is to get horizontally focused high energy monochromatic X-ray as small as 0.5mm. The bender push the crystal to a sagittally bent radius as small as 1 meter by a pair of symmetry moments. There is a twist adjustment on one side of the crystal clamp to ensure that it is parallel to the other side.

高热负载前端关键部件

束线机械工程部

“高热负载前端关键部件”是上海光源线站工程（二期）关键技术预制研究项目。项目针对热负载最高的超硬多功能光束线站 BL12SW，其首次采用超导扭摆器光源，峰值功率密度约 45 kW/mrad²，前端接收的辐射总功率高达 44.7 kW，与上海光源已运行前端相比，该前端吸收的辐射功率要高出 4~64 倍。热负载的大幅提升，对前端系统设计，尤其是光子吸收器的研制提出了前所未有的挑战。

前端总体设计

图 1 给出了 BL12SW 前端的总体布局。其中，固定光阑用于逐级吸收高功率同步辐射，同时定义输出到下游光束线站的光束张角；挡光器用于阻挡同步辐射。3 个高热负载光子吸收器，固定光阑 1、固定光阑 2 和挡光器 2 的吸收功率都超过了 10 kW。

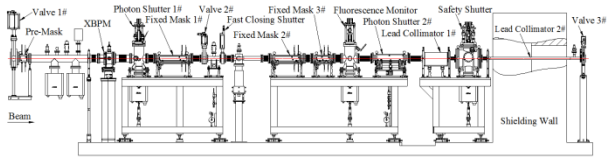

图 1 BL12SW 前端总体布局

有限元分析

高热负载光子吸收器的材料选用 GlidCop AL-15，通过热分析得到了不同参数下光子吸收器的温度和热应力分析结果。优化后的光子吸收器结构参数为：水路直径为 6 mm，水路到光照面的距离为 9 mm，光照面接线处圆角≥2 mm，且水路与光束方向基本平行[1]。

表 1 给出了固定光阑和挡光器 2 优化后的热分析结果，均满足上海光源相关失效准则。其中，σ_{max} 是等效应力，T_{max_body} 是整体最高温度，T_{max_wall} 是冷却壁最高温度。

表 1 热分析结果

	σ_{max} /MPa	T_{max_body} /°C	T_{max_wall} / °C
FM1	154.1	111	52.2
FM2	182.1	103.2	58.3
FM3	242.1	104.6	63.8
PS2	228.3	144.5	70.9

工艺研究

为了提高光子吸收器的热负载能力，固定光阑 1、固定光阑 2 和挡光器 2 的吸收体纵向长度均超过了 500 mm，而常用的慢走丝线切割的最大加工长度仅为 300 mm。因此，高热负载光子吸收器的工艺研究是 BL12SW 前端成功与否的关键。

电子束焊接是加大吸收体长度的有效途径。通过拉伸试验和疲劳试验得到了焊接接头在 20 °C、100 °C 和 200 °C 下的拉伸力学性能和疲劳性能。相比钎焊接头，电子束焊接头的强度更高，塑性更好，焊接性能更稳定，可以应用于 FM1 和 FM2。图 2 是 Glidcop 焊接接头与本体的力学性能比较[2]。

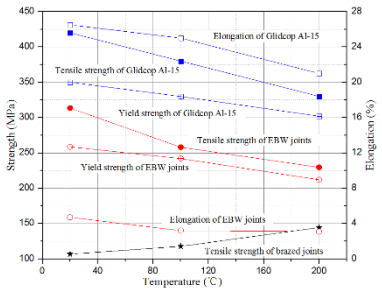

图 2 Glidcop 焊接接头与本体的力学性能比较

中走丝线切割是高热负载光子吸收器的另一种工艺方案。相比焊接式方案，中走丝型光子吸收器兼顾机械强度和加工工艺性，但尺寸精度低于慢走丝型光子吸收器，可以应用于 BL12SW 前端的 PS2[3]。通过不断调整工艺参数，现已完成光子光闸的实际研制，如图 3 所示。

图 3 光子光闸(中走丝)

参考文献

1. 李勇军, 张敏, 薛松, 等. 上海光源前端高热负载挡光器的结构设计与优化[J]. 光学精密工程, 2016, **24**(7): 1640−1646.
2. Li Yongjun, Xue Song, Zhang Min, *et al*. Vacuum joints of dispersion-strengthened copper and its applications in synchrotron radiation front end[J]. Nuclear Science and Techniques, 2016, **27**(6): 133.

High Heat Load Absorbers for Front-end at SSRF

Department of Beamline Mechanical Engineering

High heat load absorbers for front-end at SSRF is a key technology for SSRF phase-II Beamline project. A superconducting wiggler, which will be first utilized to generate high energy X-rays for the ultra-hard X-ray applications beamline, abbreviated as BL12SW, has a peak power density of 45 W/mrad^2. The front-end will handle a heat load of 44.7 kW, which is 4 to 64 times higher than the commissioned ones at SSRF. The sharply increased heat load becomes a big challenge to design of BL12SW front- end and its photon absorbers.

Overall design

Fig.1 shows the layout of BL12SW front-end. Three fixed masks (FM) confine the photon beam and protect the downstream components from a mis-steered beam. Two photon shutters (PS) intercept the photon beam. The total power on FM1, FM2 or PS2 is higher than 10 kW.

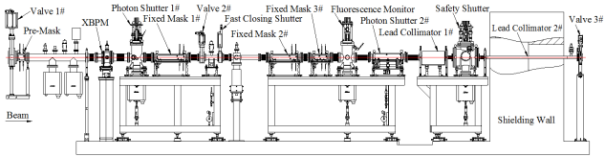

Fig.1 Layout of BL12SW front-end

Thermal analysis

Absorbers of FMs and PS2 are all made of Glidcop Al-15. The temperature and thermal stress distributions of photon absorbers with different structure parameters were simulated carefully by thermal analysis with ANSYS. The optimized parameters are: diameter of cooling channels is 6mm, distance of photon confining surfaces to cooling channel walls is 9mm, corner radiuses of two adjacent photon confining surfaces are bigger than 2mm and directions of cooling channels should be parallel to the beam approximately[1].

Table 1 Thermal Analysis Results

	σ_{max} / MPa	T_{max_body} / ºC	T_{max_wall} / ºC
FM1	154.1	111	52.2
FM2	182.1	103.2	58.3
FM3	242.1	104.6	63.8
PS2	228.3	144.5	70.9

Table 1 shows thermal analysis results of three FMs and PS2 with mis-steered beam, which fairly comply with SSRF failure criteria. Where, σ_{max} is the maximum equivalent stress on the body, T_{max_body} and T_{max_wall} are the maximum temperatures on the body and cooling wall, respectively.

Technology of manufacturing

The length of FM1, FM2 or PS2 are designed to be longer than 500 mm to minimize the grazing angles and improve heat-absorbing ability, consequently. While, the maximum available length of low speed wire-cut electrical discharge machining (WEDM-LS) in China is about 300mm. Therefore, technology of manufacturing photon absorbers becomes a key issue for BL12SW front-end.

Electron beam welding (EBW) is a way to make long absorbers. The tensile mechanical properties and fatigue properties were obtained by tensile tests and fatigue tests at 20℃, 100℃ and 200℃, as shown in Fig.2. Compared to brazed joints, EBW joints have higher tensile strength, better ductility and more stable performance and can be applied to FM1 and FM2.

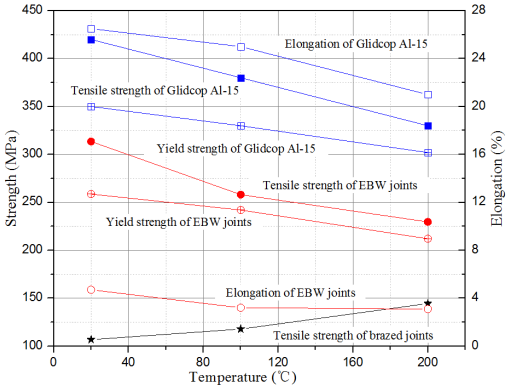

Fig.2 Tensile testing results of joints versus the Glidcop Al-15 base metal

With a higher mechanical strength and a little worse accuracy, medium speed wire-cut electrical discharge machining (WEDM-MS) becomes another effective scheme to make high heat load photon absorbers and is well suited to long photon shutters. After constantly adjusting of process parameters of WEDM-MS, the photon shutter for BL12SW front-end has been successfully developed and will be commissioned in the near future, , as shown in Fig.3, which is the first application of WEDM-MS in synchrotron radiation facility front-end.

Fig.3 PS2 (WEDM-MS)

Reference

1. Li Yongjun, Zhang Min, Xue Song, *et al*. Structure design and optimization of high heat load absorbers in SSRF front end[J]. Optics and Precision Engineering, 2016, **24**(7): 1640−1646.
2. Li Yongjun Li, Xue Song, Zhang Min Zhang, *et al*. Vacuum joints of dispersion-strengthened copper and its applications in synchrotron radiation front end[J]. Nuclear Science and Techniques, 2016, **27**(6): 133.

软 X 射线自由电子激光前端区

束线工程部前端真空组

X 射线自由电子激光实验装置(SXFEL)是上海光源(SSRF)建设的一台第四代光源，是一条独立运行的光束线站。前端区是 SXFEL 的重要组成部分，它位于诊断光束线辐射防护墙内，介于波荡器和光束线之间，上连波荡器,下接光束线，是二者的连接纽带，安全、可靠、稳定的运行时其最基本的设计要求。

光源参数

1) 光源大小和衍射角均为 RMS 值；

2) FEL 脉冲重复频率 10 Hz；

3) 8.8 nm 辐射的脉冲长度(FWHM)为 100~200 fs；

4) 此处数据仅为第二级辐射，假设第一级辐射已经被足够衰减或阻挡；

5) 红色为 1 mm·mrad 发射度结果，蓝色为 2 mm·mrad 发射度结果。

表 1　电子束参数表

电子束参数	能量/MeV	峰值电流强度	能散/RMS	归一化发射度/RMS	束团长度/FWHM
	840	≥500 A	0.1-0.15%	≤2.5 mm·mrad	≤ 1.0 ps
FEL 参数		第一级		第二级	
		调制段	辐射段	调制段	辐射段
波长/nm		265	44	44	8.8
输出功率/MV			≥100		≥100
脉冲长度/fs		<150		<150	

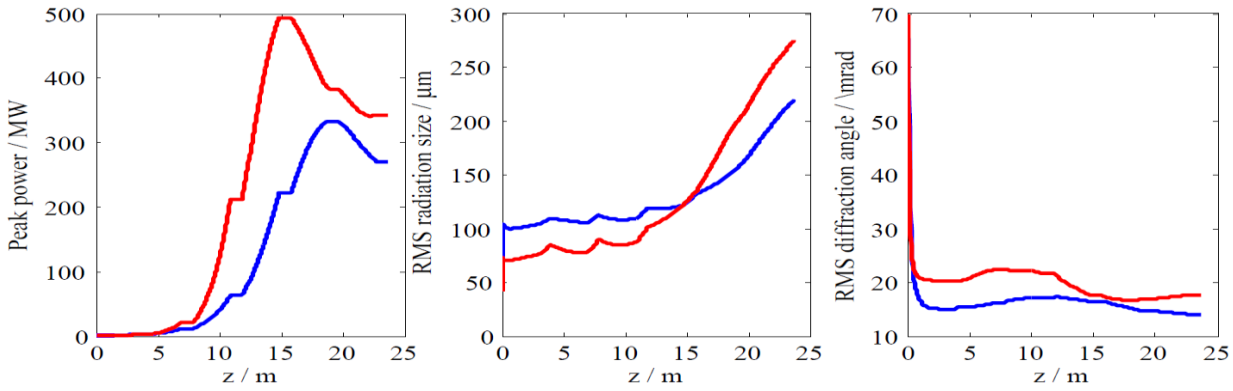

图 1　SXFEL 输出光源性能

总体布局

前端区空间有限，各种功能的安全、有效的发挥与否，与前端区的科学合理的布局密不可分。SXFEL 使用的是超短强脉冲，前端区除了关键部件结构与传统前端区不同之外，还装有气体通量衰减装置和 GMD，这布局在 SSRF 是首次采用，同时碳化硼材料作为吸收体材料也首次用于前端区。

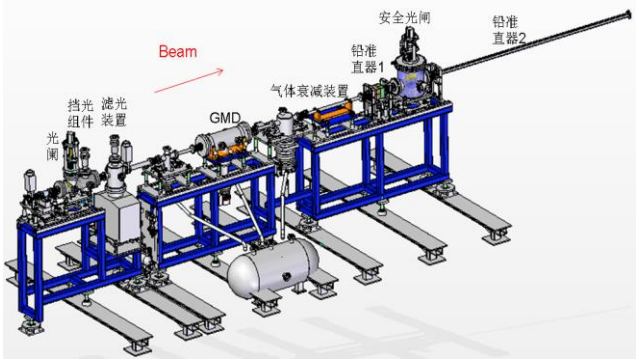

图 2　前端区总体布局

关键部件

光阑组件的吸收体材料为碳化硼，用于保护后续设备。光阑采用电动方式可以实现远程调节。

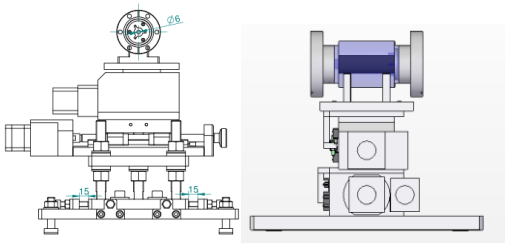

图 3　光阑组件

活动光子挡光器与 YAG 探测器共用一个腔体，挡光器吸收体材料为碳化硼，用于实现光束的阻挡和通过，YAG 探测器可以实时探测光束的位置。

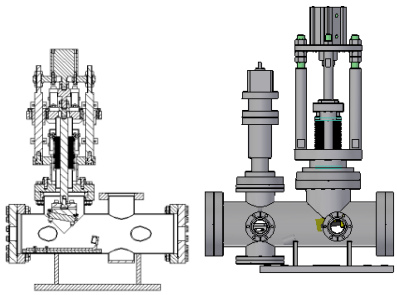

图 4　挡光组件

由于前端区前后压强要求不同，所以该前端区采用气体通量衰减装置，以实现高压强到低压强的过渡。

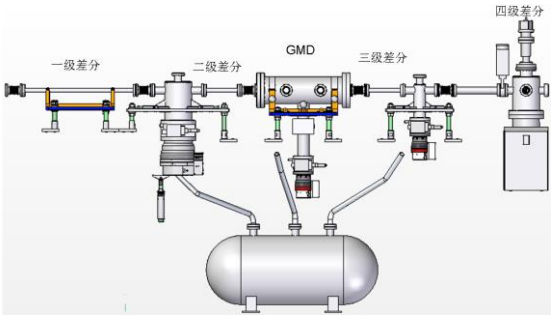

图 5　前端区安装完成图

安装调试

SXFEl 诊断线前端区已于 2016 年底安装调试完成，验收结果满足设计要求，同时该前端区也通过了通光调试。

图 6　前端区安装完成图

Front end of Soft X-ray Free Electron Laser Beamline

Front End Vacuum Group

Soft X-ray free electron laser experiment device (SXFEL) is the fourth generation light source of the SSRF, a stand-alone beamline station. The front end is an important part of the SXFEL, it is located in the radiation protection wall, an interface and connecting link between the undulator and beamline. Safe, reliable and stable operation is the most basic design requirement of the front end.

The beam parameters

Table 1 The electron beam parameters

electron beam parameters	energy MeV	intensity of peak current	energy-dispersive (rms)	normalized emittance (rms)	FWHM
	840	≥500A	0.1-0.15%	≤2.5mm·mrad	≤1.0ps
FEL parameters		The first level		The second leve	
		Modulation period	Radiation period	Modulation period	Radiation period
wavelength (nm)		265	44	44	8.8
Output power (MV)			≥100		≥100
pulse length (fs)		<150		<150	

1) Beam size and diffraction angle are the RMS values;

2) FEL pulse repetition frequency is 10 Hz;

3) 8.8 nm radiation pulse length (half full width) is 100~200 fs;

4) This data is only the second radiation, assuming that the first level of radiation has been sufficient attenuation or is blocked;

5) Red line is 1 mm·mrad launch degrees as a result, blue line for 2 mm·mrad emission results.

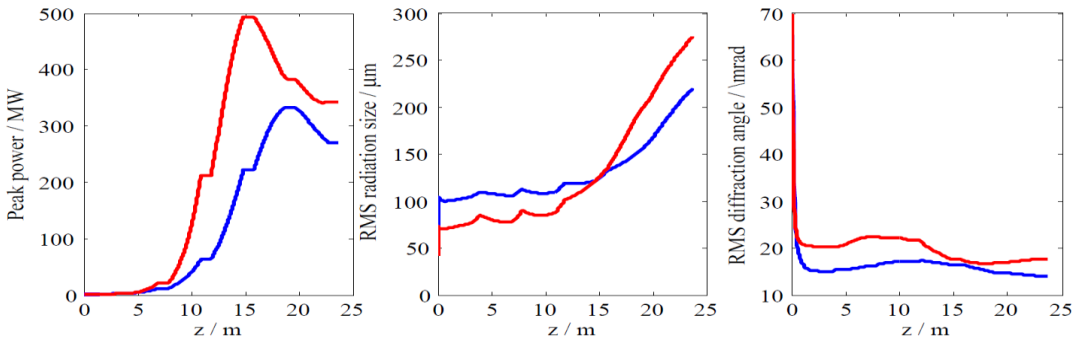

Fig.1 The output beam performance of the SXFEL

The overall layout

Front end in limited space, safe and effective play it or not, is closely connected with scientific and reasonable layout of the front end. SXFEL use ultrashort pulses, the structure of the key components of this front end is different from the traditional's. This front end include gas flux attenuation device and GMD, this layout is the first time adopted in front end of SSRF. At the same time, boron carbide as absorbers' material using in front end also is the first time.

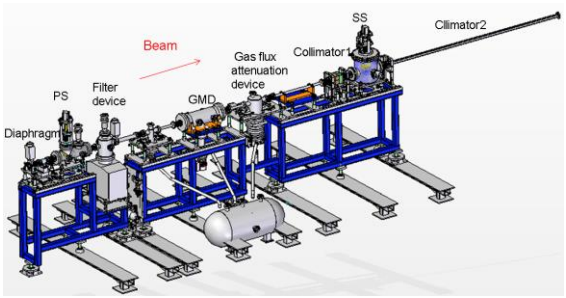

Fig.2 The overall layout

Key components

The diaphragm use the boron carbide as the absorber material, protects the following equipments. The diaphragm component adopts electric method to realize remote control.

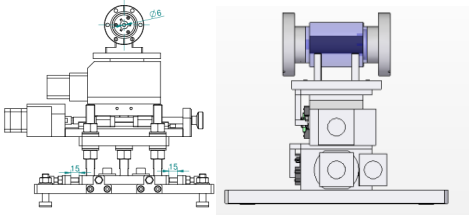

Fig.3 Diaphragm component

The photon shutter share a cavity with the YAG detector, the absorber material is boron carbide, used to achieve beam blocking or through, YAG detector can real-time detect the position of the beam.

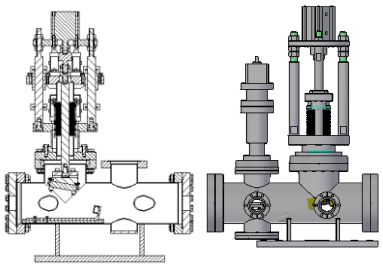

Fig.4 Photon shutter

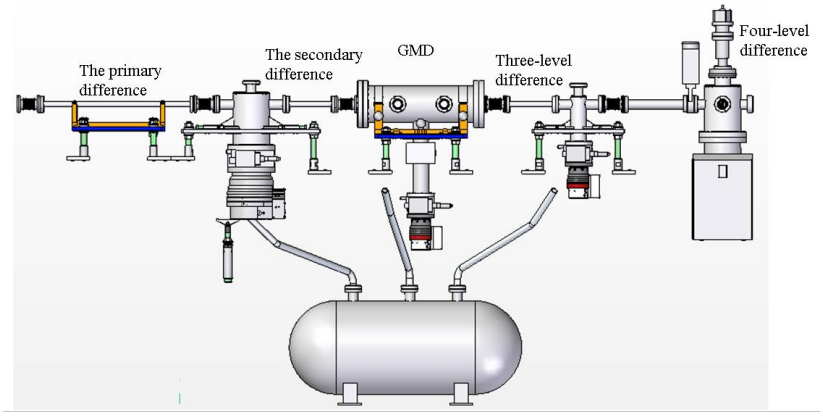

Fig.5 Gas flux attenuation device

Due to the different requirements for the pressure at the front end upstream and downstream, so the gas flux attenuation device is used to realize the transition from high pressure to low pressure.

Fig.6 Installation is complete

Installation and debugging

The front end of the SXFEL has installation completed at the end of 2016, the results meet the design requirements.At the same time the front end also passed the debugging.

棚屋防护系统

束线机械工程技术部

线站辐射防护棚屋的主要作用就是阻挡和屏蔽被光束线部件散射所产生的各种辐射，起辐射防护的作用。辐射防护棚屋是光束线站辐射防护最重要的工具和手段之一，直接关系到科研人员的人身安全和实验仪器的设备安全。

经过上海光源一期和蛋白质设施、梦之线项目辐射防护棚屋的设计、施工、建造，已经形成了一整套完整的相关方案。

设计指标方面，根据相关规定棚屋的辐射泄露率小于等于 1.2 $\mu Gy \cdot h^{-1}$，棚屋结构承重 1 t/m，棚屋内安装吊车，可满足线站绝大部分设备安装维护的吊装。

棚屋采用标准化、模块化、美观性与实用性兼具的设计原则。大部分部件采用标准部件，在有特殊需求的条件下进行非标设计，采用拼装式的方式进行安装，减少焊点数量。辐射防护棚屋的关键技术主要有：防泄漏结构工艺、材料掺杂工艺、特种粘合工艺、离线测试工艺。

防辐射泄漏是棚屋的最基本功能，需要进行一系列的结构设计来满足需求。针对棚屋内外有各种管线进出，采用管线迷宫口的设计，满足防护需求。针对设备人员进出棚屋的需求，采用双开移门、单开移门、推门的形式满足需求。

棚屋部件采用钢铅夹心板的方式加工，高纯度的铅板很软，密度很大，在垂直放置的情况下容易产生变形，时间长了容易造成辐射剂量泄漏。为了增加铅板自身的强度，避免因铅板变形或位移而产生的剂量泄漏，又不影响铅板辐射防护的性能，对铅板进行特殊惨杂处理。采用材料掺杂工艺和特种粘合工艺进行加工，解决长时间使用过程中部件变形造成辐射泄露的问题。

通常，面积较大的钢板与铅板固定采用贯穿螺钉加铅帽，虽然强度牢固，但为了防止辐射泄漏，在螺钉孔的地方用铅帽屏蔽，因此将在夹芯板的外表面突出许多铅帽，使得板表面高低不平，影响外观。较好的办法是采用粘接的工艺，用特种胶粘剂将钢板与铅板粘接，再将内外层钢板焊接，确保大尺寸的钢铅夹芯板具有足够的强度。

棚屋安装完成后进行离线测试，对不满足辐射需求的地方进行补漏，以满足辐射辐射标准，避免了因棚屋泄漏导致线站通光调试推迟的情况发生，为光束线站带光调试一次成功创造了条件，保证了线站按工程节点顺利完成建设任务。

线站棚屋建造完成后，通过棚屋内外公用设施设备的安装、棚屋内光束线站设备的安装、棚屋在线辐射泄漏测试、以及国内外实验用户的使用等情况表明，线站辐射防护棚屋的设计满足了可靠性、实用性和美观性的要求，辐射泄漏控制在允许的范围内。

在上海光源线站辐射防护棚屋的研制过程中，采用了棚屋离线辐射泄漏测试技术、特殊惨杂工艺、特殊粘接工艺等多项国内外同类装置中首次采用的关键工艺技术，确保并提高了棚屋的建造质量。

图 1　棚屋现场图

参考文献

1. 杨东, 朱卫华, 乌镇亮, 等. 一种移门驱动装置及其双移门和防护移门[P]. 中国, 201220042301.7, 2012-10- 10.
2. 杨东, 刘小栋, 朱卫华, 等. 一种钢铅夹芯板[P]. 中国, 201220066560.3, 2012-10-10.
3. 朱卫华, 苏东, 杨东, 等.辐射防护棚屋的离线辐射泄漏测试装置[P]. 中国, 201220165867.9, 2012-11-28.

Radiation Protection Hatches System

Department of Beamline Mechanical Engineering

The main function of the radiation protection hatches is to block and shield the various kinds of radiation produced by the scattering of the beam line parts. Radiation protection hatch is one of the most important tool and means for radiation protection of beamline station, which is directly related to the safety of personnel safety of scientific researchers and equipment safety of laboratory instruments.

We have formed a complete set of relevant schemes according to previously built beamline stations.

According to relevant national regulation, The radiation leakage rate of the hutch is less than or equal to 1.2 $\mu Gy \cdot h^{-1}$.The load-bearing of the hatches is 1t/m and the crane is installed in the hut, which can meet the installation and maintenance of most equipment in the beamline station.

The hutch adopts the design principle of standardization, modularity, aesthetics and practicality. Most parts adopt standard parts, and non-standard design is carried out under special requirements, and assembly is adopted to reduce the number of solder joints.

The key technologies of radiation protection hutch are: leakproof structure technology, material mixing technology, special bonding process and off-line testing technology.

Radiation leakage is the basic function of the hutch. A series of structural design is needed to meet the demand. For the inside and outside of the hutch, there are various pipelines in and out, using the design of the pipeline labyrinth mouth to meet the protection requirements.

In order to meet the needs of the equipment personnel in and out of the hutch, the double open door, single open door and push door are used to meet the demand.

Hutch parts adopt the way of lead steel sandwich board processing, whose high purity lead plate is very soft and density is very big. Radiation leaks will happen after a long time because of deformation of the vertical direction. We make special treatment for lead plate under the conditions that not affect the performance of lead plate radiation protection in order to increase the strength of the lead plate to make sure the dose leakage caused by the deformation or displacement of lead plate is avoided. The material doping process and special bonding process are used to solve the problem of radiation leakage caused by the deformation of parts during long time use.

In general, the larger steel plates and lead plates are fixed with a perforated screw and lead cap. Although the strength of strong, but in order to prevent radiation leaks, where the screw hole lead hat shielded, so will be in the outer surface of the sandwich board highlighted many lead cap, makes the plate surface is rugged and affect the appearance. The better method is to use the adhesive process, the steel plate and lead plate are glued together with special adhesive, and the inner and outer layer steel plates are welded to ensure that the large size steel lead sandwich plate has enough strength.

After the construction of the hutch completes, the offline test will be carried out to meet the radiation requirements of the place where the radiation needs are not met. Radiation leakage is avoided to avoid the delay of the adjustment of the beamline station, who can make sure that the beamline station completes the construction task smoothly according to the project.

After the completion of the hutch, we meet the design requirements of reliability, practicality and aesthetics according to the construction of utility equipment inside and outside the hut and installation of beamline station equipment in the hut and the online radiation leakage test of the hut and the use of experimental users at home and abroad.

In the process of construction of radiation protection hutch in SSRF, we adopt offline radiation leak testing technology, special miserably hybrid technology, special adhesive technology and many key technique adopted in similar equipment at home and abroad for the first time, to ensure and improve the construction quality of the hutch.

Hutch construction site

前端真空组 2015–2016 工作进展

前端真空组

前端真空组主要承担“上海光源”前端区的设计、工程建设和维护任务以及线站的真空设计和维护任务。在 2015–2016 年完成了以下项目：

微系统所插入件前端和测试线前端的机械安装

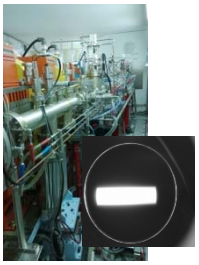

图 1 微系统所插入件前端

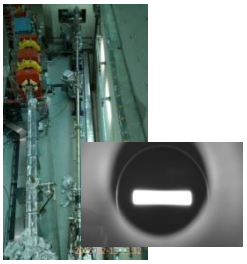

图 2 测试线前端

完成了上海光源线站工程首批 8 个线站前端区的工程设计

高性能膜蛋白晶体结构线站-表面衍射线站前端区；

时间分辨超小角散射线站-P2 生物防护蛋白线站前端区；

动力学研究线站前端区；

纳米自旋与磁学线站前端区；

硬 X 通用谱学站前端区；

纳米三维成像前端区。

表 1 前端区引出、引入张角

光束线	线站编号	光源类型	光束线使用张角 (mrad²)	前端区引出光束张角(mrad²)	前端区引入光束张角(mrad²)	前端区功率 (KW)	功率密度 (KW/mrad²)
高性能膜蛋白晶体结构线	BL02U1	IVU22	0.1×0.05	0.3×0.15	2×1	2.5	27.16
表面衍射线	BL02U2	CPMU	0.08×0.04	0.3×0.15	2×1	3.0	35.7
时间分辨超小角散射线	BL10U1	IVU20	0.1×0.06	0.3×0.15	2×1	2.65	31.4
P2 生物防护蛋白晶体学线	BL10U2	IVU22	0.1×0.05	0.3×0.15	2×1	2.6	28.4
动力学研究线	BL05U	U22	0.1×0.04	0.3×0.15	3.5×1.5	8.1	41.88
纳米自旋与磁学线	BL07U	双 EPU	0.25×0.21	0.36×0.32	3.5×1.9	8.1 / 8.1 / 7 / 4.9	
硬 X 通用谱学光束线	BL11B	BM	1.5×0.16	3×0.5	10×3	690	0.325
纳米三维成像光束线	BL18B	BM	0.22×0.22	3×0.5	10×3	690	0.325

表 2 前端区元件特性表

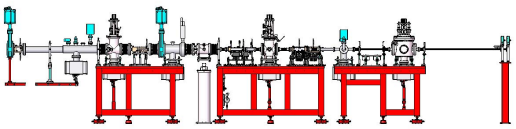

图 3　Canted 前端区

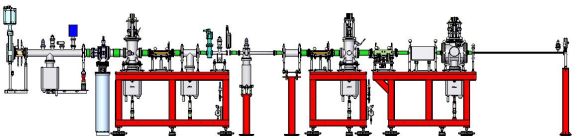

图 4　插入件前端区

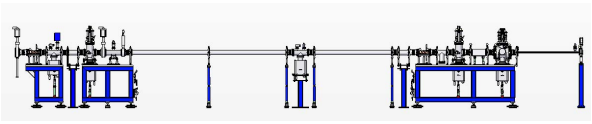

图 5　弯铁前端区

在 Canted 前端区中解决了在狭小空间内 Canted 前端区固定光阑、光子光闸二线的并列的布局和在线独立调控。

完成了软 X 自由电子激光前端工程设计和建设

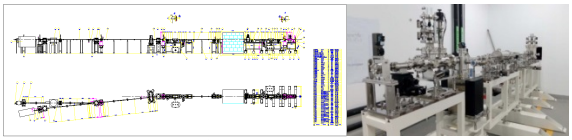

图 6　SXFEL 诊断线前端

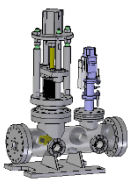

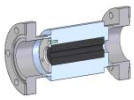

图 7　活动光子挡光器组件　图 **8**　光阑　图 **9**　安全光闸

在前端区中首次应用 B4C 作为挡光材料。

气体通量衰减器的研制

软 X 自由电子激光的气体通量衰减器 Gas Attenuator（GAT）设计对 8.8 nm 波长的 X 射线强度衰减 4~5 个量级。气体传输介质为距离 6 m、压强 80 Pa 的氮气(N_2)。由于 SXFEL 的 X 射线的材料吸收和光子通量的稳定度的要求，气体通量衰减器须采用无窗过渡方法连接至其他超高真空设备(<1×10^{-5} Pa)，气压不稳定度低于±0.08%。

研制的 GAT 采用三级差分来实现 7 个量级的差分比，通过质量流量计、蝶阀和电容式薄膜计组成的闭环控制系统来实现压强的反馈调节。

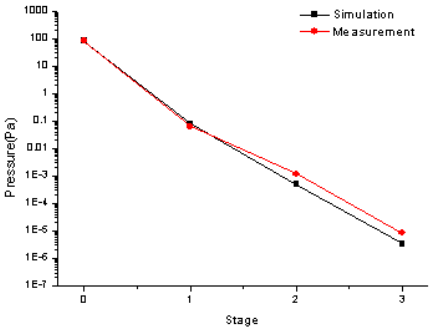

图 10　真空差分理论设计与实际测试值对比

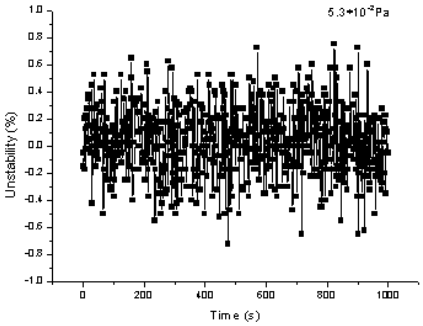

图 11　压强稳定度测试结果

研制的气体通量衰减器真空差分系统理论设计值与实际测试值相符，在限定的距离内达到了所需差分比，且实现了动态压强的精密反馈调节。

参考文献

1. 刘俊男, 吴仁智, 薛松, 等. 一种压强稳定的多级真空差分系统[J]. 真空科学与技术学报, 2017, **21**(3): 70−74.

Progress of Front End & Vacuum Group 2015-2016

Front end and vacuum group

The front end & vacuum group is mainly responsible for the mechanical design, construction and maintenance of the front-ends at SSRF, and the vacuum design and maintenance of the beamline. The following projects were completed in 2015-2016.

Construction of VUV EPU beamline 03I front end and XT-line front end

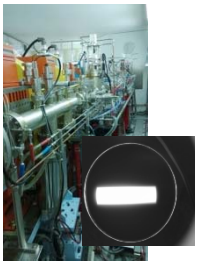

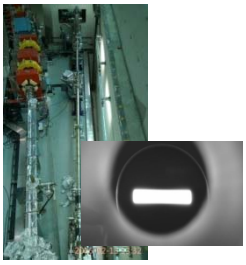

Fig.1 VUV EPU beamline 03I front end

Fig.2 XT-line front end

Mechanical design of 8 beamline front ends at SSRF

Surface Diffraction & Membrane Protein Crystallography Beamline front end

Time-resolved USAXS & P2 Beamline front end

Dynamic line front end

S2 Line front end

Hard X-Ray Spectroscopy Beamline front end

3D nano imaging beamline front end

Table1 Input and output angles of front end

光束线	线站编号	光源类型	光束线使用张角 (mrad²)	前端区引出光束张角(mrad²)	前端区引入光束张角(mrad²)	前端区功率 (KW)	功率密度 (KW/mrad²)
高性能膜蛋白晶体结构线	BL02U1	IVU22	0.1×0.05	0.3×0.15	2×1	2.5	27.16
表面衍射线	BL02U2	CPMU	0.08×0.04	0.3×0.15	2×1	3.0	35.7
时间分辨超小角散射线	BL10U1	IVU20	0.1×0.06	0.3×0.15	2×1	2.65	31.4
P2 生物防护蛋白晶体学线	BL10U2	IVU22	0.1×0.05	0.3×0.15	2×1	2.6	28.4
动力学研究线	BL05U	U22	0.1×0.04	0.3×0.15	3.5×1.5	8.1	41.88
纳米自旋与磁学线	BL07U	双 EPU	0.25×0.21	0.36×0.32	3.5×1.9	8.1 | 8.1 | 7 | 4.9	
硬 X 通用谱学光束线	BL11B	BM	1.5×0.16	3×0.5	10×3	690	0.325
纳米三维成像光束线	BL18B	BM	0.22×0.22	3×0.5	10×3	690	0.325

Table 2 Front end components characteristics

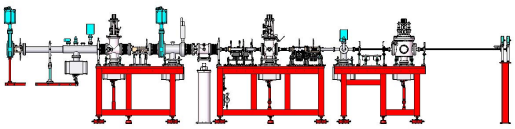

Fig.3 Canted beamline front end

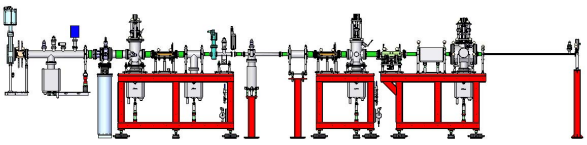

Fig.4 ID front end

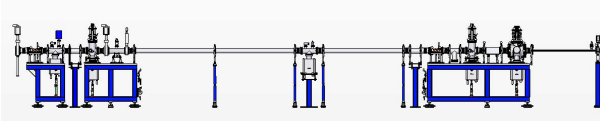

Fig.5 BM front end

They have solved the Paralleling layout and Online independent regulation of fixed mask and photon shutter on the canted beamline in small space.

Mechanical design and construction of SXFEL front end

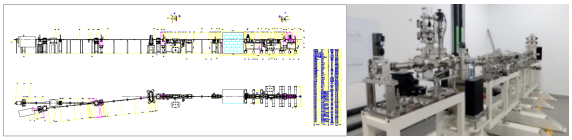

Fig.6 SXFEL front end

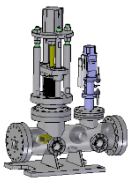

Fig.7 Photon shutter

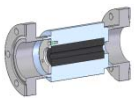

Fig.8 Fixed mask

Fig .9 Safety shutter

The B4C material is used as the front end to block beam power for the first time.

Development of gas flux attenuator

The Gas flux Attenuator (GAT) of the soft X free electron laser is intended to attenuate the X-ray intensity of the 8.8 nm wavelength by 4~5 magnitudes. The gas transmission medium is nitrogen (N_2) with a distance of 6 m and pressure of 80 Pa. Because of material X-ray absorption and the requirements of the stability of the photon flux, gas flux attenuator windowless transition method should be used in connection to other ultra-high vacuum equipment ($<1\times10^{-5}$ Pa), and stability pressure should be not less than ±0.08%.

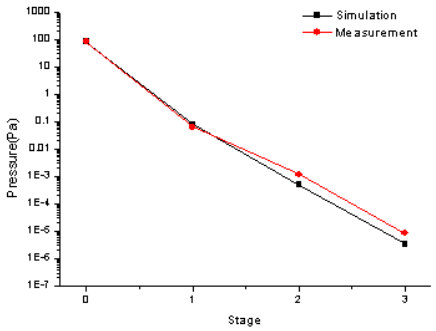

Fig.10 Differential pumping result

The developed GAT uses a three-level difference to achieve the difference ratio of 7 orders of magnitude, and the pressure feedback regulation is achieved through the closed-loop control system composed of mass flowmeter, butterfly valve and capacitive thin-film meter.

The actual test values of GAT is consistent with theoretical design value. The developed GAT realizes the difference in limited distance, and the high-precision dynamic pressure feedback regulation.

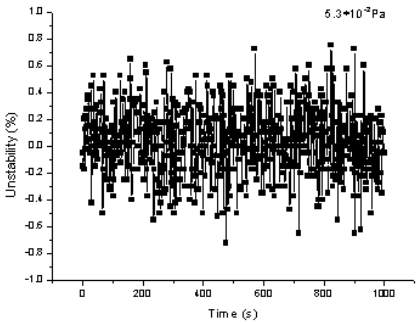

Fig.11 Pressure stability for GAT and GMD

Reference

1. Liu J N, Wu R Z, Xue S, *et al*. Highly Stable Pressure Produced by Multistage Differential Pumping Unit[J]. Chinese Journal of Vacuum Science and Technology, 2017, **21**(3): 70−74.

上海光源光束线新的运行数据管理和查询系统

电子学与探测器组

本组设计开发的上海光源光束线新的运行数据管理和查询系统，为各个线站的运行维护和故障分析提供了有力保障。这套系统基于 Web 技术，具有数据的实时显示，历史数据查询和分析功能，同时使用者可以将数据导出做进一步的数据分析。

上海光源光束线新的运行数据管理和查询系统采用 Archiver Appliance 把各条光束线的运行数据存储到数据库中。这些数据包括：XBPM 的刀片电流值、光束的中心位置值、各个设备的温度、真空和水流量状态、以及真空阀门的开关状态等参数。Archiver Appliance 运行在两台装有 CentOS 7 系统的服务器上。

系统的设计构成

本系统主要包括数据采集、数据存储和数据查看分析三部分，结构框图如图 1 所示。各部分的功能可简述如下：1) 系统中 IOC 部分主要负责数据的采集，IOC 通过串口、以太网等接口与线站的真空计、安全联锁控制系统相连，数据以记录形式保存在 IOC 的实时运行数据库中[1]；2) Archiver Applianc 主要负责数据的存储。Archiver Appliance 程序根据配置文件设置的变量名及其相应的采集频率，将需要保持的数据从 IOC 的实时运行数据库中取出来，然后保存到数据库中；3) 基于 Web 网页的数据查看系统，主要根据用户的请求，动态生成标准 Html 页面送到客户端浏览器，达到人机交互的目的；这样的优势在于各线站的工作人员只要在控制网内，通过任何一台电脑的浏览器都可以进行数据查询和分析，为使用者提供了极大的方便。

数据库的设计及数据获取

我们的数据库采用的是 Archiver Appliance 软件。它是由 SLAC、BNL、MSU 联合开发的 EPICS 框架下的数据存取管理软件，能够获取百万量级的 PV，同时也十分注重数据的提取速度。Archiver Appliance 具有组建应用程序集群的能力，同时它的分时段的存储技术使得它的存储数据的速度更快[2]。我们选用了两台 Dell 服务器 R730 作为它的硬件设备，每台服务器的内存为 64 GB，磁盘容量为 300 G，选择 CentOS7 作为服务器的操作系统。这里将两台服务器配置为一个集群来使用，两台服务器的网址分别为 10.30.50.96 和 10.30.50.97。

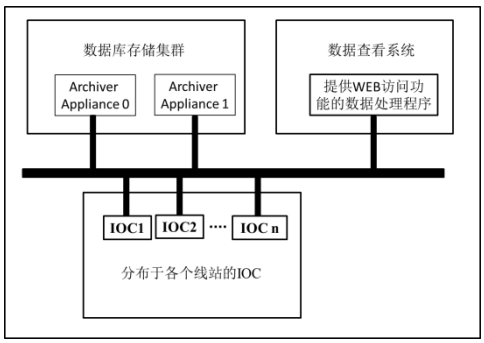

图 1 运行数据管理和查询系统的结构框图

Web 前端是指用户通过浏览器可以直接浏览和使用的 Web 界面，需要对各相应的界面进行重新设计方能满足我们的使用要求，如通过修改 index.html 代码，输入网址后的显示界面见图 2。

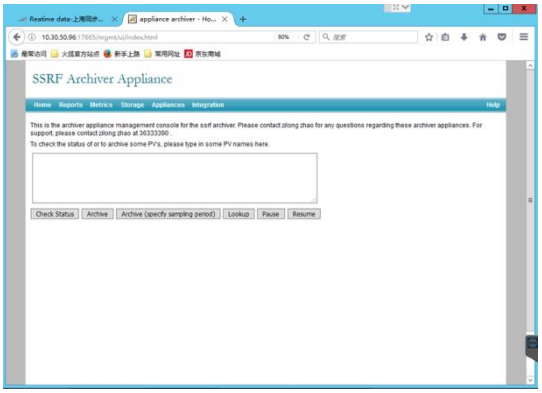

图 2 数据库查看的 Web 界面

数据查询系统功能的设计与实现

根据光源运行过程和故障排除的需要，我们建立了数据查询系统。它提供了的数据检索和导出功能，用户可方便地通过 Web 方式查询光束线相关设备运行过程中的实时数据和历史数据，同时提供了简单的数据分析功能。为了满足用户进行复杂的数据处理需求，使用者还可将数据导出后做进一步的离线分析。

本系统的开发选用了 Apache 作为 Web 服务器软件。Apache 由于其自身的高可靠性和可用性，全球有 50%以上的用户在进行 Web 开发使用，都

选择将其作为自己的服务器软件，服务端脚本语言选用 PHP。PHP 是一门开源语言，资源非常丰富且免费。同时为了提高开发效率，我们采用了 THINKPHP 开发框架。THINKPHP 是国内一款免费开源的快速简单的面向对象的轻量级 PHP 开发框架[3−4]。通过 THINKPHP 的使用，可极大地减轻开发的工作量，使我们能将主要精力放在系统本身功能的实现上。

Archiver Appliance 支持的数据提取格式有很多种，比如 JSON、CSV、MAT、RAW、TXT 等。我们使用其提供的 JSON 数据格式，开发了基于 WEB 的数据查询系统，可实现实时数据查看，历史数据回看，数据的简单分析及光源运行状态的监测。在实时数据显示上，我们使用了 Highcharts 图表库。Highcharts 采用纯 JavaScript 编写，使用它可以在在 Web 网站中方便快捷地添加交互性的图表。目前，HighCharts 支持的图表类型有曲线图、区域图、柱状图、饼状图、散状点图和综合图表。对于历史数据查询，我们仍采用 Archive Viewer 软件来查看。Archive Viewer 软件专门用来处理 EPICS 系统得到的数据，它是一个可扩展的、多线程的 java 程序。为了使用方便，我们使用了 JNLP (Java Network Launching Protocol)技术。JNLP 是 java 提供的一种可以通过浏览器直接执行 java 应用程序的途径，你可以直接通过网页上的 url 连接，打开一个 java 应用程序[5]。在历史数据查看界面上添加 JNLP 链接，点击以后就可以打开查询功能。

在光源的运行过程中，我们还需要对一些设备的运行情况定期进行评估，以便能及早地发现设备的异常，以免造成重大的事故，可主要通过关注的设备运行参量如设备的温度、真空度，以及 X 射线的位置等信息，计算这些参量的最大值，最小值和 RMS 值等方法来进行评估。

参考文献

1. 孙小影, 陈广花, 刘义勇, 等. 上海光源储存环真空数据检索系统[J]. 核技术, 2010, **33**(9): 645−648。
2. Murali Shankar, Luofeng Li, Michael Davidsaver, *et al*. The epics archiver appliance[R]. Proceedings of ICALEPCS, Melbourne, Australia, 2015.
3. 李绍静, 车广杰, 董 峰. 基于 ThinkPHP 架构的学生考核系统的设计与实现[J]. 信息技术, 2013, (5): 47–53.
4. 王青, 刘沛. 基于 ThinkPHP 技术的高校财务预算系统开发与实现[J]. 软件导论, 2013, (5): 1−103.
5. Java Network Launching Protocol[EB/OL]. https:// baike. baidu.com/item/JNLP/3678319?fr=aladdin

A New Management and Query System of the Beamline Operation Data at SSRF

Department of Beamline Optics Engineering

A new operation data management and query system of the beamline operation data at SSRF，developed by electronic and detector group， provides strong guarantee for devices maintenance and fault analysis of each beamline. This system, based on Web technology, provide the functions of the realtime display of data, the query and analysis of history data. And the users can export the data for offline analysis.

The new operation data management and query system store the running date into the dataset by Archiver Appliance. These data include: the central position of X-ray beam, the equipment temperature, vacuum and the state of water flow, the state of valve and so on. Archiver Appliance run on two DELL- servers equipped with CentOS 7 system.

The design of the system

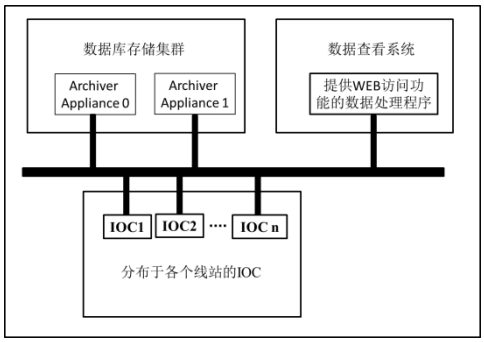

Fig.1 Management and query system architecture

This system mainly includes data acquisition, data storage and data analysis. The structural block diagram is shown in figure 1. The brief function is: 1) the IOC of the system is mainly responsible for data collection, which link with vacuum-meter and device controller via a serial port or Ethernet interface. The data is stored in real-time database of the IOC. 2) Archiver Applianc is responsible for the storage of data. Archiver Appliance program according to the configuration file set the process variable name and its related acquisition frequency, will get the needed data from the IOC's real-time database, and then save into the historical database. 3) the data view system based on the Web page, which dynamically generates standard Html pages to the client browser to realize the purpose of human-computer interaction according to user's request. It will take advantage that staff can query and analysis data though computer's browser as long as in the control network. Thus is great convenience for user.

Database design and data acquisition

Our database uses Archiver Appliance software. It is a type of data management software under the EPICS framework developed by SLAC, BNL and MSU. It can get PV on the scale of million, also pays attention to the extraction rate of the data. Archiver Appliance has the ability to assemble an application cluster, and its time-sharing storage technology makes its storage much faster. We chose two Dell servers R730 as its hardware device, and the memory of each server was 64 GB and the disk capacity was 300 G, and CentOS7 was selected as the operating system of the server. The two servers are configured to be used by a cluster, with the server address 10.30.50.96 and 10.30.50.97.

A Web front end is a Web interface that a user can browse and use directly though a browser. After the program is installed, need to redesign the corresponding interface to meet our usage. By modifying the index.html code, enter the URL to display the interface as shown in Fig.2.

Design and implementation of data query system function

According to the operation process of SSRF and the need of troubleshooting, we set up a data query system. It provides the data retrieval and export function, users can easily query beam line related equipment in the process of running real-time data and historical data through a Web. At the same time, the system provides a simple data analysis function. In order to meet the user's complex data processing requirements, the user can also make further offline analysis by exporting the data.

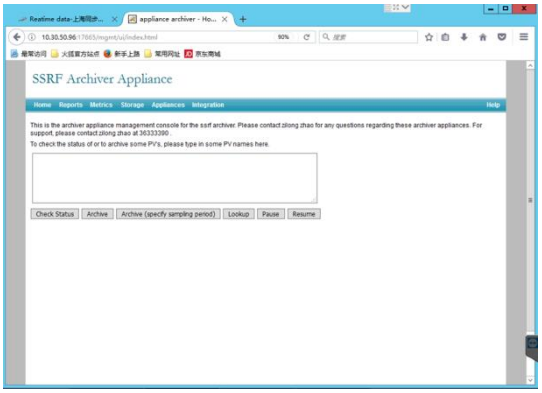

Fig.2 The home page of Archiver Appliance

This system use Apache as the Web server software. Apache, due to its high reliability and availability, has been used as their own server software by more than 50 percent of the world's users. Therefore, we also use Apache as our server software. The server-side scripting language uses PHP, which is an open source language and is very resource-rich and free of charge. In order to improve development efficiency, we also adopted the THINKPHP development framework. The THINKPHP is a fast, simple, object-oriented, lightweight PHP framework for free and open source. The use of the THINKPHP greatly alleviates the workload of development, so that we can focus on the implementation of the system itself. There are many data extraction formats supported by The EPICS Archiver Appliance, such as JSON, CSV, MAT, RAW,

TXT, *etc*. We developed data query system based on Web by using the JSON data format. The system include the features: real-time data display, the inquiry of historical data, simple data analysis and monitoring of running status of SSRF. On the real-time data display, we used the Highcharts. Highcharts is written in pure JavaScript, and it can be used to quickly and easily add interactive graphics on a web site.

In the future, we also need to evaluate the operation of some key equipment on a regular basis so as to detect the abnormality of equipment early, in order to avoid causing major accidents, the maximum value, the minimum and RMS values of these parameters can be calculated, mainly through the information of the equipment operating parameters such as temperature, vacuum degree, X-ray position and so on.

Reference

1. Sun Xiaoying, Chen Guanghua, Liu Yiyong, *et al*. A vacuum data retrieval system for SSRF storage ring[J]. Nuclear Technology, 2010, **33**(9): 645−648.
2. Murali Shankar, Luofeng Li, Michael Davidsaver, *et al*. The EPICS Archiver Appliance[R]. Proceedings of ICALEPCS, Melbourne, Australia, 2015.
3. Li Shaojing, Che Guangjie, Dong Feng. Design and implementation of student evaluation system based on ThinkPHP framework[J]. Information Technology, 2013, (5): 47−53.
4. Wang Qing, Liu Pei. Design and implementation of university financial budgeting system based on ThinkPHP framework[J]. Software Guide, 2013, **12**(5): 101−103.
5. Java Network Launching Protocol[EB/OL]. https:// baike.baidu.com/item/JNLP/3678319?fr=Aladdin

束线控制组研究进展

束线光学工程技术部

束线控制组主要承担“上海光源”已建线站光束线控制系统的运行维护和新建线站控制系统的工程建设任务。已建线站光束线控制系统运行稳定，软硬件功能不断完善，有力支持了线站总体的稳定运行。本年度完成了 14W1 实验站时间分辨 QXAFS 实验的控制与数据采集系统开发，完成了 14B1 衍射线实验站 X 射线单晶衍射实验的控制与数据获取系统的开发，完成了 SipME2 软 X 射线弯铁线光束线控制系统的工程建设任务，。

快速扫描 X 射线精细结构谱(Quick-scanning X-ray Absorption Fine Structure, QXAFS)是测定特定吸收原子临近环境结构的一个强有力的工具，已广泛应用在固体物理、催化剂和蛋白质分子等领域。双晶单色器(Double Crystal Monochromator, DCM)是上海光源 XAFS 光束线站的关键设备，它能够将一定波长范围内的白光单色化，并将单色光束稳定出射至下游光学元件。上海光源 XAFS 光束线站数据采集程序是在 Labview 环境下开发的，而采用了步进电机的 DCM 控制系统则采用了基于分布式控制的实验物理及工业控制系统[1](Experimental Physics and Industrial Control System, EPICS)。由于运行环境不同，两者在装置联动时不可避免存在网络延时的缺陷并使得 XAFS 谱发生变形和不连续的问题。解决办法是，在 EPICS 环境下产生硬件触发信号并用其同步采集电离室和步进电机的信号，实现 QXAFS 数据的实时采集与控制。对标准铜箔样品进行了实验测试，结果表明该方法不仅可以保证系统获得较高的信噪比，而且可以在小于 8 s 的时间内获取一个完整的 QXAFS 谱，在小于 500 ms 时间内获得一个近边结构谱[2–4]。该系统的实现

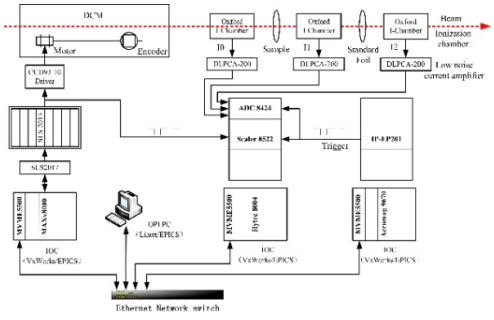

图 1　QXAFS 数据采集与 DCM 控制系统的硬件结构

对上海光源开展快速时间分辨 QXAFS 实验具有重要的应用意义。

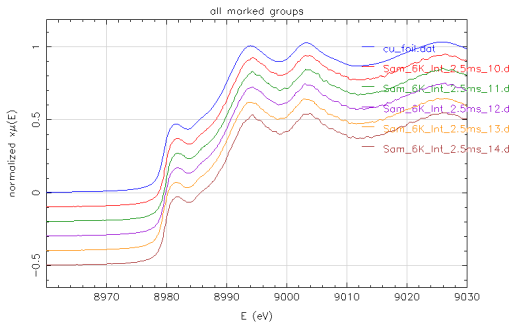

图 2　五次 QXAFS 谱与普通 XAFS 谱的比较

单晶 X 射线衍射是利用单晶体对 X 射线的衍射效应来测定晶体结构的实验方法。控制组负责完成了该实验方法的控制与数据采集系统。对衍射仪的 TTH 轴、Phi 轴和 TH 轴的控制进行了改造，实现了 EPICS 环境下的运动控制与快门的同步触发。控制器选用了美国 Galil 公司的智能运动控制器，该控制器功能强大，可以输出位置比较同步触发信号，用来同步快门开关和探测器数据采集。探测器采用的是 MARCCD，利用 EPICS SynApps 包中的面探测器控制与数据采集模块 AreaDetector 可以实现在 EPICS 下对 MARCCD 进行控制与数据采集。

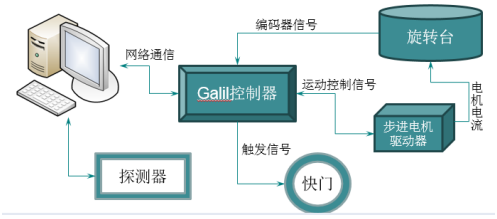

图 3　单晶衍射控制系统硬件示意图

参考文献

1. http://www.aps.anl.gov/epics/.
2. 周永年, 张招红, 刘平, 等. 基于 DCM 的 QXAFS 数据采集与控制[J]. 核技术, 2015, **38**(5): 1−7.
3. 周永年. 上海光源基于 EPICS 的 QXAFS 数据采集系统的研究与实现[D]. 上海: 中国科学院上海应用物理研究所, 2015.
4. Quintana J P G. Uncertainty determination in QXAFS measurements[C]. American Institute of Physics, 2000: 194−197.

Research Development of Beamline Control Group

Department of Beamline Optical Engineering

The beamline control group is mainly responsible for the operation and maintenance of the beamline control system and the project construction tasks of the control system for the new proposed Beamlines. The beamline control system has been running steadily and the functions of hardware and software have been continuously improved, effectively supporting the overall stable operation of the Facility. In this year, the time-resolved QXAFS experiment control and data acquisition system was developed at the 14W1 beamline station, the X-ray single crystal diffraction experiment control and data acquisition system was developed at the 14B1 beamline station. In addition, the construction of the beamline control system for the SipME2 soft X-ray bending wire beamline has been completed.

Quick-scanning X-ray Absorption Fine Structure (QXAFS) is a powerful tool for measuring and determining the environmental structure of specific absorption atoms. It has been widely applied in the fields of solid state physics, catalyst and protein molecules. Double Crystal Monochromator (DCM) is a key device at XAFS beamline of Shanghai Synchrotron Radiation Facility(SSRF). It is used to change the certain wavelength of white light to monochromatic light and pass it to follow-up optical elements. The Bragg motor of the DCM is a step motor and its control system adopts Experimental physics and Industrial Control System (EPICS[1]) while the data acquisition system (DAQ) of QXAFS is developed in Labview. The present QXAFS control system at XAFS beamline is using Labview based DAQ which contains some drawbacks, such as the energy drift and spectrum distortion. It is running in the Windows operating system environment while the DCM control system is running in linux. The newwork transmission delay occurs at the communication between the two different kinds of system. The aim of this work is to design and implement fast time-resolved QXAFS data acquisition system based on EPICS that can solve these defects. In the system, two 1-MHz hardware trigger signal is generated and used to collect the signals of ionization chambers and the step motor position synchronously in the new design. The software of the system is developed in EPICS and runs in the linux operating system environment. The experimental method is implemented by python routine which is also integrated into the Graphical User Interface (GUI). The Conventional XAFS spectrum and four QXAFS spectra with an energy of 1.2 keV at the Cu K-edge have been collected in less than 8s at the XAFS beamline. The experimental results indicate that the QXAFS system can ensure a good signal-to-noise ratio, as well as a perfect stability and repeatability[2–4]. So the QXAFS data acquisition system based on EPICS is achieved at the XAFS beamline at SSRF. It has great practical significance for carrying out fast time-resolved QXAFS experiment at SSRF.

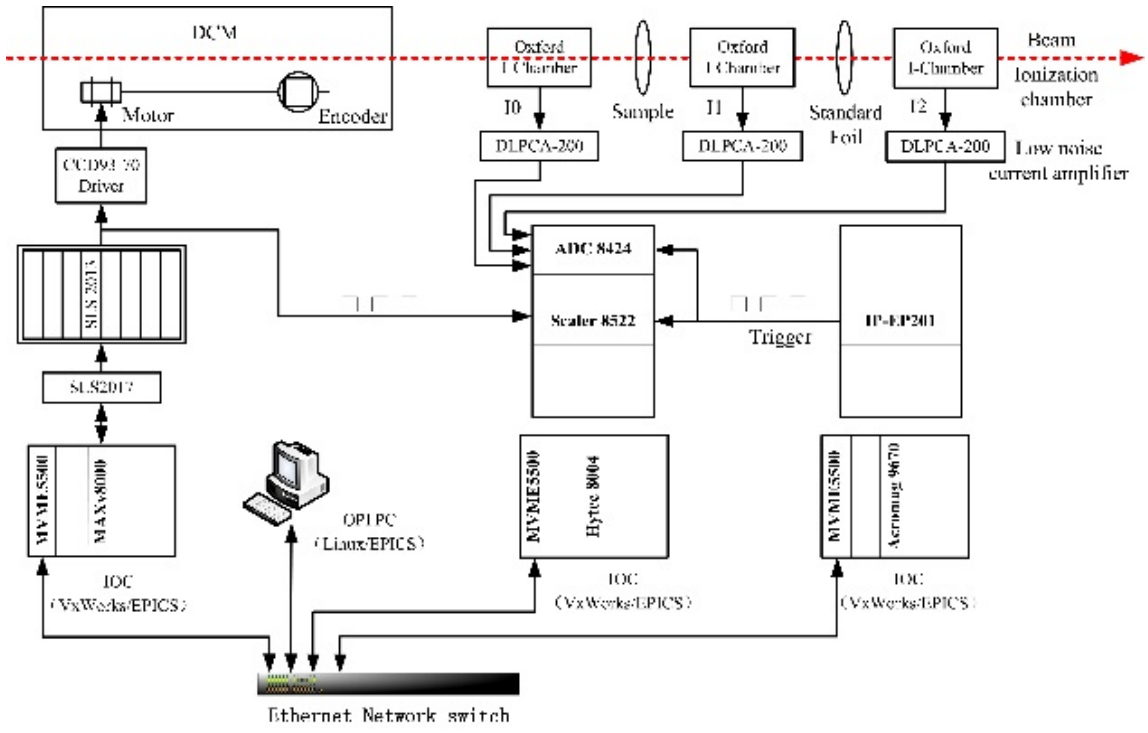

Fig.1 Hardware structure for the QXAFS system

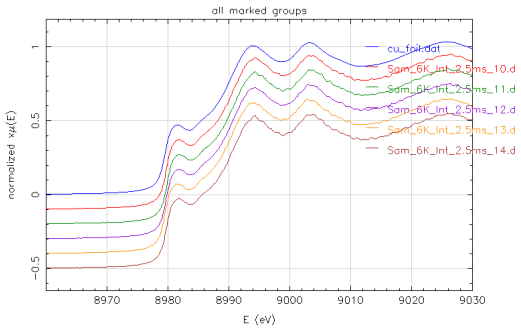

Fig.2 Comparation between five QXAFS spectra and one ordinary XAFS spectrum for the standard Cu element

The single crystal X-ray diffraction is one experimental method to use the single crystal X-ray diffraction effect to determine the crystal structure. The control group has completed the experiment's control and data acquisition system. The control system of the TTH axis, Phi axis and TH axis of the diffractometer were modified to realize the motion control and shutter synchronization trigger in EPICS environment. The controller selected is the American Galil company's intelligent motion controller, the controller is powerful, it can output trigger signals to synchronize the shutter switch and detector data acquisition with the position of the motors. The detector used is the MARCCD, the control and data acquisition of the MARCCD under EPICS can be realized by using the area detector control and data acquisition module AreaDetector in the EPICS SynApps package. The system worked well since it was put into use.

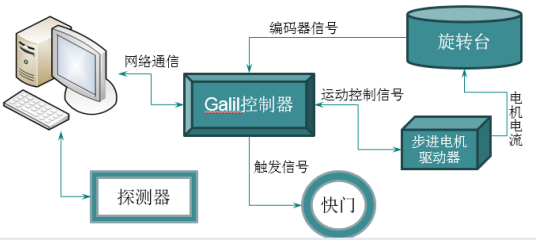

Fig.3 The hardware structure of the single crystal experiment setup

Reference

1 http://www.aps.anl.gov/epics/

2 ZHOU Yongnian, ZHANG Zhaohong, *et al*.. QXAFS data acquisition and control based on DCM [J]. Nuclear Science and Technology, 2015, **38**(5): 1-7

3 ZHOU Yongnian. Sudy and Realization on QXAFS Data Acquisition System Based on EPICS at SSRF[D]. University of Chinese Academy of Sciences, 2015

4 Quintana J P G. Uncertainty determination in QXAFS measurements[C]//American Institute of Physics, 2000: 194-197.

电子学与探测器组的研究进展(2015−2016)

束线光学工程技术部

本组开展了上海光源线站工程关键技术预研项目“高精度光束位置探测技术的研究”和大科学装置联合基金项目“基于数据挖掘的故障诊断算法”的研究，均取得了阶段性的研究成果。在做了大量测试和数据分析后，于 2015 年 4 月，就原有的光束线前端 XBPM 的联合测试验收做了内部评审，确认了光束线前端 XBPM 的探测精度为垂直方向 1 μm，水平方向 2 μm，以及分辨率达到 0.2 μm 等指标，同时指出影响现有 XBPM 测量精度的三方面因素，及其所占的比值。在此基础上，通过进一步对白光 XBPM 探测器的改进，采用较薄的探测刀片、改进组装工艺和优化数据处理方法，在 BL17U 前端达到了 X 光位置测量不确定度好于 0.4 μm，分辨率好于 0.08 μm 的水平，其测量结果如图 1(a)所示。本组所承担的单色光 QBPM 探测器的研制也取得了骄人的成绩，经过不断的摸索和试验，与相关技术人员的交流讨论，找到了合适的单晶硅探测芯片的组装工艺，完成了中心有孔和无孔两种探头的性能测试，都达到了位置测量不确定度好于 0.2 μm、分辨率好于 0.1 μm 的水平，其测量结果如图 1(b)所示。

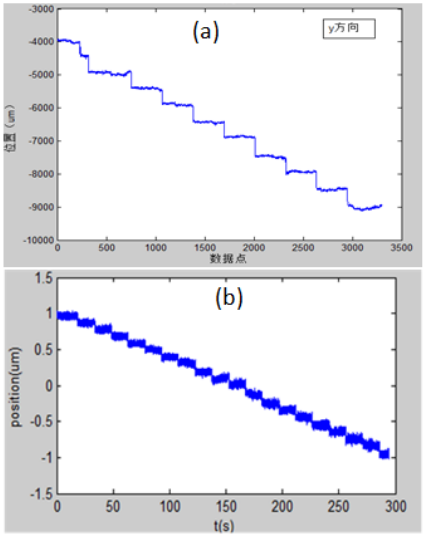

图 1　白光 XBPM(a)和单色光 QBPM(b)的测量结果

本组还结合运行研究项目的经费支持，通过测试比较和方法改进，发展了一种新的线站运行数据储存和管理系统，可快速实现各线站运行参量的查询和比较，能对感兴趣的运行参数进行相关的数据处理，可较方便地得到诸如光斑位置稳定情况的分析等，顺利地完成了联合基金项目的研究任务，所建立的新的光束线运行数据储存和分析系统较以前的系统使用更加方便、运行更加可靠，且系统的扩展性较强，其相关功能界面的截图如图 2 所示。

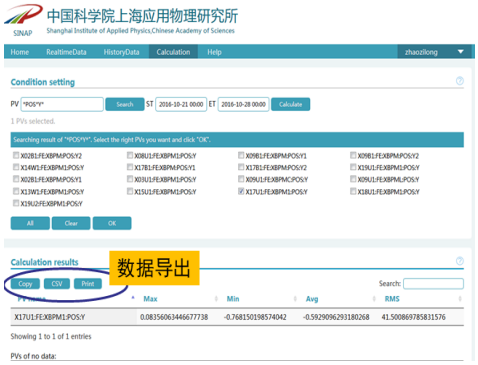

图 2　新的运行数据储存和分析界面

除此之外，本组还完成了三条新建光束线站（BL02B、BL03U 和 BL09B）的安全联锁保护系统和 XBPM 设备的安装调试，完成了各条光束线前端的性能测试和束线调光。测试结果表明：各系统的装调符合设计要求；同时还开展了丝扫描 XBPM 探测器的深入研究，可为今后设计更能满足线站使用要求的丝扫描探测器提供充分的技术支持和知识储备。

参考文献

1. 龚培荣, 徐慧超, 周剑英, 等. 上海光源光束线前端区 XBPM 探测器[J]. 核电子学与探测技术, 2015, **35**(3): 281−286.
2. 孙皓, 龚培荣. MATLAB 神经网络分析上海光源光束线的运行数据[J]. 计算机工程与应用, 2016, **52**(16):233−237.
3. 孙皓, 龚培荣. 基于MATLAB 的上海光源光束线运行状态分析与预警[J], 核技术, 2016, **39**(7): 070104.
4. 龚培荣, 何迎花, 周剑英. 丝扫描探测器测量同步辐射 X 光的位置和尺寸[J]. 核电子学与探测技术, 2016, **36**(3): 274−278.
5. 邵中尉, 韩定定, 龚培荣. 同步辐射丝扫描连续采样测量系统设计[J]. 核电子学与探测技术, 2016, **36**(10): 999−1003.
6. 邵中尉, 韩定定, 龚培荣. 丝扫描快速信号处理测量系统设计[J]. 核电子学与探测技术, 2016, **36**(12): 1245−1248.

Reasearch Development of Electronics and Detector Groups Duration 2015−2016

Department of Beamline Optics Engineering

Our group has carried out the research on the key technology pre-research project of SSRF beamline "Research on High-precision Beam Position Detection Technology" and Joint Scientific Fund project of large scientific facilities "Great data Fault Diagnosis Algorithm Based on Data Mining", and two projects have achieved periodic research results. After a lot of testing and data analysis, an internal review meeting was organized for the joint test acceptance of the original front-end XBPM in April 2015, to confirm detection accuracy of the beamline front-end XBPM is vertical direction 1um, horizontal direction 2 μm, and the resolution is 0.2 μm. The three factors affecting the accuracy of the XBPM measurement and their ratios are analyzed. On this basis, the XBPM detector was further improved by using the thin detector blade, changing the assembly process and optimizing the data processing method, the improved XBPM is tested at the front-end of BL17U, and the uncertainty of X-ray position measurement is better than 0.4 μm, the resolution is better than 0.08um, the measurement results are shown in Fig.1(a). The research and development of the monochromatic x-ray detector QBPM also made remarkable achievements. After continuous exploration, experiment and the discussion with related technician, the suitable assembly process of single crystal silicon detection chip was found, the performance test of the detecror which center with hole and center without hole was both completed, the both detectors have reached the position measurement uncertainty better than 0.2 μm and the resolution better than 0.1μm, the measurement results are shown in Fig.1(b).

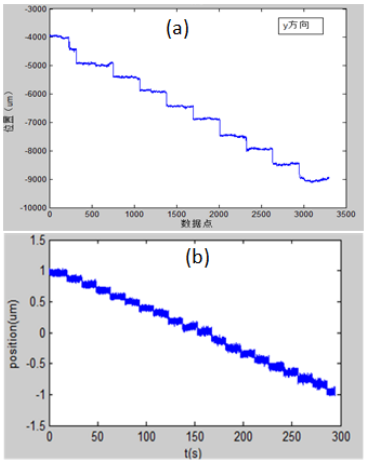

Fig. 1 Measurement results of XBPM (a) and QBPM (b)

Our group also received funding support from the operational research project. Through test comparison and method improvement, a new data storage and management system for beamlines operation has been developed, which can quickly inquire and compare the operation parameters of each beamline, and also can easily obtain the analysis of the stability of the spot position, etc. Therefore the research task of the joint fund project is completed smoothly. The new beamline operation data storage and analysis system is more convenient and reliable than the previous system, and the new system has strong expansibility. The relevant functional interface screenshot is shown in Fig.2.

In addition, our group also completed the installation and adjustment of the safety interlock protection system and XBPM equipment of three new beamlines BL02B, BL03U and BL09B, and completed the performance test of these beamline. The test results show that the installation and adjustment of each system meets the design requirements. At the same time, the further study of the wire scanning XBPM detector was carried out, which can provide sufficient technical support and knowledge reserve for the wire scanning detector designed to meet the requirements of the beamline in the future.

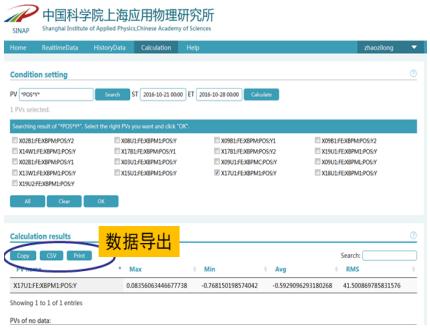

Fig. 2 New operational data storage and analysis interface

Reference

1. GONG Peirong, XU Huichao, ZHOU Jianying, *et al*. The X-ray beam position monitor used in the front end of SSRF[J]. Nuclear Electronics & Detection Technology, 2016, **35**(3): 281−286.
2. SUN Hao, GONG Peirong. MATLAB neural network analysis of the operation data of SSRF beamline[J], Computer Engineering and Applications, 2016, **52**(16): 233−237.
3. SUN Hao, GONG Peirong. Analysis of beamline running state and forewarning by using MATLAB in SSRF[J]. Nuclear Techniques, 2016, **39**(7): 070104.
4. GONG Peirong, HE Yinghua, ZHOU Jianying. The Size and Position of the X-Ray Beam Line Measured by Wire Scanning Detector at SSRF[J]. Nuclear Electronics & Detection Technology, 2016, **36**(3): 274−278.
5. SHAO Zhongwei, HAN Dingding, GONG Peirong. A New measureement system design for wire scanner monitor in SSRF[J], Nuclear Electronics & Detection Technology, 2016, **36**(10): 999−1003.
6. SHAO Zhongwei, HAN Dingding, GONG Peirong. Design of filament scanning fast signal processing measurement system[J]. Nuclear Electronics & Detection Technology, 2016, **36**(12): 1245−1248.

梦之线石墨 XBPM 的瞬态热分析

光学组

目前，超高能量分辨率及宽能量范围软 X 光束线（梦之线），已经在上海光源建成。为了监视 X 光束的轮廓，XBPM 是必不可少要安装在这条束线上，这有助于光束位置进行诊断。

一般来说，有几种 XBMP 可以用于测量光束的位置， 例如刀片型[2–3]、荧光屏[4]和丝型[5]。但刀片型 XBPM 不能得到光束的分布，而荧光屏 XBPM 通常用在束线的调试期间。

因此我们选用丝型 XBPM 用于实现上述功能。它提供光束轮廓的原理是基于光束和扫描线相互作用产生的光电流的大小。信号探测器可以显示打在丝上的光子数量。考虑到高热负载，采用具有高熔点和热导率的石墨，而不用钨作为扫描丝的材料。

为了模拟高热负载对 XBPM 的影响，使用 SPECTRA[6]软件来计算 X 光束的功率分布，如图 1 所示。它主要由储存环和 EPU 光源决定。从图 1 可以看出，最大功率密度将近 90 W/mm^2，此前上海光源所用的 XBPM 从未承受如此高的热负载。

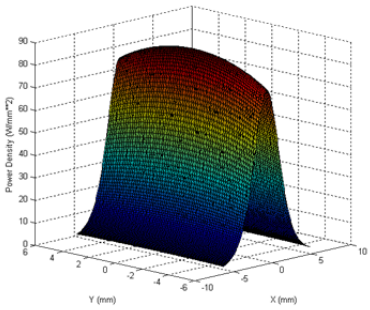

图 1 在 XBPM 处的 X 光功率分布

图 2(a)是 XBPM 的三维结构，包括步进电机、限位开关、光栅尺、真空室、C 型支撑体，观察窗和真空电接头等。两个石墨丝垂直固定在支撑体上。为了减少石墨丝吸收的热负载，选用厚度薄的石墨。本设计中石墨丝的尺寸是 50 mm (L)×2 mm (W)×0.125 mm (T)。如图 2(b)所示，丝支撑体是沿着与 X 和 Y 夹角 45°方向移动，这样就可以同时测量水平和垂直两个方向的 X 光束轮廓。从安全角度来说，主要关心的是石墨丝和高负载之间的热效应。因此需要使用 FEA 软件（如 ANSYS[7]）来模拟石墨丝扫描光束过程中的温度分布。

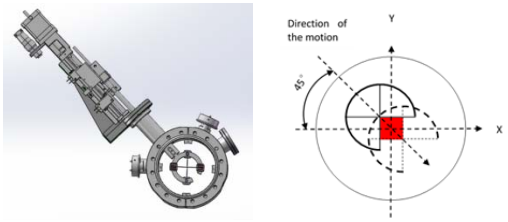

(a) (b)

图 2 XBPM 三维模型(a)和扫描 X 光示意图(b)

通常对于束线元件，例如光阑和反射镜[8]，进行稳态热分析就够了。这种方法可以得到稳态时的温度分布，但对于移动的石墨丝是不合适的。因为在扫描过程中，照射在丝上的功率密度和接受 X 光的区域都是在变化的，所以采用瞬态分析来模拟石墨丝的运动过程。

瞬态分析的关键是在扫描过程中施加对应位置的非均匀功率分布。为得到更精确的温度分布，最好是选择更多的载荷步和更小的时间步长。

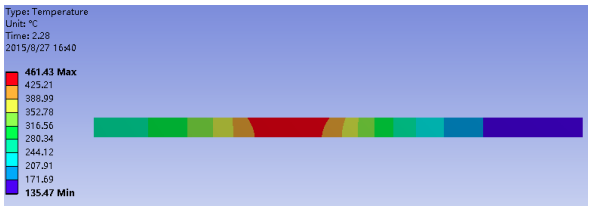

(a)

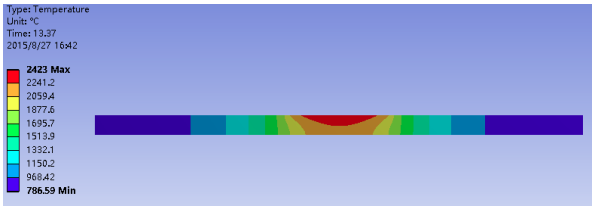

(b)

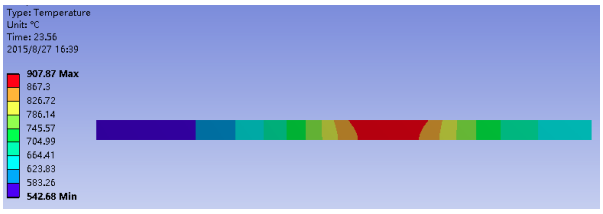

(c)

图 4 不同时刻 XBPM 上的温度分布
(a) 2.28s; (b) 13.37s; (c) 23.56s

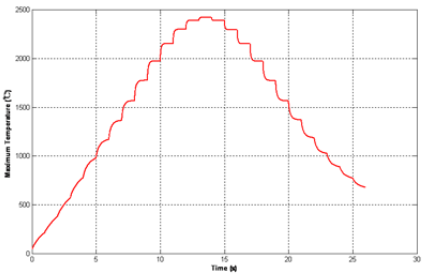

图 5　石墨丝的最高温度随时间的变化

我们可以得到XBPM在任意时刻的功率分布。图 4(a)、(b)和(c)分别对应在 2.28 s、13.37 s、23.56 s 时刻的温度分布。图 5 是整个扫描过程中最高温度随时间的变化曲线。可以看出：石墨丝上的最高温度从环境温度(30 °C)逐渐升高，大约在 13.37 s 达到最高 2 432 °C，然后温度慢慢降低。即使石墨丝移出了光束区域，它的最大温度仍然高于 500 °C。有限元分析的结果显示整个扫描过程石墨丝的最高温度都小于其熔点。XBPM 已经安装在梦之线上，并且运行良好。可以看出瞬态分析对 XBPM 设计是非常有帮助的。

参考文献

1. Lian Xue, Ruben Reininger, Yanqing Wu, *et al*. Design of an ultrahigh-energy-resolution and wide-energy-range soft X-ray beamline[J]. Synchrotron Rad, 2014, **21**: 273−279.
2. Aoyagia H, Kudoa T, Kitamura H. Blade-type X-ray beam position monitors for SPring-8 undulator beamlines[J]. Nuclear Instruments and Methods in Physics Research A, 2001, **467–468**: 252–255.
3. Sheng I C, Kuan C K, Chung Y T, *et al*. Design and analysis of EPU XBPM in TPS[C]. Proceedings of IPAC2012, New Orleans, Louisiana, USA, 894−896.
4. Jordi Juanhuix, Fernando Gil-Ortiz, *et al*. Developments in optics and performance at BL13-XALOC, the macromolecular crystallography beamline at the Alba Synchrotron[J]. J Synchrotron Rad, 2014, **21**: 679–689.
5. El Sisi A B. Wire Scanner Beam Profile Measurement for ESRF[C]. Proceedings DIPAC 2003–Mainz, Germany, 131−133.
6. Takashi Tanaka, Hideo Kitamura. SPECTRA: a synchrotron radiation calculation code[J]. Synchrotron Rad, 2001, **8**: 1221−1228.
7. ANSYS V12.0 Documentation. ANSYS Inc. 2011.
8. Xu Zhongmin, Wang Naxiu. An optimized side-cooling scheme for a collimation mirror at the SSRF[J]. Synchrotron Rad, 2012, **19**: 428–430.

Transient Thermal Analysis of an X-ray Beam Position Monitor Based on Graphite for the Dreamline

Optic Group

Currently, an ultrahigh-energy-resolution and wide-energy-range soft X-ray beamline[1], dubbed "Dreamline", has been built at SSRF. In order to monitor the profiles of the X-ray beams, X-ray beam position monitors (XBPMs) are indispensable and installed on this beamline, which help to verify beam position diagnostics.

Generally, several kinds of XBMPs, such as blade type[2–3], fluorescent screen[4] and wire type[5], can be used to measure the position of the beam. However, blade-type XBMP has no ability to get the distribution of the beam, while fluorescent screen is usually available during the commissioning of the beamline.

So we select wire scanner to implement above functionality. The principle of providing profiles is based on the amount of photocurrent generated by the interactions of the beam and the wire. The wire signal detector is to indicate the amount of photon striking the wire. Taking the high heat load from source into account, graphite with high melting point and thermal conductivity is adopted instead of tungsten used in other synchrotron facilities.

To simulate the effect of high heat load on the XBPM, the distribution of power density, mainly influenced by storage ring and elliptical polarized undulator (EPU) light source, is calculated and shown as Fig.1, using SPECTRA[6] software. From the Fig.1, we can see that the X-ray beam at 18.372 m, where the XBPM is located, has the maximum power density of nearly 90 W/mm^2 with a footprint area of 11.02×11.02 mm^2

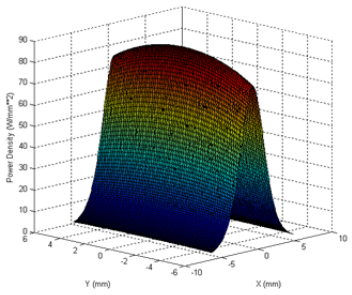

Fig.1 Spatial distribution of the power density

Fig.2(a) shows the 3D model of XBPM, consisting of stepper motor, limit switch, sylphon bellows, grating ruler, vacuum chamber, C-shaped wire holder, viewing window, and vacuum electric connector. Two graphite wires are perpendicular to each other and mounted on the wire holder. In order to reduce the thermal loads absorbed by the graphite, the small thickness of the graphite is a good choice. In this design, the dimensions of the two wires are 50 mm (L)×2 mm (W)×0.125 mm (T). As shown in Figure 2(b), the moving direction of the wire holder is 45 degrees between X and Y axis, which has an advantage of that this XBPM can measure X-ray beam (red square) in the both horizontal and vertical directions at the same time.

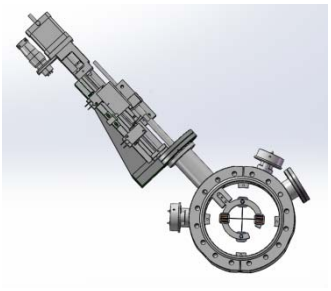

(a)

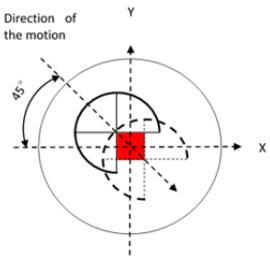

(b)

Fig.2 (a) Model of XBPM for the Dreamline; (b) Schematic view of scanning the X-ray beam

For the sake of safety, the major concern is the thermal effect between the wire and the extremely high loads from the light source. So it is indispensable to simulate the temperature distribution of two graphite wires during their moving across the beam, using FEA software like ANSYS[7].

Usually, static thermal analysis is performed for the beamline components, such as masks and mirrors[8]. Using the method, temperature distribution can be got when they reach thermal equilibrium. However, this is unsuitable for a moving graphite. Because both the power density shining on it and the zone receiving the heat load on its surface are always changing during scanning, the transient analysis is adopted to simulate the whole moving process. This kind of analysis determines temperatures that vary over time.

The key method of transient analysis is applying the corresponding non-uniform power density distribution on the surface of graphite at different position during the scanning. To get more precise temperature distribution, it is better to select more number of load steps and smaller time steps.

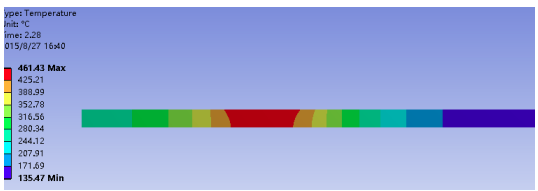

(a)

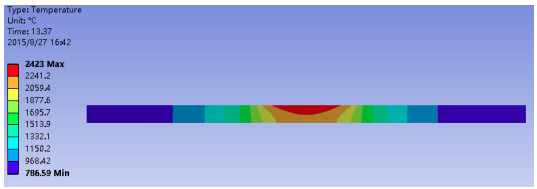

(b)

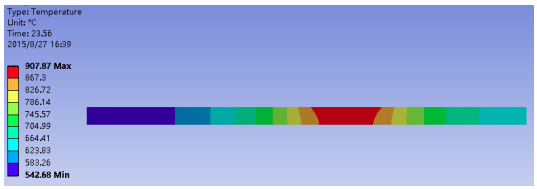

(c)

Fig.4 Temperature distribution of the graphite wire at (a) 2.28s; (b) 13.37s; (c) 23.56s

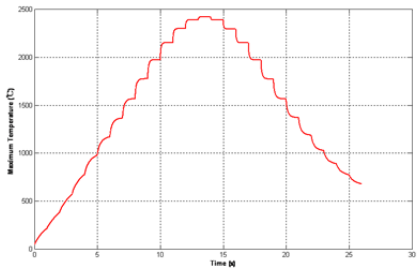

Fig.5 Maximum temperature on the graphite wire versus scanning time

We can get the temperature distribution of graphite at any time. Temperature distribution of graphite at three different time, 2.28 s, 13.37 s, 23.56 s, are shown in Fig.4 after the wire entered the scope of X-ray beam. Especially, time-dependent maximum temperature on it, shown in Fig.5, is obtained. The maximum temperature of the graphite gradually increases from ambient temperature (30 °C) after it encounters the beam. It reaches the peak of 2 432 °C at 13.37 s or so, then it decreased slowly. Even if the graphite moves out of the beam, its maximum temperature is still more than 500 °C. So temperature variation is seen clearly from the wire. It is very helpful to evaluate the design. The finite element analyses results show the maximum temperature of the graphite is below its melting point. This XBPM has been installed in the Dreamline and works well.

Reference

1. Lian Xue, Ruben Reininger, Yanqing Wu, *et al*. Design of an ultrahigh-energy-resolution and wide-energy-range soft X-ray beamline[J]. Synchrotron Rad, 2014, **21**: 273−279.
2. Aoyagia H, Kudoa T, Kitamura H. Blade-type X-ray beam position monitors for SPring-8 undulator beamlines[J]. Nuclear Instruments and Methods in Physics Research A, 2001, **467–468**: 252–255.
3. Sheng I C, Kuan C K, Chung Y T, *et al*. Design and analysis of EPU XBPM in TPS[C]. Proceedings of IPAC2012, New Orleans, Louisiana, USA, 894−896.
4. Jordi Juanhuix, Fernando Gil-Ortiz, *et al*. Developments in optics and performance at BL13-XALOC, the macromolecular crystallography beamline at the Alba Synchrotron[J]. J Synchrotron Rad, 2014, **21**: 679–689.
5. El Sisi A B. Wire Scanner Beam Profile Measurement for ESRF[C]. Proceedings DIPAC 2003–Mainz, Germany, 131−133.
6. Takashi Tanaka, Hideo Kitamura. SPECTRA: a synchrotron radiation calculation code[J]. Synchrotron Rad, 2001, **8**: 1221−1228.
7. ANSYS V12.0 Documentation. ANSYS Inc. 2011.

Xu Zhongmin, Wang Naxiu. An optimized side-cooling scheme for a collimation mirror at the SSRF[J]. Synchrotron Rad, 2012, **19**: 428–430.

生物大分子晶体学研究进展(2015−2016)

生物大分子晶体学组

生物大分子晶体学组主要承担上海光源首批线站“生物大分子晶体学光束线站(BL17U1)”的运行维护与用户实验支撑工作。该线站在 2015−2016 年度高效运行，累计总供光时间 11 016.8 h，其中用户机时 9 072 h，执行用户课题 6 2 1 次。用户共发表文章 373 篇，其中一区文章 116 篇，Cell、Nature 及 Science 顶级期刊文章 18 篇；用户解析结构总数高达 848，连续两年名列世界第一。

本研究组在保证光束线安全高效运行的同时，还积极开展光束线站新方法和新技术的研究及发展。

低温波荡器性能测试

对新安装的低温波荡器(CPMU)进行性能测试和优化，测得 6~20 keV 的能谱图（图 1）。

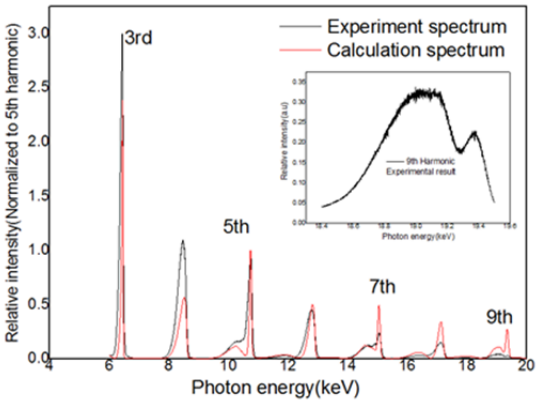

图 1　CPMU 小束流调试在 BL17U1 获得的光谱

微细光束研究

在前期一维 CRL 聚焦研究的基础上，同时基于 BL17U1 光束线光学布局，在超环面聚焦镜后增加水平偏转镜实现二维 CRL 与超环面聚焦镜聚焦情况下光斑一致性；完成了水平偏转镜安装与调试，实现二维 CRL 聚焦，聚焦光斑为 11.9 μm×6.96 μm，并提供给用户使用。

同步辐射光束线束斑形状实时分析技术研究

本课题组提出了一种基于图像处理的、实时的同步辐射光斑提取方法。该方法通过基于 OpenCV 视觉库开发的程序，经过测试和标定，获取的光斑尺寸与通过刀片扫描的方式获取的光斑尺寸大致吻合。与狭缝或刀片扫描的方式相比，这种方式更快速、更直观，而且能够同时显示光斑的二维尺寸信息、光斑的中心点及光斑的对称性，在同步辐射光束线的调试中可以作为一种有效的辅助手段[1]。

穿透型金刚石 X 射线位置灵敏探测器

X 射线位置灵敏探测器是同步辐射光束线上不可缺少的重要部件，由它所提供的光束位置和强度的实时数据是监测光束线运行状态的重要依据。为适应对高亮度同步辐射光束的测量需要，我们成功地研制了一套穿透型金刚石位置灵敏探测器，并在 BL17U1 上对其性能进行了测定。测量数据表明，在整块探测器(2.5 mm×2.5 mm)上均具有极好的线性响应，探测器的信噪比(S/N)>5×10^3，位置分辨能力为 σ=(136±11) nm，光强强度的测量精度和线性度均<0.1%，能满足第三代同步辐射和第四代光源（自由电子激光）束线上对光强、光斑位置及其运动轨迹的监测需求，是束线诊断的重要设备[2]。

除负责上海光源一期生物大分子晶体学光束线站的日常运行维护及用户实验支持外，本组还负责上海光源线站工程两条晶体学线站和一个用户辅助实验室的设计和建设工作。本年度，课题组负责完成了“P2 防护蛋白质晶体学线站”和“高性能膜蛋白晶体学线站”两条晶体学线站及生物与医学辅助实验室的可行性研究报告及初步设计报告撰写，提交发改委；邀请国内、国际专家对线站及实验室的可行性分析及初步设计方案进行评审；线站初步设计基本结束，转入工程设计阶段。

除了线站稳定运行相关技术的发展，在 In house 研究方面，课题组也不断拓展研究领域，不仅在重要蛋白质结构与功能研究方面进行了不断的研究和探索，解析了阿司匹林及其衍生物与脂肪酸结合蛋白 4 复合物及甲基转移酶 TleD 晶体结构的晶体结构[3−4]；在利用原位 XRD 及 EXAFS 合成病检测 Co@SiO_2 核壳纳米颗粒中心 Co 的氧化及 dSe 量子点从室温到 700 ºC 热膨胀合成及检测方面也取得了一定的进展[5−6]。

2015−2016 年度，本课题组在研项目主要有：

国家自然科学基金“同步辐射装置远程实验方法研究”和“具有新颖催化活性的细胞色素 P450 酶 TxtE 和甲基转移酶 TleD 的晶体结构和功能研究”；上海交大合作研究国家自然科学基金项目“古菌 RecJ-like 核酸酶参与校正 RNA 引物 3'末端错配核糖核苷酸的分子机制研究”；国家自然科学基金大科学装置联合基金“TET 蛋白的结构与功能”；上海交通大学微生物代谢国家重点实验室 2015 年开放课题“古菌 CRISPR-Cas 系统中 Cas7 蛋白的结构与功能研究”。

参考文献

1. 张春波, 汪启胜, 黄胜, 等. 同步辐射光束线束斑形状实时分析技术[J], 核技术, 2015, **38**(5): 050102.
2. 崔莹, 汪启胜, 黄胜, 等. 穿透型金刚石 X 射线位置灵敏探测器及其在同步辐射光束线上的应用[J], 核技术, 2016, **39**(7): 070101.
3. 黄佩, 李敏军, 左刚, 等. 阿司匹林及其衍生物与脂肪酸结合蛋白 4 复合物的晶体学研究[J], 核技术, 2016, **39**(8): 1−7.
4. Yu F, Li M J, Xu C Y, *et al*. Crystal structure and enantioselectivity of terpene cyclization in SAM-dependent methyltransferase TleD[J], Biochemical Journal, 2016, **473**: 4385−4397.
5. Zhang K H, Zhao Z Y, Wu Z H, *et al*. Synthesis and detection the oxidization of Co cores of Co@SiO_2 Core-Shell Nanoparticles by in-situ XRD and EXAFS[J], Nanoscale Research Letters, 2015, **10**: 37.
6. Zhao Ziyan, Zhou Ying, Bian Fenggang, *et al*. Synthesis and detection the thermal expansion of CdSe quantum dots from room temperature to 700 ℃[J] Journal of Nano Research, 2016, **35**: 11-20.

Research Development of Macromolecular Crystallography Group

Macromolecular Crystallography Group

Macromolecular Crystallography Group (MX group) is mainly in charge of operation and user support of the macromolecular crystallography beamline (BL17U1). During 2015-2016, BL17U1 provided 11 016.8 h beam time, of which 9 072 h were allocated to 621 research projects. 373 papers including 116 premium ones were published by users during this period. 848 structures have been deposited in the Protein Data Bank by the users. The number of structures deposited in Protein Data Bank by BL17U1 users still ranked first around the world in 2015 and 2016.

In order to ensure the safe and efficient operation of the beam line, research and development of the new method and technology of the beamline were carried out.

Test of the Cryogenic Permanent Magnet Undulator(CPMU)

The new CPMU was installed in the beamline of BL17U1. The energy spectrum was measured and optimized in the energy range of 6~20 keV (shown in Fig.1).

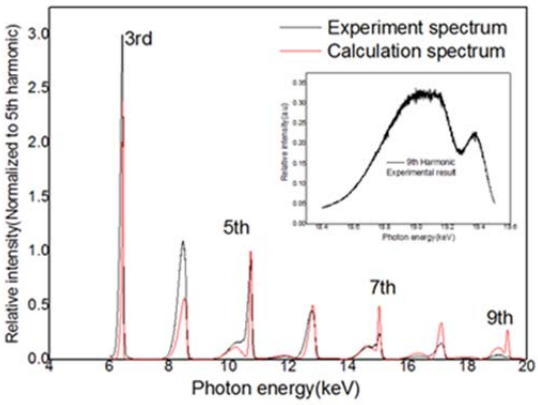

Fig.1 The spectrum of CPMU in the energy range of 6~20 keV

Micro-beam study in BL17U1

Based on the previous development of CRL focusing technique and the beamline layout of BL17U1, insertion of horizontal deflection mirror after the toroidal focusing mirror can achieve the same focusing spot consistency as before. The two-dimensional CRL focusing technique can achieve a focusing spot as small as 11.9 μm×6.96 μm and this has been used for user's experiment.

Real-time analysis technology on the shape of synchrotron radiation beam

Basic image processing method and adaptive threshold binarization method are employed to resolve the problem. The results showed that the image processing program can get the spot size correctly even the change of the spot size in a large range, and what's more, the new method can show the information about spot center and spot symmetry simultaneously. Compared with the currently used method, the new method is faster and more intuitive and it can be considered as an effective diagnosis tool during beamline operation [1].

Transmission-mode diamond X-ray position sensitive detector

X-ray position sensitive detector is indispensable for beamlines at synchrotron radiation facilities. In order to provide accurate real-time position and intensity for high-flux X-ray beams, we have demonstrated the feasibility of building a transmission-mode synthetic single-crystal diamond X-ray position sensitive detector. Based on the principle of potentiometers, the transmission-mode diamond X-ray position sensitive detector works as a "solid" ionization chamber. When the X-ray beam comes into the detector's sensitive region, electronic-holes occur due to the effect of ionization and the charges or the current pulses on the electrodes of the detector are given. According to the collected currents on the electrodes, the location of the incident X-ray can be determined by the ratio between the current difference of electrodes and the total current. A signal/noise ratio of (S/N)>5×10^3 and a position resolution of σ=(136±11) nm for the synthetic single-crystal diamond position sensitive detector with an active area of 2.5 mm×2.5 mm, respectively, have been obtained. The measurement precisions for the X-ray beam intensity and position linearity are less than 0.1% [2].

In addition to the daily operation and maintenance of the BL17U1 beamline, MX group is also responsible for the design and construction of two new macromolecular crystallography beamlines and a user laboratory in the PHASEII beamline project. During 2015−2016, MX group completed the feasibility study report and the preliminary design report of the Biosafety P2 Macromolecular Crystallography Beamline, the High Performence Membrane Protein Crystallography Beamline and the Biological and medical Auxiliary Laboratory. The reports have been reviewed both by the domestic and international experts after submission to the National Development and Reform Commission.

Besides the development of techniques for assisting the beamline operation and supporting the user's experiment, MX group also strived to expand the in house study field. During 2015−2016, MX group have reported the crystal structures of human fatty acid binding protein 4 with aspirin and its derivative[3] and terpene cyclization in SAM dependent methyltransferase TleD[4]. Furthermore, in the field of synthesis and detection the oxidization of Co cores of Co@SiO_2 Core-Shell Nanoparticles by in-situ XRD and EXAFS and synthesis and detection the thermal expansion of CdSe quantum dots from room temperature to 700 ℃, MX group also made some progress[5−6].

In these two years, the undertaken projects by MX group

included: 1) National Science Foundation of China: “Study on the remote experiment method of synchrotron radiation” , “Study on the crystal structure and function of cytochrome P450 enzyme TxtE and methyltransferase TleD with novel catalytic activity”, ”Study on the molecular mechanism of RecJ-like nuclease involved in the correction of RNA primer 3'-terminal mismatched ribonucleotide”(in cooperation with Shanghai Jiaotong University); 2) Joint Funds of the National Science Foundation of China” Structure and function of TET protein”; 3) The 2015 open subject of the National Key Laboratory for microbial metabolism of Shanghai Jiao Tong University: "study on the structure and function of Cas7 protein in the CRISPR-Cas system of Archae bacteria".

Reference

1. Zhang Chunbo, Wang Qisheng, Huan Sheng, *et al*. Real-time analysis technology on the shape of synchrotron radiation beam[J]. Nuclear Technique, 2015, **38**(5): 050102.
2. Cui Ying, Wan Qisheng, Huan Sheng, *et al*. Transmission-mode diamond X-ray position sensitive detector and its applications in synchrotron radiation beamlines[J]. Nuclear Technique, 2016, **39**(7): 070101.
3. Huang Pei, Li Minjuni, Zuo Gang, *et al*. Crystallography study of the complexes of human fatty acid binding protein 4 with aspirin and its derivative[J]. Nuclear Technique, 2016, **39**(8): 1−7.
4. Yu F, Li M J, Xu C Y, *et al*, Crystal structure and enantioselectivity of terpene cyclization in SAM-dependent methyltransferase TleD[J]. Biochemical Journal, 2016, **473**: 4385–4397.
5. Zhang K H, Zhao Z Y, Wu Z H, *et al*. Synthesis and detection the oxidization of Co cores of Co@SiO_2 Core-Shell Nanoparticles by in-situ XRD and EXAFS[J]. Nanoscale Research Letters, 2015, **10**: 37.
6. Ziyan Zhao1, Ying Zhou1, Fenggang Bian, *et al*. Synthesis and detection the thermal expansion of CdSe quantum dots from room temperature to 700 ºC[J]. Journal of Nano Research, 2016, **35**: 11-20.

光电子组研究进展

光电子组

光电子组主要承担上海光源“超高分辨宽能段光电子实验系统”（梦之线）线站的调试及运行和维护工作，以及线站工程中 S^2 线、Eline 软线、RIXS 实验站和原位环境支撑实验室的建设。

梦之线 2015 年上半年（1−7 月）处于试运行状态，未对用户正式开放。总用光时间 343 h，其中用户机时 248 h。下半年（9−12 月）进入正式运行。全年专有用户机时 2 444.73 h，故障机时 156 h。2016 年度完成运行机时 5 544.19 h，其中用户实验机时为 4 361.07 h，束线故障机时 51.57 h，故障率 0.93%。接待 19 个课题组，进行 27 个课题的研究，取得了包括“发现外尔费米子”、“首次观察到大能隙拓扑材料的边界态 $ZrTe_5$”等重要的成果。用户发表文章 13 篇，其中一区 7 篇，二区 3 篇，三区 3 篇。

本组负责二期线站“纳米自旋与磁学线站”(S^2 线站)的建设工作。确定了插入件及前端的参数，确定了所有光学元件的参数，确定了所有运动机构的技术参数要求，确定了实验站的技术参数，并完成了实验站中原位生长装置的招标工作。完成可研报告和初步设计报告。本组负责二期线站 E-line 软线分支的建设。初步设计评审于 2016 年 7 月正式通过。在初步设计报告的基础上，进一步开展了束线的技术设计。本组还负责了二期关键技术的预研项目-“软 X 射线荧光谱仪（SRXES 谱仪）”的研制，完成了谱仪的物理设计及初步设计。本组负责了上海光源二期辅助实验室中原位条件实验室的建设工作。完成了二期原位条件辅助实验室可研报告；完成了二期原位条件辅助实验室初步设计报告。本组负责的 RIXS 站，作为上海光源线站工程二期的一个实验站，在 2016 年通过实验站初步设计方案评审和国家发改委的方案概算评审。

为提高梦之线运行的性能，本组完成了运行项目 “同步辐射光下的在线氧清洗系统的研制及其对束线性能的影响”，使得在线氧清洗的方法率先在梦之线得到应用并取得良好清洗效果；实现了 GAP 运动的限制模式，尽早实现了梦之线的全能域、全极化使用；关于 MCP 探测器方法的应用获专利并发表文章一篇[1]。本组对同步辐射和 FEL 束线站相干性传播进行研究，并发展出 MOI 模型[2]。

在研项目包括国家重点研发项目“同步辐射和强磁场下量子材料的多维度测量和表征”的子课题“利用多种同步辐射测量手段研究量子材料的结构、磁性激发和动力学特性”(2016YFA0401002)，国家重点研发计划项目“先进材料多维多尺度高通量表征技术”(2016YFB0700402)[3]，国家自然科学基金项目“同步辐射原位磁场研究平台及磁性纳米点阵研究”(11475251)，国家自然科学基金项目“活体细胞的软 X 射线三维成像实验方法的研制”(11305254)[4]，国家自然科学基金联合基金项目“结合同步辐射实验和第一性原理的理论对’半晶化’过程中的晶体结构、电子结构和热力学性质进行研究”。并承担项百人计划 C 类先期支持项目。

2017 年度梦之线预计将使 ARPES 实验站升级自旋分辨功能；实现 PEEM 微区吸收谱及 XMCD 实验方法；实现 GAP 联调，以方便连续吸收谱的测量。针对本组负责的二期各条线站（S^2、E-line 软线）、关键技术预研项目及辅助实验室，进一步精炼技术参数，并开始部件的采购。

参考文献

1. Li J Q, Zou Y, Chen Z H, *et al*. Nuclear Technique, 2016, **39**: 050101.
2. Meng X, Xue C F, Yu H N, *et al*. Opt. Express 2015, **23**: 29675-29686.
3. Cao J F, Wang Y, Zou Y, *et al*. Synchrotron Rad. 2016. **23**: 436-442.
4. Miao X R, Tian F, Lin J Y, *et al*. RSC Adv 2016, **06**: 83356-83365.

Research Development of Photoelectron Group

Photoelectron Group

Photoelectron group (PE group) is mainly in charge of commission, operation and user support of the DREAMLINE beamline (High Energy Resolution and Broad Energy Range Photoelectron Experimental System) and, for the PHASE-II Beamline Projects, developing three beamlines(station) including S^2-line, Eline soft-branch and RIXS station plus one user-supporting laboratory–in-situ instrumentation lab.

In the first half of 2015, the DREAMLINE beamline was test-running and not open to the public. It has delivered supported beam time in a total of 343 h and provided 248 h for users. In the second half of 2015, this beamline has officially started its operation. All the year it provided 2 444 h beam time for exclusive users with 156 h in fault. In the year of 2016, the beamline has opened to public users, and supplied a beam time in a total of 5 544 h, provided 4 361 h for 19 users from 27 proposals, major achievements include discovery of Weyl fermion and first observation of the edge states of large energy gap topological insulators ($ZrTe_5$). The annual a fault rate is 0.93%. thirteen papers have been published during this time.

For the PHASEII beamline projects, the nanospin and magnetics beamline (S^2-line), the specifications for two IDs, front end, all optic elements, motion mechanisms, experimental stations etc have been determined. The bidding of an in-situ sample growth device for a station was concluded. The feasibility proposal and preliminary design report have been accomplished. For the E-line soft branch, the preliminary design was reviewed and passed in July 2016, the engineering design phase has been followed afterwards. As one of beforehand-research topic of PHASEII critical techniques, the soft X-ray emission spectrometer (SRXES) has been developed by our group, and its physical design and preliminary design were completed. For the in-situ instrumentation lab, the feasibility proposal and preliminary design report have been finished as well. For the RIXS station, the review on its preliminary design in 2016 was successful and got through budgetary review at NDRC.

To improve the performance of the DREAMLINE beamline, the PE group has conducted a beamline study program-“developing an in-situ oxygen cleaning system under synchrotron radiation”, and realized the cleaning method firstly at the beamline with positive results. A new GAP/SHIFT motion mode (confined mode) for undulator control was implemented at the beamline to achieve the global access to full polarization in the full energy range at its earliest operation stage. The MCP application in the beamline was studied with outcomes of a patent and a journal paper[1]. A new MOI model has been developed by our group in the study of beam coherent propagation of synchrotron radiation and FEL light[2].

The ongoing projects include two National Key R&D Programs “Crystal structure, magnetic excitation and quantum dynamic studies on the quantum materials using synchrotrons experimental methods” (2016YFA0401002) and “Multi-dimensional multi-scale high flux characterization techniques of advanced materials” (2016YFB0700402)[3]; and those supported by the National Natural Science Foundation of China “In-situ magnetic field research platform via SR for magnetic nano-array” (11475251),” Soft x-ray 3D imaging on living cells” (11305254[4]); and one project supported by Joint Funds of the National Natural Science Foundation of China “Study on crystal structure, electronic structure and thermodynamics in the process of semi-crystallization combining SR experiments with ab-initio theory”; and the CAS Pioneer “Hundred Talents Program” (type C).

In 2017，for the DREAMLINE, besides the beamline operation and user experiments support, the PE group strives to upgrade the ARPES station with spin-resolving capability, fulfil micro-zone absorption spectroscopy and XMCD at PEEM station, realize synchronized GAP adjustment. Refinement and frozen of technical specifications for all involved PHASEII-related beamlines(station/lab) shall be done, and parts procuring shall start.

Reference

1. Li J Q, Zou Y, Chen Z H, *et al.* Nuclear Technique, 2016, **39**: 050101.
2. Meng X, Xue C F, Yu H N, *et al.* Opt. Express 2015, **23**: 29675-29686.
3. Cao J F, Wang Y, Zou Y, *et al*. Synchrotron Rad. 2016. **23**: 436-442.
4. Miao X R, Tian F, Lin J Y, *et al*. RSC Adv 2016, **06**: 83356-83365.

软 X 射线组研究进展

软 X 射线组

软 X 射线组主要承担上海光源首批线站“软 X 射线谱学显微光束线站和干涉光刻分支线站”的运行维护与用户实验支持工作。该线站在 2015−2016 年度高效低故障运行，总供光机时 11 197 h，总故障率 0.07%。累计提供用户机时 9 301 h。接待用户实验人员 874 人次，执行用户课题 270 个，用户涵盖环境科学、材料科学、生物医学和物理学等领域。共发表包括 Adv. Funct. Mater.、 Particle and Fibre Toxicology、ACS NANO、Advanced Materials、Corrosion Science、Carbon、Nature Communication 等一区在内用户文章 100 篇，其中包括一区文章 21 篇。

除负责上海光源一期软 X 射线谱学显微(STXM)光束线站和干涉光刻(XIL)分支线站的日常运行维护及用户实验支持外，本组还负责上海光源线站工程一条新建线站——“中能谱学线站”的建设；国家重大科研仪器设备研制专项：SiP·ME^2 项目——弯铁软 X 射线光束线(02B)的设计和部分建设，2016 年调试出光，并内部测试达到验收指标；承担完成了国家重大科技基础设施建设项目“活细胞结构与功能成像等线站工程(SBP)”活细胞成像光束线的初步设计；参与了 X 射线自由电子激光试验装置诊断光束线的部分设计和建设任务。

为满足不同学科领域用户研究的需求，发展了实验站方法学：1) 优化了基于 STXM 的扫描相干衍射成像(CDI)实验方法学，实现了低剂量、高分辨、高效率的成像方法，将上海光源空间分辨能力由 30 nm 提升至 8.5 nm，成像剂量降低至常规 STXM 技术的 1/12，数据获取时间为 STXM 的 1/3[1]；2) 搭建了硅漂移探测器的软 X 射线荧光的探测设备，实现了用软 X 射线部分荧光产额模式测试材料的吸收谱，有助于绝缘材料、低元素含量样品、材料体相信息的研究；3) 搭建了 STXM 纳米 CT 平台，实现了 100~200 nm 的三维空间分辨；4) 完成多功能谱学测量系统的装调；增加了原位标样测量装置，均开放使用；5) 完成 STXM 新系统的设计和评审；6) 开展激光和 X 射线光子关联谱实验装置腔体的离线搭建和相关实验[2]；7) 实现了高效拼接制备大面积高深宽比结构，并成功应用于多个研究领域[3]；8) 发展了宽带泰保光刻技术，得到了最小点径为 20 nm，周期为 106 nm 的曝光图形；9) 发展了时间分辨软 X 射线激发光学发光(XEOL)方法，并实测了氧化锌样品。

在应用研究方面，依托本线站开展了纳米气泡的研究，进行了纳米气层的物理性质测量，以及纳米气泡可控生长和界面张力的原位测量[4−5]；利用激光光子关联谱，在弛豫铁电体极化团簇弛豫特性研究取得进展，进行 X 射线光子关联谱实验装置搭建；将 VUV 波段精确聚焦概念用于高性能 VUV-软 X 射线双模单色器的设计[6]；研制表面修饰闪烁体成像探测器。

本课题组承担的在研科研项目有：国家自然科学基金项目“X 射线扫描相干衍射成像方法学及其应用研究”、“亚微米周期性结构基底对纳米气泡界面特性的调控机制研究”、“基于新型宽带相干光学技术的软 X 射线干涉光刻”、“同步辐射 X 射线光子关联谱和 X 射线偏振检测实验方法研究”；大科学装置联合基金重点项目“基于同步辐射的固液界面‘纳米气泡’结构与性质研究”；国家自然科学基金青年基金项目“同步辐射软 X 射线光束线光束位置无损在线监测技术的研究及其在纳米 CT 与透射扫描显微成像中的应用”、“多孔石墨烯分离膜的粒子束制备及其性能的理论研究”、“基于同步辐射研究纳米气泡的电化学方法的发展”、“基于 XIL 技术的复杂图形光刻技术及其应用研究”、“基于同步辐射光源的扫描菲涅耳相干衍射成像方法学研究”；国家自然基金重大项目子课题“水科学先进实验技术研究”；国家自然科学基金重点项目子课题“无铅压电材料的多层次结构调控与表征技术”；973 项目子课题“弛豫铁电单晶多尺度微结构研究和巨压电性的起源”；中国科学院前沿科学重点研究项目子课题“纳米气泡同步辐射研究”。

2017 年，软 X 射线组主要任务：完成软 X 射线谱学显微和干涉光刻线站的运行维护；开展中能谱学线站的设计和建设；完成 SiP·ME^2 项目弯铁软 X 射线光束线的束线安装；发展 STXM 和 XIL 相关的束线方法学，更好为用户服务。

参考文献

1. Wang C P, Xu Z J, Liu H G, *et al.* Appl Opt, 2017, **56**: 2099.
2. Zhang M J, GUO Z, TAI R Z, *et al.* JJAP, 2015, **54**: 042401.
3. Xue C F, Wu Y Q, Zhu F Y. Rev Sci Instrum, 2016, **87**:

043303.
4. Zhao B, Wang X, Wang S, *et al*. Soft Matter, 2016, **12**, 3303，中国专利：ZL2015106665003.
5. Zhao B, Wang X, Song Y, *et al*. Phys Chem Chem Phys, 2015, **17**: 13598-13605.
6. Xue C F, Wu Y Q, Zou Y J. Synchrotron Rad, 2015, **22**: 1353.

Research Progress in Soft X-ray Group

Soft X-ray Group

Soft X-ray group is mainly in charge of operation and user support of soft X-ray scanning microscopy (STXM) beamline and soft X-ray interference lithography (XIL) branch beamline. During 2015–2016, this beamline has supported beam time of 11 197 h with a low fault rate of 0.07%. There were 9 301 h provided for 874 users from the 270 proposals, whose research fields covering environmental science, material science, biomedicine, physics and so on. During this time 100 user papers have been published on academic journals，including Adv. Funct. Mater., Particle and Fibre Toxicology, ACS NANO, Advanced Materials, Corrosion Science, Carbon, Nature Communication, etc. 21 papers were publiched on the top journals (SCI-I).

Besides the maintenance user suport work on STXM and XIL stations, soft X-ray group takes charge of the constraction of 4 new beamlines. 1) The design and construction of Medium energy spectroscopy beamline in SSRF Phase-II project; 2) The design and partial construction of Bending magnetic soft X-ray beamline (02B) of National Major Scientific Instruments and Equipment Development of NSFC (SiP·ME^2), the beam has been shed into the sample position on Junuary 23 rd, 2016; 3) The physical desigin and partial construction of SASE beamline of National major science and technology infrastructure construction project SBP project. The physical designing and its reviewing have been completed. 4) Soft X-ray group is participating the physical design and construction of the diagnostic beamline of National major science and technology infrastructure construction project X-ray free electron laser test facility.

In order to meet the demands of users in different fields , several methodologies have also been developed: 1) Our group developed and optimized the scanning coherent diffractive imaging (SCDI) methodology based on STXM, implementing a low-dose, high-resolution and high-efficiency imaging method, which improves the spatial resolution of SSRF from 30 nm to 8.5 nm, reduces the imaging dose to 1/12 that of conventional STXM imaging, and cuts down the data acquisition time to only 1/3 that of STXM; 2) The system for soft X-ray fluorescence detection is established based on the silicon drift detector (SDD) in BL08U. The soft X-ray absorption spectrum is realized by partial fluorescence yield (PFY) mode. The insulation materials, the element with low concentration, and the bulk information of materials can be well investigated with PFY study; 3) Developed the Nano-CT function based STXM and the 3D resolution is 100~200 nm； 4) The installation and debugging tasks of the spectra measurement system have been accomplished, and we also developed an in situ standard sample measurement device. All of these systems have been opened for users; 5) Design and review of the new STXM system have been completed in 2016; 6) The laser and X-ray PCS setup and related experiments have been implemented[2]; 7) Implementing the effective abrication of large area high-aspect-ratio periodic nanostructures by stiching XIL, on various substrates in dfferent studies[3]; 8) Developing Broadband Talbot lithography, obtain the dots with minimum size 20 nm in a 106nm period structure; 9) Time-resolved XEOL technique has been developed at STXM beamline. The ZnO sample was measured by using time-resolved XEOL technique.

Some in-house application researches have also been carried out. The study on nanobubbles was done based on this beamline, such as the measurement of physical properties of nano gas layers, the controllable growth of nanobubbles at different substrates and the in situ measurement of their surface tension[4–5]. Some improvements have been achieved in the relaxor characteristic of polarization clusters in relaxor ferroelectrics based on laser PCS, and X-ray PCS setup has been fabricated. The VUV extra-focus mechanism was applied on high -performance dual-mode monochromator from VUV to soft X-ray[6]; X-ray indirect imaging detector with a surface modified scintillator was investigated.

The ongoing projects include Projects of National Natural Science Foundation of China “X-ray scanning coherent diffractive imaging methodology and its applications”, “Manipulation mechanism research on the interfacial characteristics of nanobubbles by Sub-micron periodic structures”, “Soft X-ray inteference lithography based on new coherence optics”, “Researches for synchrotron radiation X-ray photon correlation spectroscopy and x-ray polarization detection method”; The joint funding key projects for large scientific facility, “research on the structure and properties of nanobubbles at the solid-liquid interface based on synchrotron radiation”; The projects of the National Science Foundation for Young Scientists of China, “The study of detection technology for online non-invasive beam position monitoring of soft X-ray beamline and its application in nano-CT and STXM”, “Theoretical research on the ion-beam fabrication and property of porous graphene membranes”, “the development of electrochemical method for nanobubbles based on synchrotron radiation”, “Research on complex periodic nano-structures based on X-ray interference lithography”, “Research on Scanning Fresnel Coherent Diffractive Imaging Based on Synchrotron Radiation Source”; National natural funding major project-sub-project, “study on advanced experimental techniques for water science”; Subproject of key projects of National Natural Science Foundation,“Regulation and characterization technology for Multi-level structure of non-lead piezoelectric material”; Subproject of the National Basic Research Program of China (973 Program),“Origin research for the multi-dimensional microstructure and ultrahigh piezoelectricity of relaxor ferroelectrics”; Research project of frontier science of Chinese academy of sciences-sub-project, “study on nanobubbles by synchrotron radiation.”

In 2017, there are the following tasks of Soft X-ray group: operation and maintenance of STXM and XIL endstation; design and construction; Completing the installation of Bending magnetic soft X-ray beamline (02B) in SiP·ME^2 project; Development of methodology in STXM and XIL endstation,

for better user support.

Reference

1. Wang C P, Xu Z J, Liu H G, *et al.* Appl Opt, 2017, **56**: 2099.
2. Zhang M J, GUO Z, TAI R Z, *et al.* JJAP, 2015, **54**: 042401.
3. Xue C F, Wu Y Q, Zhu F Y. Rev Sci Instrum, 2016, **87**: 043303, Chinese Patent ZL201506665003.
4. Zhao B, Wang X, Wang S, *et al*. Soft Matter, 2016, **12**, 3303.
5. Zhao B, Wang X, Song Y, *et al.* Phys Chem Chem Phys, 2015, **17**: 13598-13605.
6. Xue C F, Wu Y Q, Zou Y J. Synchrotron Rad, 2015, **22**: 1353.

X 射线衍射组研究进展

X 射线衍射组

X 射线衍射组主要承担“上海光源”首批线站“X 射线衍射光束线站”的运行维护与用户实验支持工作。该线站在 2015–2016 年度高效低故障率运行，总供光机时 11 084.5 h，总故障率为 0.4%。累计提供用户机时 8 964 h，接待用户实验人员 956 人次，执行用户课题 306 个，用户研究涵盖材料科学、化学、凝聚态物理、高分子科学、环境与地质等众多学科领域，共发表用户成果 169 篇，其中 SCI 一区及以上文章 70 篇。线站维护方面，完成了光束线单色器一晶、单色器 Pitch 电机驱动模块、控制器的控制模块、电控 Z 轴、探测器电源适配器的更换以及 CCD 气路清理等。2015 年寒期，束线前置准直镜由柱面镜更换为超环面镜。2016 年暑期，完成 CCD 返厂家维修，修复背底高、不均匀现象。

除负责上海光源一期 X 射线衍射线站的日常运行维护及用户实验支持外，本组还负责上海光源线站工程 2 条新建线站“白光劳厄衍射线站”和“表面衍射线站”、“超硬多功能束线工程材料实验站”及材料样品辅助实验室的设计工作，本年度完成了上述工程任务的可行性报告以及初步设计报告并通过相应评审，2016 年 11 月份上海光源二期线站工程正式开工。

为满足不同学科领域用户研究的需求，本组在 X 射线衍射方法学研究及相关应用研究方面进行了不断的研究和探索，共发表论文 19 篇[1-19]，其中 SCI 收录 16 篇，获授权专利 5 项。束线实验方法及装置发展方面，线站工作人员开展了全反射荧光、单晶衍射、衍射信号荧光探测、金属焊接原位研究、线形探测器应用、异常散射法、二维面探测器支撑系统改造、高真空高温原位热台发展等工作。应用研究方面，在石墨烯 CVD 原位生长结构研究[2]、金纳米颗粒增强有机太阳能电池材料与器件[3]、PVP 水溶性牺牲层转移印制增强性能的磁性微传感器[6]、纳米晶 GaN_xMn_3 覆盖室温的巨负膨胀效应[7]、Na 离子注入提高 SnO 薄膜 p 型导电性、Mythen 新型线探测器快速校正[8]、冷轧纳米镍铁合金的同步辐射研究[9]以及高性能钙钛矿太阳能电池研究[1]等诸多领域都有所进展。

在研项目主要有：1) 中国科学院百人计划项目；2) 国家自然科学基金青年项目“掺杂 $BiFeO_3$ 锂离子电池电极材料的同步辐射原位构效关系研究”，“关联体系的同步辐射原位研究平台及在电子铁电材料中的应用”；3) 国家自然科学基金大科学装置联合项目“利用同步辐射二维掠入射 X 射线衍射实时表征共轭聚合物薄膜微结构变化的测试平台的搭建与相关方法学研究”；4) 国家自科学基金大科学装置联合项目（重点）项目“基于同步辐射 X 射线衍射研究钙钛矿微结构”等。

新申请获批项目 10 项：1) 国家自然科学基金面上项目：“钙钛矿型太阳能电池真空制备原位实时表征”、“基于同步辐射及正电子湮没技术的 $LaNi_{1-x}M_x$ 合金储氢性能本征衰退机理的研究”；2) 上海大科学中心研发项目：“材料结构和输运的同步辐射原位表征”；3) 国家自然科学基金青年基金项目：“采用原位同步辐射衍射研究纳米结构 Cu/Ag 多层膜的微机械行为”、“利用同步辐射研究钙钛矿太阳能电池微结构”以及“同步辐射黄昆漫散射平台的建立及其在 p 型 SnO_2 薄膜内部点缺陷研究中的应用”；4) 中国科学院青年创新促进会会员人才专项；5) 上海市科委“材料基因组”工程“同步辐射应用与材料基因组科学基础研究”；6) 国家重点研发计划项目：先进材料多维多尺度高通量表征技术；7) 国家自然科学基金联合基金项目：“钙钛矿太阳能电池的结构与性能的同步辐射研究”。

2017 年度本组除了进行衍射线站的运行维护和用户实验支持、新建相关线站、实验室的工程实施以及上述科研项目外，将基于现有线站装置继续发展相关实验方法及各种原位设备，以满足相关领域用户的需求。还将在高分辨粉末衍射、新型太阳能电池研究、多铁材料构效关系、石墨烯负载二维材料以及锂/钠电池电极材料等方面继续进行深入研究。

参考文献

1. Wang Z K, Li M, Gao X Y, *et al.* High efficiency Pb–In binary metal perovskite solar cells[J]. Advanced Materials, 2016, **28**: 6695–6703.
2. Zhu D M, Gao H, Li X L, *et al.* Real-time observation of graphene layer growth: Coupling of the interlayer spacing with thickness[J]. Carbon, 2015, **94**: 775-780.
3. Yang Y G, Feng S L, Gao X Y, *et al.* Optical absorption,

and performance of organic solar cells improved by gold nanoparticles in buffer layers[J]. ACS Applied Materials & Interfaces, 2015, **7**: 24430-24437.

4. Feng S L, Yang Y G, Gao X Y, *et al.* High-performance perovskite solar cells engineered by an ammonia modified graphene oxide interfacial layer[J]. ACS Applied Materials & Interfaces, 2016, **8**: 14503-14512.
5. Yuan Z C, Yang Y G, Gao X Y, *et al.* Approximately 800-nm-thick pinhole-free perovskite films via facile solvent retarding process for efficient planar solar cells[J]. ACS Applied Materials & Interfaces, 2016, **8**: 34446−34454.
6. Zhao B, Ji G W, Gao X Y, *et al.* Transfer printing of magnetic structures with enhanced performance using a new type of water-soluble sacrificial layer[J]. RSC Advances, 2015, **5**(70) 56959-56966.
7. Lin J C, Tong P, Lin H, *et al.* Giant negative thermal expansion covering room temperature in nanocrystalline GaNxMn3[J]. Applied Physics Letter, 2015, **107**(13) 131902.
8. Gao M, Gu Y L, Wen W, *et al.* Facile usage of a MYTHEN 1K with a Huber 5021 diffractometer and angular calibration in operando experiments[J]. Journal of Applied Crystallography, 2016, **49**: 1182–1189.
9. Li L, Ungar T, Toth L S, *et al.* Shear-coupled grain growth and texture development in a nanocrystalline Ni-Fe alloy during cold rolling[J]. Metallurgical and Materials Transactions, 2016, 47A(12) 6632-6644.
10. Li H, Yang Y G, Song F, *et al.* Performance improvement of $ch_3nh_3pbi_3$ perovskite solar cell by CH_3SH Doping[J]. Nanomater and Nanotechnol, 2016, **6**: 24.
11. 季庚午, 张晓楠, 杨迎国,等. 前驱体混合比例对$CH_3NH_3PbI_3$ 钙钛矿薄膜微观结构及光伏器件性能的影响[J]. 核技术, 2016, **39**(12) 120101.
12. 刘华秋, 朱大明, 刘 星,等. 衬底温度对蒸汽辅助沉积法制备钙钛矿薄膜微观结构的影响[J]. 核技术, 2016, **39**(6) 060104.
13. 柳义,王连文. 小角 X 光散射绝对强度的两种测试方法[J]. 光散射学报. 2015, **27**(1) 59-63.
14. Jiang W L, Ying J F, Yang T Y, *et al.* A new layered nano hybrid perovskite film with enhanced resistance to moisture-induced degradation[J]. Chemical Physics Letters, 2016, **658**: 71-75.
15. Jiang W L, Yang T Y, Gao X Y, *et al.* Enhanced stability of $CH_3NH_3PbI_3$ thin films deposited on FTZO[J]. Chemistry Letters, 2016, **45**(7): 819-821.
16. Liu Y, Wang L W. Preparation and characterization of p-type transparent conducting SnO thin films[J]. Materials Letters, 2015, **139**: 39-41.
17. Jiang W L, Ying J F, Yang T Y, *et al.* Introduction of the X-ray diffraction beamline of SSRF[J]. Nuclear Science and Techniques, 2015, **26**(2): 020101.
18. Jiang W L, Yang T Y, Gao X Y, *et al.* Facile preparation of nitrogen-doped graphene sponge as a highly efficient oil absorption material[J]. Materials Letters, 2016, **178**: 95-99.
19. Yang T Y, *et al.* Synthesis of Tb_4O_7 complexed with reduced graphene oxide for Rhodamine-B absorption[J]. Materials Research Bulletin, 2016, **77**: 111-114.

Research Development of X-ray Diffraction Group

X-ray Diffraction Group

X-ray diffraction (XRD) group is mainly in charge of operation and user support at X-ray diffraction beamline. During 2015–2016, this beamline provided 11 084.5 h beam time with a fault rate of only 0.4%. There were 8964 hours allocated for 956 users from 306 proposals, whose research fields covered material science, chemistry, condensed matter physics, macromolecule science, environmental and geological sciences. 169 papers including 70 premium ones were published by users during this period. The completed beamline maintenance work included: the monochromator first crystal replacement, pitch motor drive module replacement, controller and z axis control module replacement, Mythen1K detector power adapter replacement, CCD gas system cleaning. In 2015 winter, the cylindrical pre-collimating mirror was replaced by a toroidal mirror. In 2016 summer, the CCD detector was shipped back for factory maintenance and solved the high and uneven background noise.

Besides the routine beamline maintenance and user technical support, XRD group took charge of designing two new beamlines (white beam Laue diffraction and surface diffraction), the engineering material endstation, and the sample preparation laboratory for material science in the second phase beamline project. In 2015–2016 the corresponding feasibility reports and then the preliminary design reports were finished and successfully reviewed. The second phase beamline project construction started in Nov. 2016.

In order to meet users demands from different research disciplines, XRD group was dedicated to X ray diffraction methodology developments and their applications with 19 papers published[1-19] (including 16 SCI-cited) and 5 authorized patents. Regarding the methodology and instrumentation developments, the carried-out research work included total reflection fluorescence, single crystal diffraction, XRD using fluorescence signal, *in-situ* metal welding, anomalous scattering, Mythen1k linear detector application, the upgrade of the supporting and motion-control system for two-dimensional area detector, a set of high vacuum /high-temperature *in-situ* heating system. Regarding the applied research, some achievements were obtained in many fields, such as structural research of *in-situ* CVD graphene growth mechanism[2], gold nanoparticle enhanced organic solar cells[3], transferring printed magnetic microstructures with enhanced performance by using water soluble sacrificial layer[6], studying the giant negative expansion effect of GaN_xMn_3 nanocrystal[7], improving the SnO film P type conductive properties by Na ion implantation, fast coordination correction of Mythen1K linear detector[8], synchrotron-based research of cold rolled nanocrystal NiFe alloy[9] and high performance perovskite solar cells[1].

The on-going projects were as following: 1) Hundred-Talent Program (Chinese Academy of Sciences); 2) National Science Foundation for Young Scientists of China: “Synchrotron radiation in situ structure-activity relationship studies of doping $BiFeO_3$ lithium ion battery electrode materials”, “The synchrotron radiation in situ research platform of the associated system and its application in electronic ferroelectric materials; 3) Joint Funds of the National Science Foundation of China: Construction of test platform for the real-time characterization of the microstructural changes of conjugated polymer films using synchrotron radiation two dimensional grazing incidence X-ray diffraction; 4) The State Key program of the National Science Foundation of China: Study of the microstructure and the physical properties of some perovskite oxide multilayer membrane interfaces using synchrotron radiation.

The group also has 10 new grants approved. 1) National Science Foundation of China: “Real Time Characterization of Perovskite Type Solar Cells during Vacuum Synthesis” and “The study on the decay mechanism of the of $LaNi_{1-x}M_x$ alloys based on synchrotron radiation and positron annihilation technology”; 2) Shanghai Large Scale Scientific Facility Center Research Project: “Synchrotron Based Characterization on Materials Structure and Transporting Properties”; 3) National Science Foundation for Young Scientists of China: “Study micro mechanical behavior of nanostructures Cu/Ag multilayer membrane using in situ synchrotron radiation diffraction”, “Study of the microstructure of perovskite solar cell using synchrotron radiation”, and “The establishment of the synchrotron radiation huang diffuse scattering platform and its application in the research of the internal point defect of p type SnO_2 films”; 4) Science and Technology Commission of Shanghai Municipality: “Basic research on the application of synchrotron radiation and material genomics”; 5) Youth Innovation Promotion Association (Chinese Academy of Sciences); 6) National Key Research and Development Program of China; 7) Joint Funds of the National Science Foundation of China: “Synchrotron Based Research on the Structure-Properties Relationship of Perovskite Solar Cells”.

In 2017–2018, besides the beamline operation, user experimental support, the construction of new beamline and materials sample preparation laboratory for material science, as well as the above research projects, XRD group will continue to develop automatic sample changer robot arm for the high resolution powder diffraction system, commission its matching detector’s software/hardware debugging, as well as develop other experimental methods and new *in-situ* equipment to meet user demands. In-house research will focus on high resolution X-ray powder diffraction, novel solar cells, multi-ferroic materials, two dimensional graphene supported materials, and lithium/sodium battery electrode materials.

Reference

1. Wang Z K, Li M, Gao X Y, *et al.* High efficiency Pb–In binary metal perovskite solar cells[J]. Advanced Materials, 2016, 2**8**: 6695–6703.
2. Zhu D M, Gao H, Li X L, *et al.* Real-time observation of graphene layer growth: Coupling of the interlayer spacing with

thickness[J]. Carbon, 2015, **94**: 775-780.

3. Yang Y G, Feng S L, Gao X Y, *et al.* Optical absorption, and performance of organic solar cells improved by gold nanoparticles in buffer layers[J]. ACS Applied Materials & Interfaces, 2015, **7**: 24430-24437.
4. Feng S L, Yang Y G, Gao X Y, *et al.* High-performance perovskite solar cells engineered by an ammonia modified graphene oxide interfacial layer[J]. ACS Applied Materials & Interfaces, 2016, **8**: 14503-14512.
5. Yuan Z C, Yang Y G, Gao X Y, *et al.* Approximately 800-nm-thick pinhole-free perovskite films via facile solvent retarding process for efficient planar solar cells[J]. ACS Applied Materials & Interfaces, 2016, **8**: 34446−34454.
6. Zhao B, Ji G W, Gao X Y, *et al.* Transfer printing of magnetic structures with enhanced performance using a new type of water-soluble sacrificial layer[J]. RSC Advances, 2015, **5**(70) 56959-56966.
7. Lin J C, Tong P, Lin H, *et al.* Giant negative thermal expansion covering room temperature in nanocrystalline GaNxMn3[J]. Applied Physics Letter, 2015, **107**(13) 131902.
8. Gao M, Gu Y L, Wen W, *et al.* Facile usage of a MYTHEN 1K with a Huber 5021 diffractometer and angular calibration in operando experiments[J]. Journal of Applied Crystallography, 2016, **49**: 1182–1189.
9. Li L, Ungar T, Toth L S, *et al.* Shear-coupled grain growth and texture development in a nanocrystalline Ni-Fe alloy during cold rolling[J]. Metallurgical and Materials Transactions A-Physical Metallurgy and Materials Science, 2016, 47A(12) 6632-6644.
10. Li H, Yang Y G, Song F, *et al.* Performance Improvement of $CH_3NH_3PbI_3$ Perovskite Solar Cell by CH_3SH Doping[J]. Nanomater and Nanotechnol, 2016, **6**: 24.
11. Ji Gengwu, Zhang Xiaonan, Yang Yingguo, *et al*. Influences of precursor ratio on microstructure of perovskite $CH_3NH_3PbI_3$ film and photoelectric conversion properties of perovskite solar cell[J]. Nuclear Techniques, 2016, **39**(12) 120101
12. Liu Huaqiu, Zhu Daming, Liu Xing, *et al.* Influences of substrate temperature on the structure of the perovskite films prepared using a vapor-assisted solution process[J]. Nuclear Techniques, 2016, **39**(6): 060104.
13. Liu Yi, Wang Lianwen. Determination of absolute intensity by two ways in small angle x-ray scattering[J]. Chinese Journal of Light Scattering, 2015, **27**(1) 59-63.
14. Jiang W L, Ying J F, Yang T Y, *et al.* A new layered nano hybrid perovskite film with enhanced resistance to moisture-induced degradation[J]. Chemical Physics Letters, 2016, **658**: 71-75.
15. Jiang W L, Yang T Y, Gao X Y, *et al.* Enhanced stability of $CH_3NH_3PbI_3$ thin films deposited on FTZO[J]. Chemistry Letters, 2016, **45**(7): 819-821.
16. Liu Y, Wang L W. Preparation and characterization of p-type transparent conducting SnO thin films[J]. Materials Letters, 2015, **139**: 39-41.
17. Jiang W L, Ying J F, Yang T Y, *et al.* Introduction of the X-ray diffraction beamline of SSRF[J]. Nuclear Science and Techniques. 2015, **26**(2): 020101.
18. Jiang W L, Yang T Y, Gao X Y, *et al.* Facile preparation of nitrogen-doped graphene sponge as a highly efficient oil absorption material[J]. Materials Letters, 2016, **178**: 95-99.
19. Yang T Y, *et al.* Synthesis of Tb_4O_7 complexed with reduced graphene oxide for Rhodamine-B absorption[J]. Materials Research Bulletin, 2016, **77**: 111-114.

硬 X 射线谱学组研究进展

硬 X 射线谱学组

硬 X 射线谱学组主要承担上海光源首批线站“X 射线吸收精细结构光束线站(BL14W1)”的运行维护与用户实验支持工作。该线站在 2015–2016 年度高效运行，共为用户提供机时约 8 517 h，束线研究机时约 2 558 h，束线故障率仅 0.24%。共完成了 335 个研究课题，用户发表文章 293 篇，其中 SCI-I 区文章 135 篇，占文章总数的 46%。用户研究涵盖化学、材料、物理学、环境地质等众多学科领域。

2013–2014 年度，BL14W1 线站在原有基础上，积极开展新实验技术和方法的研究，丰富了 XAFS 实验条件，拓展了研究范围，主要进展如下。

BL14W1 在原有单晶体高分辨发射谱方法基础上，搭建了一套基于竖直 Rowland 圆结构的三晶体高分辨谱仪装置，在能量分辨率、荧光计数率以及信噪比等方面达到了较好的水平。目前已经利用该装置对 3 d 过渡金属的 $K\beta_{1,3}$ 发射谱进行了测试，在 Mn-K_β 的能量分辨率小于 1 eV，光子计数率可达到 2×10^5 以上，完成了 2015 年度束线研究计划的预定目标。高分辨方法的建立，是对常规 XAFS 方法的有力补充，能够在电子自旋态、分子轨道、配体种类分辨等电子结构研究上发挥重要作用。继而在这套高能量分辨谱仪装置基础上，通过编写相应的控制程序，实现了单色器能量和高分辨谱仪能量的联动扫描，从而发展了共振 X 射线发射谱实验方法[1]。

在 BL14W1 毛细管透镜聚焦的基础上，进一步发展了共聚焦的实验方法。毛细管的传输效率可达 20%以上，样品处聚焦光斑为 40×40 μm^2@8 keV，完成了 2015 年度束线研究计划的预定目标。利用共聚焦实验装置，通过对样品的三维扫描，可以实现三维元素空间分布分析。以乾隆时期斗彩陶瓷中铁元素在不同深度位置的研究为例，可以看出毛细管透镜共聚焦是一种有效的深度分辨的结构分析方法[2]。

BL14W1 线站搭建了一套新的 QXAFS 系统。在该系统中，ADC 数据采集卡与 Scaler 计数卡均工作于 1MHz 的外部触发模式下。整个 QXAFS 谱的采集时间约为 8 s。对铜箔的 K 边吸收谱进行 QXAFS 测试，并与常规的 XAFS 谱进行对比，结果表明：QXAFS 与常规 XAFS 得到的数据基本一致，k 空间和 R 空间的比较证明 QXAFS 结果具有良好的信噪比。多次重复测试，谱型完全重合，表明单色器在连续采谱过程中，具有较好的能量重复性。

为了解决溶液体系 XAFS 实验中极易出现的样品辐射损伤和热损伤问题，以及低浓度溶液样品普遍存在的 EXAFS 数据质量较差等问题，在 BL14W1 线站搭建了一套适用于溶液样品的低温 XAFS 实验平台。该装置利用 99.99%的高纯氦气作为介质，对样品进行降温，具有不破坏样品结构、超低震动、高真空、降温速度快、温度稳定性好等特点。可以一次性放入多个样品，大大提高了实验效率。对铀酰配合物进行测试，表明在低温环境下样品的辐射损伤情况得到了明显的抑制，并且实验信噪比要远远优于常温下的测试结果。

参考文献

1. Duan Peiquan, Bao Hongliang, Li Jiong, *et al.* In-situ high-energy-resolution X-ray absorption spectroscopyfor UO_2 oxidation at SSRF[J]. Nuclear Science and Techniques, 2017, **28**(1):2.
2. ZI Ming, WEI Xiangjun, YU Haisheng, *et al.*,Stratified structure in ancient paints studied by synchrotron confocal micro-X-ray method[J], Nuclear Techniques, 2015, **38**(6): 060101.

Research Development of XAFS Group

XAFS Group

XAFS group is mainly in charge of operation and user support of X-ray Absorption Fine Structure Spectroscopy beamline (BL14W1). During 2015–2016, this beamline has supported beam time of 8 517 h for users and 2 558 h for in-house research. Users from all over the country have finished 335 proposals, whose research fields covering chemistry, material science, physics, environmental science and son on. 293 papers have been published by users during this 2 years, 135 in which were published on SCI-I journals.

A series of work has been carried out at BL14W1 to provide the optimal experimental conditions for users.

Based on the high-energy-resolution fluorescence spectrometer on the BL14W1 beamline, an in-situ high- energyresolution X-ray absorption spectroscopy technique, with an in-situ heating cell, was developed. The high-energyresolution fluorescence detection for X-ray absorption near-edge spectroscopy (HERFD-XANES) was tested in a UO_2 oxidation experiment to measure the U L_3-edge, with higher signal-to-noise ratio and higher-energy-resolution than conventional XANES. The technique has potential application for in-situ study of uranium-based materials.

On the basis of polycapillary lens-based focusing technique at BL14W1, we have developing the confocal micro-X-ray method, which is a sensitive tool for analysis of three dimensional (3D) elemental composition and chemical species, and has many important applications in the research fields such as geology, archaeology, environment, biology and materials sciences. This system has been applied to study the stratified structure of some kind of paints in the Forbidden City[2].

Time-resolved technique plays an important role on the investigations of dynamic structural changes of measured samples during the physical and chemical reactions. To meet users' demand, quick-scanning XAFS (QXAFS) method, based on the EPICS and LabVIEW systems, has been developed at BL14W1. Analog-to-digital converter and double-crystal monochromator setups have been applied to optimize the QXAFS experimental parameters. A good QXAFS spectrum with an energy range of 1.2 keV at the Cu K-edge has been collected in 2 s with stable beam position. The obtained data quality is comparable to those collected under the step mode

In order to solve the sample radiation damage and thermal damage prone solution system in the XAFS experiment, common problems and low concentration sample EXAFS data quality is poor, the BL14W1 line station to build a set of suitable solution sample low temperature XAFS experiment platform. The device uses 99.99% high pure helium as the medium. The samples were cooled, with no damage to the sample structure, low vibration, high vacuum, cooling speed, temperature stability. It can be put into multiple samples at one time, which greatly improves the experimental efficiency. The test of uranyl complex shows that the radiation damage of samples is suppressed obviously under low temperature, and the signal-to-noise ratio of experiment is much better than that of normal temperature.

Our group are responsible for 22 ongoing projects, and take on funds of 13.27 million yuan.

Reference

1. Duan Peiquan, Bao Hongliang, Li Jiong, *et al.* In-situ high-energy-resolution X-ray absorption spectroscopyfor UO_2 oxidation at SSRF[J]. Nuclear Science and Techniques, 2017, **28**(1): 2.
2. ZI Ming, WEI Xiangjun, YU Haisheng, *et al.*,Stratified structure in ancient paints studied by synchrotron confocal micro-X-ray method[J], Nuclear Techniques, 2015, **38**(6): 060101.

X 射线小角散射组研究进展

X 射线小角散射组

1 BL16B1 线站开放运行及用户工作

2015−2016 年度，BL16B1 线站共为用户提供机时约 8 862h，束线研究机时约 2 032 h。共完成 258 个研究课题，用户发表文章 237 篇，其中 SCI 一区文章 69 篇，占文章总数的 29%。

2 实验技术和方法学发展

2015−2016 年，BL16B1 线站在原来改造的基础上，开展新实验技术和方法学研究。发展了微聚焦 SAXS、时间分辨原位 SAXS/WAXS、Bonse-Hart 超小角散射、GIWAXS 等多项方法学研究；完成了滑动轨道样品台改造并正式对用户进行了开放；开展了光束线稳定性观测研究等工作；自主研制了 GISAXS 气氛保护加热样品台等小型在线实验设备，改进升级了线站控制系统。

2.1 微聚焦 SAXS 技术

基于 KB 镜聚焦系统在 BL16B1 线站发展了微聚焦 SAXS 实验方法学（图 1），在 10keV 的入射光波长下得到了 19.9 μm×13.5 μm 的聚焦光斑，通量为 1.5×10^{10} phs/s；基于 BL19U2 光束线站调试 KB 聚焦镜系统，在 12 keV 的入射光波长下得到了 10 μm×4 μm 的聚焦光斑，通量为 5.0×10^{10} phs/s。相关方法学研究工作已发表在 Chinese Physics C [1]。

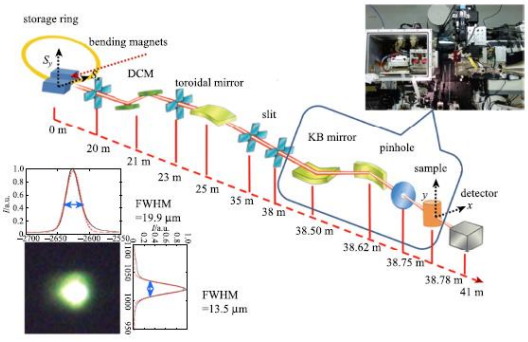

图 1 基于 BL16B1 线站的微聚焦 SAXS 技术

2.2 GIWAXS 实验方法学

同步辐射掠入射 X 射线散射技术是研究有机/无机薄膜材料微观结构的重要方法。2015−2016 年度线站一直致力于掠入射散射技术的方法学研究和发展，设计制作了 GIWAXS 专用 Beamstop、Pinhole 挡板和样品控制台（图 2）；在线站现有设备空间条件下，调试完成了 GIWAXS 实验方法学。近一年来，用户利用这一实验方法学，发表了 9 篇一区和 4 篇二区的相关文章。

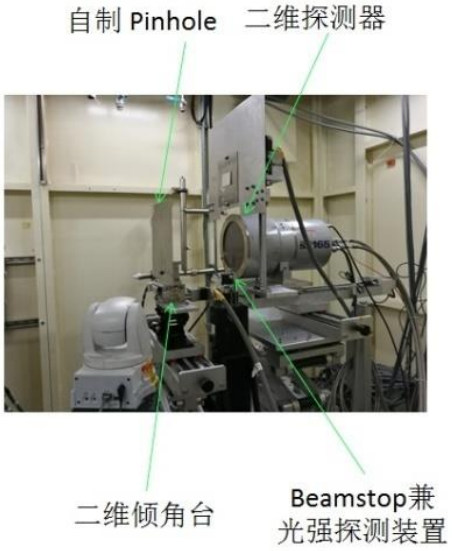

图 2 基于 BL16B1 线站的 GIWAXS 技术

3 光束线稳定性观测研究

光斑稳定性对于线站调试和实验（尤其是原位实验）用光至关重要。2015−2016 年度在 BL16B1 实验站持续测试了光束垂直方向稳定性。测试平台包括扫描光斑形状和大小的 Kohzu 二维运动平台、IC-500-50 两象限电离室和用于观察光斑形状的 Navitar 摄像头组件。测试结果表明，BL16B1 实验站在在正常实验情况下（垂直光斑尺寸 439 μm），垂直方向光束位置稳定在 5%内，满足正常实验需求。

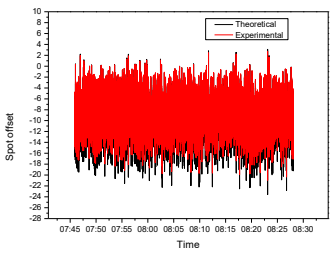

图 3 光斑垂直方向偏移量的理论和实验值

4 科研工作

2015−2016 年度散射组成员积极利用束研机时在在半导体量子点材料、纤维微观结构与性能关系、高效聚合物电池材料等领域开展了相关的 In-house 研究[2-6]，取得了一系列富有特色的研究成果，共发表 SCI 文章 22 篇。

参考文献

1. Hua Wenqiang, Wang yuzhu, Zhou Ping, *et al*. Micro-focus small-angle X-ray scattering at SSRF BL16B1[J]. Chinese Physics C , 2017, **41**(4): 048001.
2. Li Xiaoyun Li, Tian Feng, Gao Xueping, *et al*. Tuning the mechanical properties of cellulose nanofibrils reinforced polyvinyl alcohol composites via altering the cellulose polymorphs[J]. RSC Advances, 2016, **6**: 83356- 83365.
3. Li Xiaoyun, Tian Feng, Tang Zhongfeng, *et al*. In situ synchrotron small-and wide-angle X-ray study on the structural evolution of Kevlar fiber under uniaxial stretching[J], RSC Advances, 2016, **6**: 81552.
4. Li Xiaoyun, Tian Feng, Zhou Ping, *et al*. A hierarchical and gradient structured supersorbent comprising three-dimensional interconnected porous fibers for efficient oil spillage cleanup[J]. Journal of Materials Chemistry A, 2016, (4): 9635-9643.
5. Zhao Yueyue，Miao Xiaran，Lin Jinyou, *et al*. Cellulose nanofibrils extracted from the byproduct of cotton plant, Carbohydrate Polymers, 2016, (136): 841- 850.
6. Miao Xiaran, Lin Jinyou, Tian Feng, *et al*. Probing the surface microstructure of layer-by-layer self- assemblychitosan/poly (L-glutamic acid) multilayers: A grazing-incidencesmall-angle X-ray scattering study[J]. Materials Science and Engineering C, 2016, **58**(352).

Progresses in Research of X-ray Scattering Group

Department of Materials and Energy, X-ray scattering Group

1 Operation status and user results of BL16B1 beamline

In the two years of 2015 and 2016, BL16B1 provided about 8 862 h user beamtime，and about 2 032 h for beamline study. At the beamline, 258 user subjects have been finished in 2015 and 2016; the users have published 237 papers (SCI indexed) based on the research results of the beamline, in which 69 papers published on top 5% Journals.

2 Beamline upgrading and Developing in Experimental techniques and methodologies

In 2015−2016, some new experimental techniques and methodologies have been developed, containing microbeam SAXS, time-resolved SAXS/ WAXS, ultra-SAXS based on Bonse-Hart system， GIWAXS, etc. In addition, study on the beamline stability has been developed.

2.1 Microbeam SAXS

Based on KB focusing mirror system, microbeam SAXS technique has been developed at BL16B1; at the energy of 10 keV, the microbeam spot size is 19.9 μm×13.5 μm and the flux is 1.5×10^{10} phs/s. The technique was also developed at BL19U2; At the energy of 12 keV, the microbeam spot size is 10 μm×4 μm, and the flux is 5.0×10^{10} phs/s。The work has been published on Chinese Physics C [1]。

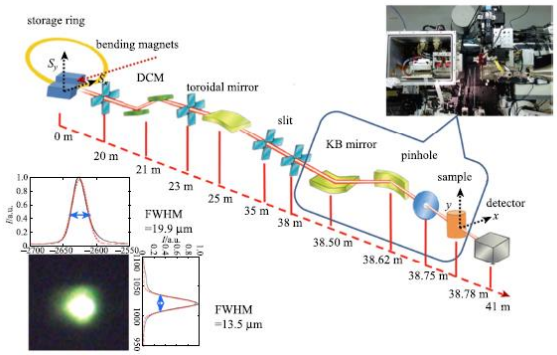

Fig.1 Microfocus technique at BL16B1

2.2 WAXS technique

In 2015−2016, the scattering group was dedicated to develop GIWAXS technique. GIWAXS Beamstop, pinhole baffle and sample console were shown (Fig.2); at the endstation existing space conditions, Commissioning GIWAXS technique. By GIWAXS，the users have published 13 papers, in which 9 papers published on top 5% Journals.

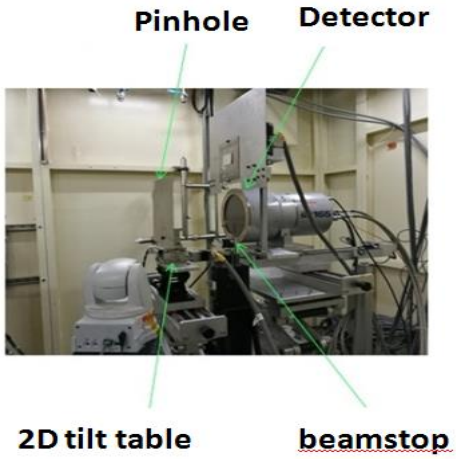

Fig.2 GIWAXS technique at BL16B1

3 Study on the beamline stability

Beam stability is very important for user experiments, especially for *in-situ* experiments. From 2015 to 2016, the vertical beam stability has been insistently tested at BL16B1. The measurement results showed that, at the normal experimental conditions (the vertical spot beamsize is 439 μm), the beam position stability can be controlled within 5%（Fig.3），which meets the requirements of the user experiments.

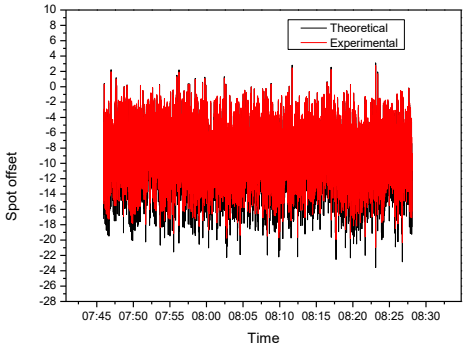

Fig. 3 The vertical beam position stability measurement of at BL16B1

4 Research activities

In the two years of 2015 and 2016, In-house study has been developed at BL16B1 in the field of high-perfomance fibers, semiconductor quantum dots and high efficiency polymer batteries[2-6]. The X-ray scattering group has published 22 papers (SCI indexed) in the two years.

Reference

1. Microfocus small-angle X-ray scattering at SSRF BL16B1, Chinese Physics C, 2017, **41**(4): 048001.
2. Tuning the mechanical properties of cellulose nanofibrils reinforced polyvinyl alcohol composites via altering the cellulose polymorphs, RSC Advances, 2016, **6**: 83356- 83365.
3. In situ synchrotron small-and wide-angle X-ray study on the structural evolution of Kevlar fiber under uniaxial stretching, RSC Advances., 2016, **6**: 81552.
4. A hierarchical and gradient structured supersorbent comprising three-dimensional interconnected porous fibers for efficient oil spillage cleanup, Journal of Materials Chemistry A, 2016, (4): 9635-9643.
5. Cellulose nanofibrils extracted from the byproduct of cotton plant, Carbohydrate Polymers, 2016, (136): 841- 850.
6. Probing the surface microstructure of layer-by-layer self-assemblychitosan/poly (L-glutamic acid) multilayers: A grazing-incidencesmall-angle X-ray scattering study, Materials Science and Engineering C, 2016, **58**(352).

时间分辨组 2015-2016 年进展报告

时间分辨组

时间分辨专业组的研究方向是基于同步辐射技术的时间分辨 X 射线谱学实验方法，2015−2016 年度的主要研究内容围绕上海光源线站工程建设展开，并集中在硬 X 射线通用谱学线站和动力学线研究站(Dynamics-Line，简称 D-Line)。

硬 X 射线通用谱学线站的建设目的是满足日益增加的硬 X 射线吸收精细结构谱学(XAFS)用户的科学需求，并配备在亚秒(0.1 s)量级的快扫 XAFS 功能。2015−2016 年度已完成了可行性研究报告和初步设计报告的评审工作，重点解决了关键光学设备——单色器的物理参数要求的确定和物理设计等问题，冻结了主要设备的技术参数。作为二期中首个出光的线站（2018 年底通光、2019 年开始试运行），从 2016 年 11 月光束线正式开工建设以来，先后完成了 4 元硅漂移探测器、双平晶单色器、快扫单色器、36 元锗探测器及电子学系统、镜子及压弯机构等设备的采购工作。

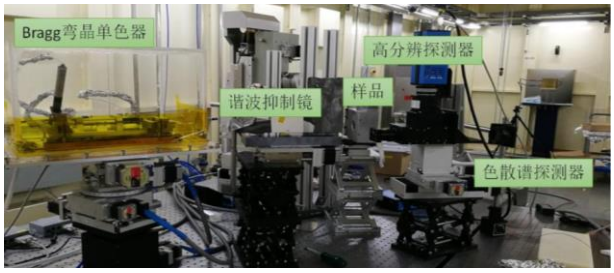

图 1　色散弯晶单色器测试验收现场

D-Line 的总体目标是建设一条基于波荡器光源的能量色散 X 射线吸收谱线站(ED-XAS)和一条基于弯铁边缘辐射的红外光谱光束线站(IR)，并将两束光耦合在同一样品点，实现动态过程分子结构、原子结构及电子结构的同步采集。总体布局方案为两线三站，其中时间分辨组负责组合站以及硬 X 射线站的建设任务。2015 年，完成了线站设计方案的国内和国际两次评审，根据评审意见优化了线站设计方案；启动了色散弯晶单色器以及红外-X 射线耦合系统两项关键技术的预研。2016 年，完成了线站可行性研究报告及初步设计的评审，冻结了初步设计参数；色散弯晶单色器以及红外-X 射线耦合系统两项关键技术预研进展顺利，其中色散弯晶单色器已完成离线测试验收，红外-X 射线耦合系统完成了完成了工程设计评审，正在加工制造。作为首批启动建设的光束先站之一，D-Line 将于 2019 年底完成实验站通光，2020 年开始试运行。

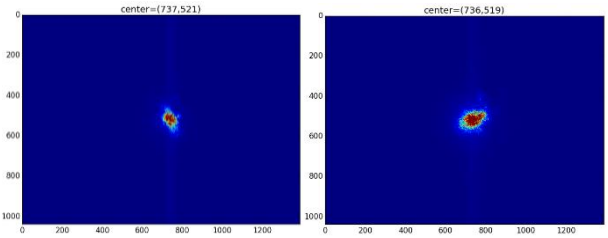

图 2　耦合系统测试结果（左：模拟 X 光斑；右：模拟红外光斑）

时间分辨组承担了化学与环境实验室的工程任务，并于 2015 年完成国内专家评审，2016 年底开始建设。另外，时间分辨组参与了中能谱学线站的建设，该光束线站于 2015 年完成了国内和国际评审。

在运行维护方面，时间分辨组还参与了 BL14W1 线站的日常值班与用户实验支持工作。2015−2016 年度完成了基于 EPICS 的 XAFS 实验方法控制系统编程测试，以及针对关键实验设备——32 元高纯锗荧光探测器的 XIA 电子学系统测试模式的研发，并完成了 7 元高纯锗荧光探测器在线调试与程序编写。

在 in-house 研究方面，时间分辨组依托上海光源 XAFS 线站，与国内催化等领域用户深入开展合作研究，2015−2016 年度共计发表了通讯作者 SCI 论文 16 篇，其中一区 5 篇[1−5]，包括 Nature Communications (1 篇)、ACS Catalysis (3 篇)、Nanoscale (1 篇)等国际著名期刊。

参考文献

1. Guo L W, Du P P, Si R, *et al*. Nat Commun, 2016, 7: 13481.
2. Yang Q, Wang X, Si R, *et al*. ACS Catal, 2016, **6**: 3072-3082.
3. Ke J, Si R, *et al*. ACS Catal, 2015, **5**: 5164-5173.
4. Wang W W, Du P P, Si R, *et al*. ACS Catal, 2015, **5**: 2088-2099.
5. Guo Y, Du P P, Si R, *et al*. Nanoscale, 2015, **7**: 4920-4928.

Progress Report of Time-Resolved Technique Group (2015-2016)

Time-Resolved Technique Group

The research motivation of time-resolved technique group is to develop synchrotron X-ray time-resolved techniques, and its main task during 2015-2016 is to construct related beamlines for the SSRF phase-II project, particularly Hard X-ray Spectroscopy Beamline and Dynamic-Line (D-Line).

The construction purpose of Hard X-ray Spectroscopy Beamline is to meet the requirement from increased number of users on the demand of beamtime for X-ray absorption fine structure (XAFS). In 2015-2016, we have completed the review of the feasibility study report and the preliminary design report, of which the focus is on the determination of the physical parameters and the design of the monochromators. Then, all the technical parameters of key instruments have been frozen. As the first completed beamlines in Phase II project (end of installation in 2018 and start of commissioning in 2019), since the start of construction in Nov. 2016, we have successively completed the ordering of key instruments, including 4-element silicon drift detector, double-crystal and channel-cut monochromators, 36-element germanium detector and electronic system, as well as the mirrors and bending mechanism.

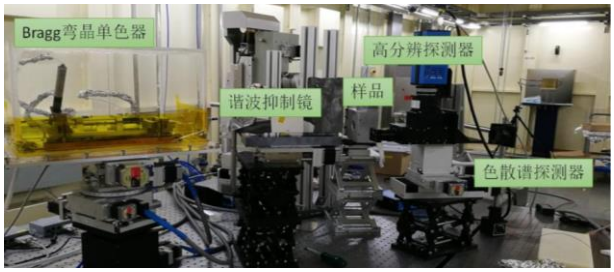

Fig.1 Picture of tests and adjustment on polychromator

The major goal of D-Line is to construct a beamline combining time-resolved energy-dispersive X-ray absorption spectroscopy (XAS), on the basis of on undulator source and synchrotron radiation IR based on edge radiation from bending magnet together, in order to capture the rapid evolution of non-equilibrium structures during dynamic process by detecting the atomic and molecular structure at the same sample point. D-Line is designed as two beamlines with three end-stations, of which we are in charge of construction tasks on combined station and hard X-ray station. International and domestic beamline design meetings were held in March and April 2015, respectively. Beamline design was upgraded according to the comments on the review report. Pre-research of the two critical techniques of the beamline, polychromator and the coupling system of IR and X-ray, started in early 2015. The feasibility research report and the primary design report were reviewed in 2016. The primary design and budget were approved by the government in October 2016. Beamline construction started formally in November 20th 2016. Two pre-research projects were going smoothly. For the pre-research of polychromator, off-line tests and adjustment had been finished (Fig.1); for the coupling system of IR and X-ray, final design had been completed and had gone into the manufacture period. As one of the 1st run beamlines starting the construction, D-Line will complete the installation in the end of 2019, and will be commissioned in 2020.

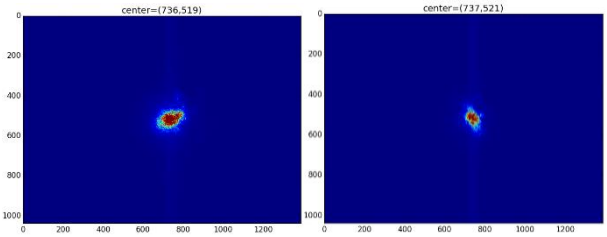

Fig.2 Images of testing results on coupling system (left: mimic X-ray spot; right: mimic IR spot)

The time-resolved technique group has another task for Phase II project, chemical and environmental laboratory, which has completed domestic design meeting in 2015 and started construction in 2016. Meanwhile, we participated in the construction of Medium Spectroscopy Beamline, of which the international review has been completed in 2015.

The time-resolved technique group also participated in the routinely on-duty and user support for beamline BL14W1. We completed the following work during 2015-2016: development of a software controlled system (EPICS) for XAFS measurements; research on 32-element high purity germanium solid fluorescence detector and completed the XIA electronics system testing mode; Realization of online debugging and programming on 7-element high purity germanium solid fluorescence detector.

For in-house research, the time-resolved technique group carried out collaborated work with domestic catalysis groups on the basis of XAFS beamline at SSRF. Totally 16 SCI papers of co-corresponding author were published during 2015-2016, of which 5 papers are first rank in CAS system,[1–5] including Nature Communications (1), ACS Catalysis (3) and Nanoscale (1).

Reference

1. Guo L W, Du P P, Si R, *et al*. Nat Commun, 2016, 7: 13481.
2. Yang Q, Wang X, Si R, *et al.* ACS Catal, 2016, **6**: 3072-3082.
3. Ke J, Si R, *et al.* ACS Catal, 2015, **5**: 5164-5173.
4. Wang W W, Du P P, Si R, *et al.* ACS Catal, 2015, **5**: 2088-2099.
5. Guo Y, Du P P, Si R, *et al*. Nanoscale, 2015, **7**: 4920-4928.

硬 X 射线微聚焦组研究进展

硬 X 射线微聚焦组

硬 X 射线微聚焦组主要承担上海光源首批线站“硬 X 射线微聚焦及应用光束线站”的运行维护与用户实验支持工作。该线站在 2015−2016 年度高效低故障率运行，总供光机时 11 100.5 h，总故障率为 0.22%。累计提供用户机时 8 817 h，执行用户课题近 300 个，用户研究涵盖环境与地球科学、材料科学、生命科学、地质学、考古学、凝聚态物理众多学科领域，共发表用户成果 155 篇，其中一区文章 32 篇，发表在如 Nature、PNAS、Advance Materials、J. Am. Chem. Soc.、Biomaterials 等知名期刊。线站维护方面：更换光束线末端真空 Be 窗、更换 KB 镜片、维修棚屋空调、Zoneplate 运动控制器加装光栅尺、单色器维护等。升级方面：在微聚焦光学平台之前，开发出和现有设备匹配的高分辨单色器，用于硬 X 射线非弹性散射实验。

新线站建设方面，2015−2016 年度本组负责完成了上海光源线站二期工程“硬 X 射线纳米探针线站和超硬多功能线站”的项建书、可研报告国内国际评审、完成了线站的初步设计；并在现有的微聚焦实验站进行了预研工作，开展了低温条下多层膜单色器材料应变和稳定性研究[1]，波前特性的表征技术以及纳米聚焦装置控制系统的研究；超硬多功能线启动了高能劳厄单色器和液氮冷却子午压弯劳厄单色器的预研，完成了弧矢压弯劳厄单色器的初步设计，并开始设计加工压弯原型机。

为满足不同学科领域用户研究的需求，本组在 X 射线微纳聚焦方法学研究及相关应用研究方面进行了不断的研究和探索，发展了超高灵敏全反射 X 射线荧光技术。在应用研究方面开展了燃料电池催化氧还原反应机理研究[2]、合金损伤机理研究[3,4]、相变存储薄膜材料的结构研究[5]、材料内部残余应力测试实验方法的研究、基于 X 射线散射技术的原子分子动力学研究[6−8]，以及金属有机骨架和稀土氧化物的高压行为的研究，以上 in-house 研究共发表文章 19 篇，申请专利 13 项。

硬 X 射线微聚焦组 2015−2016 年在研项目涵盖国家自然科学基金项目、中科院及地方资助项目，其中国家自然科学基金青年基金、面上基金以及联合基金共计 11 项，资助额 588 万；中科院及地方资助项目 5 项，资助额 46.5 万。2016 年新增 2 项国家自然基金青年基金项目。

2017 年度本组除了进行硬 X 射线微聚焦及应用光束线站的运行维护和用户实验支持、新建相关线站的设计以及执行上述科研项目外，还将发展非弹性散射实验方法、自适应的压电变形反射镜对硬 X 射线波前调制的研究等工作。

参考文献

1. Jiangh Hui, He Yan, He Yumei, *et al*. Structural characterization and low-temperature properties of Ru/C multilayer monochromators with different periodic thicknesses[J]. Journal of Synchrotron Radiation, 2015, **22**: 1379−1385.
2. Qing Haiying, Chen Kaijian, Zhu Cai, *et al*. High electrocatalytic activity for borohydride oxidation on palladium nanocubes enclosed by {200} facets[J]. Journal of Power Sources, 2015, **299**: 241−245.
3. Li Xiaoli, He Shangming, Zhou Xingtai *et al*. High-temperature corrosion behavior of Ni–16Mo–7Cr–4Fe superalloy containing yttrium in molten LiF–NaF–KF salt[J]. Journal of Nuclear Materials, 2015, **464**: 342−345.
4. Li Xiaoli, He Shangminge, Zhou Xingtai, *et al*. Improving oxidation resistance of Ni-16Mo-7Cr-4Fe nickel-based superalloy by yttrium microalloying[J]. Nuclear Science and Techniques, 2015, **26**: 030201.
5. Zhang Ling, Song Sannian, Xi Wei, *et al*. Local structure of $AlSb_2Te_3$ thin film studied by experimental and theoretical methods[J]. Journal of Physics and Chemistry of Solids, 2015, **83**: 52−57.
6. Zhao Xiaolio, Yang Ke, Xu Longquan, *et al*. Investigation of Compton profiles of molecular methane and ethane[J]. The Journal of Chemical Physics, 2015, **142**: 084301.
7. Dongdong Ni, Xu Kang, Ke Yang, *et al*. Squared form factors for the $A^1\pi$ and $B^1\Sigma^+$ vibronic bands of carbon monoxide studied by high-resolution inelastic x-ray scattering[J]. Physical Review A, 2015, **91**: 042501.
8. Liu Yawei, Kang Xu, Xu Longquan, *et al*. Oscillator strengths of vibrionic excitations of nitrogen determined by the dipole (γ, γ) method[J]. The Astrophysical Journal, 2016, **819**(2): 142−146.

Research Development of Hard X-ray Micro-focusing Group

Hard X-ray Micro-focusing Group

Hard X-ray micro-focusing group is mainly in charge of the operation and user support of hard X-ray micro-focusing beamline. During 2015–2016, the beamline has supported beam time of 11 100.5 h with a low fault rate of 0.22%. 8 817 h are provided for nearly 300 proposals with research fields covering environmental and earth science, material science, life science, geology, archaeology, condensed matter physics, and so on. 155 papers have been published by users during this period and part of them on the famous periodicals such as Nature, PNAS, Advance Materials, J. Am. Chem. Soc., Biomaterials. The completed work about beamline maintenance includes the replacement of the vacuum be window at the end of the beamline, the replacement of K-B mirrors, the maintenance of the monochromator and the air conditioning of the experimental hutch, and the installation grating ruler for the zoneplate motors and etc.

In addition, hard X-ray micro-focusing group is in charge of the design and construction of new beamlines of SSRF phase-II project named as “Hard X-ray nano-focusing beamline” and “Ultra-hard X-ray beamline”. During 2015-2016, X-ray imaging group completed the project proposals, the internal and international review of feasibility report, and the preliminary designs. The preliminary research was carried out at the hard X-ray micro-focusing beamline, including the strain and stability of multilayer monochromater under low temperature[1], characterization of wavefront and the control system of nano-focusing device. For ultra-hard x-ray beamline, pre-researches of sagittal and meridional bending Laue monochromator were carried out. Prototype of sagittal bending was designed and started manufacturing.

In order to meet the demands of users, ultra high sensitive total reflection X-ray fluorescence technique has been developed. Some application researches have also been carried out, including the mechanism of catalytic oxygen reduction for fuel cells[2], the damage mechanism of alloy[3,4], the structure of phase change storage thin film materials[5], the atomic and molecular dynamics study based on X-ray scattering technology[6-8], the residual stress study in metallic material, the high pressure research of MOFs (Metal organic Framework) and rare earth oxide[7,8], and so on. A total of 19 articles were published and 13 patents were applied based on the above in house research.

The ongoing projects cover the National Natural Science Foundation, Chinese Academy of Sciences and local Foundation. Among them, 11 National Natural Science Foundations were granted and the funding was 5,880,000 RMB; 5 Chinese Academy of Sciences and local Foundation were granted and the funding was 465,000 RMB. In 2016, 2 new National Natural Science Foundation were granted.

In 2017, besides the beamline operation and user support, the design of new beamlines and the performing of the above research projects, the group will continue to develop the inelastic scattering technique, to carry out the research about the adaptive piezoelectric deformable mirror for hard X-ray wavefrontmodulation, and so on.

Reference

9. Jiangh Hui, He Yan, He Yumei, *et al*. Structural characterization and low-temperature properties of Ru/C multilayer monochromators with different periodic thicknesses[J]. Journal of Synchrotron Radiation, 2015, **22**: 1379−1385.
10. Qing Haiying, Chen Kaijian, Zhu Cai, *et al*. High electrocatalytic activity for borohydride oxidation on palladium nanocubes enclosed by {200} facets[J]. Journal of Power Sources, 2015, **299**: 241−245.
11. Li Xiaoli, He Shangming, Zhou Xingtai *et al*. High-temperature corrosion behavior of Ni–16Mo–7Cr–4Fe superalloy containing yttrium in molten LiF–NaF–KF salt[J]. Journal of Nuclear Materials, 2015, **464**: 342−345.
12. Li Xiaoli, He Shangminge, Zhou Xingtai, *et al*. Improving oxidation resistance of Ni-16Mo-7Cr-4Fe nickel-based superalloy by yttrium microalloying[J]. Nuclear Science and Techniques, 2015, **26**: 030201.
13. Zhang Ling, Song Sannian, Xi Wei, *et al*. Local structure of $AlSb_2Te_3$ thin film studied by experimental and theoretical methods[J]. Journal of Physics and Chemistry of Solids, 2015, **83**: 52−57.
14. Zhao Xiaolio, Yang Ke, Xu Longquan, *et al*. Investigation of Compton profiles of molecular methane and ethane[J]. The Journal of Chemical Physics, 2015, **142**: 084301.
15. Dongdong Ni, Xu Kang, Ke Yang, *et al*. Squared form factors for the $A^1\pi$ and $B^1\Sigma^+$ vibronic bands of carbon monoxide studied by high-resolution inelastic x-ray scattering[J]. Physical Review A, 2015, **91**: 042501.
16. Liu Yawei, Kang Xu, Xu Longquan, *et al*. Oscillator strengths of vibrionic excitations of nitrogen determined by the dipole (γ, γ) method[J]. The Astrophysical Journal, 2016, **819**(2): 142−146.

红外组研究进展

红外组

红外组目前承担了 Dline 动力学线站的红外分支线站的建设工作，完成了初步设计报告并完成了国际评审，完成了实验站相关的初步设计报告。

在同步辐射红外谱学显微研究方面，红外组开展了同步辐射红外谱学显微的新方法学研究如 3D 成像技术、光声光谱学等研究，并对束线优化设计、空间分辨率等方面进行了研究。应用研究方面开展了利用同步辐射红外谱学显微方法研究彩绘文物的保护及修复问题，药物小球的红外谱学显微研究等，发表文章 6 篇，获得发明专利 2 项，另有两项发明专利申请中。

已有科研项目包括：国家自然科学基金面上项目“基于同步辐射红外光源的三维红外谱学显微 CT 技术及其应用”(No.11475252)、国家自然科学基金青年科学项目“同步辐射红外光束线降噪技术研究”(No.11405258)、上海市自然科学基金“同步辐射红外 3D 成像技术在骨组织细胞中的应用”(No.15ZR1448200)和“基于 SR 红外显微的帕金森症(PD)药物治疗机制研究”(No.15ZR1448900)。新获一项项目资助：国家自然科学青年基金项目“基于同步辐射显微红外光谱的故宫彩绘传统工艺及保护技术研究”(No.11505267)。

在 2017 年度，红外组除了完成 Dline 红外分支线的建设任务，还将继续开展同步辐射红外谱学显微的方法学研究如 3D 红外谱学显微在细胞中的应用、光声谱学等，在应用研究领域继续开展彩绘文物、生物细胞等领域的同步红外谱学显微研究。

参考文献

1. Ji Te, TONG Yajun, ZHU Huachun, *et al*. The status of the first infrared beamline at Shanghai Synchrotron Radiation Facility[J]. Nuclear Instruments and Methods in Physics Research, A, 2015, **788**:116–121.
2. Manli Wang, Xiaolong Lu, Xianzhen Yin, *et al*. Synchrotron radiation based Fourier-transform infrared spectromicroscopy for characterization of the protein/peptide distribution in single microsphere[J]. Acta Pharmaceutica Sinica B, 2015, **5**: 270-276.
3. Wu Li, Yin Xianzhen, Guo Zhen, *et al*. Hydration induced material transfer in membranes of osmotic pump tablets measured by synchrotron radiation based FTIR[j]. European Journal of Pharmaceutical Sciences, 2016, **84**: 132-138.
4. 张增艳，吉特，朱智勇，等. 一种有效提高太赫兹时域光谱装置成像空间分辨率的方法[J]. 光谱学与光谱分析, 2015, **35**(1): 1-4
5. 张增艳，吉特，肖体乔， 等，基于平均吸收的太赫兹波振幅成像研究[J]. 光谱学与光谱分析，2015, **12**: 3315-3318
6. 朱华春，佟亚军，吉特，等. 小接收角同步辐射红外光束线的优化设计[J]. 光学学报，2016, **36**(11): 1122002-(1-7).
7. 去除恒流注入对同步辐射红外光束线站影响的系统及方法，中国，发明专利，专利号：ZL201410654932.8.
8. 一种同步辐射 X 射线 CT 校轴系统及方法，中国，发明专利，专利号：ZL201410706151.9.

Research Development of Infrared Group

Infrared Group

The infrared group currently undertakes the construction of the infrared branch station of the dynamic line (D-line) bemline and have completed the preliminary design report, the international review, and the preliminary design report of the experimental station.

In synchrotron infrared microspectroscopy research, the infrared group has carried out new methodological researches, such as 3D imaging technology and photoacoustic spectroscopy of synchrotron infrared microspectroscopy, optimization of beamline design and spatial resolution of the infrared microspectroscopy station, etc. In terms of applied research, synchrotron infrared microspectroscopy methods are used to study the protection and restoration of painted cultural relics and drug pellets etc. The infrared group has published six papers and obtained two invention patents.

The research projects include: National Natural Science Foundation of China, "3D Infrared Spectroscopy Micro-CT Technology Based on Synchrotron Radiation Infrared Light Sources and Its Applications" (No.11475252), Young Scientists Fund of National Natural Science Foundation of China Project “Synchrotron Radiation” Research on Noise Reduction Techniques of Infrared Beam Lines" (No.11405258), Shanghai Natural Science Foundation “Application of Synchrotron Radiation 3D Imaging Technology in Bone Tissue Cells” (No.15ZR1448200) and “Based on SR Infrared Microscopy Study on the Mechanism of Drug Treatment for Parkinson Disease (PD) (No.15ZR1448900). New project funding: Young Scientists Fund of National Natural Science Foundation of China “Research on Traditional Chinese Painting and Protection Technology of the Forbidden City Based on Synchrotron Radiation Infrared microspectroscopy” (No.11505267).

In 2017, infrared group is in charge of the construction of the D-line infrared branch beamline, and the infrared group will continue to carry out methodological and application research such as 3D infrared microspectroscopy of biological cells, photoacoustic spectroscopy, the heritage restoration and biological cells of the infrared microspectroscopy.

Reference

1. Ji Te, TONG Yajun, ZHU Huachun, *et al*. The status of the first infrared beamline at Shanghai Synchrotron Radiation Facility[J]. Nuclear Instruments and Methods in Physics Research，A, 2015, **788**:116–121.
2. Manli Wang, Xiaolong Lu, Xianzhen Yin, *et al*. Synchrotron radiation based Fourier-transform infrared spectromicroscopy for characterization of the protein/peptide distribution in single microsphere[J]. Acta Pharmaceutica Sinica B, 2015, **5**: 270-276.
3. Wu Li, Yin Xianzhen, Guo Zhen, *et al*. Hydration induced material transfer in membranes of osmotic pump tablets measured by synchrotron radiation based FTIR[J]. European Journal of Pharmaceutical Sciences, 2016, **84**: 132-138.
4. ZHANG Zeng-yan, JI Te, ZHU Zhi-yong, *et al*. An Effective Method for Improving the Imaging Spatial Resolution of Terahertz Time Domain Spectroscopy System, Spectroscopy and Spectral Analysis, 2015，**35**(1):1-4.
5. ZHANG Zengyan, JI Te, XIAO Tiqiao, *et al*. Study of Terahertz Amplitude Imaging Based on the Mean Absorption[J]. Spectroscopy and Spectral Analysis，2015，**12**：3315-3318
6. Zhu Huachun, Tong Yajun, Ji Te, *et al*. Optimized Design for Synchrotron Radiation Infrared Beamline with Small Extraction Angle[J]. Acta Optica Sinica, 2016, **36**(11): 1122002-(1-7).
7. A method for removing influence induced by the qusi-constant current injection mode on synchrotron radiation infrared beamline station, China，Patents of invention, Authorization number：ZL201410654932.8.

   A method for calibration axis of Synchrotron radiation X-ray CT，China, Patents of invention, Authorization number：ZL201410706151.9.

X 射线成像组研究进展

X 射线成像光学组

X 射线成像组负责“上海光源”首批线站“X 射线成像及生物医学应用光束线站”的运行维护与用户开放。该线站在 2015−2016 年度高效低故障率运行，总供光机时 9 982.34 h，总故障率为 0.86%。累计提供用户机时 8 733.6 h，接待用户实验人员 1 500 人次，执行用户课题 339 个，用户研究涵盖生物医学、材料科学、地质考古学等众多学科领域，共发表用户成果 143 篇，其中 SCI 二区及以上论文 64 篇。线站维护方面：单色器二晶夹持机构经厂商升级后，晶体变形严重。通过晶体在安装条件下根据光学检测结果调节至最佳状态后解决晶体变形严重的问题。更换单色器 Bragg 电机驱动器和编码器。完成了滤波器的日常维护。实验站建立了光强自动反馈系统，提高了单色器稳定性；完成了 X 射线成像探测器的升级，实现帧频 100 fps、探测器闪烁体厚度优化[1]等。

新线站建设方面，X 射线成像组负责上海光源线站工程二条新建线站“快速 X 光成像线站”和“纳米三维成像线站”的设计建造工作。此外，X 射线成像组还负责“X 射线成像搬迁线站”的设计和相关工程工作。2015−2016 年度本组负责完成了相关线站的项建书、可研报告国内国际评审，完成了所有线站的初步设计。

为满足不同学科领域用户研究的需求，本组在 X 射线成像方法学研究及相关应用研究方面进行了不断的研究和探索，共发表论文 29 篇，其中 SCI 收录 21 篇、SCI 影响因子大于 3 的论文 5 篇、申请发明专利两项。发展和建立了全场荧光 CT 方法[2−3]、2 Hz 动态显微 CT 方法[4−6]、三维血管定量分析方法，并对用户开放[7−8]；建立了分辨率 100 nm 的全场 Nano-CT 方法[9]、高能定量相衬 CT 方法[10]、三维 X 射线衍射方法、小角散射 CT 方法、X 射线体视成像方法；开展了 X 射线成像在昆虫呼吸机理[4]、柴油机气缸碳沉积[11]、中药材显微鉴定[12−13]、页岩孔隙特性、胶体自组装机理、竹材结构和功能等方面的应用研究。

在研项目主要有：CAS-CSIRO 合作研究项目“基于同步辐射显微 CT 的肿瘤血管三维结构定量分析” (No.GJHZ1303)；国家自然科学基金项目“基于’飞行’扫描与 OSEM 加速 X 射线荧光 CT 成像” (No.11275257)、“毫秒级动态定量显微 CT 研究” (No.11375257)、“基于 X 射线定量显微 CT 研究中药显微特征结构与有效成分关系” (No.11475248)、联合基金项目“基于 EST 的全场纳米 CT 方法研究”(No.U1532118)；联合基金重点项目“小动物缺血性脑卒中模型的原位活体动态研究” (No.U1232205)；国家林业公益性行业专项“基于 X 射线成像的木竹材无损检测技术研究 ” (No.201304513)；基金重点项目“桥接细胞和整体的纳米药代动力学研究” (No.81430087)等。新申请获批项目有：国家重点研发计划项目“金属材料多场耦合制备与极端使役环境原位实验集成系统” (No.2017YFA0403801)、国家重大科研仪器研制项目（部委推荐）“材料内部变形损伤过程的超快时、高分辨、强穿透同步辐射原位表征分析系统” (No.11627901)等。

2017 年度本组除了进行成像线站的运行维护和用户开放、新建线站工程以及执行上述科研项目外，还将在动态显微 CT、全场纳米 CT、三维 X 射线衍射、小角散射 CT、小动物原位活体动态研究以及中药材显微鉴别、木材无损检测等方法学和相关应用领域继续进行深入研究。

参考文献

1. Xie H L, *et al*. Study of Scintillator thickness optimization of lens-coupled X-ray imaging detectors[J]. Journal of instrumentation,2016, **11**: C03057
2. Deng B, *et al*. 3D elemental sensitive imaging by full-field XFCT[J]. Analyst, 2015, **140**(10): 3521- 3525
3. Sun P F, *et al*. X-Ray Spectromet, **44**(6): 442–446 2015
4. Xu L, *et al*. Scientific Reports, 2016, **6**: 32380
5. Xu L, *et al*. Journal of instrumentation，2015, **10**: C03010
6. Chen R C, *et al*. Proc. SPIE, 2016, Vol. 9967, 99671B
7. Tan H, *et al*. Journal of Synchrotron Radiation, 2016, 23: 1216-1226
8. Tan H, *et al*. Nuclear Science and Techniques, 2016, **27**: 125
9. Feng B G, *et al*. Chinese Optics Letters, 2016, **14**(9): 093401-5
10. Liu H Q, *et al*. Med. Phys, 2015, **42**(10): 5595-5603
11. Zhang X S, *et al*. Fuel , 2015, **142**, 173–179
12. Ye L L, *et al*. Journal Ginseng Research, 2016, 41(3): 290-297
13. Xue Y L, *et al*. Microscopic identification of Chinese medicinal materials based on X-ray phase contrast imaging: from qualitative to quantitative[J]. Journal of instrumentation, 2016, 11: C07001

Research Development of X-ray Imaging Group

X-ray Imaging Group

X-ray imaging group is mainly in charge of operation and user support of X-ray imaging and biomedical applications beamline at Shanghai Synchrotron Radiation Facility. During 2015–2016, this beamline operated with high efficiency and low fault rate, and has supported beam time of 9 982.34 h with the fault rate of 0.86%. There are 8 733.6 hours provided for 1 500 users from the 339 proposals, whose research fields covering biomedicine, material science, archeology paleontology and so on. And 143 papers have been published by users during this time, in which there are 64 papers attributed to top 20% papers. The completed work about beamline maintenance includes: the clamping device of the second crystal of the monochromator has severe deformation after the manufacturer's upgrade. This problem has been resolved through adjusting to the best position of the crystal according to the optical testing under the installing condition. Other maintenance includes: replacement of the Bragg motor driver and the encoder of the monochromator, maintenance of the filters, development of the automatic feedback system of the flux to increase the stability of the monochromator, upgrading of the X-ray imaging detector to achieve the 100 fps frame rate and optimize the thickness of the scintillator[1] and so on.

In addition, X-ray imaging group is in charge of the design and construction of the two new beamlines of SSRF phase-II project named as "Fast X-ray imaging beamline" and "Nano 3D imaging beamline" and the design and project work of "X-ray imaging movement beamline". During 2015−2016, X-ray imaging group completed the project proposals, the internal and international review of feasibility report, and the preliminary designs.

In order to meet the demands of users for different samples, many X-ray imaging methodologies and application research have also been developed and explored with 29 papers (21 SCI-cited papers and 5 IF>3 papers) and two patents. The full-field X-ray fluorescence micro-CT[2−3], 2 Hz dynamic micro- CT[4−6] and 3D quantification of vasculatures[7−8] have been developed and opened to users. The full-field nano-CT with 100 nm resolution[9], quantitative phase retrieval CT with high energy X-ray[10], 3DXRD, small- angle x-ray scattering CT, X-ray stereoscopic imaging have been established. The application research included the mechanism of insect respiration[4], the structures of piston carbon deposits in diesel engine[11], identification of traditional Chinese medicine[12−13], pore property of shale, mechanism of colloidal self-assembly, the structure and function of bamboo, and so on.

The ongoing projects include the CAS-CSIRO cooperation research project "Automated Quantitative Analysis of 3D Angiogenesis for Early Diagnosis of Tumors using Synchrotron Radiation X-Ray Microtomography" (No.GJHZ1303), the projects supported by National Natural Science Foundation of China including "Accelerating X-ray fluorescence CT based fast scanning and OSEM" (No.11275257), "Study on millisecond dynamic quantitative microscopic CT" (No.11375257), "Study on the relationship between the microstructure and effective components of traditional Chinese medicine based on X ray quantitative microscopic CT" (No.11475248), the projects supported by Joint Funds of the National Natural Science Foundation of China including "Study of full field nano CT method based on EST" (No.U1532118), "In vivo and in vivo dynamic study of ischemic stroke in small animals" (No.U1232205), Special Funding Projects of Forestry Nonprofit Industry Research "Nondestructive testing technology of wood and bamboo based on X ray imaging" (No.201304513), the project supported by Key National Natural Science Foundation of China "Study on the nanoscale pharmacokinetics of bridged cells and the whole" (No.81430087). The new approved projects include National key research and development program "A multi-field coupling preparation and in situ experimental system integrated extreme working environment of the metal material" (No.2017YFA0403801) and National project for research and development of major scientific instruments "A synchrotron-based system with dynamic loading and in situ, real-time, X-ray characterization instrumentations for investigating deformation, damage and failure within material interiors" (No.11627901).

In 2017, besides the beamline operation and user experiments support, the construction project of new beamlines and performing the above research projects, the group will focus on the following research aspects including dynamic micro-CT, full-field nano-CT, 3DXRD, small-angle scattering CT, in situ dynamic research of small animals in-vivo, identification of traditional Chinese medicine, nondestructive characterization of wood.

Reference

1. Xie H L, *et al*. Study of Scintillator thickness optimization of lens-coupled X-ray imaging detectors[J]. Journal of instrumentation,2016, **11**: C03057
2. Deng B, *et al*. 3D elemental sensitive imaging by full-field XFCT[J]. Analyst, 2015, **140**(10): 3521- 3525
3. Sun P F, *et al*. X-Ray Spectromet, **44**(6): 442–446 2015
4. Xu L, *et al*. Scientific Reports, 2016, **6**: 32380
5. Xu L, *et al*. Journal of instrumentation，2015, **10**: C03010
6. Chen R C, *et al*. Proc. SPIE, 2016, Vol. 9967, 99671B
7. Tan H, *et al*. Journal of Synchrotron Radiation, 2016, 23: 1216-1226
8. Tan H, *et al*. Nuclear Science and Techniques, 2016, **27**: 125
9. Feng B G, *et al*. Chinese Optics Letters, 2016, **14**(9): 093401-5
10. Liu H Q, *et al*. Synchrotron-based High Energy X-ray Phase Sensitive Micro-tomography for Biomedical Research[J], Med. Phys, 2015, **42**(10): 5595-5603
11. Zhang X S, *et al*. Investigating the microstructures of piston carbon deposits in a large-scale marine diesel engine using synchrotron X-ray microtomography [J]. Fuel, 2015, **142**, 173–179
12. Ye L L, *et al*. Journal Ginseng Research, 2016, 41(3): 290-297
13. Xue Y L, *et al*. Microscopic identification of Chinese medicinal materials based on X-ray phase contrast imaging: from qualitative to quantitative[J]. Journal of instrumentation, 2016, 11: C07001

自由电子激光物理研究取得系列进展

自由电子激光

1　相位汇聚型自由电子激光

外种子机制是短波长自由电子激光的一个重要发展方向。目前，人们已经相继提出了高增益高次谐波放大(HGHG)和回声高次谐波放大(EEHG)等外种子自由电子激光机制。但是，外种子自由电子激光的谐波转换次数通常会受到直线加速器所产生电子束能散的限制，较难向更短的波长发展。自由电子激光部科研人员于 2013 年提出了相位汇聚高次谐波放大(PEHG)自由电子激光运行模式(Phys Rev Letts, 2013, **111**: 084801)，能够有效地克服电子束能散的限制，从而大大提高谐波转换次数。PEHG 为未来全相干 X 射线自由电子激光装置的建设提供了一种非常有吸引力的方案。

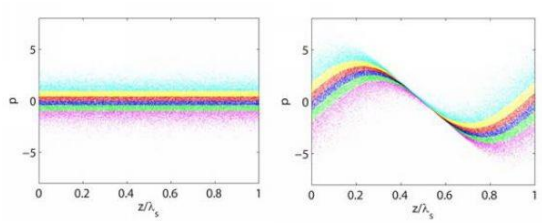

PEHG 机制电子束相空间演化过程示意图：不同颜色代表不同能量电子，可见在一个种子激光波长范围内，中间部分电子束能散得到了压缩。

在后续研究中，研究人员从三维的束流物理学出发，详细分析了相位汇聚(phase-merging)的物理机制，系统地研究了 PEHG 对种子激光、电子束、波荡器的各种参数的依赖关系(New J Phys, 2014, **16**: 043021)；并提出了种子激光相位倾斜等实现 PEHG 原理的新方案(Phys Rev ST-AB, 2014, **17**: 070701)。研究发现：相位汇聚原理不仅可以提高外种子自由电子激光的高次谐波转换效率，在粒子加速器领域中还有着更为广阔的应用前景。

2　外种子型 FEL 中的噪声放大问题

外种子自由电子激光的主要优势是可以继承种子激光的优秀特性，具有优异的横向相干性、纵向相干性和波长稳定性等。同时，和任意一个信号系统类似，在外种子 FEL 的高次谐波转换过程中，种子激光和电子束团的微小噪声和缺陷也会被继承，并被进一步放大。一般认为，外种子 FEL 的输出信噪比与其谐波转换次数的平方成反比，即随着谐波次数的增大，外种子 FEL 频谱等性能会严重退化，也就是所谓的噪声演化问题。因此，噪声问题被认为是限制外种子 FEL 向 X 射线扩展的一个重要因素。

自由电子激光部的研究人员通过引入种子激光和电子束团之间的相对滑移修正，揭示了外种子 FEL 的噪声演化规律，相关研究成果发表在 Phys Rev ST-AB, 2013, **16**: 060705、Nucl Instr Meth A, 2014, **737**: 237、Nucl Instr Meth A, 2014, **753**: 56。研究人员发现：种子激光相位噪声的放大并非简单地遵守 N 平方规律，可以通过增加调制段波荡器周期数来有效抑制，从而改善外种子 FEL 性能。当种子激光为超短脉冲情况下，理论和模拟均证明，外种子 FEL 可以完全补偿种子激光的相位噪声，从而输出纵向相干性非常优秀的辐射脉冲。同时，研究人员还系统地分析了不同模式外种子 FEL 对电子束团噪声的响应，发现 PEHG 和 EEHG 两种模式可以做到对电子束能量噪声较小的响应。

外种子 FEL 噪声问题的研究修正了以前的理论预期，证明目前的激光技术可以非常好地满足外种子 FEL 对种子激光的要求，并为全相干 FEL 装置向更短波长发展提供了理论依据，对建设中的大连相干光源和上海软 X 射线试验装置都有积极意义。

3　外种子型 FEL 的基于光学准直技术

短波长自由电子激光的饱和出光，不单需要直线加速器提供高品质电子束团，而且需要确保电子束团在波荡器系统中高精度扭摆，这就涉及到波荡器系统准直、波荡器间隙设定、波荡器段间相位匹配和尾场补偿等问题。因此，在交付用户之前，FEL 装置都要经历漫长的调束阶段，以便掌握和优化整个 FEL 装置的性能。

基于电子束团的准直(BBA)是粒子加速器领域常用的准直方法。利用 BBA 技术，美国 LCLS 自由电子激光在 132 m 波荡器达到了小于 5 μm 的束流轨道。波荡器的 BBA 过程需要改变电子束能量、读取大量 BPM 数值和复杂的数值算法，鉴于此，LCLS 是目前唯一成功运行 BBA 的 FEL 装置。

基于电子束团自发辐射的准直(PBA)，是近年发展起来的 FEL 波荡器准直方法。利用波荡器下游的光学系统，独立测量各段波荡器的自发辐射谱，推出束流轨道相关信息，从而加以反馈调整。日本 SACLA 自由电子激光利用 PBA 在 110 m 波荡器达到了 1 μm 的束流轨道。

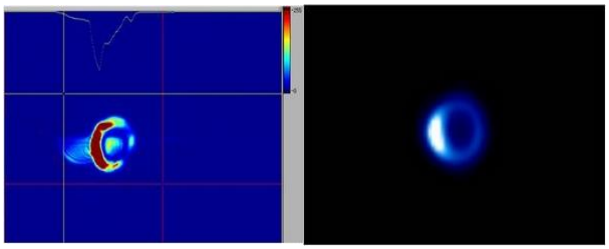

左：SDUV-FEL 实验结果；右：从头至尾的数值模拟结果

在基于电子束团相干辐射的外种子 FEL 波荡器准直调试方法中，当电子束在水平方向以一个倾角进入波荡器，并且波荡器的 gap 大于 FEL 共振关系所需时，在下游 CCD 上看到的电子束团相干辐射的空间分布。

由于其优越的全相干性和波长稳定性，外种子 FEL 已经成为紫外至软 X 射线波段用户装置的首选工作模式。外种子 FEL 电子束团能量相对较低，通常在 0.3~1 GeV 量级，电子束刚性差，大幅改变电子束能量的 BBA 几乎无法正常工作；另外，外种子 FEL 的工作波段没有可用的晶体单色仪，无法进行类似 SCALA 的自发辐射准直。因此，对于外种子 FEL，探索新的波荡器系统调试方法，是极具意义的一个科学问题。

在这样的前提下，我们提出了基于电子束团相干辐射的外种子 FEL 波荡器调试方法，并在 SDUV-FEL 试验装置上完成了实验验证，相关研究成果近日发表在 Phys Rev ST-AB, 2014, **17**: 100702。研究表明：通过分析已群聚电子束在辐射段波荡器的相干辐射性能，同样能得到波荡器内的束流轨道和共振关系等信息，便可以实现外种子 FEL 波荡器系统的束流轨道准直。另外，基于电子束团相干辐射的准直技术与整个 FEL 调试浑然一体，更为直观，除波荡器准直之外，还可以用来设定波荡器的工作磁间隙和波荡器的段间相位匹配等。

目前，我国首个高增益 FEL 用户装置（大连相干光源）和首个 X 射线 FEL（上海软 X 射线 FEL 试验装置）均采用外种子 FEL 工作模式，并在 2~3 a 内进入 FEL 调试阶段。因此，基于电子束团相干辐射的波荡器准直和调试方法的提出，对我国 FEL 装置建设有十分重要的实际意义。

4 发展全光学自由电子激光

相对于射频电子加速器驱动的 X 射线光源，发展全光学 X 射线光源，对减小同步辐射和自由电子激光的装置规模很有好处。所谓全光学光源，即利用激光等离子尾场加速原理获得高能量电子束团，并用激光电场来替代常规的波荡器。激光等离子加速能产生比常规射频加速器高 2~3 个量级的加速梯度，而激光波荡器的周期长度比常规磁铁波荡器小 2~3 个量级，因此，全光学方法可以将光源规模急剧缩小，是桌面型 X 射线光源的可行方案，对于同步辐射和自由电子激光等光源的普及应用具有十分重要的意义。

激光等离子加速产生电子束团峰值流强高（一般可达数千安培），束团长度短（一般仅有几个飞秒），横向发射度极低（如 0.1 微米弧度），这些特性均十分符合高亮度 X 射线光源对电子束团的要求。然而，目前激光等离子体加速产生的电子束团能散在 1%以上，尚远大于 X 射线 FEL 的需求，这就限制了其在高增益 X 射线 FEL 方面的应用。

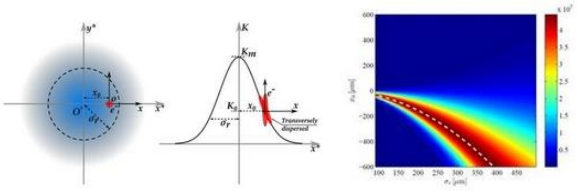

左图：全光学光源中，电子束团（红色圆点）以一个横向偏移进入激光波荡器场扭摆；中图：纵向能量和横向位置关联的电子束团在激光波荡器梯度场中符合共振关系；右图：全光学光源辐射功率随激光束斑大小和横向偏移的变化情况，红色区域为优化区域。

通过耦合电子能量和横向位置，并调节电子束在激光场中扭摆的中心位置，便可以补偿全光学 X 射线光源中电子束团的能散效应，相关研究成果近日发表在 Optics Express, 2014, **22**: 13880。具体原理如下：首先利用横向色散元件将电子束团的纵向能量映射到横向分布；其次激光场在横向天然具有高斯分布，即场强从横切面中心位置向四周递减，只要入射电子束团不在激光场中心扭摆，便自然感受到横向场梯度的存在，也就是所谓的具有横向梯度的激光波荡器。这样安排下，不同能量电子均满足自由电子激光共振条件，便可将能量转换效率提高 2~3 个量级，并改善 FEL 横向模式。

参考文献

1. Deng H X, Chao F. Using off-resonance laser modulation for beam-energy-spread cooling in generation of short-wavelength radiation[J]. Physical Review Letters, 2013, **111**(8): 084801.
2. Feng C, Deng H, Wang D, *et al*. Phase-merging enhanced harmonic generation free-electron laser[J]. New Journal of Physics, 2014, **16**(4): 043021.
3. Feng C, *et al*. Three-dimensional manipulation of electron beam phase space for seeding soft x-ray free-electron lasers[J]. Physical Review Special Topics-Accelerators and Beams, 2014, **17**(7): 070701.
4. Feng C, Deng H, Wang G, *et al*. Slippage effect on energy modulation in seeded free-electron lasers with frequency chirped seed laser pulses[J]. Physical Review Special Topics-Accelerators and Beams, 2013, **16**(6): 060705.
5. Wang G, Feng C, Zhang T, *et al*. Study on the seed laser phase error multiplication in seeded free electron lasers[J]. Nuclear Instruments and Methods in Physics Research Section A: Accelerators, Spectrometers, Detectors and Associated Equipment, 2014, **737**: 237−241.
6. Wang G, Feng C, Deng H, *et al*. Beam energy chirp effects in seeded free-electron lasers[J]. Nuclear Instruments and Methods in Physics Research Section A: Accelerators, Spectrometers, Detectors and Associated Equipment, 2014, **753**: 56−60.
7. Feng C, Deng H, Dai Z, *et al*. Coherent photon beam based diagnostics for a seeded extreme ultraviolet free-electron laser[J]. Physical Review Special Topics-Accelerators and Beams, 2014, **17**(10): 100702.
8. Zhang T, Feng C, Deng H, *et al*. Compensating the electron beam energy spread by the natural transverse gradient of laser undulator in all-optical X-ray light sources[J]. Optics express, 2014, **22**(11): 13880−13888

Progresses in Research of FEL Physics

Free-Electron

1 Phase-merging enhanced harmonic generation free-electron

To improve temporal coherence in electron beam based light sources, various techniques employ frequency up conversion of external seed sources via electron beam density modulation; however, the energy spread of the beam may hinder the harmonic generation efficiency. A novle method is described for cooling the electron beam energy spread by off-resonance seed laser modulation, through the use of a transversely dispersed electron beam and a modulator undulator with an appropriate transverse field gradient. With this novel mechanism, it is shown that the frequency up-conversion efficiency can be significantly enhanced. We present theoretical analysis and numerical simulations for seeded soft X-ray free- electron laser and storage ring based coherent harmonic generation in the extreme ultraviolet spectral region. Together with one of its variants, the recently proposed phase-merging enhanced harmonic generation (PEHG) FEL is systematically studied. Different from a standard high-gain harmonic generation scheme, a transverse gradient undulator is employed to introduce a phase-merging effect into the transversely dispersed electron beam in PEHG. The analytical theory of the phase-merging effect and the physical mechanism behind the phenomenon are presented. Using a representative set of beam parameters, intensive start-to-end simulations for soft X-ray FEL generation are given to illustrate the performance of PEHG. Moreover, some practical issues that may affect the performance of PEHG are also discussed.

2 Study on the seed laser phase error multiplication in seeded free electron lasers

Free-electron lasers seeded with external lasers hold great promise for generating high power radiation with nearly transform-limited bandwidth in the soft X-ray region. However, it has been pointed out that the initial seed laser phase error will be amplified by the frequency up-conversion process, which may degrade the quality of the output radiation produced by a harmonic generation scheme. Theoretical and simulation studies on frequency chirp amplification in seeded FEL schemes with slippage effect taken into account are presented. It is found that the seed laser imperfection experienced by the electron beam can be significantly smoothed by the slippage effect in the modulator when the slippage length is comparable to the seed laser pulse length. This smoothing effect allows one to preserve the excellent temporal coherence of seeded FELs in the presence of large frequency chirp in the seed laser. Our studies show that the tolerance on frequency chirp in the seed laser for generating nearly transform-limited soft x-ray pulses in seeded FELs is much looser than previously thought and fully coherent radiation at nanometer wavelength may be reached with current technologies.

3 Coherent photon beam based diagnostics for a seeded extreme ultraviolet free-electron laser

Independently from conventional electron beam based procedures, the photon beam based diagnostic is an alternative way for electron trajectory alignment and commissioning of numerous undulator cells in high-gain short-wavelength free-electron lasers (FELs). Using the microbunched electron beam and the undulator fine-tuning technique, a novel method based on the spatial profile analysis of coherent harmonic radiation from individual or two consecutive undulator segments, the so-called coherent photon beam based diagnostic, is proposed for undulator alignment and commissioning in seeded FELs. The preliminary experimental results at the Shanghai deep ultraviolet FEL test facility shows that the proposed method is effective and convenient in the electron beam trajectory control, the undulator magnetic gap verification, and the phase match between two undulator segments.

4 All-optical x-ray light sources

All-optical ideas provide a potential to dramatically cut off the size and cost of x-ray light sources to the university-laboratory scale, with the combination of the laser-plasma accelerator and the laser undulator. However, the large longitudinal energy spread of the electron beam from laser-plasma accelerator may hinder the way to high brightness of these all-optical light sources. The beam energy spread effect is proposed to be significantly compensated by the natural transverse gradient of a laser undulator when properly transverse-dispersing the electron beam. Theoretical analysis and numerical simulations on conventional laser-Compton scattering sources and high-gain all-optical x-ray free-electron lasers with the electron beams from laser-plasma accelerators are presented.

Reference

1. Deng H X, Chao F. Using off-resonance laser modulation for beam-energy-spread cooling in generation of short-wavelength radiation[J]. Physical Review Letters, 2013, **111**(8): 084801.
2. Feng C, Deng H, Wang D, *et al*. Phase-merging enhanced harmonic generation free-electron laser[J]. New Journal of Physics, 2014, **16**(4): 043021.
3. Feng C, *et al*. Three-dimensional manipulation of electron beam phase space for seeding soft x-ray free-electron lasers[J]. Physical Review Special Topics-Accelerators and Beams, 2014, **17**(7): 070701.
4. Feng C, Deng H, Wang G, *et al*. Slippage effect on energy modulation in seeded free-electron lasers with frequency chirped seed laser pulses[J]. Physical Review Special Topics-Accelerators and Beams, 2013, **16**(6): 060705.

5. Wang G, Feng C, Zhang T, *et al*. Study on the seed laser phase error multiplication in seeded free electron lasers[J]. Nuclear Instruments and Methods in Physics Research Section A: Accelerators, Spectrometers, Detectors and Associated Equipment, 2014, **737**: 237−241.
6. Wang G, Feng C, Deng H, *et al*. Beam energy chirp effects in seeded free-electron lasers[J]. Nuclear Instruments and Methods in Physics Research Section A: Accelerators, Spectrometers, Detectors and Associated Equipment, 2014, **753**: 56−60.
7. Feng C, Deng H, Dai Z, *et al*. Coherent photon beam based diagnostics for a seeded extreme ultraviolet free-electron laser[J]. Physical Review Special Topics-Accelerators and Beams, 2014, **17**(10): 100702.
8. Zhang T, Feng C, Deng H, *et al*. Compensating the electron beam energy spread by the natural transverse gradient of laser undulator in all-optical X-ray light sources[J]. Optics express, 2014, **22**(11): 13880−13888

自由电子激光实验研究取得进展

核物理研究室

1　自由电子激光偏振控制实验研究取得重要进展

偏振状态可以任意调控，高亮度、全相干 X 射线自由电子激光是研究物质的结构、磁性、电性、自旋和手型等各种不均匀性的有效工具。目前，国际上短波长自由电子激光多数采用平面波荡器，只能产生线偏振光，且偏振状态不可改变。而采用螺旋波荡器的自由电子激光，偏振状态调节依靠机械机构传动，速度较慢，而且调节后的辐射波长也会发生改变。因此，美国 ANL 实验室的 Kim K J 提出了交叉平面波荡器的概念(Nucl Instr Meth A, 2000, **445**: 329)，将两个交叉放置的平面波荡器产生的水平与垂直光场相干叠加，同步辐射光源和高增益自由电子激光辐射光场偏振状态的改变，通过调节交叉平面波荡器中间的移相器实现，若移相器采用脉冲磁铁结构便可实现偏振状态的快速调节。

自由电子激光团队完成了一项新的自由电子激光实验，基于上海深紫外自由电子激光实验装置(SDUV-FEL)，在国际上首次利用交叉平面波荡器实现了自由电子激光脉冲偏振态的任意调控。研究成果发表在《Physical Review Special Topics: Accelerator & Beams》(Phys Rev ST-AB17, 2014, 020704)。

在光源用户需求的驱动下，交叉平面波荡器原理得到了国际自由电子激光界的高度关注，近年来开展了一系列的相关理论研究。2012 年，自由电子激光团队提出了在 SDUV-FEL 开展交叉平面波荡器控制辐射偏振状态的实验方案(Nucl Instr Meth A, 2012, **680**: 112)。经过近两年的努力，成功将交叉平面波荡器、高精度电磁移相器和分振幅偏振测量仪等设备集成到 SDUV-FEL，使其成为世界首个配备交叉平面波荡器的自由电子激光装置。2013 年 11 月，研究人员经过精心调试，国际首次利用交叉平面波荡器，成功实现了自由电子激光脉冲在圆偏振和线偏振之间的任意切换，并进行了全相干自由电子激光脉冲光谱和偏振度的精确测量。

交叉平面波荡器的实验验证对自由电子激光科学用户具有重大的实际价值，并有望在近期建设的大连极紫外相干光源和上海软 X 射线自由电子激光装置等研究中得到应用。

SDUV-FEL 交叉平面波荡器实验束线

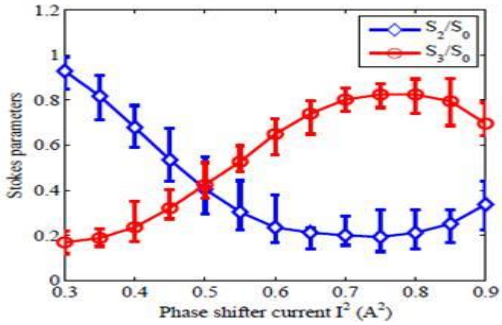

SDUV-FEL 辐射脉冲偏振态调控

2　电子束非线性补偿研究取得重要进展

作为第四代先进光源，自由电子激光由高亮度电子束团驱动，然而由于微波电场加速和束团长度压缩，直线加速器产生的电子能量在束团纵向尺度上不可避免地呈非均匀分布。电子束团的这种不均匀性，将减缓自由电子激光增益，并破坏其纵向相干性。因此在短波长自由电子激光装置中，人们提出了偏峰加速和高次谐波结构两种方法，来分别补偿电子束团纵向相空间的线性和非线性变化。

由电子激光团队完成了一项新的自由电子激光实验，在上海深紫外自由电子激光装置上，利用相对论电子束团在沟槽金属结构中激起的尾场，对电子束纵向相空间的非线性进行了补偿，并成功实现了自由电子激光辐射光谱的操控和改善。该项研究成果发表在《物理评论快报》上。

2012 年，美国 SLAC 实验室的 Bane K 和 Stupakov G 提出了金属沟槽结构补偿电子束团能量的概念(Nucl Instr Meth A, 1012, **690**: 106)，束流

在经过沟槽结构时激起尾波场，可以补偿电子束团纵向相空间的线性耦合。相对于其他方法，沟槽结构由于其简单、被动性、高性价比等特点，得到了国际加速器界的高度关注。2013 年，美国 SLAC 和 LBNL 实验室的科学家通力合作，在韩国 PAL 实验室 70 MeV 直线加速器上，成功地利用沟槽结构补偿了电子束团纵向相空间的线性耦合（Phys Rev Lett, 2014, **112**: 034801）。

2012 年，中国科学院上海应用物理研究所自由电子激光团队研究发现，通过匹配金属沟槽结构参数，也能补偿电子束团纵向相空间的非线性耦合(GU Qiang, *et al*. Proceedings of LINAC2012, Tel-Aviv, Israel, 525−527)。2013 年，自由电子激光团队提出在 SDUV-FEL 开展电子束团非线性补偿的实验方案，并经过一年的努力，将金属沟槽真空腔等硬件集成到了 SDUV-FEL。2014 年 4 月，经过精心调试，研究人员利用金属沟槽结构，成功地补偿了电子束团纵向相空间的非线性耦合，同时完成了自由电子激光辐射光谱改善和电子束团能散降低的测量。这是国际上首次将金属沟槽结构运行在自由电子激光装置中。

金属沟槽结构在 SDUV-FEL 的成功实验运行，对当前及未来自由电子激光等大科学装置的发展具有重要的实际意义并且产生深远的影响。目前，美国 SLAC 实验室已经准备将金属沟槽结构应用到其 X 射线 FEL 用户装置中；在国内，金属沟槽结构有望在建设中的大连相干光源、上海软 X 射线自由电子激光、以及上海交通大学超快电子透镜等装置中得到应用。

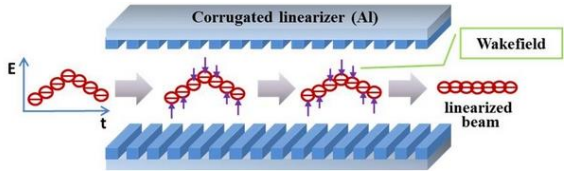

电子束团通过金属沟槽结构时，纵向相空间的非线性被尾波场补偿

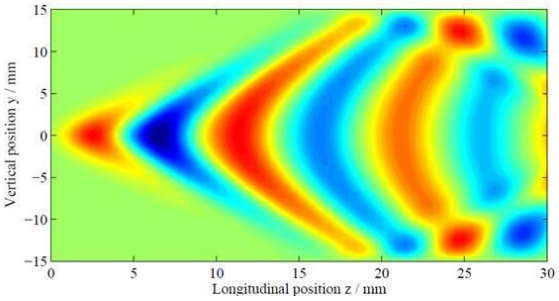

电子束团在金属沟槽结构中激起的纵向尾波场

参考文献

1. Zhang T, Deng H, Chen J, *et al*. Polarization control proposal for Shanghai deep ultraviolet free electron laser[J]. Nuclear Instruments and Methods in Physics Research Section A: Accelerators, Spectrometers, Detectors and Associated Equipment, 2012, **680**: 112−116.
2. Deng H, Zhang T, Feng L, *et al*. Polarization switching demonstration using crossed-planar undulators in a seeded free-electron laser[J]. Physical Review Special Topics-Accelerators and Beams, 2014, **17**(2): 020704.
3. Deng H, Zhang M, Feng C, *et al*. Experimental demonstration of longitudinal beam phase-space linearizer in a free-electron laser facility by corrugated structures[J]. Physical Review Letters, 2014, **113**(25): 254802.

Progresses in FEL Experiments

Free Electron Laser

1 Polarization switching demonstration using crossed-planar undulators in a seeded free- electron laser

Polarization switching of light sources is required over a wide spectral range to investigate the symmetry of matter. A fully coherent radiation option with controllable polarization is proposed for the Shanghai deep ultraviolet free electron laser test facility. Intensive start-to-end simulation suggests that the two crossed planar undulators which generate the horizontal and vertical linear polarized FEL, should be placed as close as possible for avoiding the polarization performance degradation of the final combined FEL radiation. With the existence of the phase-shifter between the two crossed radiators, Fourier-Transform-Limited output radiation with 100 nJ order pulse energy, 5 ps full pulse length and circular polarization degree above 90% could be achieved. We have also performed the first experimental demonstration of the crossed-planar undulators technique at a seeded free-electron laser, which holds great promise for the full control and fast switching of the polarization of short-wavelength radiation. In the experiment, the polarization state of the coherent radiation at the second harmonic of the seed laser is switched successfully. The experimental results confirm the theory and pave the way for applying the crossed-planar undulators technique for seeded x-ray free-electron lasers.

2 Experimental Demonstration of Longitudinal Beam Phase-Space Linearizer in a Free-Electron Laser Facility by Corrugated Structures

Removal of the undesired time-energy correlations in the electron beam is of paramount importance for efficient lasing of a high-gain free-electron laser. Recently, it has been theoretically and experimentally demonstrated that the longitudinal wake field excited by the electrons themselves in a corrugated structure allows for precise control of the electron beam phase space. We have performed the first utilization of a corrugated structure as a beam linearizer in the operation of a seeded free-electron laser driven by a 140 MeV linear accelerator at the SDUV-FEL, where a gain of ~10 000 over spontaneous emission was achieved at the second harmonic of the 1 047 nm seed laser, and a free-electron laser bandwidth narrowing by 50% was observed, in good agreement with the theoretical expectations.

Reference

1. Zhang T, Deng H, Chen J, *et al*. Polarization control proposal for Shanghai deep ultraviolet free electron laser[J]. Nuclear Instruments and Methods in Physics Research Section A: Accelerators, Spectrometers, Detectors and Associated Equipment, 2012, **680**: 112−116.
2. Deng H, Zhang T, Feng L, *et al*. Polarization switching demonstration using crossed-planar undulators in a seeded free-electron laser[J]. Physical Review Special Topics-Accelerators and Beams, 2014, **17**(2): 020704.

Deng H, Zhang M, Feng C, *et al*. Experimental demonstration of longitudinal beam phase-space linearizer in a free-electron laser facility by corrugated structures[J]. Physical Review Letters, 2014, **113**(25): 254802.

上海质子治疗装置治疗头设计

电子学组

电子学组在 2015–2016 年主要承担了上海质子治疗装置治疗头设计（包括束配系统和治疗控制系统）。治疗头的主要功能是将加速器引出束流转换为治疗束流，并将治疗束流准确照射在目标组织上。

我们采用点扫描作为治疗头的技术路线，在治疗头的结构与参数设计中，我们需要根据目前的设计水平和工艺加工能力，能够保证实现所设计的治疗指标，并且确保系统能够长期稳定运行。同时，通过结构和关键部件的优化设计，使系统关键参数（如扫描速度、束斑尺寸）在国外已有的质子治疗装置中属于领先水平，确保投入运行后仍然可以达到当时的国际先进水平。

2016 年 12 月–2017 年 3 月进行了固定束扫描治疗头样机的安装与部件测试。部件测试包括扫描磁铁静磁测试、扫描磁铁动态测试、电离室离线测试和治疗头机械变形测试。

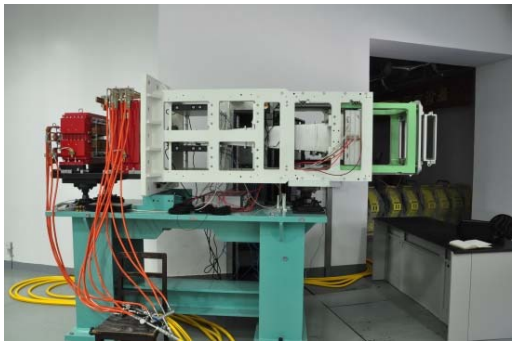

扫描磁铁静磁测试的磁场均匀性满足设计指标；在设计的扫描磁场范围内，扫描磁铁没有进入饱和区；扫描磁场沿束流方向分布符合计算。

为了测量扫描磁场动态性能，我们搭建了扫描磁场动态测试平台。采用治疗头扫描磁场测量模块，霍尔探头采用瑞士 SENIS 公司 I1A-0YK01F-Z02T2K5Z，数据采集与电源控制指令同步。磁场测量系统的模拟带宽为 4 kHz，数据采样率为 50 kHz，磁场测量分辨率为±0.3 Gauss。扫描磁场动态测试结果如下图所示：

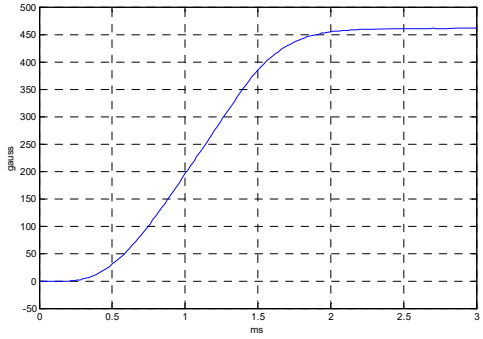

剂量电离室设计高压为−2 500 V。剂量电离室电子学量程为 0~3 400 nA；850 Hz 模拟带宽；75 Hz 采样率。采用激光测距仪测量剂量电离室膜窗平整度，如下图所示。

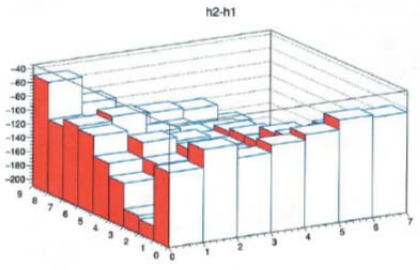

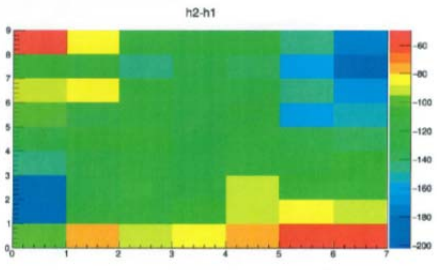

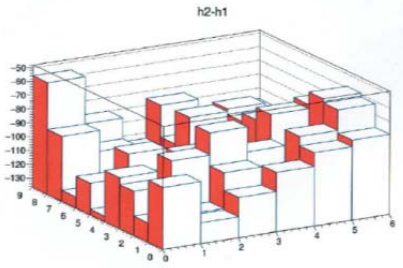

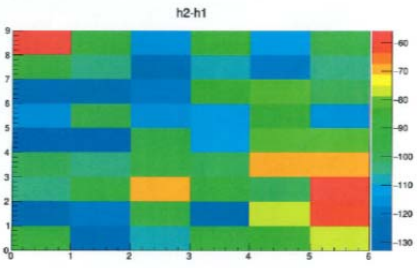

次剂量电离室膜窗平整度在膜窗信号面积内为±20 μm；在整个膜窗面积内为±60 μm。主剂量电离室膜窗平整度在膜窗信号面积内为±30 μm；在整个膜窗面积内为±40 μm。

剂量电离室电子学积分非线性为±0.04 nA，即好于 0.07%。剂量电离室加载−2 500 V 高压后的实测分辨率为 0.14 nA (RMS)。测试结果如下图所示。

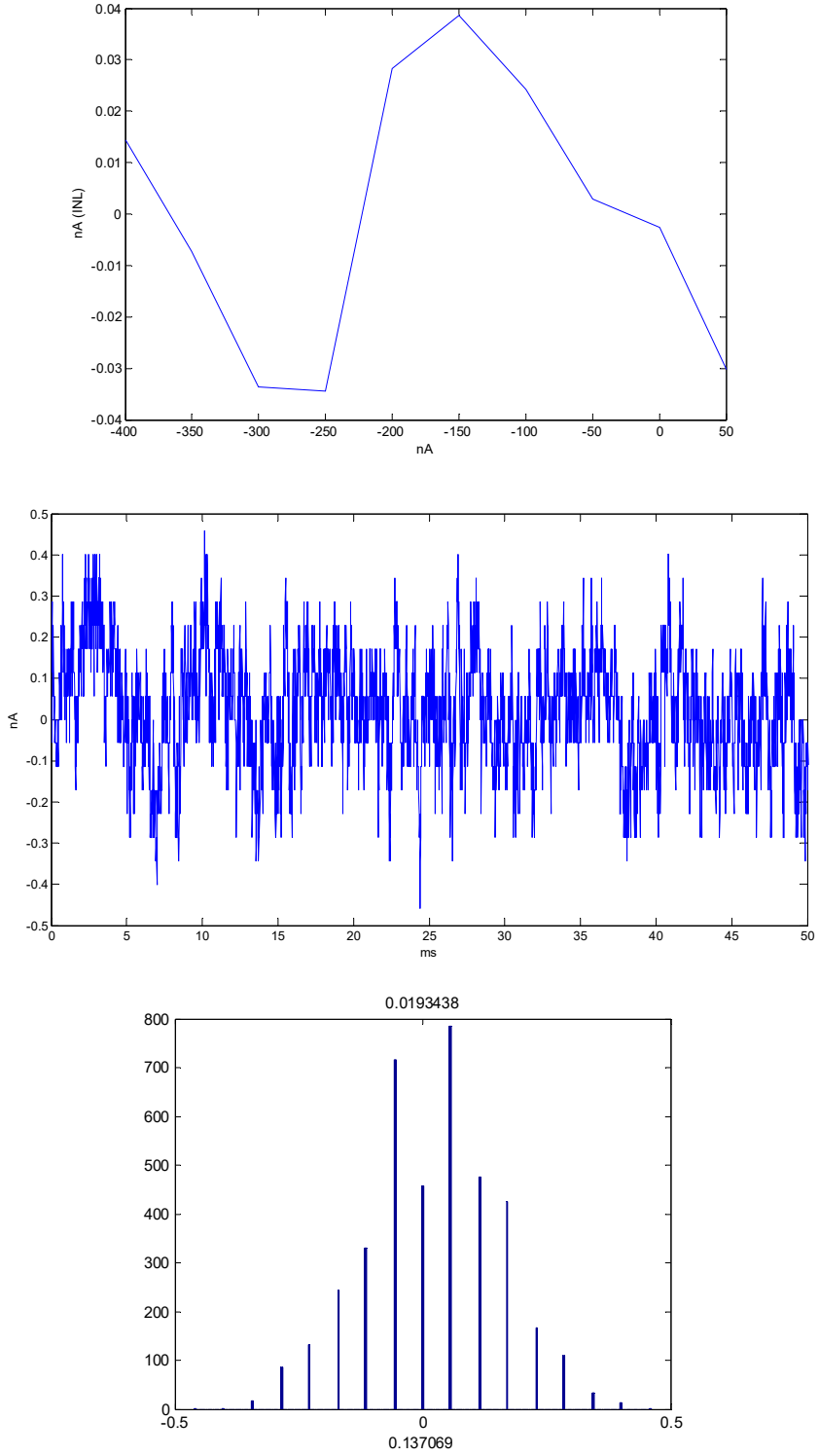

剂量电离室噪音本底

治疗头部件测试结果表明治疗头实测结果都满足设计指标。

Electronics group

Electronics group

Electronics group mainly undertook the design of the treatment head for the SAPT from 2015 to 2016, including the beam delivering system and treatment control system. The main function of the treatment head is to convert the beam extracting from the accelerator to the treatment beam and focus the treatment beam on the target tissues correctly.

We had adopted the spot-scanning technique for our treatment head. In this way, we have designed the structure and parameters of the treatment head according to current design level and process capability so that we can ensure the designed treatment specifications to be achieved and the system to run stably in a long term. Meanwhile, through the optimum design for the structure and the critical components, we can make the key parameters of the system, such as the scanning speed and the size of the beam spot, keep the leading level in the existing proton treatment facilities overseas and make sure that the treatment head can also achieve the international advanced level after being put into operation.

We had installed the prototype of the scanning treatment head for the fixed beam and tested the components from December of 2016 to March of 2017, including the static magnetic tests of the scanning magnet, the dynamic tests of the scanning magnet, the off-line tests of the ionization chamber and the mechanical deformation tests of the treatment head.

For example, the magnetic uniformity for the static magnetic test of the scanning magnet had met the design criteria; the scanning magnet was not in the saturation region in the range of the designed scanning magnetic field; the distribution of the scanning magnetic field along the beam direction was in accordance with the calculation.

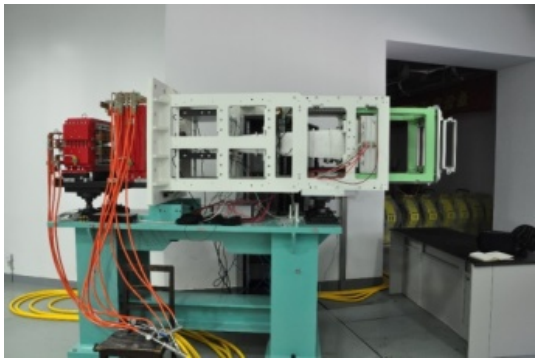

We established a dynamic test platform of the scanning magnetic field to measure the dynamic properties of the scanning magnetic field. First of all, we used a measuring module of the scanning magnetic field of the treatment head. And then, we adopted the product of SENIS (a Swiss company), that the model is I1A-0YK01F-Z02T2K5Z, as the Hall probe. Finally, we synchronized the data acquisition with the power control instruction. The specific parameter setting is as follows: the analog bandwidth of the magnetic measuring system was 4 kHz; the data sampling rate was 50 kHz; the magnetic field measurement resolution was ±0.3 Gauss. The following figure shows the dynamic testing result of the scanning magnetic field:

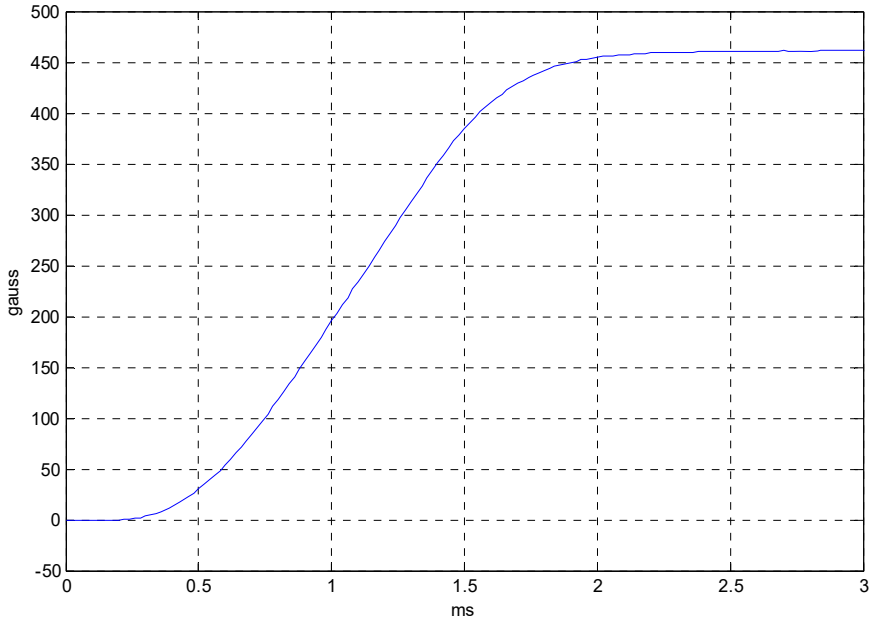

The designed high voltage of the dose ionization chamber was -2 500V, and the electronics range of the dose ionization chamber was 0–3 400 nA; also the analog bandwidth was 850 Hz and the acquisition rate was 75 kHz. We used the laser distance measuring instrument to measure the flatness of the film window as below.

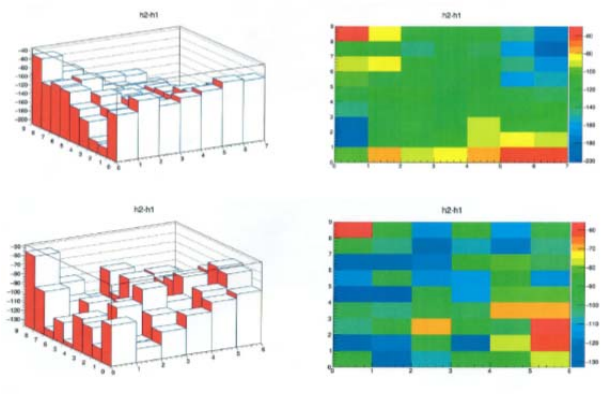

On one hand, the flatness of the film window of the sub dose ionization chamber in the film window signal area was ±20 μm; the flatness in the whole film window area was ±60 μm. On the other hand, the flatness of the film window of the main dose ionization chamber in the film window signal area was +/- 30 μm; the flatness in the whole film window area was ±40 μm.

The electronics integral nonlinearity of the dose ionization chamber was ±0.04 nA, which is better than 0.07%. After the dose ionization chamber was loaded high voltage of -2 500V, the measured resolution was 0.14 nA (rms). The test result is as below.

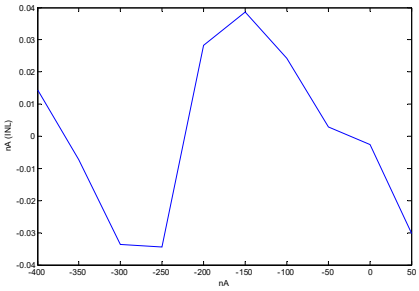

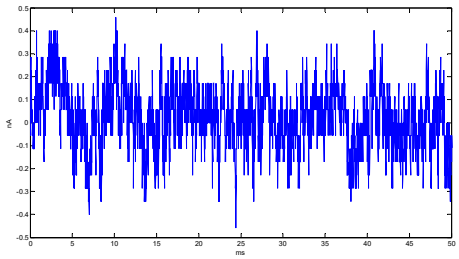

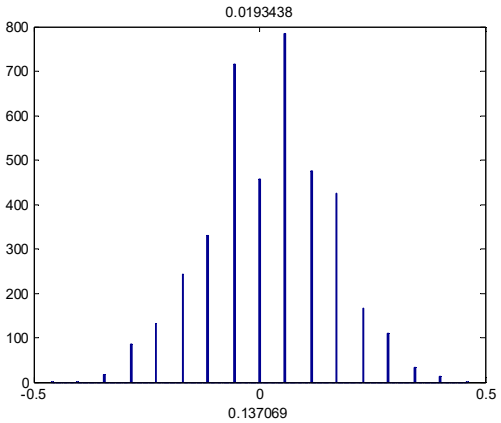

The background noise of the dose ionization chamber

The test results of the components of the treatment head show that the measured results of the treatment head all meet the design specifications.

基于平面绝缘芯变压器的新型高压电源研究

应用加速器研究室

PICT 电源简介

绝缘芯平面变压器(Planar Isolated Core Transformer, PICT)是一种大功率开关电源变压器，核心功率转换部分由逆变电路和 PICT 构成。PICT 的磁芯采用铁氧体材料，次级绕组和整流电路布置在印刷电路板(PCB)上。多层 PCB 输出串联后可获得数百千伏的直流输出。

PICT 电源具有体积小、功率密度高、储能低、可靠性高和组装性能好的许多优点，有望成为 1 MV 以下大功率直流高压电源的重要发展方向[1-3]。

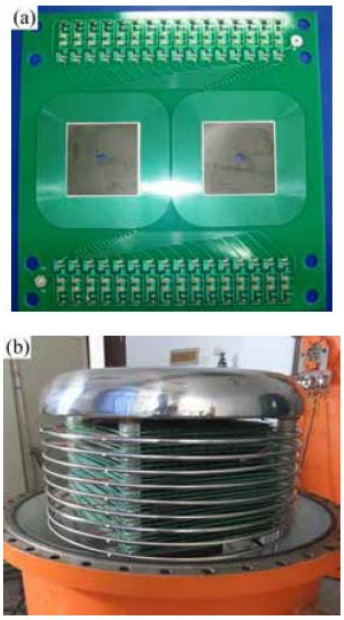

图 1 PICT 电源 (a) PCB 单元，(b) PICT 样机

PICT 调试及优化[1,4]

我们建造的电源其设计指标为：初级线圈匝数 N_p=5，次级线圈匝数 N_s = 1728，工作频率 f =33 kHz，输入电压范围 20~380 V，方波占空比 δ=0.45，铁氧体相对磁导率 μ_r=2400，初级电感量 L_p=70 μH，最大输出电压 U_{out}=300 kV，最大输出电流 I_{out}= 100 mA，PCB 板间耐压 V_{PCB} = 25 kV。

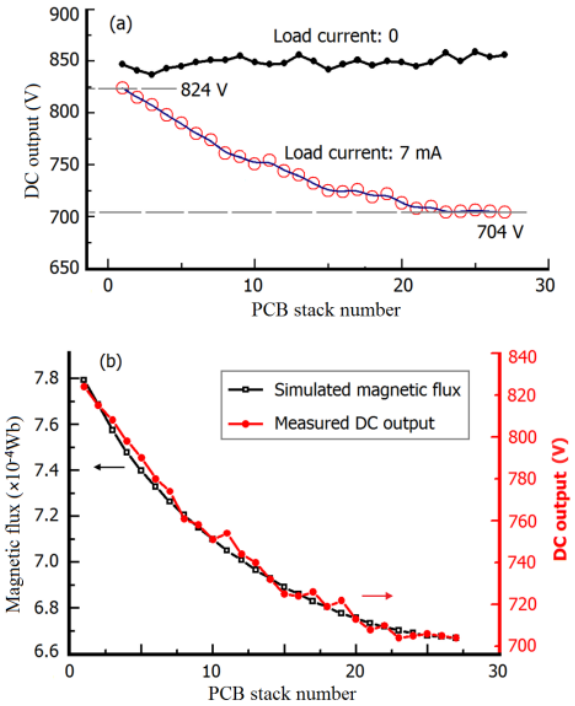

图 2 直流输出测试和各级磁通仿真

测试结果表明通过次级线圈并联补偿电容的手段可以改善各层线圈输出电压的均匀性。

参考文献

1. Kang C, Liu Y H, Li D M. Analysis of output voltage on a planar insulating core transformer[J]. Nuclear Science and Techniques, 2012, **23**(1): 15-18.
2. 康成, 刘永好, 黄建鸣, 等. 绝缘磁芯平面变压器的漏磁补偿[J]. 强激光与粒子束, 2012, **24**(7): 1595-1598.
3. 田佳甲, 刘永好, 张金玲, 等. 基于绝缘芯平面变压器的新型高压直流电源的调试及输出特性[J]. 核技术, 2015, **38**(7): 44-48.
4. Tian J J, Liu Y H, Li R, *et al*. Magnetic flux leakage analysis and compensation of high-frequency planar insulated core transformer[J]. Nuclear Science and Techniques, 2015, **26**(3): 21-25.

Research on a Novel HV Power Supply Based on Planar Insulated Core Transformer

Department of Applied Accelerator

Introduction of PICT

Planar isolated core transformer (PICT) is a kind of high power switching power supply transformer. Its core structure power conversion is PICT circuit driven by an inverter. The magnetic core of the PICT is made of ferrite material, and the secondary winding and rectifier circuit are arranged on the printed circuit board (PCB). We can obtain hundreds of kV high-voltage DC output by multilayer PCB output in series.

The PICT power supply has many advantages, such as small size, high power density, low energy storage, high reliability and good assembly performance[1-3]. It is expected to become the important development direction of high-power and high-voltage DC power supply below 1 MV.

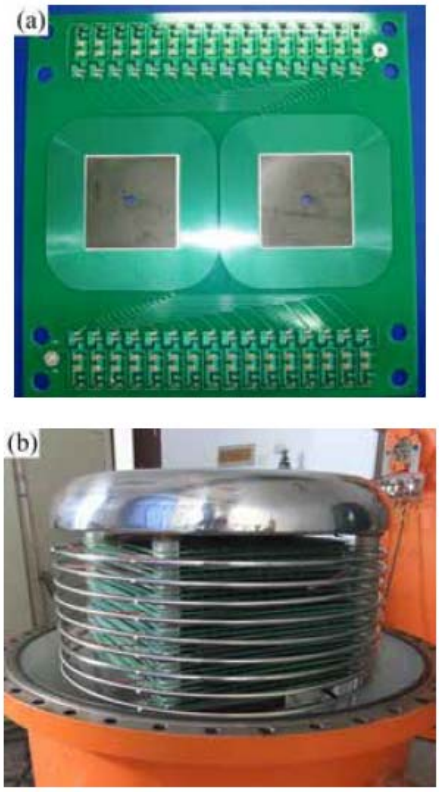

Fig.1 PICT power supply (a) PCB unit, (b) prototype.

Commissioning and optimization for PICT[1,4]

The design specifications of the power we build are as follows: primary coil turns N_p = 5, driving frequency f =33 kHz, input voltage range is about 20~380 V, duty ratio of the square wave δ=0.45, relative permeability of the ferrite μ_r = 2400, primary inductance L_p=70 μH, maximum output voltage U_{out}=300 kV, maximum output current I_{out}=100 mA and insulation voltage between PCB V_{PCB}=25 kV.

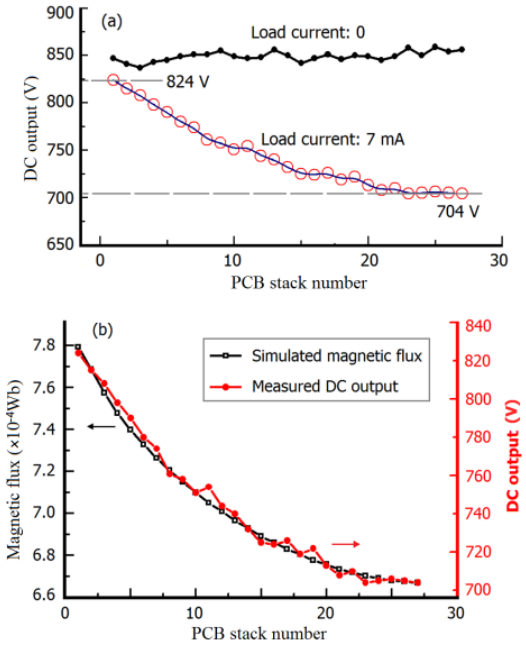

Fig.2 Test of the DC output and magnetic flux simulation for each layer of PCB

The test results show that the output voltage uniformity of each coil can be improved by means of parallel compensation capacitor to the secondary coil.

Reference

1. Kang C, Liu Y H., Li D M. Analysis of output voltage on a planar insulating core transformer[J]. Nuclear Science and Techniques, 2012, **23**(1): 15-18.
2. Kang Cheng, Liu Yonghao, Huang Jianming, *et al.* Compensation of leakage flux on insulated core flat winding transformer[J]. High Power Laser and Particle Beams (Chinese), 2012, **24**(7): 1595-1598.
3. Tian Jiajia, Liu Yonghao, Zhang Jinling, *et al.* Test and output characteristics research on high voltage DC generator based on High-frequency planar insulated[J]. Nuclear Techniques (Chinese), 2015, **38**(7): 44-48.
4. Tan J J, Liu Y H, Li R, *et al.* Magnetic flux leakage analysis and compensation of high-frequency planar insulated core transformer[J]. Nuclear Science and Techniques, 2015, **26**(3): 21-25.

TMSR

钍基熔盐堆设计平台

反应堆物理部

背景

本课题面向钍基熔盐堆核能系统先导专项需求，建设 TMSR 设计计算分析能力，为系列钍基熔盐堆提供设计工具和平台。课题科研进展主要在熔盐堆设计分析软件研发方面，先后完成了适用于液态燃料熔盐堆的 RELAP5 程序二次开发、基于 DRAGON 的宏观群常数加工流程、基于 GPU 加速的固态堆的堆芯中子时空动力学程序 GAND、多孔介质热工水力 GPU 并行计算程序 GATH、并联通道核热耦合稳态分析程序等，并完成了 TMSR-LF1 软件适用性分析初步研究。

熔盐堆确定论分析软件研发

2015、2016 年度熔盐堆确定论分析软件研发以具体功能软件二次开发或研发为主。针对 RELAP5 软件进行了二次开发，植入了包含缓发中子先驱核迁移项的点堆中子动力学模型，使其适用于液态燃料熔盐堆的瞬态分析，随后用 MSRE 基准题对其进行了验证，如图 1 所示。

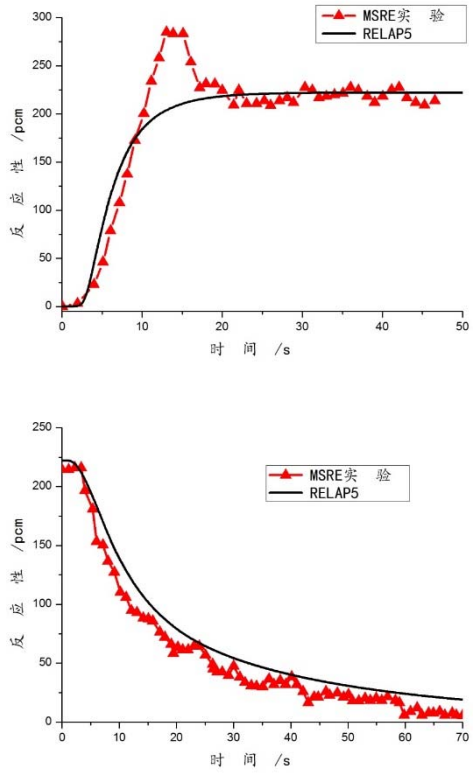

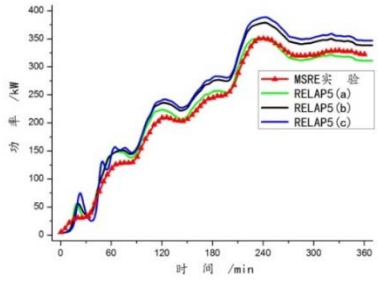

图 1 MSRE 零功率启泵(上)、停泵(中)及自然循环(下)基准题验证

基于开源程序 DRAGON 建立 TRISO 颗粒燃料球物理模型，完成了固态燃料球床熔盐堆的宏观群常数加工流程，针对高温气冷堆的 k-inf 基准题计算表明，在此流程下使用 DRAGON 加工的宏观群常数与 VSOP99、APOLLO2 等程序加工结果一致，相对偏差在 1.05 %以内，如表 1 所示。

表 1 DRAGON 程序宏观群常数加工流程的高温气冷堆燃料球 k-inf 基准题验证

基准程序	核数据库	基准 k-inf	本工作 k-inf
VSOP99	ENDF/B-V	1.5060	1.5180 (+0.80%)
SCALE	ENDF/B-V	1.5075	1.5180 (+0.70%)
MCNP-4B	ENDF/B-6	1.5018	1.5164 (+0.97%)
APOLLO2	JEF2.2	1.5223	1.5203 (-0.13%)
WIMS9	JEF2.2	1.5176	1.5203 (+0.18%)
MONK9	JEF2.2	1.5364	1.5203 (-1.05%)

基于 GPU 加速的固态堆的堆芯中子时空动力学程序 GAND 以多维多群瞬态及稳态中子扩散理论为基础，结合 GPU 并行计算技术，可快速求解固态堆堆芯的中子通量及功率分布，可用于堆芯稳定运行工况下的及事故工况下的安全分析。GAND 程序内部采用的物理数学模型基于多群中子扩散理论，TMSR-SF1 堆芯稳态的中子通量密度分布及功率密度分布如图 2 所示。

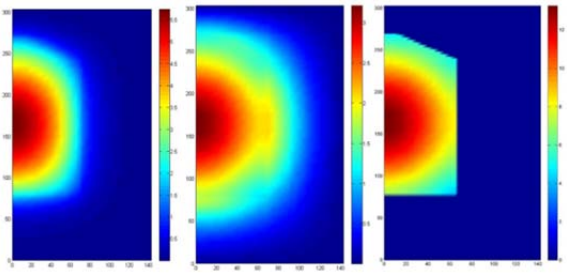

图 2 TMSR-SF1 堆芯稳态的快群(左)、热群(中)中子通量密度分布及堆芯活性区功率密度分布(右)

GPU 并行计算堆芯热工水力程序 GATH 基于计算流体力学方法，采用非热平衡多孔介质模型建立堆芯结构，采用 SIMPLEC 算法求解流体动量方程。为了更准确地模拟球床内流体的热弥散现象，该程序引入多孔介质的湍流模型。TMSR-SF1 堆芯冷却剂温度及燃料温度如图 3 所示。

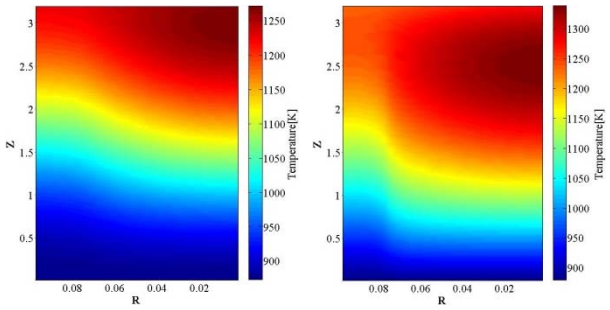

图 3　TMSR-SF1 堆芯冷却剂温度(左)及燃料温度(右)

GAND 和 GATH 程序均采用 GPU 加速；其中中子动力学程序 GAND 采用不同求解算法时的加速比如图 4 所示；热工水力学程序 GATH 计算不同规模网格模型时的加速比如图 5 所示。

并联通道核热耦合稳态分析程序采用一维模型求解燃料盐在各并联通道内的水力学问题，计算压强平衡条件下的流量和压降，采用三维传热模型计算固相区域（即石墨组件）传热，并充分考虑各燃料通道之间的热传导。该程序用于 TMSR-LF1 堆芯的热工水力稳态分析，堆芯活性区石墨与熔盐的温度分布如图 6 所示。

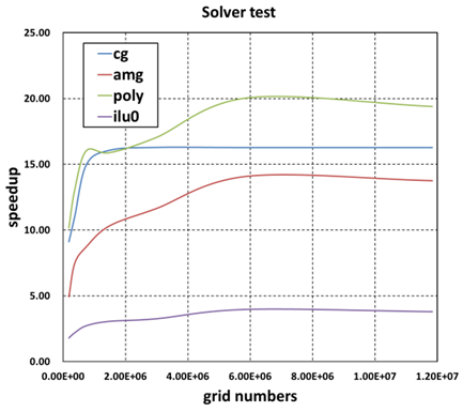

图 4　GAND 采用不同求解算法时的加速比

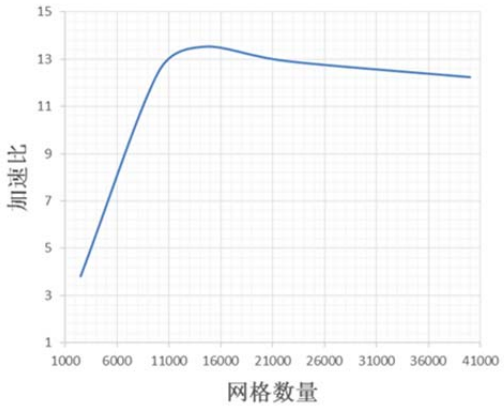

图 5　GATH 计算不同规模网格模型时的加速比

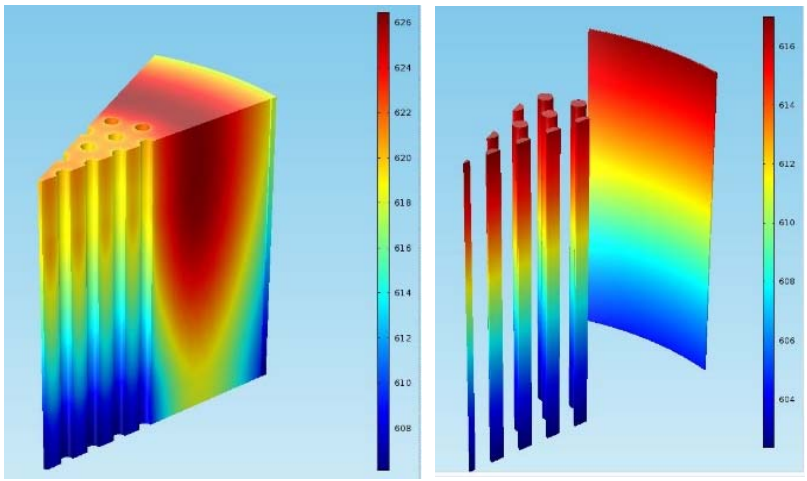

图 6　TMSR-LF1 堆芯活性区石墨(左)与熔盐(右)的温度分布

在 2014 年度完成的《10MW 固态燃料钍基熔盐实验堆（TMSR-SF1）设计与安全分析软件适用性研究报告》工作基础上，2015 年度完成了 TMSR-LF1 的设计与安全分析软件适用性初步研究。与 TMSR-SF1 软件适用性研究相比，TMSR-LF1 软件适用性研究的范围有所变化，在堆物理设计及分析、热工水力设计及分析、结构力学计算与抗震分析、放射性源项与辐射计算、安全分析五个方面之外，增加了燃料循环相关设计分析软件的适用性研究。课题完成了 TMSR-LF1 软件适用性研究的框架设计，参照 TMSR-SF1 软件适用性研究完成了 TMSR-LF1 设计分析软件需求和完

备性研究，并完成了初步的软件适用性研究报告，内容涵盖 TMSR-LF1 的核设计、燃料循环设计、热工水力设计和瞬态分析四个主要方面；涉及到的程序包括 MCNP、SCALE、SRAC、ORIGEN-2、ORIGEN-S、MOCBurnup、ANSYS、CINSF1D 等主要设计分析程序。模型方面主要包括 TMSR-LF1 各版本的堆芯初步设计、TMSR-LF1 系统设计、TMSR-LF1 回路关键部件设计、TMSR-LF1 燃料循环设计等；数据方面包括核数据、材料数据、热物性数据。

TMSR 超算系统运行

TMSR 超算系统部署了反应堆中子学、热工水力学、辐射防护、材料科学等学科的计算分析软件。截至 2015 年底平台用户 186 余人，总共运行近 34.8 万个作业，总作业时间 1600 万处理器小时；截至 2016 年底平台用户 202 人，总作业数 42.7 万条，总作业时间 3 000 万处理器小时。2015、2016 年度超算系统 CPU 资源利用率分别如图 7、图 8 所示。

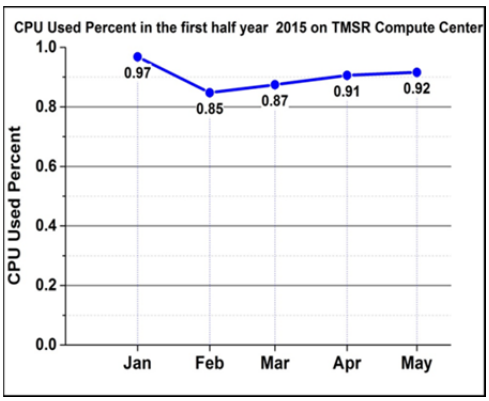

图 7 TMSR 超算系统 2015 年度 CPU 资源利用率

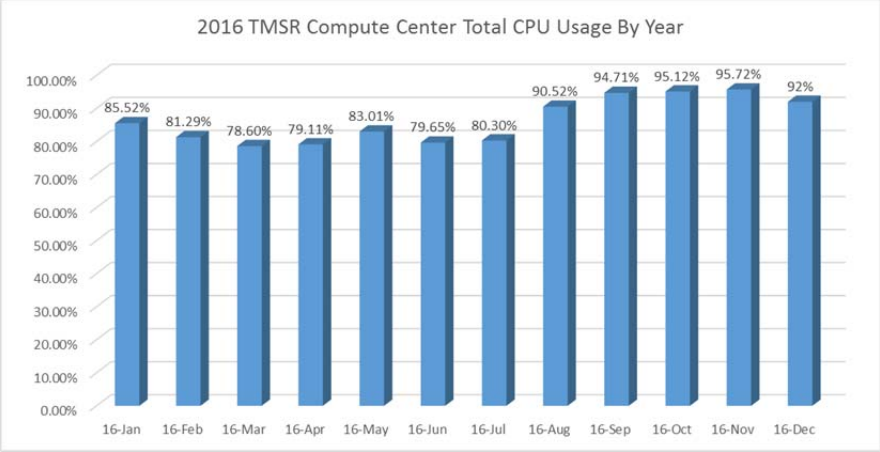

图 8 TMSR 超算系统 2016 年度 CPU 资源利用率

2016 年中，TMSR 超算系统针对不同的需求做了相关技术的部署，具体包括：1) PBS 作业调度系统的 HOOK 技术；2) 为软件迁移做准备的 YUM 数据源；3) 基于 GPU 的调度队列配置 VNODE 技术。配置 VNODE 技术后，混合计算节点的 CPU 计算资源得到充分挖掘，进一步拆分出 2CPU 核心+2GPU 单元运算资源用于 GPU 并行计算应用，剩余 10CPU 核心运算资源可归入 CPU 资源池。

TMSR Design Platform

Department of Reactor Physics

Background

Driven by needs of TMSR project, the TMSR Design Platform sub-project has vision to provide design codes and tools for design & analysis of Molten Salt Reactors (MSR), as well as long-term ability build-up. The sub-project advances mainly in reseach and development of MSR design & analysis software, such as modification of neutron kinetics model in RELAP5, method and procedure of macroscopic group constant generating based on DRAGON, GPU accelerated neutron spatial-temporal kinetic program for the core of solid fueled MSR (GAND), parallel thermal-hydraulic GPU program for the porous media core (GATH), neutronic thermal-hydraulic coupled program for steady state analysis of multi-channel liquid-fueled MSR core. Also, preliminary study on the applicability of designing softwares for liquid-fueld MSR has been conducted.

Research and development of the deterministic analysis code package for MSR

During year 2015 and 2016, the R&D of the deterministic analysis code package for MSR focused on development or re-development of code and software with specific physical functions. Redevelopment of RELAP5 has been done, by incorporating a modified point kinetic model with drift terms of delayed neutron precursors; by such a modification, the RELAP5 program is capacitated with transient-state analysis function of liquid-fueld MSR core. The modified RELAP5 program is tested with MSRE benchmarks, as shown in Fig.1.

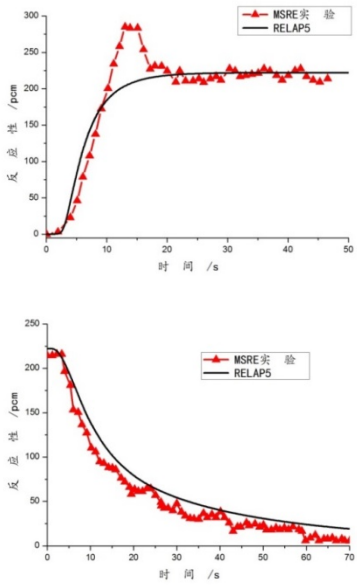

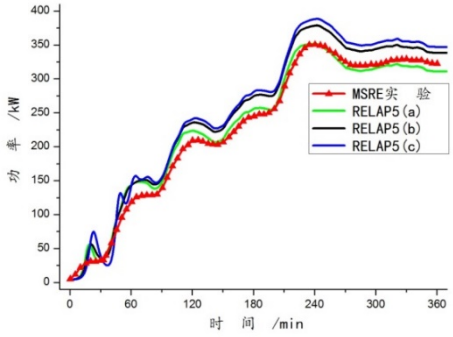

Fig.1 MSRE benchmarks for modified RELAP5. Top down: , zero-power pump start-up, zero-power pump coast down, and natural circulation.

The TRISO fuel-pebble adopted by solid-fuel MSR has been modeled and the procedure of macroscopic group constant (MaGC) generating based on open-source neutronic program DRAGON has been established. Benchmark calculations of k-inf for High Temperature Gas-cooled Reactor (HTRG) fuel pebble show that the DRAGON-based macroscopic group constants are equivalent to constants generated by other programs such as VSOP99, APOLLO2, etc., the relative deviations are within 1.05%, as shown in Table 1.

Tabel 1 k-inf benchmarking of DRAGON-based MaGC generating of HTGR fuel-pebble

Benchmark Program	Nuclear Data Lib	Benchmark k-inf	k-inf by DRAGON
VSOP99	ENDF/B-V	1.5060	1.5180 (+0.80%)
SCALE	ENDF/B-V	1.5075	1.5180 (+0.70%)
MCNP-4B	ENDF/B-6	1.5018	1.5164 (+0.97%)
APOLLO2	JEF2.2	1.5223	1.5203 (-0.13%)
WIMS9	JEF2.2	1.5176	1.5203 (+0.18%)
MONK9	JEF2.2	1.5364	1.5203 (-1.05%)

A GPU accelerated neutron spatial-temporal kinetic program for the core of solid fueled MSR, GAND, has been developed. The GAND program realizes 3D multi-group neutron diffusion model, and is able to perform both steady-state analysis and transient-state analysis for solid-fueled MSR core. The flux-density distributions of fast-neutron (left), thermal-neutron (middle) and power-density (right) for a steady-state TMSR-SF1 core are shown as Fig.2.

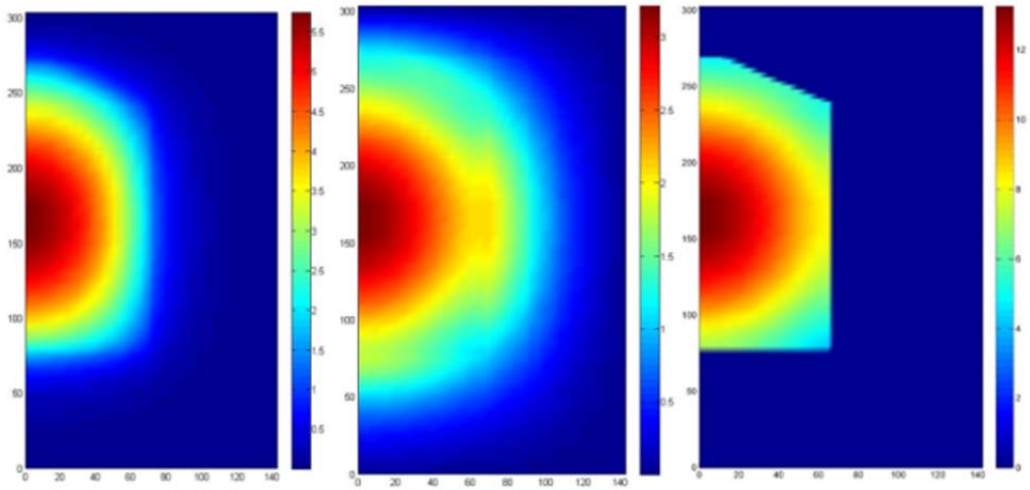

Fig.2 The neutron flux and power density of TMSR-SF1 core, calculated by GAND

A parallel thermal-hydraulic GPU program for the porous media core, GATH, has been developed. The GATH program is based on computational fluid dynamic (CFD) methods, and a non-equilibrium porous media model is chosen to represent the pebble-bed core of solid-fuel MSR. The distributions of coolant temperature (left) and fuel temperature (right) of TMSR-SF1 core are shown as Fig.3.

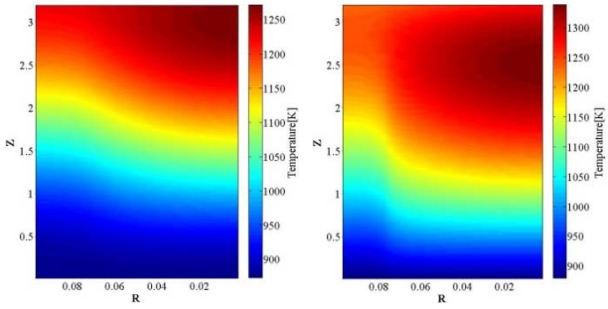

Fig.3 The temperature distributions of TMSR-SF1 core, calculated by GATH

Both GAND and GATH uses GPU accelerating technique. The speed-up ratio using different algorithms in GAND is shown as Fig.4. The speed-up ratio solving meshes of different scale in GATH is shown as Fig.5.

A neutronic thermal-hydraulic coupled program for steady state analysis of multi-channel liquid-fueled MSR core has been developed. A 1D model is adopted to calculate hydraulic features (flow rate, pressure drop, etc.) of fuel salt in each channel, and the hydraulic calculations on all channels are ballenced assuming that the pressure drops on every channel are equal. A 3D model is adopted to solve the thermal conduction in solid graphite structures using unstructured meshes. The program is coupled to neutronic program SCALE which provides power-density and takes temperature distribution as feed-back. The program is applied in the steady-state analysis for TMSR-LF1, the temperature distributions of graphite zone (left) and fuel zone (right) are shown as Fig. 6.

Based on the technical report “Studies on applicability of design and analysis softwares for a 10 MW solid-fueld thorium-based molten salt experimental reactor (TMSR-SF1)”, a preliminary study on applicability of design and analysis softwares for TMSR-LF1 has been made. Comparing to the software applicability study for TMSR-SF1, scope of the software applicability study for TMSR-LF1 is expanded, the applicability of software used in fuel cycle simulation and investigation. The framework of software applicability study for TMSR-LF1 is established, covering nuclear design, fuel cycle design, thermal-hydraulic design and transient analysis; major programs and codes are listed, such as MCNP, SCALE, SRAC, ORIGEN-2, ORIGEN-S, MOCBurnup, ANSYS, CINSF1D, etc; important models are included, such as core models, hydraulic system models, loop models, fuel handling models, etc; fundamental data set are suggested, such as nuclear data, material data, and thermophysical properties.

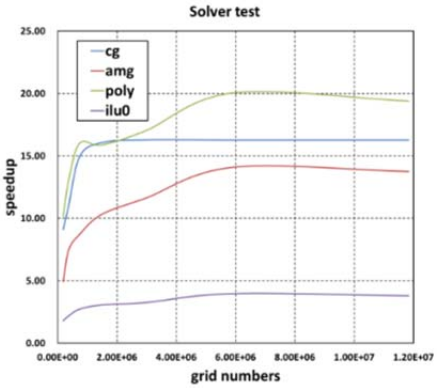

Fig.4 GAND speed-up ratio, using solvers with different algorithms

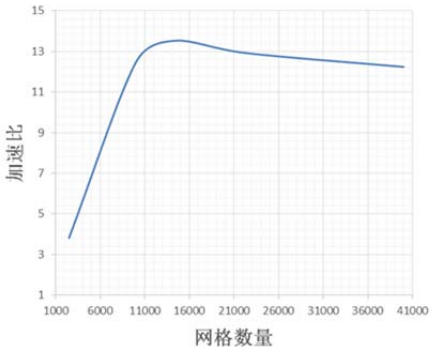

Fig.5 GATH speed-up ratio, solving meshes of different scales

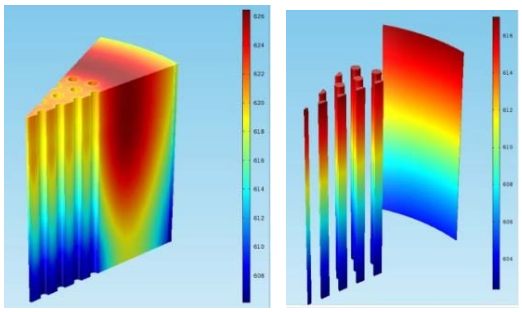

Fig. 6 Temperature distributions of TMSR-LF1 core

Operation of TMSR Super Computer System

Numerous softwares and codes of reactor neutronics, thermal-hydraulics, shielding, and ma-terial scince are deployed on TMSR Super Computer System (TMSR SCS). By the end of FY 2015, numbers of total user accounts on TMSR SCS reached 186, more than 348,000 computing jobs were executed, the overall walltime reached 16,000,000 processor hours; by the end of FY 2016, number of total user accounts on TMSR SCS reached 202, more than 427,000 computing jobs were executed, the overall walltime reached 30,000,000 processor hours. The CPU load ratio of TMSR SCS during FY 2015 and FY 2016 are shown as Fig.7 and Fig.8, respectivly.

During year 2016, several new IT features are incorporated on TMSR SCS, including: 1) HOOK technique for PBS job scheduling, 2) YUM data source for software migration and 3) VNODE technique for GPU queue scheduling. The VNODE technique releases the CPU resources in each GPU hardware nodes, the GPU programs can run on a virtual 2 CPU+2 GPU configuration, and the rest 10 CPU are added to the CPU resource pool.

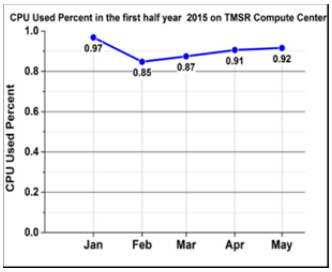

Fig.7 CPU load reatio of TMSR SCS, FY2015

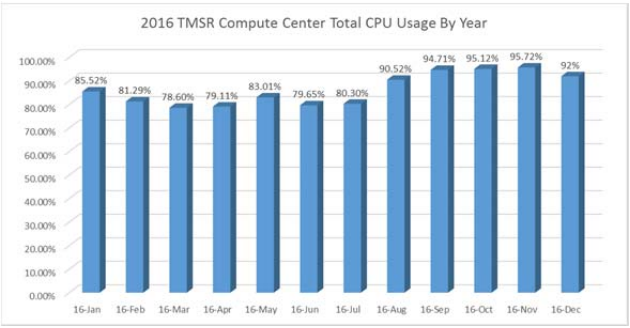

Fig.8 CPU load reatio of TMSR SCS, FY2016

TMSR

背景

钍铀核安全与工程项目分为钍基熔盐核能系统核安全、辐射安全、钍铀放射性三废处理、钍铀职业健康与环境影响、钍基熔盐实验堆安全审评关键技术研究等任务。 2015–2016 年度，项目主要目标是 10 MW 固态钍基熔盐实验堆（简称 TMSR-SF1）的安全研究，各任务在 2013–2014 年的基础上进一步深化，均取得了实质性进展。

钍基熔盐核能系统核安全

2015–2016 年度，钍基熔盐核能系统核安全课题进展主要包括：TMSR 研究堆分类论证、TMSR 研究堆安全设计准则、事故分析、固态熔盐堆初设及安全分析报告、熔盐自然循环实验研究五个方面。

在 TMSR 研究堆分类论证方面，开展了将固态熔盐实验堆和液态熔盐实验堆论证为二类堆的工作。两份安全分类报告已通过正式审评，获得国家核安全局正式批复文件，明确 TMSR 两个实验堆可归为二类堆范畴。

在 TMSR 研究堆安全设计准则方面，10 MW 固态燃料熔盐堆安全相关的安全设计准则已由苏州核安全中心进行了评阅，依据核安全中心审查意见进行了修改。其将作为编制审评原则的基础性文件，已达到初步设计阶段的深度。

在 TMSR 研究堆事故分析方面，开展了固态熔盐堆相关的事故分析计算、概率风险评价等工作。完成超设计基准事故分析。通过这几方面的工作，具备了开展固态熔盐堆最终安全分析的能力。

在 TMSR 初设阶段事故分析及安分报告方面，依据 2015 年度经专家评审的《TMSR-SF1 初步安全分析报告格式与内容》，开展了 TMSR-SF1 初步安全分析报告的撰写工作。本年度共撰写初步安全分析报告 14 章内容，完成了除厂址特征外 PSAR 要求的内容。

在 TMSR 熔盐自然循环实验研究方面，2015 年完成了自然循环实验回路调试，并成功连续运行了 1 400 多个小时。2016 年度继续以 NNCL 回路为平台，连续运行了 2 000 多个小时，开展了一系列实验研究工作。取得了较好的进展。

国 家 核 安 全 局

国核安函〔2015〕128 号

关于钍基熔盐实验堆以Ⅱ类研究堆开展前期工作有关问题的复函

中国科学院上海应用物理研究所：

你所《关于钍基熔盐实验堆以Ⅱ类研究堆开展前期工作的请示》（应物发核字〔2015〕6 号）收悉。根据《民用核设施安全监督管理条例》及其实施细则之三，以及研究堆的有关安全规定，我局对你所提交的相关技术资料进行了审查。经研究，函复如下：

一、10MWt 固态燃料钍基熔盐实验堆和 2MWt 液态燃料钍基熔盐实验堆的安全分类论证报告符合《研究堆安全分类（试行）》（国核安发〔2013〕165 号）关于Ⅱ类研究堆的要求。

二、在后续工作中，如反应堆的最终设计方案与申请文件有较大变化，你所应按照有关规定重新向我局提交申请文件。

特此函复。

2015 年 11 月 26 日

图 1 核安全局对 TMSR 二类堆论证批复

钍基熔盐核能系统辐射安全

2015–2016 年度,钍基熔盐核能系统辐射安全课题取得的阶段性研究成果如下：

在 TMSR-SF1 设计方面，与中国核动力研究设计院联合开展了源项、辐射屏蔽、辐射防护与监测、新燃料与乏燃料暂存库的联合设计，共同及自主完成了辐射屏蔽、防护与监测相关的设计准则、方案设计和初步设计(初稿)，提交了 14 份初步设计文件，并完成专家评审，进行了意见的回复与修改。

在 TMSR 嘉定园区在线辐射监测系统方面：完成了相应的测试与验收，实现了对全园区放射性工作场所和园区环境辐射水平的实时监测，为 TMSR 新园区辐射监测系统的设计与建设积累了经验。

在中子物理仿真实验装置辐射防护方面：完成了中子物理仿真实验装置局部屏蔽的设计与建设。

在 TMSR 高温熔盐安全模拟实验系统设计与建设方面，完成了方案设计和初步设计，提交了 13 份初步设计文件，并完成专家评审，正开展设备加工与制造。

此外，还开展了放射性气体气溶胶监测样机相关实验，为熔盐堆辐射安全系统设计提供了有力的

支持。

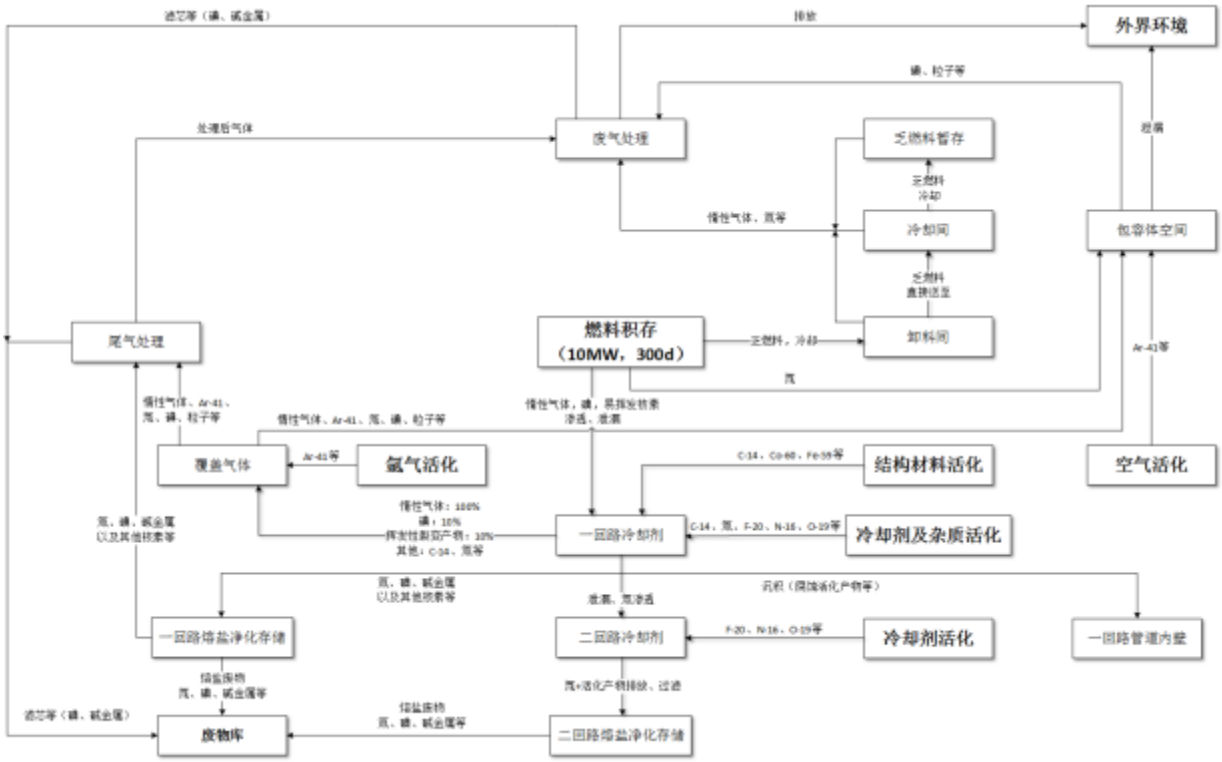

图 2　TMSR-SF1 堆放射性物质迁移途径

钍铀放射性三废处理

2015−2016 年度钍铀放射性三废处理课题主要在 TMSR 热基地放射性三废处理设施初步设计、熔盐堆放射性废物处理工艺基础研究、嘉定园区放射性废物处理设施的运行维护、TMSR 综合仿真实验平台堆仓废气处理这四方面取得了显著性进展，具体如下。

在 TMSR 热基地放射性三废处理设施初步设计方面，与核动力院一所联合开展了初步设计，完成了《TMSR 新园区三废处理设施设计输入》、《TMSR-SF1 标准规范清单-放射性三废处理部分》、《三废处理系统初步设计说明书》、《初步设计图册》、《初步设计设备材料清单以及初步设计概算书（工艺部分）》等。2016 年 6 月 TMSR 组织相关专家对初步设计报告进行了内部评审，联合设计组根据评审意见对初步设计内容进行修改。

在熔盐堆放射性废物处理工艺基础研究方面，关于放射性废物处理的实验研究平台进一步完善，熔盐堆放射性废物处理方法与工艺研究取得显著进展，在含氟废物磷酸盐玻璃/陶瓷固化方法，超临界水氧化处理放射性废液等方面也取得了阶段性研究成果。

在嘉定园区放射性废物处理设施的运行维护方面，嘉定园区放射性废物处理设施的调试、验收与维护工作顺利开展，单工艺设备调试与系统的联合调试均已完成，系统试运行满足设计要求，已达到运行标准，可接收园区内放射性废物。

此外，本课题组提交了 TMSR 综合仿真实验平台堆仓废气处理实验系统初步设计报告，并开展了相关设备的设计、采购与加工等工作。

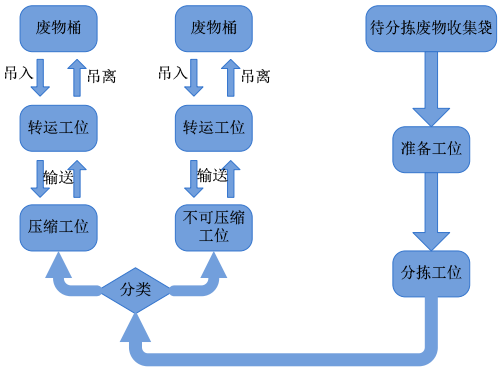

图 3　低放固体废物分拣系统工艺原理流程

钍铀职业健康与环境影响

2015−2016 年度钍铀职业健康与环境影响课题具体取得进展如下：

初步完成了 10 MW 固态钍基熔盐实验堆环境影响评价报告和厂址选择安全分析报告及深度的

专家论证研究工作。2016年度与国家电投共建（热）基地选址工作推进要求，针对钍基熔盐堆（热）基地预选厂址（山东海阳厂址）进行了 TMSR 海阳厂址选址案例、选址审评要求、容量分析等初步研究工作，为 TMSR 预选厂址的确定提供了参考依据。

初步完成了 10MW 固态钍基熔盐实验堆职业安全和职业病危害因素分析及评价研究；

30 份适用于 TMSR 项目的质量保证程序和 1 份实施细则，经过 TMSR 中心审核，已于 2015 年 6 月份批准，编制适用于固态燃料熔盐实验堆（简称 TMSR-SF1）的质量保证程序。

为了规范 TMSR-SF1 设计和建造阶段质量保证活动，质保部门积极参与各个总体、系统、设备部门开展的工程任务。

钍基熔盐实验堆安全审评关键技术研究

本项目邀请环境保护部核与辐射安全中心开展了与固态燃料熔盐堆安全评审相关的课题进行了研究。主要进展情况包括：

根据计算结果及调研的相关资料给定了关键核设计参数反应性系数与停堆裕量的限值。

编写了《固态钍基熔盐实验堆堆芯关键热工限值和具体验收准则研究报告》。

完成研究报告《辐射源项理论模型研究及其在固态钍基熔盐实验堆中适用性研究报告》。

固态燃料熔盐堆的 PSA 以一、二级 PSA 结合的方式开展，以始发事件分析和分组为起点，开展事故序列分析和定量化，以释放类和源项分析为终点，然后将源项分析作为输入开展三级 PSA 分析。

编制完成了《固态燃料钍基熔盐堆随机分布堆芯燃耗计算及功率分布分析评价方法研究》报告、《熔盐堆中多孔介质流动及传热分析方法及评价方法研究》报告。

在研究已有堆型对于氚的计算分析方法方面，结合固态熔盐堆特点，编制完成了《熔盐堆一回路氚源计算方法调研分析》报告。

在初步研究固态燃料钍基熔盐堆系统功能及安全要求分析评价方面，编制完成了《固态燃料钍基熔盐堆系统功能及安全要求分析研究》报告等。

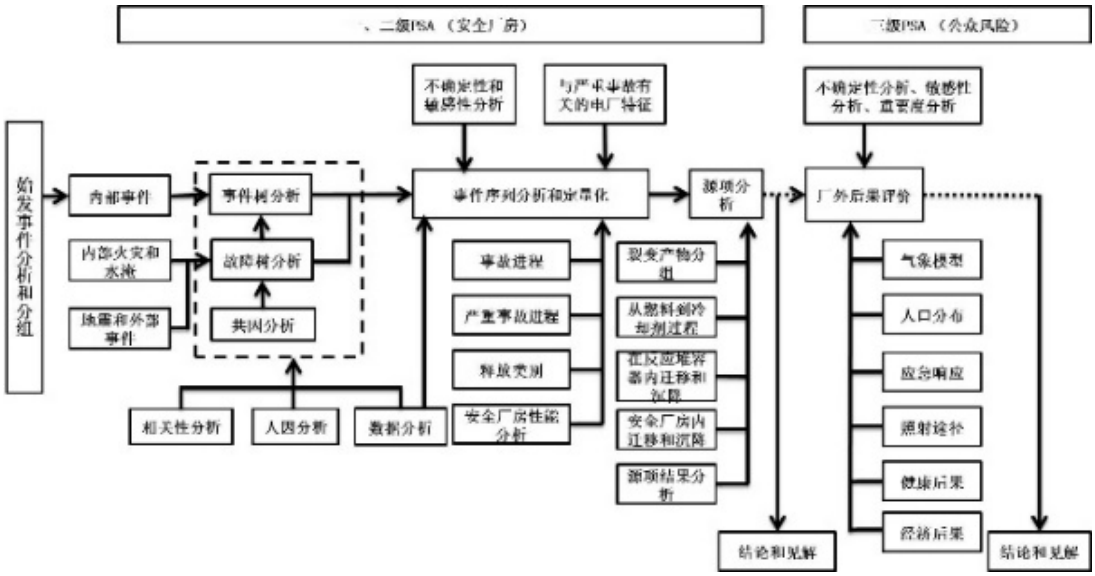

图 4　固态燃料熔盐堆 PSA 框架

TMSR

Background

Thorium-uranium nuclear safety and engineering project is divided into five parts: nuclear safety、radiation safety、radioactive waste treatment、occupational health and environmental impact、key technology research for reactor safety review. From 2015−2016, the main goal of the project is the safety research of 10MW Thorium-based Molten Salt Experiment Reactor with Solid Fuel（TMSR-SF1）. The tasks have gone further on the basis of 2013−2014 years, and substantial progresses have been made.

Nuclear safety

The year 2015 to 2016, the progress of nuclear safety issues mainly include: classification demonstration for MSR, safety design criteria for TMSR-SF1, accident analysis for TMSR-SF1, preliminary design and safety analysis report for TMSR-SF1, experimental research for molten salt natural circulation.

The Thorium-based Molten Salt Experiment Reactor with Solid Fuel (and with liquid fuel)(TMSR-SF1 and LF1)have been proved to be the second type of reactors. Safety classification reports have been formally reviewed by the National Nuclear Safety Administration (NSA), and official approval documents haved been obtained. It's cleared that TMSR-SF1 and LF1 can be classified as second category.

The reactor safety design criteria for TMSR-SF1 was underreviewed by the Suzhou nuclear security center, the revised work was also finished according to the nuclear safety center review.

The accident analysis and probabilistic risk assessment of SF1 were carried out. Beyond Design Basis Accident was completed. The ability to carry out the final safety analysis of the solid state molten salt reactor has received.

According to the《TMSR-SF1 preliminary safety analysis report format and content》, approved by the experts in 2015, TMSR-SF1 preliminary safety analysis report was written. During this period, the 14 chapters of the preliminary security analysis reports have been written, which meet the content of the PSAR requirements except the site characteristis.

The test of natural circulation experiment circuit was completed in 2015, and it has been successfully run for more than 1 400 h. In 2016, it continued to operate for more than 2 000 h and a series of experimental research work were carried out.

Radiation safety

During 2015-2016，the main achievements for radiation safety were as follows:

At the aspect of the TMSR-SF1 design, the source term, radiation shielding, radiation protection and monitoring, temporary storage of new fuel and spent fuel were carried out jointly with Nuclear Power Institute of China (NPIC). The conceptual design and preliminary design were completed (Draft). 14 preliminary design documents were submitted, under the expert's review, the revise was also completed.


国 家 核 安 全 局

Fig.1 The approval by NSA for TMSR

The tests of online radiation monitoring system of TMSR at Jiading Park were completed and the acceptance was received, the real-time monitoring of radiation levels of radioactive workplace and environment of the park in the park was realized.

The design and construction of neutron physics simulation experiment device of partial shielding was completed.

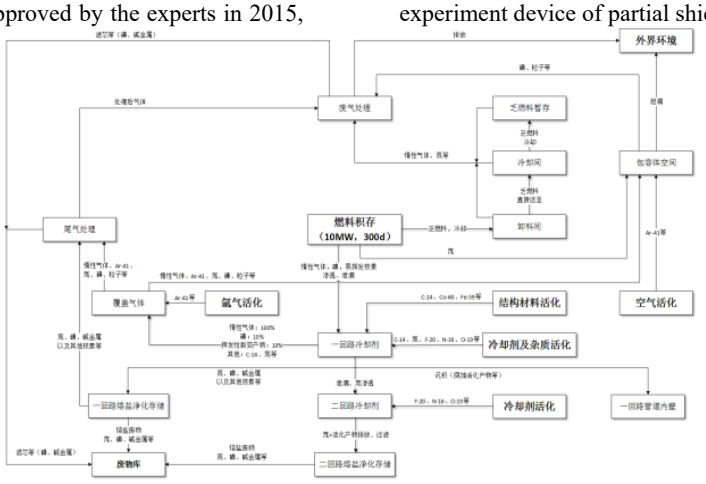

Fig.2 Migration of radioactive material

At the aspects of design and construction of TMSR high temperature molten salt safety simulation experiment system the design and preliminary design which related to radiation safety were completed, 13 preliminary design documents were submitted, and experts review was completed, processing and manufacturing equipment were on the way.

In addition, the related experiments of the radioactive gas aerosol monitoring prototype have been carried out, which provides a powerful support for the design of the radiation safety system of the MSR.

Radioactive waste treatment

During 2015−2016, the significant progress in radioactive waste treatment were as follows: the preliminary design base of radioactive waste treatment for TMSR、waste facilities and technologies for radioactive waste treatment of MSR 、radioactive waste treatment facilities operation and maintenance of Jiading Park、Disposal of waste gas in TMSR-SF0,etc.

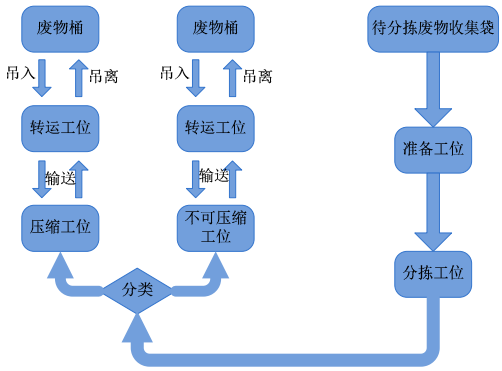

Fg.3 Sorting system process for low-level solid waste

At the preliminary design of radioactive waste treatment facilities at TMSR thermal base, combined with Nuclear Power Institute of China, the preliminary design was carried out.《The design input for TMSR waste treatment facilities》、《Standard specification list for radioactive waste treatment of TMSR-SF1》、《Preliminary design for waste treatment system》、《Preliminary design atlas for waste treatment system》、《Preliminary design of equipment and materials list and preliminary budgetary estimate》 were carried out. In June 2016, an internal review of the preliminary design report was conducted by the TMSR organization, the reply and revise were also carried out.

The experimental platform for radioactive waste treatment was further improved, the molten salt of radioactive waste disposal methods and technology have made significant progress. The curing method of phosphate glass/ceramic for fluorine waste, and supercritical water oxidation for radioactive liquid waste, have also made gradual research results.

The radioactive waste treatment facilities commissioning, inspection and maintenance work were carried out smoothly at Jiading Park, the single equipment and system equipment debugging have both been completed, according to a series of work, the radioactive waste which produced by jiading park can now be received.

In addition, our research group has submitted the preliminary design report of the radioactive gas treatment of TMSR-SF0, and related equipment design, procurement and processing have been carried out.

Occupational health and environmental impact

The specific progresses in the issue of the occupational health and environmental impact of thorium and uranium in 2015-2016 were as follows:

The environmental impact assessment report and the safety analysis report of site selection and the expert demonstration research on depth for of TMSR-SF1 were completed preliminarily. In 2016, combined with State Power Investment Corporation Limited, site selection、review requirements、capacity analysis and preliminary research work for Haiyang location were conducted, which provided a reference for determining the site of the TMSR.

The analysis and evaluation of the occupational safety and occupational hazards of the TMSR-SF1 were preliminarily completed.

30 quality assurance procedures and 1 implementation rules for TMSR projects were approved by TMSR center in June 2015, and the quality assurance procedures for TMSR-SF1 were compiled.

In order to standardize the TMSR-SF1 design and construction phase quality assurance activities, the quality assurance department actively participates in the engineering tasks carried out by the various aspets、systems and equipment departments.

Research on key technology for safety review

The project invited the Nuclear And Radiation Safety Center to carry out a research on the issues related to the safety review of the TMSR-SF1. The main progresses include:

According to the results of the calculation and the relevant data of the investigation, the limit of the reactivity coefficient and the shutdown margin of the key nuclear design parameters is given.

The three levels PSA of TMSR-SF1 analysis which took the source term analysis as input has been carried out.

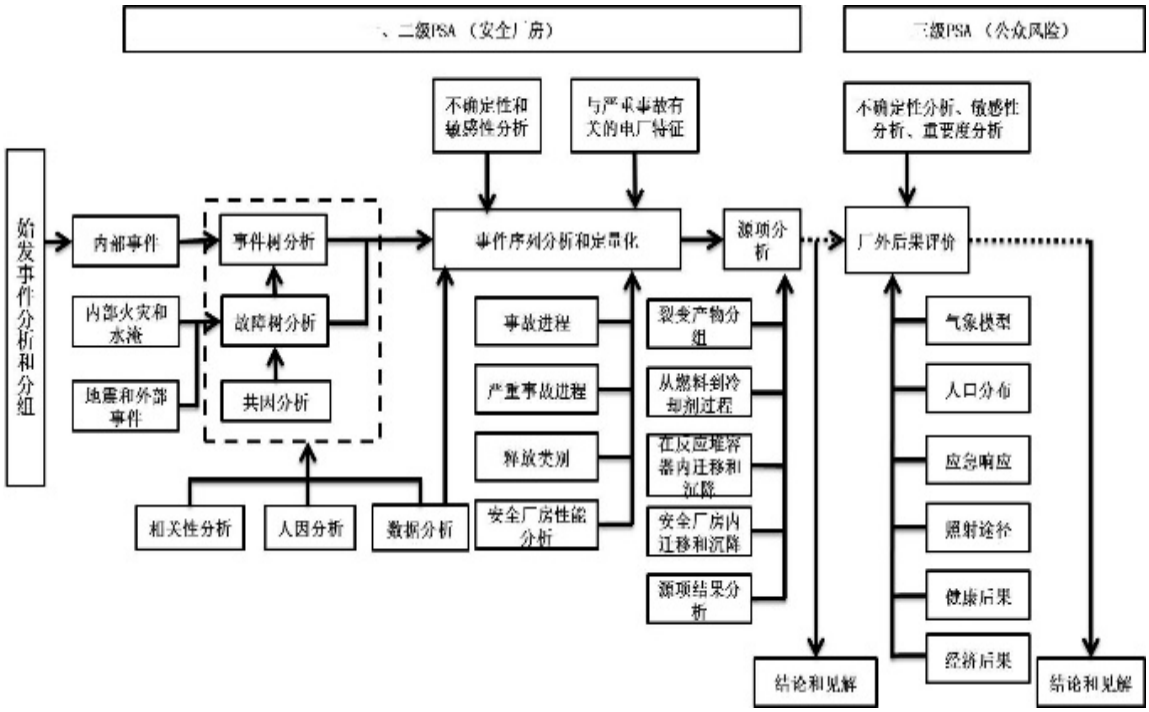

Fig.4 PSA frame for TMSR-SF1

《The research on the key thermal limits and the specific acceptance criteria of the TMSR-SF1》, 《The research on the theoretical model of radiant source term and its applicability in TMSR-SF1》, 《Evaluation method for burnup calculation and power distribution analysis of TMSR-SF1》, and 《the study of porous media flow and heat transfer analysis method and evaluation method of TMSR-SF1》 were completed.

Considering the characteristics of MSR, the research and analysis report of 《the first loop tritium source calculation method of TMSR-SF1》 has completeed.

On the function and safety requirements of TMSR-SF1, report-《the analysis and research report on the function and safety requirements of the TMSR-SF1》 have been completed.

钍铀循环物理研究

反应堆物理部

背景

本课题基于“TMSR 专项”钍资源核能利用的战略部署，继续深入开展不同堆型钍资源利用模式、性能及相关物理课题研究。在钍铀燃料循环物理、钍铀核燃料循环关键核数据及中子物理实验装置建设方面取得了重要进展。

在熔盐堆钍铀循环物理研究方面，根据专项钍利用战略及路线部署开展相关课题的研究工作。升级及开发熔盐堆燃料循环物理分析工具，着重解决熔盐堆燃料流动性、在线换料、在线后处理问题的理论模拟，及其对熔盐堆中子物理学的影响。TMSR 专项钍利用基本方案为：在固态燃料熔盐堆中初步利用钍部分节省天然铀；在液态燃料熔盐热堆、快堆中以现有易裂变燃料为基础，大规模利用钍，实现节省天然铀、生产 ^{233}U 以及嬗变次锕系核素，进而实现钍铀核燃料闭循环的远期目标。

针对 Th 系列、Pa 系列和熔盐的全套中子核数据、裂变产额、衰变数据和热中子散射数据进行了评价更新，并对截面加工平台进行了更新，初步完成了 ACE 光核数据库的研制，制定了 SCALE238 群数据库加工方案，并开展了相关的宏观检验，完成了 ACE 格式数据库的研制。初步完成了钍铀循环核数据评估，建立裂变产额和热中子散射数据数据库，初步完成 CENDL-TMSR-V1.0 库 Beta 版，并完成了 SCALE 44 群协方差数据库的加工，开展了不同燃耗时期钍铀循环核数据不确定度评价。

为了提高中子物理实验装置的实验测量能力，对中子探测器屏蔽进行了改造，并进行了铍靶、石墨靶的总截面测量实验；完成了 ^{7}Li，^{232}Th 中子总截面测量工作；开展了石墨硼当量实验方案的理论模拟研究；完成计划的装置升级改造工作，提高了装置运行稳定性及数据可靠性。

钍铀核燃料循环物理软件

在固态燃料熔盐堆方面，对基于确定论方法的燃料球流动模式下燃耗计算方法进行了改进，有效提高了燃料球平衡态燃耗的搜索速度（图 1）；在液态燃料熔盐堆方面，针对前期开发的在线加料及后处理模式的物理模块进行了升级，扩展了工具适用范围，综合考虑了燃料流动性及在线添料、后处理等功能。基于上述改进的软件平台及计算工具，在熔盐堆物理及钍利用性能方面进行物理分析及优化。

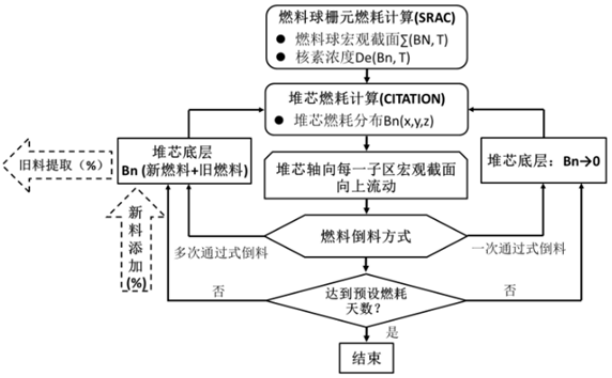

图 1 固态堆倒料计算流程图

钍铀核燃料循环物理分析

基于上述两个主要软件平台，课题针对固态燃料熔盐堆、液态燃料熔盐堆以及部分新概念反应堆开展了钍铀核燃料循环物理分析。

基于 FHR 平衡态燃耗计算方法，通过对燃料球中钍铀燃料配比、铀燃料富集度、C/HM 及 triso 颗粒直径等参数的优化，分析了钍铀混合燃料在 FHR 中的利用率，并从燃料利率的角度为下一步固态堆钍利用率研究提供了方向。在反应堆中，燃料球中钍铀燃料配比，直接关系到燃料球在堆内可停留时间，停留时间越长，有利于 ^{232}Th、^{238}U 等增殖材料获得充分的中子辐照，直接影响重金属燃耗和燃料利用率（图 2）。

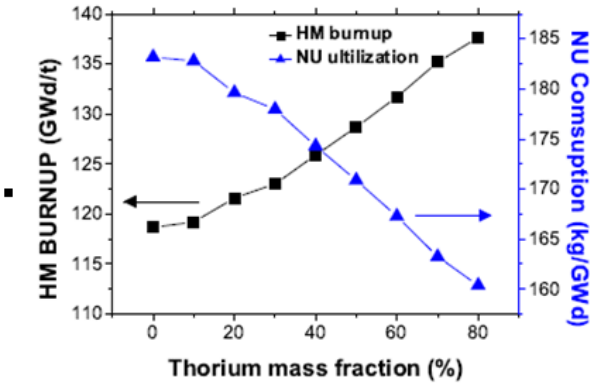

图 2 重金属燃耗与钍质量比关系及对应天然铀消耗率

为了确定液态燃料熔盐堆中 Xe 行为对堆芯中

子学及钍铀转换增殖性能的影响，从理论上初步研究了 Xe 在堆芯中的行为。分析了不同氙分离效率、氦泡在熔盐中不同空泡比例下氙毒的变化规律。图 3 结果表明，在提高空泡比例和氙分离效率的情况下，可以降低氙的中子毒性，提高熔盐堆的中子经济性。

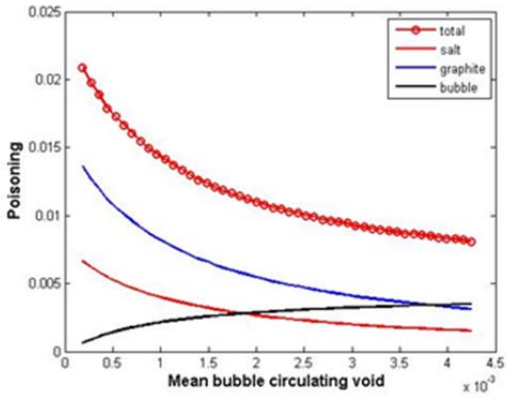

图 3　氙毒与氦气在熔盐中的空泡比例的关系

完成了熔盐堆钍铀循环过渡分析工作。为了解决熔盐堆启动阶段 ^{233}U 短缺问题，分析了用富集 ^{235}U 启堆并过渡到 ^{233}U 的可行性，并给出了优化过渡方案。图 4 可以看出，^{233}U 净积累量与富集度大小密切相关。

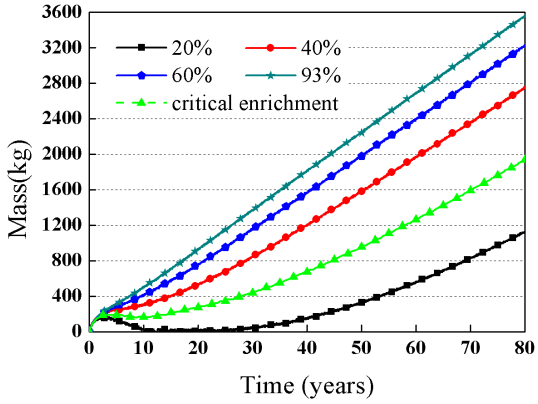

图 4　不同富集度下 ^{233}U 净积累量变化

基于氯化物熔盐的液态燃料反应堆（氯盐堆）进行了燃料利用性能研究，结合氯盐载体盐和快堆的优势，以实现钍铀循环、铀钚循环的高增殖和高嬗变性能为设计目标，给出了氯盐快堆的概念设计。

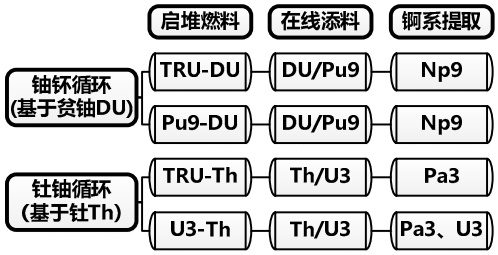

图 5　氯盐堆装料方式及后处理方式

完成不同种类熔盐的液态燃料熔盐快堆嬗变性能计算分析；开展了 LiF 和 LiNaKF 两种载体盐对长寿命高放射性核废料 MA 的影响研究，为解决 TMSR 专项中核废料最小化问题提供可靠的理论依据。

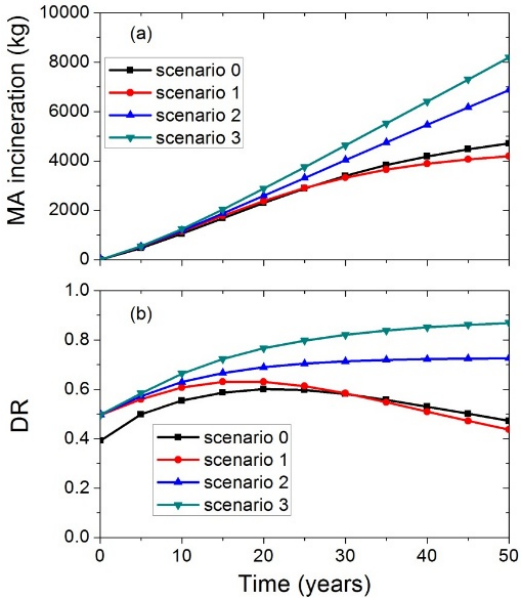

图 6　MA 焚毁量（a）和 DR（b）随燃耗时间演化

在其它先进堆型钍利用方面，对先进固态燃料堆 EM^2 在不同初始装料模式下的的多代堆增殖、转换性能进行了深入分析，给出了燃料燃耗性能与堆芯转换比 CR 之间的关系，图 7 结果表明在堆芯初始装料设计中，设置合理的 CR 值有利用提高燃料燃耗性能。

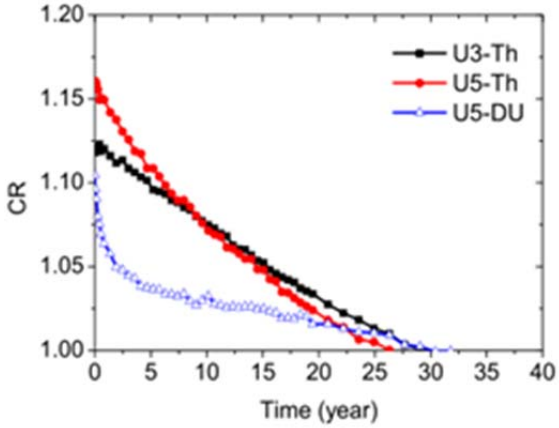

图 7　EM^2 一代堆 CR 对比

此外，分析了铀燃料启堆的 CANDLE 堆在理想燃料状态下的重金属利用率，对 CANDLE 堆堆芯燃烧模式进行了分析（图 8），研究在固态燃料熔盐堆上借鉴其优势用于钍铀燃料循环。

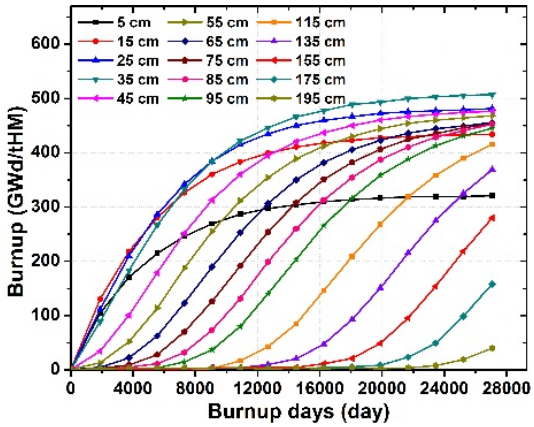

图 8 铀燃料启堆的 CANDLE 堆不同几何位置燃耗演化

钍铀核数据研究

基于 TMSR 专用核数据库一期（CENDL-TMSR-V1）的研究计划，继续开展中子核数据评价加工及 CENDL-TMSR-V0 的检验等相关研究。现已完成 ^{7}Li、^{233}Th 和 Pa 系列的全套中子核数据更新评价（图 9）。^{231,234,235,236}Th、^{234,234m}Pa 等的基态或同质异能态的半衰期的比对评价及推荐及石墨固态熔盐的热中子散射数据的初步研究，并完成了对上述数据的检验入库(CENDL-TMSR-V0)，完成对截面加工平台的更新，制定了 SCALE238 群数据库研制方案，并完成 ^{9}Be、^{12}C、^{27}Al 等 47 个核素的 ACE 光核数据库的初步研制。研发了基准检验平台(Gen-Benchmark)，并以该平台为基础，完成了对现有 ACE 数据库部分核素的检验。

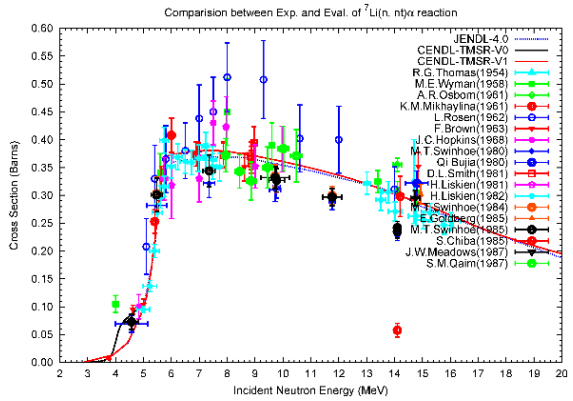

图 9 ^{7}Li(n, nt)α 评价数据与实验数据对比

开展了 ^{232}Th，^{233}U 和 ^{235}U 裂变产额的核数据评价和更新。采用国际比对推荐的 IAEA 光核数据库，制作 ACE 格式光核数据库。利用 SCALE 程序对基准题数据的正确性进行了验证，结果与 SCALE6.1 自带的数据库的结果对比显示一致性较好，验证了加工的数据库的正确性。基于 1 GWth 钍基熔盐堆，利用 SCALE 程序中的 TRITON 和 TSUNAMI-3D 模块开展不同燃耗时期核数据引起的 keff 不确定度分析，结果表明随着燃耗增加核数据引起的 keff 不确定度由 0.49%增大到 0.55%。基于 ENDF/B-VII.0、ENDF/B-VII.1 以及 JENDL4.0 评价数据库，利用自主开发的截面处理系统(Gen-TMSR-ACE)制作了一系列的 ACE 格式数据库。

加速器驱动中子物理实验装置

2015 年中子物理仿真实验装置继续进行实验调试和装置的改进，对探测器进行了总体组装和探测器单元的性能测试，相继进行了 In，Cd 吸收峰分布，C 靶、Be 靶的总截面测量等实验工作（图 10），开展了中子探测器刻度及性能研究等，同时由于辐射防护等问题，2015 年下半年集中开展了装置的屏蔽与辐射防护改进（图 11：TOF 探测器局部屏蔽）。2015 年运行时间约 500 h（6-10 月份因屏蔽升级改造停机）。

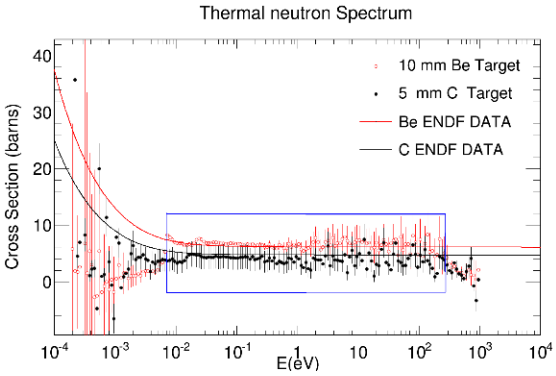

图 10 石墨靶、铍靶总截面测量结果与评价数据对比

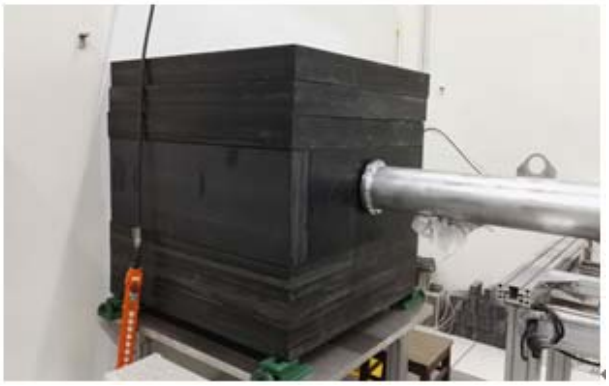

图 11 TOF 探测器屏蔽方案及完成照片

2016 年完成了 LiF，ThO_2 靶中子总截面测量工作，^{7}Li 的中子总截面实验结果如**错误!未找到引用源。**所示。实验结果在 0.01~0.03 eV 能量范围内具有较好的统计误差；开展了石墨硼当量实验方案的理论模拟研究（图 13）；完成计划的装置升级改造工作，提高了装置运行稳定性及数据可靠性。

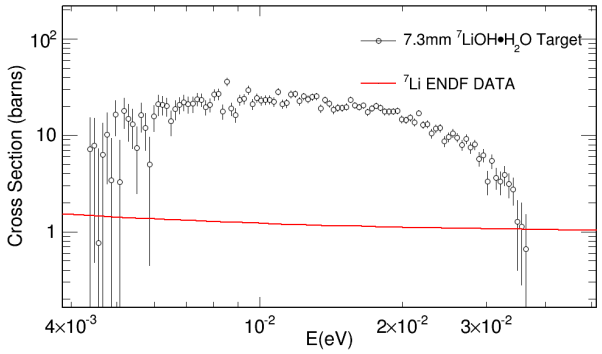

图 12 实验测量的 7Li 中子总截面（数据点）与评价数据比较（实线，来自 ENDF/B-VII.1）

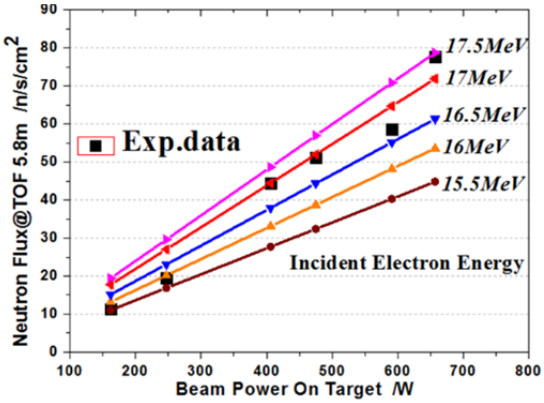

图 13 功率为 162、247、406、475、591、657、1500W，通量的实验测量值（黑色）与模拟计算值（红色）

Research on Thorium-Uranium Fuel Cycle

Reactor Physics Department

Background

This research is under the framework of the TMSR strategic pioneer science and technology project of CAS, aiming at the optimization of thorium resource utilization in various kinds of reactors. Progresses have been achieved in several aspects, such as thorium uranium fuel cycle analysis, thorium uranium nuclear data research and accelerator driven neutron physics experiments.

Based on the goals and strategies of TMSR, several aspects of thorium-uranium fuel cycle re-search have been carried out. The software platform has been improved aiming at the problems of molten salt fuel flowability, online refueling and online processing. The basic scheme of thorium utilization in TMSR is to save nature uranium in solid fuel TMSR by using Th and to generate ^{233}U and transmutate MAs in order to achieve closed fuel cycle in liquid fuel TMSR.

The neutron nuclear data, decay data and thermal neutron scattering data of Th, Pa and molten salt has been updated. And the ACE optical nuclear database is developed. The relevant macroscopic examination is carried out based on the developed SCALE 238 database. The thorium uranium nuclear data evaluation is preliminary finished and the database of fission yield and thermal neutron scattering data is established. The CENDL TMSR - V1.0 Beta is completed as well as the processing of SCALE 44 group of covariance database. Nuclear data uncertainty evaluations have been carried out in different periods of burnup.

In order to improve the experimental measurement capability of the neutron physics experiment device, the neutron detector shielding is modified, and the total cross section measurement experiments of beryllium target and graphite target are carried out. The total cross section measurements of ^{7}Li and ^{232}Th are completed. The theoretical simulation study of graphite boron equivalent experimental scheme is carried out. Completion of the planned installation renovation can improve the device operation stability and data reliability.

Thorium uranium fuel cycle physical analysis soft-ware

In terms of solid fuel molten salt reactor, the fuel flow mode based on deterministic method is improved, which can effectively enhance the search speed of pebbles at equilibrium (Fig.1). In terms of liquid fuel molten salt reactor, online refueling and processing modules are upgraded, which can expand the application scope. Based on the above improved software platforms and calculation tools, physical analysis and optimization of the physical and thorium utilization performance of molten salt reactor are carried out.

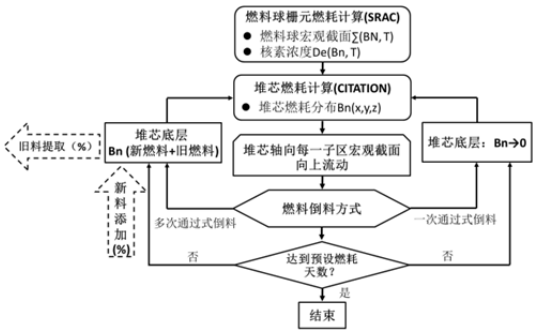

Fig. 1 flowchart of solid fuel reactor shuffling

Physical analysis of thorium uranium fuel cycle

Based on the above two main software platforms, physical analysis of thorium uranium nuclear fuel cycle is carried out on the solid fuel molten salt reactor and liquid fuel molten salt reactor as well as some new concept reactors.

The utilization of Th-U fuel in FHR is analyzed based on the equilibrium burnup calculation method and the ratio of Th and U, enrichment of U fuel, C/HM and diameter of triso particles are optimized. These results can be used to provide the research direction for solid fuel reactors from the fuel utilization point of view. As can be seen from Fig.2, the ratio of uranium and thorium fuel is directly related to the time of pebble staying within the reactor. The longer the residence time, the more the neutron irradiation will be gained by ^{232}Th, ^{238}U,, which will directly affect the heavy metal burnup and fuel efficiency.

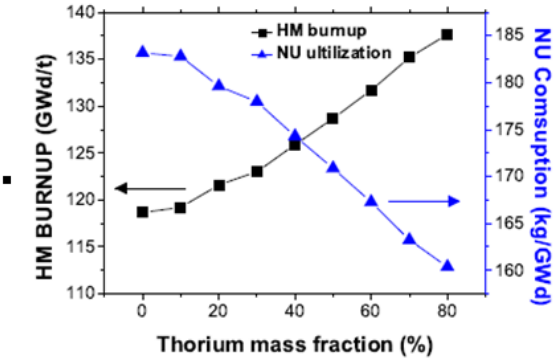

Fig.2 The relationship between heavy metal burnup and thorium mass and corresponding natural uranium consumption rate

In order to determine the effect of Xe in liquid fuel molten salt reactor, the behavior of Xe in the core is studied theoretically. The variation patterns of xenon in different air bubbles in molten salt are analyzed. Fig.3 shows that the neutron toxicity of xenon can be reduced and the neutron economy of molten salt reactor can be improved by increasing the cavitation ratio and xenon separation efficiency.

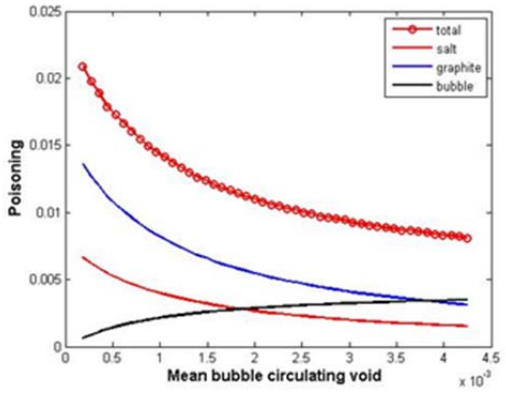

Fig.3 The relationship between xenon and helium gas in molten salt

The transition of thorium uranium in molten salt is analyzed. In order to solve the shortage problem of ^{233}U in the start-up phase of molten salt reactor, the feasibility of using enriched uranium to start up and transiting to ^{233}U is analyzed, and the optimal transition scheme is given. As can be seen from Fig.4, the net accumulation of ^{233}U is closely related to the uranium enrichment.

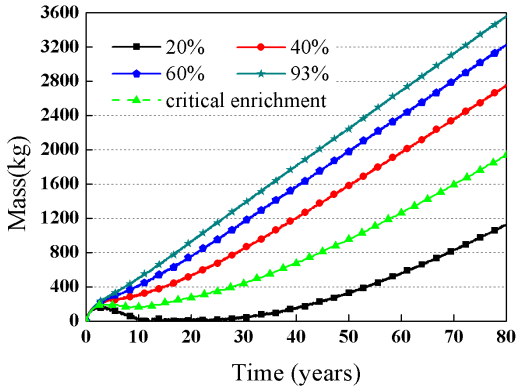

Fig.4 U-233 accumulation for various kinds of enrichment

Based on the liquid chloride molten salt reactor, the fuel performance study is carried out in order to realize high breeding and transmutation capacity. The concept design of chlorine slat fast reactor is completed.

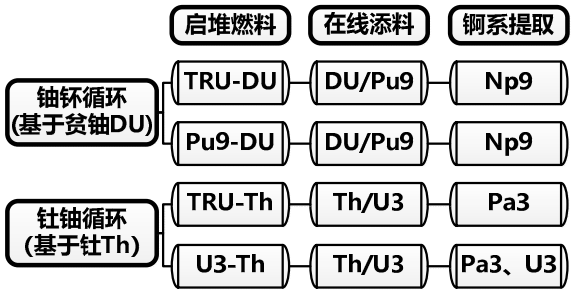

Fig.5 Chlorine salt reactor feeding and processing schemes

The transmutation performance of molten salt in different types of MSR is analyzed. The research on the influence of LiF and LiNaKF carrier salt on long-life high radioactive waste MA is carried out, which provides a reliable theoretical basis for solving the problem of minimization of nuclear waste in TMSR.

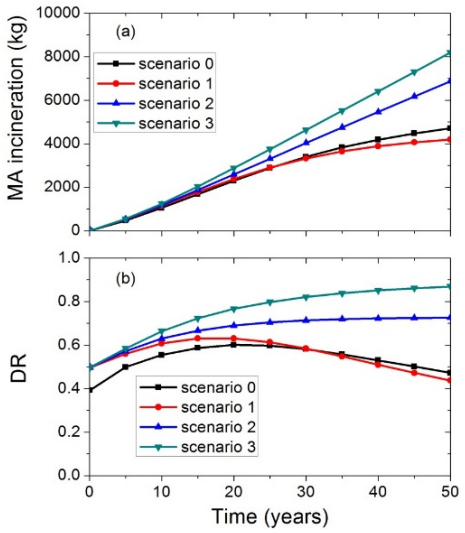

Fig.6 MA incineration (a) and DR (b)

In term of other advanced reactor, a solid fuel EM^2 start up with different kinds of fuel is analyzed. The conversion capacity based on multi-generation is studied. Fig.7 shows that a reasonable CR can effectively improve the burnup performance.

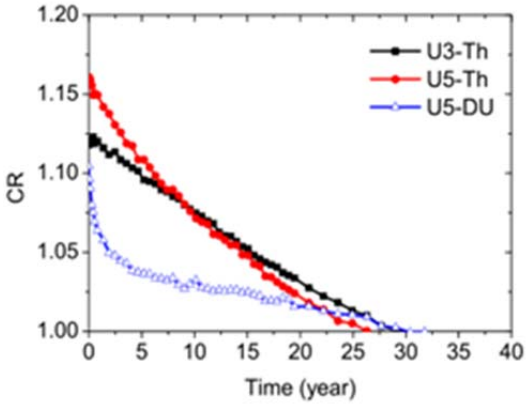

Fig.7 CR comparison of GEN-I EM^2

Besides, the heavy metals utilization of CANDLE reactor at ideal burnup condition is analyzed, which can be used as reference of Th utilization in solid fuel reactor. (Fig.8)

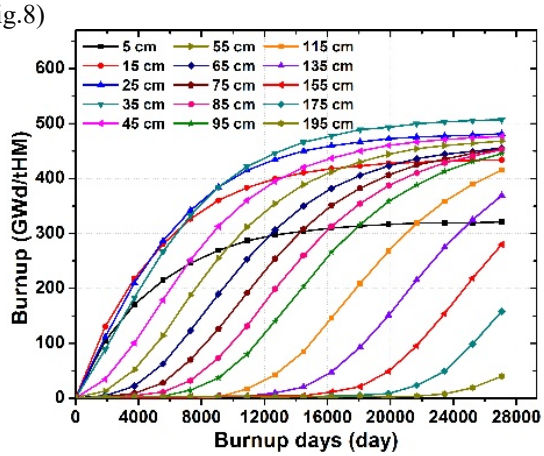

Fig.8 The burnup evolution of the CANDLE initiating by Uranium

Thorium-uranium nuclear data research

Based on the phase I plan of TMSR special nuclear database (CENDL-TMSR-V1), the evaluation and processing of neutron nuclear data of CENDL-TMSR-V0 are carried out. A complete set of neutron nuclear data update evaluation of ^{7}Li, ^{233}Th and Pa series is completed (Fig.9). Half-life comparisons of ground state and isomeric state of ^{231,234,235,236}Th, ^{234,234m}Pa are completed and preliminary research on the thermal neutron scattering data of molten salt is finished to complete the CENDL-TMSR-V0 database. SCALE238 group database is established and the ^{9}Be、^{12}C、^{27}Al etc. (47 species in total) are developed to complete the ACE database. The Benchmark test platform (Gen-Benchmark) is developed and based on this platform, the tests of some nuclides in the existing ACE database are completed.

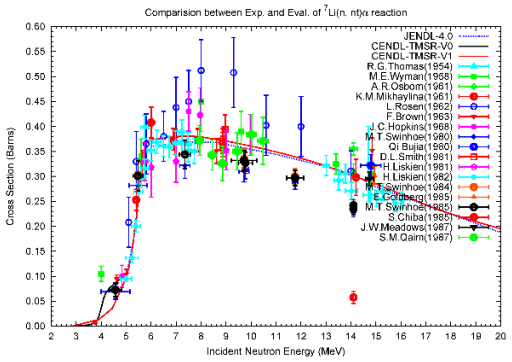

Fig.9 α data evaluation and comparisons of ^{7}Li (n, nt)

The nuclear data evaluations of the fission yield of ^{232}Th, ^{233}U and ^{235}U are carried out. The recommended IAEA photonuclear database is used to produce the ACE optical database. The correctness of the benchmark data is verified using the SCALE program since the results have good coherence with that of SCALE6.1.

Based on the 1 GWth thorium base molten salt reactor, using the TRITON and TSUNAMI-3D module, the keff uncertainty analysis caused by nuclear data at different burnup period is carried out. The results show that with the increase of burnup, keff uncertainty increased from 0.49% to 0.55%. Based on ENDF/B-VII.0, ENDF/B-VII.1 and JENDL4.0 evaluation database, a series of ACE format databases are made using the self-developed cross-section processing system (Gen-TMSR-ACE).

Photo-neutron Source Driven by 15 MeV Electron Linac

Debugging and improvement of the neutron physics simulation experiment device is carried out. The general performance of detector unit is tested while the In, Cd absorption cross-section peak distribution measurements, C target, Be target total cross-section measurements are finished (Fig.10). Due to the radiation protection requirements, a device shielding and radiation improvement is completed (Fig.11). The total operation time in 2015 is about 500 hours (shutdown from Jun. to Oct. due to shielding upgrade).

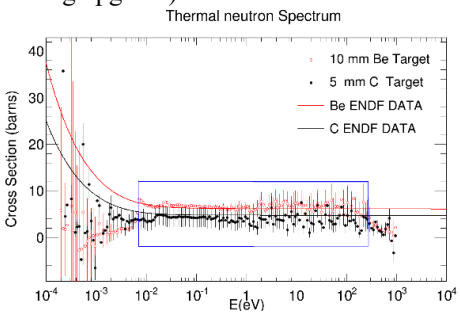

Fig.10 Total cross section measurement of graphite target and beryllium target compared with the evaluation data

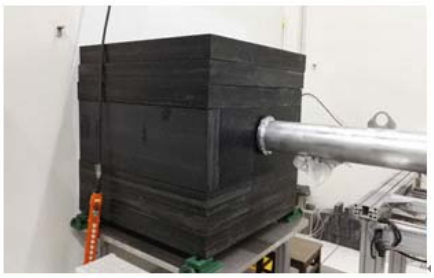

Fig.11 TOF detector shielding scheme

In 2016, the total cross section measurement of LiF and ThO_2 targets is completed. The experimental results of the total cross section of ^{7}Li are shown in Fig.12. The experimental results have good statistical error in the range of 0.01~0.03 eV. A theoretical simulation study of the graphite boron equivalent experimental is carried out (Fig.13). The planned installation upgrade and renovation work is completed to improve the device operation stability and data reliability.

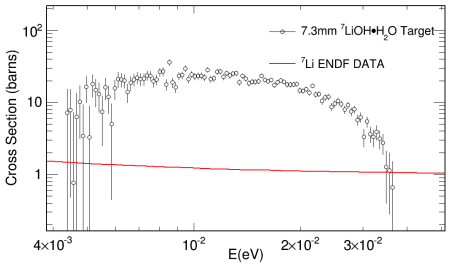

Fig.12 Total neutron cross-section of ^{7}Li (dot) and evaluation data (line: from ENDF/B-VII.1)

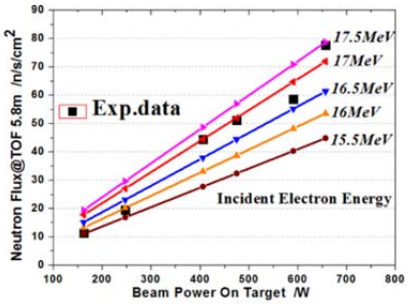

Fig.13 Neutron flux comparisons of experimental values(black) and modeling value(red) for the power of 162, 247, 406, 475, 591, 657, 1500W

反应堆物理部

本课题以熔盐堆关键工程技术研发与设备研制、完成熔盐实验堆工程设计为核心目标，主要包括固态熔盐堆的堆本体结构设计与结构力学评定、控制系统设计与研制、测量系统工程样机的研制。

钍基熔盐堆的堆本体结构设计方面，根据物理设计方案，完成了 SF0 仿真实验平台堆本体系统部分的结构设计演变，并已经进行了制造加工，将于 2018 年 6 月进行现场安装。此外根据项目需要，完成了堆本体上各关键样机设备的研制，并开展了相关的实验。

熔盐堆控制系统设计与研制方面，完成了 TMSR SF1 控制系统的方案设计与初步设计，仿真平台软件开发，CRDM 系统棒控棒位实验测试，保护系统样机第三方鉴定及高温步进电机工程样机的研制及测试。完成了 TMSR SF0 仿真堆控制系统方案设计，初步设计及工程评审，其中包括控制系统、保护系统和主控室及仪控仿真。

熔盐堆测量系统设计与研制方面，完成便携式惰性气体监测仪、高温中子测量系统样机以及满足 TMSR-SF1 熔盐堆要求的热工参数测量工程样机地研制，同时，完成了基于气压驱动原理的高温超声波流量计标定平台工程设计并完成了设备的加工。

固态熔盐堆的堆本体结构设计

1 堆本体系统的设计、分析和制造工作

1.1 SF1 反应堆本体结构优化工作

通过对 N10003 合金材料的市场制造能力的确认以及评估，以及前期初步设计工作内容的总结，对 SF1 反应堆容器设备顶盖进行了分析和计算，确认了更换材料更符合实际情况的路线方针，并进行了反应堆本体和反应堆容器结构的更改和优化工作。

针对设计情况，对安分报告进行了撰写和改进。

1.2 SF0 堆本体系统设计分析和研制

SF0 堆本体系统是用于尽可能多的验证 SF1 相关的设计和技术。SF0 堆本体系统结合物理、热工和工艺的相关需求，对 SF0 堆本体系统的主容器及其支撑、堆内上部构件、堆芯构件（包括堆芯石墨构件、堆芯围筒组件、石墨压紧钢板组件、下腔室填充体组件等）进行了针对性设计，对相关设备进行了详细的力学分析和评估工作，完成了 SF0 堆本体系统的方案设计和初步设计评审工作，提交了一整套 SF0 堆本体系统各设备的施工图纸。通过招投标程序，选定了相应设备的制造厂商，完成了合同的签订工作，正在进行相关各设备的制造，后续将在仿真实验平台上陆续进场安装。

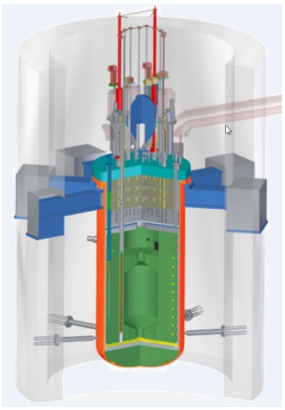

图 1 TMSR-SF1 的堆本体工程设计方案

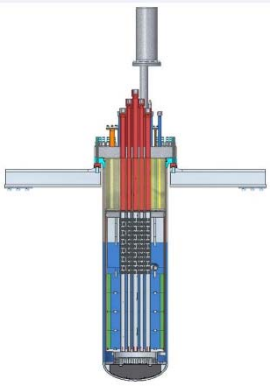

图 2 TMSR-SF0 的堆本体工程设计方案

2 堆本体相关样机研制

2.1 卸料装置关键技术研究

通过搭建静水试验装置及试验，验证了双腔室的结构设计配合球匙及液位面的合适位置能够实现堆芯模拟球的自稳，双腔室的结构设计也能确保在卸料过程中球匙的下插不会对堆芯球床产生较大的扰动。

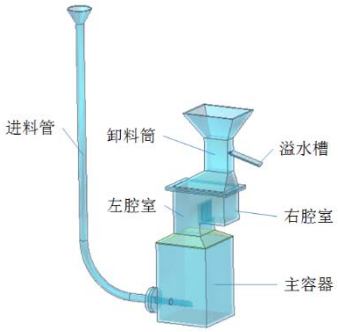

图 3 静水试验装置

通过卸料机构水循环试验装置的搭建及试验、验证了水的流动不会对双腔室结构内模拟球的数量及排列规则产生较大的影响，保证了卸料机构连续卸料的可行性。同时试验了几种不同的球匙结构形式，球匙结构对卸球效率影响较大。

图 4 卸料机构水循环试验装置

2.2 调节棒/补偿棒驱动机构单项关键技术研究

根据 SF1 的特点和驱动机构运行环境的综合分析，确定了控制棒在堆内运行环境以及控制棒的主要结构；开展了控制棒在熔盐中、水中、空气中的落棒时程分析；通过实验与分析的对比校验，验证了控制棒落棒性能分析的准确性、结构设计的可行性。

图 5 调节棒/补偿棒驱动机构

2.3 堆芯构件 C/C 箍紧带研究

针对反应堆石墨散体结构的特点，通过调研地震情况下石墨构件的运动趋势；分析了石墨堆内构件与金属构件在常温安装与高温运行环境下，因为材料膨胀系数的不同，引起的进行位移，以及高温下材料力学性能的变化；分析石墨构件因为安装定位误差、制造误差、设计公差等因素引起的石墨构件的可能进行位移，设计了 C/C 箍紧带的机械结构；根据 C/C 材料的特点、以及综合力学估算，初步确定了 C/C 材料的制造工艺、力学分析方案、样机实验测试内容等。

2.4 调节棒/补偿棒驱动机构工程样机常温实验研究

针对控制棒驱动机构工程样机的技术特点，反应堆的运行工况、环境，分析、总结了驱动机构工程样机常温测试内容。根据这些内容，初步设计了驱动机构常温测试台架（在原台架基础上）的改造内容，编制了常温下实验内容测试方案报告。

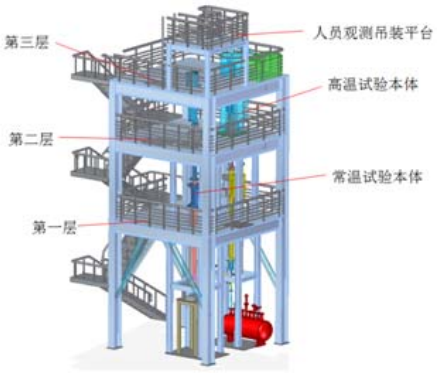

图 6 控制棒常温实验台架

2.5 控制棒驱动机构熔盐蒸汽抑制及控制棒运行影响研究

通过对熔盐在高温下的蒸发量的估算，熔盐蒸汽在控制棒系统内不同工作温度的分析，分析了熔盐蒸汽可能的凝结部位及可那的影响后果。设计了一整套熔盐蒸发及控制棒运行影响实验装置，进行可能的影响评估。

图 7 熔盐蒸发环境下的控制棒实验台架

固态熔盐堆的堆本体结构力学评定

对于目前的 TMSR-SF1 设计版本，已完成包括石墨构件、压力容器、控制棒、熔盐泵和管道等设备或部件的结构力学评定工作。其中石墨堆芯进行了抗震分析（见图 8）；

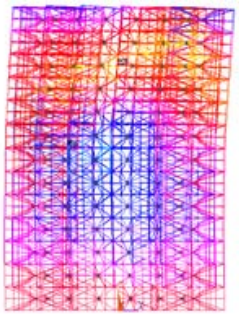

图 8　石墨堆芯抗震分析模型

压力容器进行了开孔补强分析、设计工况与正常运行工况下的应力分析与评定；控制棒进行了落棒动力学程序 TMSR-CRD 的开发；GH3535 工程样泵进行了相关的分析与评定（见图 9）等。对于 TMSR-SF0，进行了压力容器（见图 10）、回路管道、一、二回路熔盐泵的分析与评定。

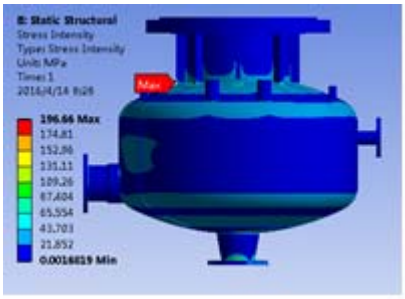

图 9　GH3535 工程样泵的分析与评定

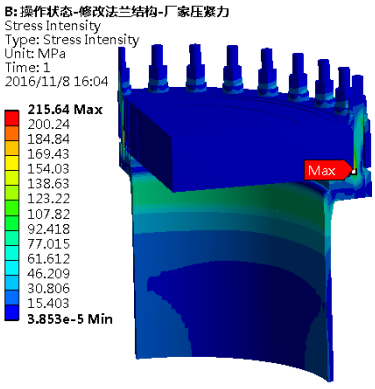

图 10　压力容器的应力分析与评定

石墨堆芯进行了多散体抗震分析，主要包括石墨堆芯多散体建模研究；控制棒孔道在地震载荷下的变形研究；以及石墨砖、销的应力分析。由于熔盐环境下反应堆多散体石墨堆芯结构在受到地震载荷时会呈现出复杂非线性效应，传统方法难以对其进行分析，我们在气冷堆（如清华大学 HTR-PM）研究的基础上，采用“多刚体非线性弹簧阻尼”与附加质量（阻尼）相结合的新方法，成功克服了由于石墨散体结构的移动与碰撞，和流固耦合效应导致的分析困难，对 TMSR-SF1 的石墨堆芯进行了初步的抗震分析。

对于压力容器、回路管道等部件，由于 TMSR 的高温特点，我们采用 ASME-NH、ASME BPVC.III.5 等规范来代替 ASME NB 规范（传统的压水堆所采用的）来进行分析与评定，不仅考虑了这些部件的应力限值评定、还考虑了应变评定，以及疲劳—蠕变评定。其研究范围大大拓展，研究难度大大增加。

对于控制棒部件，在传统压水堆研究的基础上，我们还针对 TMSR 特点，进行了控制棒在高温熔盐环境中落棒分析研究，以及控制棒落棒时熔盐反冲高度的研究等等。

熔盐堆控制系统设计与研制

棒控棒位系统样机及台架试验完成了关键设备高温步进电机工程样机、选装变压器原理样机的电气性能测试、高温性能测试，对测试中出现的线缆辐照问题找到了解决办法；CRDM 系统棒控棒位实验测试主要完成了磁尺标定、旋转变压器标定、控制棒运行时电机内部温度测量、控制系统性能初测、驱动机构稳定性、定位精度、机电延迟性能、运行回程差等，证明系统功能达到设计要求。控制棒高温试验台架原型样机控制系统整体规划图如图 10 所示。

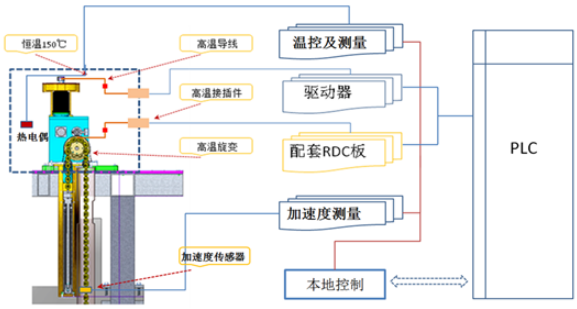

图 10　控制棒高温试验台架原型样机控制系统整体规划图

保护系统样机研制完成，并进行了第三方鉴定，第三方鉴定测试完成了电磁兼容试验、高低温试验、振动试验等，实验结果表明保护系统样机研制符合设计要求，第三方鉴定检测报告如图 11 所示。

图 11 保护系统样机第三方鉴定检测报告

围绕 TMSR-SF0 方案设计及初步设计，SF0 控制系统主要完成了仿真堆及关键样机和台架的控制工作，包括 SF0 堆芯加热器监控、堆本体监测、一二回路监控、气路监控等；控制棒驱动机构试验台架、熔盐蓄热装置、安全模拟系统试验装置等。

以 SF0 及部分台架实际信号为基础，辅以相关系统仿真信号，从界面上整体仿真 TMSR-SF1，以主控室为展示平台，整体构建 TMSR-SF1 仪控仿真平台。TMSR SF0 控制系统整体架构如图 12 所示。

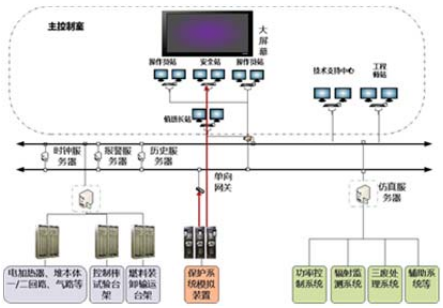

图 12 TMSR-SF0 仪控系统整体架构

控制系统结构基于 EPICS 架构，采用国产商用成熟的 DCS 控制器及模块，采用虚拟化集群的服务器设备。完成了 EPICS 和 DCS 的硬件接口开发。

保护系统主体采用工程原型样机硬件架构，扩展断路器柜、主控盘台、定期试验装置等，完成了信号处理流程需求分析、接口分析、原理图设计、PCB 设计、机柜布局设计等，保护系统原理结构如图 13 所示。

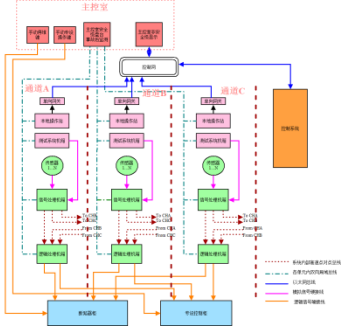

图 13 TMSR-SF0 保护系统原理结构

主控室设计按照核电厂要求设计，根据现有厂房提供区域，完成了系统布局设计和主要设备的规格要求，确定了大屏幕的功能设计及 HMI 模板。

熔盐堆测量系统设计与研制

完成了便携式惰性气体监测仪样机的研制如图 所示。该仪表不仅测量反射性元素的活度，而且还能区分不同的核素。该仪表采用双 PIPS 探测器，通过符合电路可以分别测量 β 射线和 γ 射线。核素测量灵敏度如下：^{85}K：2.0×10^{-5}cps/（Bq/m^3）；^{133}Xe：1.0×10^{-5}cps/（Bq/m^3）。

图 14 便携式惰性气体监测仪

高温熔盐压力计采用耐氟盐腐蚀的 GH3535 合金材料作为传感器的膜片，GH3535 尚未有加工成膜片的经验，常规的膜片加工技术不适用于 GH3535 材料。通过样机的研制，掌握了 0.1mm GH3535 膜片的加工工艺和 NaK 合金填充工艺，成功研制了基于三层 GH3535 膜片的填充 NaK 式熔盐压力计，其量程为 0~0.5MPa，精度为 0.25%FS，最高温度范围为~700℃。同时，研制了国内首个 750℃的高温压力标定平台如图 15 所示，其标定量程为 0~0.5MPa，精度为 0.02%FS，标定介质为水、油、气、熔盐。

图 15 熔盐压力计工程样机及标定装置

针对 TMSR 熔盐堆其高温、高腐蚀以及高辐照环境的特殊工况，研制了具有弯曲波导管的雷达液位计工程样机如图 16 所示:

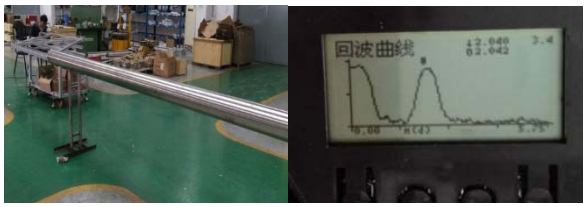

图 16　熔盐液位计工程样机

掌握了高频雷达波导管的设计方法和关键部件的制作工艺。产品经实验测试，参数如下：弯曲波导 长度：4.5m；精度：±0.1%F.S；测量介质温度：600-700℃；

研制成功了外夹式高温超声波流量计工程样机，样机采用国产化的元器件，数据处理方法在以互相关算法的基础上改进了数据滤波方法，提高了系统的精度和抗干扰能力。另外，通过对超声波导波板的结构、加热和保温结构的优化，实现了通过自然冷却的方式，确保超声波探头在测量高温熔盐流体的可靠性。系统性能指标：流速测量范围：0.1~5m/s，测量精度 <3%。

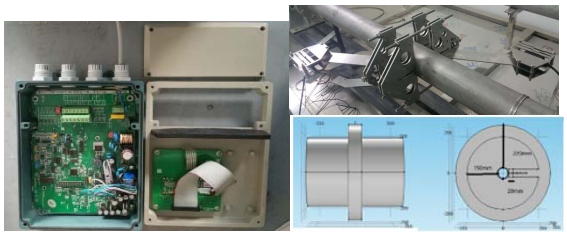

图 17　高温超声波流量计工程样机

针对原有的高温熔盐超声波流量计标定平台的结构复杂和价格昂贵的缺点，设计了基于气压驱动的高温氟盐超声波流量计标定平台方案，并通过开发专用的软件仿真计算了相应的设计参数和性能指标，计算结果与国外的 TRACE 软件计算结果一致：最大工作压力<0.5MPa;工作温度<700℃，系统标定精度 <3%。同时，完成了标定装置的设备研制和验收工作。

图 18　高温超声波流量计标定平台方案

The research of reactor engineering technology

Reactor physics department

This project focused on the research and development of molten salt reactor's key engineering technology and equipment, as well as the engineering design of molten salt experimental reactor. The progress of this subject mainly included solid reactor design, structural mechanics evaluation, instrumentation and control system design and development.

According to the physical design, the structure of the SF1 design is optimized and the system structure design of SF0 simulation experiment platform is completed. The simu-lation device of the SF0 reactor will be on-site installation in June 2018. In addition, according to the requirements of the project, the development of the key prototype equipment is completed and the related experiments are carried out.

For the design and development of the molten salt re-actor control system, the design and preliminary design of the TMSR SF1 control system was completed. The software development of the simulation platform, the stick-control rod test of the CRDM system, the third-party identification of the protection system pro-totype, and the development and testing of the high-temperature stepper motor engineering prototype were completed. In the TMSR SF0 simulation reactor control system, the program design, preliminary design and engineering review was completed, including con-trol system, protection system and main control room and instrument and control simulation.

In the design and development of the molten salt reactor instrumentation system, the portable inert gas monitorM has been developped , as well as the main engineering prototype of thermodynamical instruments , which can satisfy the re-questment of TMSR-SF1. Meanwhile, the design optimization of the high temperature ultrasonic flowmeter calibration plat-form, based on the pneumatic driving principle, has been completed and the platform equipments have been manufac-tured.

Reactor body structure design of solid molten salt re-actor

1 The design, analysis and manufacturing of reactor system

1.1 Optimization of SF1 reactor structure

Through summary of the contents of the preliminary de

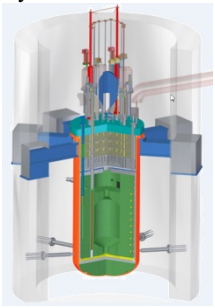

Fig.1 Engineering design scheme of TMSR-SF1

sign work, the SF1 reactor vessel equipment roof is an-alyzed and calculated. The modification and optimiza-tion of reactor body and reactor vessel structure are car-ried out.. According to the design situation, the safety re-port was written and im-proved.

1.2 Optimization of SF0 reactor structure

The SF0 reactor system is used to verify the design and technology related to SF1 as much as possible. SF0 reactor system combines the related requirements of physics, thermal engineering and technology, and designs the main container and its support, upper components and core components of the SF0 reactor system. Detailed mechanical analysis and evaluation of related equipment were carried out, and the scheme design and preliminary design review of SF0 reactor ontology system were com-pleted. A complete set of construction drawings for each equipment of SF0 heap ontology system is presented. Through bidding program, equipment manufacturers are selected. On the simulation experiment platform, the re-actor is installed suc-cessively.

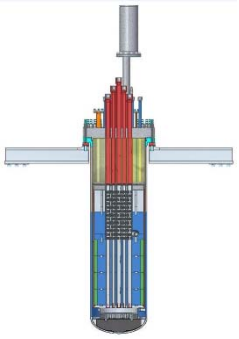

Fig.2 Engineering design scheme of TMSR-SF0

2 Prototype of the reactor

2.1 Key technology research of the unloading device

Through hydrostatic test equipment and the experi-ments, it can be verified that, double chamber structure design, with a reasonable ball-spoon structure and appro-priate liquid level position enables the self- stabilization of the reactor ball-bed.

Fig.3 Hydrostatic test device

The structural design of the double chamber also ensures that, during the unloading process, the insertion of the ball-spoon will not cause much dis-turbance to the core reactor ball-bed.

Through the water circulation test of the unloading mechanism, it is verified that the flow of water does not have a great influence on the number and arrangement of the analog balls in the double chamber structure, ensuring the continuous discharge of the unloading mechanism. In the tests, several different ball-spoon-shape structures were tested. The ball-spoon-shape structure has a great influence on the un-loading efficiency.

Fig.4 Unloading mechanism water cycle test device

2.2 Key technology research of the control rod/compensation rod drive mechanism

According to the characteristics of SF1 and the compre-hensive analysis of the operating environment of the driving mechanism, the main structure of the control rod in the reactor and the control rod is determined. The control rod is analyzed in the molten salt, water and air situation. Through the comparison between experiment and analysis, the accuracy and the feasi-bility of the structure design are verified.

Fig.5 Control rod/compensation rod drive mechanism

2.3 Design and manufacturing of C/C belt

In view of the characteristics of the graphite internals structure of the reactor, the mechanical structure of C/C belt is designed. According to the characteristics of C/C materials and the comprehensive mechanical estimation, the manufacturing process, mechanical analysis scheme and prototype test con-tents of C/C materials are prelimi-narily determined.

2.4 Experimental study on the normal temperature of the control rod/compensation rod drive mechanism

Aiming at the technical characteristics of the control rod drive mechanism engineering prototype, the normal tempera-ture test content of the driving mechanism engi-neering proto-type is analyzed and summarized. According to these contents, the modification content of the driving mechanism's normal temperature test bench (on the base of the original platform) was designed, and the test pro-gram report of experimental content under normal tem-perature was prepared.

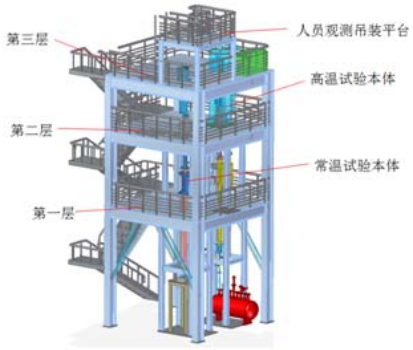

Fig.6 Temperature experimental bench of control rod normal

2.5 The study of the control rod drive mechanism on In-fluence of Molten Salt Steam Suppression and influence of control rod operation

Through the estimation of the evaporation of molten salt at high temperature, and the analysis of the different operating temperatures of the molten salt vapor in the control rod system, the possible condensation sites of the molten salt vapors and the possible consequences are analyzed. A set of molten salt evap-oration and control rod operation impact experimental devices is designed to perform possible impact assessments.

Fig.7 Control rod drive mechanism on Influence of Molten Salt Steam Suppression

Structure Evaluation of TMSR-SF1 Reactor

Based on the current design version of TMSR-SF1, the safety assessment of equipment structures has been completed, including the graphite core components, reactor vessel, control rod, molten salt pump and loop piping, etc. The seismic analysis of graphite is considered (shown in Fig.8), the analysis of opening reinforcement, and the stress analysis and evaluated under the design condition and normal operating condition of pressure vessel are conducted, the dynamic drop program for control rod is developed, the stress analysis and evaluated of GH3535 engineering sample pump (shown in Fig.9) and pressure vessel are finished, etc. Based on the current design version of TMSR-SF0, the stress analysis and evaluated of pressure vessel (shown in Fig.10), loop pipe, and molten-salt pump are conducted.

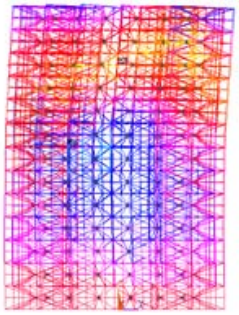

Fig.8 The finite element modeling with multi-body structure of graphite core

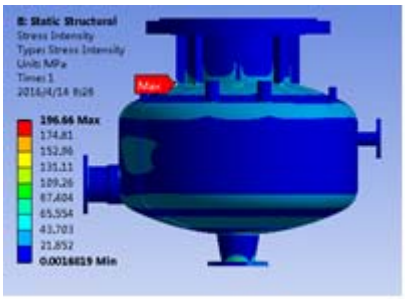

Fig.9 The evaluated of GH3535 engineering sample pump

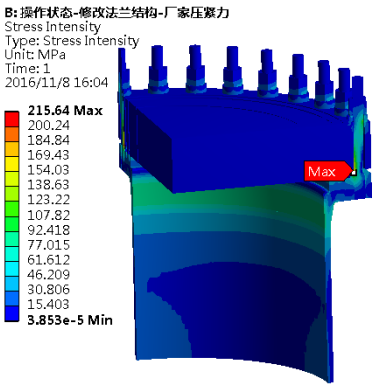

Fig.10 The stress analysis and evaluated of pressure vessel

The specification of ASME-NH, ASME BPVC.III.5 have been used to analyze and evaluate for the components with high temperature characteristics such as pressure vessel, loop pipeline in TMSR, which replace the specification ASME NB used in the traditional pressurized water reactor. The scope of the research has expanded greatly and the difficult of the research has increased significantly since these research not only include the load-controlled stress limits, but also the strain and deformation limits, and the fatigue and creep limits.

According to the characteristic of the control rod in TMSR, the research of drop time analysis in the high temperature environment and the recoil height of the molten salt have been done based on the research of the traditional pressurized water reactor.

Design and Development of the Molten Salt Reactor Control System

In the control rod I&C system prototype and bench test, the electrical performance test and high temperature performance test of the key equipment, such as high-temperature stepper motor engineering prototype and optional transformer prototype were completed, and the method was found to solve the the cable radiation problems that appeared during the test; The CRDM system experiment test mainly completed the calibration of magnetic scale and resolver, motor internal temperature measurement during control rod operation, initial test of control system performance, stability of drive mechanism, positioning accuracy, electromechanical delay performance, poor operation return, etc. The test result shows that the system function meets the design requirements. The overall plan of the control rod high temperature test bench prototype control system is shown in Figure 11.

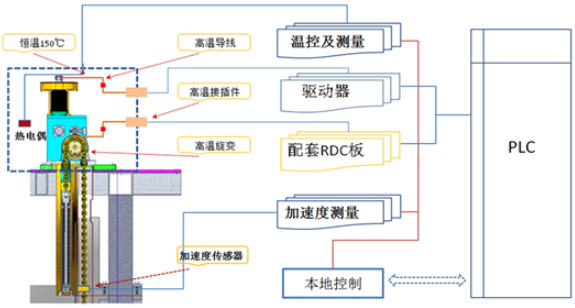

Fig.11 The overall architecture of the TMSR SF0 control system

The development of the protection system prototype was completed, and a third-party appraisal test was carried out. The third-party appraisal tests inclued electromagnetic compatibility tests, high and low temperature tests, and vibration tests. The experimental results showed that the development of the protection system prototype met the design requirements. The third-party appraisal test report is shown in Figure 12.

Fig.12 The third-party appraisal test report

According to the TMSR-SF0 scheme design and preliminary design, the control of simulation reactors and key prototypes and benches in the SF0 control system were completer,

including the SF0 core heater monitoring, reactor body monitoring, the first and second loop monitoring, and gas-circuit monitoring, and the control of CRDM test bench, molten salt heat storage device, safety simulation system test device, etc.

Based on the actual signals of SF0 and some of the gantry, with the relevant system simulation signals, the overall simulation of the TMSR-SF1 was shown in the interface, the overall TMSR-SF1 instrument control simulation platform was constructed and displayed in the main control room. The overall architecture of the TMSR SF0 control system is shown in Figure 13.

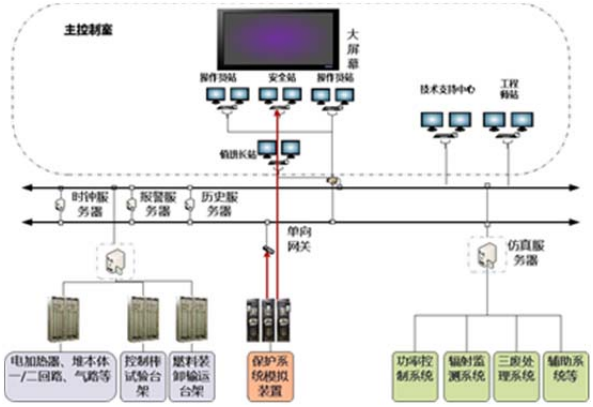

Fig.13 TMSR-SF1 I&C System Overall Architecture

The control system structure is based on the EPICS architecture, using domestically-developed and mature DCS controllers and modules, and virtual clustered server devices. The hardware interface development of EPICS and DCS was completed.

The main body of the protection system adopts the prototype hardware architecture, expands circuit breaker cabinets, master control panel stations, and periodic test equipment. And the requirements analysis of signal processing flow, interface analysis, schematic design, PCB design, cabinet layout design was completed. The principle structure is shown in Figure 14.

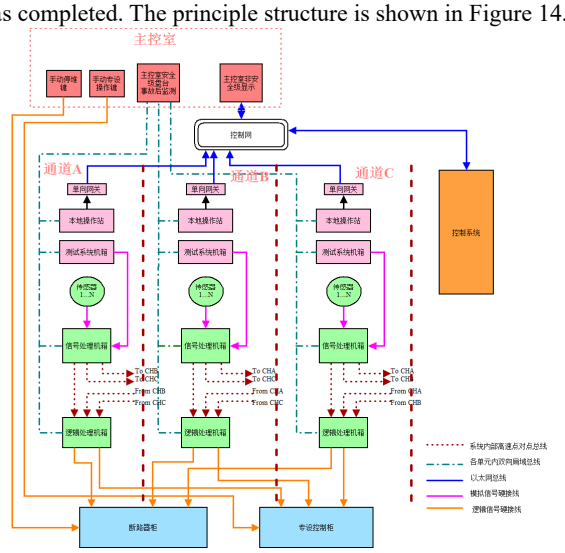

Fig.14 The principle structure of TMSR SF0 protection system

The main control room was designed according to the requirements of the nuclear power plant. According to the existing factory building area, the system layout design and the specifications of the main equipment were completed, and the function design of the large screen and the HMI template were determined.

Design and development of Instrumentation system

The portable inert gas monitor has successfully developed,as shown in Figure . It not only measures the activity of reflective elements, but also distinguishes different nuclides. The instrument uses a dual PIPS detector, which can be used to measure beta ray and gamma ray respectively through a coincidence circuit. The sensitivity of the nuclide measurement is as follows: 85K, 2.0×10^{-5} cps/(Bq/m^3); 133Xe, 1.0×10^{-5} cps/(Bq/m^3).

Fig.15 The portable inert gas monitor

The high temperature molten salt pressure gauge uses fluoride resistant salt corrosion GH3535 alloy material as the diaphragm of the sensor, At present there is not any experience of processing GH3535 diaphragm, and the conventional diaphragm processing technology is not suitable for GH3535 material. Through the development of the prototype, we have mastered the processing technology of 0.1mm GH3535 diaphragm and NaK alloy filling process. The filling NaK pressure transmitter with three-layer GH3535 diaphragm have been manufactured, of which measurement range is 0~0.5mpa, the precision is 0.25%FS and the maximum working temperature is about ~700℃. At the same time, a high temperature pressure calibration device is developed, of which high temperature is 750 ℃, the calibration range is 0~0.5MPA, the precision is 0.02%FS, the calibration medium is water, oil, gas and molten salt.

Fig.16 The filling NaK pressure transmitter and calibration bench

Aiming at the special conditions of high temperature, high corrosion and high irradiation environment of TMSR, a prototype of radar liquid level meter with curved waveguide has been developed, and the design method of high-frequency radar waveguide and the manufacturing process of key parts are mastered. The products are tested by experiment, the parameters are as follows: Bending waveguide length: 4.5m; precision: ±0.1%f.s; measuring medium temperature: 600-700 ℃;

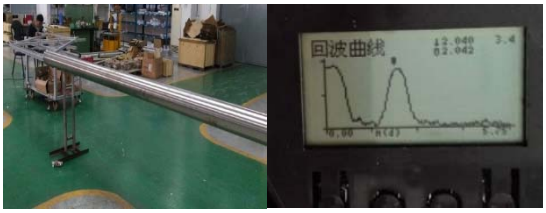

Fig.17 The prototype of radar level meter

The prototype of the external clamp high temperature ultrasonic flowmeter is successfully developed. The prototype adopts the homemade components. The data processing method improves the data filtering method on the basis of intercorrelation algorithm, and improves the precision and anti-interference ability of the system. In addition, through the optimization of the structure, heating and thermal insulation structure of the ultrasonic guided wave plate, the mode of natural cooling is realized to ensure the reliability of the ultrasonic probe in the measurement of the high temperature molten salt fluid. System performance is as following as : the flow velocity measurement range is 0.1~5m/s, and the measurement accuracy is <3%.

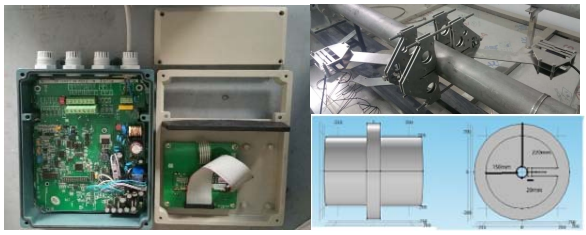

Fig.18 The prototype of high temperature ultrasonic flowmeter

In view of the complicated structure and high price of the original high temperature molten salt ultrasonic flowmeter calibration platform, a New calibration platform scheme for high temperature fluorine ultrasonic flowmeter based on air pressure is designed, and the corresponding design parameters and performance are calculated through the development of special software simulation. The calculation results are in agreement with the results of TRACE software : the maximum working pressure <0.5MPa; The temperature is <700 C, and the calibration accuracy is <3%. At the same time, we completed the development and acceptance of the calibration device.

Fig.19 The high temperature ultrasonic flowmeter calibration platform

熔盐堆物理研究

反应堆物理部

背景

本课题基于钍基熔盐堆核能系统先导专项关于熔盐堆研发的“实验堆—示范堆—商用堆”总体技术路线，以完成系列熔盐实验堆物理设计为核心目标，在熔盐堆中子物理、热工水力学方面开展物理研究，同时展开 10 MW 固态燃料熔盐实验堆(TMSR-SF1)、2 MW 液态燃料熔盐实验堆(TMSR-LF1)、小型模块化熔盐堆(TMSR-LF2、TMSR-SF2)、TMSR 仿真堆(TMSR-SF0)的设计分析工作。

10 MW(th)固态燃料熔盐实验堆设计方面，形成详细的核设计和热工水力设计参数及接口参数清单，形成工程设计阶段的核设计报告和热工水力设计报告。

2 MW(th)液态燃料熔盐实验堆设计方面，给出连续加料方案的燃料循环规律研究、堆芯选型方案研究和热工水力设计初步研究内容，形成初步核设计分析和热工水力分析报告。

小型模块化熔盐堆设计方面，开展百兆瓦级液态熔盐示范堆(TMSR-LF2)的初步物理分析工作，给出连续加料方案的燃料循环规律研究、堆芯选型方案研究和热工水力设计初步研究内容，形成初步核设计分析和热工水力分析报告。完善 100 MW 级固态钍基熔盐堆(TMSR-SF2)初步物理设计。

仿真堆方面，完成 TMSR-SF0 物理和热工水力的方案设计工作，确定 SF0 所需开展的热工实验，并完成实验方案的模化分析和评审，完成相应的物理和热工水力方案，开展加热装置的设计与样机加工工作。

10 MW(th)固态燃料熔盐实验堆设计

10 MW(th)固态燃料熔盐实验堆(TMSR-SF1)将是 TMSR 专项的首个实验堆，也是世界上首个有明确建造计划的氟盐冷却高温堆。

TMSR-SF1 的总体方案和参数有：1）反应堆功率：设计总功率为 10 MWt，装燃料球 13 000 个，使用一次装载一次卸料的方式。2）燃料元件：使用高温气冷堆的 TRISO 包覆颗粒燃料球。正常运行情况下最高燃料温度限值为 1 250 ℃。3）冷却剂：一回路冷却剂为 2LiF-BeF2 熔盐，熔盐中 7Li 的丰度大于 99.99%。4）堆芯：堆芯包括燃料区及其外围的反射层，堆芯外有围桶。燃料区中燃料球为随机排列。堆芯冷却剂质量流速 82 kg/s，出口温度为 650 ℃。5）反应性控制：反应性控制采用控制棒实现温度调节、功率调节、燃耗补偿和停堆等功能。6）堆本体：堆本体由内向外主要由以下部分组成：堆芯活性区、反射层、堆芯围筒、堆芯冷却剂下降环腔与上下腔室、反应堆主容器、氩气层、反应堆保护容器、热屏蔽层和隔热层。反应性控制系统、堆内相关测量系统、堆芯冷却剂流道等布置在相应的结构件中。反应堆容器内最大压力小于 5atm。7）回路系统：包括一回路、二回路、气路和熔盐检测设施等。8）余热排出：正常余热排出利用回路；失流事故情况下的余热排出由非能动堆外壳散热实现。9）燃料球装卸：从堆芯正下方通道依靠熔盐浮力进球，采用逐球装载方式；从堆芯正上方通道卸球。10）材料：堆容器、堆内结构和回路材料主要为哈氏-N 合金，反射层材料为核石墨，控制棒套管采用 SiC/SiC 复合材料或者 C/C 复合材料。11）安全设施：包括包容体、非能动反应堆容器外壳散热系统等设施。

TMSR-SF1 的物理方案如图 1 所示。

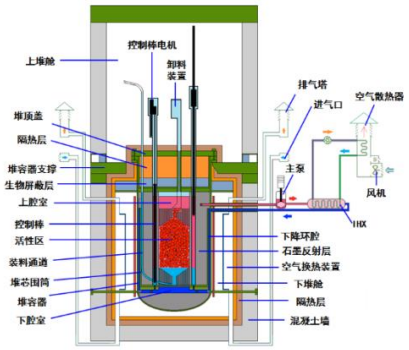

图 1 10 MW(th)固态燃料熔盐实验堆(TMSR-SF1)物理方案

2 MW(th)液态燃料熔盐实验堆设计

2 MW(th)液态燃料熔盐实验堆(TMSR-LF1)是继美国橡树岭国家实验室 MSRE 项目结束 50 年之后，人类重拾液态燃料熔盐堆技术的首堆。

TMSR-LF1 基本参数主要包括：1）^{235}U 富集度低于 20%；2）初装堆熔盐燃料为 LiF-BeF_2-UF_4，摩尔比为 68%-30.69%-1.31%，其中燃料富集度为

19.75%，Li-7 丰度为 99.95% at；3）限制初始剩余反应性为 2000 pcm；4）燃烧一定时间后，可以在熔盐燃料中添加少量 Th，以验证钍铀转换；5）堆芯石墨组件采用与 MSRE 相同的四棱柱体堆芯石墨组件，侧面开田径场型槽作为燃料盐流道；实验堆活性区高度和直径均为 180cm，实验堆堆芯主容器和下支撑板等堆内金属结构件使用 ASME-N10003 镍基合金材料。TMSR-LF1 的系统总体布局示意如图 2 所示。

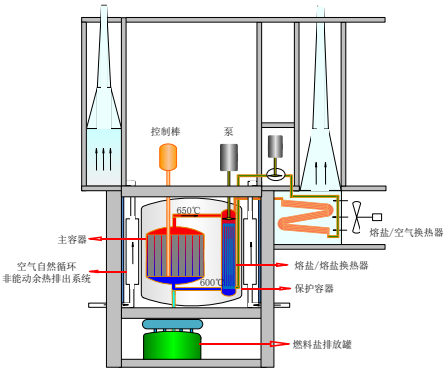

图 2 TMSR-LF1 系统总体布局示意

小型模块化熔盐堆设计

小型模块化熔盐堆是 TMSR 专项框架内连接实验堆向商用堆发展的重要环节，示范熔盐堆的安全性、经济性、可持续发展等先进性能。

TMSR-LF2 采用紧凑式回路设计，主要包括核热产生单元、中间热量传输单元、发电单元、非能动余热排出单元以及各辅助系统。核热产生单元建设于地下，由堆本体、主泵、主换热器和钢制安全壳组成，安全壳做为一道重要的安全屏障，将带有放射性的一回路总体包含在其中。核热产生单元底部设置紧急燃料盐排放罐，用于部分严重的事故下的停堆和余热排出。中间热量传输单元主要用于隔离带放射性的核热产生单元和热能利用单元（蒸汽发生单元、发电单元等），包括放射性隔离、化学隔离和压力隔离。反应堆核岛建设于地下，以降低占地面积和提高反应堆的安全性。TMSR-LF2 主要方案和参数：（1）单堆热功率为 373MWth，电功率为 168 MWe。（2）采用四个回路式布局，一回路（泵和主热交换器）位于安全壳内部。（3）TMSR-LF2 使用 LiF-BeF_2-UF_4.ThF4 做为燃料，^{235}U 富集度为 19.75%，Li-7 丰度为 99.995at%。（4）堆本体模块设计寿命为 10 年，堆运行初期使用低浓度的燃料运行，以保持较低的后备反应性，在运行过程中逐渐添加燃料。在堆运行过程中在线去除 Xe、T 等气态产物。使用气压装载和卸载燃料。（5）每炉燃料总运行时间为 40 年，其中每 10 年进行一次后处理，将其中有用的铀、钍、载体盐提取出来，进行多次循环的回堆利用。（6）使用石墨做为慢化剂，堆内构件采用简单的金属构件，有利于进行模块化设计和提高堆的结构稳定性。图 3 是 TMSR-LF2 总体系统示意图。

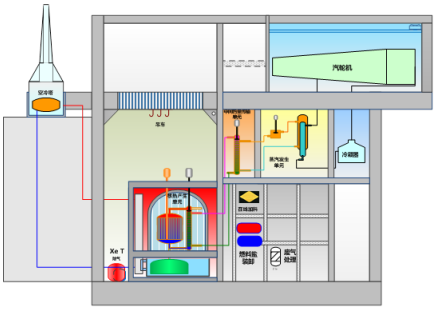

图 3 TMSR-LF2 系统总体布局示意图

TMSR 仿真堆

TMSR 仿真堆(TMSR-SF0)是以 TMSR-SF1 为原型的缩比实验装置，使用电加热器模拟反应堆核裂变热源，主要用于开展与 TMSR-SF1 相关的设计、安全、技术、设备的设计分析验证与研究。TMSR-SF0 的堆本体主要由以下部分组成：堆芯、堆芯围筒及隔板、堆芯冷却剂下降环腔、下腔室、上腔室、上下腔室填充体、流量分配装置、氩气覆盖层、堆内上部隔热层、熔盐注入和排出管道、反应堆容器、反应堆容器贯穿件和反应堆容器支撑结构等。TMSR-SF0 加热功率 0-400 kW，主容器及一回路设计温度 700 ℃，模拟堆熔盐出入口温度 600~650 ℃，非能动余排系统额定功率 12.8 kW。已完成了加热器样机的研制与初步测试，完成了缩比仿真堆堆芯加热装置的初步设计、技术规格说明书、招投标计合同签订，施工方案审阅等。图 4 为 TMSR-SF0 物理方案示意图。

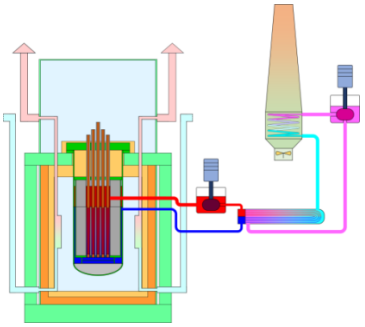

图 4 TMSR-SF0 物理方案示意图

Progress in Reactor Physics

Reactor Physics Division

Background

This project is based on the general technical route "Technology of Experimental Reactor - Demonstration Reactor - Commercial Reactor", which is planned by the center for Thorium Molten Salt Reactor system (TMSR) for the research and development of Molten Salt Reactor (MSR) nuclear energy system. This project is aimed to complete the physical design of a series of molten salt experimental reactors and research in neutron physics and thermal hydraulics in MSR. Meanwhile,10 MW solid fuel molten salt experimental reactors(TMSR-SF1), 2 MW liquid fuel molten salt experimental reactors (TMSR-LF1), small modular molten salt reactor（TMSR-LF2、TMSR-SF2）, and the TMSR Simulator (TMSR-SF0) are designed and analyzed.

For the design of 10 MWth solid fuel molten salt reactors, a detailed parameter list of design and interface for design of nuclear and thermal hydraulic will be formed, the design report of nuclear and thermal hydraulic will be formed at engineering design stage.

For the 2 MWth liquid fuel molten salt experimental reactor design, the regularity of fuel cycle by continuous feed, selection of reactor type and preliminary research of thermal hydraulic design will be given. The preliminary design report of nuclear and thermal hydraulic will be formed

For the small modular molten salt reactor design, the preliminary physical analysis of the 100 MW liquid molten salt demonstration reactor (TMSR-LF2) will be carried out, the regularity of fuel cycle by continuous feed, selection of reactor type and preliminary research of thermal hydraulic design will be given. The preliminary design report of nuclear and thermal hydraulic will be formed. The preliminary physical design of a 100MW TMSR-SF2 will be improved.

For the TMSR Simulator, the physical and thermal hydraulic design of TMSR-SF0 will be completed, thermal experiments required will be determined, the model analysis and review of the experimental plan will be formed, the corresponding physical and thermal hydraulic solutions will be completed. The design of heating device and the machining of prototype work are in process.

Design of 10 MWth solid fuel fluoride salt experimental reactor

The 10 MWth solid-fuel test reactorsis the important experimental reactor for the TMSR project and also be the first fluoride-cooled high-temperature reactor in the world with a well-constructed plan.

The overall scheme and parameters of TMSR-SF1 are as follows. 1) Reactor power: The design power is 10 MW. 13000 fuel pebbles will be loaded and unloaded all at once. 2) Fuel element: TRISO coated fuel of HTGR is used, with the temperature limit of 1 250 ^{o}C during normal operation. 3) Coolant: Primary coolant is 2LiF-BeF_2, abundance of Li-7is approximately 99.99%. 4) Reactor core: The core includes fuel zone and the reflector in its periphery. There is core barrel outside the reactor core. Fuel pebbles in the fuel zone are randomly arranged. The mass flow rate of coolant in reactor core is 82kg/s, and the outlet temperature of TMSR-SF1 is 650^{o}C. 5) Reactivity control: the reactivity control adopts the control rod to achieve the functions of temperature regulation, power adjustment, burnup compensation and shutdown. 6) Reactor body: from inner to outer, the reactor consists: core active zone, the reflector, the core barrel, the downcomer and the upper and lower chambers, the reactor vessel, the argon layer, the reactor container, thermal shield layer and heat insulation layer. The reactivity control system, some measurement system and the primary coolant flow channel are appropriately arranged in the reactor body. The maximum pressure in the reactor vessel is less than 5 atm. 7) Loop system: including the primary loop, secondary loop, gas circuit and molten salt detection facilities.8) Decay heat removal: The decay heat is removed by the primary loop under normal condition. Under the loss of flow accident, the passive decay heat removal system is used to discharge the decay heat. 9) Fuel handling process: the fuel pebbles are loaded in turn by the buoyancy of molten salt and discharged from the channel directly in the top of the core. 10) The materials of reactor container, inner structure and the pipelines are mainly Hastelloy-N alloys. The reflector is made out of nuclear graphite, the control rod sleeves are made of SiC/SiC composites or C/C composites. 11) Safety facilities: include containment bodies, passive decay heat removal system and other facilities. The physical scheme of TMSR-SF1 is shown in Fig.1.

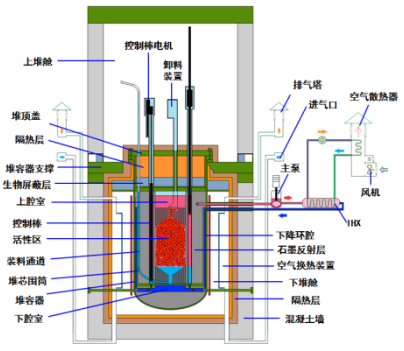

Fig.1 Physical solution of 10 MWth solid fuel molten salt experimental reactor (TMSR-SF1)

The design of 2 MWth liquid fuel molten salt experimental reactor

The 2 MWth liquid fuel molten salt experimental reactor (TMSR-LF1) will be the first reactor in 50 years after the end

of the MSRE project at the Oak Ridge National Laboratory in the United States.

The basic parameters of TMSR-LF1 mainly include: 1) the U-235 enrichment is less than 20%. 2) The molten salt fuel is LiF-BeF_2-UF_4, and the molar ratio is 68.00%-30.69%-1.31%, in which the enrichment of U-235 and the abundance of Li-7 is 19.75% and 99.95 %, respectively.3) The initial residual reactivity is 2 000 pcm. 4) After burning for a certain time, a small amount of Th should be added to the molten salt fuel to verify the thorium-uranium conversion. 5) The core graphite assembly is tetrahedral graphite assembly which is the same as MSRE's core assembly. Its lateral track is field groove as fuel salt channel.The height and diameter of the reactor's active zone are both 180cm, The ASME-N10003 nickel base alloy is used in the metal structure of the core main vessel and the lower support plate of the experimental reactor. The overall layout of the TMSR-LF1 is illustrated in Figure 2.

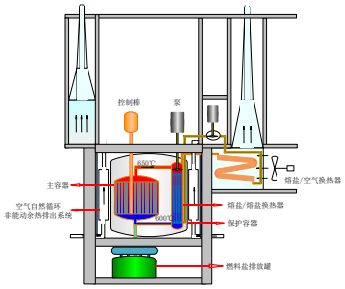

Fig.2 System Overall Layout of TMSR-LF1

Design of small modular molten salt reactor

The small modular molten salt reactor is an important part in the development of the experimental reactor to the commercial reactor in the TMSR project. It can demonstrate the safety, economy, sustainable development of molten salt reactor.

TMSR-LF2 adopts a compact loop design, which mainly includes nuclear heat generation system, intermediate heat transfer system, power generation system, passive decay heat removal system and various auxiliary facilities. The nuclear heat generation system is built underground and consists of the reactor body, the main pump, the main heat exchanger and the steel containment. As an important safety barrier, the nuclear heat generation system contains the primary circuit with radioactivity in it as a whole. An emergency fuel salt discharge tank is arranged at the bottom of the nuclear heat generating system for shutdown and waste heat discharge in some serious accidents. The intermediate heat transfer system is mainly used to isolate the radioactive nuclear heat generation system from thermal energy utilization system (steam generation system, power generation system, etc.), including radioactive isolation, chemical isolation and pressure isolation. Reactor nuclear island is built underground to reduce floor space and improve reactor safety. TMSR-LF2 main scheme and parameters: (1) the thermal power of single reactor is 373 MWth and the electric power is 168 MWe. (2) a four-loop arrangement is adopted, and the primary loop (pump and main heat exchanger) is located inside the container. (3) TMSR-LF2 uses LiF-BeF_2-UF_4-ThF_4 as fuel, ^{235}U enrichment is 19.75%, and Li-7 abundance is 99.995%. (4) The design life of the reactor proper module is 10 years. In the early stage of operation, low concentration fuel was used to maintain low reactivity and fuel gradually during operation. The gas products such as Xe and T are removed on line during the operation of the reactor.(5) The total operating time for each furnace fuel is 40 years, and a reprocessing is carried out to extract the useful uranium, thorium and carrier salts in every 10 years, and recycle it for multiple cycles. (6) Using graphite as a moderator, the internal components of the reactor adopt simple metal components, which is conducive to modular design and improve the structural stability of the reactor. Figure 3 is a schematic diagram of the overall system of TMSR-LF2.

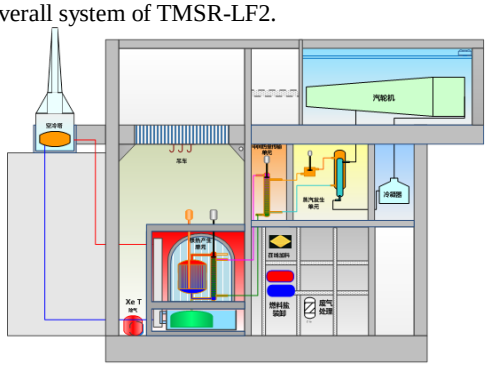

Fig.3 Overall layout of TMSR-LF2 system

TMSR Simulator

The TMSR Simulator (TMSR-SF0) is a reduced-ratio experimental device based on TMSR-SF1. It uses an electric heater to simulate the reactor nuclear fission heat source and is mainly used to carry out analysis verification and research in design, safety, technology and equipment related to TMSR-SF1.

The reactor of TMSR-SF0 is mainly composed of the following components: core, core barrel and separator, core coolant descending ring cavity, lower chamber, upper chamber, upper and lower chamber filling objects, flow distribution device, argon gas blankets, upper in-stack insulation, molten salt injection and discharge piping, reactor vessels, reactor vessel penetrations, and reactor vessel support structures. TMSR-SF0 heating power 0~400 kW, main vessel and primary circuit design temperature 700 °C, simulated reactor molten salt inlet and outlet temperatures 600~650 ℃, passive residual heat removal system rated power 12.8 kW. The development and preliminary test of the heater prototype have been completed, the preliminary design of the simulation reactor core heating device, the technical specifications, the signing of the bidding contract, and the review of the construction plan have been completed. Figure 4 is theTMSR-SF0 physical scheme diagram

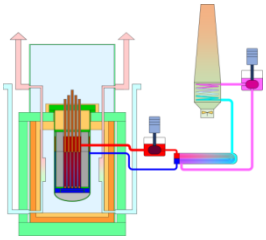

Fig.4 TMSR-SF0 physical scheme diagram

熔盐化学与工程技术部

工程样机为立式液下机械离心泵，泵与泵罐一体化设计。为方便维护检修，除泵罐外，其余部分可抽芯设计。叶轮为悬臂式安装，采用导叶式压水室。为阻挡高温熔盐的热辐射，采用屏蔽塞隔热。为防止泵罐内放射性气体的逸出，主轴轴封采用气体吹扫加迷宫密封的气封方式。轴承采用强制润滑冷却，轴承体上下端有机械密封充当油封。泵与电机采用膜片式联轴器挠性联接，联轴器外部设置保护罩。电机采用隔爆型变频电机，电机通过支架支撑于主法兰上方。泵组支架支撑于主法兰下方。总体结构见图 1。

完成熔盐泵工程样机的结构方案的初步设计，设计温度 500~700 ℃，设计流量 300m^3/h，适用氟盐介质。按照安全 2 级的规范要求，完成压力边界的焊接结构设计，提交焊接及无损检测技术条件 8 篇，并按照 QA1 要求，完成质保大纲的升版。

熔盐泵熔盐试验回路目的是为熔盐泵及样机提供高温熔盐试验平台，主要任务是对泵进行熔盐介质下的高温试验研究。

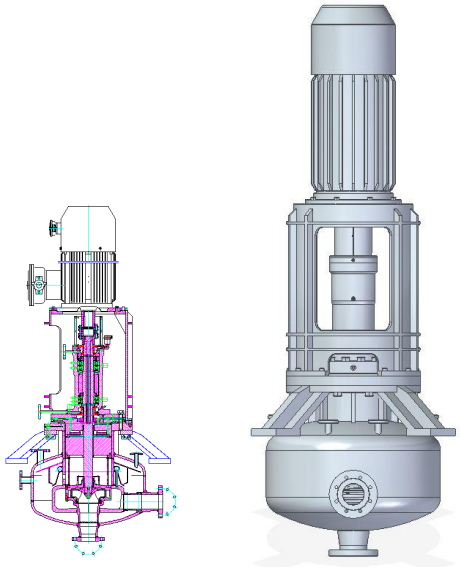

图 1　工程样机总体结构示意图及三维实体图

熔盐泵熔盐试验台架主要由主回路系统、熔盐储存与加载系统、气路系统、预热及散热系统、测控系统、支撑系统 6 个子系统组成，系统原理、管路布置如图 2 所示。

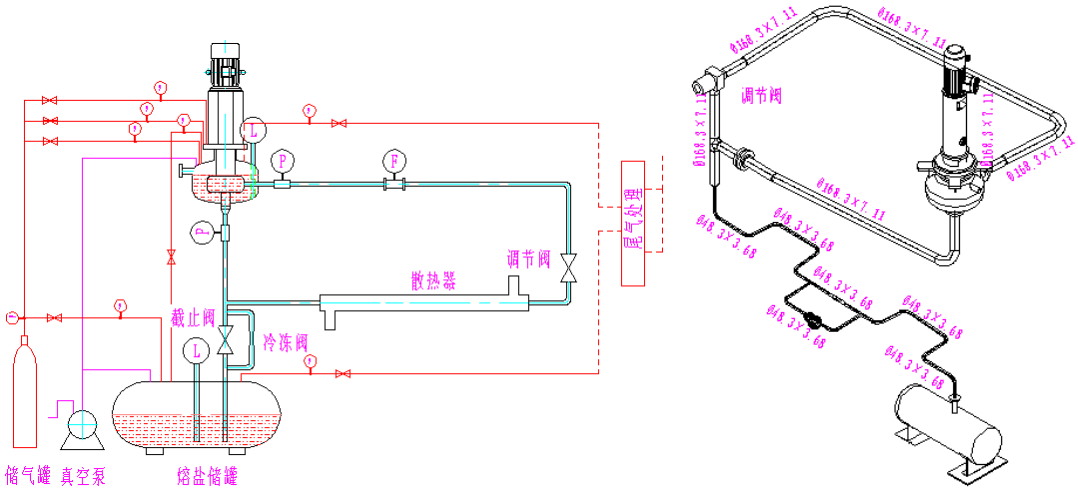

图 2　熔盐泵熔盐试验台架系统原理及管路布置图

完成泵熔盐试验台架工程设计，设计温度 500~700 ℃，主管道规格 DN150，适用氟盐介质，并开始土建基础施工，主要设备如储罐等开始加工。完成《熔盐泵熔盐试验回路系统方案评审报告》，《熔盐泵熔盐试验台架机械系统工程设计报告》、《熔盐泵台架鉴定试验大纲》等技术报告。

建立了蒸汽抑制研究方法,配套研制了蒸汽抑制专用实验台架模拟工程环境和变量控制，并开展了吹扫气量与蒸汽抑制效果影响关系的实验研究，获取了可靠的实验数据。实验结果显示，单边 1 mm 间隙，3.2 L/min 的吹扫气量可实现 99.78%的抑制率，继续增大吹扫流量抑制效果提升不明显，该结果可为工程设计中蒸汽抑制吹扫气流量的确定提供设计依据。

通过机械调节阀工程样机的研制，掌握了调节阀中关键的节流部件的设计方法，完成了节流部件的结构设计，并通过 CFD 方法分析出了调节阀的流量调节特性，进而分析出了熔盐泵台架的工作特性，获得了熔盐泵台架的 Q-H 曲线。通过对调节阀进行热学与应力分析评定及相关结构的改进设计，最终的分析计算结果满足设计要求，完善了调节阀的结构设计。最终完成了机械调节阀的加工制造。

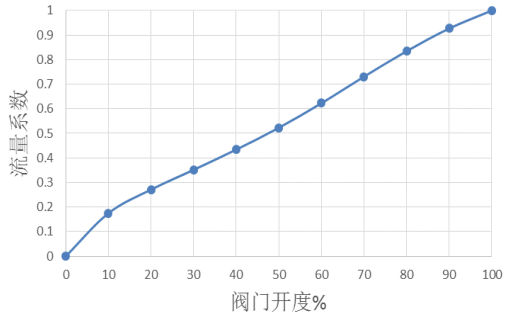

图 3 调节阀的流量特性曲线

管道预热保温样机累计进行了 3200 小时长期运行。实验测得管道内外壁温度分布均匀，无局部过热的情况发生。实验获得了不同加热功率下加热器的升温速率，为以后反应堆的运行提供了参考数据。实验测试数据指出管道支撑处可不设加热器，利用实验测得的数据校核了前期的设计计算是可靠的，并对相关参数的选取提供了参考。

管道预热保温样机高温性能试验中，分别设定加热目标温度为 500 ℃、550 ℃及 600 ℃三组实验参数，测得加热器温度控制点到达设定温度时管道内外壁的温度分布，绘制试验测得的温度数据如下图所示，由图及数据可以分析得出每次实验下被测点的温度数值分布均匀，无局部过热点。

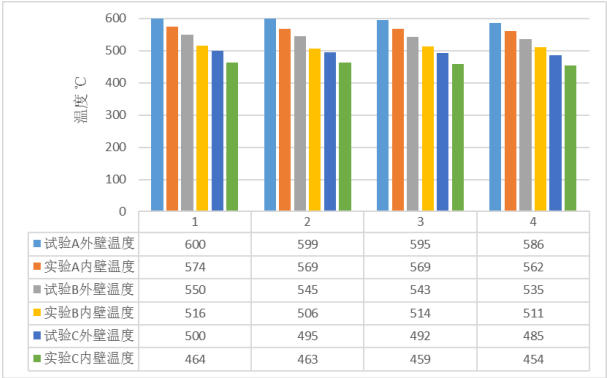

	1	2	3	4
试验A外壁温度	600	599	595	586
实验A内壁温度	574	569	569	562
试验B外壁温度	550	545	543	535
实验B内壁温度	516	506	514	511
试验C外壁温度	500	495	492	485
实验C内壁温度	464	463	459	454

图 4 管壁温度分布统计图

完成冷冻阀工程样机的性能试验，包括开关性能试验、冻堵稳态试验和耐压试验。获得相关性能数据，作为 SF1，LF1 冷冻阀设计支撑。

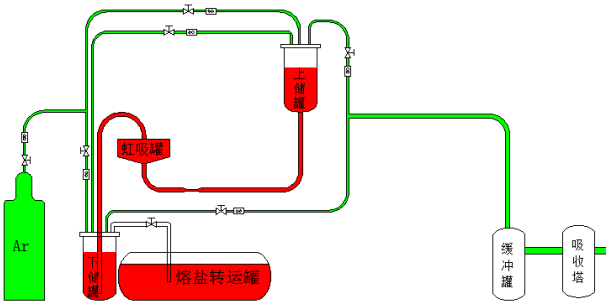

图 5 试验台架示意图

The Molten Salt Loop Technology

Molten Salt Chemistry and Engineering Technology Department

The engineering prototype pump is a vertical-shaft sump centrifugal pump with an overhung impeller and radial vaned diffuser, a pump tank and a shaft seal (see Fig. 1). For the convenience of maintenance, the rotary assembly can be pulled out from the pump tank by loosening the flange bolts. To stop the thermal radiation of the molten salt, shielded plugs are set in the upper part of the pump tank. In order to prevent the radioactive gas of pump tank escaping, shaft portion to the pump tank is sealed by a labyrinth gland with auxiliary purge gas. Bearings are cooled by the forced lubrication. A mechanical seal as oil seal is set at both at ends of bearing. The diaphragm coupling which has middle section connects the motor shaft and pump shaft，with an external shield. The motor is supported on the top of the pump tank flange. Compared with supporting upper bearing, supporting on pump tank flange is more stable and reliable.

The preliminary structure design of engineering prototype pump have been completed with the design temperature of 500~700℃, the design flow rate of 300 m^3/h, the medium of fluoride salt. According to the requirements of the level 2 safe specification, welded structure design of stress boundary has been completed. The 8 articles about welding and nondestructive testing technology have been submitted, and the quality assurance program has been completed according to the requirements for QA1.

The molten salt test loop for pump is used to provide high temperature molten salt test platform for the prototype pumps. The main task is to test and research the performances of pumps under molten salt medium and the high temperature.

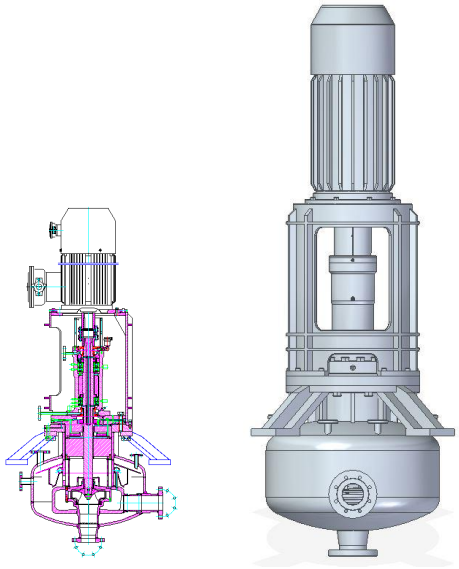

Fig.1 Structure diagram and 3D entity graph of engineering prototype pump

The molten salt test loop for pump is mainly composed of the primary loop systems, molten salt storage and loading system, pneumatic system, preheating and cooling systems, measurement and control system and the support system. The system principle, piping layout is shown in Fig. 2.

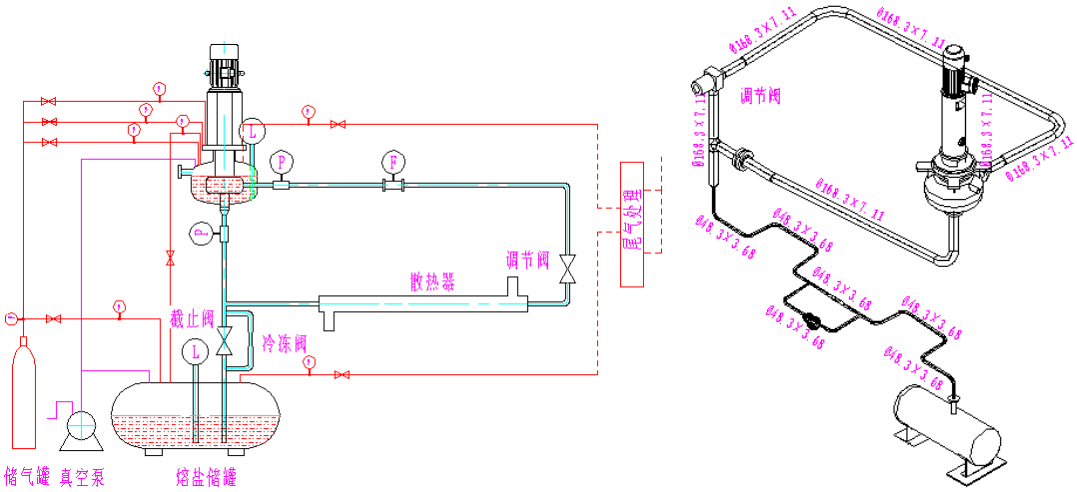

Fig.2 System principle diagram and Piping layout

The engineering design of molten salt test loop for pump has been completed, with the design temperature of 500 ~ 700℃, the main pipe specifications of DN125, he medium of fluoride salt. The foundation construction and the main equipment such as tank have started to manufacture. Some technical reports such as“The system audit report of molten salt test loop for pump”,“the mechanical system engineering design report of molten salt test loop for pump”，“the appraisal test outline of molten salt test loop for pump ”have been completed.

A method for experimental study on inhibition of molten salt steam by purge gas is developed. Moreover, a special experimental bench has been established at the same time, which can simulate the conditions of true engineering environment and variable control. On the bench, the relationship between purging gas flow and steam inhibition effect have been studied and much reliable experimental data have been obtained. The results show that the purging gas flow at 3.2 L/min could reach to 99.78% inhibition rate with the clearance of unilateral 1mm. While continuously the purge flow increases, the inhibition rate increases not obviously. It provides a design basis for the determined value of the purge gas flow in engineer design.

The design methods of the main components for throttling valve have been mastered by the development of throttling

valve. The structure design of the main throttling components has been completed and the flow characteristics have been analyzed through CFD method. Then the working characteristics and the Q-H curve of the molten salt pump test loop have been obtained from the analysis results. The structural of the throttling valve has been optimized by thermal and stress analysis, and the final results met the design requirements. The optimized structure of throttling valve was completed. At last the throttling valve was finished manufacture.

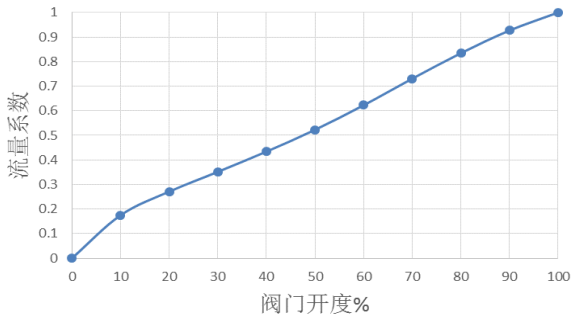

Fig.3 Flow curve of the throttling valve

The pipe heat and insulation prototype has been run for 3200 hours in all. The temperature of the inner and outer surface of the pipe is well-distributed as the test results show, and there is no local overheating.

The heating rates of the heater at different heating power have been obtained, which provide reference data for the reactor further operation. The test results indicate that there is no need to heat at the pipe support. The previous design has been verified by the test data, and the value setting of some parameters can refer to the test data.

During the test of the pipe heat and insulation prototype, the temperature distributions of the inner and outer surface of the pipe when the control temperature reached the setting valves which were 500℃、550℃ and 600℃ have been obtained. The test data is shown in the following figure .From the figure, it can be concluded that the temperature distribution is uniform, and there is no local overheating.

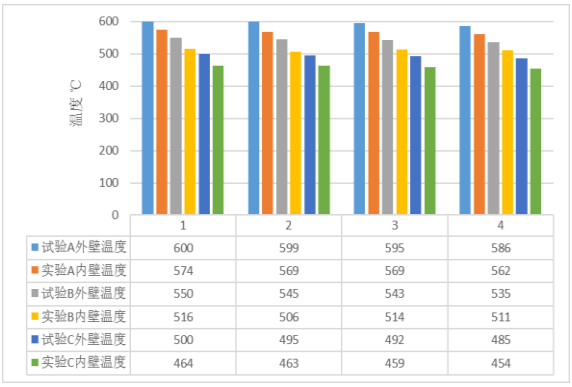

Fig.4 Distribution of the pipe temperature

The performance test for the engineering prototype of freeze valve has been completed, including on and off time, the temperature of the static freezing station and pressure test. The getting data from test is used to support for freeze valve design of SF1, LF1.

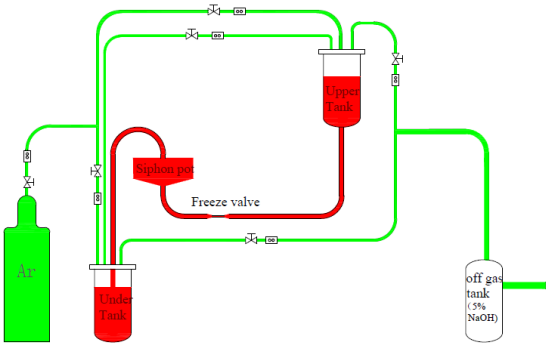

Fig.5 Schematic diagram of the test bench for freeze valve

熔盐化学研究平台

熔盐化学与工程技术部

为了满足熔盐堆设计、建造过程中对熔盐材料及相关技术、知识的需求，我们建立了熔盐化学研究平台。其主要任务是为熔盐堆建造提供合格的熔盐材料，同时为堆设计提供熔盐相关物理化学性质参数及化学安全知识。通过熔盐化学研究平台的建设，我们具有全面评估熔盐冷却剂各方面性能的能力，可以为熔盐堆冷却剂的选择及质量标准的制定提供建设性意见。2015-2016 年度，熔盐化学研究平台课题取得如下重要进展。

针对 FLiBe 和燃料盐物性测试需求，建立了完善的熔盐热物性测试平台及可靠的铍防护措施。在此基础上，采用阿基米德法、旋转法、激光闪光法、差示扫描量热法开展 FLiBe 熔盐密度、粘度、导热系数、比热的实验测试，测试误差分别为 1%、±0.2 cP、15%和 5%。

鉴于国际上还没有完备的有关 $LiF\text{-}BeF_2\text{-}ThF_4\text{-}UF_4$ 熔盐的相图与热物性数据包，因此完成这类数据包对于液态堆的工程研究与建设意义重大。本年度我们全面搜集与评估文献中有关 $LiF\text{-}BeF_2\text{-}ThF_4\text{-}UF_4$ 各子体系所有的实验密度粘度数据， 筛选准确度较高的密度粘度数据，优化模型参数。先后完成 $LiF\text{-}BeF_2$ 体系、$LiF\text{-}ThF_4$ 体系、$LiF\text{-}UF_4$ 体系、$BeF_2\text{-}ThF_4$ 体系、$BeF_2\text{-}UF_4$ 体系和 $ThF_4\text{-}UF_4$ 体系等二元系物性数据的模拟计算，具备了燃料盐关键热物性参数的理论计算能力。

另外，我们研制了熔盐蒸气压测试装置。采用 Knudsen 隙透-TG-沸点法联用的测试方案，设计出高温熔盐蒸汽压测试仪。工作温度可达 1 200℃，工作压力 10^{-5} Pa~10^{5} Pa 且连续可控，微量热重天平量程 50 g，精度 0.1 mg，灵敏度不低于 1 微克。蒸汽压测试范围 10^{-2}~10^{5} Pa，测试精度 500 Pa 以上为 10%，10~500 Pa 精度可达 20%，1Pa 以下精度小于 10%。

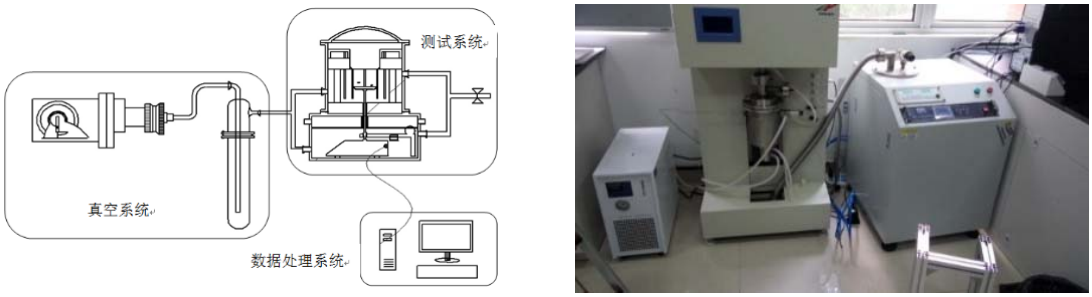

图 1 熔盐饱和蒸汽压测试系统

为确保进堆 FLiNaK 和 FLiBe 熔盐的质量满足熔盐堆冷却剂使用要求，提高熔盐产品质量的稳定性，合理利用资源，提高经济效益，根据物理设计要求结合净化工艺水平，腐蚀测试结果，制定了 $H_2\text{-}HF$ 工艺生产 FLiNaK 和 FLiBe 熔盐的质量标准，明确了质量检验规则，作为进堆熔盐组织生产和产品检验的依据。

在项目已有 FLiBe 熔盐、ThF_4 和 UF_4 分析方法的基础上，建立了 FLiBeThU 燃料盐的样品前处理方法，研究了高浓度锂、铍、钍和铀基体对杂质定量分析的影响，建立了 FLiBeThU 熔盐中痕量金属杂质和 Si、B、P、S 非金属杂质的分析流程，并考察了分析方法的准确度和精密度。

利用熔盐电化学技术建立了熔盐体系铀及氧离子的原位测试方法，并成功用于氟盐体系中氧化铀沉淀形成规律的研究。这一研究结果有助于理解熔盐堆燃料盐核燃料氧化物沉淀的形成机制，进而制定合理的燃料盐质量控制标准，避免铀燃料的沉淀及其所可能引发的安全问题。

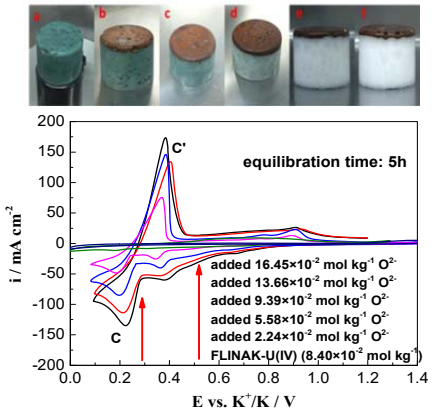

图 2 FLiNaK -U(IV)体系添加不同浓度 O^{2-}后所观测的现象（上图）及测定的循环伏安曲线（下图）

2015-2016 年度，在充分考虑了 FLiBeThU 燃料盐制备实验的化学、辐射危险性特征的基础上，在乙级放射化学实验室建立了公斤级燃料盐制备平台，解决了熔盐脱模取样与固体杂质分离等技术难题。采用“一锅煮”工艺制备了符合液态堆设计要求的 FLiBeThU 燃料盐（LiF-BeF_2-ThF_4-UF_4 68-28-0.1-3.9 mol%），核心指标硼当量低于 8 μg/g，其余各关键杂质含量亦符合指标（Fe < 50 μg/g，Ni < 50 μg/g，Cr < 10 μg/g，SO_4^{2-} < 10 μg/g，PO_4^{2-} < 10 μg/g，NO_3^- < 100 μg/g，Cl^- < 10 μg/g）。除此之外，FLiBeThU 燃料盐对堆用合金材料的静态腐蚀速率低于 10 μm/y，与石墨共存的电化学加速腐蚀速率不高于 25 μm/y。

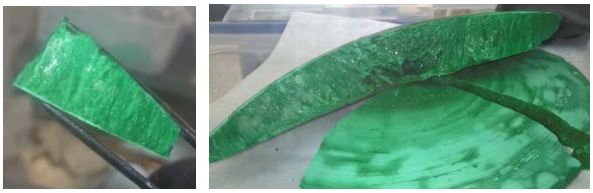

图 3 通过“一锅煮”法制备的燃料盐样品

从技术层面，高纯 FLiNaK 与哈 N 合金材料的相容性问题已经得到解决。2015−2016 年的目标是降低 FLiNaK 工程应用的成本。一方面，进一步优化 FLiNaK 制备工艺，采用工业级原料替代实验室级原料，获得氧元素含量低于 100 μg/g 的高纯 FLiNaK 产品，大幅降低了原料采购成本。另一方面，采用 316L 不锈钢替代价格高昂的哈 N 合金，依据多组分氟化物熔盐化学平衡原理，使用化学反应体系自由能计算，创新设计并制备了以 Cr^{2+}为主体的 $Cr^{3+}/Cr^{2+}/Cr^0$ 氧化还原缓冲体系，显著降低了高纯 FLiNaK 对 316L 不锈钢的腐蚀速率。

2015-2016 年铍安全与防护处理子课题主要开展了三方面的工作：（1）研究、优化含铍废气处理工艺；（2）确立实验室规模含铍废气处理装置的方案；（3）完成涉铍实验人员的培训和体检工作。研究、优化了超声增湿撞击流泡沫捕捉塔的含铍废气净化能力，出口浓度小于 10 μg/m^3，满足考核指标；经过改进，超声波增湿撞击流泡沫捕捉塔对细颗粒物有较好的去除效果，当铍颗粒物粒径达到 0.26 μm 以上时，铍的去除效率能达 60 %以上，在铍颗粒物粒径在 0.65 μm 以上时，铍去除效率达到 95 %以上并趋于平稳。通过对嘉定园区 107 楼涉铍实验室不同规模含铍尾气处理装置的效果评估，制定了实验室尾气处理方案（如图 1-4（a）所示）。监测尾气处理装置改进前后（改进前未加碱液吸收罐）尾气中锂的浓度（如图 1-4（b）所示），经过改进后的尾气处理装置对尾气中熔盐颗粒的去除效果十分明显，排放的熔盐颗粒浓度符合国标规定。

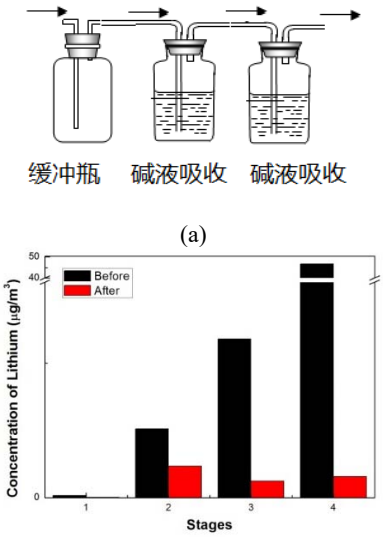

图 4 涉铍实验装置尾气处理工艺
(a) 装置示意图；(b) 处理效果对比

2015−2016 年度化学安全与监测子课题主要开展了两方面的工作：（1）涉铍实验监测体系的优化和规范；（2）铍和氟在线监测设备的研制。优化了涉铍实验的监测方案，改进了监测方法，形成技术报告。确立了铍、氟在线监测设备的研制方案，并在已有设备的基础上，初步完成了装置的搭建（如图 1-5 和 1-6 所示），检出限可达到：铍：6 ng/m^3，氟：0.1 μg/m^3。

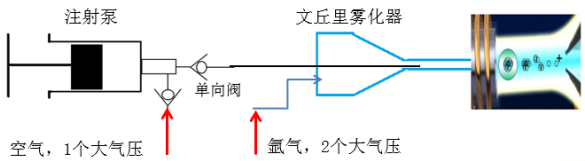

图 5 铍在线监测设备组成示意图

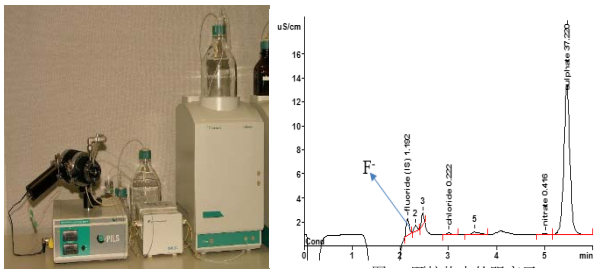

(a) (b)

图 6 氟在线监测系统 (a) 装置实物图；(b) 测量结果

2016 年度氯苯废水废气治理子课题主要开展

了两方面的工作：（1）气相、液相中氯苯检测方法的确定；（2）含氯苯废水、废气处理的研究。通过配置电子捕获检测器的气相色谱对氯苯进行分析。空气中氯苯的检测限达 0.01 mg/m^3，水中氯苯的检出限达 0.5 μg/L，均达到目标要求。利用过硫酸盐技术和纳米碳材料相互作用，开展亚铁离子活化过硫酸盐处理含氯苯废水的工艺研究，5mg/L 的氯苯水溶液经过活化过硫酸盐降解后，去除率为 82 %，排放达到国标的要求。建成基于过硫酸盐氧化法的氯苯类废气治理装置（如图 1-7 所示），治理后氯苯废气浓度低于国标 GB16297-1996 规定的排放限值（60 mg/m^3），表明该氯苯废气治理装置的有效性。

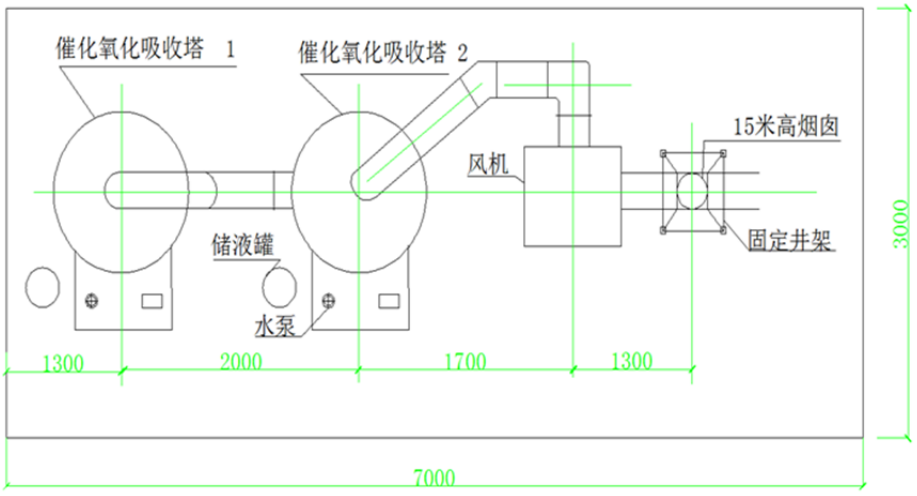

图 7　含氯苯类废气处理设备平面布置图

Molten Salt Chemistry Study Platform

Department of Molten Salt Chemistry and Engineering

A molten salt chemistry study platform was built to meet the knowledge and technology demand of molten salt reactor design and construction. The main task of this study platform is to provide qualified molten salt for the experimental reactor along with various physical and chemical property data and chemical safety knowledges. These studies will help us have the ability to fully evaluate the performance of molten salt coolant, which can provide constructive suggestions for the selection of molten salt reactor coolant and the development of quality standards. In the year 2015−2016, we made following important progresses.

A complete platform for testing thermal physical properties of molten salt and reliable anti-tank protection measures have been established to satisfy the FLiBe and fuel salt properties test requirements. The density, viscosity, thermal conductivity, specific heat capacity of FLiBe molten salt has been tested using Archimedes method, rotation method, laser flash method, differential scanning calorimetry, the error was 1%, ± 0.2 cP, 15% and 5%, respectively.

In view of the fact that there are no complete phase diagrams and thermal physical properties data packages for $LiF-BeF_2-ThF_4-UF_4$ molten salt in the world, the completion of such data packages is of great significance for the engineering research and construction of liquid reactors. In this year, we comprehensively collected and evaluated all experimental density and viscosity data of $LiF-BeF_2-ThF_4-UF_4$ and its sub-systems in the literature, and model parameters were optimized on these data. The simulations of the $LiF-BeF_2$, $LiF-ThF_4$, $LiF-UF_4$, BeF_2-ThF_4, BeF_2-UF_4 and ThF_4-UF_4 systems were successively completed, the theoretical calculation ability of the parameter was established.

In addition, we have developed vapor pressure testing device of molten salt that uses a Knudsen-TG-boiling point test scheme to design a high-temperature molten salt vapor pressure tester with a working temperature of 1 200 °C, working pressure range of 10^{-5}~10^{5} Pa, continuously controllable, micro-thermometer: range 50g, precision 0.1mg, sensitivity no less than 1 microgram, steam pressure test range: 10^{-2}～10^{5}Pa, test accuracy: >500 Pa: 10%, 10~500 Pa: 20 %, <1Pa: less than 10%.

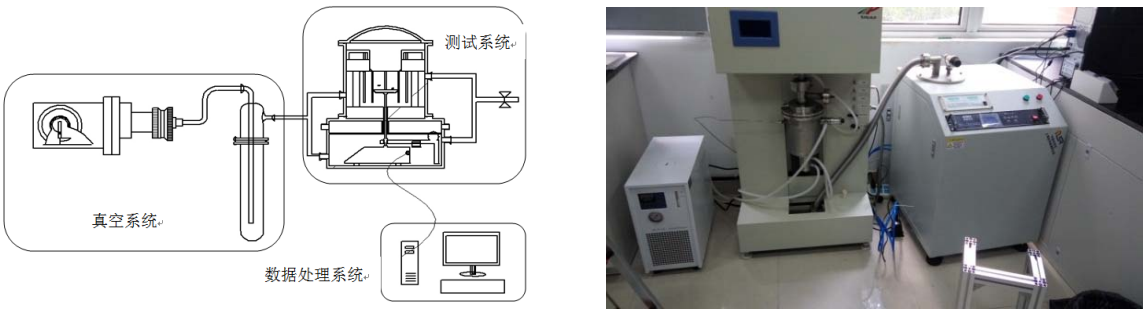

Fig.1 Test system for saturation vapor pressure of molten salt

To make sure the prepared FLiNaK and FLiBe qualified as reactor coolant, the quality standard of FLiNaK and FLiBe produced by the H_2-HF method was established. The physical requirements of molten salt reactor, the preparation and purification technological level and the corrosion test results between FLiNaK and structural alloy were comprehensively considered for determining the detailed specifications. The quality inspection methods have also been made clear as the basis for organizing production and analyzing products. This standard can help to rationally utilize the resources and improve the stability of the quality of the molten salt.

The sample pretreatment method of FLiBeThU fuel salt was established based on the experience on FLiBe and UF_4. The influence of high concentration lithium, beryllium and uranium matrix on the quantitative analysis of trace metal impurities was studied. Based on this, the analysis flow of trace metal impurities in FLiBeThU salt was determined. The accuracy and precision of the analytical methods were also investigated.

The in-situ test method of uranium and oxygen ion in molten salt system was established by the electrochemical technique and successfully used in the study of the formation phenomena of uranium oxide precipitation in the fluorine salt system. The results will help to understand the formation mechanism of the oxide deposition in fuel salt and to formulate a reasonable quality standard of fuel salt avoiding the precipitate of uranium and any possible safety problems that may arise.

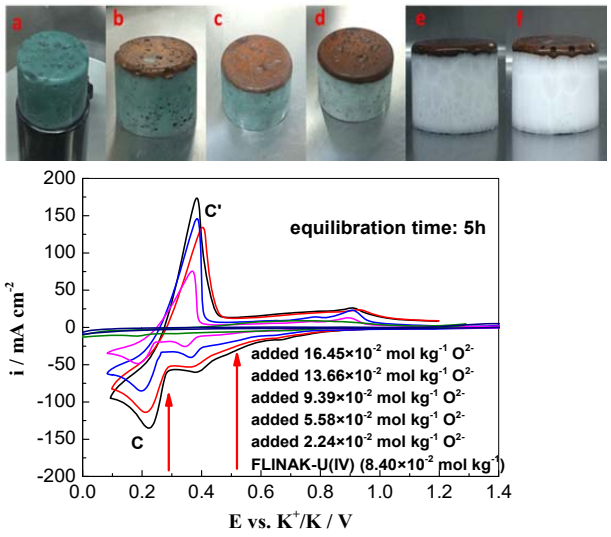

Fig.2 the phenomena observed in the FLiNaK -U (IV) system after adding different concentrations of O^{2-} (above) and corresponding cyclic voltammetry curves (below).

Radiation and chemical safety strategies were thoroughly analyzed before the fuel salt FLiBeThU was trial - produced at 1 kg per batch level in Grade B radiochemistry laboratory. Challenging technical problems such as demolding, sampling and impurity separating were solved, and the optimum technological parameters were ascertained after numbers of experiments. Purity content of the product (LiF-BeF_2-ThF_4-UF_4 68-28-0.1-3.9 mol%) met the design requirements of nuclear reactor (boron equivalent < 8μg/g, Fe<50 μg/g, Ni<50μg/g, Cr<10 μg/g, SO_4^{2-}<10 μg/g, PO_4^{2-}<10 μg/g NO_3^-<100 μg/g, Cl^-<10 μg/g). Static corrosion rate and graphite – accelerated corrosion rate of the product to Hastelloy N alloy was controlled to lower than 10 μm/year and 25 μm/year, respectively.

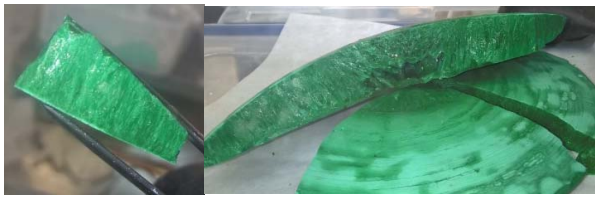

Fig.3 Photo of the fuel salts prepared by "one pot process"

On the technical side, the compatibility of high-quality FLiNaK and Hastelloy N alloy was good enough for engineering applications. However, the economic cost needed to be reduced by technical innovation. On one hand, the cost of raw materials was greatly reduced by replacing laboratory grade raw materials with industrial grade raw materials after optimizing the preparation process. On the other hand, the high cost Hastelloy N alloy was replaced by 316L stainless steel after new corrosion inhibitor $Cr^{3+}/Cr^{2+}/Cr^0$ redox equilibrium system was developed in FLiNaK.

Three aspects of beryllium safety protection and treatment subproject have been carried out during 2015 and 2016: (1) Treatment technology of beryllium-contained waste gas has been studied and optimized; (2) Beryllium-contained waste gas processing plant has been established on laboratory scale; (3) Work of training and examination beryllium-involved experiment personnel has been completed. The processing capacity of impinging stream bubble capture tower has been studied and optimized. The export concentration of tower is lower than 10 μg/m3, which meets the assessment indicator; Impinging stream bubble capture tower has been improved for a more effective removal efficiency of fine particulates. When the size of beryllium particles is bigger than 0.26 μm, removal efficiency of beryllium is more than 60%. When the size of beryllium particles is bigger than 0.65 μm, removal efficiency is more than 95% and starts to level off. Beryllium-contained waste gas processing plant (as shown in Fig.1-4(a)) has been established on laboratory scale, through evaluating the effect of beryllium-contained waste gas processing device on different scales for beryllium-involved lab of building 107 in Jiading campus. The lithium concentration of waste gas from the devices has been monitored before and after improvement (as shown in Fig.1-4(b)). It shows that the removal efficiency of molten salt particles in waste gas has been now much improved. The emission concentration of molten salt particles complies with national standard.

Two aspects of chemical safety and monitoring subproject have been carried out during 2015 and 2016: (1) Optimization and specification of beryllium-involved experimental monitoring system; (2) Development of beryllium and fluorine online monitoring equipment. The monitoring scheme of beryllium-involved experiments has been optimized, monitoring method has been improved. The development scheme of beryllium and fluorine online monitoring equipment has been established. The construction of the device has been completed on the basis of in-use equipment (as shown in Fig.1-5 and 1-6). The detection limit of beryllium and fluorine can be reached to 6 ng/m^3 and 0.1 μg/m^3, respectively.

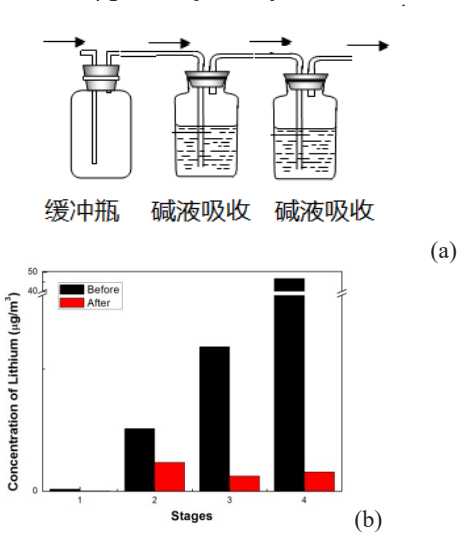

Fig.4 Waste gas treatment technology of beryllium-involved device: (a) schematic diagram of experimental set-up; (b) comparison of treatment effect

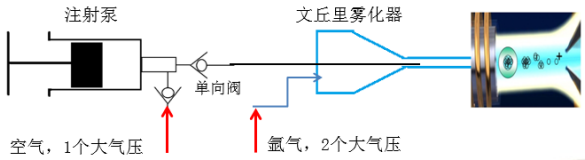

Fig.5 Composition diagram of beryllium online monitoring equipment

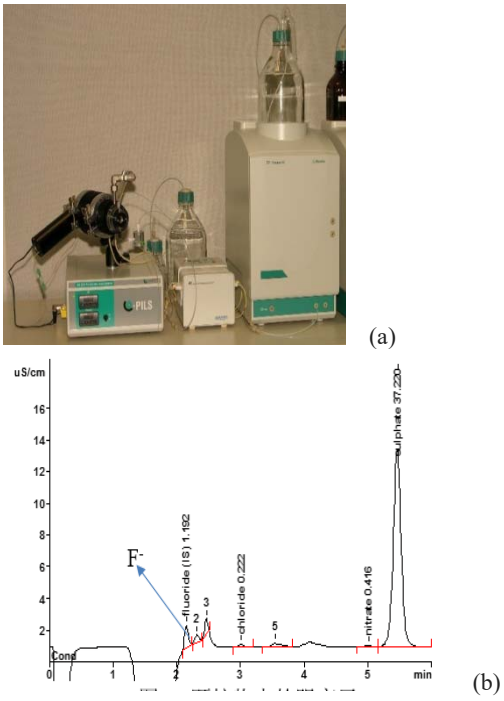

Fig.6 Fluorine online monitoring system: (a) device photo; (b) measuring result

Two aspects of waste water and gas of chlorobenzene treatment subproject have been carried out during 2015 and 2016: (1) Determination of chlorobenzene detection method in gas phase and liquid phase; (2) Research of treatment of chlo-

robenzene-contained waste water and gas. Chlorobenzene is analyzed by gas chromatography configuring electron capture detector. The detection limits of Chlorobenzene in gas phase and liquid phase are 0.01 mg/m3 and 0.5 μg/L respectively, which have both achieved the target and requirement. Advanced oxidation processes with $Fe^{2+}/Na_2S_2O_8$ were applied to treat chlorobenzene in aqueous, by interaction between persulfate technique and multi-walled carbon nanotubes (MWCNTs). The removal efficiency can reach to 82 % to meet the national emission standard, when the chlorobenzene concentration was 5 mg/L degradation by Fe^{2+} /MWCNTs system.

The processing equipment of chlorobenzene-contained waste gas has been completed based on persulfate oxidation method (as shown in Fig.1-7). The chlorobenzene concentration of waste gas after processing is lower than 60 mg/m^3 (The emission limit of national standard GB16297-1996), which indicates that the processing equipment of chlorobenzene-contained waste gas is very effective.

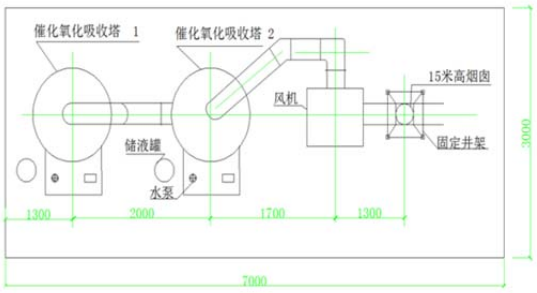

Fig.7 Layout of the processing equipment of chlorobenzene-contained waste gas

熔盐回路试验平台

熔盐化学与工程技术部

熔盐回路试验平台主要围绕着两个领域：（1）熔盐净化处理；（2）先进热-功转换关键技术及系统，开展研究工作。

1 熔盐净化处理

由于使用 FLiBe 作冷却剂，熔盐堆在运行过程中，会产生大量的气态放射性核素，包括氚、氪、氙等。为了确保堆的正常运行，降低气态放射性核素的排放量，需要对堆中气态放射性核素进行在线处理。2015–2016 年度，熔盐净化处理主要研究了 TMSR 气态放射性核素处理工艺，包括：熔盐中气态放射性核素的脱除、分离、纯化、与储存，以及整个工艺流程中的在线监测。取得如下进展：

1.1 研制了石墨对氢气的吸附与解析实验装置

我们研发了高温下石墨对氢气的吸附与解析实验装置，解决了高温下，低浓度氢气的本底控制与测量问题。并获得了初步实验结果。

(a)

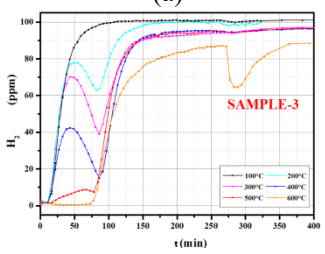

(b)

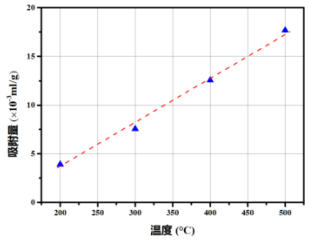

(c)

图 1 a) 高温真空吸附与解析系统实物图，b）不同温度下的吸附曲线；c）计算后的吸附量与温度的关系

结果表明，在 200~500 ℃ 时，石墨对氢的吸附量与温度成正比，这表明在此温度段内对氢的吸附是物理吸附；氢的吸附量与石墨的结构直接相关，石墨孔隙率、结构差异会导致吸附量存在巨大差异。

1.2 熔盐中放射性气体的脱除

依托现有水回路实验台架，进行升级改造，如图 2 所示。在循环泵出口缓冲罐处以 5 mL/min 的流速通入氢气，用鼓泡器通入氩气作为载气，经气液分离器将水中气体分离出来，使用仪器分析尾气浓度。

通过鼓泡脱气可以稳定的将大多数氢气提取出来，尾气分析结果见图3。通过对尾气进行检测，得到尾气中氢气和氩气的变化关系曲线。长期稳定运行后，通入氢气基本被完全脱除，水中氢气浓度达到平衡后维持在较低浓度。平均气泡直径为 0.5 mm，水中载气含气率为 0.2%，经分离器分离后，保持氢气浓度在 10 ppm 以下，完成系统脱气性能测试。

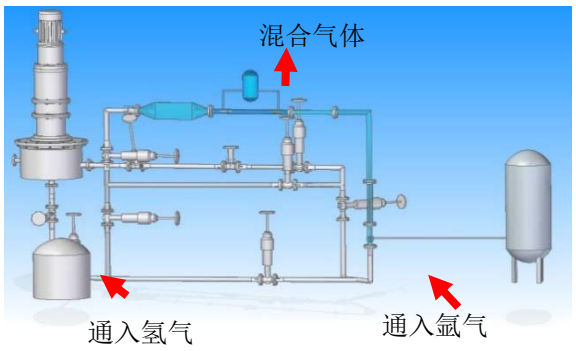

图 2 鼓泡脱气实验回路

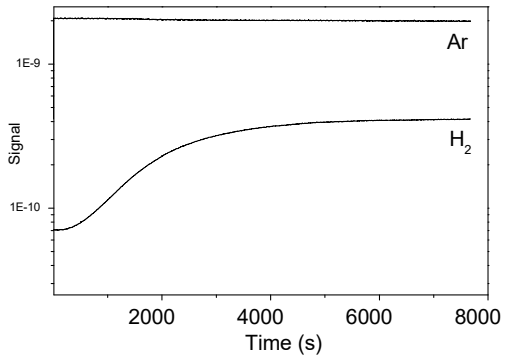

图 3 氢气和氩气浓度变化

1.3 熔盐堆中放射性气体的分离

熔盐堆中脱除出来的放射性气体拟采用低温分离系统进行分离。经多次实验验证，低温分离系统的温度和压力控制精度达到预期。低温系统一级冷冻罐内温度达到 40 K，二级冷冻罐和二级冷头温度分别达到 4.6 K 和 3.1 K。

以氦气中添加 100 pm 的 Kr，Xe，H_2 的杂质作为原料气开展分离系统性能测定，尾气测量结果显示 H_2 的浓度下降 3 个数量级(H_2 浓度低于 0.1 ppm)，而 Kr 和 Xe 均低于 RGA 的检测下限(20 ppb)。

1.4 氢同位素储存研究

对 Zr 基合金进行了改性研究，采用电弧熔炼炉制备了 $ZrCo_{0.8}M_{0.2}$(M=Co、Cu、Cr、Mn、Al)合金，并对合金的放氢性能进行测试，如图 4 所示。$ZrCo_{0.8}M_{0.2}$ 合金的放氢量随着 Cr、Mn 和 Al 的替代下降幅度大，主要原因是合金内第二相放氢量太低。这几种元素替代对合金放氢平台压的影响不明显，放氢平台压基本无变化。

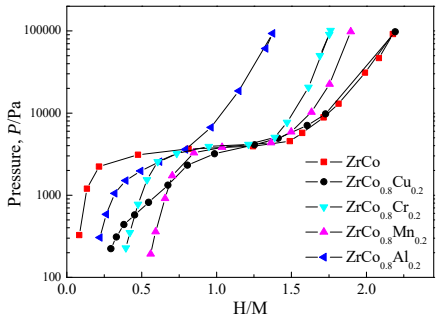

图 4 $ZrCo_{0.8}M_{0.2}$ 合金 563 K 下放氢 PCT 曲线比较

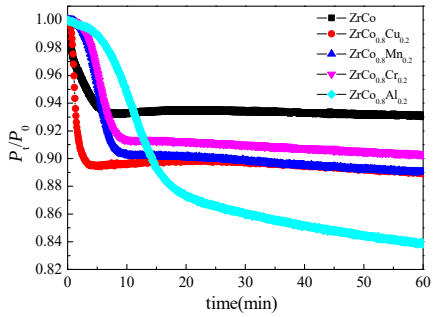

图 5 823 K 下 $ZrCo_{0.8}M_{0.2}$ 合金的歧化曲线

此外，还对合金的歧化性能进行测试，如图 5 所示 $ZrCo_{0.8}M_{0.2}$ 合金的歧化反应程度随着不同元素的添加而出现了不同程度的增大。但 Cr 和 Mn 元素的添加能够降低歧化反应速率。

在合金优化的基础上对合金储氢器的结构设计进行了优化，设备采用内部加热。增加二级保护层，采用 Ar 气对保护层吹扫，降低设备运行过程中氢的向外渗透。进气管先流经加热装置，起到提前预热作用，提高其处理效果。在合金储氚器进出口加装过滤器，防止合金粉进入气路中，同时，在进气口前端加装过滤片，用于支撑合金粉，并保证气体可以与合金粉充分接触，提高效率。

1.5 氚在线监测

研制了塑料闪烁体氚探测器，该塑料闪烁体探测器对 HTO 的最低探测下限达到 1.3μCi/L，能够满足探测下限 1mCi/L 的要求。

2 先进热-功转换关键技术及系统研究

2015−2016 年度，依托熔盐回路试验平台，先进热-功转换关键技术及系统研究取得如下进展：（1）仿真实验装置熔盐换热器设计、熔盐空气换热器设计、熔盐空气换热器系统设计，并启动加工。（2）完成 MW 级氦气闭式布雷顿循环验证示范系统建设，开展氦气闭式布雷顿循环系统运行规律调节研究。（3）完成开展氦气轮机氦气/空气模化研究。（4）完成 TMSR 新型复合布雷顿循环优化方法研究以及核心部件设计。

2.1 TMSR 换热器研制

熔盐-熔盐换热器为卧式设备，壳-U 型管式结构，采用平封头。管束规格为 Φ13.72×1.65 mm，有效换热管长为 1.9 m，管间距 20 mm，正三角形排列，U 形换热管根数为 18 根，有效换热面积 3 m^2；壳体外径为 212 mm，内径为 200 mm，采用单弓形折流板，切口 25%，折流板间距为 120 mm，折流板 14 块。

熔盐-熔盐换热器结构型式如图 6 所示。熔盐-空气换热器为垂直放置，选择纯错流形式。

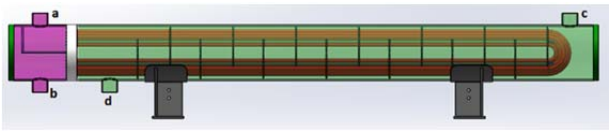

图 6 熔盐-熔盐换热器结构型式
(a) 一回路熔盐入口, (b) 一回路熔盐出口,
(c) 二回路熔盐入口, (d) 二回路熔盐出口

同时还完成了空冷系统的设计，以及小孔径内孔焊加工工艺研究，并完成性能测试。

2.2 氦气布雷的循环系统及关键技术研究

2016 年完成了氦气压气的模化试验，并完成了氦气透平试验回路的安装调试，进行了 10 MW 氦气轮机的系统循环优化设计以及一维气动设计

和初步结构设计。

氦气透平试验回路主要设备包括发电机、减速齿轮箱、透平、电加热器、回热器、气动快开快闭阀门、膨胀节，如图 7 所示。验证和分析氦气透平在不同工质时的透平特性，以及闭式循环试验控制和运行策略。

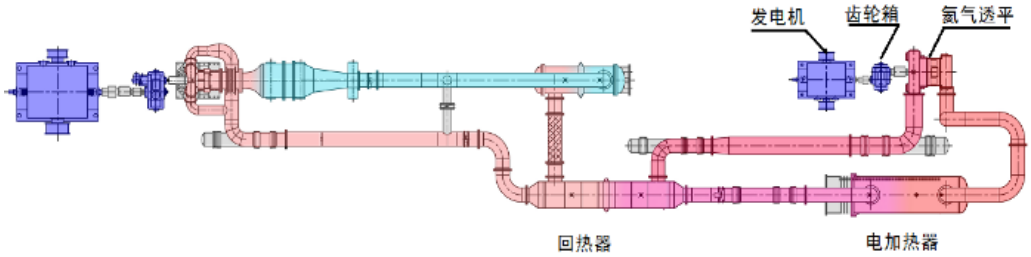

图 7　氦气闭式布雷顿系统

Test Platform of Molten Salt Loop

Molten Salt Chemistry and Engineering Technology Department

In 2015-2016, two series studies are mainly investigated based on the molten salt test platform: (1) the purification of molten salt; (2) the key technology of advanced thermal power conversion.

1 The purification of molten salt

A large amount of gaseous radionuclides, including tritium, krypton and xenon, are generated during the operation of TMSR, due to the use of FLiBe as the coolant. In order to ensure the safe operation of reactor and reduce the emission of these gaseous radionuclides, it is necessary to establish the on-line treatment of gaseous radionuclides in the reactor. During 2015−2016, the on-line treatment of gaseous radionuclides including the removal, separation, purification, storage and the monitoring through the entire process, was investigated by the molten salt purification group. The major progress can be listed as follows:

1.1 The experimental device for the determination of adsorption and desorption of hydrogen by graphite was developed

In order to accurately determine the hydrogen with low concentration at high temperature, which should be affected by the background of water, hydrogen in the atmosphere, we developed the experimental device for the adsorption and desorption of hydrogen by graphite. The tests by the blank and standard gases demonstrated that the results were reliable. The preliminary results of the adsorption and desorption were obtained.

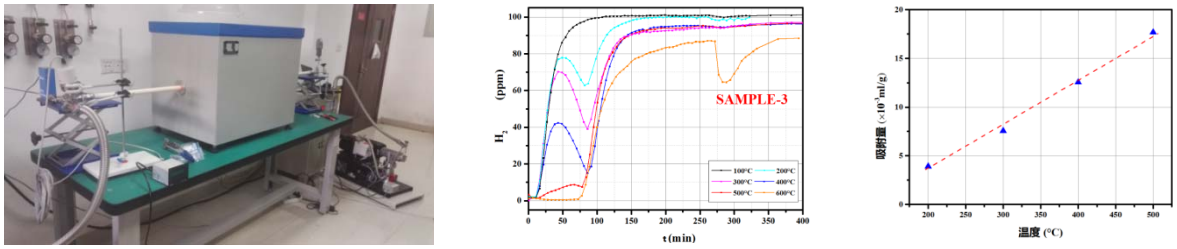

(a) (b) (c)

Fig.1 (a) The adsorption and desorption system, (b) the adsorption curves at different temperature, (c) the relationship between the adsorption and temperature

The results showed that the amount of hydrogen absorbed by graphite is proportional to the temperature in the region of 200-500℃, which indicates that the adsorption of hydrogen is physical adsorption in this temperature range. The adsorption amount of hydrogen varies largely depends on the structure, pores of the graphite.

2 The removal of radioactive gas in molten salt

The water circuit test bench was upgrade and reformed as shown in Fig.2. Hydrogen was injected with a flow rate of 5 ml/min at the outlet of the circulation pump. Ar was injected through a bubbler was the carrier gas. The hydrogen was separated with the carrier gas and separated by the gas-liquid separat

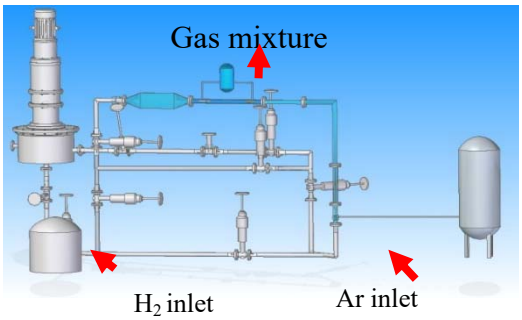

Fig.2 The test loop for removal of radioactive gas

or. The concentration of the exhaust gas was analyzed using the gas chromatography.

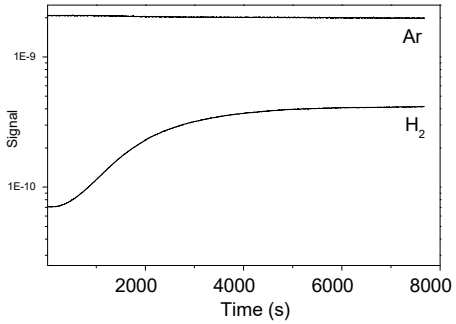

Fig.3 The concentration of H_2 and Ar

2.1 The separation of radioactive gas

The mixture of radioactive gas separated using the cryogenic separation system. The results demonstrated that the control accuracy of the temperature and pressure reached the design expectations. The temperature of the primary refrigeration tank reached 40K, and the secondary freezing tank and the secondary coldhead reached 4.6K and 3.1K, respectively.

The performance of the separation system was tested with the helium (adding 100ppm of Kr, Xe, and H_2). The results showed that the concentration of H_2 decreased by three orders of magnitude (lower than 0.1 ppm), and the concentration of Kr and Xe were lower than the limit detection (20 ppb) of RGA.

2.2 The storage of the hydrogen isotope

The modification of Zr-based alloys was studied. The alloy of $ZrCo_{0.8}M_{0.2}$ (M=Co, Cu, Cr, Mn, Al) was prepared by the arc smelting furnace, and the hydrogen release properties of the alloys were tested. As shown in Fig.4, the amount of hydrogen released decreases with the substitution of Cr, Mn and Al, which should be attributed to the low hydrogen content of the second phase in the alloy. No obvious effect on the hydrogen depressurization plateau pressure due to the substitution of these elements.

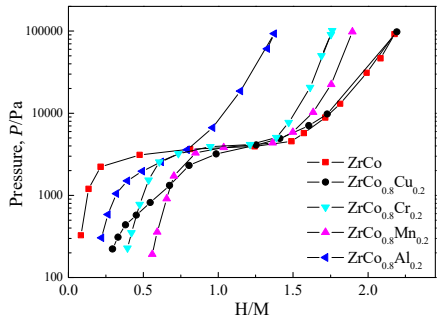

Fig.4 The PCT curves at 563K

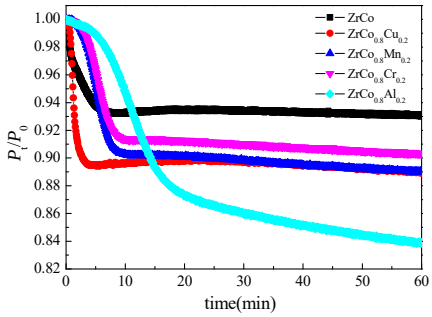

Fig.5 The disproportionation curves at 823K of $ZrCo_{0.8}M_{0.2}$

In addition, the disproportionation performance of the alloy was tested. As shown in Fig.5, the degree of disproportionation of the $ZrCo_{0.8}M_{0.2}$ increased with the addition of these elements. However, the addition of Cr and Mn will decrease the rate of the disproportionation reaction.

The structural design of the alloy hydrogen storage vessel was optimized as follows: the vessel can be heated internally; the secondary protective layer was added, which is purged by Ar continuously to avoid the permeation of H_2 during the operation. The exhaust was heated flowing through the heating device to improve the treatment effect. A filter was installed at the inlet of the vessel to prevent the entrance of alloy power to the gas pipes. At the same time, a filter plate is installed at the front of the air inlet to support the alloy powder and ensure that the gas can fully contact with the alloy powder.

2.3 On-line monitoring system

The plastic scintillator detector was developed. The minimum detection limit of the plastic scintillator detector for HTO is 1.3 μCi/L, which satisfies the need of TMSR (detection limit of 1 mCi/L).

3 The key technology of advanced thermal power conversion

In 2015-2016, the following progress was achieved in the research of the key technologies of advanced thermal power conversion based on the test platform of molten salt loop: (1) complete the design of molten salt heat exchangers and molten salt-air heat exchangers; (2) complete the construction of closed MW helium Brayton cycle demonstration system and carry out the studies of system operation; (3)complete helium / air modeling research of helium turbine; (4) investigate the optimization of new composite Brayton cycle in TMSR and design the core components.

3.1 Development of TMSR heat exchanger

The molten salt molten salt heat exchanger is designed as a horizontal equipment. A flat head is adopted to the exchanger while a U tube structure is applied. The tube bundle specification is 13.72 x 1.65mm, the effective heat transfer tube length is 1.9m, the tube spacing 20mm. The arrangement of the tubes is triangle. The number of U shaped heat transfer tube is 18, which results 3M2 effective heat transfer area. The outer and inner diameter of the shell are 212mm and 200mm respectively. The single arch baffle is used and the incision is 25%.

The structure of molten salt-molten salt heat exchanger is as shown in Fig. 6. The molten salt air heat exchanger is vertically placed and the pure cross flow mode is selected.

At the same time, the design of air cooling system and the studies of welding process in small bore were completed.

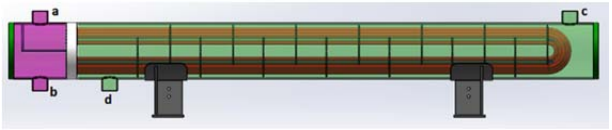

Fig.6 Structure of molten salt-molten salt heater exchanger (a) Inlet of first molten salt loop, (b) Outlet of first molten salt loop, (c) Inlet of second molten salt loop, (d) Outlet of second molten salt loop

3.2 The key technology of helium Brayton cycle system

The model test of the helium gas pressure regulation was evaluated, and the installation and commissioning of the helium turbine test circuit was completed. The optimization design of the 10MW helium turbine system and the preliminary structure design were carried out.

The main equipment of the helium turbine test circuit consists of generator, gear box, turbine, electric heater, regenerator, valves, expansion joint, as shown in Fig. 7. The characteristics of helium turbine in different working fluids are verified and analyzed. Also the control and operation of helium turbine closed cycle test was studied.

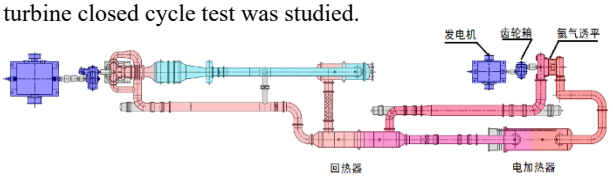

Fig.7 The closed Helium Brayton system

放射化学与工程技术部

2015−2016 年度反应堆燃料技术研究课题组在前期工作的基础上，进一步开展了以下工作：（1）TMSR-SF0 燃料元件输运系统；（2）钍基燃料元件研制，包括钍基燃料核芯制备工艺研究，包覆燃料颗粒研制以及燃料元件研制；（3）燃料性能检测与化学分析。

TMSR-SF0 燃料元件输运系统

确定燃料元件预处理及燃料输运装置的设计功能、设计参数及燃料装卸料和在线循环主要工艺流程。确定燃料输运子系统与设备空间布局，明确关键设备燃料输运管道、燃料预处理装置、碎球分离器、分配器、气氛切换阀、过球计数器(图 1)参数与关键指标设计，完成设备订购。

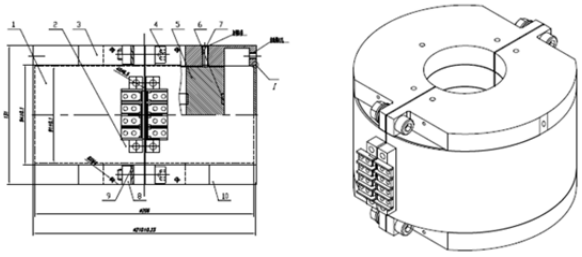

图 1　过球计数器设计结构图

钍基燃料元件研制

钍基熔盐堆核燃料研制包括钍燃料核芯、包覆燃料颗粒及燃料元件等三个主要工艺流程。

钍基燃料核芯制备：重点解决了凝胶颗粒在热处理过程中容易破碎以及粒形粒度均一性等问题。优化了胶凝小球的干燥、焙烧及烧结条件，重点考察焙烧及烧结温度、升温速率、保温时间、反应气氛等的影响，得到了直径约为 500 μm，密度>95%TD 的 ThO_2 陶瓷核芯。同时，开展了 ThCO 燃料核芯的制备工艺研究，制备得到了球形度良好的 ThCO 陶瓷小球。

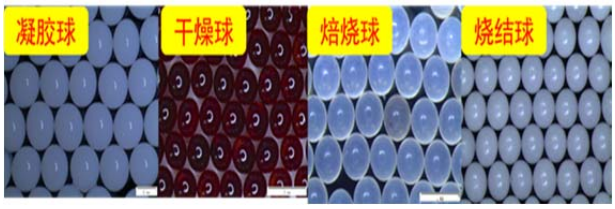

图 2　ThO_2 陶瓷核芯照片

包覆颗粒制备：完成了包覆颗粒制备装置的加工、安装和调试，并开展了包覆燃料颗粒的研制工作。重点研究了致密纯相 β-SiC 制备工艺，在优化的工艺参数下获得了各层厚度符合设计指标(图 3)、力学性能较好的包覆层。计算和测量表明，现有样品符合设计值标准偏差的概率为：缓冲层、内致密热解炭层、碳化硅层大于 99%，外致密热解炭层大于 97%。

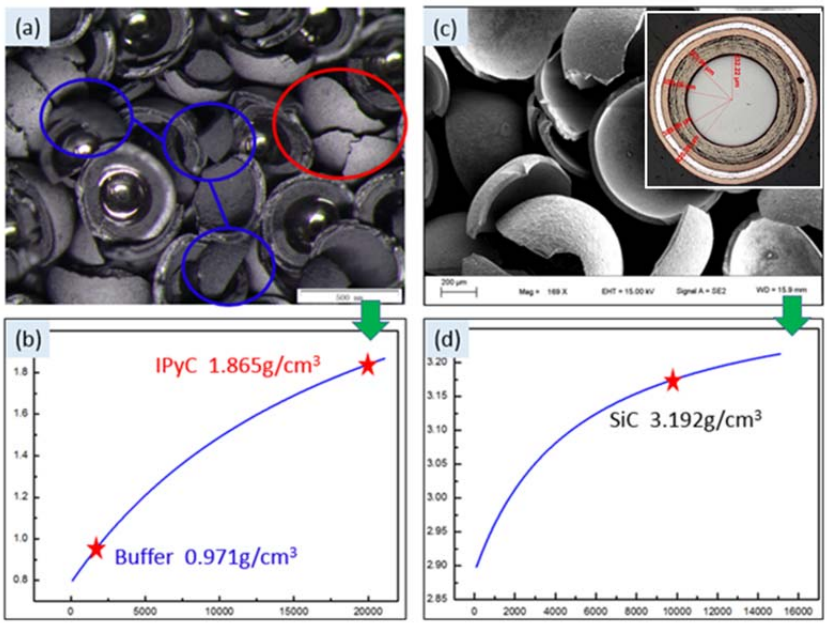

图 3　缓冲层、致密热解碳层和碳化硅层的密度

球形燃料元件制备：设计加工或购置了球形燃料元件压制的关键实验设备，建立了球形燃料元件压制工艺研究的实验条件。针对熔盐堆对球形燃料元件低密度、高功率和耐熔盐浸渗的要求，采用准等静压、基体石墨造孔和固相增密相结合的工艺路线制备原型燃料元件(图 4)，基本解决了球环型燃料元件制备的几个技术难点（元件内部低密度球芯的预置；次外层燃料区的弥散分布；外层石墨的致密化调控），得到了球（环）形燃料元件原型。图 5 中所示原型元件的直径为 60±0.3 mm，整球体密度≤1.7 g/cm^3。

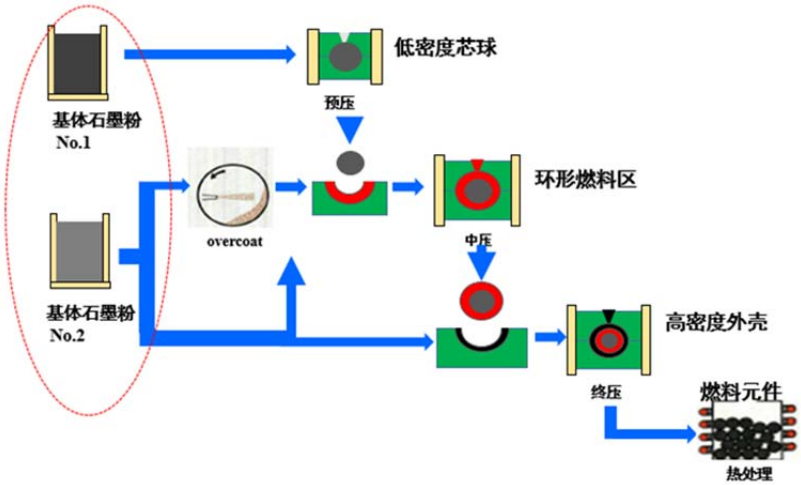

图 4　球环型燃料元件制备流程示意图

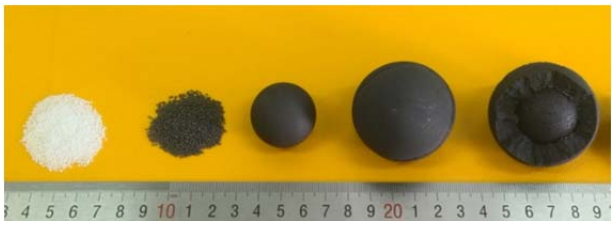

图 5　球环形燃料元件的宏观照片

燃料性能检测与化学分析

建立了包覆颗粒粒径和密度的测试方法：用激光脉冲拍照获得批量包覆颗粒投影，统计分析其粒径和球形度；用密度梯度法测试疏松热解炭层密度；用滴定法测试致密热解炭层密度。

建立了二氧化钍粉末中硼镉等杂质元素测定以及痕量稀土元素测定的内部标准，研究了四氟化钍中痕量金属杂质元素的多种分析方法。所建立的分析流程，其分析检测限、检测范围、精密度等参数都能满足核纯钍基材料的质量控制要求。

Reactor Fuel Technology for Thorium Molten Salt Reactor

Department of Radiochemistry and Engineering

During 2015−2016, the reactor fuel technology research group carried out mainly the following work among others: TMSR-SF0 fuel element transport subsystem design; the development of thorium-based fuel pebbles, including the preparation of thorium fuel kernels, the design and the manufacture of a Fluidized Bed-Chemical Vapor Deposition (FB-CVD) system, the pressing of spherical fuel elements; the characterization methods of fuel pebbles and the chemical analysis of impurities in thorium compounds;

TMSR-SF0 fuel element transport subsystem design

The function and design parameters for the fuel element pretreatment and transport devices were confirmed. And the main processes of fuel loading, on-line circulation and fuel unloading were established. The equipment layout of fuel transportation subsystems was designed. The key devices, including pipelines, fuel pretreatment device, fuel separators, fuel distributors, gas valves, and fuel counters have all been ordered from suppliers.

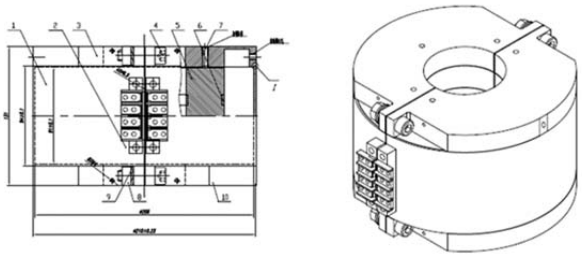

Fig.1 The design structure pictures of counters

The development of thorium-based fuel pebbles

The preparation of thorium-based fuel pebbles process includes three processes: the preparation of thorium fuel kernels, the design and the manufacture of a Fluidized Bed-Chemical Vapor Deposition (FB-CVD) system and the pressing of spherical fuel elements.

The preparation of the thorium-based fuel kernel The research was focused on solving the problem that the gel particles are easily broken during the heat treatment process and achieving the uniformity of the particle size. Through the optimization of the calcination and sintering conditions, such as the calcination and sintering temperatures, heating rates, holding times, reaction atmospheres, etc., high quality ThO_2 kernels with a diameter of approximately 500 μm and a density of >95% TD were fabricated. And research on the preparation of ThCO fuel kernels was also carried out, and ThCO kernels with good sphericity were prepared.

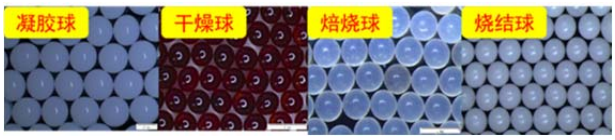

Fig.2 The microphotographs of ThO_2 kernels

The Preparation of coated particles The manufacture, installation and testing of the FB-CVD equipment were completed, and the preparation study of coated fuel particles was carried out. The preparation process for dense and pure phase β-SiC was studied, and the processing parameters were optimized. Finally, the coatings with thicknesses meeting the design requirements and excellent mechanical properties were prepared. Measurements and calculation showed that more than 99% of the buffer layer, the inner compact pyrolytic carbon layer and the silicon carbide layer, and more than 97% of the outer compact pyrolytic carbon layer are within the predetermined standard deviation range, respectively.

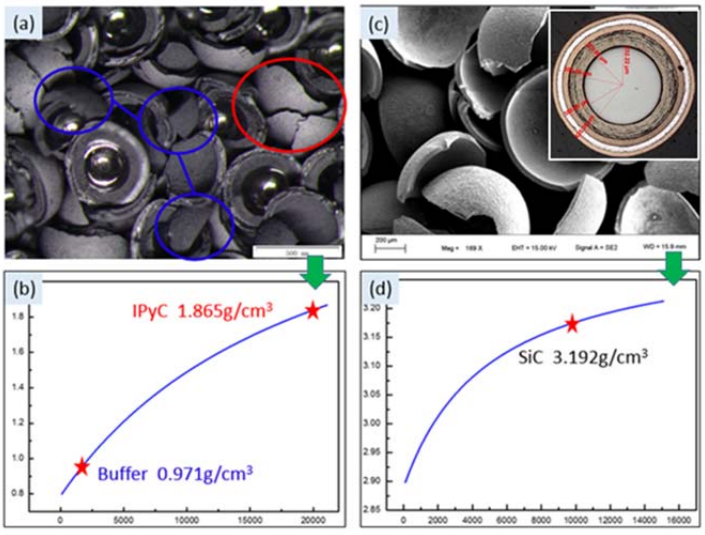

Fig.3 The density of the buffer layer, dense pyrolytic carbon layer and the silicon carbide layer

Fabrication of spherical fuel elements The experimental equipment for spherical fuel element compaction were designed and established. Spherical fuel element with high power and resistance to molten salt infiltration were prepared using quasi-isostatic pressure method. The fabrication of prototype fuel elements by the combination of graphite pore making and solid phase densification (Fig.4) solved several technical difficulties in the preparation of spherical ring fuel elements (preset of low density spherical cores within elements, particle dispersion in the secondary outer fuel zone, and densification of the outside cell). A spherical (ring) fuel element prototype has been obtained (Fig.5). The diameter of the type element is 60±0.3 mm, and the density of the whole sphere is less than 1.7 g/cm^3.

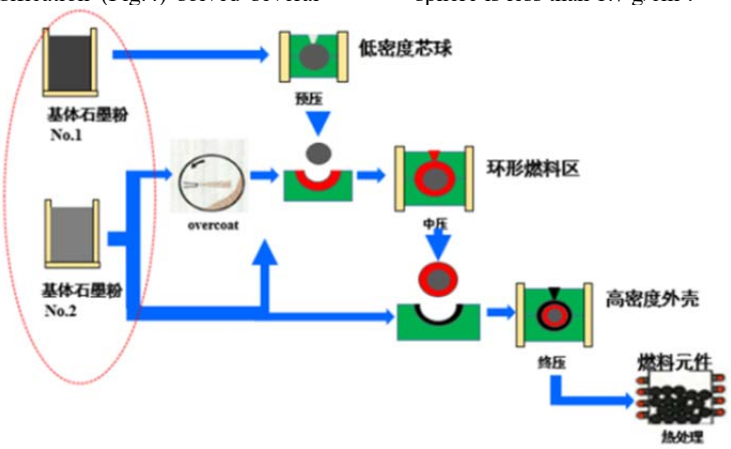

Fig.4 Diagram of preparation process of spherical Ring fuel element

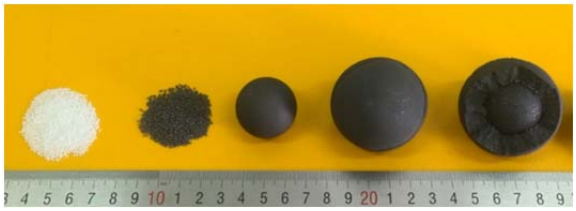

Fig.5 Photos of spherical ring fuel elements

Fuel characterization

The measurement methods concern the particle size and the density of coated particles were established: the projection of coated particles was obtained by laser pulse photography, and then the particle size and spherical degree of the samples were analyzed statistically; the density of loose pyrolytic carbon layer was measured by density gradient method. The density of dense pyrolytic carbon layer was measured by titration.

Two internal standards were established for impurity analysis in ThO_2 powders (i.e., procedures for the determination of boron, cadmium, and other elements in ThO_2 by ICP-AES and for the determination of trace rare earth elements in ThO_2 by ICP-MS). And several methods for analyzing impurities in ThF4 were also tried. The test limit, detection range, precision and other parameters of the established procedures are all satisfactory for the quality control requirements of nuclear-grade thorium materials.

熔盐机械部和堆材料部

熔盐堆用结构材料，如高温镍基合金、细颗粒核石墨、C/C 复合材料等，是目前熔盐堆研究的焦点，在中科院战略先导专项《未来先进核裂变能—钍基熔盐核能系统》资助下开展了相关材料的国产化和性能评估。

对 GH3535 合金管件进行加工工艺优化，解决了热加工开裂及热加工工件性能稳定性问题，所获得的宽厚板、环件及主管道弯管力学性能良好，满足技术条件要求。

固化熔盐堆用核级石墨 NG-CT-50 的制备工艺，获得大规格核级石墨，其结构和力学性能满足相关技术指标要求。掌握了 FLibe 熔盐在 TMSR 国产致密核石墨(NG-CT-50)中的浸渗规律及对该石墨性能的影响。

对熔盐堆用构件工艺优化、性能评估过程中的关键科学问题进行了梳理，并对相关科学问题进行扩展性研究，例如通过合金改性优化材料抗辐照性能、通过晶界工程改善合金抗碲脆性能等相关技术积累为优化现有熔盐堆材料、研发新型熔盐堆用材料提供技术支撑。

1　合金结构材料

1.1　合金加工工艺

(1) 获得了国产 GH3535 合金宽厚板、环件等管件构件制造工艺。板材制造能力可以覆盖 4~25 mm 的厚度，板材宽度可达 2 200 mm。掌握了重量规格在 1 吨以内的铸锭的锻造工艺。完成了长达 4 m 的 DN150 主管道（图 1）及换热管首批试制，并获得了基础力学性能工艺参数。各项力学性能均满足技术条件要求。

图 1　DN150 主管材

(2) 获得了进口 Hastelloy N 合金主管道弯管加工工艺。对 Φ141.3*6.55mm 的国产及进口合金无缝管材采用 3D、6D 弯曲半径进行了弯管试验，实验结果表明其可以满足表面质量、椭圆度、褶皱高度、波浪间距等尺寸要求，减薄率不高于 12%。弯管后需在 1 180℃进行热处理，消除加工硬化，调整组织及力学性能。弯管的力学性能均满足技术条件要求（表 1）。

表 1　弯管力学性能

项目	室温			600℃			650℃			700℃		
	屈服	抗拉	延伸率	屈服	抗拉	延伸率	屈服	抗拉	延伸率	屈服	抗拉	延伸率
实测值	300	790	56.6	278	607	36	259	557	32	236	501	30.5
预期值	280	690	40	210	590	35	205	530	30	200	480	30

(3) 对窄间隙自动钨极氩弧焊焊接工艺进行了优化。对两组试板的焊缝进行液体渗透、射线、超声检测，结果未发现未熔合缺陷，焊缝质量达到要求。母材、热影响区、焊缝的碳化物的形貌表征如图 2 所示。焊接接头的力学性能如图 3，其抗拉强度和延伸率都比常规自动钨极氩弧焊好。

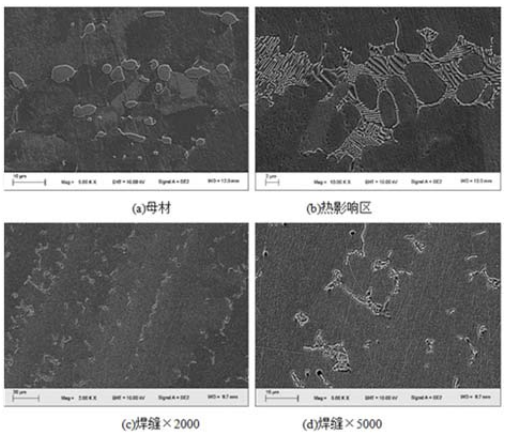

图 2　优化后窄间隙自动钨极氩弧接头各区碳化物形貌

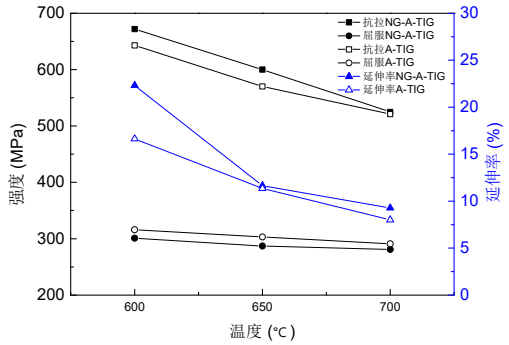

图 3　优化后窄间隙自动钨极氩弧接头和常规自动钨极氩弧焊高温拉伸结果对比

1.2 合金力学性能评估

(1) 完成了 Hastelloy N 合金蠕变第二阶段的线性应力应变关系、蠕变极限、持久曲线、平均等时应力-应变曲线的测试。**错误!未找到引用源。** 4 是 Hastelloy N 合金的蠕变持久性能。 650 ℃的寿命-应变以 0.5%应变范围为转折点，在应变范围为 0.5%以上时，满足线性关系，在 0.5%以下时，也满足线性关系。650 ℃下，Hastelloy N 合金的拉伸延伸率不到 30%，只有 25 ℃下拉伸延伸率的一半，因而高应变范围的疲劳寿命较室温下降很多；650 ℃下 Hatelloy N 合金的抗拉强度与室温较为接近，因而低应变范围下材料的疲劳寿命逐渐趋于与室温相近。

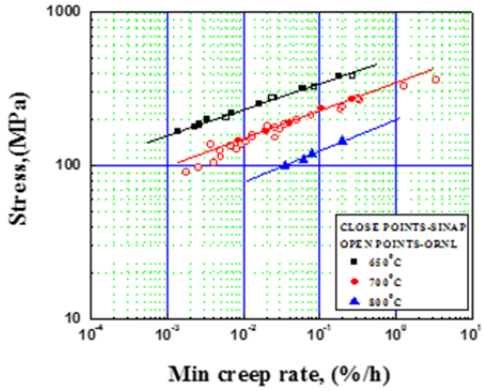

图 4 Hastelloy 合金的蠕变持久性能

(2) 依据 ASTM E606 对 Hastelloy N 合金 650 ℃疲劳性能进行了测试，对实验结果进行统计学分析，S-N 曲线如图 5 所示，该曲线具有 75%以上的置信度。

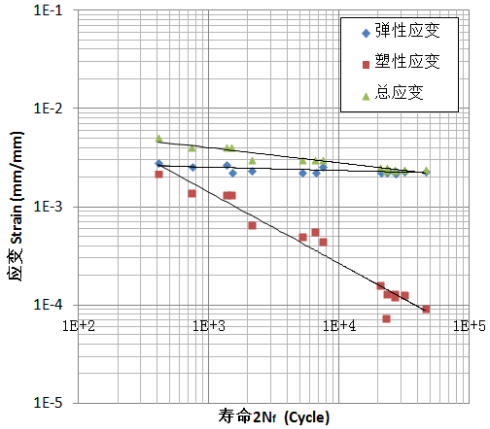

图 5 Hastelloy N 合金 650℃的 75%置信度的 S-N 曲线

1.3 合金抗碲脆及辐照性能优化

通过晶界工程(GBE)，在不改变 GH3535 合金成分的基础上对材料进行改良，提高材料抗碲脆性能。GBE 处理能够在不改变晶粒尺寸的条件下大幅提高低 Σ 晶界的比例，特别是 Σ3 晶界从 47.3%提高至 64.4%（图 6）；此外，在组织中引入了大尺寸的团簇，尺寸范围为 119.5 微米，团簇内包含取向关系确定的 Σ3 晶粒；改良后合金单位长度上的渗 Te 的晶界数目从 1.26 降至 1.03，证明 GBE 处理能够有效的抑制 Te 的渗入。

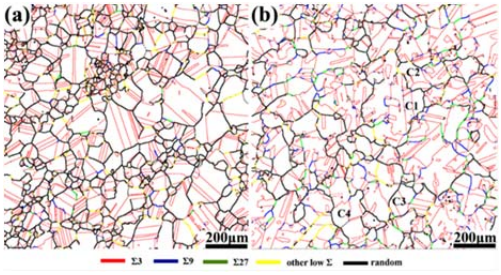

图 6 原始样品(a)和 GBE 处理(b)样品中的晶界特征分布

通过元素微调进行合金改性研究，以优化 GH3535 合金的抗氦脆性能。在此次优化方案中，将 Mo 含量降低至 12%，并添加 1.8%的 Ti。通过研究改性后 GH3535 合金的碳化物分布及结构演化规律，以理解 Ti 改善合金 He 脆的机制。结果表明 650 ℃、750 ℃ 条件下合金晶界上析出细小的 MC 碳化物（图 7），且晶界上的 MC 与基体存在半共格的界面，能够更进一步地固氦，有效降低其扩散，提高材料抗氦脆性能。

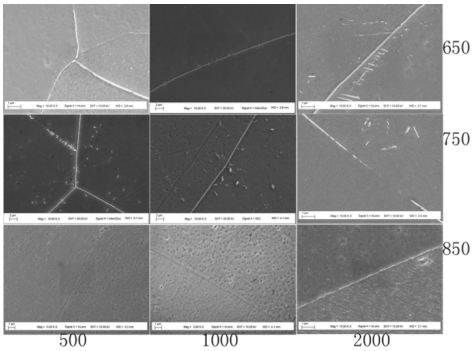

图 7 不同温度不同时效时间下的含 Ti 合金中晶界 MC 碳化物的形态

2 石墨材料

2.1 NG-CT-50 核石墨工艺固化

2016 年 6 月 15 日，熔盐堆核石墨的研制及性能指标通过了工艺评审（图 8），专家一致认为煤化所特种炭/石墨团队研发的液态熔盐堆核石墨的热物理性能满足堆内慢化剂石墨的要求，通过了大规格熔盐堆核石墨制备的工艺评审，对该石墨材料的整个制备工艺流程：配料、混捏、破碎、成型、焙烧、浸渍和石墨化提纯等进行了工艺固化。

图 8　低孔径防熔盐浸渗细颗粒石墨材料 400×400×600 mm 工艺见证图片

NG-CT-50 的各向性能指标满足熔盐堆要求。如图 9 所示，Weibull 分布是核石墨分散性重要的性能指标。根据德国 DIN 51914 抗拉强度测定标准，通过对尺寸为 400×400×600 mm 的石墨坯块进行取样，取样数量为 100 个样品，测定了 NG-CT-50 抗拉强度 Weibull 分布，特征强度 26.37 MPa，满足熔盐堆提出的指标要求。

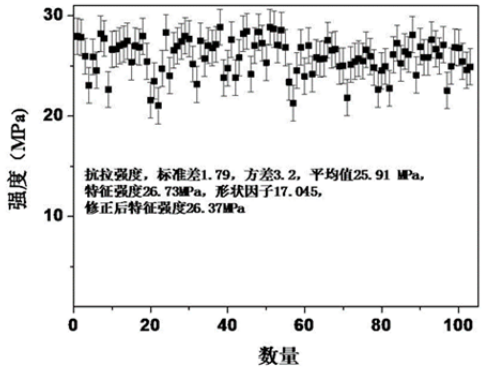

图 9　石墨性能测试

2.2　核石墨耐熔盐浸渗性能评估

获得了不同型号核石墨的熔盐浸渗特性，图 10 所示为 IG-110，NBG-18，NG-CT-10，NG-CT-50 以及 T220 石墨随压强变化的 FLiBe 熔盐浸渗曲线。其中超细颗粒石墨 NG-CT-50 及 T220 石墨临界浸渗压强介于 6~7 atm，明显高于其它牌号石墨。随着压力的增加，石墨熔盐浸渗量有一定的增加趋势，直至平衡。

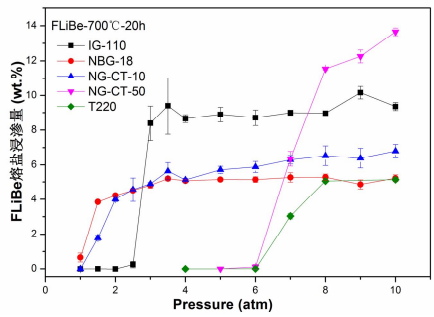

图 10　压强对核石墨 FLiBe 熔盐浸渗规律的影响

预充压(1 atm)与抽真空、温度(600 vs. 700 ℃)和时间(20 h *vs.* 500 h)对 NG-CT-10 核石墨样品在 FLiBe 熔盐浸渗量的影响见图 11。当最终浸渗压强较低时(＜6 atm＝，预充压对石墨熔盐浸渗量的影响较大，其熔盐浸渗量明显低于抽真空条件下；随着最终浸渗压强的增大，预充压对 NG-CT-10 石墨熔盐浸渗量的影响变小。由图可知，不同温度(600 ℃，700 ℃)及不同时间(20 h, 500 h)条件下，核石墨 FLiBe 熔盐浸渗量几乎不变，表明温度对石墨的熔盐浸渗量影响不大，20 h 的浸渗时间足以使石墨熔盐浸渗达到平衡。

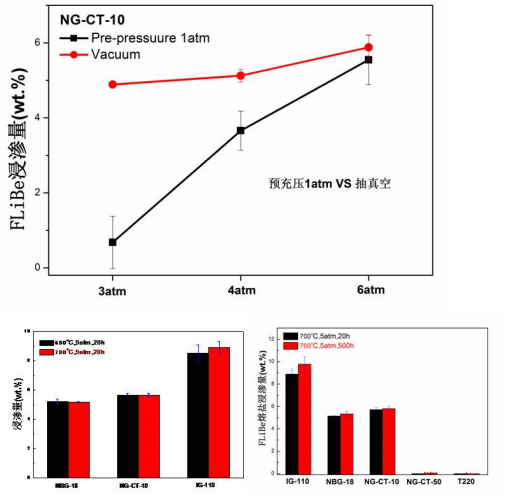

图 11　预充压(1 atm)与抽真空、温度(600 ℃ vs. 700 ℃)和时间(20 h vs. 500 h)对核石墨 FLiBe 熔盐浸渗量的影响

3　C/C 复合材料

利用热等静压工艺以及树脂浸渍工艺研制了 1:1 C / C 复合材料控制棒套管原理样机（图 12），并获取了相应的密度均匀性、工艺稳定性和常规性能数据。

图 12 原理样机: (a)热等静压工艺；(b)树脂浸渍工艺

获得了控制棒套管样件用材料的密度均匀性、热学和力学性能分布等性能数据。在较低浸渗压力下，C/C 中基本没有发生的熔盐浸渗。提高浸渗压力至 6 atm 时，只有极少量的熔盐沿纤维束间的孔隙浸渗入复合材料的内部（图 13）。熔盐浸渗后，C/C 复合材料的断裂方式没有发生改变，仍然为假塑性断裂。

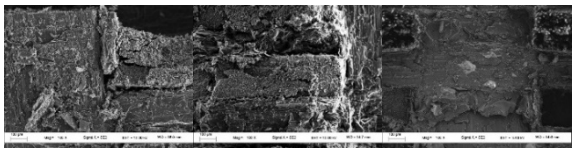

图 13 不同浸渗压力下 C/C 复合材料的断口形貌

4 SiC/SiC 复合材料研究

研制出了高温 FLiNaK 回路热工水力段用的 SiC / SiC 复合材料管及短帽，建立了 SiC/SiC 复合材料加热段管的评估方法并完成了主要性能评估；耐水压实验揭示该 SiC/SiC 复合材料管可被应用到高温回路中。

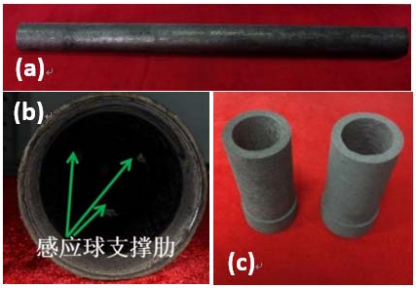

图 14 热工水力段 SiC/SiC 复合材料器件，（a）管，（b）管内部结构，（c）端帽

研究了熔盐中 CrF_3 对碳化硅的腐蚀影响，结果如图 15 所示。熔盐中的 CrF_3 会与 SiC 反应形成铬的碳化物(Cr_3C_2, Cr_7C_3)。SiC 在原始 FLiNaK 熔盐中的腐蚀深度约为 2.5 μm，在添加了 CrF_3 的 FLiNaK 熔盐中的腐蚀深度约为 14 μm（图 15），腐蚀后熔盐中的 Si 含量增加，揭示 CrF_3 会加速碳化硅的腐蚀。

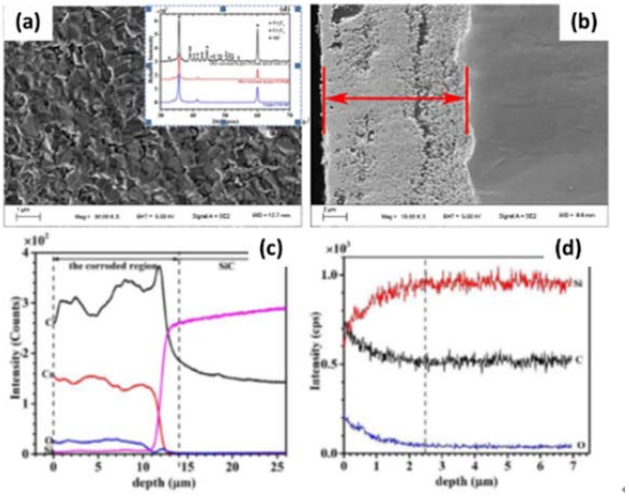

图 15 （a）在 FLiNaK-CrF_3 熔盐中腐蚀后 SiC 表面 SEM、（b）截面 SEM、（c）截面线扫描 EDS，（d）在 FLiNaK 熔盐中腐蚀后 SiC 截面线扫面 EDS

5 SiC 陶瓷研究

根据 TMSR 换热系统设计方案，开展了大尺寸、复杂形状碳化硅陶瓷换热板的研制。如图 16 所示，完成了 SiC 陶瓷换热板缩比件（1:2，尺寸 300×200×8 mm）及全尺寸 SiC 陶瓷换热板（500×200×8 mm）的制造，完成了 SiC 陶瓷换热器缩比件的高温焊接封装制造。实现了 SiC 陶瓷换热板与镍基合金的机械连接和密封。

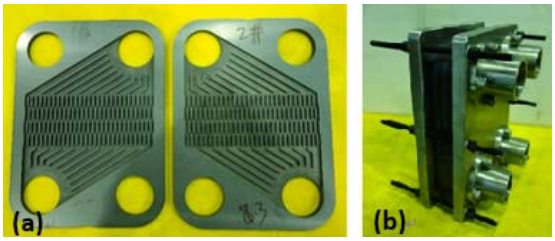

图 16 （a）碳化硅陶瓷换热板的 A 板和 B 板；（b）高温焊接封装后的碳化硅陶瓷换热器

6 结论

(1) 完成了国产 GH3535 合金宽厚板、环件等管件构件、Hastelloy N 合金主管道弯管的工艺优化，相关构件力学性能均满足技术条件要求。对窄间隙自动钨极氩弧焊焊接工艺进行了优化，焊接接头的抗拉强度和延伸率优于常规自动钨极氩弧焊。

(2) 获得了 Hastelloy N 合金长周期蠕变疲劳数据。获得了 650 ℃下，1.0%应变范围时的蠕变-疲劳包络线。获得了 650 ℃下 Hastelloy N 合金 75%置信度的 S-N 曲线。获得 Hastelloy N 合金在 650 ℃的超过 10 000 h 长周期及不同炉次的蠕变性能数据。

(3) 固化了熔盐堆用国产核石墨 NG-CT-50 的基本制备工艺，掌握了 FLibe 熔盐在 TMSR 国产致密核石墨(NG-CT-50)中的浸渗规律及对该石墨性能的影响。

上述熔盐堆材料的关键工艺和性能评估为熔盐堆安全服役提供了有力保障。此外，通过对熔盐堆用采用研发过程中的关键科学问题进行梳理并进行扩展性研究，在优化材料抗辐照性能、耐熔盐腐蚀性能等多个方面的技术积累将进一步为研发新型熔盐堆用材料提供技术支撑。

Molten Salt Reactor Structural Materials

Departments of Molten salt Engineering and Reactor Materials

Current researches on molten salt reactors (MSRs) are focused on the structural materials, such as high-temperature nickel-based alloys, fine-grained nuclear graphite, C/C composites et al. With the development of the "Future Advanced Nuclear Fission Energy — Thorium-based Molten-Salt Reactor Nuclear Energy System (TMSR)", a leading science and technology project launched by the Chinese Academy of Sciences, the localization and performance evaluation of relevant materials have been carried out.

The processing technology of GH3535 alloy pipe fittings was optimized to solve the problems of hot work cracking and improve the stability of hot working workpiece. The mechanical properties of the obtained wide plate, ring and bent pipe are excellent, which meet the technical requirements.

The preparation process of the nuclear grade graphite NG-CT-50 for MSRs has been determined. The large-scale nuclear grade graphite was obtained. And the structure and mechanical properties meet the requirements of relevant technical specifications. The infiltration rules of FLibe molten salt in the nuclear graphite (NG-CT-50) and its influence on the performance has been revealed.

The key scientific issues in process optimization and performance assessment of components used for MSRs are reviewed. The related scientific issues are studied in an expansive manner. For example, alloy modification and grain boundary engineering are used to improve respectively the irradiation and Te-embrittlement resistance of the alloy. The accumulation of relevant technologies provides technical support for the optimization of existing materials and the further development of new materials for MSRs.

1 Alloy materials

1.1 Processing technology of nickel-based alloys

(1) The manufacturing processes of the GH3535 thick plate, ring piece and other pipe components were optimized. The plate manufacturing capability can cover a thickness of 4~25 mm with the plate width reaching to 2 200 mm. The forging process of casting ingot with weight specification within 1 ton was also obtained. The first batch of DN150 main pipe (see Fig. 1) and heat exchange tube were completed. Meanwhile, the basic technological parameters were obtained. The mechanical parameters of DN150 pipe meet the technical requirements of TMSR.

Fig.1 The DN150 pipe

(2) The bent pipe technology of Hastelloy N was obtained. The bending tests of Φ 141.3×6.55 mm UNS N10003 alloy seamless pipes with bending radius of 3D and 6D were carried out. It shows that the product qualities, such as surface quality, ellipticity, fold height, wave distance et al., meet the technical requirements. Moreover, the thinning rate of the bend pile is less than 12%. An heat treatment of bend pipe at 1180 °C after bending is generally required to eliminate the work hardening, which could further adjust their microstructures and mechanical properties. The mechanical properties of bend pipes after heat treatment are also measured and shown in Table 1. It shows that all the mechanical properties under different temperatures meet the technical requirements.

Table 1 Mechanical properties of bend seamless pipes

项目	室温			600℃			650℃			700℃		
	屈服	抗拉	延伸率	屈服	抗拉	延伸率	屈服	抗拉	延伸率	屈服	抗拉	延伸率
实测值	300	790	56.6	278	607	36	259	557	32	236	501	30.5
预期值	280	690	40	210	590	35	205	530	30	200	480	30

(3) The welding process of narrow gap automatic tungsten argon arc was optimized. The liquid penetration test, ray detection and ultrasonic inspection of the two groups of test plates show that the weld qualities meet the standard requirements and no incomplete fusion defects were detected. The morphologies of carbides in difference regions (parent metal, heat affected zone and weld zone) were characterized by scanning electron microscope (SEM), as shown in Fig.2. The mechanical performance of the welding joint are shown in Fig.3. It is revealed that both of tensile strength and elongation rate are better than that of the conventional automatic tungsten argon arc welding.

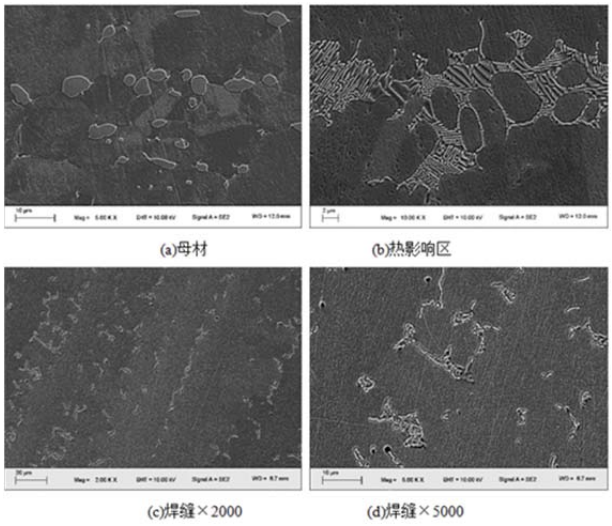

Fig.2 Morphologies of carbide in narrow gap automatic tungsten argon arc joint after optimization

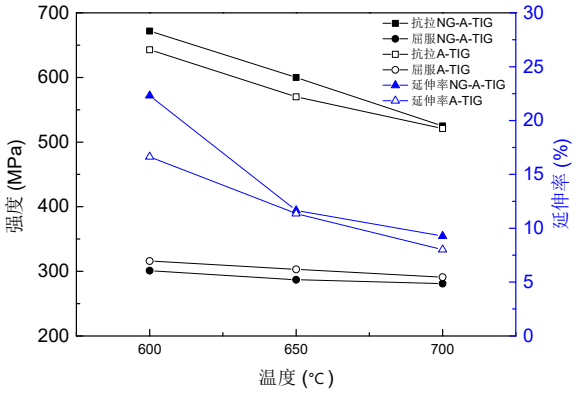

Fig.3 Comparison of high-temperature tensile results between optimized narrow gap automatic tungsten argon arc joint and conventional automatic tungsten inert gas arc welding

1.2 Evaluation of mechanical properties of nickel-based alloys

(1) The creep and fatigue properties of Hastelloy N alloy at high-temperature were studied. The linear stress-strain relations, creep limit, duration curve and average isochronous stress-strain curves were measured in the second stage of creep test. The creep properties of the Hastelloy N alloy are shown in Fig.4. It shows that there is a turning point at 0.5% in strain in the life-strain curve with temperature of 650 ºC. The linear relations existed when the strain was lower or above than 0.5%. The tensile elongation of the Hastelloy N alloy at 650 °C is less than 30%, which is only one half of that at 25 °C, indicating that the high-temperature fatigue life of materials in the high strain range is much lower than that at room temperature. Moreover, the tensile strength of Hastelloy N alloy at 650 °C is close to that at 25 °C, which shows that the fatigue life of materials under low strain range gradually tend to be more close to that at room temperature.

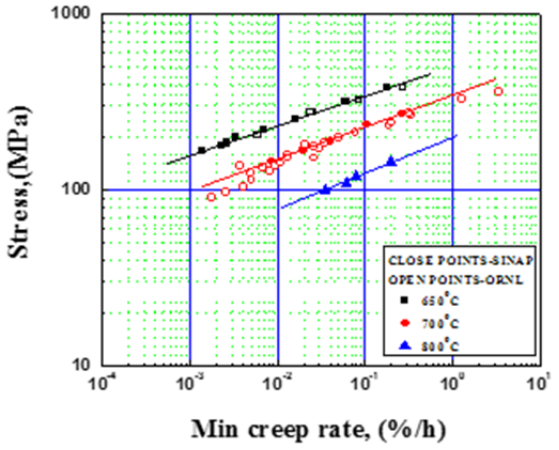

Fig.4 The creep endurance performance of Hastelloy N

(2) The fatigue properties of Hastelloy N alloy at 650 °C were tested according to ASTM E606. The experimental results were statistically analyzed. The S-N curve with more than 75% degree of confidence was shown in Fig.5.

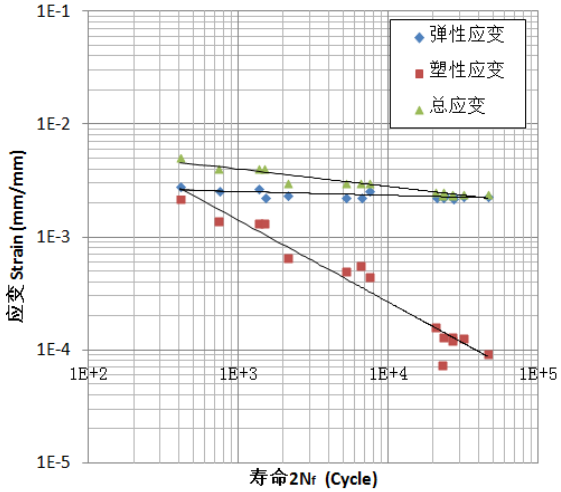

Fig.5 S-N curve of Hastelloy N alloy at 650 C with 75% confidence

1.3 Improvement properties of Te/He embrittlement resistance of nickel-based alloy

Based on the grain boundary engineering (GBE), GH3535 alloy was modified to enhance their resistance to Te-embrittlement in molten salt environment. The GBE can greatly increase the proportion of lower Σ grain boundaries (GBs) in alloys without changing the grain size and alloy compositions. As shown in Fig. 6, the proportion of Σ3 increases from 47.3% to 64.4%. In addition, the larger size (119.5 μm) clusters containing Σ3 GBs were introduced. The numbers of GBs with Te infiltrated per unit length decreased from 1.26 to 1.03, indicating that the GBE treatment could effectively inhibit the Te infiltration.

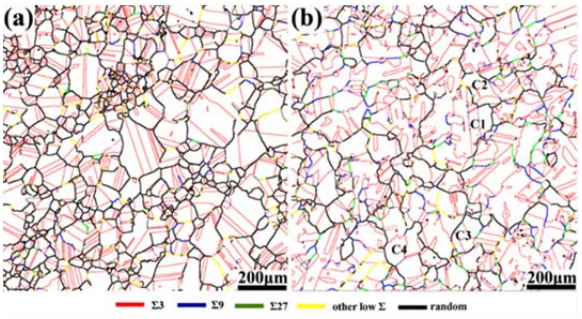

Fig.6 The grain boundary distributions in sample before (a) and after (b) GBE treatment

Alloy modification of GH3535 alloy, with reduction of the Mo content to 12% and addition of Ti to 1.8%, was used to improve their resistance to He embrittlement. Comparative studies of structural modification as well as carbides evolution in the modified GH3535 alloys were performed to understand the underlining mechanisms. The results show that fine MC carbides are precipitated on the GBs at 650 °C and 750 °C, and there are no secondary MC carbides in the matrix, as shown in Fig.7. The semi-coherent interface between MC carbide and matrix could trap atomic helium, which enhance the resistance to helium embrittlement of the alloy.

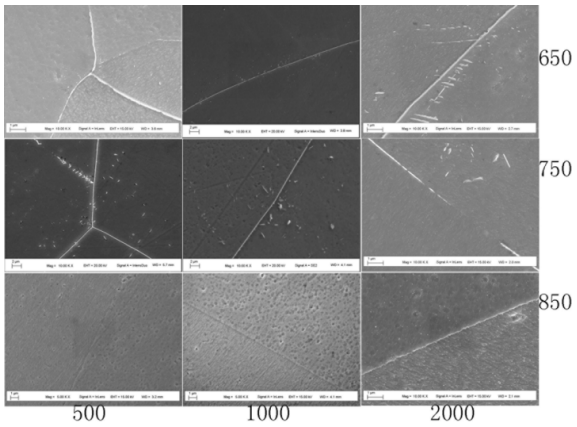

Fig.7 Morphologies of MC carbide neat the GBS in the alloy containing Ti at different temperatures and different aging time

2 Nuclear graphite materials

2.1 Solidifying of producing process of NG-CT-50 nuclear materials

The producing processes and performance of the fine-grade graphite for MSRs passed the assessment on June 15, 2016 (Fig.8). The experts agreed that the thermo-physical properties of the nuclear graphite produced by the Key laboratory of carbon materials meet the requirements of the MSRs and complete the process witness of the large scale nuclear graphite for the MSRs. The experts also witnessed the whole producing processes, namely the graphite ingredients mixing, kneading, broken, compression molding, calcinations, impregnating, graphitization and purifying processes.

Fig.8 The witness of producing process of anti-molten salt infiltration of fine graphite material with size of 400×400×600 mm

Weibull distribution is one of the important indicators of nuclear graphite mechanical strength dispersion. According to the German tensile strength measurement standards DIN 51914, the tensile strength of 100 samples taken from bulk graphite NG-CT-50 (bulk size is 400×400×600 mm) were measured and shown in Fig.9. The characteristic strength of NG-CT-50 nuclear graphite was 26.37 MPa, which satisfies the requirements of the TMSR.

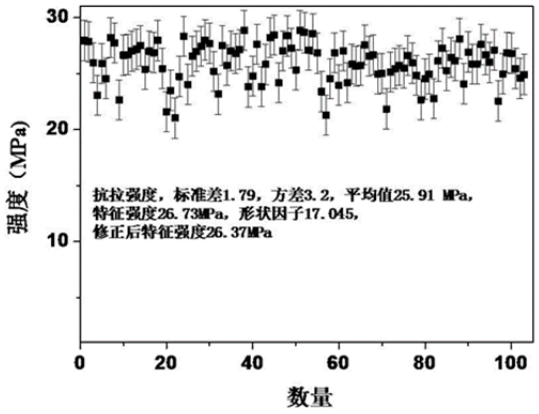

Fig.9 Graphite mechanical properties

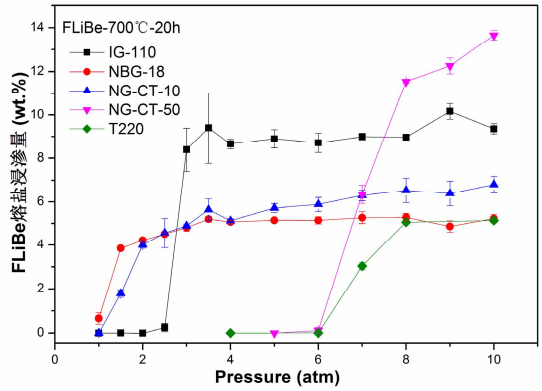

Fig.10 The weight gain ratios of different graphites under different pressures

2.2 Evaluation on the infiltration of nuclear graphite by molten salts

The infiltrations of nuclear graphite by molten FLiBe salt were systematically studied. As shown in Fig.10, the weight gain ratios for the nuclear graphite of IG-110, NBG-18, NG-CT-10, NG-CT-50 and T220 after being immersed into molten FLiBe salt at 700 ℃ for 20 h under different pressures. With the increase of the pressure, the weight gain ratios of all five grades increased, while the increase amplitude decreased gradually. For the ultrafine-grained graphite NG-CT-50 and T220, the threshold pressures for FLiBe salt infiltration are 6 and 7atm respectively, indicating that NG-CT-50 and T220 nuclear graphite have better resistance to salt infiltration in MSRs.

Effects of pre-pressure (1 atm), temperature (600 & 700 °C) and time duration (20 ~2 000 h) on molten FLiBe salt infiltration behaviors of nuclear graphite were also investigated, as shown in Fig.11. When the infiltration pressure was lower than 6atm, the weight gain ratio of the pre-gas-filled samples of NG-CT-10 was less than that of degassed sample, indicating that the gas inner the graphite sample affect the infiltration. However, while the infiltration pressure was higher than 6 atm, the weight gain ratios of the pre-gas-filled samples of NG-CT-10 were nearly equal to that of degassed sample, indicating that pre-pressure had little effect on infiltration behavior. The weight gain ratios of different types of graphite after molten salt infiltration tests in different temperatures (600 & 700 °C) and durations (20~2 000 h) showed no significant difference,

indicating both factors of temperature and duration had little effects on infiltration behaviors of nuclear graphite.

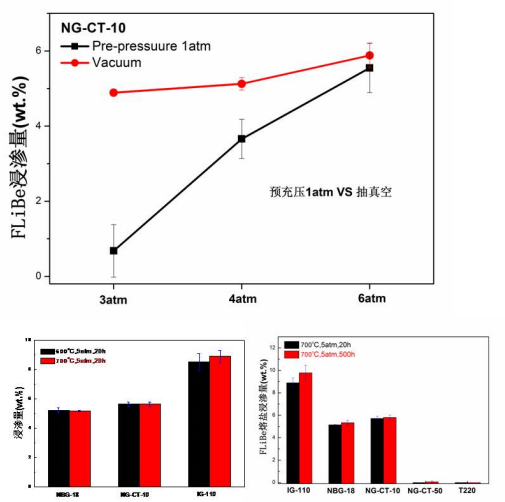

Fig.11 Effects of pre-pressure (1 atm), temperature (600 & 700 ℃), and time duration(20~2 000 h) on molten FLiBe salt infiltration behaviors

3 C/C composite materials

A prototype (1:1) of C/C composite control rod was manufactured by hot isostatic pressing and resin impregnation technologies. Relevant data, such as density uniformity, process stability and conventional performance characters were obtained. Static immersion in FLiNaK molten salt experiments indicates that the C/C prototype of control rod casing prepared by hot isostatic pressing process can prevent salt impregnation at higher press of 1.0 MPa.

Fig.12 Prototype of control rod casing developed by hot isostatic pressing (a) and resin impregnation(b) process

Besides, the density uniformity, thermal and mechanical property distribution were also obtained. When the pressure was increased to 6 atm, only a little FLiNaK salt was immersed into the C/C composites through the poles along fiber bundle, as shown in Fig.13. It shows that the C/C composites still keeping pseudo plasticity after immersion.

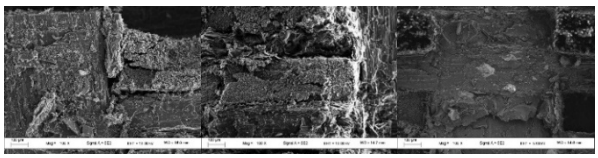

Fig.13 Fracture morphology of C/C composites under different infiltration pressures

4 SiC/SiC composite materials

Pipes and short caps were developed from SiC/SiC composite materials, which were used in thermal hydraulic section of FLiNaK loop. The evaluation system of SiC/SiC pipes were built and their conventional performance were evaluated. The tests of resistance to water pressure showed that the SiC/SiC pipes could be used in FLiNaK molten salt loops.

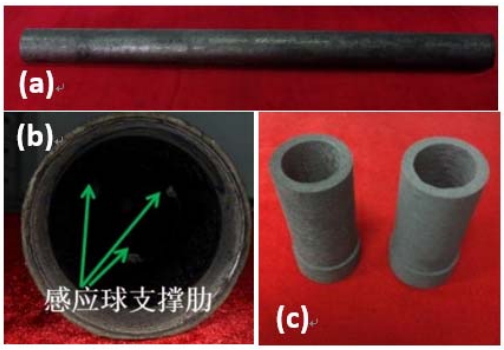

Fig.14 SiC/SiC components for thermal hydraulic section, (a)pipe; (b)pipe internal structure; (c)end cap

The effect of CrF_3 on the corrosion behavior of silicon carbide in molten salt was studied and shown in Fig.15. The CrF_3 in molten salt could react with SiC to form chromium carbide (Cr_3C_2, Cr_7C_3). The corrosion depth of SiC was about 2.5 μm in the as received FLiNaK molten salt. The corrosion depth was increased to 14 μm in the FLiNaK molten salt with CrF_3 (Fig.15). The content of Si is increased after corrosion in the molten salt, which revealed that CrF_3 would accelerate the corrosion of silicon carbide.

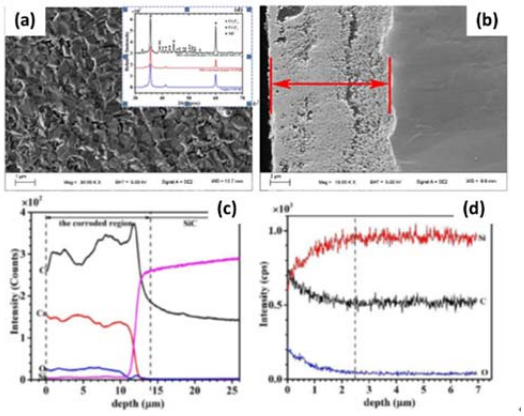

Fig.15 (a) Surface SEM, (b) cross sections SEM, (c) of EDS line scan of cross sections and (d) EDS line scan of cross sections of SiC after corrosion in FLiNaK molten salt.

5 SiC ceramic materials

SiC ceramic heat exchanger plates were developed according to the previous design proposal of TMSR heat exchanger system. As shown in Fig. 16, Scaling prototype of SiC ceramic heat exchanger with A/B plates (1:2, 300×200×8 mm) and one full size SiC ceramic heat exchanger plate (500×200×8 mm) were manufactured. High temperature joining and packaging of SiC ceramic scaling heat exchanger plate were completed. Mechanical joining and sealing between SiC

ceramic heat exchanger plate and nickel-based alloy were also finished.

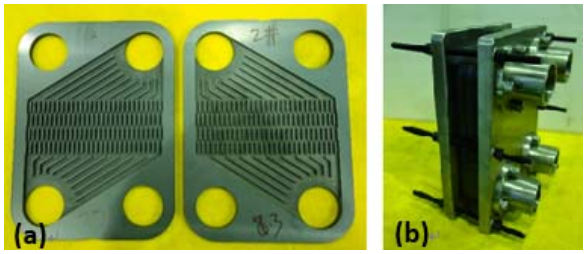

Fig.16 (a) SiC ceramic heat ex-changer A/B plates; (b) bonded and packaged SiC ceramic heat ex-changer plate

6 Conclusions

(1) The process optimization of the GH3535 alloy wide plate, ring and the main pipe elbow of the Hastelloy N alloy has been performed. The mechanical properties of related components meet the technical requirements. The welding process of narrow gap automatic TIG welding has been optimized. The tensile strength and elongation of the welded joint are better than that of conventional automatic TIG welding.

(2) The long-term creep fatigue data at 650 ℃ for the Hastelloy N alloys has been obtained, including the creep-fatigue envelope at 1.0% strain range, an S-N curve of 75% confidence and the creep performance data for more than 10 000 h.

(3) The preparation process of the nuclear grade graphite NG-CT-50 for MSRs has been determined. The infiltration rules of FLibe molten salt in the nuclear graphite NG-CT-50 and its influence on the performance has been revealed.

The above-mentioned critical process and performance evaluation of materials provide a powerful guarantee for the safe service of MSRs. In addition, the key scientific issues in process optimization and performance assessment of components used for MSRs are reviewed and the related scientific issues are studied in an expansive manner. The accumulation of relevant technologies provides technical support for the optimization of existing materials and the development of new materials used for MSRs.

堆材料工程物理组在理论模拟、辐照，腐蚀三个方向开展了研究，旨在为 TMSR 设计提供依据。

材料理论计算模拟与预测

镍基合氦脆效应的理论研究

通过对密度泛函理论计算结果进行拟合，建立了 Ni-He 原子间相互作用势，可以很好的描述氦在金属镍体材料中的稳定性、扩散等性质。应用分子动力学方法，研究了氦与镍基合金中的位错、晶界等相互作用机制，得到了氦在不同类型位错和晶界的相互作用强度，以及氦在晶界上的扩散情况。通过模拟含有氦泡的镍金属纳米线拉伸过程的应力-应变曲线，评估氦泡对金属镍力学性能降低的机制。这些结果为进一步研究材料的宏观氦脆效应提供研理论支持。

$$E_{Ni-He}(r_{ij}) = \begin{cases} ZBL\,potential, & r_{ij} < r_1, \\ p_3 r_{ij}^3 + p_2 r_{ij}^2 + p_1 r_{ij} + p_0, & r_1 \le r_{ij} < r_2, \\ f_{fit}(r_{ij}) + f_{Switch}(r_{ij}). & r_2 \le r_{ij} < r_d, \\ 0, & r_{ij} \ge r_d. \end{cases}$$

$$f_{Switch}(r_{ij}) = A(r_{ij} - r_d)^2 + B(r_{ij} - r_d)^3,$$

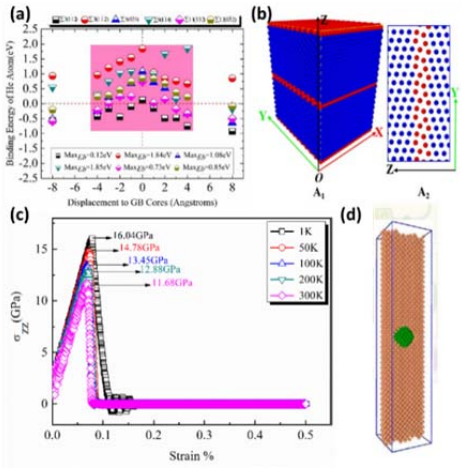

图 1 (a) 氦在金属镍不同境界上的结合能；(b) 金属镍中的典型晶界；(c)含有氦泡的镍纳米线在不同温度下的应力-应变曲线；(d)含有氦泡的镍纳米线模型示意图

熔盐杂质对于镍基合金腐蚀机制

对于镍基合金在熔盐环境下的腐蚀机制，一般认为熔盐杂质在腐蚀初期起重要作用。本工作以熔盐杂质分解后成分氟为例，采用第一性原理方法研究了其在 Ni-Cr 合金表面吸附、扩散等行为。首先氟在 Cr 掺杂的 Ni(111)表面上的吸附能为 3.52 eV，远大于其在纯净 Ni(111)表面上的吸附能(1.04 eV)，表明 Cr 原子提供了氟的最稳定吸附位，且 Cr 元素高出金属表面 0.41Å。氟的表面扩散行为验证了吸附能的结果。进一步的电子结构分析表明 F 2p–Cr 3d 杂化轨道占据了较深的能级，在 F-Cr 相互作用过程中起主要作用。F-Cr 键的形成使得 Cr-Ni（周围 Ni 原子）键长伸长，其相互作用减弱，有利于 Cr 从金属表面的脱附。相关结果有助于理解镍基合金在氟盐等强腐蚀环境下的初期相互作用机制。

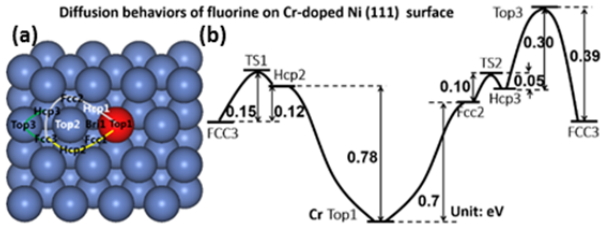

图 2 (a) 氟在 Cr 掺杂 Ni(111)表面扩散路径示意图；(b)氟合金表面相应的迁移路径和势垒

碲致合金晶界脆化效应

熔盐堆中的裂变产物碲(Te)会引起结构材料镍基合金的脆化。Te 脆化和低扩散势垒的协同效应会造成熔盐堆中严重的腐蚀问题。我们采用第一性原理方法研究探索 Te 原子沿四种不同种类晶界（Σ3 (111)，Σ5 (021)，Σ9 (221)和 Σ11 (11-3)）的扩散行为。Te 原子沿晶界的扩散势垒值对晶界类型非常敏感，在没有应力作用时，Te 原子的扩散势垒依 Σ11 (11-3)，Σ9 (221)，Σ3 (111)和 Σ5 (021)的次序增大。Te 沿 Σ11 (11-3) 晶界扩散时势垒最低，为 0.40 eV。当在晶界施加应力时，Te 沿晶界扩散的势垒发生明显变化。压缩应力会使得 Te 原子扩散势垒增大，拉伸应力会使得 Te 原子扩散势垒变小。在应力保持在较小范围时，Te 原子沿不同晶界扩散势垒的变化斜率依 Σ5 (021)，Σ11 (11-3)，Σ9 (221)和 Σ3 (111)的顺序减小。在无应力作用和有应力作用两种情况下，Te 原子都在 Σ11 (11-3)晶界的扩散势垒最低。

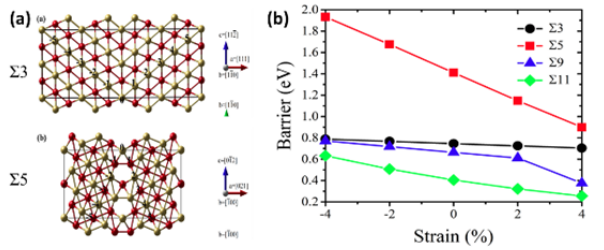

图 3 (a) 金属镍中典型的晶界示意图；(b) 碲在不同境界中扩散能垒随应变的规律

裂变气体与核燃料相互作用研究

惰性气体是核燃料中常见的裂变产物，它们在核燃料中可聚集成气泡导致燃料颗粒肿胀等从而影响其性能。研究惰性气体在燃料中的溶解、扩散和聚集行为对于提高反应堆的安全性能具有重要的意义。我们采用第一性原理方法研究了惰性气体原子在二氧化钍完美晶体中以及缺陷情况下的稳定性。研究表明，随着惰性气体原子体积的增大，其间隙位掺杂能也随之增大（从 He 的 0.75 eV 到 Xe 的 9.94 eV），从而说明原子间应力的增大使得大体积惰性气体的原子难以溶解在 ThO_2 中。而当 ThO_2 中存在肖特基空位时，由于掺杂引起的应力在缺陷处得到了释放，从而大大降低了能量，使得表明惰性气体原子很容易被肖特基缺陷俘获。同时，我们发现氪(Kr)和氙(Xe)原子并入肖特基缺陷的结合能大于肖特基缺陷自身在晶体中的形成能，说明 ThO_2 晶体中裂变产生的氪、氙更有利于肖特基缺陷结构的形成。

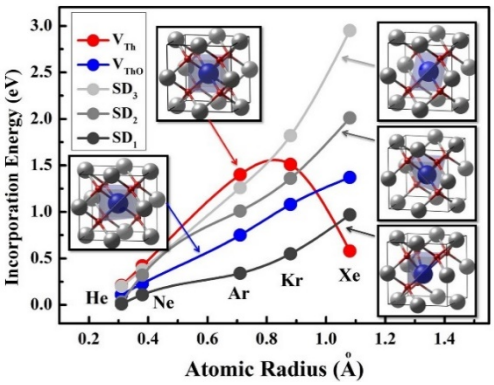

图 4 惰性气体在各种空位缺陷中的掺入能随着原子尺寸变化的比较，对应的缺陷构型也置于图中。

钍基燃料相变机制研究

核燃料的稳定性对反应堆的安全运行却至关重要，其在高温、高压、辐照等极端环境中的物性是使用钍基燃料时必须了解的性质。我们采用密度泛函理论和结构搜索演化算法，在不同压强和温度范围对钍基燃料的晶格结构、电子能带结构、声子散射谱以及热力学性质进行了理论计算。我们的计算预测出了在高压下其晶体结构及其随压强的演化和相变规律。同时，我们预测了钍基不同相间可能发生的半导体-金属相变。我们的研究了钍基燃料在压强与温度影响下的结构和电子性质，分析了相变机理，为其进一步研究以及实际应用提供了理论基础。同步辐射 XRD 开展的相应材料的高压试验验证了理论上 ThO_2 材料在不同压强下的结构相变机制。

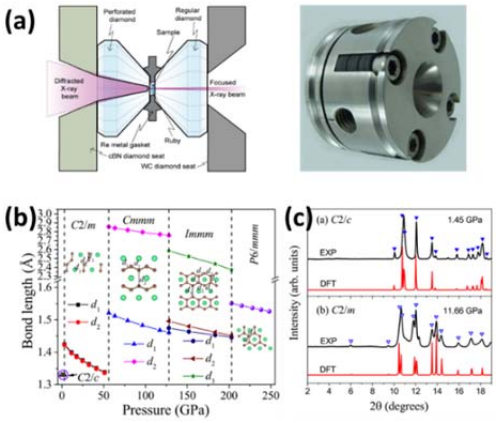

图 5 (a) 同步 XRD 高压实验设计示意图；(b) 不同相中 C-C 键长随压强的变化规律；(c)不同压强下样品结构的理论和实验值对比

材料辐照性能评价与测试

合金中子辐照后测试

哈氏 N 合金于 2014 年在核动力院进行了辐照剂量为 2.5×10^{19} n/cm^2 (E > 0.1 MeV)，辐照温度范围为 609.5- 670.7 ℃的中子辐照。目前，经过辐照装置的冷却、切割、样品分拣，已完成辐照后测试。测试项目包括合金辐照后的尺寸、密度、硬度测试，室温拉伸测试，350 ℃以下的夏比冲击测试，测试结果总结于 TMSR 技术报告——《镍基合金中子辐照进展技术报告》。

石墨辐照试验和辐照后测试

2016 年 4 月完成了在核动力院进行的中子辐照方案调整。调整后以国产超细颗粒石墨 NG-CT-50 和国产 C/C 复合材料为主。2016 年 6 月完成样品制备和辐照前尺寸和重量表征（图 6）。8 月完成样品装载和辐照装置组装（图 7）。9 月完成第一批石墨和 C/C 复合材料的堆内辐照试验。经过 3 个月的冷却，辐照装置即将切割，辐照后测试将在随后开展。

图 6 辐照前石墨和 C/C 复合材料样品照片

图 7 样品组装和辐照装置照片

2016 年 4 月完成了在 MIT 开展的石墨中子辐照样品装载设计，如图 8 所示。通过设计，保证样品浸没在熔盐中并且表面与熔盐充分接触。7 月完成样品制备和辐照前测试(SEM、尺寸、重量、Raman、XRD)。图 9 为 MITR 中子辐照实验所需样品。9 月完成样品和熔盐装载和辐照装置加工组装。从 10 月底到 12 月辐照装置在 MITR 中进行了 1000 小时的辐照。目前辐照装置已经出堆，正在冷却。辐照后测试将在 2017 年上半年开展。

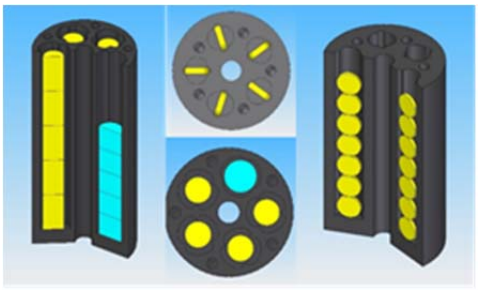

图 8 MITR 中子辐照实验样品装载方式设计

图 9 MITR 中子辐照实验所需样品

材料腐蚀性能评价与测试

腐蚀测试规范

为了将金属材料在高温熔盐中的腐蚀实验方法及腐蚀数据的分析更科学化和规范化，参照与腐蚀相关的 ASTM 标准、JIS 标准和国家标准来制定了《金属材料在静态 LiF-NaF-KF 熔盐中的腐蚀测试规范》，本规范适用于金属材料在静态 LiF-NaF-KF 熔盐中的高温腐蚀性评价。规范对腐蚀相关的定义进行了说明，并对腐蚀的实验条件进行了一一规定，包含：样品的尺寸、制备、清洗与储存，熔盐的成分、转运与储存，坩埚的尺寸、选材依据，手套箱，高温炉，浸泡，实验安全等。同时对实验步骤、实验结果与实验报告进行了详细说明。目前，本规范已经按照同行专家的意见完成修改。基于该规范框架的腐蚀测试相关内容已经通过 CNAS 认证。

316 不锈钢在氟化物熔盐中的应力腐蚀开裂评价

采用改进型弯梁试样装置（图 10），测试 316 的腐蚀性能及焊接件（图 11）的应力腐蚀敏感性，评估金属在给定环境下对应力腐蚀破裂是否敏感。国标和 ASTM 标准提出弯梁试验的试样表面的初始拉应力须达到屈服点，参考 316L 应力应变曲线（图 12）和压水堆环境的材料应力腐蚀敏感性测试条件，采用 5%变形量进行弯梁应力腐蚀试验。目前，浸泡腐蚀正在持续进行中。

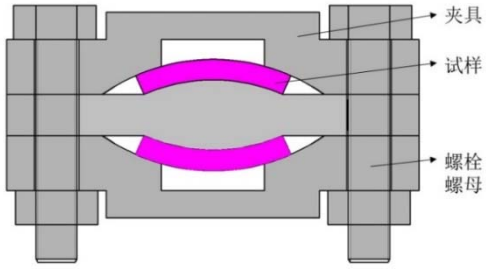

图 10 改进型弯梁试样装置图

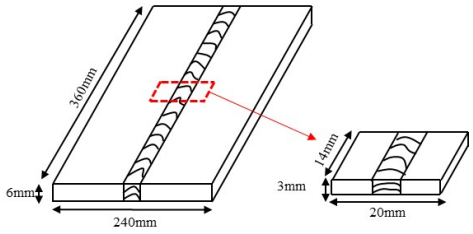

图 11 来料及焊接试样

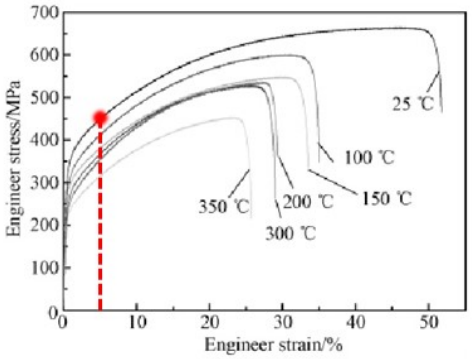

图 12 不同温度条件下 316L 不锈钢的应力-应变曲线

304LN 不锈钢在熔盐及熔盐蒸汽中的腐蚀评估

以腐蚀后的失重、形貌，以及熔盐组分等为指标，进行对比。结论如下：

304LN 在 700℃的 FLiNaK 中腐蚀严重，但熔盐蒸汽腐蚀速率相比熔盐腐蚀速率来说微乎其微；

304LN-Hastelloy N 电偶对中 304LN 腐蚀速率成倍增加；

304LN-Hastelloy N 电偶对中 Hastelloy N 的腐蚀速率受到抑制。

316 不锈钢腐蚀控制

利用 FTD(Fluoride Thermal Diffusion)技术可以对 316 不锈钢进行表面改性。改性后基材表层及近表层的晶界处形成了 BCC 结构。从而，316 不锈钢的表层和近表层形成了 BCC 和 FCC 复合结构，并与基体冶金结合。改性后的 316 不锈钢的抗拉强度没有下降（图 13），但腐蚀抗力大幅度提升（图 14）。

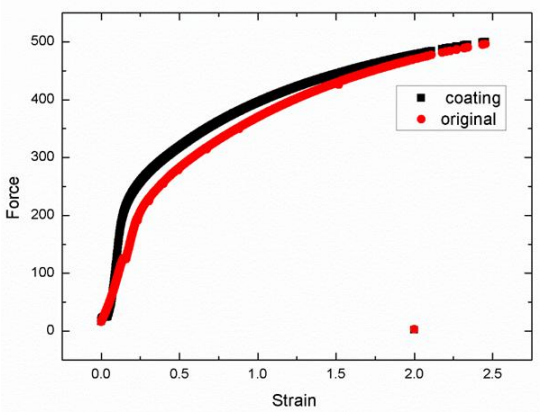

图 13 316 不锈钢样品拉伸曲线

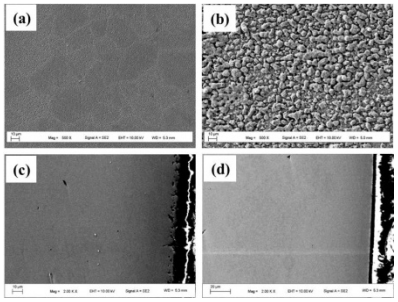

图 14 腐蚀((Flinak, 700 ℃, 90 hours))样品 SEM 图：(a) 未改性 316 不锈钢样品表面；(b) 改性 316 不锈钢样品表面；(c) 未改性 316 不锈钢样品剖面；(d) 改性 316 不锈钢样品剖面

总结

（1）完成哈氏 N 合金与 GH3535 合金在冷却剂熔融氟盐中的腐蚀评价，并制定了相关测试规范；证实高纯熔盐蒸汽几乎不腐蚀 304LN 不锈钢；采用熔盐热扩散的方式，原位改性 316 不锈钢的表面，可以明显抑制 316 不锈钢的晶间腐蚀。未来将深入研究 316 不锈钢表面改性机理。

（2）完成第一批国产碳基材料（包括超细颗粒石墨和 C/C 复合材料）的堆内辐照试验。由于放射性活度太高，待辐照样品冷却完成后才能切割辐照后的装置。拟在 2017 年第一季度进行装置切割并开展辐照后测试。

（3）发展了 Ni-He 原子间相互作用势，获得氦在金属镍中典型晶界上的行为，并进一步评估氦聚集对材料力学性能的影响。针对镍基合金在熔盐环境下的腐蚀机制，理解氟盐杂质引起的合金初期腐蚀机制，获得碲在金属镍不同晶界上的行为机制。获得气体裂变产物在锕系化合物的分布及稳定性；通过理论计算和同步辐射共同阐述了锕系燃料的高压相变机制。

Research on Material Engineering Physics for TMSR

Division of Material Engineering and Technology

The group of reactor material engineering and physics conducted theoretical simulation, irradiation and corrosion test, aiming to provide a basis for the design of TMSR.

Theoretical Simulation and Property Prediction of Nuclear Materials

Theoretical study of helium embeittlement in nickel-based alloy

An interatomic potential for helium in bulk nickel was developed by fitting first-principles calculation results, which can give a good description of relative stability and migration of interstitial and substitutional He defects in bulk nickel. Furthermore，the helium interactions (binding and diffusion) with typical dislocations and grain boundaries (GBs) were explored by using molecular dyanmics simulations. The mechanical properites of nickel nanowires containing helium bubbles are also clarified, as an typical stress-strain curves shown in Fig.1. The current results help to understand the helium behavior in nickel-based alloy.

$$E_{Ni-He}(r_{ij}) = \begin{cases} ZBL\,potential, & r_{ij} < r_1, \\ p_3 r_{ij}^3 + p_2 r_{ij}^2 + p_1 r_{ij} + p_0, & r_1 \le r_{ij} < r_2, \\ f_{fit}(r_{ij}) + f_{Switch}(r_{ij}). & r_2 \le r_{ij} < r_d, \\ 0, & r_{ij} \ge r_d. \end{cases}$$

$$f_{Switch}(r_{ij}) = A(r_{ij} - r_d)^2 + B(r_{ij} - r_d)^3,$$

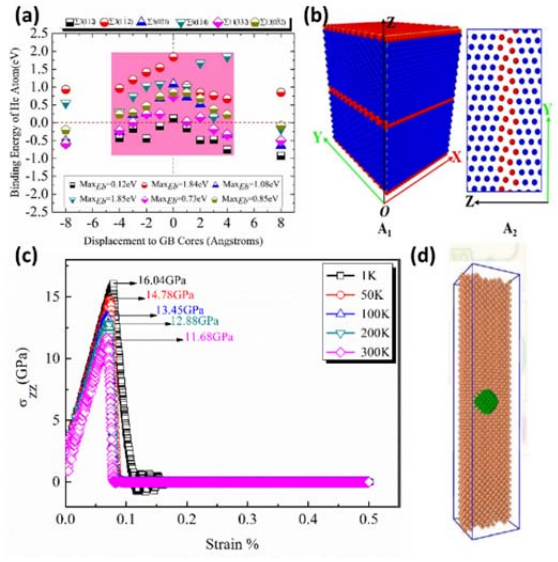

Fig.1 (a)Binding of He at different grain boundaries of nickel; (b) typical GB in nickel; (c) stress-strain curves of nickel nanowires containing with helium bubble; (d)the schematic model of nickel nanowire containg with a helium bubble.

The initial corrosion behavior of nickel-based alloy in fluoride salt environments

The adsorption and diffusion behaviors of molten salt impurities on Cr-doped Ni(111) surface are investigated by using first-principles simulation. It shows that the Cr in the Cr-doped Ni(111) surface serve a trap site for fluorine with adsorption energy 3.52 eV, which is 1.04 eV higher than that on Ni(111) surface. Moreover, the Cr atom is pulled out the surface for 0.41 Å after the fluorine adsorption, much higher than that on Ni(111) surface. Further diffusion behaviors analysis confirms the conclusion because the fluorine diffusion from neighbored sites onto the Cr top site is an energy barrierless process. Detailed electronic structure analysis shows that a deeper hybrid state of F 2 p-Cr 3 d indicates a strong FCr interaction. The NiCr bond is elongated and weakened due to the new formed FCr bonding. Our results help to understanding the basic fluorine-induced initial corrosion mechanism for Ni-based alloy in molten salt environment.

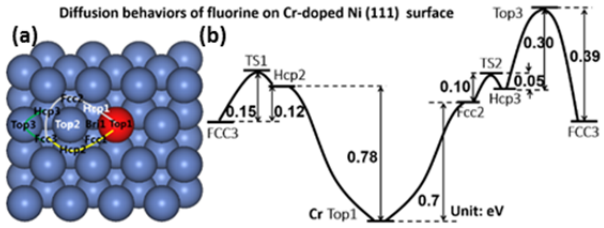

Fig.2 (a) Schematic setup for fluorine diffusions on Cr-doped Ni(111) surface; (b) diffusion energy barriers and corresponding diffusion paths of fluorine on Cr doped Ni(111) surface.

Te-induced embrittlement of grain boundary in nickel

The knowledge of the behavior of Te in nickel grain boundaries (GB) is of significant importance for the application of nickel alloys in molten salt reactors. The atomic structures, stabilities, segregation behaviors and diffusion barriers of Te are studied for the bulk, surfaces and four kinds of GBs of nickel. Our first-principles calculations indicate the segregation of Te is most favorable at Σ5 (021) GB and the weakest at Σ3 (111) GB. The diffusion barriers of Te increase in sequence: Σ11 (11-3), Σ9 (221), Σ3 (111) andΣ5 (021). The calculated diffusion barrier of Te on Σ11 (11-3) is 0.35 eV lower than in the bulk, indicating a fast diffusion of Te along this GB. We also consider the effect of strain on the diffusion and find it to be sensitive to the different GB types. When the tensile strain is up to 4%, the diffusion barriers of Te are lowered by 0.51 eV and 0.15 eV for Σ5 (021) and Σ11 (11-3), respectively. In contrast, this effect for Σ3 (111) is negligible.

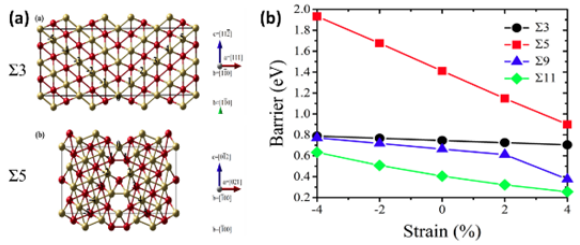

Fig.3 (a) Typical grain boundaries in nickel; (b) diffusion energy barriers of Te in different GBs as functional of lattice strains.

Studies of the interaction between fission products and actinide oxide

The stability of noble gases (He, Ne, Ar, Kr and Xe) in thorium dioxide is studied by means of density functional theory. The computations are performed considering insertion sites of ThO_2, including the interstitial sites, the thorium vacancies, the oxygen-thorium di-vacancy and three types of Schottky defects. Our results show that there is an approximately linear relation between the energies and the atomic radii. As the size of the noble gas atom increases, the noble gas atoms energetically prefer to incorporate into large vacancy defects rather than into interstitial positions. Moreover, the binding energy of Kr or Xe interstitial in a Schottky defect is larger than the formation energy of a Schottky defect, suggesting the Schottky defects are thermodynamically favorable in the presence of these noble gas atoms. The charged defects are also considered for noble gas atoms trapped in Th and O vacancies.

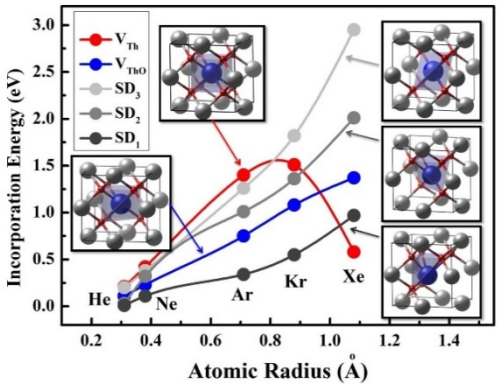

Fig.4 The Incorporation energies of noble gas in defect site of ThO_2

Pressure-induced structural transformations in ThC_2

Thorium-carbon systems have been thought as promising nuclear fuel for Generation IV reactors which require high-burnup and safe nuclear fuel. Existing knowledge on thorium carbides under extreme condition remains insufficient and some is controversial due to limited studies. Here we systematically predict all stable structures of thorium dicarbide (ThC_2) under the pressure ranging from ambient to 300 GPa by merging ab initio total energy calculations and unbiased structure searching method, which are in sequence of C2/c, C2/m, Cmmm, Immm and P6/mmm phases. Among these phases, the 2/m is successfully observed for the first time via in situ synchrotron XRD measurements, which exhibits an excellent structural correspondence to our theoretical predictions. The transition sequence and the critical pressures are predicted. The calculated results also reveal the polymerization behaviors of the carbon atoms and the corresponding characteristic C-C bonding under various pressures. Our work provides key information on the fundamental material behavior and insights into the underlying mechanisms that lay the foundation for further exploration and application of ThC_2.

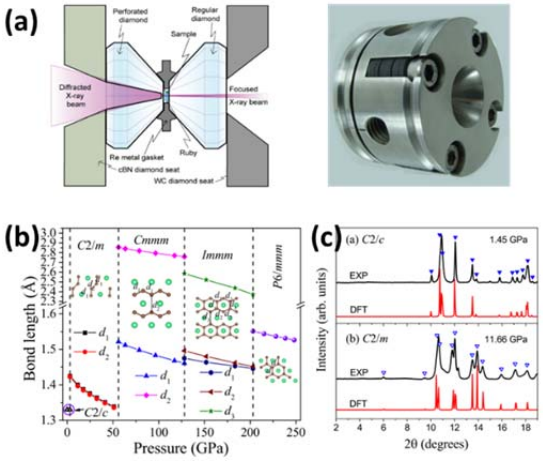

Fig.5 (a) The schematic setup for high pressure XRD measurements; (b) Change of C-C bond lengths for different phases with pressure increasing; (c) XRD patterns and volume versus pressure relation.

Materials Irradiation Test and PIE

Post irradiation examination of alloys

In the year of 2014, Hastelloy N alloys irradiation experiment was started at the high flux engineering test reactor (HFETR) in Nuclear Power Institute of China. The irradiation was conducted at the temperature ranged between 609.5-670.7 ^{o}C, and the collective dose was 2.5 × 10^{19} n/cm^2 (E > 0.1 MeV). The post irradiation examination of alloys followed the cooling and cutting of the irradiation equipment. The measurements of dimensions, density and hardness, tensile test at room temperature, and Charpy impact test below 350 ^{o}C are finished. The test results and the evaluation of irradiation resistance of Hastelloy are summarized in the TMSR technique report titled as " the progress of neutron irradiation of nickel based alloys".

Graphite irradiation test and post irradiation examination

The irradiation test plan in Nuclear Power Institute of China was adjusted in Apirl 2016. The Ultrafine particles graphite NG-CT-50 and homemade C/C composite material were selected for irradiation. The samples were well prepared, and the dimension and weight of the samples were measured before irradiation in July 2016 (see Fig.6). The samples were placed into the irradiation equipment, and the irradiation equipment was inserted into the reactor in August (see Fig.7). Irradiation test on the first batch was finished in September.

The irradiation equipment would be ready for cutting after three months' cooling. The post irradiation examination was under way.

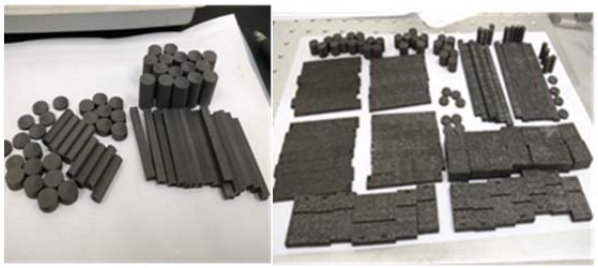

Fig.5 The samples of graphite and C/C composite before irradiation

Fig.7 The assembling of samples and the irradiation equipment

The design of the irradiation equipment in MITR for grahite irradiation test was finished in Apirl 2016, as shown in Fig.8. In this design, samples are completely immersed in the molten salt. The samples were well prepared, and the measurements before irradiation were conducted including SEM, dimension and weight measurement, Raman, XRD. The samples prepared for neutron irradiation in MITR are shown in Fig.9. The assembling of samples, molten salt and irradiation equipment were finished in September. The samples were irradiated for 1000 hours, from October to December. The irradiation equipment has been taken out of the reactor and is under cooling. The post irradiation examination will be conducted in the first half year of 2017.

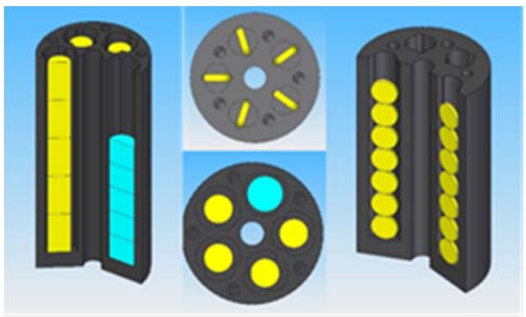

Fig.8 The design of irradiation samples assembling in MITR

Fig.9 The samples prepared of neutron irradiation in MITR

Materials Corrosion Test and Evaluation

Specification for corrosion testing

In order to make the test methods and data analysis of metal corrosion in high temperature molten salt more scientific and standardized, the corrosion testing specification of metal materials in static LiF-NaF-KF molten salt is formulated. This specification is consuled to ASTM standard, JIS standard and national standard, and suitable for the high temperature corrosion evaluation of metal materials in static LiF-NaF-KF molten salt. The specification of corrosion related definitions was explained, and the experimental conditions of corrosion were specified, including the size, preparation, cleaning and storage of the samples, the composition, transport and storage of the molten salt, the size of the crucible, the material selection basis, the glove box, the high temperature furnace, soaking, experimental safety and so on. In addition, the experimental steps, results and reports are explained in detail. At present, this specification has been modified according to the opinions of the peer experts. The content of corrosion testing based on this specification has been approved by CNAS.

Stress corrosion cracking evaluation of 316 stainless steel in fluoride molten salt

The modified bending beam specimen device (Fig.10) was used to test the corrosion resistance of 316 and the stress corrosion sensitivity of the welded parts (Figure 11), and to evaluate the sensitivity of the metal to the stress corrosion cracking under a given environment. In the national standard and ASTM, the initial tensile stress of the specimen surface on the bending beam test must reach the yield point. With reference to the 316L stress strain curve (Figure 12) and the stress corrosion sensitivity test condition of the material in the pressurized water reactor environment, the stress corrosion test of the bending beam was finally conducted with 5% deformation quantities. At present, immersion corrosion is ongoing.

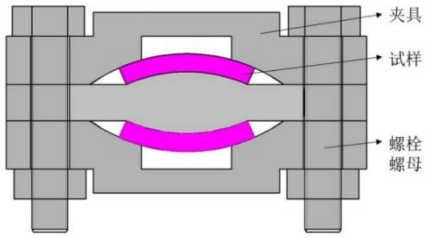

Fig.10 A set-up diagram for stress corrosion test

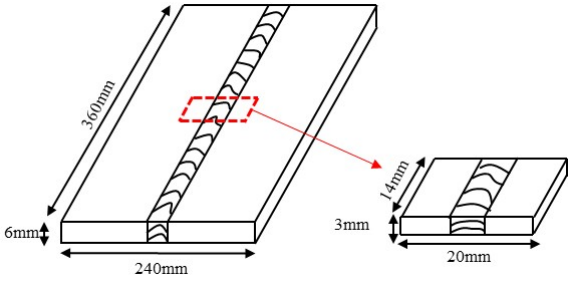

Fig.11 A diagram of welding specimen tor stress corrosion test

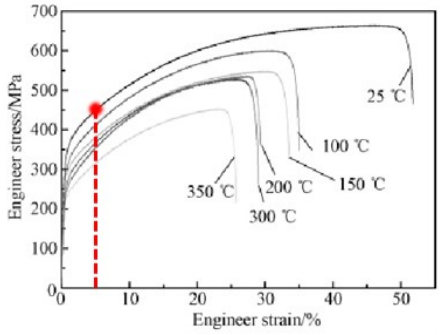

Fig.12 Stress-strain curves of 316L stainless steel at different temperatures

Corrosion evaluation of 304LN stainless steel in molten salt and its vapor

The weight loss and morphology of the corroded alloys, and the composition of the post corrosion molten salts were compared. The conclusions are as follows.

304LN suffered a severe attack in FLiNaK molten salt at 700 ℃, while the corrosion in molten salt vapor is negligible.

The corrosion rate of 304LN in 304LN-Hastelloy N couple increased double.

The corrosion of Hastelloy N in the 304LN-Hastelloy N couple is inhibited.

Corrosion control of 316 stainless steel

The surface modification of 316 stainless steel was conducted by FTD (Fluoride Thermal Diffusion) technology. The BCC structure was formed at the grain boundary of the substrate and near surface after modification. Thus, the composite structure of BCC and FCC combined with matrix metallurgy was formed on the surface and near surface of 316 stainless steel and. The tensile strength of the modified 316 stainless steel did not decrease (Fig.13), but the corrosion resistance increased significantly (Fig.14).

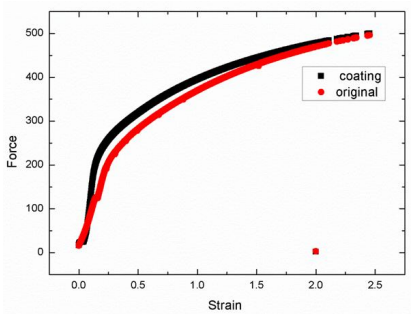

Fig.13 Tensile curves of 316 stainless steel samples

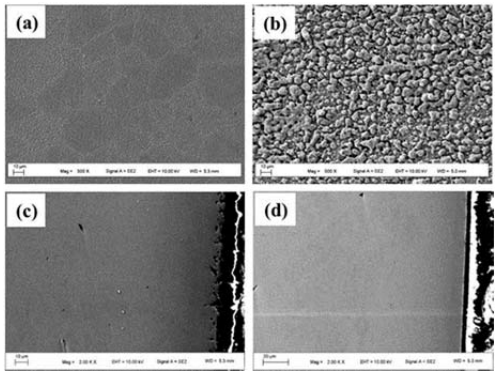

Fig.14 Post corrosion (Flinak, 700℃, 90 hours) SEM images: (a) unmodified 316SS front surface; (b) modified 316SS front surface; (c) unmodified 316SS section; (d) modified 316SS section.

Conclusion

Test specification on coolant molten salt corrosion was formulated. Based on this specification, corrosion evaluation on the hastelloy N and GH3535 was completed. It was proved that the high purity molten salt steam was almost uncorroded to the 304LN stainless steel. Thermal diffusion in molten salt situ could modify the 316SS surface, and inhibit its intergranular corrosion significontely. The mechanism of surface modification will be studied in the future.

Irradiation examinations for the first batch of domestic carbon based materials, including ultrafine graphite and C/C composite materials, were completed. Because the radioactivity is too high, the irradiated device has to be cut after the samples cooled. Device cutting and post irradiation examination will be conducted in the first quarter of 2017.

An interatomic potential for helium in bulk nickel was developed. The helium interactions with typical grain boundaries (GBs) were explored. The mechanical properties of nickel nanowires containing helium bubbles were also clarified. The initial corrosion arising from impurities in molten salts as well as the Te-induced embrittlement of GBs in nickel-based alloy were understood. Moreover, the distributation and stabilities of nobel gas (fission products) in actinide oxide were obtained. The pressure-induced structural transformations of actinide carbides were investi-gated via both theoretical calculation and synchrotron XRD measurments.

堆用聚合物材料研究进展

堆材料科学与工程二部

堆其它材料设两个子课题，分别开展高性能碳化硅纤维制备工艺研究、堆用聚合物研究。

高性能 SiC 纤维研究制备工艺研究

1、聚碳硅烷(PCS)纤维的辐照。2015−2016 年的原料 PCS 纤维均采购自苏州赛力菲陶纤有限公司，2015 年共采购 3 次，每次 25~30 筒纤维，共 15 kg。PCS 纤维非常脆弱，绕于丝筒后必须小心移动和运输，避免晃动、振动等对纤维的损伤，运达辐照车间后直接进行辐照处理，期间避免触碰纤维。为此，要求纺丝工艺和辐照工艺相匹配，避免纺好的 PCS 纤维因搬运和触碰受到损伤。经过不断改进，解决了纺丝和辐照工艺的衔接问题。2016 年共采购了 2 次 PCS 纤维，共约 10 kg。为了避免损伤，采购工作派专人负责，从纺丝、取货到辐照现场全程跟踪，充分做好纤维交接和运输工作，尽量避免纺好的 PCS 纤维因搬运和触碰受损伤。辐照 PCS 纤维的工作依照固定程序开展，实现了对 PCS 纤维的及时辐照处理。辐照设备运转正常，辐照成功率大幅提高，2016 年共辐照 20 余批次，整体辐照效果良好。

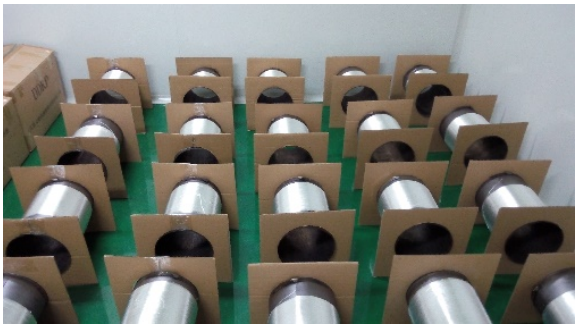

图 1　批量采购和辐照 PCS 纤维

2、掌握了 PCS 纤维的烧结工艺。将辐射固化 PCS 纤维进行烧结（热解）得到目标产物 SiC 纤维。烧结过程分为两步：第一步低温烧结，实现 PCS 纤维从有机物向无机物的转变，纤维的化学组成改变；第二步高温加张烧结，将预烧纤维在一定张力牵伸状态下经高温热处理，完成 SiC 纤维的热定型，进一步提升纤维的力学性能。2016 年针对高温烧结中的工艺问题，对烧结设备和上浆设备进行了改造，并开展了工艺的优化，获得了理想的实验效果。纤维的整体烧结能力获得提高，纤维产品的性能尤其是模量获得较大提高，产品的断头率和品相获得了较大改善。2016 年较好的完成了公斤级的批量制备，形成了稳定烧结制备第二代 SiC 纤维的能力。截至年底，获得 SiC 纤维样品 3 kg。

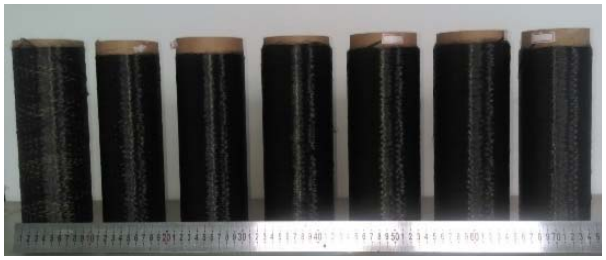

图 2　实验室烧结 SiC 纤维

3、开展第三代 SiC 纤维的试制，获得了实验室样品。第三代 SiC 纤维被认为更适于核环境，课题组在实现第二代 SiC 纤维批量制造的基础上，开展了第三代 SiC 纤维的试制工作。在研制出小型氢气氛烧结炉的基础上，通过改变烧结条件试制第三代 SiC 纤维，经过对烧结条件的筛选和优化，初步明确了烧结条件对纤维脱碳过程的影响规律，获得了符合第三代 SiC 纤维特征的实验室样品。硅碳比从 1:1.3 降低到 1:0.9－1.1 可控，纤维模量从第二代纤维的 200 GPa 提高到现在的 300 GPa。

4、建成两步法烧结制备 SiC 纤维的实验线。PCS 纤维的烧结线包括低温批次烧结设备和高温连续加张烧结设备。批量低温烧结炉从 2015 年初进行设备安装，之后用于烧结实验，6 月完成烧结试验工艺的优化。加张烧结的主体设备用于生产 1 K 碳化硅纤维，实验线高温烧结的最高温度为 1 600 ℃。该实验线于 2014 年底开始设备进场安装，2015 年 3 月基本完成安装调试，2015 年 6 月进行第一次开车实验，并根据烧结过程中存在的问题进行了设备改造，2015 年 11 月进行第二次开车。两次开车对纤维的烧结工艺参数进行了系统的考察，对炉体温度分布、牵伸张力、走丝速度控制、上浆和收卷等关键工艺进行了优化，该线于 2015 年开始正式投入使用。

图 3　加张烧结 SiC 纤维的实验现场图

聚合物材料

堆用聚合物材料子课题主要开展常规（服役温度约为 90°C）、高温（服役温度约为 250°C）电缆料研制，2015−2016 年主要进展如下。

1、完成了双层绝缘、双层护套结构的核电 K1 电缆制备，优化核电电缆结构，根据三代核电电缆双层结构，采用 60 年设计寿命的核电电缆内外绝缘材料、内外护套材料，制备了 2 km 双层绝缘、双层护套结构的核电 K1 电缆。

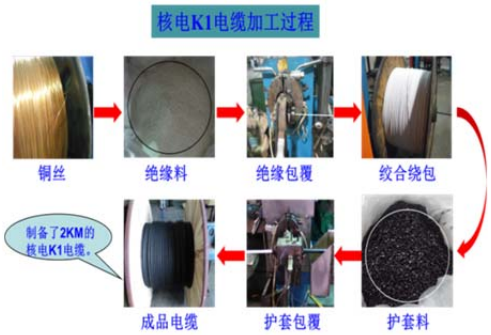

图 4　双层绝缘、双层护套结构的核电 K1 电缆加工流程图

2、双层结构核电 K1 电缆全性能检测

双层结构核电 K1 电缆已由 2015 年 5 月送国家电线电缆质量监督检验中心(CT15-2354)进行机械性能、电性能、阻燃性能、热老化性能（电缆 60 年使用寿命）、耐辐射性能（累计吸收剂量 1 500 kGy）等全性能检测，2016 年 6 月已完成以上性能检测。

图 5　双层结构核电 K1 电缆耐辐照试验报告（γ 射线）

3、核电电缆按“华龙一号”标准要求进行了 LOCA 试验(15d)及浸没试验(15 d)，经过 LOCA 试验的核电 K1 电缆浸入 2428 mg/L 硼酸水溶液中，温度 85.2 ℃进行 15 d 的浸没试验，试验结束后进行性能测试，按 40 倍外径成圈，进行浸水 1 h 的电压试验不击穿(3.5 kv，时间 5 min)，绝缘电阻不小于 1 MΩ/km，按 40 倍弯曲护套可以开裂，但不能脱落或护套绝对断裂伸长率不小于 5%。2016 年 11 月 30 日完成并顺利通过了以上试验，检测报告预计在 2017 年完成。

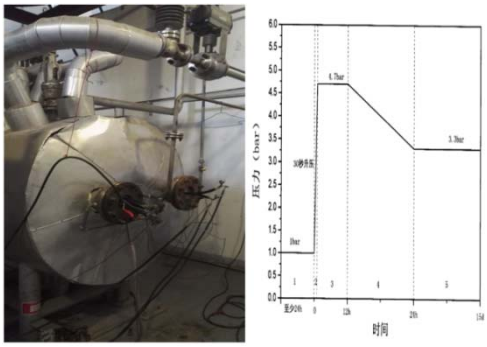

图 6　华龙一号 LOCA 试验炉和压力鉴定曲线

4、完成了进口高温电缆聚醚醚酮性能检测

采用进口聚醚醚酮(PEEK)原料制备了 PEEK 高温电缆，已取得国家电线电缆质量监督检验中心(CT14-2984)全性能检测报告。

图 7　高温 PEEK 电缆样品、试验报告

5、开展低剂量率β射线辐照对核电电缆材料损伤机理研究。

β射线辐射 LDPE 的氧化机理如图 8，LDPE 在受到辐照时产生自由基，然后这些自由基与氧气反应（图中(a)），或自由基之间相互偶合形成交联网络（图中(b)）。在相同的吸收剂量下，高剂量率β射线辐照时空气中的氧气参与反应较少，故聚合物(LDPE)以图中(b)反应为主；相应地，低剂量率下，由于相同吸收剂量所需用的时间长，因而有更多的

氧气参与辐射氧化，故低剂量率辐照时在聚合物基材中以图中(a)的反应所占比例较大，这也是其辐照损伤较大的原因。而在低剂量率β射线辐照下，聚丙烯主要以降解为主，聚丙烯的降解同时发生在无定形区与结晶区。

$$P\ (polymer) \xrightarrow{Radiation} R\bullet\ (radical)$$

$$R\bullet + O_2 \longrightarrow RO_2\bullet \quad (a)$$

$$R\bullet + R\bullet \longrightarrow R-R \quad (b)$$

In case of no chain reaction with antioxidant

$$RO_2\bullet \longrightarrow \text{Oxidation Products}$$

In case of chain reaction

$$RO_2\bullet + P \longrightarrow ROOH + R\bullet$$

图 8　LDPE β 射线辐射氧化机理图

保证 1.5 MeV 电子束辐照平台的正常运行，同时，添加一套往返式束下辐照装置和温度气氛辐照箱，可以更好的开展动态高剂量率β射线和不同温度气氛辐照试验，挖掘装置潜力，扩展应用范围。

图 9　往返式束下辐照装置和温度气氛辐照箱

Progresses in Developing Other Materials forthe Reactor

Reactor Materials Science and Engineering DivisionII

There are two subtopics in the other reactor materials for the reactor, the study on the high performance carbon silicon fiber，and the polymer materials for the reactor.

Study on preparation technology of high performance sic fiber

In 2015 to 2016, PCS green fiber was purchased from Suzhou Ceiramic Fiber Co., Ltd., In 2015, we purchased 3 times, each time 25~30 barrels of fiber, a total of 15 kg. PCS green fibers are very fragile. They must be carefully moved and transported around the cylinder to avoid sloshing, vibration and other damage to the fiber. After the radiation shop is transported to the radiation workshop, it is directly irradiated to avoid further touching the fiber. Therefore, it is necessary to match the spinning process with the irradiation process so as to avoid the damage of the PCS fiber. After continuous improvement, the connection between spinning and irradiation technology has been solved. In 2016, a total of PCS green fibers were purchased with 2 times, totaling about 10 kg. In order to avoid damage, the purchasing work is responsible for the whole process of tracking from spinning, taking goods to the irradiation site, making full use of fiber handover and transportation to avoid the damage to the spun PCS fibers from handling and touching. The irradiation of PCS fiber was carried out in accordance with the fixed procedure, and the PCS fiber was irradiated in a timely manner. The irradiation equipment was well established, and the irradiation processing was greatly improved. In 2016, more than 20 batches were irradiated, and the overall green fibers were irradiated successfully.

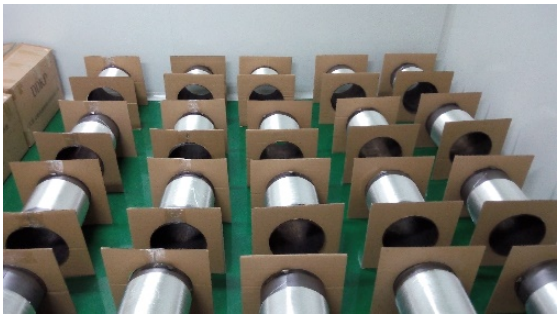

Fig.1 PCS green fibers

Study on the sintering process of PCS fibers. The radiation cured PCS fibers were sintered (pyrolyzed) to obtain the target product SiC fiber. The sintering process is divided into two steps: the first step is low temperature sintering to realize the transformation of PCS fibers from organic matter to inorganic one, and the second step is used to heat the prefired fiber under a certain tension and heat treatment to complete the thermal shape of the SiC fibers, and this step can further enhance the mechanical properties of the SiC fiber. In 2016, aiming at the technological problems in high temperature sintering, the sintering equipment and sizing equipment were reformed, and the optimization of the process was carried out, and the ideal experimental results were obtained. The overall sintering ability of the fibers has been improved, especially the modulus of the fiber products has been greatly improved, and the breakage rate and quality of the products have been greatly improved. In 2016, the batch production of kg class was completed better, and the ability of stable generation of second generation SiC fibers was formed. By the end of the year, 3 kg of SiC fiber was obtained.

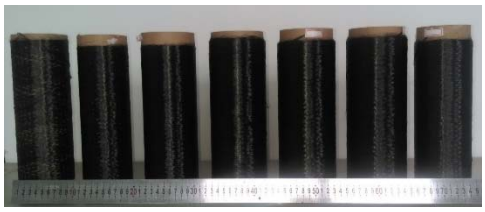

Fig.2 SiC fibers

Study on the preparation of the third generation SiC fiber, and laboratory samples were obtained. The third generation of SiC fiber is considered to be more suitable for the nuclear environment. On the basis of the second generation of SiC fiber manufacturing, our group has carried out the perparation of the third generation of SiC fibers. On the basis of developing a small hydrogen atmosphere sintering furnace, the third generation SiC fibers were produced by changing the sintering conditions. After screening and optimizing the sintering conditions, the influence of sintering conditions on the decarbonization process was preliminarily clarified, and the samples were obtained in accordance with the characteristics of the third generation of SiC fibers. The ratio of silicon to carbon decreased from 1:1.3 to 1: 0. 9 to 1 1, and the fiber modulus increased from 200GPa of the second generation fiber to the present 300GPa.

Built an experimental line for preparing SiC fiber by two step sintering process. The sintering line of PCS fiber includes low temperature batch sintering equipment and high temperature continuous sintering equipment. The batch low- temperature sintering furnace was installed in early 2015, and then used in the sintering experiment. The sintering process was optimized in June. The main equipment of sintering is used to produce 1 K silicon carbide fiber. The highest temperature of high temperature sintering line is 1 600 ^{o}C. The experiment line began to install the equipment at the end of 2014, completed the installation and debug in March 2015. The first experiment was carried out in June 2015, and the equipment was transformed according to the problems in the sintering process, and second times in November 2015 were carried out. The sintering process parameters of fiber were systematically investigated. The key technologies, such as temperature distribution, drawing tension, wire speed control, sizing and winding, were optimized. The line began to be formally put into use in 2015.

Fig.3 SiC Fiber sintering Laboratory

Polymer materials for the reactor

The main course of polymer materials for the reactor is the conventional (the service temperature is about 90 ℃) and the high temperature (the service temperature is about 250 ℃) nuclear powercable materials study and preparation. The main progress is as follows from 2015 to 2016.

1) In order to optimize the structure of nuclear power cables, the preparation has been completed for the K1 nuclear power cable with double insulation and double covering structure. According to the structure of three-generation nuclear power cable, the 2 km two-layer insulation and the two-layer covering structure K1 nuclear power cable is prepared by using the inner and outer insulation and covering materials of the nuclear power cable with the 60 years design life.

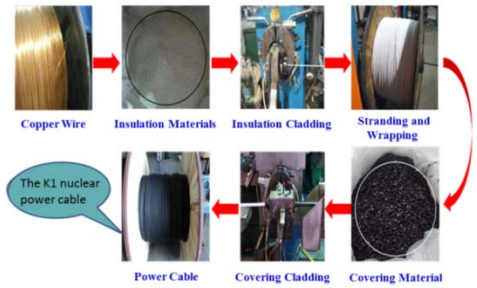

Fig.4 The K1 nuclear power cable with double insulation and double covering structure processing flow chart

2) Full performance test of double-layer nuclear power K1 cable. The two-layer nuclear power K1 cable has been sent to the national electric wire and cable quality supervision and inspection center (CT15-2354) in May 2015 for full performance test, such as mechanical performance, electrical performance, flame retardant property, thermal aging performance(60 cable years service life), irradiation resistant property(absorbed dose 1 500 kGy), and so on.

Fig.5 The irradiation resistant test report of double-layer structure nuclear K1 cable

3) The nuclear power cable is required to carry out the LOCA test (15 days) and the immersion test (15 days) according to the specific standard of Hualong first nuclear power plant. After the LOCA test, the K1 nuclear power cable have been evaluated the 15 d immersion test with 2 428 mg/L boracic acid solution and 85.2 ℃ temperature. Then the performance evaluation was conducted with a circle according to 40 times the outer diameter. The voltage test of the 1h submerging in water is not punctured(3.5 kv, 5 min). The insulation resistance is not less than 1 m Ω/km. Moreover, the covering can crack, but not fall off and the absolute breaking elongation is not less than 5%. In November 30, 2016, the above performance tests have been completed. Therefore, the test report is expected to be completed by 2017.

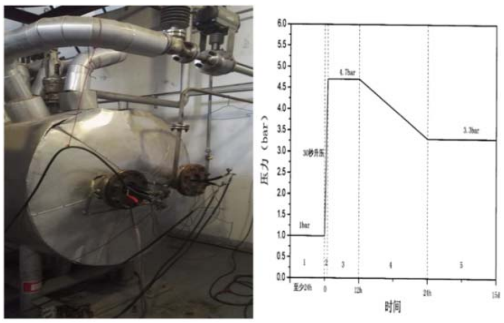

Fig.6 The LOCA test furnace for Hualong First nuclear power plant and the pressure evaluation curve

4) The performance of high temperature cable with imported polyether ether ketone was fulfilled. The PEEK high temperature cable was prepared by using imported polyether ketone (PEEK) raw material, and the whole performance test report by national power cable quality supervision and inspection center (CT14-2984) has been obtained.

Fig.7 The high-temperature PEEK cable sample and the test report

5) Study on the damage mechanism of nuclear power cable materials with low dose rate beta-ray irradiation.As in Fig.8, the oxidation mechanism of beta-ray irradiation LDPE. LDPE produces free radicals when irradiated, and then these free radicals react with oxygen (a in the diagram) or form cross linking networks (b in the diagram).Under the same absorbed dose, the oxygen is less involved in the reaction by high dose rate beta-ray irradiation. Therefore, the main reaction of the polymer (LDPE) is process (b). Accordingly, at low dose rate, more oxygen is involved in radiation oxidation due to the longer time required for the same absorbed dose, so the ratio of the process a in the polymer substrate is larger for the low dose

rate irradiation, which is also the reason of the larger irradiation damage. But PP is mainly degraded under low dose rate beta-ray irradiation, which occurs in amorphous and crystalline regions.

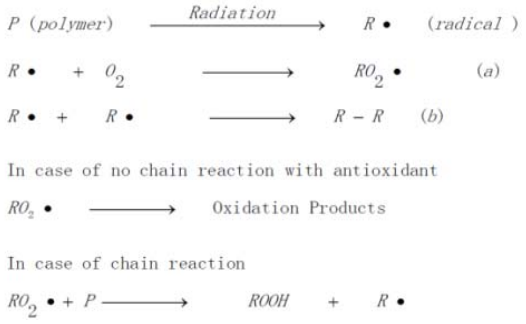

Fig.8 LDPE Beta-ray radiation oxidation mechanism

It is guaranteed that the the normal operation of 1.5 MeV electron beam irradiation platform. At the same time, a set of round trip beam device and the irradiation box with different temperature and atmosphere was supplied, which can be used to carry out the beta-ray irradiation tests with the dynamic high dose rate, the different temperature or atmosphere. The application of the equipment can excavate the potential of the platform and extend its application scope.

Fig.9 The round trip beam device and the irradiation box with different temperature and atmosphere

材料评估测试平台

堆材料一部　上海光源

在中科院战略先导专项《未来先进核裂变能-钍基熔盐核能系统》资助下，围绕国内首个熔盐堆材料的性能评估及特殊工艺参数要求，开发研制/购置了一系列熔盐堆用材料测试设备，建立了堆材料评估测试平台。材料评估测试平台涵括：热学/力学测试平台、成分分析平台、微观结构分析平台、材料腐蚀性能测试平台、高温离子束辐照平台和同步辐射原位实验平台。平台现有仪器设备 100 余台（套），固定资产价值约 1 亿元。

材料评估测试平台可精确测定堆设计及堆安全评估所需的各类材料数据，具备了熔盐堆用镍基高温合金、高致密核石墨等材料的综合测试评估能力，实现了对堆材料批量评估、筛选的能力，为 TMSR 专项的顺利实施提供了有力支撑。

材料评估测试平台 CNAS 认可资质申请

根据 TMSR 工程需要，利用“材料评估测试平台”积极推进实验室认可项目，并顺利完成了申请材料递交、文件审核和现场评审等环节。已申请检测项目涵盖了反应堆材料如金属材料、石墨材料、复合材料等材料的力学性能、热学、密度和孔隙率等参数的检测，项目的开展将极大推进实验室标准化建设，为 TMSR 用材料评估提供可靠数据。截止 2016 年年底，已完成实验室认可现场评审工作，正在进行现场评审不符合项的整改工作。2016 年 12 月 26~29 日中国合格评定国家认可委员会委派专家组对我所实验室认可项目进行了现场评审（图 1）。实验室管理层、质量负责人和技术负责人等全程协调配合专家现场检查工作。

图 1　评审组现场评审情况

通过本次现场评审，我所工作人员的工作态度、严谨精神给专家组成员留下了深刻印象。经过数天的评审工作，专家组一致认为：

(a) 我所参与认可项目人员是具有高素质人员的团队，拥有高精尖的设备平台，具备开展规范的分析测试的扎实基础；(b) 部分检测项目填补了国内 CNAS 认可领域的空白，并愿意向其他单位进行推荐；(c) 申报项目达 57 项的情况下仅给出 6 个局部不符合项，能力水平高，属于实验室初评阶段比较罕见的优秀结果；(d) 综合上述各项，专家组形成一致意见，对申报项目全部予以推荐。

按照不符合项整改提交情况和 CNAS 对不符合项整改的审核情况，预计 2017 年 3 月份可以取得 CNAS 授权的实验室认可证书。

测试标准、规范建立

随着科学技术的不但发展，已有的 ASME 标准无法完全满足完成指导工作的需求。材料评估测试平台积极推动 ASME HHA-3217 的修订工作，对于 TMSR-SF1 的石墨堆芯安全评定有重要意义。1）ASME HHA-3217 是石墨失效评定的权威规范之一，使其能够适用于熔盐堆用细晶石墨甚至熔盐堆专用的新型超细颗粒石墨，2）能够更好的方便 TMSR 熔盐堆相关评定工作的开展，并提升 TMSR 安分报告中相关内容的可靠性。3）为在未来制定熔盐堆技术规范提供经验。石墨是第四代熔盐堆堆芯反射体结构材料，石墨中的熔盐量在高温下对石墨力学性能具有较大影响，已有石墨强度测试标准，只适合常温下性能测试，因此，需要建立高温测试标准。

表 1　起草的相关测试标准

标准名称	标准类型	进展情况
石墨熔盐浸渗测试标准	ASTM	已通过，D8091-16
小样品石墨的拉伸测试	ASTM	已投票 inter-laboratory study
石墨高温拉伸强度测试	ASTM	进行中
金属材料蠕变-疲劳试验方法	GB	2016.11 已立项

因此，加入 ASME 协会和 ASTM 协会的部分标准工作组，参与熔盐堆相关标准的制定，直接推动了熔盐堆专用核石墨国际规范的建立。2016 年 11 月，金属材料蠕变疲劳测试方法获立项审批，如表 1 所示。上述工作引领国内外熔盐堆用合金、石墨测试标准的建立，弥补了该领域的空白。

TMSR-SEED 材料数据库

1.1 TMSR 材料数据库系统

为了给熔盐堆的工程建设和科学研究提供可靠的材料数据，建设 TMSR 材料数据库系统。基于数据存储安全性和并发处理能力等方面的需求，数据库系统硬件设施搭建 4 节点高性能服务器，包括一个登陆管理节点，两个数据存储节点和一个数据处理节点。其中数据处理节点 CPU 核数>40 核，四节点总核数>80 核。硬件系统能够保障数据存储的长期安全性，满足多线程同时访问的并发处理能力。采购执行政府集中采购的形式，数据库服务器实物图如图 2 所示。

数据库服务器

1.2 TMSR-SEED 材料数据库

TMSR-SEED 材料数据库包括基本库和专题库两个部分（图 3），基本库包括实验数据库和工程标准库。专题库中包括熔盐专题库、辐照专题库、加工专题库和焊接专题库等。每个库中包含合金材料、核石墨材料以及复合材料等，以及其各项性能。实验数据库拟采集所有 TMSR 的材料测试数据；而工程标准库中只包含与 TMSR 工程设计相关的材料数据，这些数据具有权威性。

TMSR－SEED V1.0 的数据库表空间结构中包含合金、石墨、熔盐三个 TMSR 项目中核心物项的标准参数数据表，还包括合金腐蚀试验数据、熔盐成分测试数据、合金辐照三个试验数据表，其它是支撑表格，如参数定义列表、试验报告列表等。

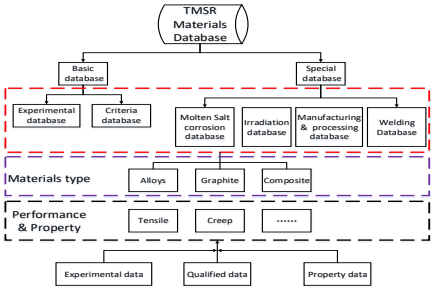

图 3 TMSR-SEED 数据库结构示意图

数据库的界面如图 4 所示，能够同时并发 180 个线程，数据库设计存储能力达到 10TB 以上，已实现了各子数据库之间的交互关联，可交叉查询数据，测试信息可追溯，分析结果可以图表形式呈现。

图 4 TMSR-SEED V1.0 数据库界面

TMSR-SEED V1.0 目前包含熔盐堆用合金(UNS N10003)、4 种核石墨、65 批次 FLiNaK 熔盐等材料的物性、力学性能、中子辐照以及腐蚀性能等 110 种性能数据集，总数据量达到 8 200 多条。

材料辐照监测与安全连锁系统

4 MeV 加速器辐射剂量 γ 射线固定监测系统

完善 4MeV 加速器辐射剂量γ射线固定监测系统（图 5），并使监测仪具有剂量率显示及报警功能。4MeV 加速器辐射监测系统建立后，经过调试已投入使用。当加速器厅剂量率超过阈值时，可以触发加速器自动停束。当实验厅剂量率超过阈值时，相应的就地报警单元可以发出警报。系统投入使用后，工作正常，有效保证了实验人员的辐射安全。

图 5 γ 探测器

实验室辐射安全联锁系统

4 MV 加速器改造后，最高端电压由 3 MV 提高到 4.3 MV，束流强度提高，新建了专用的辐照装置，这些将会引起 4 MV 加速器实验室辐射水平的变化。因 4 MV 加速器实验室原辐射剂量安全联锁系统已经损坏多年，为了确保加速器运行时人员安全，按照上海应用物理研究所新的辐射防护工作有关规章制度要求，新建了 1 套实验室辐射安全联锁系统，平面局图如图 6 所示，实验室剂量监测布点如图 7 所示。

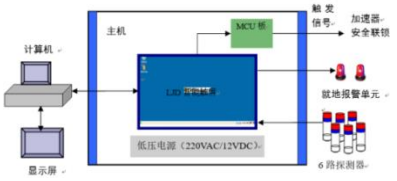

图 6　辐射监测系统框图

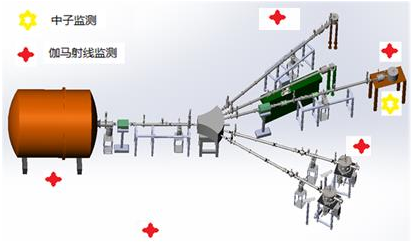

图 7　4 MV 加速器实验室剂量监测布点示意图

正电子多普勒展宽系统研制

在开展反应堆材料的辐照损伤缺陷研究中，正电子湮没光子具有较高的能量，能穿透较厚的体材料，由湮没能谱的多普勒展宽（图 8(a)）的线型参数，可以获得材料内部电子动量密度分布的信息，得知辐射损伤所产生缺陷的类型。利用它研究金属材料辐照后产生大量微结构缺陷的形成机理是一个非常有效的手段。因此，根据实验室现有一套高纯锗探测器可以利用，另购置电子学插件 659 5-KV Detector Bias Supply、928 Multichannel Buffer、672 Spectroscopy、4001C/4002D NIM Bin 和各种规格电缆线等，搭建了一套正电子多普勒展宽系统（如图 8(b)所示）。

(a) 多普勒展宽　　(b) 正电子多普勒

图 8　正电子多普勒展宽系统

原位实验装置

穹顶高温镍基合金研究装置

穹顶高温镍基合金研究装置如图 9 所示。2015 年度重新加工了铍窗和镀膜，并解决了装置温度控制上的易过冲和不稳定的问题。从发来的报告和视频上看，装置最高可控温度达到了 1 400℃，700-1200 ℃ 范围内的温度稳定性在±2℃ 以内，真空度达到了 3×10^{-6} mbar。

图 9　穹顶高温镍基合金研究装置

熔盐环境下原位蠕变-疲劳设备

结合原位拉伸试验机的运行经验，对熔盐环境下原位蠕变试验机的设计方案进行了更改。有原先通过氩气气压将熔盐从储盐罐转移到试验釜里的方案改为更为简单有效的波纹管整体提拉式设计，见图 10(a)。如图 10(b)所示，进行实验时，现将让波纹管出于拉伸状态，将固态盐装在釜的底部。加热将盐熔化后，将整个釜体上升，波纹管出于压缩状态，让试样浸没在熔盐中进行蠕变实验。实验完成后，将釜体降下，波纹管拉伸，等待熔盐冷却，最终取出试样和废盐。这样的设计简化了气路，避免了可能的泄露，并使实验流程加简单。2016 年 3 月份完成装配调试。装置试验单元的设计图和试验流程示意图见下图。

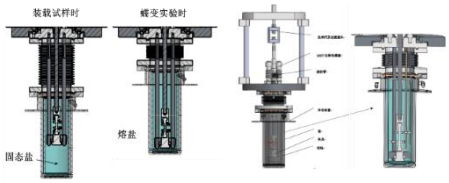

（a）设计图　　**（b）试验流程示意图**

图 10　波纹管整体提拉式熔盐蠕变试验机试验单元

高温真空万能实验系统

图 11　真空高温万能试验机

蠕变持久试验机

50 KN 高温蠕变持久试验机用于测试合金材料的高温蠕变持久性能。依据 TMSR-SF1 熔盐堆的物理设计要求，测试周期最长达 60 000 h。虽然现有的 12 台蠕变持久试验机全年每天 24 时不间断运行，但蠕变试验机需求缺口较大，国内没有第三方检测提供超过 10 000 h 的测试服务，因此购置了 12 台试验机，以同时开展进行不同参数测试，尽快获得熔盐堆工程设计所需的合金材料基本力学参数。

在采购过程中，蠕变持久试验机采用招投标方式进行，中标方为长春机械科学研究院有限公司，包含 10 台电子式蠕变持久试验机和 2 台机械式蠕变持久试验机（图 12），中标金额 190 万元。设备厂家已于 2016 年 9 月完成设备的内部调试，2016 年 10 月，我方袁广宙工程师前去设备厂家进行预验收，并现场安装了不锈钢美标试样，开展高温蠕变性能试验。

图 12 蠕变持久试验机采购及预验收

上海光源联动装置

同步原位试验装置

图 13 部分同步原位实验装置

依托上海同步辐射光源，研制十余套同步辐射联用实验装置实现了核能材料的原位、在线、动态研究，如高温熔盐原位测试装置、高温固液界面原位装置、穹顶高温合金原位装置、原位焊接实验装置、疲劳裂纹扩展实验装置、拉曼光谱联用装置等。图 13 为部分设备的现场调试情况。

原位分子振动光谱与同步辐射联用装置

2015-2016 完成了联用装置的采购、改造、安装、调试、验收，验收性能达到预定指标。设备总体运行良好，提升了原位表征技术的应用。图 14 是原位分子振动光谱与同步辐射联用装置联用装置，2014 年采购，11 月份送货安装，2015 年 3 月份开始改造，8 月份开始投入调试，2016 年 5 月份正式开始投入工作；经过原位池、漫反射系统、外置样品仓的改造，气路控制、温控装置、循环水的离线和在线调试，目前已经处于稳定运行状态。该套联用装置设计针对 XAFS 测试的透射模式，配有 6 路进气系统和快速切换阀，原位测试条件下，常压下，可承受的最高温度为 350 ℃，升温速率可认为调控。目前已经成功地将其应用到 CuO/CeO_2 催化体系中，后续将继续探究催化剂体相-表面原位表征的应用和研究

图 14 原位分子振动光谱与同步辐射联用装置

总结和展望

材料评估测试平台逐渐完善，完成了新购置设备安装、调试、验收，每台设备由固定人员进行日常使用及维护管理，每年或每两年定期校核。目前设备数量 130 余台（套），固定资产约 8000 万元。能够精密测定堆设计及安全评估所需的材料数据，实现材料批量评估与筛选，具备了开发新一代高温合金、高致密核石墨的能力。同时，在确保材料评估测试平台设备正常运行的基础上，积极发展了新的熔盐堆用材料的测试方法，起草了 3 项 ASTM 测试标准、1 项 GB 国家测试标准，完成了实验室 CNAS 认可资质现场评审，并建成了国内首个熔盐堆专用材料数据库共享平台。

Material Assess Platform

Nuclear Materials Division SSRF

Under the funding of the "Future Advanced Nuclear Fission Energy-Strontium-Based Molten Salt Nuclear Energy System" of the Chinese Academy of Sciences, a series of molten salt reactors were developed around the performance evaluation and special process parameters of the first molten salt reactor in China. Material evaluation test platform includes: thermal/mechanical test platform, component analysis platform, microstructure analysis platform, material corrosion performance test platform, high-temperature ion beam irradiation platform and synchrotron radiation in-situ experiment platform. The platform has more than 100 sets of equipment, and the value of fixed assets is about 100 million yuan.

CNAS Application

For promoting the development of TMSR project, we actively push forward the Laboratory Accreditation Certificate on Material Evaluation Test Platform, and have accomplished such works as application, material assessment, on-site assessment, and so on. The applied test items cover the mechanical property, thermal property, density and porosity of metal matrials, graphite materials and composite materials, which are widely used in reactors. The project has greatly promoted the standardization construction of laboratory, and which will ensure the reliability of the test results provided for TMSR. The evaluation experts assigned by CNAS carried out a three days on-site assessment on December 26~29, 2016(Fig.1), the administrator, quality personnel and technical directors attend the on-site assessment.

Fig.1 CNAS evaluation photograph

The working attitude of staff left a deep impression on the evaluation experts during on-site assessment, and they consider that:

(a) The participants are excellent, the equipments are advanced.

(b) Part of the test items filled the domestic gaps of CNAS accreditation area.

(c) Only six nonconformities were found for fifty-seven test items, which indicated that the team is excellent.

(d) All the applied test items will be recommended to CNAS.

We will rectify the six nonconformities on the relevant regulations, and submit a correction report to CNAS, then it is expected that we will get the laboratory accreditation certificate authorized by CNAS in March 2017.

Test standards Establishment

With the development of science and technology, the existing ASME standards cannot meet the need of the guidance work.Materials evaluationtest platformpromotesrevision of ASME HHA-3217 actively, which has important significancefor TMSR - SF1 graphite core security assessment.1) Revised ASME HHA-3217is one of the standard specificationsfor failure evaluation of graphite, which can be suitable for molten salt reactor with new type of super-fine grain graphite; 2)Revised ASME HHA-3217 can make the TMSR molten salt reactor-related evaluation workconveniently, and promote the reliability ofTMSR SAR (safety analysis report);3) providedexperience forestablishing the Molten Salt Reactor Code in the future. Graphite is the fourth generation of molten salt reactor core reflector structure materials. Graphite in the molten salt at high temperature has great influence on mechanical properties of graphite.Test standards ofgraphite strength are only suitable for room temperature, therefore, and it needs to establishthe high-temperature mechanical test standards of graphite.

So, join the ASME association and thepart of the working group in theassociation of ASTM standard, to participate in the molten salt reactor-related standards, promotethe establishment of the international norms of the special molten salt reactor nuclear graphite

In November 2016, the metal material creep-fatigue test method for project approval, as shown in Table 1. The above work leads the molten salt reactor at home and abroad with the alloy, the establishment of the graphite test standard, make up the blank of the field.

Table 1 Test standards draft

Standard	Type	Progress
Standard Guide for Impregnation of Graphite with Molten Salt	ASTM	Publish , D8091-16
Standard Test method for splitting tensile strength of Carbon and Graphite Specimens	ASTM	Voted, inter-laboratory study
Standard Guide for high-temperature strengths of Carbon and Graphite Specimens	ASTM	In progress
Test method of Creep-fatigue for metal materials	GB	2016.11

TMSR-SEED

TMSR-SEED Material Database System

TMSR Material Database Hardware System

In order to provide reliable material data for construction and scientific research of molten salt reactors, the TMSR material database system was constructed. Based on the requirements of data storage security and concurrent processing capabilities, the database system hardware infrastructure was designed as a 4-node high-performance server, including a login management node, two data storage nodes, and a data processing node. Among them, the number of CPU cores for data processing nodes is >40 cores, and the total number of four-node nodes is >80 cores. The hardware system can guarantee the long-term security of data storage and meet the concurrent processing capability of simultaneous access by multiple threads. Purchasing implements the form of centralized government procurement. A photo of the database server is shown in Fig.2.

Fig.2 The materials database server

TMSR-SEED materials database

TMSR-SEED material database consists of two parts, i.e. basic database and specialdatabase (Fig.3). The basic database includes the experimental database and the engineering standard database. Special database includes molten salt database, irradiation database, processing database and welding database. Each database contains alloys, nuclear graphite and composite materials, and their various properties and performance data. The experimental database is designed to collect all the material test data of TMSR, while the engineering standard database only contains data related to engineering design for TMSR, which are authoritative.

The table of TMSR-SEED V1.0 database contains standard parameters of alloys, nuclear graphite and molten salt, which are the key materials for TMSR project. It also includes tables for the corrosion data of alloys, chemistry of molten salt and irradiation data of alloy. In addition, support information such as parameter definition and test reports are also listed in the database.

The table of TMSR- SEED V1.0 database contains standard parameters of alloys, nuclear graphite and molten salt, which are the key materials for TMSR project. It also includes tables for the corrosion data of alloys, chemistry of molten salt and irradiation data of alloy. In addition, support information such as parameter definition and test reports are also listed in the database.

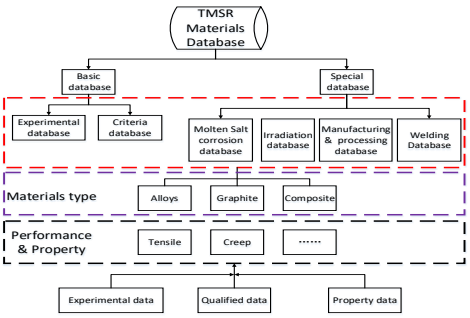

Fig.3 Schematic of TMSR-SEED materials database

Fig.4 UI of TMSR-SEED V1.0

The UI of TMSR-SEED is shown in Fig. 4. TMSR-SEED can concurrently hold 180 threadsat the same time, and storage capacity is more than 10 TB. The connectionbetween the sub databaseshas been realized, which make it easy to query data cross different database. The details of test data is traceable and the analysis results can be shown in chart form.

TMSR-SEED V1.0 database contains 110 classes of properties of one type of alloy (UNS N10003), four types of nuclear graphite and 65 batches of FLiNaK salts, including mechanical properites, neutron irradiation data and molten salts corrosion data. The total amount of data is more than 8200.

Radiation monitoring and safety interlocking system

Fig.5 Gamma detector of the radiation monitoring system

Radiation safety interlock system of 4MV accelerator laboratory

Because the 4MV accelerator was modified, the highest voltage was increased from 3MV to 4.3MV, and the beam intensity was increased. The special ion radiation device was built. These will change of the radiation level in the 4 MV accelerator laboratory. The original radiation dose safety interlock system of the 4MV accelerator laboratory has been damaged. In order to ensure the safety of the accelerator laboratory, new radiation safety interlock system was established according to “the radiation protection work regulations of the Shanghai Institute of Applied Physics”.

The system and the sketch map are shown in Fig.6, and the layout of radiation dose is shown in Fig.7.

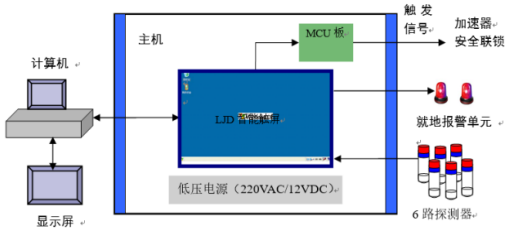

Fig.6 The sketch map of radiation monitoring system

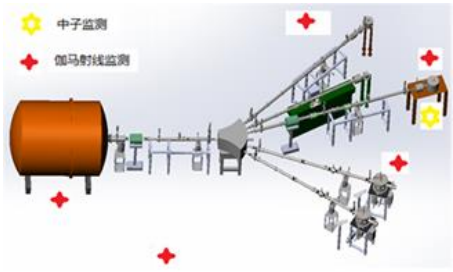

Fig.7 The layout of radiation dose

Development of positron Doppler broadening system

In the study of radiation damage defects in reactor materials, positron annihilation photons have high energy and can penetrate the thicker body materials. The information of the distribution of electron momentum density within the material can be obtained by the linear parameters of Doppler broadening (Fig.8(a)) of annihilation energy spectrum, and the types of defects produced by radiation damage can be found. It is a very effective method to study the formation mechanism of a large number of microstructural defects after irradiation. Therefore, according to the laboratory's existing set of high-purity germanium detectors, a set of positron Doppler broadening systems (shown in Fig.8 (b)) can be constructed by purchasing additional electronics plug-ins 659 5-KV Detector Bias Supply, 928 Multichannel Buffer, 672 Spectroscopy, 4001C/4002D NIM Bin and various cable sizes.

Fig.8 Positron Doppler broadening system

In-situ testing machine

High temperature beryllium dome hotstage for nickel-base alloys research

The high temperature beryllium dome hotstage for nickel-base alloys research is shown in Fig.9. The beryllium windows and coatings were re-processed, and the problems of overshoot and instability of the device were solved in 2015. From the reported report and video, the maximum controllable temperature of the device reached 1 400^{o}C, the temperature stability in the range of 700-1 200 ^{o}C was within ±2 ^{o}C, and the vacuum pressure reached 3×10^{-6} mbar.

Fig.9 High temperature beryllium dome hotstage

Molten salt in-situ creep tester

The original design of molten salt in-situ creep tester was modified based on the previous operation experiences. In the original design, the molten salt was transferred from the storage tank to the test autoclave by argon gas pressure before experiment. While a bellow type autoclave as is shown in Fig.10(a) is used in the new design, which allows a more convenience installation of the salts. As it is shown in Fig.10(b), the bellow is in the elongated state during setup of the device so that the solid salts can be placed at the bottom of the autoclave. After mounting the sample and salts, the autoclave is heated to melt the salts. Then the autoclave is lifted up to immerse the sample in the molten salts, and the bellow is in the compression state. Finally, after the experiment finishes, the autoclave is lowered, enabling the separation of the sample and salts, and the sample and salts are taken out for further examinations. This kind of design simplifies the gas path system, avoids the possible leakage of molten salt, and makes the whole experimental process less complicated. The installation and adjustment of the new tester was finished in March 2016.

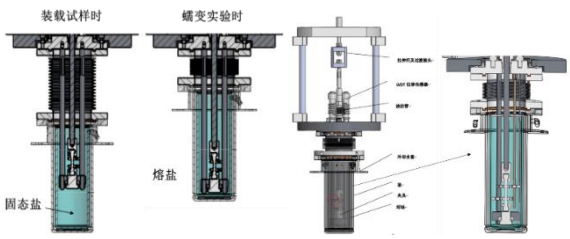

(a) Design drawing (b)Schematic of experimental procedure

Fig.10 The test section of molten salt creep tester with a bellow type autoclave design

High-temperature and vacuum universal experiment system

Complete the acceptance of vacuum high-temperature universal testing system. High-temperature vacuum universal testing machine consists of a high-temperature vacuum furnace and universal testing machine. In November 2015, complete the acceptance of universal testing machine, the main technical

indicators: Force Value Range:100 kN, Accuracy class0.5, meet the target requirements. June 2016, complete equipment acceptance of high-temperature vacuum universal testing machine, as shown in Fig.11. The main technical indicators: vacuum≤ 10^{-3} Pa; Temperature range: 25~1 600 ℃, meet the target requirements. After high-temperature vacuum universal testing machine can be used in mechanics performance evaluation of the molten salt impregnated graphite at high temperature.

Fig.11 High-temperature and vacuum universal experiment system

Creep testing mahchine

The 50KN creep machinesare used to test the high temperature creep performance of alloy. According to the physical design requirements of the TMSR-SF1 molten salt reactor, the test period is up to 60 000 h. Although the existing 12 machines operate 24 h a day throughout the year, there is a large gap in the demand. There is no third-party testing in china to provide more than 10 000 h of testing services. Therefore, the12 creep machineswere purchased. Different parameters were tested simultaneously to obtain the basic mechanical parameters of the alloy materials required for the design of the molten salt reactor as soon as possible.

In the procurement process, the creep machines adopts the bidding method. The successful bidder is Changchun Machinery Science Research Institute Co., Ltd., which consists of 10 electronic and 2 mechanical machines (Fig.12). The bid amount is 1.9 million yuan. The equipment manufacturers completed the internal commissioning in September 2016. In October, Guangzhou Yuan went to the equipment manufacturer for per-acceptance and installed stainless steel samples of ASTM on site to carry out high-temperature creep performance tests.

Fig.12 Creep experiment

In situ Molecular Vibration Spectrum and Synchronous Radiation combined device

The procurement, modification, installation, commissioning and acceptance of the combined device were completed from 2015 to 2016, and the acceptance performance reached the predetermined target. The equipment generally worked well, and improved the application of in situ characterization technique. Fig. 13 shows the in situ molecular vibration spectrum and synchronous radiation combined device, procured in 2014, delivered and installed in November 2014, reconstructed from March 2015, commissioned from August 2015, and officially started to work in May 2016. After the modification of in situ cell, diffuse reflection system and external sample warehouse, and the debugging of gas control device, temperature control device, and off-line and on-line circulating water system, the combined device has been in a stable operating state. The combined device is designed for XAFS transmission mode and equipped with 6-way gas inlet system and fast switching valve. Under in situ test condition, the maximum temperature at ambient pressure reached 350 ℃ with regulable heating rate. It has been successfully applied to CuO/CeO_2 catalyst system, and will be further explored for the application and research of bulk-surface in situ characterization of catalyst.

Fig.13 In situ Molecular Vibration Spectrum and Synchronous Radiation combined device

Conclusions

The material assessment and test platform was gradually improved, and the installation, commissioning and acceptance of newly purchased equipment were completed. Each equipment was routinely used and maintained by a fixed staff and regularly checked every year or every two years. It can accurately measure the material data required for stack design and safety assessment, realize material batch evaluation and screening, and has the ability to develop a new generation of high-temperature alloys and highly dense nuclear graphite. At the same time, on the basis of ensuring the normal operation of materials assessment and test platform equipment, some new test methods for molten salt stack materials were actively developed. Three ASTM test standards, a GB national test standard were drafted, and laboratory CNAS accreditation was completed. On-site assessment of qualifications, and built the first shared database of molten salt reactor-specific material databases.

钍基熔盐干法在线处理

放射化学与工程技术部

钍基熔盐堆核能系统(TMSR)的首要科学目标是“钍基核能”，即实现钍基核燃料的循环利用。TMSR 实现钍基核燃料循环利用的技术路线是液态燃料钍基熔盐堆加燃料干法处理。“钍基熔盐干法在线处理”以建立适用于钍基熔盐核能系统的燃料盐干法处理流程为目标，开展氟化挥发、减压蒸馏、熔盐电化学等干法技术的工艺可行性研究，进行干法设备放大和工艺集成，并开展关键支持技术研发，重点解决氟化挥发和减压蒸馏技术从实验室走向工程应用的关键技术问题。并形成燃料盐干法处理流程设计能力，干法工艺设备设计、研发、调试和运行能力。2015−2016 年取得的进展如下：

1　干法关键技术

1.1　氟化挥发技术

在氟盐体系铀氟化挥发研究中，考察了温度、自由 F^-浓度对氟化反应过程的影响规律，实现了氟化反应、产物纯化、冷凝收集的全流程工艺贯通，确定了氟化挥发全流程的工艺条件，氟化产物 UF_6 的冷凝回收率达 95%以上，产物中 Sr、Nd、Ce、Sm 元素的去污系数达 10^5，Nb 的去污系数达 10^2，Ru、Zr 的去污系数为 10^3。重点在 FLiBe 熔盐体系中，开展了从小到大（从十克级至公斤级），逐级放大的铀氟化挥发工艺研究，在公斤级 FLiBe 铀氟化挥发分离实验中实现 UF_6 总回收率达 95%以上（图 1），裂变产物 Nb 去污系数大于 10^3，Cs 去污系数达 10^4，Sr、Ce、Nd、Sm 去污系数大于 10^7。建立了 MgF_2 吸附剂颗粒的合成制备工艺，确定其对 MoF_6 的最佳吸附温度为 125°C，最大吸附容量为 60 mg/g。在 U/Mo 吸附分离工艺研究中，确立了吸附温度、载气与 UF_6 吸附、脱附行为间的依赖关系，为实现氟化产物 UF_6 的吸附纯化提供重要依据。

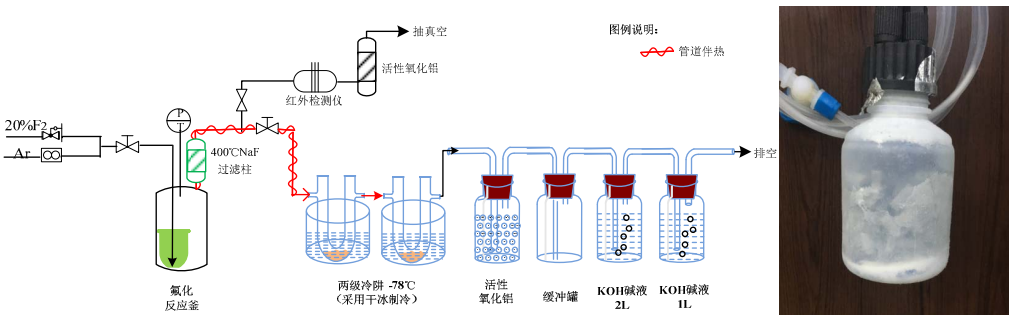

图 1　公斤级 FLiBe 熔盐体系氟化挥发工艺流程图（左）和冷凝产物（右）

1.2　冷冻壁技术

为降低干法工艺对设备材质的腐蚀，发展了熔盐冷冻壁技术用于干法处理工艺，在初步完成硝酸盐冷冻壁形成及维持工艺研究基础上，顺利实现了熔盐冷冻壁实验装置的升级改造，开展了空气冷却工况下的氟盐冷冻壁技术研究，掌握了氟盐冷冻壁形成、维持的关键工艺和传热规律，并利用温度梯度、热量衡算、实时摄像等多种手段实现氟盐冷冻壁厚度在线监测，为冷冻壁技术在干法后处理工艺中的成功应用奠定了良好基础。重点考察了氟气环境下氟盐冷冻壁对 304 不锈钢、Inconel600 合金等材质的防护效果，在冷冻壁防护下材料的腐蚀速率可降低一个数量级。后续将进一步优化冷冻壁工艺，增强其防护性能，并开展耦合冷冻壁技术氟的化挥发反应装置概念设计工作。

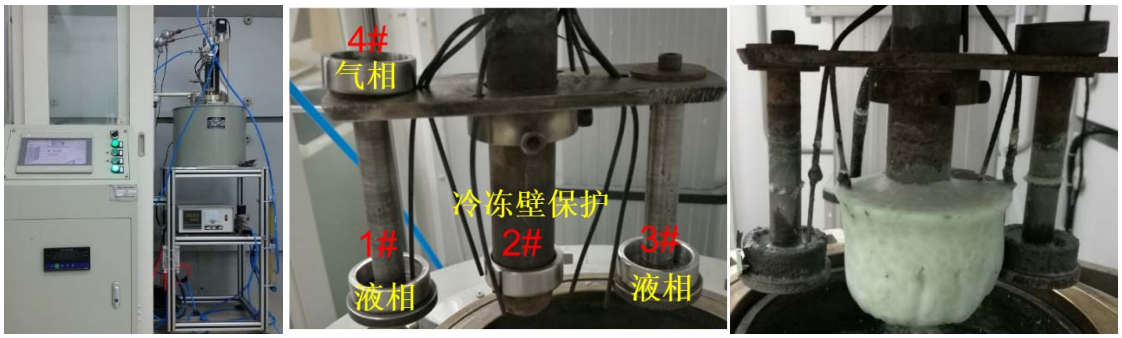

图 2 （左）中心冷却式冷冻壁实验装置实物图；（中）装置内金属试样的排布位置；（右）氟盐冷冻壁形成后的试样状态

1.3 熔盐减压蒸馏技术

减压蒸馏技术的开发在完成了氟盐蒸馏工艺的初步获取和挥发性数据的测量后，继续开展载体盐减压蒸馏行为研究，确定了蒸馏温度、裂变产物价态、钍元素浓度对载体盐蒸发行为的影响规律。为进一步开展涉铍熔盐的蒸馏工艺研究，自行研制了手套箱相连的密闭式蒸馏装置（如图 3），并开展百克级氟盐蒸馏实验，1 000 ℃时蒸馏速率为 1.2 g/cm^2·h，具备开展 FLiBe 熔盐蒸馏实验的研究能力。基于该装置开展的 FLiBe 熔盐减压蒸馏分离研究中，实现了 FLiBe 熔盐蒸馏收集率达 99%，收集盐中稀土、钍元素的去污系数大于 10^3。在采用卧式减压蒸馏装置开展的公斤级氟盐蒸馏研究中，建立了高温熔盐定量、匀速输运技术，输运量精度达 0.1 kg，利用熔盐质量、温度、气压等多种手段实现熔盐蒸馏进程的在线监测，熔盐收集率进一步提升至 98%以上，蒸馏速率超过 6 g/cm^2·h.，收集盐中稀土裂变产物的去污系数达 10^2 以上。后续将开展冷态条件下干法处理流程贯通实验研究。

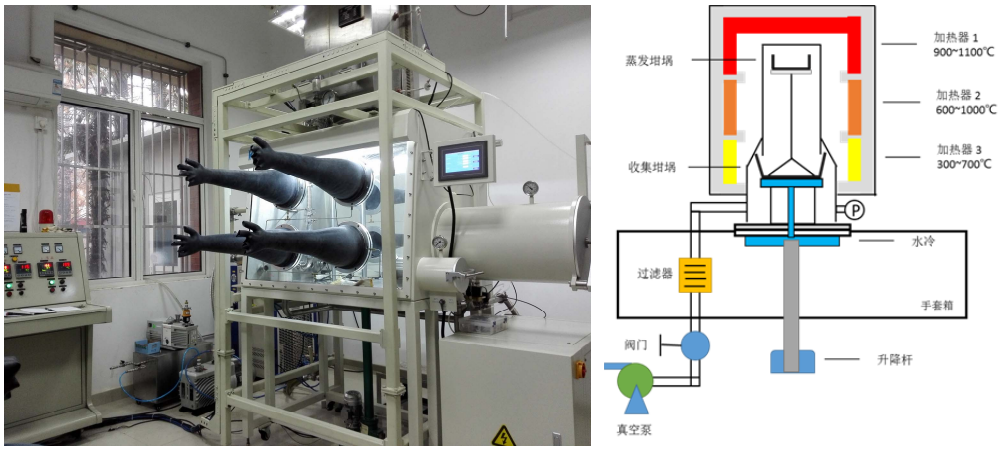

图 3 手套箱相连的密闭式蒸馏装置（左：实物照片；右：结构示意图）

1.4 氟盐体系电化学技术

铀的分离是熔盐堆燃料盐干法处理的关键步骤和目标，课题组主要致力于采用电化学方法分离熔盐堆载体盐 FLiBe 中的 UF_4。在 FLiBe 熔盐中，U^{4+}经两步电化学还原为金属 U，我们针对 U^{4+}离子直接电解还原困难的问题，开发了一种预还原+电解的分离方法。通过向 FLiBe-UF_4 熔盐中加入还原性金属（Li 或者 Be 单质等），化学反应使 U^{4+}首先还原成 U^{3+}，再进行电解取得了良好的效果。FLiBe-UF_4 熔盐在电解过程中的不同阶段分别获得了 UF_3、U 金属和 UBe_{13} 三种电解产物。在 FLiBe-UF_3 熔盐中通过改进电解方法和设计新的收集坩埚，U 的回收率可达到 96%。这些结果为在熔盐堆燃料盐 FLiBe-UF_4 中通过电解方法来分离铀奠定了良好的技术基础。

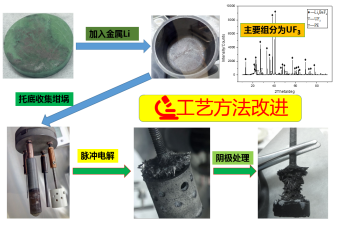

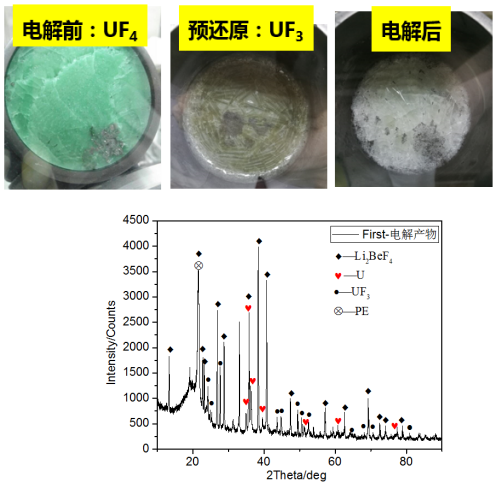

图 4　电解工艺、电解前后熔盐和电解产物图

2　展望

针对 TMSR 燃料循环的需求，对可能适用于氟盐处理的技术或工艺进行了原理验证和筛选，确定了以氟化挥发分离铀和减压蒸馏纯化载体盐为优先发展技术、熔盐电化学技术作为备用技术的发展思路。就目前来说，所有的研究装置和研究主要是面向实验室级水平（百克级至公斤级），离真正的实用化还有一段距离。除了实验量的差异，在可供热室内使用方面还有不少的功能未被实现，热室内实验装置的远程操控和过程监测一直是干法设备使用过程中的主要难点之一。

后续的工作重点用模拟燃料或真实燃料进行基本工艺单元的验证和优化，包括氟化挥发、减压蒸馏和熔盐电化学工艺单元。研发从冷态实验到示范实验的关键技术，重点研发可远程操控的干法分离设备。掌握不同输入条件下盐、An 和 FP 在各工艺单元中的轨迹或走向，废物类型与产生量，在此基础上进行干法分离全流程物质平衡动态模似，评估和优化 TMSR 燃料处理流程。

Pyroprocessing Technologies for on-Line Treatment of TMSR Fuel

Department of Radiochemistry Engineering and Technology

The primary scientific goal of the Thorium-based Molten-Salt Reactor system (TMSR) is “thorium-based nuclear energy”, that is, the thorium-based fuel cycle. The technical route to realize the thorium-based fuel cycle in TMSR is liquid fueled TMSR coupled with pyroprocessing facility. This study has been devoted to establishing a fuel processing flowsheet suitable for TMSR system and to achieving the following purposes: i) demonstration of process feasibility of pyroprocessing technologies, such as fluoride volatility, low pressure distillation, molten salt electrochemistry, etc; ii) the enlargement of process equipments and the integration of pyroprocessing technologies; iii) solution of the key technical problems in the industrialization of fluoride volatility and low pressure distillation; iv) qualification of the ability of designing TMSR process flowsheet and the R&D, commissioning and operation of pyroprocessing equipments.

The main progresses obtained in recent two years are listed as follows:

1 Key pyroprocessing technologies

1.1 The fluoride volatility technology

In the study of the fluoride volatility process for recovering uranium from molten fluoride salt, the effects of temperature and free fluorine anions on the fluorination were investigated. The complete process contained the fluorination reaction, product purification and condensation recovery were established, and the process conditions was determined. The results shown the recovery rate of UF_6 was more than 95%, decontamination factors (DF) for Sr, Nd, Ce, and Sm in the product were 10^5, DF for Nb was 10^2, and DFs for Ru and Zr were 10^3. In the FLiBe molten salt system, the study scale of the fluorination process was amplified step-by-step and was from small to large (from 10 g to kilograms). The UF_6 total recovery was above 95% (Fig. 1) in the Kg-scale fluoride volatility process. The DF for fission product Nb was more than 10^3, the DF for Cs was 10^4, and the DFs for Sr, Ce, Nd, and Sm were more than 10^7. The preparation process of MgF_2 adsorbent was determined. The optimum adsorption temperature was 125°C and the maximum adsorption capacity was 60 mg/g. In the study of U/Mo adsorption separation technology, the dependences of adsorption temperature, carrier gas and UF_6 adsorption and desorption behavior were established, which supported for the developing of the product purification technology by adsorption.

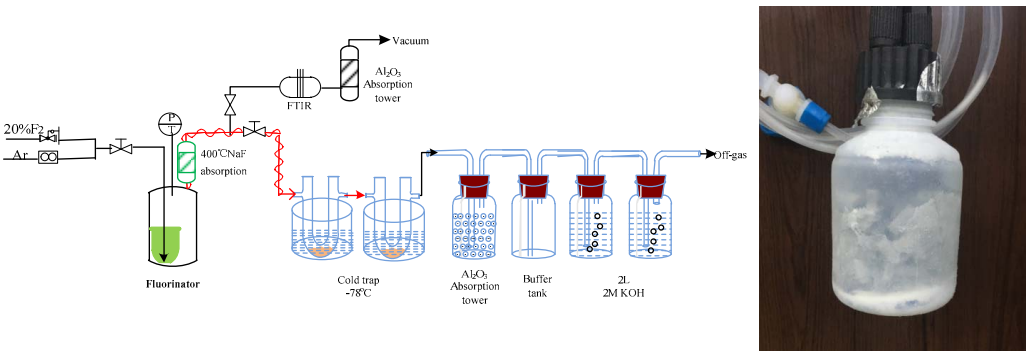

Fig.1 The flowsheet of fluoride volatility process in the Kg-scale FLiBe molten salt system (left) and the condensation product (right)

1.2 Frozen-wall technology

The molten salt frozen-wall technology was developed for protecting the metallic walls from corrosion by a layer of frozen salt during the pyroprocessing of spent fuel. Based on the preliminary research on frozen wall forming and maintaining process with nitrate salt, the experiment device was upgraded smoothly, which could be used for fluoride molten salt. Then research of fluoride salt freozen-wall has been carried out by air cooling. The heat transfer law and key technique of formation and maintain was mastered. The thickness of frozen-wall can be measured by various on-line methods, such as temperature gradient, heat balance, and real-time video. This research results of fluoride molten salt frozen-wall tech

nology laid a good foundation for the successful application in pyroprocessing. In addition, the protection performance study of molten salt frozen-wall were conducted in molten FLiNaK, the 304 stainless steel and Inconel 600 alloy was test. The corrosion rate of the materials under the protection of frozen wall could be reduced by an order of magnitude. In future, protective performance could be improved by optimizing frozen-wall controlling process. Furthermore, the concept design of fluorinated reaction device coupled with frozen-wall technology will be carried out.

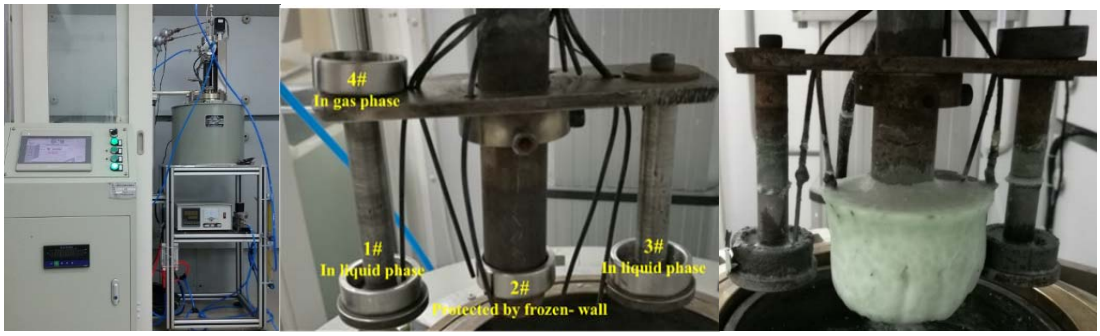

(a) (b) (c)

Fig.2 (a) Molten salt frozen wall device with central cooling rod; (b) Placement of test samples and thermal couples on central cooling rod; (c) The protection state of frozen-wall

1.3 Low pressure distillation technology

The vaporization behavior of carrier fluoride salt was further investigated after the distillation condition of fluoride salts was determined, and the volatility data were achieved. Up to now, the valence of some rare earth fission products was confirmed and the effect of thorium content on the vaporization of carrier salt was illustrated. To observe the distillation behavior of FLiBe melts, we setup a closed–chamber distillation system combined with a glove box as Fig.3, which can carry out a hundred-gram scale distillation experiment. Based on this system, the distillation rate at 1000°C was measured to 1.2 g/cm^2·h, the recovery ratio of collection was up to 99% and the decontamination factor of both rare earth and thorium was more than 10^3. The kilo-gram scale distillation experiment was carried out using the horizontal distillation system. The transport technology of high temperature molten salt was established. The accuracy was 0.1kg. Moreover, the online detection method was developed using the one or several parameters, such as mass, temperature and pressure. The results showed that the recovery can up to more than 98% and the distillation rate at 1000°C was over 6 g/cm^2·h. The pyroprocess methods such as fluorination and distillation technology will be integrated to further explore the experiment condition and to improve the separation efficiency.

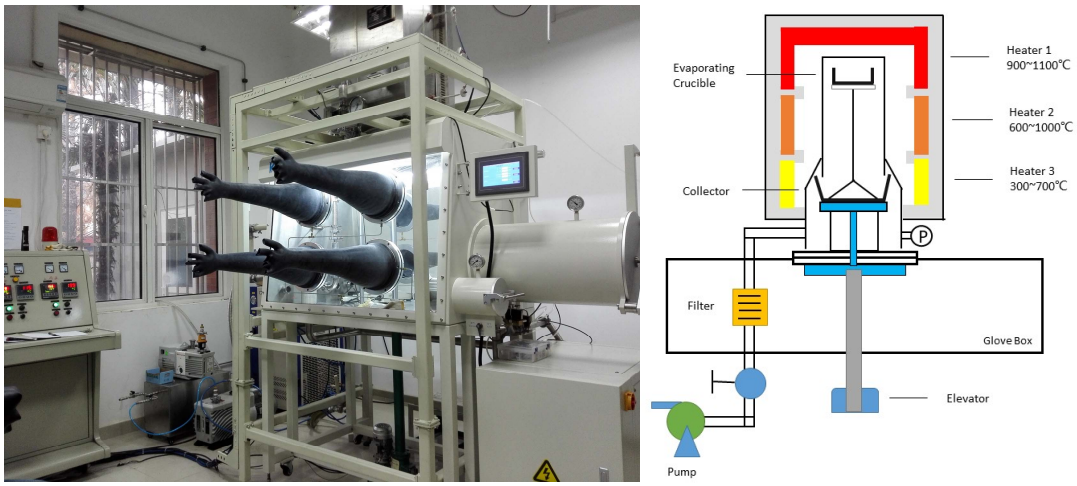

Fig.3 The closed chamber distillation equipment combined with a glove box (Left :equipment photo; Right: the schematic diagram)

1.4 Electrochemistry technology in fluoride salt system

The separation of uranium is the key step and prime target of the fuel salt pyroprocessing of the molten salt reactor, and our research is mainly devoted to the separation of UF_4 from the salt FLiBe of the molten salt reactor by electrochemical method. In FLiBe molten salt, U^{4+} can be reduced to U metal by two step electrochemical reaction, and we have developed a pre-reduction combined electrolysis separation method for solving the problem of U^{4+} direct electrolysis in the fluoride salt. By adding some reducing metal (Li or Be) to FLiBe-UF_4 molten salt, U^{4+} was first reduced to U^{3+} by chemical reaction, and then electrolyzed to U with good effectiveness. Three kinds of electrolysis products of UF_3, U metal and UBe_{13} alloy were obtained at different stages of the electrolytic process in FLiBe-UF_4 molten salt. In the pre-reduced FLiBe-UF_3 molten salt, the recovery rate of uranium can reach 96% by this improved electrolysis method and new designed collection crucible. These results provide a good technical basis for the separation of uranium by electrochemical method in the FLiBe-UF_4 fuel salt of the molten salt reactor.

2 Prospect

According to the demand of TMSR fuel cycle, the feasibility verification and screening of technologies and procedures that may be suitable for fluoride fuel salt treatment have been carried out. The fluoride volatility and low pressure distillation methods to separate uranium and carrier salt, respectively, have been determined as the priority technologies, while the electrochemical technology has beeb selected as alternative. Currently, all the researches and experiment devices are at laboratory scale (100 g to 1 kg), which is far away from the engineering application. In addition to the scale difference, many functions for the operation in hot cell still have not been realized, and the remote handling and process monitoring in hot cell are always the main challenges in the development of pyroprocessing equipments.

The later work will be focused on the verification and optimization of basic process units with simulated fuel or real fuel, including fluoride volatility, low pressure distillation and molten salt electrochemistry. The development of key technologies will be performed from cold experiment to demonstration experiment, focusing on developing remotely handling pyroprocessing equipments. A variety of parameters should be obtained in the process demonstration: the distribution and flow direction of salt, An and FPs in every process units under different conditions, and the waste type and amount. On this basis, the dynamic model of material balance in the pyroprocessing flowsheet will be established, and the TMSR fuel process flowsheet will also be evaluated and optimized.

钍基核燃料水法后处理方法研究

放射化学与工程技术部

钍基熔盐堆干法尾料的后处理中的核心问题是钍、铀的分离和回收。为了使水法技术能够应用于干法尾料的后处理，重点开展了少量辐照氧化钍中的 ^{233}U 分离提取、钍基氧化物乏燃料中 Th、U 回收，离子交换工艺、Thorex 流程台架、新萃取剂筛选、不同氟化物高温水解性质的研究等工作。同时，负责研发与钍基熔盐堆核热相匹配的铀-碳热化学循环制氢技术，拟利用熔盐堆产生的高温热制备 H_2。

^{233}U 是钍铀燃料循环中的关键裂变材料，为获得少量 ^{233}U 开展后续研究，制备了 10g 氧化钍辐照靶件进堆辐照，累积热中子注量率为 3.7×10^{19} n/cm^2，初步计算其中含 ^{233}U 约 2.5 mg。通过冷实验对辐照氧化钍的后续溶解及 ^{233}U 离子交换分离工艺进行了优化、验证。结果表明，利用浓盐酸作为溶解试剂，在其中加入适量 NaF，110 ℃下冷凝回流，氧化钍的溶解率可达到 98%；利用 Dowex1 阴离子交换+Dowex50 阳离子交换工艺，可以从辐照氧化钍溶解液中进行微量 ^{233}U 的分离提取，铀收率大于 99%，钍铀分离系数大于 1.0×10^6，稀土裂变产物去污系数大于 1.0×10^3，具体流程如下图 1 所示。实际辐照氧化钍中的 ^{233}U 分离热实验待实验条件成熟后进行。

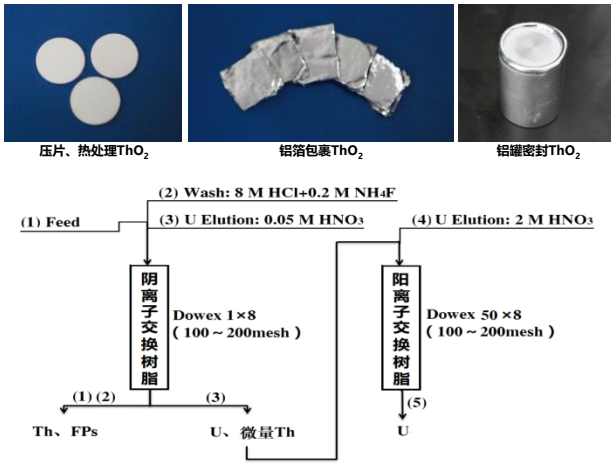

图 1 辐照 ThO_2 靶件制备过程（上）及辐照氧化钍中 ^{233}U 离子交换分离工艺流程（下）

Thorex 流程是钍基燃料水法后处理工艺中最重要的流程，可以同时回收钍基乏燃料中的 Th、U。在前期单级及串级萃取实验研究的基础上，采用离心萃取器完成了酸式进料单循环 Thorex 流程的台架实验验证。实验结果表明（如图 2 所示）：钍回收率为 99.99%，铀回收率为 99.30%，钍中去铀分离系数 $SF_{U/Th}$ 为 1.5×10^2，铀中去钍分离系数 $SF_{Th/U}$ 为 2.2×10^4，钍、铀和裂片走向正常，各级样分布合理，说明离心萃取器的使用能够保证 Thorex 流程高流比工艺参数下的流程稳定运行。

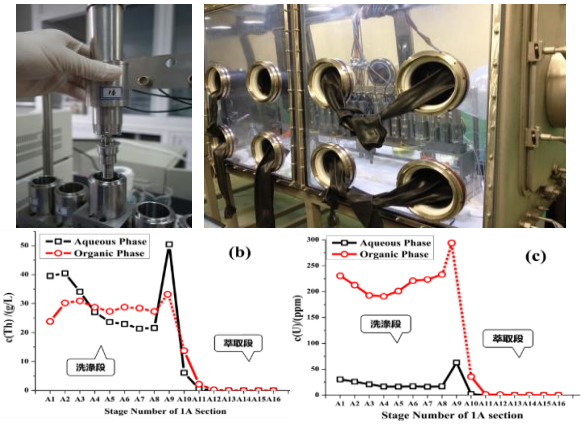

图 2 Thorex 流程离心萃取器台架（上）及 Thorex 流程 1A 段 Th、U 级分布（下）

TBP 在 Purex 流程中已经得到了商业化应用，但其用于钍基燃料处理时存在着钍的分配比及萃取容量低，钍铀分离系数不高，容易出现“第三相”，萃取流程设计较为复杂，产生有机废液较多等缺点。因此，有必要筛选和发展适用于钍基燃料处理的萃取剂及萃取流程。在前期研究中发现，P350 具有较好的综合物理性质、辐照稳定性和钍铀分离性能，且不形成“第三相”。在 P350 串级萃取实验基础上，建立了具有自主知识产权的 P350 钍基乏燃料后处理流程，经台架实验验证，该流程主要技术指标与 Thorex 流程相当，但其具有不使用盐析剂，流程简单，萃取剂用量较低、流程运行酸度低等优点，在钍基乏燃料处理中有较大应用前景。

表 1. 基于 P350 及 TBP(Thorex)的钍基燃料处理流程主要工艺参数对比

1A（钍铀共萃取去污）段主要工艺参数						
	萃取剂浓度 (mol/L)	料液酸度 (mol/L)	洗涤液酸度 (mol/L)	盐析酸 (HNO_3)	流比（料液:萃取剂:洗涤液）	体系酸度 (mol/L)
P350 流程	0.73	0.4	0.2	无	1:7:0.8	0.2~0.4
TBP 流程	1.1	1.0	0.1	13 mol/L	1:9:1	1.0~4.0
1B（钍铀分离）段主要工艺参数						
	钍反萃液酸度 (mol/L)	补萃液浓度 (mol/L)	流比（钍铀有机相产品:钍反萃液:补萃液）			
P350 流程	0.08	0.73	1:2:0.25			
TBP 流程	0.4	1.1	1:0.83:0.17			
1C（铀反萃）段主要工艺参数						
	铀反萃液酸度(M)	流比 （铀有机相产品：反萃液）				
P350 流程	0.001	1:1				
TBP 流程	0.01	1:0.7				

表 2　基于 P350 及 TBP 的钍铀回收流程主要技术指标对比

	Th 收率 (%)	U 收率 (%)	Th 中去 U 分离系数	U 中去 Th 分离系数
P350 流程	99.70%	99.98%	7.1×103	5.9×10^{2}
TBP 流程	99.99%	99.30%	1.5×102	2.2×10^{4}

利用高温水解技术可将氟化物转化为氧化物，前期在小型实验装置上开展的研究结果表明，高温水解技术在干法尾料处理中具有较好的应用前景，能够将目标氟化物转化为氧化物并为后续流程所利用，因此该技术也被列为 TMSR 液态燃料后处理流程中。为了继续开展氟化物燃料高温水解工艺放大的实验研究，在研制的公斤级高温水解实验装置上开展了小批量氟化物高温水解性质的研究（结果如下图 3 所示），通过一系列的实验研究确定了最优的反应参数，并最终实现四氟化钍和四氟化铀的高温水解反应，且转化率大于 90%。

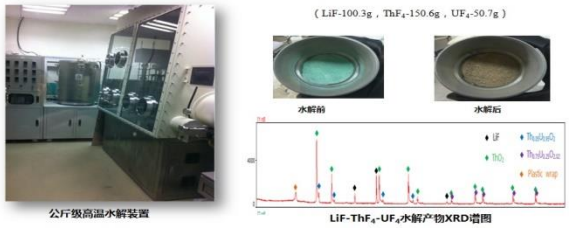

图 3　公斤级高温水解实验装置及水解产物的结果

为制备清结能源 H_2，针对能与熔盐堆产生的高温热相匹配的铀－碳热化学循环制氢流程进行了系统的研究。首先在实验室内完成了铀－碳热化学循环制氢的原理性验证，在其基础上完成了三套原理样机的研制、调试和试运行，并在原理样机上完成了该流程的工艺可行性研究（如图 4 所示），确定了各关键反应的工艺参数。提出的沉淀－析出方法，优于原流程中的离子交换分离法，大大提高了铀－钠分离中铀的收率，减少了液体操作体积及固体废物量，可简化工艺并降低能耗。

图 4　铀－碳制氢百克级工艺验证

发展合适的钍铀分离技术对于钍铀燃料循环的最终实现具有重要意义。离子交换分离、新萃取剂筛选、基于离心萃取器的萃取流程研究以及高温水解实验的结果表明，我们已经基本掌握了钍基燃料水法处理的关键技术。与此同时，铀－碳热化学循环制氢流程中一系列的研究成果可为后续该流程的放大提供理论指导和参考依据。

Aqueous Reprocessing for Thorium Based Nuclear Fuel

Department of Radiochemistry and Engineering

The aqueous separation technique is a reliable method to process the tailing after the TMSR fuel pyroprocessing. The core issues in aqueous reprocessing for Th-based fuel is the separation and recovery of Th and U. In order to achieve the application of aqueous separation techniques in the reprocessing of tailing after the TMSR fuel pyroprocessing, the separation of ^{233}U from a small amount of irradiated ThO_2 and the recovery of Th/U from Th-based oxide spent fuel were studied, mainly including ion exchange process, Thorex process, extractant screening, pyrohydrolysis of fluoride, and so on. Meanwhile, We have also conducted the research of uranium-carbon thermochemical cycles for hydrogen production that match the high temperature generated by the thorium molten salt reactor (TMSR).

^{233}U is a key fissile material in Th/U fuel cycle. In order to obtain a small amount of ^{233}U for the further study, 10 g of ThO_2 was irradiated, and the cumulative thermal neutron flux was $3.7\times10^{19}n/cm^2$. The amount of ^{233}U is about 2.5mg according to the preliminary calculation. The process for the dissolution of irradiated ThO_2 and ion exchange separation of ^{233}U were optimized and verified by using cold simulated experiments. It is found that the dissolution rate of ThO_2 could reach 98% by using concentrated hydrochloric acid as dissolution reagent, adding appropriate amount of NaF and refluxing at 110 ℃. Trace uranium could be separated and extracted from dissolved solution of simulated irradiated ThO_2 by using Dowex1 anion exchange and Dowex50 cationic exchange process(As shown in Fig.1). The recovery of uranium is greater than 99%, the separation factor of thorium and uranium is greater than 1.0×10^6, and the decontamination factor of rare earth fission products is greater than 1.0×10^3. The "hot" separation of ^{233}U from irradiated ThO_2 will be carried out when the experimental conditions are available.

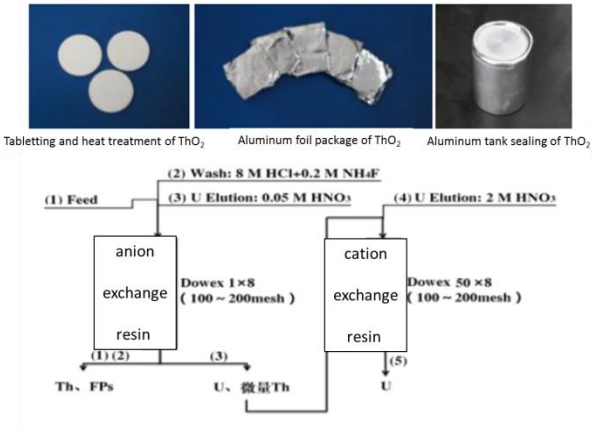

Fig.1 Preparation process of irradiated ThO_2 target (up) and ion exchange separation of ^{233}U from irradiated ThO_2 (down)

Thorex process is the most important process in the aqueous reprocessing of Th-based fuel, and it can be used to recover both Th and U. On the basis of previous single and batch multistage countercurrent extraction experiments, the bench test of single cycle acid Thorex process was completed by using centrifugal extractors. The results(as shown in Fig.2) show that the recovery of Th and U is 99.99% and 99.30%, respectively. The separation factor of U from Th and Th from U is 1.5×10^2 and 2.2×10^4, respectively. The flow of Th, U and fission products is normal, and the stage profiles are reasonable. It is indicated that the use of centrifugal extractor can ensure the stable operation of Thorex process with high flow ratio.

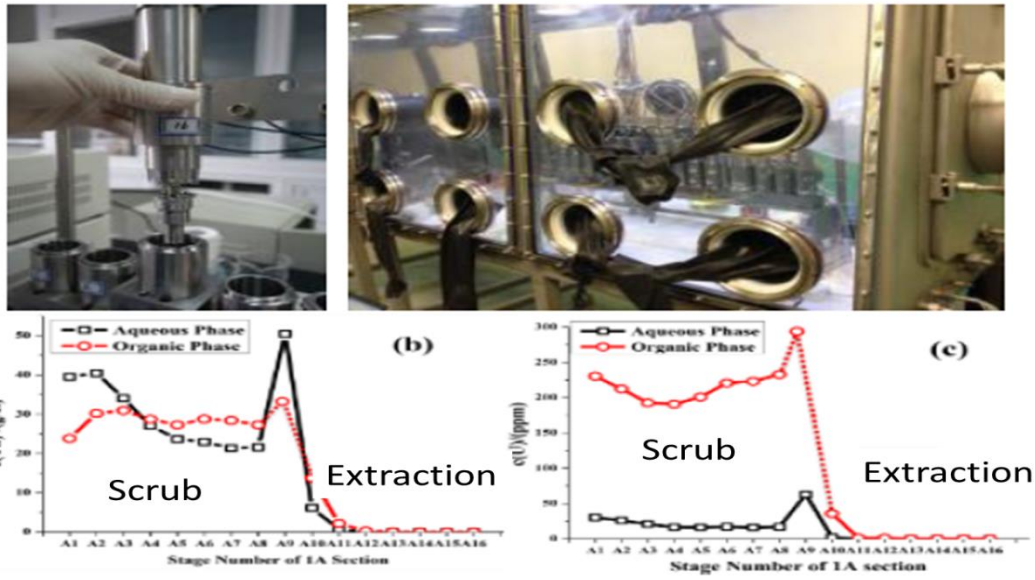

Fig.2 The bench of centrifugal extractors for Thorex process(up)and the stage profiles of Th, U in 1A cycle (down)

TBP has been commercialized in the purex process. However, there are some defects when it is used for Th-based spent fuel reprocessing, such as low distribution ratio and extraction capacity for Th, low separation factor of Th and U, “third phase” information, complex process design, and large amount of organic waste liquid. Thus, it is necessary to screen and develop suitable extractant and extraction process for Th-based spent fuel reprocessing. In previous studies, it was found that P350 possesses good physical properties, radiation stability and separation performance of Th and U. Especially, the "third phase" would not be formed when P350 was used. On the basis of batch multistage countercurrent extraction experiments, the P350 Th-based spent fuel reprocessing process with independent intellectual property rights was established. By bench experiment test, it is found the main technical index of the process was equivalent to that of Thorex process. However, the process based P350 is more simple due to the absent of salting-out agents. Furthermore, the process also has the advantages of lower amount of used extractant and lower operation acidity. Thus, it has great application potential in Th-based spent fuel reprocessing.

Table 1 Comparison of main process parameters in Th-based spent fuel reprocessing process based P350 and TBP(Thorex)

The main process parameters in 1A（Co-extraction and decontamination of Th and U）cycle						
	Extractant concentration mol/L	1AF acidity (M)	1AS acidity (M)	salting-out agent (HNO_3)	Flow ratio (1AF：1AX：1AS)	Operation acidity (mol/L)
P350 process	0.73	0.4	0.2	non-use	1:7:0.8	0.2~0.4
TBP process	1.1	1.0	0.1	13mol/L	1:9:1	1.0~4.0
The main process parameters in 1B (Separation of Th and U) cycle						
	1BX acidity (M)	1BS concentration (M)	Flow ration (1AP:1BX:1BS)			
P350 process	0.08	0.73	1:2:0.25			
TBP process	0.4	1.1	1:0.83:0.17			
The main process parameters in 1C (Stripping of U)cycle						
	1CX acidity (M)	Flow ration (1BU:1CX)				
P350 process	0.001	1:1				
TBP process	0.01	1:0.7				

Table 2 Comparison of main technical indexes in Th-based spent fuel reprocessing process based P350 and TBP (Thorex)

	Recovery of Th (%)	Recovery of U (%)	The separation factor of Th from U	The separation factor of U from Th
P350 process	99.70%	99.98%	7.1×10^3	5.9×10^2
TBP process	99.99%	99.30%	1.5×10^2	2.2×10^4

Using pyrohydrolysis, fluorides can be converted to therir corresponding oxides. According to the results of preliminary small-scale tests, pyrohydrolysis holds promise for possible applications in the recycle of usful materials from TMSR fuel after pyroprocessing. Therefore, this technique is included in the post-processing procedures of TMSR fuel. For continuing the research on scale-up pyrohydrolysis on fluorides, a series of experiements were performed on a small amount of fluorides through the kilogram-level pyrohydrolysis device. (The results are shown in Fig.3) According to the results, the best reaction parameters are confirmed, and pyrohydrolysis of ThF_4 as well as UF_4 are realized, with a conversion rate over 90%.

Apparatus for pyrohydrolysis experiments

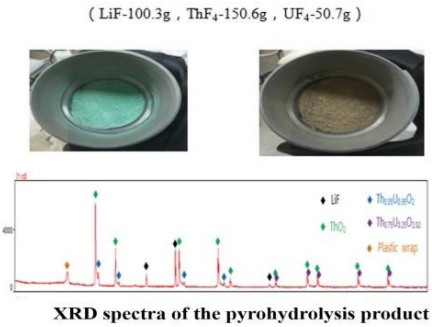

XRD spectra of the pyrohydrolysis product

Fig.3 Apparatus for pyrohydrolysis experments and XRD analysis of the pyrohydrolysis product

To make H_2, the clean energy, research on uranium-carbon thermochemical cycles for hydrogen production that match the high temperature generated by the thorium molten salt reactor (TMSR) was performed. Firstly, the principle of uranium-carbon thermochemical cycles for Hydrogen production was verified in our lab. Then three sets of prototypes were designed, debugged and operated. Based on the prototypes, the feasibility of thermochemical cycles for Hydrogen production was verified (shown in Fig.4), making sure processing parameters in every key reaction. The proposed precipitation method is better than the ion-exchange method in the original process because it significantly improves the yield coefficient of uranium in the separation of uranium and sodium and reduces the liquid volume for operation as well as solid pollutions, simplifying the process and reduce the energy consumption.

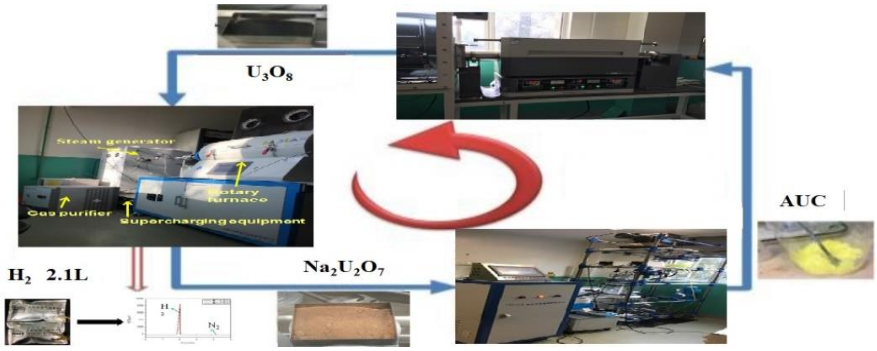

Fig.4 The uranium-carbon thermochemical cycle for production hydrogen

The development of suitable Th/U separation technology is of great significance for the ultimate realization of Th-U fuel cycle. The results of ion exchange separation, extractant screening, extraction process based on centrifugal extractor and pyrohydrolysis experiment show that we have basically mastered the key technology of aqueous reprocessing for Th-based spent fuel. At the same time, the results of uranium-carbon thermochemical cycles for hydrogen production can provide theoretical guidance and reference for subsequent scale-up tests.

钍铀燃料循环研究平台

放射化学与工程技术部

钍铀燃料循环研究平台是开展 TMSR 燃料研发、干法分离技术研发以及钍铀燃料循环相关核化学与放射化学研究的基础实验设施。总体目标是建设先进放射化学分析测试平台及核化学与放射化学综合研究设施，形成一个较为完善的钍基核能系统放射化学研究基地。主要任务包括放化分析测试平台建设与运行、103 放化实验室运行、TMSR-LF1 热室系统设计等。2015−2016 年的工作进展如下：

1 放射化学分析测试平台

放射化学分析测试平台是为钍铀燃料循环研究相关放射化学分析测试提供由多种仪器设备构成的较为完备的分析测试平台。放射化学分析测试平台主要包括以下仪器：电感耦合等离子体光谱(ICP-AES)、电感耦合等离子体质谱(ICP-MS)、X 射线衍射仪(XRD)、原子吸收光谱(AAS)、氧分析仪、离子色谱(IC)、高温拉曼光谱(Raman)、同步热分析质谱联用仪(TG-MS)、γ 谱仪、α 谱仪等。2015−2016 年放射化学分析测试平台总体运行良好，较好地完成了 TMSR 相关研究的分析测试任务，为 TMSR 相关科研任务的完成提供了很好的技术支持。

为提高放射化学分析测试平台的分析测试能力与水平，开展了实验室认可(CNAS)申报工作，放射化学分析测试平台申报的项目如表 1 所示。目前，目前 CNAS 实验室认可文审已通过，2016 年底完成了现场评审，即将获得证书。

表 1 CNAS 实验室认可项目汇总

序号	项目	限制范围
1	铀化合物中铀的测定（滴定法）	铀：20~200 mg
2	铀化合物中铀同位素组分分析（ICP-MS 法）	^{233}U、^{234}U、^{235}U、^{236}U、^{238}U
3	铀化合物中杂质元素的测定（ICP-MS 法）	67 种杂质（含硼）
4	铀化合物中 24 种杂质元素的测定（ICP-AES 法）	Ag/Al/Ba/Be/Bi/Ca/Cd/Cr/Cu/ Fe/Mg/Mn/Mo/Ni/Pb/Ru/Sb/Sn/Sr/Th/Ti/V/W/Zn,共 24 种
5	铀化合物中杂质元素的测定（AAS 法）	Al/Cd/Ca/Cr/ Co/ Cu/ Fe/ Pb/ Mg/ Mn/Ni/ K/Na/Zn,共 14 种
6	铀化合物中杂质元素的测定（ICP-AES 法）	Al/Ca/Cd/Co/Cr/Cu/ Fe/Mg/Mn/Mo/Ni/Pb/Sn/Ti/V/Zn, 共 16 种
7	铀化合物中钆、钐、镝、铕的测定（ICP-AES 法）	Sm, Eu, Gd, Dy
8	铀化合物中游离酸的测定（滴定法）	H+
9	铀化合物中硼的测定（ICP-AES 法）	0.05~33 μg B/g
10	钍化合物中钍的测定（滴定法）	Th
11	钍化合物中金属杂质的测定（ICP-MS 法)	稀土外金属杂质
12	钍化合物中杂质元素的测定（ICP-MS 法)	La/Ce/Pr/Nd/Sm/Eu/Gd/Tb/Dy/Ho/Er/Tm/Yb/Lu/U/Sc/Y, 共 17 种
13	钍化合物中硼的测定(ICP-AES)	B
14	放射性物质中总 α 活度的测定（α 谱仪法）	总 α 活度
15	放射性物质中放射性核纯度的测定（HPGe 法）	放射性核纯度
16	放射性核素标记化合物核纯度的测定（HPGe 法）	放射性核纯度
17	放射性核素标记化合物 γ 放化纯度的测定（TLC 法）	γ 放射化学纯度
18	放射性核素标记化合物 β 放化纯度的测定（HPGe 法）	β 放射化学纯度
19	放射性核素标记化合物 γ 活度的测定（活度计法）	γ 活度

2 103 放化实验室运行

2015−2016 年 103 放化实验室总体运行情况良好，基本满足了 TMSR 燃料处理工艺研究及其它放射性相关研究工作的需求。实验室主要系统及设备均未见异常，各项技术指标均达到设计要求。

个别设备出现故障后也能及时维修，未影响实验室的正常运行。103 放化实验室运行期间，对“103 放射化学实验室辐射安全管理规定”、“103 放射化学实验室放射性废物管理规定”、“103 放射化学实验室放射源使用管理规定”、“103 放射化学实验室放射事故应急预案”、“103 放射化学实验室实验与设备操作规程”等进行了修订，同时针对放射性废物管理方面的问题，制定了“103 放射化学实验室放射性废物管理规定实施细则”，进一步细化了放射性废液以及放射性固体废物的分类要求、收集与集中暂存流程。

3 TMSR-LF1 热室系统设计

由于 TMSR-LF1 总体方案的调整，干法处理实验设施的设计任务调整为 TMSR-LF1 热室系统的设计。在保留燃料盐干法处理热验证和 TMSR-LF1 燃料盐质量分析等功能的基础上，增加堆运行维护以及辐照材料分析测试等功能。热室系统中各主要热室的功能、数量、类型、气氛要求等如表 2 所示。

表 2 TMSR-LF1 热室系统

主要功能	热室名称	数量	类型	气氛
干法工艺	氩气热室	1	α-γ	氩气
热验证	放化辅助热室	1	α-γ	空气
燃料盐	分析热室 A	1	α-γ	氩气
质量分析	分析热室 B	3	α-γ	空气
TMSR-LF1	去污热室	1	α-γ	空气
运行维护	维修热室	1	α-γ	空气
	切割热室 A	1	α-γ	空气
材料	切割热室 B	1	α-γ	空气
分析测试	探伤检测热室	1	β-γ	空气
	力学性能测试热室 A	1	β-γ	空气
	力学性能测试热室 B	1	β-γ	空气

完成了干法热室关键技术验证装置的设计。该装置是干法热室关键技术研发中技术方案验证的实验平台，主要用于热室密封、气氛净化控制相关技术测试、方案验证、设计优化等方面的实验工作，为干法热室工程设计获取关键技术参数。同时预留充足的接口，便于后续开展物料转运、远程操作等的技术方案验证工作。干法热室关键技术验证装置主要由箱体和气氛净化控制系统两部分构成，箱体由不锈钢加工而成，包含窥视窗、检修门、机械手穿管、工艺/电气管线接口等主要贯穿件，气体净化控制系统由气体供应、气体循环净化、压力保护及排气等功能单元构成。系统构成如图 1 所示。

图 1 干法热室关键技术验证系统

完成了数字化仿真热室系统的研制。系统采用 Unity3D 引擎，可实现基于真实设计数据的虚拟环境快速搭建以及热室操作的准确模拟（图 2）。系统可实现热室及干法工艺设备设计数据的直接导入，并对设备数据模型进行仿真远程操作。仿真操作过程中可对热室内主动设备（机械手、吊车、工程机械手）的布局、选型以及工艺设备布局进行分析评估，为热室系统的设计和设备选型提供技术支持。仿真操作过程中还对热室内干法工艺设备的设计、操作空间、可视性、可达性等进行技术分析与评估，为干法工艺设备设计方案的确定以及工艺设备布局提供重要参考。

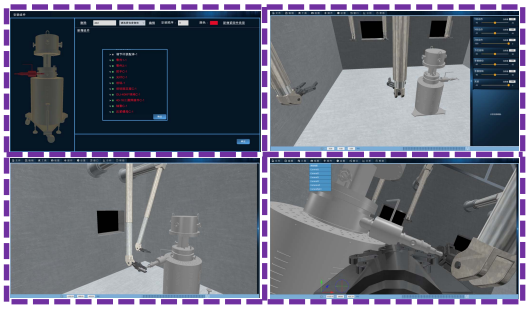

图 2 数字化仿真热室系统

4 小结与展望

放射化学分析测试平台运行良好，较好地完成了 TMSR 相关研究的分析测试任务。CNAS 实验室认可申请工作进展顺利，即将获得证书。103 放化实验室主要系统与设备运行良好，基本满足了 TMSR 燃料处理工艺研究及其它放射性相关研究工作的需求。确定 TMSR-LF1 热室系统方案，开展氩气热室关键技术的研发，完成干法热室关键技术验证装置的设计和数字化仿真热室系统的研制。下一阶段将围绕 TMSR-LF1 热室系统的工程设计，重点开展干法热室密封方案及气氛控制方案的技术验证工作。

Research Platform of Thorium-Uranium Fuel Cycle

Department of Radiochemical Engineering and Technology

The Research Platform of Thorium-Uranium Fuel Cycle is a basic experimental facility for research and development of TMSR fuel, pyroprocessing technology of depleted fuel, and other nuclear chemistry and radiochemistry for thorium-uranium fuel cycle. The main objective is to establish an advanced radiochemical analysis platform and thorium-uranium fuel cycle experiment facility, thus to build a complete research base for TMSR radiochemical research. The main tasks include construction and operation of the radiochemical analysis platform, reconstruction of radiochemical laboratory in building 103 and design of pyroprocessing experimental facilities. The progress of the work during 2015and 2016 are as follows:

1 Radiochemical analysis platform

The radiochemical analysis platform is a relatively complete analysis platform for thorium-uranium fuel cycle research, which contains a variety of relative instruments. The main instruments are: Inductively cupled plasma atomic emission spectrometry (ICP-AES), inductively coupled plasma mass spectrometry (ICP-MS), X-ray diffractometry (XRD), atomic absorption spectroscopy (AAS), oxygen analyzer, ion chromatography (IC), high temperature Raman spectroscopy (Raman), simultaneous thermal analysis mass spectrometry (TG-MS), gamma spectrometer, alpha spectrometer, etc.. During 2013−2014, the radiochemical analysis platform has worked well, completed all the analysis tasks for TMSR related research, and provided excellent technical support for the TMSR related research.

In order to improve the analysis and testing capability and level of the radiochemical analysis platform, the application for China National Accreditation Service for Conformity Assessment (CNAS) was conducted. The items declared by the radiochemical analysis platform are shown in Table 1. At present, the CNAS has approved the file review and the on-site review has been completed at the end of 2016. The certificate will soon be obtained.

Table1 Acrredited Testing Scope

No.	Item	Scope
1	Determination of uranium in uranium compounds (titration)	U：20~200 mg
2	Isotopic composition of uranium in uranium compounds (ICP-MS)	^{233}U、^{234}U、^{235}U、^{236}U、^{238}U
3	Impurites inuranium compounds(ICP-MS)	67 elements
4	24 Impurites inuranium compounds(ICP-AES)	Ag/Al/Ba/Be/Bi/Ca/Cd/Cr/Cu/Fe/Mg/Mn/ Mo/Ni/Pb/Ru/Sb/Sn/Sr/Th/Ti/V/W/Zn
5	14 Impurites inuranium compounds(AAS)	Al/Cd/Ca/Cr/Co/Cu/Fe/Pb/Mg/Mn/Ni/ K/Na/Zn
6	16 Impurites inuranium compounds(ICP-AES)	Al/Ca/Cd/Co/Cr/Cu/ Fe/Mg /Mn/Mo/Ni/Pb/Sn/Ti/V/Zn
7	Sm/Eu/Gd/Dy in uranium compounds(ICP-AES)	Sm, Eu, Gd, Dy
8	Free acid in uranyl nitrate solutions(titration)	H^+
9	Boron in uranium compounds(ICP-AES)	0.05~33 μg B/g
10	Thorium in thorium compounds(titration)	Th
11	Metallic impurities in thorium compounds(ICP-MS)	Li/B/Be/V/Mn/Co/Ga/Ge/Rb/Sr/Zr/Nb/Mo/Ag/Cd/ In/Sn/Sb/Cs/Ba/Hf/Re/Pb/Bi
12	Rare earth impurities in thorium compounds(ICP-MS)	La/Ce/Pr/Nd/Sm/Eu/Gd/Tb/Dy/Ho/Er/Tm/Yb/Lu/ U/Sc/Y, 共 17 种
13	Boron in thorium compounds(ICP-AES)	B
14	Total alpha activity in radioactive materials(α spectrometric method)	Total alpha activity
15	Activity concentration of gamma-emitting radionuclides(HPGe)	Gamma activity
16	Radionuclide purity in radioactive materials(HPGe)	Radionuclide purity
17	Radiochemical purity of radiopharmaceuticals(TLC)	Radiochemical purity
18	Total gamma activity of radiopharmaceuticals(dose calibrator)	Total gamma activity

2 Radiochemical laboratory in building 103

During 2015 and 2016, the overall operation of the 103 radiochemical laboratory goes well, and basically meet the requirement of TMSR fuel treatment process research and other related research work. No major abnormalities situation occurred in the laboratory's main systems and equipment, and all technical indicators met the design requirements. Some slight failure occurred but had been fixed in time, and hadn't affected the operation of the laboratory. Some of the rules had been modified such as "Regulations for Radiation Safety Management of 103 Radiochemical Laboratories", "Administrative Regulations for Radioactive Waste Management of Radiochemical Laboratory 103", "Administrative Regulations for the Use of Radioactive Sources in 103 Radiochemical Laboratories", "103 Radiochemistryn Laboratory Emergency Plan for Radiological Accidents"and"103 Radiochemical Laboratory Experiments and Equipment Operating Procedures". At the same time, in accordance with the issues related to radioactive waste management, the"103 radiochemical laboratory regulations for the implementation of radioactive waste management regulations" was formulated, which further refined the classification requirements for radioactive waste liquids and radioactive solid wastes, and collection and centralization procedures.

3 Design of Hot Cells system

As the overall TMSR-LF1 solution was adjusted, the design task for the dry process laboratory facility was adjusted to the TMSR-LF1 hot cell system. Based on retaining the functions of fuel salt pyroprocessing experimental verification and TMSR-LF1 fuel salt quality analysis, the functions such as stack operation and maintenance, Post-Irradiation Examination were added. The function, quantity, type, and atmosphere requirements of each major hot cell in the hot cell system are shown in Table 2.

Table 2 TMSR-LF1 Hot cell System

Main function	Hot Cell name	Number	Type	Atmosphere
Pyroprocessing hot verification	Argon Hot Cell	1	α-γ	Ar
	Radiochemical Auxiliary Hot Cell	1	α-γ	Air
Quality analysis of fuel salt	Analysis Hot Cell A	1	α-γ	Ar
	Analysis Hot Cell B	3	α-γ	Air
TMSR-LF1 Operation	Decontamination Hot Cell	1	α-γ	Air
	Maintains Hot Cell	1	α-γ	Air
	Cutting Hot Cell A	1	α-γ	Air
Post-Irradiation Examination	Cutting Hot Cell B	1	α-γ	Air
	Flaw Detection Hot Cell	1	β-γ	Air
	Mechanical properties test Hot Cell A	1	β-γ	Air
	Mechanical properties test Hot Cell B	1	β-γ	Air

The design of the key technology verification device for the dry hot chamber was completed. This device is an experimental platform for the verification of key technologies in pyroprocessing hot cells. It is mainly used for the test, validation and design optimization of hot cells sealing and atmosphere purification control technologies. It is designed for dry hot chamber engineering, by which we can get the key technical parameters. At the same time, sufficient interfaces are reserved to facilitate the follow-up of technical program verification such as material transfer and remote operation.

This device is mainly composed of two parts - the box body and the atmosphere purification control system. The box body is made of stainless steel, including the window, access door, Wall-through Tube for manipulator, process/electrical pipeline interface, and other main penetration parts. The gas purification control system is composed of gas supply, gas circulation purification, pressure protection and exhaust gas and other functional units. The system configuration is shown in Fig.1.

Fig.1 The key technology verification device of the pyroprocessing hot cells

The development of a digital simulation hot cell system was completed. The system used the Unity 3D engine to realize the rapid building of virtual environments based on real design data and accurate simulation of hot cell operations (Fig.2). In the system, hot cell and pryoprocessing equipment design data can be directly imported, the simulate can be remotely operated. During the simulation operation, the layout, selection of the remote operation equipments (Master-Slave manipulator, cranes, and Power manipulator) can be analyzed and evaluated to provide technical support for the design and equipment selection of the hot cell system. During the simulation operation, technical analysis and evaluation of the design, operation space, visibility, and accessibility of the pyroprocessing equipment in the hot cells were also performed, which provided important reference for the design of the pyroprocessing equipment design and the layout of the process equipment.

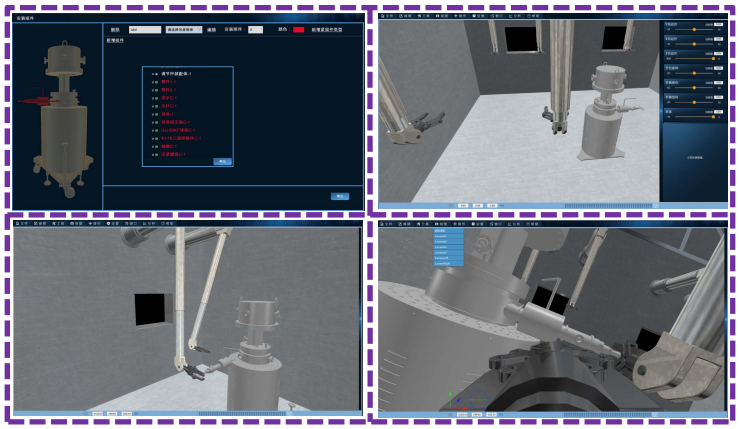

Fig.2 Digital simulation hot cell system

4 Summary and Prospect

The radiochemical analysis platform is running well t and it has completed the analysis task for TMSR related research. The CNAS laboratory accreditation application process is progressing smoothly and will soon receive a certificate. The main systems and equipments of the radiochemical laboratory in 103 building were well-operated, basically meeting the requirements of the TMSR fuel treatment process and other radiological related research work. The TMSR-LF1 hot-cell system plan was determined, the development of key technologies for the argon hot cell was carried out, and the design of the key technology verification device for the pyroprocessing hot cell and the development of the digital simulation hot cell system were completed. The subsequent work is the engineering design of TMSR-LF1 hot cell system, focusing on the technical validation of sealing scheme and the atmosphere control scheme for the pyroprocessing hot cells

基础与交叉

相对论重离子对撞物理研究

核物理研究室

位于美国布鲁克海汶国家实验室的相对论重离子对撞机上(RHIC)产生了类似于宇宙大爆炸早期的物质形态，是研究宇宙早期新物质形态的理想实验场所。2015−2016 年我们在 RHIC-STAR 上首次直接测量了反质子-反质子之间的相互作用，这对理解反物质的构成具有十分重要的意义。

为深入理解 RHIC 对撞机以及欧洲核子中心的大型强子对撞机 LHC 上的一系列重要的实验数据，开展物理唯象模型的理论研究是十分必要的。我们借助粒子输运模型和流体力学等理论工具，深入理解夸克胶子等离子 QGP 产生的机制和具有的特性。

RHIC-STAR 实验研究

我们利用 RHIC-STAR 质心系能量为 200 GeV 的金核-金核碰撞中产生的丰富的反质子，通过反质子-反质子动量关联函数的测量，并扣除了通过其他粒子衰变过来的次级反质子与其他反粒子关联的污染，精确地构建了反质子-反质子关联函数[1]。然后，结合量子多粒子关联理论，提取出反质子-反质子的有效力程和散射长度这两个基本作用参数。研究表明：在实验精度内，反物质间的相互作用与正物质并没有差别。即反质子-反质子之间的强相互作用存在着吸引，它们可以克服由于同号（负电荷）的反质子-反质子之间的库伦排斥而结合成反物质原子核。该研究对于理解自然界中物质-反物质不对称性提供了新的基础。人类所认识的自然界充满了普通物质，而反物质却非常稀少，这是一直以来困扰科学家的一个难题。在宇宙大爆炸初期，夸克、反夸克是成对产生的，然后演化到现在，在物质空间缺失了数量上的对称性。而这项研究又指出，反物质之间的作用与正物质作用是对称的。也就是说，在相互作用的层次上，反物质作用仍然满足“电荷共轭-空间反射-时间反演(CPT)”对称性。因此，要彻底解决正反物质粒子产额不对称的这个难题，需要科学家全面地研究正反物质的产生、相互作用及其演化机制。因此，反物质的研究有着广阔的前景。此外，我们也通过 π 介子椭圆流差别测量发现了手征电磁波效应[2]，通过双电子不变质量研究了 QCD 物质的电磁属性[3]，通过 Ω/ϕ 能量扫描测量研究奇异夸克动力学与 QCD 相变的对照关系[4]。

RHIC 物理唯象动力学研究

集体流是研究夸克胶子等离子 QGP 的一个重要实验探针。我们使用多相粒子输运 AMPT 模型和 3+1 维粘滞性流体动力学模型预言了 LHC 能量下质子＋铅核碰撞中不同运动方向的集体流的区别，发现铅核运动方向比质子运动方向有更大的带电粒子椭圆流和三角流[5]，已被 LHC-ALICE 实验组 μ 介子探测器实验结果所证实[6]。我们合作开展使用 AMPT 模型和 3+1 维理想流体动力学模型研究了相对论重离子碰撞早期的纵向涨落造成的各项异性流的纵向退关联效应，并提出使用长程关联函数作为实验探针[7]，也被 LHC-CMS 实验结果所证实[8]。我们合作研究发现：一套新的参数可以很好地同时描述 200 GeV 能量下金核+金核和 2.76 TeV 能量下铅核+铅核碰撞中的基本实验观测量，我们对 5.02 TeV 的铅核+铅核碰撞中的不同种实验观测量，包括粒子产额、横向动量分布、各向异性流、长程关联因子化进行了理论预言[9]。我们使用 AMPT 模型，采用 1.5~3 mb 的部分子弹性碰撞截面，很好地解释了 LHC 能量下 CMS 实验测量的两粒子长程关联结构、椭圆流、三角流，从而证明部分子散射是产生粒子发射各向异性的直接原因[10]。我们研究了 200 GeV 下金核+金核碰撞中的初始的部分子的几何各向异性分布的性质，对不同碰撞中心度下采用累积矩和传统的参加核子计算，提取初始的几何各向异性分布系数之间的比值和末态各阶各向异性流之间比值，研究了各阶几何各向异性分布系数及其涨落的横向动量和快度依赖性，有助于理解相对论重离子碰撞初态几何分布的信息[11]。在最高的 RHIC 能量下，我们研究了修正的组分夸克标度率，发现除了考虑逐事件的初态涨落之外，还需要考虑强子相的作用。同时，我们推广了 AMPT 模型，在考虑了部分子相和强子相的平均场效应下研究了正反粒子的椭圆流劈裂的能量依赖性。结果表明，可能需要平均场以外的机制的帮助来理解现有的实验数据[13]。我们利用 AMPT 模型研究了氘核+金核 200 GeV 碰撞能量下 ϕ 介子

在前向和后向的产额的快度和横向动量、系统尺寸的依赖性，表明初始状态和后续的部分子散射是对于描述相关实验数据很必要的[14]。由于相对论重离子碰撞早期产生强大的电磁场，所以理论上预言了会有很多强磁场下的手征反常现象会发生。例如：我们将手征电荷分离效应引进到 AMPT 模型中 200 GeV 的铜核＋金核碰撞中初始部分子分布中去，建议了两种新的实验观测量（两粒子方位角关联因子和正反电荷事件平面），研究了它们对不同的手征电磁效应的敏感程度[15]。我们合作研究了同质异位素碰撞中手征磁效应的实验观测量，基于 Glauber+参数化模型，假设在 2/3 的背景比例下，研究发现 4 亿个事件的基础下，两种不同的同质异位素碰撞中手征磁效应的实验观测量的相对区别可以达到 5%左右，并且有 5σ 的实验显著性[16]。

参考文献

1. Adamczyk L, Adkins J K, Agakishiev G, *et al.* (STAR Collaboration) Measurement of interaction between antiprotons[J]. Nature 2015, **527**: 345-348.
2. Adamczyk L, Adkins J K, Agakishiev G, *et al.* (STAR Collaboration) Observation of Charge Asymmetry Depdendence of Pion Elliptic Flow and the Possible Chiral Magnetic Wave in Heavy-Ion Collisions[J]. Physical Review Letter 2015, **114**: 2523002.
3. Adamczyk L, Adkins J K, Agakishiev G, *et al.* (STAR Collaboration) Measurements of dilepton production in Au+Au collisions at 200 GeV from the STAR experiment[J]. Physical Review C 2015, **92**: 024912.
4. Adamczyk L, Adkins J K, Agakishiev G, *et al.* (STAR Collaboration) Probing parton dynamics of QCD matter with Omega and Phi production[J]. Physical Review C 2016, **93**: 021903(R).
5. Bozek P, Bzdak A, Ma G L. Rapidity dependence of elliptic and triangular flow in proton–nucleus collisions from collective dynamics[J]. Phys Lett B, 2015, **748**: 301-305.
6. Adam J, *et al.* (ALICE Collaboration), Forward-central two-particle correlations in p-Pb collisions at $\sqrt{s_{NN}}$= 5.02 TeV[J]. Physics Letter B, 2016, **753**: 126-139.
7. Pang L G, Qin G Y, Roy V, *et al*. Longitudinal decorrelation of anisotropic flows in heavy-ion collisions at the CERN Large Hadron Collider[J]. Physical Review C, 2015, **91**, 044904.
8. Khachatryan V, *et al*. (CMS Collaboration), Evidence for transverse-momentum-and pseudorapidity-dependent event-plane fluctuations in PbPb and pPb collisions[J]. Physical Review C, 2015, **92**: 034911.
9. Ma G L, Lin Z W. Predictions for √sNN=5.02 TeV Pb + Pb collisions from a multiphase transport model[J]. Physical Review C, 2016, **93**: 054911..
10. Ma G L, Bzdak A. Flow in small systems from parton scatterings[J]. Nuclear Physics A, 2016, **956**: 745-7488.
11. Ma L, Ma G L, Ma Y G. Initial partonic eccentricity fluctuations in a multiphase transport model[J]. Physical Review C, 2016, **94**: 044915.
12. Zhang C J, Xu J. Investigating the scaling of higher-order flows in relativistic heavy-ion collisions[J]. Physical Review C, 2016, **93**: 024906.
13. Xu J, Ko C M. Collision energy dependence of elliptic flow splitting between particles and their antiparticles from an extended multiphase transport model[J]. Physical Review C, 2016, **94**: 054909.
14. Ye Y J, Chen J H, Ma Y G, *et al*. Phi-meson production at forward/backward rapidity in high-energy nuclear collisions from a multiphase transport model, Physical Review C, 2016, **93**: 044904.
15. Ma G L, Huang X G. Possible observables for the chiral electric separation effect in Cu + Au collisions[J]. Physical Review C, 2015, **91**: 054901.
16. Deng W T, Huang X G, Ma G L, *et al*. Testing the chiral magnetic effect with isobaric collisions[J]. Physical Review C, 2016, **94**: 041901.

The Researches on Relativistic Heavy-Ion Collisions

Division of Nuclear Physics

The Relativistic Heavy-Ion Collider at Brookhaven National Laboratory created a condition similar to the earlier universe at a few microseconds just after the Big Bang, thus it is the ideal lab to understand the early state of the universe. During 2015 and 2016, we measure the interaction between antiproton and antiproton for the first time at RHIC-STAR, which has significant importance for understanding the structure of anti-matter.

In order to understand the physics behind plentiful experimental data from RHIC and the Large Hadron Collider (LHC) at CERN, theoretical phenomenal studies are strongly required. By taking the advantage of some models, e.g. transport model and hydrodynamical model, we can learn more about the production mechanism and properties of Quark Gluon Plasma (QGP).

Experimental researches at RHIC-STAR

With abundantly produced anti-nucleons after the hadronization of QGP, RHIC offers the excellent capability of conducting the study of interaction between antiprotons. By using from STAR Au+Au collisions data at $\sqrt{s_{NN}}$ =200 GeV, we can measure and identify the antiprotons, and then construct the correlation function of antirproton-antiproton pairs[1]. After considering the residual correlation due to the secondary antiproton that decayed from other particles, we obtain the pure antiproton-antiproton correlation function. By applying the quantum theory of multi-particle correlation, two key parameters that characterize the corresponding strong interaction: namely, the scattering length (f_0) and effective range (d_0) were extracted. This measurement is for the first time on anti-matter interaction in the world. We found that within errors, the f_0 and d_0 for the antiproton-antiproton interaction are consistent with their antiparticle counterparts - the ones for the proton-proton interaction. Like the force that holds ordinary protons together within the nuclei of atoms, the force between antiprotons is attractive and strong. The current measurement offers a new way to test the matter-antimatter symmetry. In order to understand the asymmetry between matter and antimatter, ned more analysis on the production, interaction and evolution mechanism of matter. Thus, the study on antimatter has broad prospects. In addition, we measure the elliptic flow difference of charge pion to discovery the chiral magnetic wave[2]; analyze the di-electron pair invariant mass continue to study the electromagnetic effect in QCD matter[3]; measure the Ω/ϕ production in STAR BES experiment to probe the connection between strange quark dynamics and QCD phase structure[4].

Phenomenological study on partonic dynamics in relativistic heavy-ion collisions

Collective flow is one of important experimental observables to study the properties of QGP. Using the AMPT model and 3+1D viscous hydrodynamical model, we predict a larger flow in Pb-going direction than that in p-going direction in p+Pb collisions at the LHC energy[5]. It has been verified by the experimental measurements using the muon detector in the ALICE[6]. With the AMPT model and 3+1D viscous hydrodynamical model, we also investigate the decorrelation of anisotropic flow due to the longitudinal fluctuations in early state of heavy-ion collisions and propose a long-range correlation function as the corresponding experimental observable[7], which whereafter has been measured by the CMS experiment[8]. We find a new setting of parameters, which can simultaneously describe many basic experimental observables from Au+Au 200 GeV and Pb+Pb 2.76 TeV. We then implement it to predict the observables for Pb+Pb 5.02 TeV, including particle multiplicity, ρ_T spectra, anisotropic flow, decorrelation etc[9]. With a parton elastic scattering cross section about 1.5~3 mb, we describe the long-range correlation, elliptic flow and triangular flow in p+Pb collisions measured by the CMS experiment well, which indicates that parton scatterings leads to anisotropic flow of final particles in AMPT[10]. We study the properties of initial partonic geometry for Au+Au collisions at 200 GeV, by calculating particle cumulants in the initial and final states. We also investigate the pT and rapidity dependences of anisotropic flow coefficients and fluctuations, which can help us understand more information about initial geometry of relativistic heavy-ion collisions[11]. The modified number of constituent quark (NCQ) scaling has been investigated at top RHIC energy. It has been found that the modified NCQ scaling can not be obtained from the naive coalescence even by taking into account event-by-event fluctuations but may be due to hadronic afterburner or thermal freeze-out[12]. Based on an extended multiphase transport model, which includes mean-field potentials in both the partonic and hadronic phases, we have studied the collision energy dependence of the elliptic flow splitting between particles and their antiparticles. The results indicate the existence of other mechanisms for the elliptic flow splitting besides the mean-field potentials[13]. We also study the ϕ-meson production is studied in d+Au collisions at 200 GeV in the forward and backward direction in AMPT. Detailed investigations including the rapidity, transverse momentum and collision system size dependencies of ϕ-meson nuclear modification factor indicate that a combination of the initial state effect and a follow-up parton cascade is required in the AMPT model to describe the experimental data[14]. Because extremely large electromagnetic fields are produced in the early state of heavy-ion collisions, many interesting chiral effects have been predicted inside the environment. With introducing a chiral electric separation effect into the AMPT model, we propose two new sensitive observables (i.e. two-particle azimuthal correlation and charge-dependent event plane) to investigate the different chiral effects in Cu+Au collisions at 200 GeV[15]. We investigate the experimental observables related to chiral magnetic effect in isobaric collisions. Based on a Glauber + parameterization model, if we assume the background contribute to 2/3 of signal, we demonstrate that the relative difference of experimental observable between two isobaric collisions can achieve 5%

with a 5σ significance under an event statistics of 400 M[16].

Reference

1. Adamczyk L, Adkins J K, Agakishiev G, *et al.* (STAR Collaboration) Measurement of interaction between antiprotons[J]. Nature 2015, **527**: 345-348.
2. Adamczyk L, Adkins J K, Agakishiev G, *et al.* (STAR Collaboration) Observation of Charge Asymmetry Depdendence of Pion Elliptic Flow and the Possible Chiral Magnetic Wave in Heavy-Ion Collisions[J]. Physical Review Letter 2015, **114**: 2523002.
3. Adamczyk L, Adkins J K, Agakishiev G, *et al.* (STAR Collaboration) Measurements of dilepton production in Au+Au collisions at 200 GeV from the STAR experiment[J]. Physical Review C 2015, **92**: 024912.
4. Adamczyk L, Adkins J K, Agakishiev G, *et al.* (STAR Collaboration) Probing parton dynamics of QCD matter with Omega and Phi production[J]. Physical Review C 2016, **93**: 021903(R).
5. Bozek P, Bzdak A, Ma G L. Rapidity dependence of elliptic and triangular flow in proton–nucleus collisions from collective dynamics[J]. Phys Lett B, 2015, **748**: 301-305.
6. Adam J, *et al.* (ALICE Collaboration), Forward-central two-particle correlations in p-Pb collisions at $\sqrt{s_{NN}}$= 5.02 TeV[J]. Physics Letter B, 2016, **753**: 126-139.
7. Pang L G, Qin G Y, Roy V, *et al*. Longitudinal decorrelation of anisotropic flows in heavy-ion collisions at the CERN Large Hadron Collider[J]. Physical Review C, 2015, **91**, 044904.
8. Khachatryan V, *et al*. (CMS Collaboration), Evidence for transverse-momentum-and pseudorapidity-dependent event-plane fluctuations in PbPb and pPb collisions[J]. Physical Review C, 2015, **92**: 034911.
9. Ma G L, Lin Z W. Predictions for √sNN=5.02 TeV Pb + Pb collisions from a multiphase transport model[J]. Physical Review C, 2016, **93**: 054911..
10. Ma G L, Bzdak A. Flow in small systems from parton scatterings[J]. Nuclear Physics A, 2016, **956**: 745-7488.
11. Ma L, Ma G L, Ma Y G. Initial partonic eccentricity fluctuations in a multiphase transport model[J]. Physical Review C, 2016, **94**: 044915.
12. Zhang C J, Xu J. Investigating the scaling of higher-order flows in relativistic heavy-ion collisions[J]. Physical Review C, 2016, **93**: 024906.
13. Xu J, Ko C M. Collision energy dependence of elliptic flow splitting between particles and their antiparticles from an extended multiphase transport model[J]. Physical Review C, 2016, **94**: 054909.
14. Ye Y J, Chen J H, Ma Y G, *et al*. Phi-meson production at forward/backward rapidity in high-energy nuclear collisions from a multiphase transport model, Physical Review C, 2016, **93**: 044904.
15. Ma G L, Huang X G. Possible observables for the chiral electric separation effect in Cu + Au collisions[J]. Physical Review C, 2015, **91**: 054901.
16. Deng W T, Huang X G, Ma G L, *et al*. Testing the chiral magnetic effect with isobaric collisions[J]. Physical Review C, 2016, **94**: 041901.

上海激光电子伽玛源（SLEGS）

核物理研究室

上海激光电子伽玛源(SLEGS)是基于激光康普顿散射原理建设的高质量γ光装置，γ光的能区为0.4~20 MeV。经过多年技术积累，SLEGS在2015年4月获得国家发改委批复。2015−2016年，我们主要专注SLEGS的工程设计和关键设备的预制研究[1]。主要工作进展如下。

1 开展光源和前端区初步工程设计

SLEGS采用外部激光和上海光源储存环(SSRF)电子束以一定的夹角发生康普顿散射产生伽玛光，并通过连续改变激光和电子束夹角的办法实现伽玛光能量连续可调；高极化度(~100%)伽玛光采用激光和电子束康普顿背散射产生。SLEGS光源主要包括激光器及其光路和检测系统，位于相互作用点处的靶室等。光源系统的初步工程设计如图1所示。

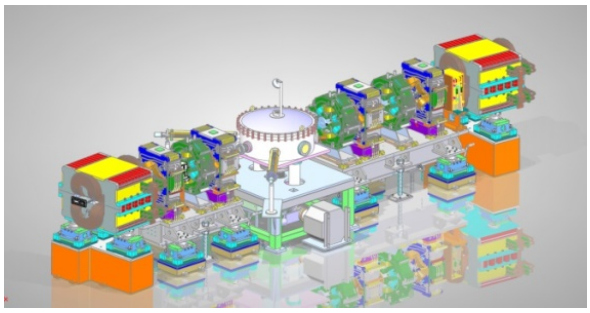

图1 光源系统初步工程设计

前端区位于储存环隧道内，介于储存环和光束线之间，它上连电子储存环，下接光束线，是二者的连接纽带。SLEGS前端区主要作用为吸收弯铁产生的同步辐射光，引入背散射激光光束，引出伽玛光束，以及真空和连锁等保护功能。前端区工程设计如图2所示。

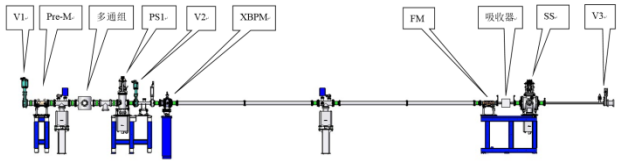

图2 前端区系统初步工程设计

2 开展光束线初步工程设计

光束线的功能是将伽玛光成功传输到实验站，并根据实验的需要对伽玛光的性质进行调整和检测。光束线主要设备设置有准直器、衰减器、辐射和屏蔽块、γ位置探测器、γ能谱探测器、γ流强探测器等。光束线系统的初步工程设计如图3所示。

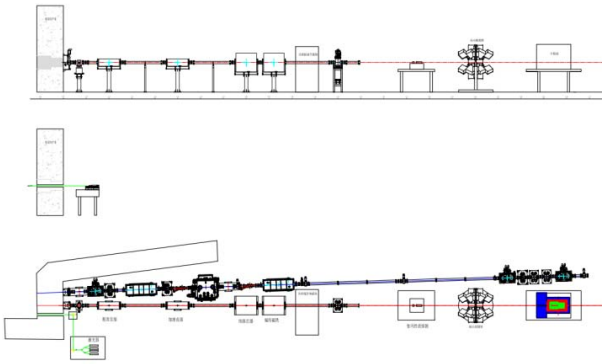

图3 光束线系统初步工程设计

3 完成实验站初步工程设计

实验站为开展光核物理实验及应用实验研究而设计，如通过光核反应开展核天体物理、核物理、极化物理等领域中的基础研究，特别是解决核物理、核天体物理中具有重大科学价值的问题；此外，还开展与航天、国防、核能等战略需求相关的应用基础研究，如利用伽玛射线开展航天电子元器件空间辐照效应中的总剂量效应、抗辐射加固评估的研究，以及航天伽玛探测器的精确定标，核能关键光核截面，核废料嬗变截面研究等。因此实验站的设备设计和探测器布局主要基于这样的一些物理目标的实现。实验探测器装置：包括(γ, n)中子测量探测器，(γ, p/α)带电粒子探测器及真空靶室，(γ,γ)伽马探测器以及核共振荧光NRF探测器等。实验站布局如图4所示。

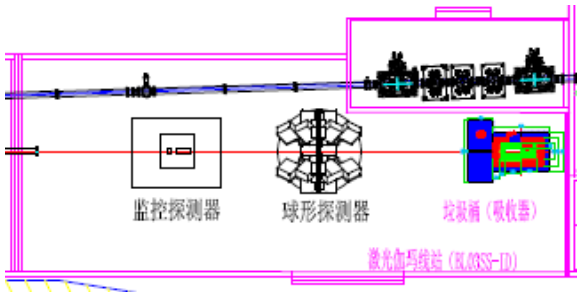

图4 实验站布局

参考文献

1. 上海光源二期工程设计报告：上海激光电子伽玛源2016, (SLEGS).

Shanghai Laser Electron Gamma Source (SLEGS)

Department of Nuclear Physics

Shanghai Laser Electron Gamma Source (SLEGS) is one of the high quality gamma sources based on Laser Compton Scattering (LCS). The energy region of SLEGS is 0.4~20 MeV. Based on several years of technical accumulation, SLEGS was finally approved by the National Development and Reform Commission (NDRC) in April 2015. During 2015−2016, we mainly focus on the technical design of SLEGS and the pre-research of key equipment[1]. The main results are as follows.

1 Technical design of light source and front end

The gamma ray of SLEGS are produced by the slanting Compton scattering between electron beam in storage ring (SSRF) and external laser. And the gamma energy can be continually tuned by changing the incident angle of laser. The high polarizable (~100%) gamma ray are generated by Compton back scattering. The light source system includes high power laser and laser detection system, LCS chamber at collision point *et al*., The preliminary technical design of light source system shown in Fig.1.

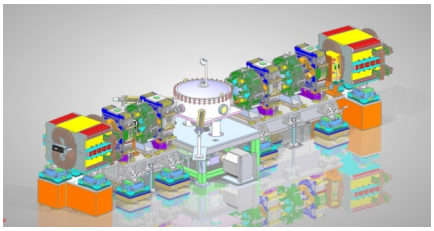

Fig.1 The preliminary technical design of light source system

The front end system is located in the storage ring tunnel, which connects the storage ring and the beam line. The main functions of front end system are absorbing the synchronous radiation, introducing the laser beam of back scattering, as well as the protection of vacuum. The preliminary technical design of front end system shown in Fig.2.

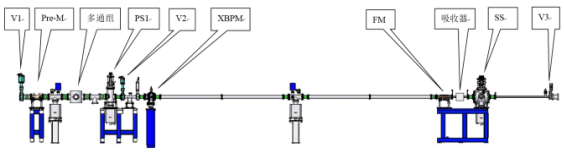

Fig.2 Preliminary technical design of front end system

2 Technical design of beam line

The main functions of the beam line system are connecting the storage ring tunnel and the experimental station, and adjusting the properties of gamma ray according to the requirements of experiment. The beam line system is composed of gamma collimators, gamma attenuator, γ position detectors, γ energy detector, as well as γ flux detector. Preliminary technical design of beam line shown in Fig.3.

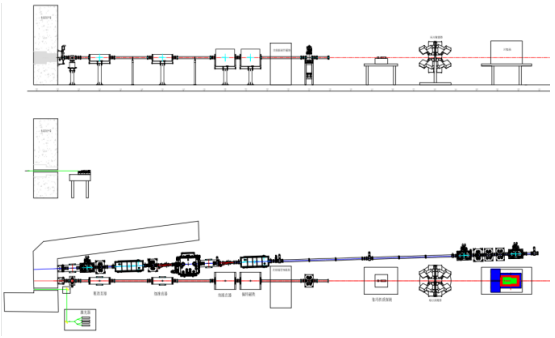

Fig.3 Preliminary technical design of beam line

3 Technical design of experimental station

Based on different experiment detector system, experimental station aims at basic physics researches, such as nuclear astrophysics, nuclear physics, and polarization physics. In addition, experimental station also tends to carry out applied research relating to aerospace, national defense, nuclear energy and other strategic demand of our country, such as space radiation effect research of the aerospace electronic components, and accurate calibration of the gamma detector for aerospace. So, technical design of experimental station is mainly based on the physical objects mentioned above. According to different experimental requirements, experimental station will include following detectors: (g, n) neutron detectors, (γ, p/α) charged particle detectors, and (γ,γ) gamma detectors. The experimental station layout is shown in Fig.4.

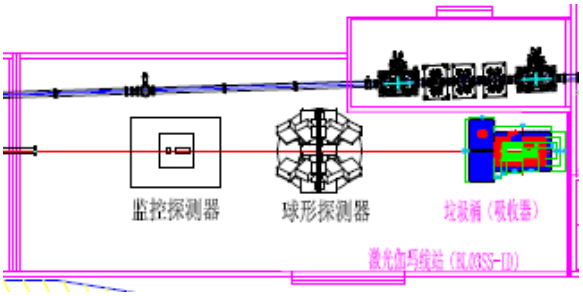

Fig.4 Layout of experimental station

Reference

1. Technical Design Report of SSRF-II Beamlines: Shanghai Laser Electron Gamma Source, 2016, LEGS.

CUORE(CUPID)及 PandaX 合作实验

核物理研究室

本研究主要在非加速器物理前沿的无中微子双贝塔衰变及暗物质直接测量两个方向参与国际及国内大型实验合作，在无中微子双贝塔衰变参加CUORE(CUPID)国际合作，在暗物质直接测量方面参加国内 PandaX 实验。核物理室不仅在这些国际、国内合作中做出了重要贡献，与此同时锻炼青年人才队伍，发展非加速器物理探测技术及理论模拟，提升国际影响力。

1 中微子国际合作（CUORE&CUPID实验）

CUORE(Cryogenic Underground Observatory for Rare Events)实验研究目标是测量 130 Te 极其稀有的无中微子双贝塔衰变(0νDBD)事件，关于 CUORE 实验可见 CUORE 的在线网站[1]。

核物理室邓先概于 2014 年 11 月 15 日至 2015 年 1 月 23 日访问意大利 LNGS 国家地下实验室，参加 CUORE-0 实验低温器运行维护、在线数据获取及离线数据分析工作。CUORE-0 实验的目的是为了检验 CUORE 所采用新技术和验证科学目标的可行性，CUORE-0 完全采用 CUORE 一样的晶体及组装方法，CUORE-0 从 2013 年 3 月~2013 年 8 月, 2013 年 9 月~2015 年 3 月在 LNGS 的 HallA 取数据，得到的半衰期灵敏度超过了之前 CUORICINO 的灵敏度，结合 CUORICINO 的数据 CUORE 合作组于 2015 年 9 月在 Phhys Rev Lett 上发表了目前最为灵敏的 130 Te 的 0VDBD 半衰期大于 4.0×10^{24} yr@90%置信度，结合核矩阵元计算，可以得到 $m_{\beta\beta}< 270-760$ meV[2]，CUORE-0 达到了最初的计划，证实 CUORE 技术是可靠的。

专为 CUORE 设计的大型低温器于于 2016 年 3 月实现了低温期的长时间试运行(70 d)，可以达到 6.3 mK 的稳定运行温度，2016 年 8 月完成了 19 个 TeO_2 塔在低温器内的安装工作。预计 2017 年初开始取物理数据。

最近 CUPID(CUORE Upgrade with Particle Identification)合作组成立，目前通过各种 R&D 研究寻找增加灵敏度的方法，使 0VDBD 半衰期达到 $(2\sim5)\times10^{24}$ yr，相应得出 $m_{\beta\beta}$ 处于 6~20 meV 的约束，最终达到探测中微子整个反转质量区的目的[3]。复旦大学黄焕中教授组织了国内 0VDBD 相关研究力量组建了 CUPID-China 合作组，2016 年 11 月 10 日在复旦大学召开首次 CUPID-China 合作组会议，合作组成员来自复旦大学、中国科学院上海应用物理研究所、宁波大学、中国科学院上海硅酸盐研究所、清华大学、中国科学技术大学、上海交通大学，CUPID-China 目标一方面参与 CUPID 的 R&D 研发，另一方面计划在中国锦屏地下实验室开展具有较强国际竞争力的 0VDBD 实验。

2 暗物质探测（PandaX实验）

PandaX 实验（Particle AND Astrophysical Xeon experiments, 粒子和天体物理液氙探测实验），又称“熊猫 X 计划”，是利用液氙作靶物质组建大型时间投影室探测器 Xe-TPC（吨级）探测暗物质及无中微子双贝塔衰变的系列性实验。其一期实验 PandaX-I 在 2014 年已经完成，以 54.0 kg×80.1 day 的曝光量，取得了当时国际前沿的暗物质探测结果[4–5]。二期实验 PandaX-II 利用 500 kg 级的液氙进行更大规模的 WIMP 暗物质测量，截至 2016 年是世界上最大的正在运行中的液氙暗物质探测实验，PandaX-II 探测器示意图如图 1 所示。

在 PandaX-II 合作实验中我们主要负责 ^{3}He 中子正比计数器的模拟分析、环境中子本底的测量；锦屏实验室的维护、值班工作、数据获取；数据分析工作，具体包括：探测器中子本底的模拟计算、电子反冲本底的分析计算、电子反冲刻度等等。

2015 年进行一系列的测试运行来调试新的探测器系统。2015 年 9~12 月在锦屏实验室测试 ^{3}He 正比计数器，进行环境中子本底测量；同时完成一个试运行数据获取（Run8, 19.1 d 活时间）[6]。2016 年年初运行精馏塔提纯液氙。2016 年 3~6 月完成第一个物理数据获取(Run9, 79.6 天活时间)，加上试运行数据，以 3.3×10^4 kg/day 的曝光量，在 Phys Rev Lett 上发表了当时国际领先的暗物质探测结果[7]。2016 年 7–10 月进行电子反冲与核反冲的刻度数据获取，并进行 PandaX-II 的数据分析工作。2016 年 11 月在现场开始第二次运行精馏塔提纯液氙。

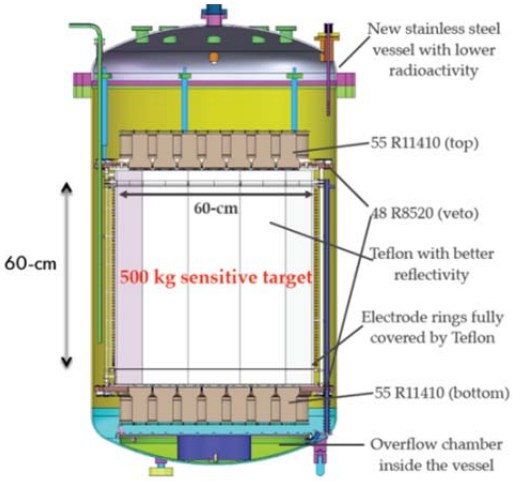

图 1　PandaX-II 探测器示意图

参考文献

1. https://wiki.wlab.yale.edu/cuore/.
2. Alfonso K, *et al*. (CUORE collaboration), Search for Neutrinoless Double-Beta Decay of ^{130}Te with CUORE-0, Phys Rev Lett, 2015, **115**(10), 102502.
3. G Wang, *et al.* The CUPID Interest Group, CUPID: CUORE (Cryogenic Underground Observatory for Rare Events) Upgrade with Particle IDentification, arXiv: 1504.03599v1.
4. M Xiao, *et al.* (PandaX) Sci China Phys Mech Astron, 2014, **57**: 2024.
5. Xiao X, *et al.* (PandaX) Phys Rev D, 2015, **92**: 052004.
6. Tan A, *et al.* (PandaX collaboration), Dark matter search results from the commissioning run of PandaX-II[J]. Phys Rev D, 2016, **93**(12), 122009.
7. Tan A, *et al.* (PandaX-II collaboration) , Dark Matter Results from First 98.7 Days of Data from the PandaX-II Experiment, Phys Rev Lett, 2016, **117**(12): 121303.

CUORE(CUPID) and PandaX Collaborations

Nuclear Physics Division

This study direction mainly involved in international and domestic large-scale experimental collaborations in neutrinoless double beta decay (0νDBD) and dark matter direct measurement in the non-accelerator physics frontier. We participated in CUORE (CUPID) international collaboration on 0νDBD, as well as domestic dark matter PandaX experiment. Nuclear physics division not only made important contributions to these international and domestic collaborations, but also train young talents, develop detection technology and theoretical simulation of non-accelerator physics, enhance our international influence.

1 International collaboration

The goal of the CUORE (Cryogenic Underground Observatory for Rare Events) experiment is to measure the extremely rare 0νDBD event of ^{130}Te. For a detailed introduction of the CUORE experiment, please see CUORE's online site[1].

Xiangai Deng from Nuclear physics divison visited LNGS of Italy from November 15, 2014 to January 23, 2015. He participated in CUORE-0 experiments, including cryostat operation and maintenance, online data acquisition and offline data analysis. The purpose of the CUORE-0 experiment is to test the new technology adopted by CUORE and to verify it's scientific objectives feasibility. CUORE-0 fully adopted CUORE-like crystals and assembly line. CUORE-0 took data from March 2013 to August 2013, from September 2013 to March 2015, located at HallA of LNGS. It's sensitivity has surpassed the sensitivity of previous CUORICINO experiment. In conjunction with CUORICINO data, the CUORE team published the most sensitive 0νDBD half-life of 130 Te larger than 4.0×10^{24} yr @ 90% confidence level in September 2015, and $m_{\beta\beta}$ <270~760 meV obtained by combining with nuclear matrix elements calculation[2]. CUORE-0 has achieved its initial plan, confirming the technology adopted in CUORE is reliable.

A large-scale custom-built cryostat for CUORE has achieved long-term commissioning (70 days) in March 2016 and obtained a stable operating temperature of 6.3 mK. 19 TeO_2 towers were installed inside cyrostat in August 2016. It is estimated that the physics data will be taken in early 2017.

Recently, CUPID (CUORE Upgrade with Particle Identification) interest group has been established. Recently, various R&D studies are undergoing in order to increase the sensitivity to reach haf life of $(2\sim5)\times10^{27}$ yr, resulting in the constraint $m_{\beta\beta}$ 6~20 meV, finally reaching the entire inverted mass zone of neutrino[3]. Professor Huanzhong Huang from Fudan University organized the domestic people related with 0νDBD research to form a CUPID-China collaboration group recently. Collaboration members, from 7 institutes such as Fudan University, Shanghai Institute of Applied Physics, Chinese Academy of Sciences, Ningbo University, Shanghai Institute of ceramics, Chinese Academy of Sciences, Tsinghua University, University of Science and Technology of China, Shanghai Jiaotong University, had the first CUPID-China collaboration collaboration meeting in Fudan University on November 10, 2016. CUPID-China team has two goals: one is to to participate in R&D of CUPID, and on the other hand, it plans to build a 0νDBD experiment with strong international competitiveness in Jinping Underground Laboratory in China.

2 PandaX collaboration for dark matter search

PandaX (Particle and Astrophysical Xeon experiments) is designed to build and operate a ton-scale liquid xenon experiment to search elusive dark matter particles and neutrinoless double beta decay. The first phase of the experiment, PandaX-I has performed an international advanced WIMP search in 2014 with a 54×80.1 kg-day exposure[4–5]. The second phase of the experiment, PandaX-II, with a half-ton scale LXe target, is the largest running dual-phase xenon detector by 2016. The schematic figure of PandaX-II is shown by Fig.1.

We are mainly responsible for the simulation of ^{3}He neutron proportional counter and the measurement of environmental neutron background in the lab; the maintenance， shift and DAQ work in CJPL; data analysis work, including simulation and calculation of neutron background in PandaX-II detector, ER background calculation, ER calibration and so on.

In 2015, a series of engineering runs were carried out to test the new detector system. From Sep to Dec in 2015, we tested the ^{3}He neutron proportional counter and measured the environmental neutron background inside CJPL; and meanwhile a brief physics commissioning run was taken (Run 8, 19.1 live days)[6]. In early 2016, a krypton distillation campaign was carried out. From Mar to June in 2016, we accomplished data taking of the first physics run (Run 9, 79.6 live days); and in combination with the data set during the commissioning run, with a total exposure of 3.3×10^4 kg/day, we reported a world leading WIMP search result at that time in Phys Rev Lett[7]. From July to Oct in 2016, the ER and NR calibration data were taken and data analysis was ongoing. A re-distillation of xenon was carried out on site since Nov 2016.

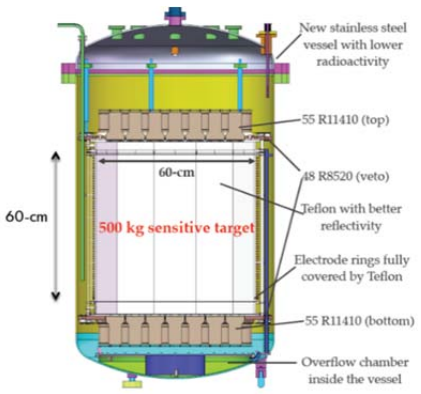

Fig.1 The schematic diagram of PandaX-II

Reference

1. https://wiki.wlab.yale.edu/cuore/.
2. Alfonso K, *et al*. (CUORE collaboration), Search for Neutrino-less Double-Beta Decay of 130Te with CUORE-0, Phys Rev Lett, 2015, **115**(10), 102502.
3. G Wang, *et al*. The CUPID Interest Group, CUPID: CUORE (Cryogenic Underground Observatory for Rare Events) Upgrade with Particle IDentification, arXiv: 1504.03599v1.
4. M Xiao, *et al*. (PandaX) Sci China Phys Mech Astron, 2014, **57**: 2024.
5. Xiao X, *et al*. (PandaX) Phys Rev D, 2015, **92**: 052004.
6. Tan A, *et al*. (PandaX collaboration), Dark matter search results from the commissioning run of PandaX-II[J]. Phys Rev D, 2016, **93**(12), 122009.
7. Tan A, *et al*. (PandaX-II collaboration) , Dark Matter Results from First 98.7 Days of Data from the PandaX-II Experiment, Phys Rev Lett, 2016, **117**(12): 121303.

低中能重离子碰撞物理

核物理研究室

本研究方向主要在丰质子核的双质子发射机制、不稳定核的共振能级结构、中能重离子碰撞中的自旋物理与中质子有效质量劈裂等方面开展了实验或理论研究。

不稳定核的结构与奇异衰变方式实验研究

双质子发射是质子滴线区原子核的奇特衰变方式之一，主要有 ^{2}He 集团发射、三体发射及级联发射三种机制，对其进行实验研究具有重要意义。我们分析了在日本理化学研究所 RIPS 束流线上完成的 ^{23}Al 与 ^{22}Mg 的质子-质子关联及双质子发射实验测量数据，得到了处于激发态的 ^{23}Al 与 ^{22}Mg 衰变发射的两个质子的相对动量、相对角度，并通过余核及两个质子的三体系统重构得出 ^{23}Al 与 ^{22}Mg 衰变时的激发能，发现奇 Z 核 ^{23}Al 不同激发态的双质子衰变模式基本为三体衰变或级联衰变，但 ^{22}Mg 在 14.044 MeV 激发态附近存在约 30%的 ^{2}He 集团发射机制[1]。同时，基于质子-质子动量关联函数分析，发现 ^{23}Al 与 ^{22}Mg 的两个质子发射时间差存在很大差别，即 ^{23}Al 的两质子发射时间差很长，主要为级联发射，而 ^{22}Mg 的两质子发射时间差很短，几乎为同时发射[2]。我们指出利用关联函数分析方法并结合两质子的相对动量及相对角度分析方法可以对双质子发射的三种机制进行清楚的判别。该工作提供了新的稀有的双质子发射的实验数据，对鉴别和理解极端丰质子原子核的双质子发射机制与核子-核子关联具有重要意义。

我们在兰州 RIBLL 束流线上利用逆运动学的共振弹性散射方法进行了 ^{10}Be+^{1}H->^{11}B*->p+^{10}Be 的实验，测量了 ^{11}B 的共振能级结构。通过数据分析并结合 R-Matrxi 理论计算，在共振能级谱实验数据上观测到 ^{11}B 激发态中，激发能为 14.53 MeV 处具有一个明显的共振峰，对应自旋宇称为 $5/2^{+}$；在激发能为 15.23 MeV 处有一个矮小的峰，并指认该能级自旋宇称为 $3/2^{-}$。观测到的这两个能级与现有实验结果符合。同时观测到一个激发能为 13.46 MeV 的可能新能级[3]。

中能重离子碰撞中的自旋动力学与中质子有效质量劈裂研究

自旋动力学的研究一直是许多物理领域的热门课题。自旋轨道耦合是在相对论体系的动力学过程中普遍存在的相互作用，会影响不同自旋粒子的动力学行为，这称为自旋霍尔效应。在原子核体系中，核子的自旋轨道耦合对解释幻数和壳结构至关重要。我们近年来关注核自旋轨道耦合在核反应中的效应，研究重离子碰撞中的自旋霍尔效应。受《物理学前沿》邀请，我们撰写了重离子碰撞中自旋动力学方面的综述，并作为杂志当期封面文章发表[4]。我们同时对 BUU 输运理论进行了拓展，从自旋依赖的玻尔兹曼方程出发，利用试验粒子方法得到体系自旋依赖的运动学方程，这成为自旋动力学模拟的理论基础[5]。我们在量子化极限下对该运动学方程进行了应用[6]。最近，除了自旋依赖的平均场，我们还将自旋依赖的核子-核子散射截面引入到输运模型模拟计算中[7]。

由于受到核介质的相互作用，核子的有效质量一般比真空中的小。在丰中子核物质中，中子和质子的有效质量哪个大一直受到学术界的关注。中质子有效质量劈裂和对称能都是同位旋物理的重要课题，影响着放射性核反应的同位旋动力学、丰中子原子核的性质、及核天体物理中的许多现象。基于一套动量相关的有效核势，我们研究了中质子有效质量劈裂对丰中子核物质热力学性质[8]、输运性质[9]、及核反应中质子产额比的影响[10]。最近，我们用动力学方法研究了铅原子核的巨共振，并基于相关实验数据对核物质对称能与中质子有效质量给出了一定的约束[11]。

参考文献

1. Ma Y G, Fang D Q, Sun X Y, *et al.* Different mechanism of two-proton emission from proton-rich nuclei ^{23}Al and ^{22}Mg[J]. Phys Lett B, 2015, **743**: 306.
2. Fang D Q, Ma Y G, Sun X Y, *et al.* Proton-proton correlations in distinguishing the two-proton emission mechanism of ^{23}Al and ^{22}Mg[J]. Phys Rev C, 2016, **94**: 044621.
3. Liu Y D, Ma y G, *et al.* New measurement of the excited states in ^{11}B via elastic resonance scattering of ^{10}Be + *p*. Phys Rev C, 2015, **91**: 044302.
4. Xu J, Li B A, Shen W Q, *et al.* Dynamical effects of spin-dependent interactions in low-and intermediate- energy heavy-ion reactions[J]. Front Phys, 2015, **10**: 102501.
5. Xia Y, Xu J, Li B A, *et al.* Equations of motion of test particles for solving the spin-dependent Boltzmann–

Vlasov equation[J]. Phys Lett B, 2016, **759**: 596.
6. Xia Y, Xu J, Li B A, *et al.* Simulating spin dynamics with spin-dependent cross sections in heavy-ion collisions[J]. Nucl Phys A, 2016, **955**: 41.
7. Xia Y, Xu J, Li B A, *et al.* Simulating spin dynamics with spin-dependent cross sections in heavy-ion collisions[J]. Phys Rev C, 2017, **96:** 044618.
8. Xu J, Chen L W, Li B A. Thermal properties of asymmetric nuclear matter with an improved isospin and momentum-dependent interaction[J]. Phys Rev C, 2015, **91**: 014611.
9. Xu J. Isospin splitting of nucleon effective mass and shear viscosity of nuclear matter[J]. Phys Rev C, 2015, **91**: 037601.
10. Kong H Y, Xia Y, Xu J, *et al.* Reexamination of the neutron-to-proton-ratio puzzle in intermediate-energy heavy-ion collisions[J]. Phys Rev C, 2015, **91**: 047601.
11. Kong H Y, Xu J, Chen L W, *et al.* Constraining simultaneously nuclear symmetry energy and neutron-proton effective mass splitting with nucleus giant resonances using a dynamical approach[J]. Phys Rev C, 2017, **95**: 034324.

Low and Intermediate Energy Heavy Ion Collision Physics

Division of Nuclear Physics

This research field focuses on the following subjects: mechanism of two-proton emission in proton-rich nuclei, resonance state in unstable nuclei, spin dynamics and neutron-proton effective mass splitting in intermediate energy heavy-ion collisions.

Experimental study on structure and exotic radioactivity in unstable nuclei

Two-proton emission is one of the exotic radioactivity modes in nuclei close to the proton dripline. There are three main mechanism, *i.e.*, ^{2}He, three-body democratic and sequential emission. It is significant to study these mechanisms experimentally. We have analyzed the data of proton-proton correlation and two-proton emission for ^{23}Al and ^{22}Mg obtained on the RIPS beamline in RIKEN. The relative momentum and opening angle distributions between two protons from the excited states of ^{23}Al and ^{22}Mg were obtained. The excitation energies of the projectile were constructed from the three-body kinematics. For the odd-Z nucleus ^{23}Al, the sequential decay is overwhelmingly dominant. However, about 30% ^{2}He emission probability was observed clearly in ^{22}Mg at excitation energies around the 14.044 MeV state [1]. By the proton-proton correlation function analysis, it is found that the emission time difference between two protons is quite different for ^{23}Al and ^{22}Mg. The results indicated that the mechanism of two-proton emission from ^{23}Al was dominantly sequential, while that for ^{22}Mg was mainly three-body simultaneous[2]. Based on these results, it is possible to distinguish clearly the mechanism of two-proton emission by investigating the proton-proton momentum correlation function, the two-proton relative momentum, and the opening angle distributions. This work provides the experimental data on the exotic radioactivity in proton-rich nuclei and is significant for the studies on the two-proton emission mechanism in proton-rich nuclei close to the dripline.

The elastic resonance scattering protons decayed from ^{11}B to the ground state of ^{10}Be were measured by using the inverse kinematics at RIBLL beamline in Lanzhou. By comparing with the R-matrix calculations, a state around Ex=14.55 MeV [$J^{\pi}=5/2^{+}$] was observed in the excitation energy of the resonant states. Another state around Ex=15.23 MeV [$J^{\pi}=3/2^{+}$] was seen. These two states are consistent with the existing data. A possible new state with Ex=13.46 MeV was also seen[3].

Studies of spin dynamics and neutron-proton effective mass splitting in intermediate-energy heavy-ion collisions

The study of spin dynamics has been a hot topic in many fields of physics. The spin-orbit coupling is a general interaction existing in the dynamics of relativistic systems. It affects the dynamics of particles with different spins, and this is called the spin hall effect. In nuclei, the nucleon spin-orbit coupling is important in explaining the magnetic number and the shell structure. In recent years, we have been focusing on the effect of nuclear spin-orbit coupling in nuclear reactions, and studying the spin hall effect in heavy-ion collisions. Invited by the Journal of Front. Phys., we wrote a review paper on spin dynamics in heavy-ion collisions, and this was selected as a cover story of the journal[4]. We have also extended the BUU transport theory. Starting from the spin- dependent Boltzman equation, we have obtained the spin-dependent equations of motion from the test-particle method, and this becomes the theoretical foundation of the simulation of spin dynamics[5]. We have applied these equations of motion in the quantum limit[6]. Except for the spin-dependent mean-field potential, recently we have also incorporated the spin-dependent nucleon-nucleon scattering cross section into transport model calculations[7].

Due to the interaction in nuclear medium, nucleons have a smaller effective mass than that in vacuum. In neutron-rich medium, whether neutrons or protons have a larger effective mass has attracted considerable interest. Similar to the nuclear symmetry energy, the neutron-proton effective mass splitting is also an important topic in isospin physics, and it affects the isospin dynamics in nuclear reactions with radioactive beams, properties of neutron-rich nuclei, as well as many phenomena in nuclear astrophysics. Based on an effective momentum-dependent nuclear interaction, we have studied the effect of neutron-proton effective mass splitting on thermodynamical properties[8] and transport properties[9] of neutron-rich nuclear matter, and the neutron/proton ratio in nuclear reactions[10]. Very recently, we have studied the giant resonances of ^{208}Pb nuclei from a dynamical approach, and constrained the nuclear symmetry energy as well as the neutron-proton effective mass splitting based on the corresponding experimental data[11].

Reference

1. Ma Y G, Fang D Q, Sun X Y, *et al.* Different mechanism of two-proton emission from proton-rich nuclei ^{23}Al and ^{22}Mg[J]. Phys Lett B, 2015, **743**: 306.
2. Fang D Q, Ma Y G, Sun X Y, *et al.* Proton-proton correlations in distinguishing the two-proton emission mechanism of ^{23}Al and ^{22}Mg[J]. Phys Rev C, 2016, **94**: 044621.
3. Liu Y D, Ma y G, *et al.* New measurement of the excited states in ^{11}B via elastic resonance scattering of ^{10}Be + *p*. Phys Rev C, 2015, **91**: 044302.
4. Xu J, Li B A, Shen W Q, *et al.* Dynamical effects of spin-dependent interactions in low-and intermediate- energy heavy-ion reactions[J]. Front Phys, 2015, **10**: 102501.
5. Xia Y, Xu J, Li B A, *et al.* Equations of motion of test particles for solving the spin-dependent Boltzmann–Vlasov equation[J]. Phys Lett B, 2016, **759**: 596.
6. Xia Y, Xu J, Li B A, *et al.* Simulating spin dynamics with spin-dependent cross sections in heavy-ion collisions[J]. Nucl Phys A, 2016, **955**: 41.
7. Xia Y, Xu J, Li B A, *et al.* Simulating spin dynamics with spin-dependent cross sections in heavy-ion collisions[J]. Phys Rev C, 2017, **96:** 044618.

8. Xu J, Chen L W, Li B A. Thermal properties of asymmetric nuclear matter with an improved isospin and momentum-dependent interaction[J]. Phys Rev C, 2015, **91**: 014611.
9. Xu J. Isospin splitting of nucleon effective mass and shear viscosity of nuclear matter[J]. Phys Rev C, 2015, **91**: 037601.
10. Kong H Y, Xia Y, Xu J, *et al*. Reexamination of the neutron-to-proton-ratio puzzle in intermediate-energy heavy-ion collisions[J]. Phys Rev C, 2015, **91**: 047601.
11. Kong H Y, Xu J, Chen L W, *et al*. Constraining simultaneously nuclear symmetry energy and neutron-proton effective mass splitting with nucleus giant resonances using a dynamical approach[J]. Phys Rev C, 2017, **95**: 034324.

中子物理实验装置（白光中子源）

核物理研究室

中子物理实验装置（又称为光中子源，Photo Neutron Source, PNS），2015 年中子物理仿真实验装置的设备调试工作基本完成；对加速器输运线及实验终端区域，TOF 探测器进行了局部屏蔽，在低功率运行条件下满足辐射防护的要求，实验厅内伽马剂量降低了一个量级；完善了中子、伽马射线的形状甄别，完成了数据获取与自动换靶控制软件的结合，实现了总截面测量数据的全自动获取，完成了探器的局部屏蔽的设计和部分安装；完成了总截面验证实验测量，获得了 C、Be、In 靶等总截面测量数据，实验测量结果和 ENDF 评价数据库符合一致；2015 年中子物理仿真实验装置全年运行时间近 500 h。

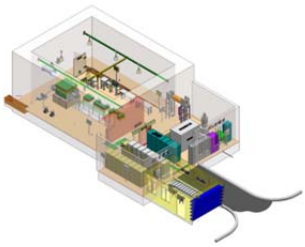

图 1　中子物理实验装置

1　实验终端的调试及数据测量

实验终端经过仔细调试和刻度，Digitizer 获取系统获得的 TOF 飞行时间谱，如图 2 所示，目前的 Digitizer 获取具有简单快速，以及和反应靶控制相结合的全自动获取系统[1−4]。

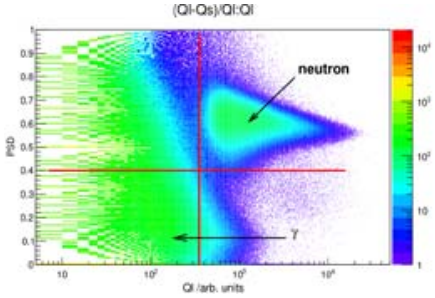

图 2　TOF 探测器的中子/伽马甄别

2　实验刻度及 GEANT4 模拟分析

光中子源的中子能谱是连续的，中子能量通过中子飞行时间测量得到，利用吸收片的中子吸收峰刻度能量、刻度飞行时间、计算等效飞行距离和扣除实验本底等。实验采 In (0.05 mm，99.99%，1.457 eV)，Cd (0.125 mm，99.99%，0.177 eV)，Ag (0.1 mm，99.95%，5.19 eV)，Co (0.05 mm，99.9%，132 eV)，Block-off (12.8 cm，5% Boron loaded PE)[5−6]，测量结果如图 3 所示。

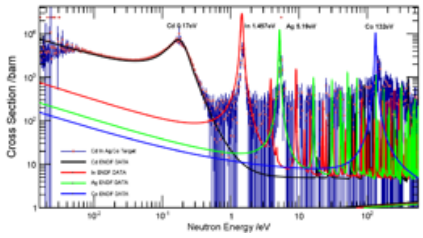

图 3　Cd/In/Ag/Co 吸收片实验测量

3　实验厅屏蔽改进

中子物理仿真实验装置偏转段电子输运线作了屏蔽，并加强了电子入口处的屏蔽，增加了 10 cm 含硼聚乙烯遮挡；实验区组合屏蔽体将采用大块含硼聚乙烯材料加水泥块体组合的形式，现场用固定支架固定；TOF 探测器的局部屏蔽。

图 4　TOF 中子探测器的屏蔽

参考文献

1. 常乐, 刘龙祥, 王宏伟, 等. EJ339A 俘获门控中子探测器双脉冲特性[J], 核技术, 2015, **38**: 050403.
2. 常乐, 刘应都, 杜龙, 等. EJ301 液体闪烁体探测器的波形甄别和能量刻度[J], 核技术, 2015, **38**: 020501.
3. 王宏伟，陈金根，蔡翔舟，等. 15 MeV 电子直线加速器驱动的光中子源研究进展[C]. 中国核科学技术进展报告(第 4 卷), 中国核学会 2015 年会.
4. 刘龙祥, 王宏伟, 马余刚, 等. 波形数字采样器测量中子飞行时间谱[C]. 中国核科学技术进展报告(第 4 卷), 中国核学会 2015 年会.
5. 朱亮, 刘龙祥, 王宏伟, 等. 光中子源上吸收片功能研究[J], 原子核物理评论, 2016, **33**: 251−256.
6. Liu L X, Wang H W, Ma Y G, *et al.* Neutron time-of-ight spectroscopy measurement using a waveform digitizer[J], Chinese Physics C, 2016, **40**: 056202.

Neutron Physics Experimental Facility (White Light Neutron Source)

Nuclear Physics Division

The neutron physics experimental facility, a Photo Neutron Source (PNS), some time call as White Light neutron Source. Equipment installation and primarily commissioning basically finished in 2015. The partly shielding for transport line of accelerator and experimental zone, and Time-Of-Flight (TOF) neutron detector shielding decreased the background dose rate to about one order of magnitude, new DAQ combined with the target control code, finished the total neutron cross section test measurement of calibrated north filter and C, Be, In element target with this DAQ system, and get well agreement with ENDF/B-VII evaluated Lib data. The total run time is nearly 500 h in 2015 year.

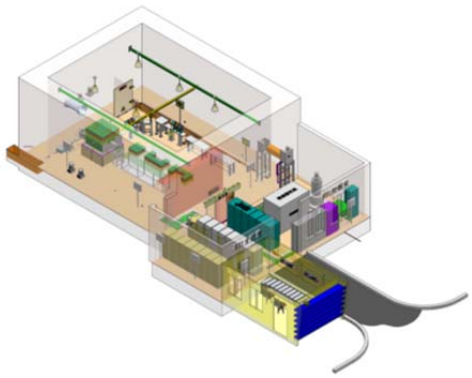

Fig.1 Photo of neutron physics experimental facility

1 Commissioning and Data Measurement

The experimental device have been tested and calibrated, included the neutron detector, DAQ system, reaction target control system, neutron production target temperature control system and CCD camera, and so on. Fig.2 shows the neutron/gamma discrimination spectrum. New digitizer DAQ system have a perfect characters of auto record data file and change the target in a setting time[1–4].

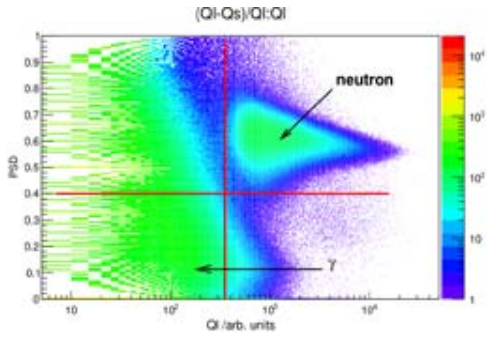

Fig.2 n/γ discrimination of TOF detector

2 Notch filter calibration and GEANT4 Simulation

The neutron energy spectrum in continues and neutron energy can be obtained from the TOF signal in a effective flight path about 5.8 m, some notch filter be used as calibrator, for example: In (0.05 mm, 99.99%, 1.457 eV), Cd (0.125 mm, 99.99%, 0.177 eV), Ag (0.1 mm, 99.95%, 5.19eV), Co (0.05 mm, 99.9%, 132 eV) and Block-off target (12.8 cm, 5% Boron loaded PE)[5–6].

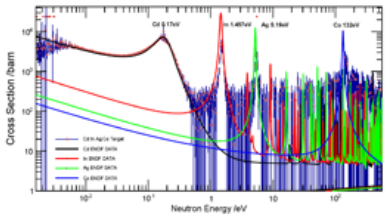

Fig.3 Cd/In/Ag/Co notch filter Calibration

3 Improvement of Shielding

The transport line and entrance of electron beam, add another 10 cm thickness Boron loaded Polythene for radiation protection, and the detector box and L shape shielding wall be used in for reduced the neutron and gamma background.

Fig.4 The neutron detector box design

Reference

1. Chang L, Liu L X, Wang H W, *et al.* Double pulse waveform spectrum of EJ339A capture-gated neutron detector[J], Nuclear Techniques, 2015, **38**: 050403.
2. Chang L, Liu Y D, Du L, *et al.* Pulse shape discrimination and energy calibration of EJ301 liquid scintillation detector[J]. Nuclear Techniques, 2015, **38**: 020501.
3. Wang H W, Chen J G, Cai X Z, *et al.* Establishing the Photo-neutron Facility Driven by 15 MeV Electron LINAC in sinap[C], Progress Report on China Nuclear Science & Technology, 2015, 70-74.
4. Liu L X, Wang H W, Ma Y G, *et al.* neutron time of flight spectrum measurement with a waveform digitizer[C], Progress Report on China Nuclear Science & Technology, 2015, 75-79.
5. Zhu L, Liu L X，Wang H W, *et al.*, A Study of the Filter Functions Used in the Photo-neutron Source, Nuclear Physics Review，2016, **33**: 308-314.
6. Liu L X, Wang H W, Ma Y G, *et al.* Neutron time-of-ight spectroscopy measurement using a waveform digitizer，Chinese Physics C, 2016, **40**: 056202.

应用理论物理研究

计算物理组

应用理论物理研究组从事理论物理学与生物学的交叉研究，主要是纳米生物学和纳米尺度界面水的特性研究。本组以上海光源和我所重要研究方向为导向，利用长期积累的微纳尺度界面水性质等研究基础，与相关实验组密切结合开展应用基础理论研究，并建设相关的模拟计算平台，为实验提供模拟计算支持。另外，与所内其他课题组合作，目前已取得了部分科研成果。

电解质溶液提高含芳香环氨基酸和多肽的溶解度的研究

中国科学院上海应用物理所石国升博士、赵红卫博士、方海平研究员和澳大利亚 ANSTO 的 Dehong Yu 博士等研究发现：色氨酸、色氨酸-苯丙氨酸和苯丙氨酸-苯丙氨酸等芳环氨基酸和多肽在氯化铜溶液中的溶解度可以达到是其纯水中的 2~5 倍。

通过理论模拟计算发现：水合金属阳离子与芳香环之间的离子-π 作用依然足够强，这导致芳香环氨基酸容易吸附水合离子，显著增加芳香环结构的亲水性，从而增加其溶解度（图 1）。基于以上基础，课题组设计了系列实验，观测到了含芳香环氨基酸和多肽在氯化铜等二价离子溶液中的显著增加。他们进一步用中子散射证实含芳香环氨基酸在氯化铜溶液中水分子亲和力增强，用同步辐射软 X 射线吸收谱、太赫兹以及红外证实含芳香环氨基酸没有变性，用荧光和紫外证实了其中离子-π 作用的存在。

这个工作的最重要贡献在于改变了人们对芳香环氨基酸不溶于金属电解质溶液的传统认识，提出了水环境下金属阳离子与芳香环之间离子-π 作用的新机制发现将唤起人们对电解质溶液中疏水相互作用的重新认识，提供了理解金属离子生理功能和毒性的新观点，有望在理论模拟蛋白折叠、分析蛋白生理条件下的功能、药物分子设计等方面有重要的启迪作用。相关研究工作近期发表在美国物理学会的 Phys Rev Lett[1]。

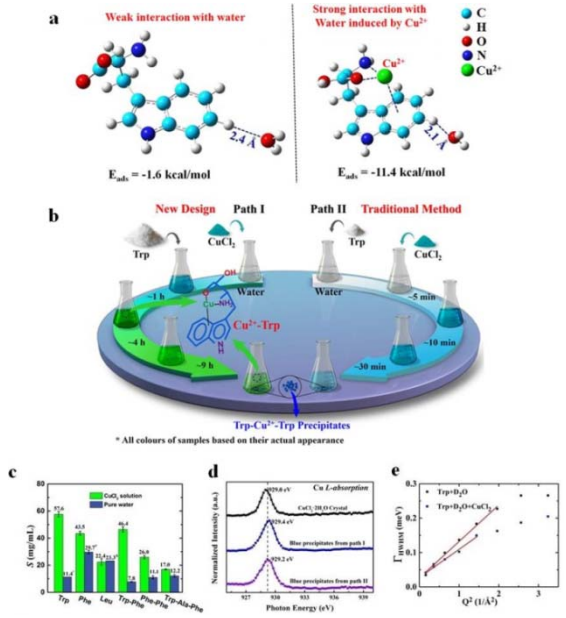

图 1 芳香环氨基酸和多肽在电解质溶液中溶解度意想不到的显著增加

抗冻蛋白对冰晶成核的 Janus 效应

抗冻蛋白是生活在寒冷区域的生物经过长期自然选择进化产生的一类用于防止生物体内结冰而导致生物体死亡的功能性蛋白质。对于抗冻蛋白抗冻机制的研究有助于揭开冰晶成核、生长和冰晶形貌调控的分子层面的机理。但是，科研人员对抗冻蛋白在调控冰晶成核的机制一直有争议。

中国科学院化学所的王健君研究员课题组与中国科学院上海应用物理所的王春雷副研究员、方海平研究员和新疆大学的马纪教授合作，根据抗冻蛋白的冰结合面(ice-binding face)和非冰结合面(non-ice-binding face)具有截然不同官能团的特性，将抗冻蛋白定向固定于固体基底，选择性地研究了抗冻蛋白冰结合面与非冰结合面对冰核形成的影响。研究表明抗冻蛋白的不同面对冰核的形成表现出完全相反的效应：冰结合面促进冰晶成核，而非冰结合面抑制冰晶成核。通过分子动力学模拟进一步研究了抗冻蛋白的冰结合面和非冰结合面界面水的结构，发现了冰结合面上羟基和甲基有序间隔排列使得冰结合面上形成类冰水合层，从而促进冰核生成；而非冰结合面上存在的带电荷侧链及疏水性侧链，使得非冰结合面上的界面水无序，从而抑

制冰核形成。揭示了抗冻蛋白对冰成核“Janus”效应分子层面的机制。该研究大大加深了人们对抗冻蛋白分子层面防冻机制的理解，同时对仿生合成防覆冰材料和低温器官保存材料有着重要的指导意义。相关结果已发表在《美国科学院院报》[2]。

大统一模型揭示配体金纳米团簇生长机制

长期以来，配体金纳米团簇因其独特的结构和物理化学性质以及在催化、纳米技术及生物医学等领域广泛的应用前景得到了广泛关注。近 10 年来，随着一系列大尺寸的配体金纳米团簇被成功结晶，人们试图提出理论模型解释其结构稳定性，但并未获得普遍成功。

中国科学院上海应用物理研究所的许文武博士、朱倍恩博士在高嶷研究员指导下，与美国内布拉斯加大学林肯分校和中国科技大学的曾晓成教授合作，建立了一个普适模型，实现了对迄今为止报道的所有 71 个配体金纳米团簇的基本理解。该模型认为每个金原子有三个不同的电子价态，三个或者四个金原子可以满足 2 电子的满壳层电子态，从而构成基本的结构单元（三角形 Au3 和四面体 Au4）。当这些基本单元堆积在一起时，就形成了结构各异的稳定的金纳米团簇。该模型的建立，有力的证明了金纳米团簇的结构和生长遵循着基本的化学规律，从而为进一步理解金以外的金属纳米团簇打开了新的思路。由于这个模型非常类似于粒子物理中的基本粒子模型（即夸克有不同的“味”，三个夸克构成质子和中子，并进一步构成原子核和原子），所以被称为“大统一模型”(Grand Unified Model)。研究人员利用该模型预测了一系列高度稳定的金团簇，从而为实现基于化学规则的纳米金团簇可控合成提供了基础。相关研究工作已发表在 Nature Communation[3]。

水蒸汽环境下硅量子点的奇异荧光机制

当前，硅量子点由于其价格便宜、无毒、生物相容性和硅基电子市场巨大而引起了广泛的研究。而水作为无处不在的环境，大量实验数据显示水环境对硅量子点的光学特性具有明显的影响。

中国科学院上海应用物理研究所水科学与技术研究室的博士生杨金荣在高嶷研究员和方海平研究员的指导下，运用含时密度泛函理论计算，解释了一个关键问题：在水环境下水分子如何通过影响硅量子点的电子结构，进而导致了其荧光特性的奇异变化。此外，从分子尺度理解了水吸附在硅量子点的荧光现象，揭示了水分子与硅量子点之间的相互作用对基于硅涂层的光电子器件具有重要的影响，同时将进一步促进硅量子点在荧光标记和太阳能电池等方面的应用。相关研究工作已发表于《物理化学快报》[4]。

界面水的微观性质研究取得系列进展

饮用水短缺、土壤保湿、植物抗旱、生物分子功能的理解以及药物分子的水溶性等都是目前工业社会面临的问题，因此理解微观尺度水的行为及其基本性质具有重要的意义。中国科学院上海应用物理研究所水科学与技术研究室在相关领域取得系列进展，三篇论文发表在《物理评论快报》[5–7]，英国的 Chemistry World 就其中的部分工作进行了专门报道。

海水脱盐是解决水资源危机的重要手段之一。尽管现在已有商业化的过滤技术，但是如何降低能耗依然是大问题。自 2005 年以来，多个实验表明：碳纳米管膜具有很好的水透过能力，因而人们预期碳纳米管可以作为性能极佳的海水脱盐膜材料。至今 10 年过去，尽管碳纳米管膜的合成制造技术已经有了极大的提高，然而并没有相关实验表明碳纳米管膜具有海水脱盐效果。博士生刘健、石国升博士和方海平研究员等，采用经典力场与量子力学计算结合的手段，提出造成这一困局的关键是离子会阻塞碳纳米管。造成这种阻塞的关键原因是离子与碳纳米管中的芳香环之间存在 20 世纪 80 年代才发现的阳离子-p 相互作用。研究者发现了即使离子水合以后仍然与碳纳米管之间存在着强的阳离子-p 相互作用，并建立了相关计算软件。基于此物理机理，研究人员提出了两种可能的改进方案，即管口修饰饱和基团以及施加电场，两者都可以在保持 100% 的脱盐率的条件下，将碳纳米管在盐水中的水渗透性能提高到接近(>60%)其在纯水中的性能。该研究工作被英国的 Chemistry World 以“纳米碳管海水脱盐膜研究可以重回正轨”为题进行了专门报道(Nanotube desalination could be put back on track)。

水分子在细胞组织中占据比例高达 70%，在蛋白、核酸、生物膜结构的形成、稳定以及功能的实现中发挥着重要作用，然而人们对水分子如何具体发挥生物功能却知之甚少。即使对于由羧酸为终端的烷链自组装而成的二维仿生膜表面，在 25 年以

来的相关理论和实验研究中，人们也无法理解其表面水的行为和性质。博士生郭盼、方海平研究员等与扬州大学物理科学与技术学院的涂育松教授合作，运用量子力学计算和分子动力学模拟研究，发现在室温环境下水分子能够嵌入这个自组装膜表面，与表面的羧酸形成完整稳定的复合结构,这种结构增强了仿生膜的稳定性并使原本超亲水表面展现显著的疏水特性。该项研究是国际上首次发现水分子主动嵌入并形成仿生表面复合结构，解决了以羧酸为终端的烷链自组装仿生表面水性质这个长达 25 年的谜团。更重要的是，该工作研究的二维自组装仿生膜与真实生物分子（包括生物膜）有着高度的相似性，此项研究提供一个理解“生物水”以及生物水可能承载生物功能方面的新视角。

自然界中生物和材料表面，比如植物表面、土壤表面以及细菌表面等普遍存在少量甚至纳米尺度的水。这些表面绝大多数的亲疏水性质并不均一，通常是亲水和疏水区域相间的结构。因此表面亲疏水区域相间结构上的少量水蒸发对植物的抗旱，土壤的沙化以及细菌的生存等产生决定性的影响。万荣正博士，方海平研究员等与浙江农林大学理学院的周国泉教授合作，运用分子动力学模拟方法，将纳米尺度三角形亲疏水区域相间结构作为模型研究了纳米尺度水在其表面的蒸发情况，发现在一些特定亲疏水区域相间表面，纳米尺度水的蒸发比所有均一性质表面都快。这一快速蒸发的关键在于亲疏水边界的扩散行为，因此亲疏水区域相间表面上水的蒸发速度会与亲疏水区域边界的总长度相关。此项研究深入了对动植物非均一性质表面上纳米尺度水蒸发的理解。

参考文献

1. Shi G S, Dang Y R, Pan T T, *et al*. Unexpectedly enhanced solubility of aromatic amino acids and peptides in an aqueous solution of divalent transition-metal cations[J]. Physical Review Letters, 2016, **117**: 238102.
2. Liu K, Wang C L, Ma J, *et al*. Janus effect of antifreeze proteins on ice nucleation[J]. Proc Natl Acad Sci USA, 2016, **113**: 14739.
3. Xu W W, Zhu B E, Zeng X C, *et al.* A grand unified model for liganded gold clusters[J]. Nat Commun, 2016, 7: 13574.
4. Yang J R, Fang H P, Gao Y. Effect of water adsorption on the photoluminescence of silicon quantum dots[J]. J Phys Chem Lett, 2016, **7**: 1788.
5. Liu J, Shi G S, Guo P, *et al*. Blockage of water flow in carbon nanotubes by ions due to interactions between cations and aromatic rings[J]. Phys Rev Lett, 2015, **115**: 164502.
6. Guo P, Tu Y S, Yang J R, *et al*. Water-COOH composite structure with enhanced hydrophobicity formed by water molecules embedded into carboxyl-terminated self- assembled monolayers[J]. Phys Rev Lett, 2015, **115**: 186101.
7. Wan R Z, Wang C L, Lei X L, *et al*. Enhancement of water evaporation on solid surfaces with nanoscale hydrophobic-hydrophilic patterns[J]. Phys Rev Lett, 2015, **115**: 195901.

Theoretical Physics for Nanobiology and Interfacial Water

Group of Computational Physics

The group is engaged in interdisciplinary studies on theoretical physics and nanobiology, focusing on molecular dynamics simulation and other computational studies on biomolecules and interfacial water. These provide theoretical assistance to synchrotron radiation studies and other experimental research programs at SINAP. Collaborating well with the experimental groups, the group has made remarkable progresses.

Improvement of solubility of aromatic ring amino acids and peptides by electrolyte solution

Dr. Guosheng Shi, Dr. Hongwei Zhao and Prof. Haiping Fang from Shanghai Institude of Applied Physics, Chines Academy of Science (CAS), and Dehong Yu from ANSTO investigated the unexpectedly enhanced solubility of aromatic amino acids and peptides in an aqueous solution of divalent transition-mental cations, which could reach about 2~5 times the solubility in pure water.

Theoretic studies showed that the strong cation-π interaction between hydrated mental ions and aromatic rings enhance the significantly the water affinity of aromatic amino acids and peptides, which resulted in the enhancement of their solubility. Based on these results, the research group designed series of experiments to observe the unexpectedly enhanced solubility of aromatic amino acids and peptides in an aqueous solution of divalent transition-mental cations. They further confirmed the water affinity of aromatic amino acids and peptides in $CuCl_2$ solution by neutron scattering and the unchangeable property of precipitates by synchrotron radiation soft X-ray absorption spectrum, THz spectra and infrared spectra and the existence of cation-π interaction by fluorescence and UV adsorption spectra.

This work make important contribution to change the traditional understanding of the insolubility of aromatic amino acids in metal electrolyte solution and proposed the new mechanism of cation-π interaction between metal cation and aromatic amino acids in aqueous solution. Our findings enrich the view of biomolecular solubility in aqueous electrolyte solution and provide new insights for the understanding of physiological functions of multivalent metal ions and are expected to play important roles in the functions of proteins, such as protein folding, maintaining protein structure, and protein-ligand interactions. This work has been published on Phys. Rev. Lett. 2016,117,238102[1].

Janus effect of antifreeze proteins on ice nucleation

Antifreeze proteins (AFPs) protect a broad range of biological organisms inhabiting subzero environments via controlling ice formation. Since the discovery of AFPS in 1960s, a vast body of experimental and theoreticalworkshavebeen undertaken to investigate the molecular level mechanism of the AFPs in controlling ice formation. However, the exact effect of AFPs on ice nucleation is under intense debates.

Based on the fact that ice-binding face (IBF) and non-ice-binding face (NIBF) of the AFPS possess distinct functional groups, Prof. Jianjun Wang from Institute of Chemistry, Chinese Academy of Sciences(CAS), Dr. Chunlei Wang and Prof. Haiping Fang from Shanghai Institute of Applied Physics, CAS, and Prof. Ji Ma from Xinjiang University investigated the effect of IBF and NIBF of AFPs on ice nucleation by selectively tethering IBF and NIBF of AFPs to solid substrates[2]. The experimenta lresults revealed that the IBF of AFPs facilitates ice nucleation, whereas the NIBF depresses ice nucleation.

The results of molecular dynamics simulations showedthat there are distinct molecular hydrationwater structures around IBF and NIBF. For the IBF of AFPs, water molecules form ice-like interfacialwater structure due to the special arrangement of hydrophobic methyl and hydrophilic hydroxyl groups on the IBF.In strong contrast, almost no ice-like water structure is formed on the NIBF, which is possibly due to the absence of regular hydrophobic/ hydrophilic patterns as well as the existence of charged groups and bulky hydrophobic groups. This helpsestablish the molecular level understanding of AFPs in tuning ice nucleation

Revealing the growth mechanism of liganded gold nanoclusters

For a long time, liganded gold nanoclusters have attracted extensive attention due to their unique structure and physicochemical properties, as well as their wide applications in catalysis, nanotechnology and biomedicine. In the recent 10 years, with the success of crystallization of a series of large size gold nanoclusters, attempts have been made to explain the structural stability of the gold nanoclusters, but they have not been generally successful.

Dr. Xu Wenwu and Dr. Zhu Bienen at the Shanghai Institute of Applied Physics, under the guidance of Prof. Gao Yi, cooperated with Prof. Zeng Xiaocheng at the University of Nebraska at Lincoln and the University of Science and Technology of China, established a universal model to achieve a basic understanding of all the 71 ligand gold nanoclusters reported so far. The model considers that the gold atom has three different valence states, and three or four gold atoms can satisfy the electronic states with two electrons shell closure, which constitute the basic structural unit (triangular Au3 and tetrahedral Au4). When these basic units are stacked together, stable gold nanoclusters with different structures are formed. The establishment of the model strongly prove that the structure and growth of gold nanoclusters follow the basic chemical laws, which opens a new way for the further understanding of metal nanoclusters except gold nanoclusters. Since this model

is very similar to the basic particle model in particle physics, such as quarks have three different "flavor", three quarks or four quarks constitute nuclei, and further constitute the nucleus and atoms, it is termed Grand Unified Model. The researchers used the model to predict a series of highly stable gold clusters, which provides a basis for the realization of controlled synthesis of nano-gold clusters based on chemical rules. The results of the research have been published in the journal of Nature Communication. (A grand unified model for liganded gold clusters, Nat. Commun. 2016,7, 13574[3].)

Singular photoluminescence emission of water vapor adsorbed on Si QDs

Silicon quantum dots (Si QDs) are under intense investigation because of their inexpensive, nontoxic, biocompatible and huge silicon electronics market. Optical properties of Si QDs are strongly influenced by circumjacent surface-adsorbed molecules, which would highly affect their applications in electronics, biology and solar cell. However, water, as the ubiquitous environment, has not received enough attention yet.

Based on the TDDFT method, Jinrong Yang, Haiping Fang and Yi Gao from Shanghai Institute of Applied Physics have resolved a critical fundamental question for Si QDs is whether and how the electronic structure and hence the PL properties is altered on the nanoscale, in particular, with the presence of water. Our study of the detailed water molecule clusters effect on the fluorescence of Si QDs not only provides new explanations for the fluorescence mechanism of Si QDs at a particular size, but also shed light on the Si-water interaction that is important for the development of optical devises based on Si coated surfaces. This work was published in J. Phys. Chem. Lett. 2016, 7, 1788[4].

A series of progress in the study of the microscopic properties of interface water

Seawater desalination is one of the major methods to solve the water crisis. Even the desalination technologies have been commercialized now, unfortunately, those technologies are still too expensive and inefficient. Filtering nanotechnology based on nanotube is believed to be a potential approach in producing clean and affordable water. Along with this direction, great efforts have been made in the past ten years including that an ultrafast water flow rate through carbon nanotube (CNT) has been actually observed by experiment since 2005 and numerical simulations have shown that CNT is capable of rejecting ions while allowing fast water flow. However, up to now, there is still no experiment demonstrating that the CNT is adequate for desalination even though the fabrication technology of CNT membranes has been greatly improved.

Recently, Dr. Jian Liu, Dr. Guosheng Shi, Prof. Haiping Fang and other scientists at SINAP show that water flow in CNT will be blocked by cations in solutions since cations are bound at the entrance or trapped in the interior of the CNT by combining classical simulations with density functional theory calculations. The key to this behavior is the strong non-covalent interactions between cations in solution and aromatic rings in CNT. Based on this understanding, new methods are proposed to prevent blocking of CNT by ions while allowing ultrafast water flow with ion rejection. These findings provide new insight for the CNT-based water desalination and purification, individual ions detecting and ions selective transporting. The results have been published in Physical Review Letters (PRL 115, 164502 (2015))[5]. This work has been specially reported as a research in Chemistry World with a title “Nanotube desalination could be put back on track”.

Water is essential to life, as it constitutes seventy percent of the content of all living cells, within the structural formation, stability and function of proteins, nucleic acids and membranes, but it still remains little known how water engages, interacts with biomolecules, and even carries the biological functionalities. Even for the two dimensional biomimetic surfaces, e.g., the carboxyl-terminated self-assemble monolayers (COOH-SAMs), its interfacial behaviors of water can always not be understood well, though with numerous relevant experimental and theoretical efforts over the past 25 years.

SINAP researchers Pan Guo and Prof. Haiping Fang, collaborating with Prof. Yusong Tu at Yangzhou University, have recently combined molecular dynamics simulations and quantum mechanics calculations, and succeeded in demonstrating that water molecules can be embedded into the COOH matrix to form a composite structure on COOH-SAMs at room temperature. This composite structure enables COOH-SAMs to behave like a stable and integral surface with an integrated hydrogen bond network inside, reduces the hydrogen bonds with the water above to make an “apparent” enhancement of the hydrophobicity of COOH-SAM, though with super hydrophilic COOH groups. For the first time water is found to be able to embed into the surface and participate in the arrangement of the composite structure, and as inseparable part enclosed within this composite structure, embedded water becomes determinative to the wetting characteristics on COOH-SAMs. The results resolve a long-standing puzzle on seemingly contradictory experimental observations on COOH-SAMs in basic surface physics. More importantly, since the surface of COOH-SAMs with the flexible COOH-terminated alkyl chains is much analogous to a wide variety of biological surfaces, including membranes, and the COOH group itself occurs widely in biomolecules as a main component, the finding may provide a new perspective in understanding of how water becomes an active participant in interacting with biomolecules with finely tuning adaptation for the biological processes during the cell life and in stabilizing the surface of biological systems. The above results have been published in Physical Review Letters (PRL 115, 186101 (2015))[6].

There is usually a tiny and even nanoscale volume of water on various biological and material surfaces, such as the surfaces of leaf, soil and even bacteria, and most of these surfaces have hydrophobic-hydrophilic patterns. The evaporation of nanoscale water on these surfaces will cause distinct effects, e.g., plant withering, desertification, and bacterial sterilization. Dr. Wan Rongzheng and Researcher Fang Haiping *et al*. cooperated with Prof. Zhou Guoquan from Zhejiang A&F University, employed a nanoscale triangular hydrophobic-hydrophilic pattern as a model to study the evaporation of water on a patterned surface by molecular dynamics (MD) simulations[7]. They showed that the evaporation of a na-

noscale volume of water from certain hydrophobic-hydrophilic patterns is faster than that from any surface with uniform wettability. The key to this phenomenon lies in the diffusing of water near pattern boundaries. Thus, the evaporation rate of nanoscale water on patterned surface is related to the total length of pattern boundaries. These findings expand the fundamental understanding of nanoscale water evaporation on biological patterned surface.

Reference

1. Shi G S, Dang Y R, Pan T T, *et al*. Unexpectedly enhanced solubility of aromatic amino acids and peptides in an aqueous solution of divalent transition-metal cations[J]. Physical Review Letters, 2016, **117**: 238102.
2. Liu K, Wang C L, Ma J, *et al*. Janus effect of antifreeze proteins on ice nucleation[J]. Proc Natl Acad Sci USA, 2016, **113**: 14739.
3. Xu W W, Zhu B E, Zeng X C, *et al*. A grand unified model for liganded gold clusters[J]. Nat Commun, 2016, 7: 13574.
4. Yang J R, Fang H P, Gao Y. Effect of water adsorption on the photoluminescence of silicon quantum dots[J]. J Phys Chem Lett, 2016, **7**: 1788.
5. Liu J, Shi G S, Guo P, *et al*. Blockage of water flow in carbon nanotubes by ions due to interactions between cations and aromatic rings[J]. Phys Rev Lett, 2015, **115**: 164502.
6. Guo P, Tu Y S, Yang J R, *et al*. Water-COOH composite structure with enhanced hydrophobicity formed by water molecules embedded into carboxyl-terminated self- assembled monolayers[J]. Phys Rev Lett, 2015, **115**: 186101.
7. Wan R Z, Wang C L, Lei X L, *et al*. Enhancement of water evaporation on solid surfaces with nanoscale hydrophobic-hydrophilic patterns[J]. Phys Rev Lett, 2015, **115**: 195901.

太赫兹技术及应用研究

水科学 太赫兹实验组

本组主要从事太赫兹技术及其应用基础研究工作。利用太赫兹光谱对不同物质结构和弱相互作用进行光谱探测，开展太赫兹技术在水的微观结构和动力学方面的研究工作。发展和完善太赫兹实验室建设，以满足不同领域包括固体、液体和气体等样品的探测。

生物分子的太赫兹探测

物质在太赫兹波段包含有丰富的物理化学信息。利用太赫兹时域光谱技术能够非接触灵敏探测获得不同物质在太赫兹低频区域的信息。不同组成和结构的色氨酸及其衍生物在太赫兹波段呈现特有的指纹图谱，利用这些特征谱能够有效揭示分子间氢键、范德华力等弱相互作用，以及晶格和声子振动，有助于加深理解生物分子结构特点，该技术在生物无标记探测和医药的在线检测中具有重要的应用前景[1-3]。

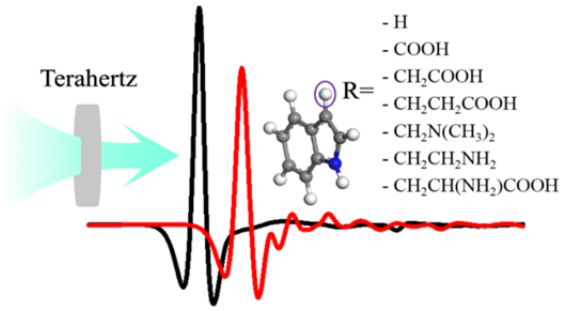

图 1 太赫兹对不同物质结构具有敏感响应

受限空间水的太赫兹响应

受限空间水在生物、化学及能源催化等方面发挥独特的作用，因此理解水的微观结构和动力学具有重要的意义。水在太赫兹波段具有强吸收。研究发现在太赫兹电磁场中，受限于碳纳米管中的水，在界面不同方向上的氢键分布明显不同，这种各向异性会影响氢键网络动力学，进而带来不同方向上介电弛豫的差异[4]。

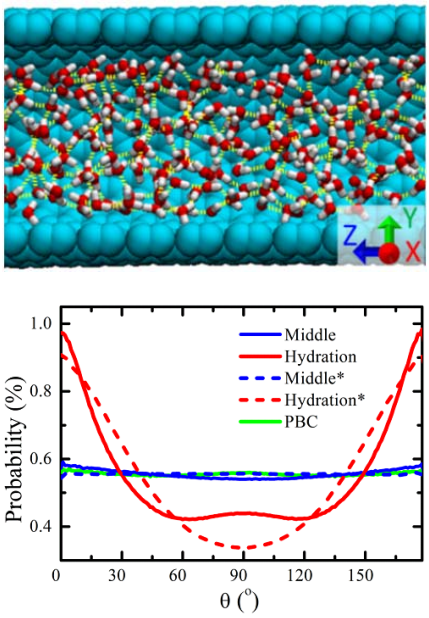

图 2 （上）碳纳米管中的水示意图，(下)受限在不同碳管和一定周期边界条件 PBC 中水氢键的取向分布.

太赫兹超材料传感探测

太赫兹波段水的吸收，影响到溶液体系的探测。太赫兹超材料对周围介质介电环境改变能够产生敏感响应。利用太赫兹超材料诱导电磁透明，实现了水和有机 1,4 二氧六环混合溶液的定量探测与分析，提示能够用于太赫兹生物传感检测[5]。

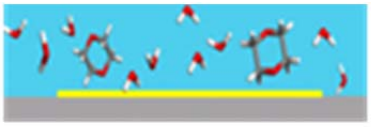

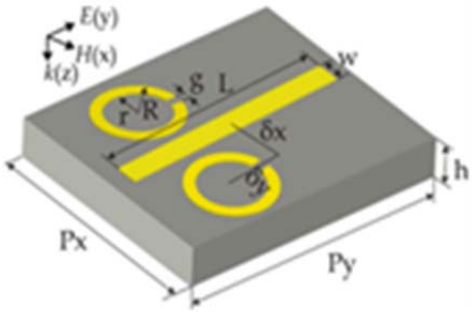

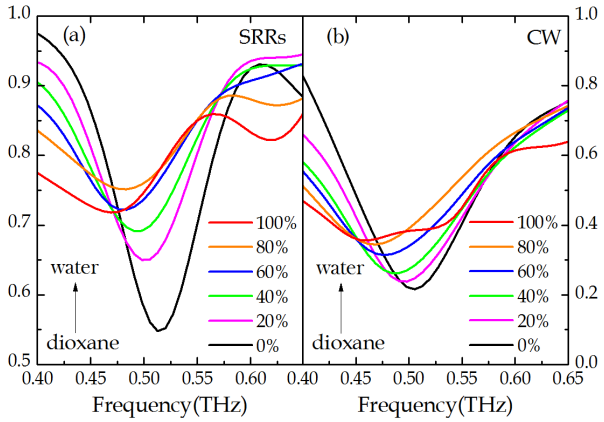

图 3 （上） EIT 超材料传感器；（下）水/二氧六环混合体系的太赫兹透射信号 (a) SRRs (b) CW.

太赫兹实验室建设

2015−2016 年，在中国科学院修缮仪器设备项目支持下，建设完成：1) 一套宽频太赫兹红外光谱仪（图 4），带宽 0.1~18 THz，动态范围>60 dB，频谱分辨率<2 GHz。2) 一套太赫兹时域光谱及成像装置（图 5），带宽 0.5~7 THz，动态范围>60 dB，频谱分辨率 1.9 GHz，成像分辨率~200 μm。

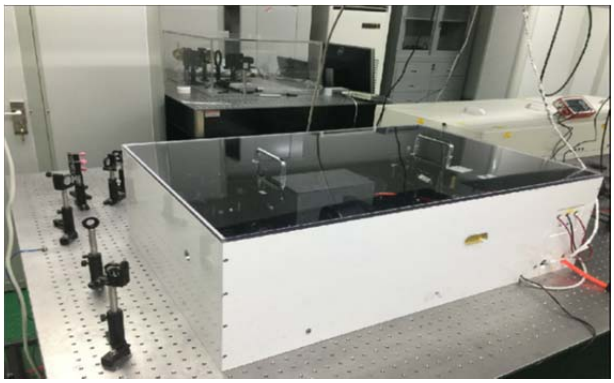

图 4 太赫兹红外光谱仪

图 5 太赫兹时域光谱及成像装置

参考文献

1. Dang Y R, Li S P, Liu H, *et al*. Low-frequency vibrations of indole derivatives by Terahertz time-domain spectroscopy[J]. Journal of Electronic Science and Technology, 2016, **14**(4): 329−336.
2. Li S X, Yang J Q, Zhao H W, *et al*. Terahertz time-domain spectroscopy and quantitative analysis of metal gluconates[J]. Applied Spectroscopy, 2015, **69**(1): 52−57.
3. Shi G S, Dang Y R, Pan T T, *et al*. Unexpectedly enhanced solubility of aromatic amino acids and peptides in an aqueous solution of divalent transition-metal cations[J]. Physical Review Letters, 2016, **117**: 238102.
4. Qi W P, Zhao H W. Hydrogen bond network in the hydration layer of the water confined in nanotubes increasing the dielectric constant parallel along the nanotube axis[J]. The Journal of Chemical Physics, 2015, **143**(11): 114708.
5. Li S X, Zhao H W, Han J G. Terahertz metamaterial sensor based on electromagnetically induced transparency effect[J]. Physical Review Letters, 2015, **13**(2): 117−121.

Terahertz Technique and Applications

THz Experimental Group

The group is engaged in the studies on terahertz (THz) technique and its applications. THz time- domain spectroscopy was applied to investigate the structures and interactions of biomolecules. The studies of microstructure and dynamics of water molecules by THz spectroscopy were also carried out. We have built and improved the THz spectroscopy laboratory to meet the needs of various fields including the detection of solid, liquid and gas samples.

Terahertz detection of biomolecules

Substances contain a wealth of physicochemical information in the THz range. The use of THz time-domain spectroscopy technology can be non-contact sensitive detection of different substances. The tryptophan and its derivatives with different compositions and structures show unique THz fingerprints. These characteristics can effectively reveal the weak interactions such as hydrogen bond and van der Waal's force as well as lattice and phonon vibration. The study can help understanding of the structure and interaction of biomolecules. THz spectroscopy has important applications in marker-free probe of biomolecules and on-line detection of medicine[1-3].

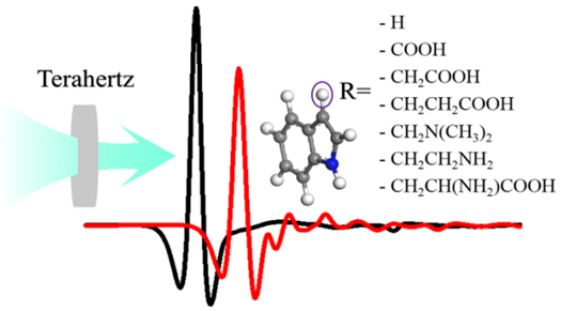

Fig.1 THz spectroscopy has a sensitive response to different compounds.

THz response of confined space water

Water in confined spaces plays a unique role in biological, chemical and energy catalysis. Water has strong absorption in THz band. It is found that the distribution of water in carbon nanotubes is obviously different in different directions of the interface. Such anisotropy will affect the hydrogen-bond network kinetics, and then lead to the difference of dielectric relaxation in different directions[4].

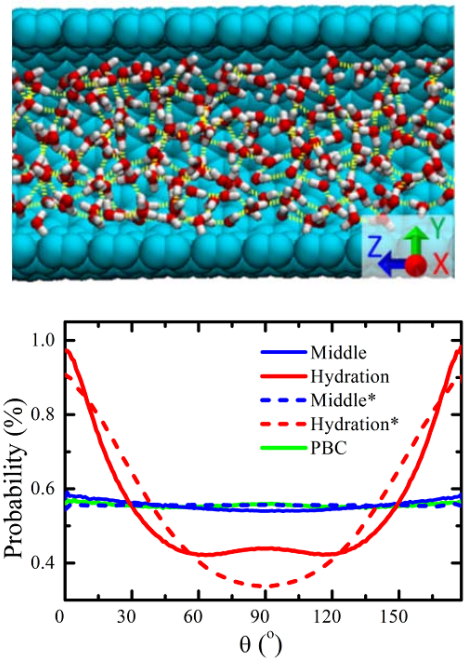

Fig.2 (First) Water in carbon nanotubes. (Second) Orientation distribution of hydrogen-bond in water molecules confined in different nanotubes SWCNT, SWCNT*, and water in PBC.

Terahertz Metamaterial Sensing

The highly absorption of water in THz range always makes it difficult for identification and quantitative analysis for aqueous biosystems. Metamaterial-based THz biosensor has attracted great attention as a promising tool in biological research. The very strong confinement of electromagnetic fields in the metamaterial allows one to detect the small changes of the dielectric environment, leading to high sensitivity and high resolution for material recognition. A THz metamaterial sensor based on electromagnetically induced transparency (EIT) effect is presented for sensing different concentration of 1,4-dioxane aqueous solution. The result indicates the THz label free sensor has potential applications in biochemistry[5].

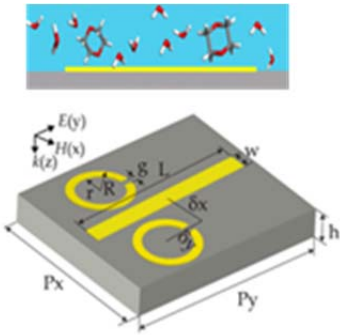

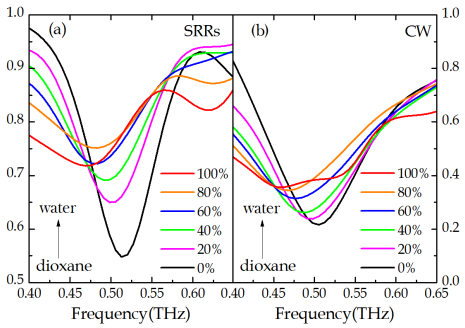

Fig.3 (left) Schematic diagram of the EIT metamaterial senor. (right) Experimentally measured THz transmission spectra in different water/dioxane mixtures (a) SRRs and (b) CW.

Terahertz spectroscopy laboratory construction

In 2015−2016, with the support of the Chinese Academy of Sciences, we built 1) A broadband terahertz infrared spectrometer (Fig.4), it possesses the bandwidth 0.1~18 THz, dynamic range >60 dB, spectral resolution <2 GHz. 2) A terahertz time- domain spectroscopy and imaging device (Fig.5), it possesses the bandwidth 0.5~7 THz, dynamic range >60 dB, spectral resolution 1.9 GHz, imaging resolution ~200 μm.

Fig.4 The broadband THz infrared spectrometer system.

Fig.5 The THz time-domain spectrosc

Reference

1. Dang Y R, Li S P, Liu H, *et al*. Low-frequency vibrations of indole derivatives by Terahertz time-domain spectroscopy[J]. Journal of Electronic Science and Technology, 2016, **14**(4): 329-336.
2. Li S X, Yang J Q, Zhao H W, *et al*. Terahertz time-domain spectroscopy and quantitative analysis of metal gluconates[J]. Applied Spectroscopy, 2015, **69**(1): 52-57.
3. Shi G S, Dang Y R, Pan T T, *et al*. Unexpectedly enhanced solubility of aromatic amino acids and peptides in an aqueous solution of divalent transition-metal cations[J]. Physical Review Letters, 2016, **117**: 238102.
4. Qi W P, Zhao H W. Hydrogen bond network in the hydration layer of the water confined in nanotubes increasing the dielectric constant parallel along the nanotube axis[J]. The Journal of Chemical Physics, 2015, **143**(11): 114708.
5. Li S X, Zhao H W, Han J G. Terahertz metamaterial sensor based on electromagnetically induced transparency effect[J]. Physical Review Letters, 2015, **13**(2): 117-121.

水科学研究室 纳米材料研究组

本组长期从事糖类物质的辐射化学基础应用研究、生物材料及纳米材料的研制、高分子材料的辐射改性研究、过滤膜结构与性质研究等。主要研究：高分子材料改性及其在膜过滤技术及有机无机复合材料制备中的应用、同步辐射技术应用和水科学应用基础。

通过控制石墨烯液滴与固体基底的接触线运动调节氧化石墨烯自组装结构

微液滴在衬底上的可控溶解是可以用于调控液滴内部溶解的结构单元自组装微观结构的有效的方法。在这项工作中，我们研究了二维石墨烯氧化物(GO)薄片的自组装行为。这些石墨烯薄片溶解与水滴中，水滴位于固体基底上并浸泡于液体环境中。液体环境能从液滴中吸收水分，导致液滴不断溶解，从而使石墨烯薄片在此过程中沉淀并自组装。我们发现，虽然在液-液界面石墨烯自组装成了均匀的显微结构，液滴和基板之间的接触可以在液滴的基地附近形成各种不同的形貌。特别是在逐渐溶解的液滴边界上的钉扎效应导致了非球形的石墨烯自组装结构的形成。在这项工作的结果表明：通过溶解液滴的方法量身定做不同的三维石墨烯纳米结构是可行的。控制固体基底材料对石墨烯液滴的润湿性能可以调控石墨烯的自组装结构。

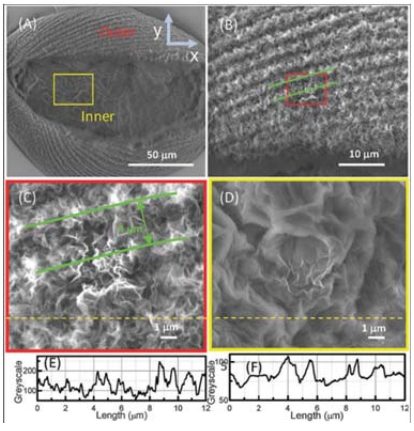

图 1 开口的橄榄形氧化石墨烯自组装结构的扫描电镜图像：（A） 全貌，（B） 外表面，（C） 和 （D）为 (B) 和 (A) 中选定区域的放大视图。（E） 和 (F) 为(C) 和 (D) 中标记相应位置的轮廓图。在衬底上液滴的接触面积在溶解过程中沿 x 方向拉伸。

力模式蘸笔纳米刻蚀技术中的力漂移

蘸笔纳米刻蚀技术(DPN)是近年来用于制造生物分子或化学材料的微/纳米结构的一种广泛应用的技术。力漂移是影响 DPN 中力的精确控制的一个关键因素，并且在 DPN 过程中经常发生。然而，力漂移的潜在机制尚不清楚。在这项工作中，基于分析力曲线和轻敲模式(TM)针尖反射信号随针尖在基底的停留时间（即“表面延迟”期）的变化规律，我们深入研究了力模式蘸笔纳米刻蚀技术(FMDPN)的力漂移现象。当使用开环的原子力显微镜(AFM)扫描管实施 FMDPN 时，当针尖在基底上的停留时间为 2 s，在柔软的聚二甲基硅氧烷(PDMS)基底上，力漂移值可达其预设值的 30%左右；而在刚性的硅晶片上其值可达 400%。AFM 扫描管在 *z* 方向上的蠕变效应对力漂移起决定作用；而 AFM 的热漂移在仪器稳定后对力漂移几乎没有影响。当扫描管为闭环时，由于系统对扫描管在 *z* 方向上的蠕变有实时补偿作用，力漂移现象无论在 PDMS 还是刚性的硅基底上都不会发生。本研究有助于解决如何正确利用 DPN 技术在固体基底上制备微米和纳米图案化结构的问题。

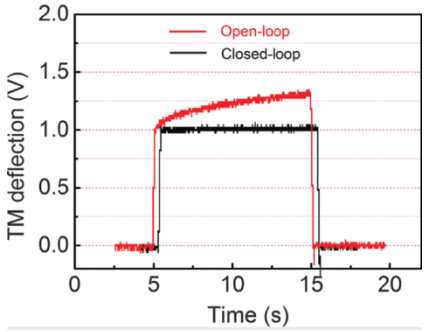

图 2 TM 挠度曲线记录在 FMDPN 进行刚性的硅晶片上。在 *z* 方向的闭环反馈是打开 （闭环） 或关闭 （开环） 由软件控制。为清楚起见，TM 偏转信号对应于开环模式稍微转向左边

参考文献

1. Yang H J, Song Y T, Downton M T, *et al*. Tailoring Q1 Q2 graphene oxide assemblies by pinning on the contact line of a dissolving microdroplet[J]. Soft Matter, 2015, **11**(43): 8479−8483.
2. Yang H J, Zhang C, Zhang J J, *et al*. Force Drift in Force Mode Dip-Pen Nanolithography[J]. Journal of Nanoscience and Nanotechnology, 2016, **16**(7): 7030−7036.

Industrial Application of Interfacial Water Research

Department of Water Science

Basic and applied research radiation chemistry of carbohydrates has long been engaged in this group, the development of biological materials and nano- materials, radiation modification of polymer materials, filtration membrane structure and properties research. The main research area includes as follows: modification of polymer materials and its application in filtration membrane technology and organicinorganic composite materials, synchrotron radiation applications and scientific applications of water based technology.

Tailoring graphene oxide assemblies by pinning on the contact line of a dissolving microdroplet

The controlled dissolution of microdroplets on a supporting substrate is an effective approach that can be used to tune the assembled microstructure of basic units suspended within the droplet. In this work, we studied the self-assembly of two-dimensional graphene oxide (GO) nanosheets driven by the dissolution of a microdroplet situated at the interface between a solid substrate and the surrounding liquid

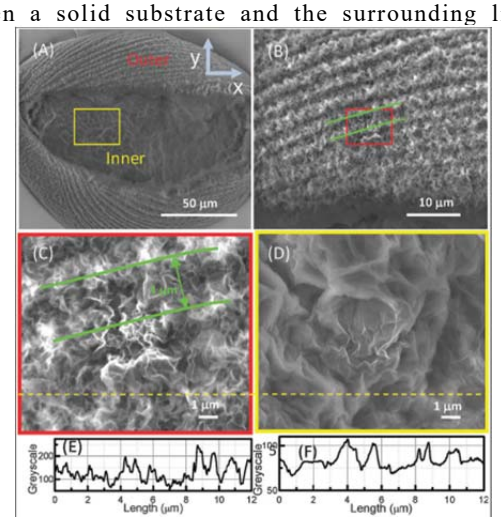

Fig.1 SEM images of an open GO olive with ridges on its surface. (A) An overview, (B) the outer surface, (C) and (D) close up view of the selected areas in (B) and (A). (E) and (F) The corresponding profiles of marked lines in (C) and (D). The contact area of the droplet on the substrate is stretched along the x-direction during the dissolution process.

phase. We found that although uniform microstructures form at the liquid–liquid interface of the droplets, the contact between the droplet and the substrate can give rise to a variety of different morphologies near the base of the droplet. In particular, pinning effects at the boundary of the dissolving droplet on the substrate lead to non-spherical GO assemblies. The results in this work demonstrate the possibility that tailored three-dimensional architectures of nanosheets assembled in a dissolving droplet may be achieved through control of the wetting properties of the droplet on the supporting substrate.

Force drift in force mode dip-pen nanolithography

Dip-pen nanolithography (DPN) is a widely employed technique in fabricating micro- and nanopatterns composed of biological molecules or other chemical materials. Force drift, a key factor affecting the force control, therefore the performance of DPN, is commonly happened in DPN. However, the underlying mechanism of force drift is not well understood yet. In this work, based on analyzing the force curve and tapping mode (TM) deflection signals varying with dwell time (i.e., the 'surface delay' period), the force drift during force mode dip-pen nanolithography (FMDPN) was studied in depth. For an open-loop atomic force microscope (AFM) scanner the force drift is about 30% of its preset value on a soft polydimethylsiloxane (PDMS) substrate while it can reach 400% on a rigid silicon wafer during the dwell time of 2 seconds. The creep effect of the scanner in the z direction determines the force drift and the thermal drift of AFM system is negligible in comparison with the preset loading force when the AFM system is stabilized. For a closed-loop scanner the loading force can nearly keep constant on either a soft PDMS substrate or a rigid silicon wafer during the whole dwell time due to the compensation for the creep effect of piezoelectric tube in the z direction of the AFM scanner. This study is helpful for properly employing DPN technique to fabricate micro- and nano-patterned structures on solid substrates.

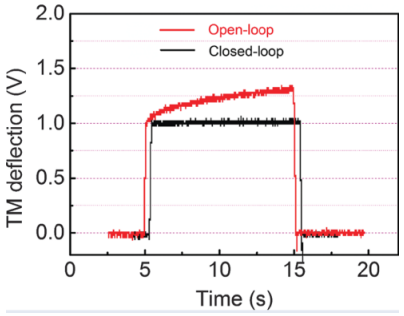

Fig.2. TM deflection curves recorded during FMDPN conducted on a rigid silicon wafer. The closed-loop feedback in the z-direction is turned on (closed-loop) or turned off (open-loop) by software control. For clarity, the TM deflection signal corresponding to the open-loop mode is slightly shifted to the left side.

Reference

1. Yang H J, Song Y T, Downton M T, *et al*. Tailoring Q1 Q2 graphene oxide assemblies by pinning on the contact line of a dissolving microdroplet[J]. Soft Matter, 2015, **11**(43): 8479−8483.
2. Yang H J, Zhang C, Zhang J J, *et al*. Force Drift in Force Mode Dip-Pen Nanolithography[J]. Journal of Nanoscience and Nanotechnology, 2016, **16**(7): 7030−7036.

金属纳米结构 SERS 传感探针的研究

物理生物学研究室

本研究课题依托上海光源和物理生物学实验室，主要开展了纳米科学、化学、物理学和生物科学领域的交叉研究，包括功能化纳米探针的制备、生物分子的检测分析，纳米探针的生物传感应用等方向。旨在结合纳米材料的理化性质与生物的分子识别功能及生物相容性构建新型的纳米生物传感器件。

具有表面等离子共振性质的纳米结构制备

金属纳米材料具有优异的表面等离子体共振的性质。入射光通过与纳米颗粒内的自由电子相互作用从而使得电子发生重排。通过构建特定形貌金纳米结构，就可以使得表面电子在某些限域空间内富集从而使得局域电场发生增强，而增强的电场则可以使得处于这一位置的分子的拉曼振动信号发生放大。这里我们通过 DNA 调控制备了纳米金-银“蘑菇”的结构[1]，可以在金与银的界面获得较强的电场增强，金-银“蘑菇”结构对与拉曼分子的信号增强达到了 10^9。同时金纳米颗粒上游离的 DNA 保留了杂交的性能所以可以用于生物检测及纳米光子学基元的构建。

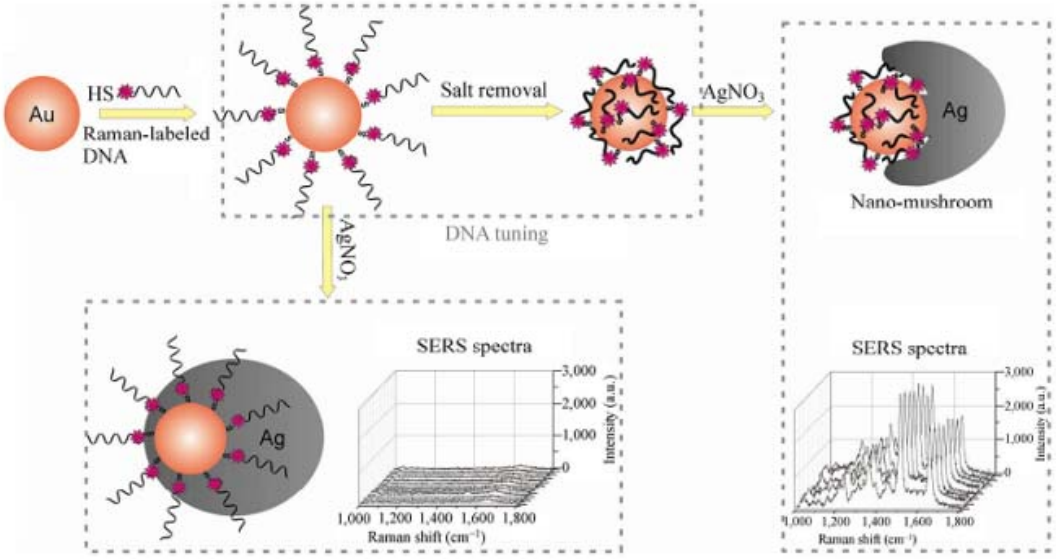

金-银“蘑菇”拉曼探针

复杂形貌纳米材料生长过程的表征

传统的纳米材料表征手段包括透射电子显微镜(TEM)，扫描电子显微镜(SEM)等，这些表征手段往往受到制样的复杂性，分辨率，三维形貌重构等的限制。这里我们结合 X 射线小角散射(SAXS)，TEM 及紫外-可见吸收，表面增强拉曼光谱(SERS)等手段获得具有 1 nm 厚度内空腔的纳米金花结构的精细形貌，同时揭示了具有 1 nm 厚度内空腔结构的纳米材料的生长机理[2]。结构内的 1 nm 空腔对于拉曼分子拉曼信号具有很好的增强效应。另外，由于结构的密闭性，使得密闭于空腔内的拉曼分子可以保持较好的稳定性。结构的稳定性与均一性使得这种纳米材料可以作为一种稳定的 SERS 探针。

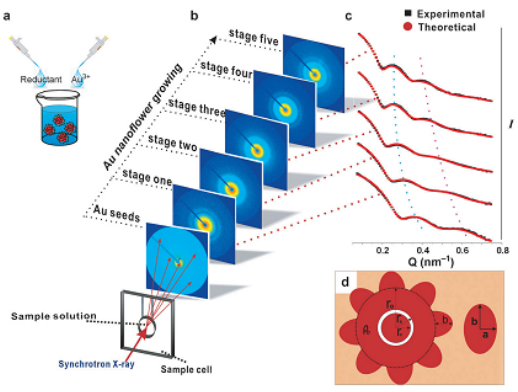

SAXS 揭示纳米金花的精细形貌

SERS 探针用于生物分子的检测

传统的 SERS 探针具有信号低，结构复杂，重复性差等缺陷，这里我们获得了一种具有 1 nm 空腔的金纳米结构[3]。这种结构具有较强的拉曼增强功能，拉曼增强因子可达 10^8。相比于其它的纳米结构，这种结构具有更好的稳定性及重复性。同时，合成后的结构尺寸在 45 nm 左右且新生表面可以进行化学修饰和物理吸附而对包裹在内的拉曼分子没有影响。这就使得颗粒具有很强的适用性。通过改变嵌入空腔内拉曼分子的种类，就可以获得多色的探针，相比于传统的荧光探针，我们的拉曼探针具有较窄的半峰宽，从而使得多元检测具有更好的分辨率。

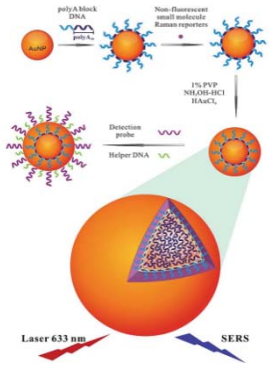

SERS 探针的制备及修饰

本工作中，利用制备好的纳米生物探针分别检测了核酸物质、蛋白质及小分子，证明了结构具有良好的普适性。同时，通过制备三种探针可以实现对于三种目标物的同时检测，通过调节检测物浓度发现对目标物的检测具有很好的线性关系和较高的灵敏度。对 miRNA-141、PDGF、cocaine 的检测线分别达到了 1.77 pmol·L^{-1}、143.4 pg·mL^{-1} 和 3.9 μmol·L^{-1}。

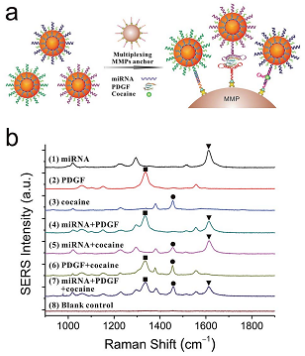

多色拉曼探针用于多元检测

参考文献

1. Shen J L, Su J, Yan J, *et al*. Nano Res, 2015, **8**(3): 731–742.
2. Shen J L, Xu L F, Wang C P, *et al*. Angew Chem Int Ed, 2014, **53**: 8338−8342.
3. Zhao B, Shen J L, Chen S X, *et al*. Chem Sci, 2014, **5**(11): 4460−4466.

Preparation of the Nano-Scale Bio-Prober

Division of Physical Biology

Here, we combined the physical-chemical properties of the inorganic nanomaterials with recognition ability, biocompatibility of biomolecular to fabricate new nano-biology biosensing device.

Preparation of plasmonic gold nanoparticle

Duo to its excellent localized surface plasmon resonant property, the incident light would induce the rearrangement of the surface charge in nanoparticles. For modulating the arrangement of the surface charges to enhance the near field electromagnetic field at certain position, the nanostructure with specified geometry was needed. The enhanced EM field could enhance the Raman signal of molecular extensively (known as SERS). Here, we fabricated Au-Ag "mushroom" under mediating of the DNA[1]. The inter-gap between Au and Ag could lead the enhance of the EM field which further amplified the Raman signal of molecular in the gap. The enhance factor was calculated reached to 10^9. Moreover, the DNA on Au side without covering by the Ag kept its hybridization ability.

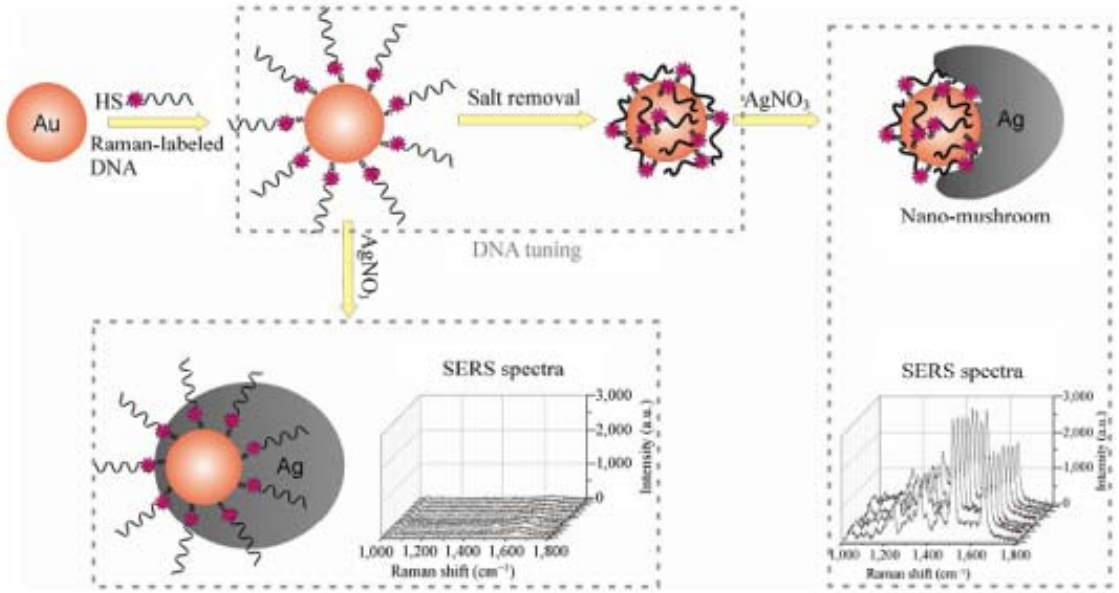

Au-Ag mushroom as Raman bio-prober

The characterization of the nanostructure

The existed methods for characterization of nanostructures often resorted to the electron microscopy (TEM, SEM) which often confronted with complex sample preparation, resolution, three dimensions reconstruction, etc. Here, X-ray small angle scatter was combined with TEM, UV-vis, SERS et, al to character the fine geometry of Au core-shell nanostructures with 1 nm gap between its core and shell. The mechanism of the nanostructure's growth was been elucidated simultaneously[2]. The 1 nm gap within the nanostructure offered the stable sealed room for the SERS and molecular stability and these properties made the Au core-shell nanostructures as the good candidate as SERS tags.

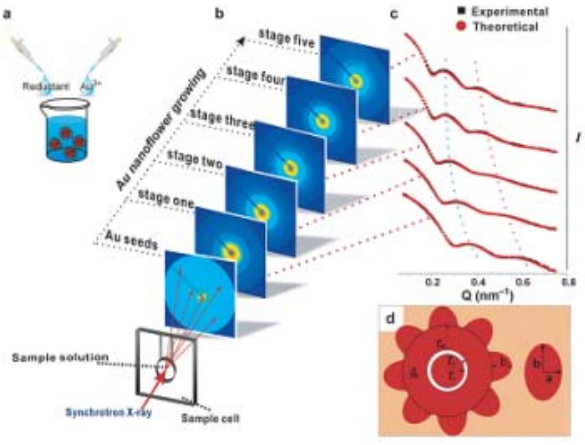

Elucidating of the gold nanoflower growth's mechanism with SAXS.

The bio-detection with SERS tags

The traditional SERS tags often confront with the low signal intensity, geometry complexity and poor reproducibility, *etc*. The Au core-shell nanostructure with 1-nm hollow gap was fabricated here to overcome the above mentioned drawbacks[3]. The enhance factor of this nanostructure can reach to 10^8. The fabricated nanostructure with diameter about 45 nm and freshly born Au shell offered the versatile platform for the subsequent chemical or physical modification and these operations would cause little influence to the Raman reporter in gap.

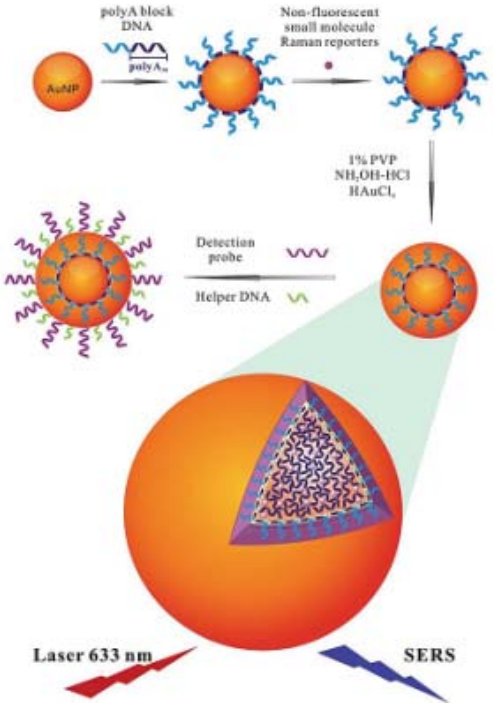

Prepration of SERS nanoprobes

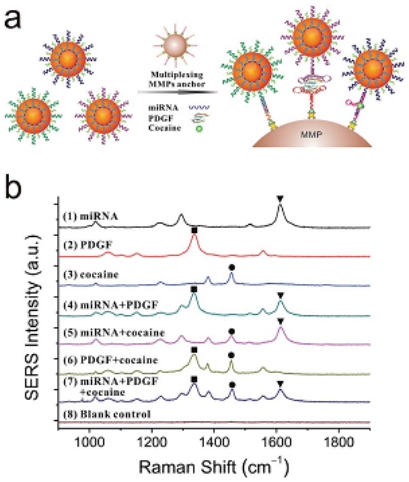

Multi-color Raman tags for the multi-molecular detection.

Different Raman tags would get through loading different molecular in the gap. The Raman peaks own the narrower half band width than the fluorescence, so it was more practical to use multi-color Raman tags for multi-molecular detection.

In this study, we make use of the prepared SERS nanoprobes for the detection of nucleic acids, proteins and small molecule, respectively. The limits of detection (LODs) for the miRNA-141, PDGF and cocaine were reached to 1.77 pM, 143.4 pg/mL and 3.9 μM. These results proved the universality of this method. Additionally, there bioactive analytes were analysis simultaneously with there SERS nanoprobes.

Reference

1. Shen J L, Su J, Yan J, *et al*. Nano Res, 2015, **8**(3): 731–742.
2. Shen J L, Xu L F, Wang C P, *et al*. Angew Chem Int Ed, 2014, **53**: 8338−8342.
3. Zhao B, Shen J L, Chen S X, *et al*. Chem Sci, 2014, **5**(11): 4460−4466.

DNA 纳米技术的研究进展

物理生物学研究室

在 2015−2016 年，我们课题组基于前期生物传感和生物检测的积累，设计和构建了一系列新型生物传感和生物检测新方法。主要研究成果包括以下几个方面：

DNA 纳米泵

分子级别的纳米泵在生物体内发挥着重要的生物学功能，如细胞内外水分子的输运以及离子的输运等。针对纳米泵问题，充分利用 DNA 纳米结构精确可调的特点，左小磊研究员通过与樊春海、胡钧研究员等的合作，构建了一种质子响应性的动态 DNA 四面体纳米结构，通过精确界面组装技术将该结构组装到金界面上，实现了质子驱动的 DNA 纳米泵。该纳米泵可用于驱动水分子以及离子的定向运动。这种三维、动态以及有序的界面在生物传感、逻辑器件、以及合成生物学中具有重要的应用潜力[1]。研究结果发表之后，被《Nature Reviews Materials》杂志作为研究亮点，以“Pump fiction”为题进行了专题报道[2]。

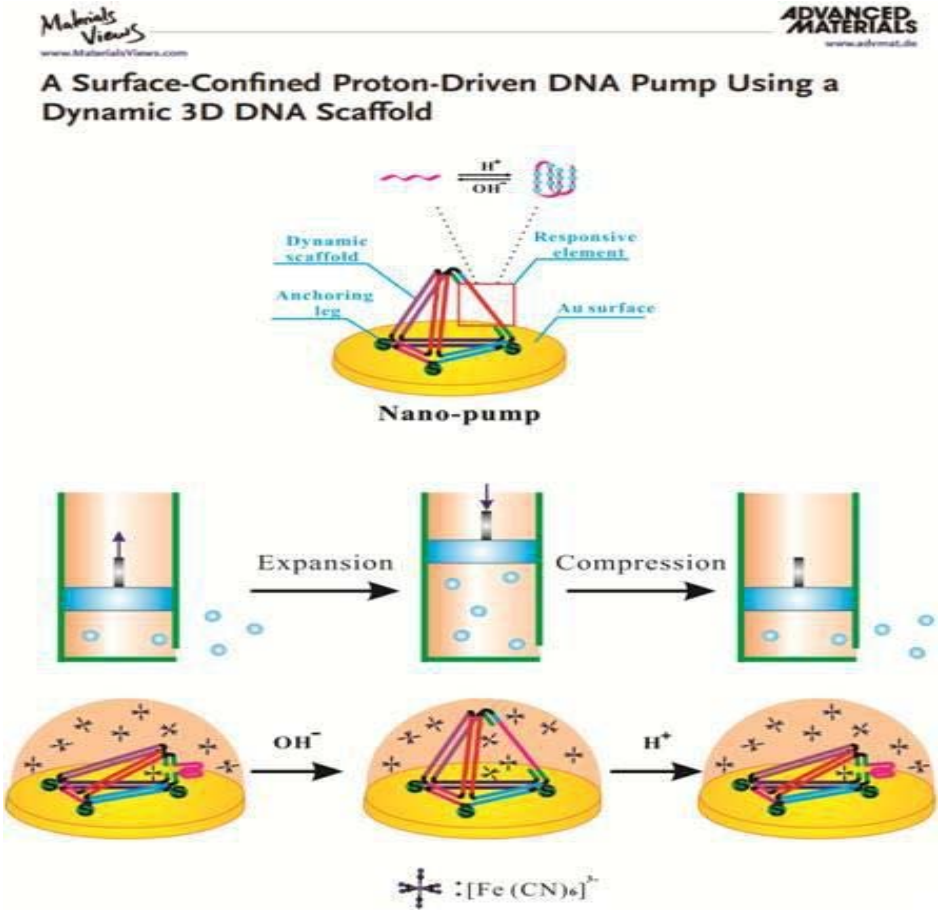

DNA 质子泵作用原理示意图

DNA 计算

DNA 分子具有强大的序列可编程性及精确的分子识别能力，被认为是发展下一代生物计算机的理想材料。现有的原型 DNA 计算机往往存在输入输出不一致、信号串扰、运算效率低等问题，并且缺乏直观的输出模式，其运算过程与结果往往难以解读，限制了 DNA 计算领域的发展。课题组柳华杰、樊春海等研究人员与 Kurt Gothelf 教授合作，提出了基于组合学原理建立类似“查找表”的全新 DNA 计算模式，显著提高了 DNA 计算的效率。DNA 构建的查找表具有超大的变量容纳能力。利用 DNA 强大的平行计算能力则可以高效地访问查找表。研究人员以乘法运算为例对该模式进行了演

示，并采用了类似电子计算器的可视化数字输出形式。运算结果以明确的数字结果在多尺度的显示器上均可以得到解读。这一 DNA 计算模型具有模块化设计的特点，有望通过设计人性化的输入、计算、输出等模块，成为一种适合于普通用户的原型 DNA 计算机，并在生物传感、数据存储与处理等方面得到应用[3]。

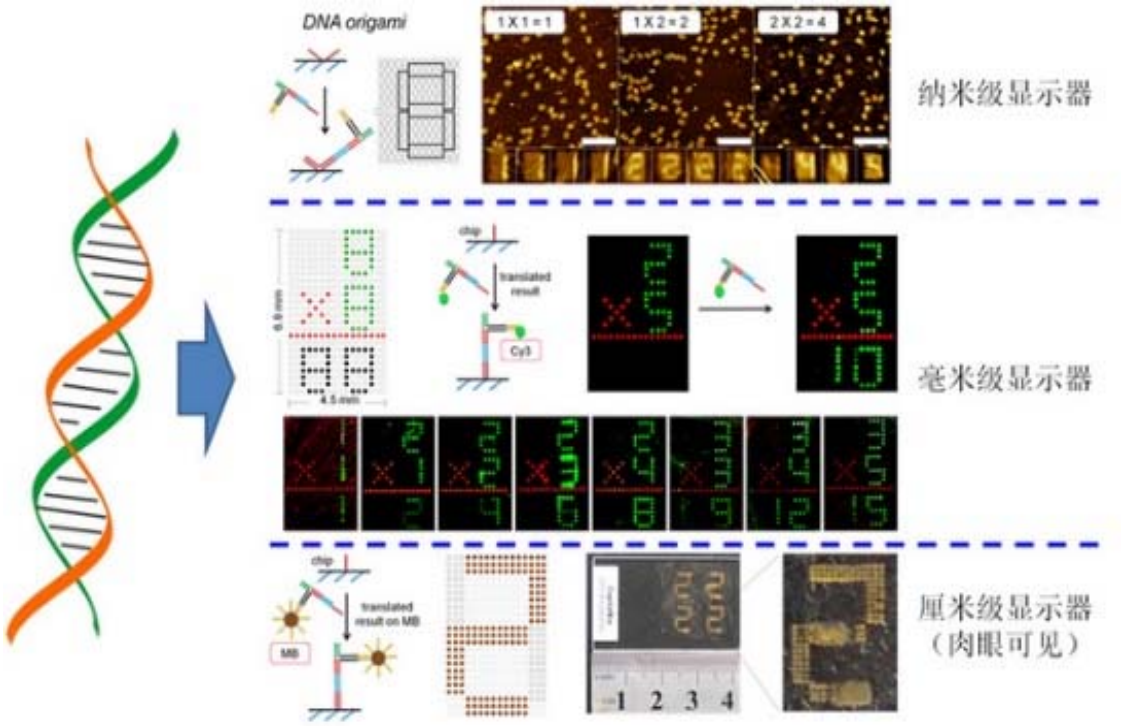

在多尺度显示器上得到的 DNA 计算结果

基于“DNA 折纸术”的等离子体纳米结构

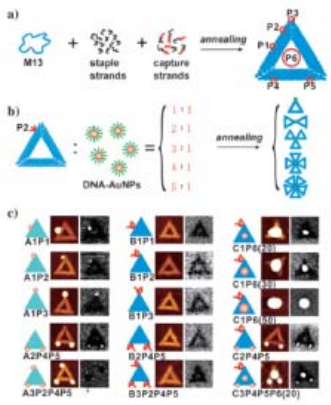

金纳米粒介导折纸拼图合成示意图

在纳米尺度自下而上构建高度有序且具有奇异光学性质的等离子体结构是纳米光子学领域的重要目标。课题组博士研究生姚广保和李江、晁洁副研究员等设计了一种三角形 DNA 折纸结构，并以特定序列 DNA 修饰的纳米金粒子作为桥梁可控有序地拼装出一系列复杂结构。这些结构表现出独特的表面等离子体耦合效应。展示了 DNA 纳米技术与金属纳米材料的结合在构建有序的超分子结构方面的强大能力，为实现更加精细的多功能纳米超结构提供了有价值的参考[4]。

参考文献

1. Zhu D, Pei H, Yao G, *et al.* A surface-confined proton-driven DNA pump using a dynamic 3D DNA scaffold[J]. Adv Mater, 2016, **28**: 6860.
2. Pacchioni G. Nature Reviews Materials, 2016, DOI: 10.1038/natrevmats.2016.47
3. Liu H, Wang J, Song S, *et al*. A DNA-based system for selecting and displaying the combined result of two input variable[J]. Nature Commun. 2015, **6**: 10089.
4. Yao G B, Li J, Chao J, *et al*. Gold-nanoparticle-mediated jigsaw-puzzle-like assembly of supersized plasmonic DNA origami[J]. Angew Chem Int Ed, 2015, **54**: 2966.

Research Progress of DNA Nanotechnology

Division of Physical Biology

In 2013−2014, we continued our research on design, synthesis of DNA-based nanomaterials, as well as their potential applications. Some accomplishments were summarized in the following.

DNA Nano-pump

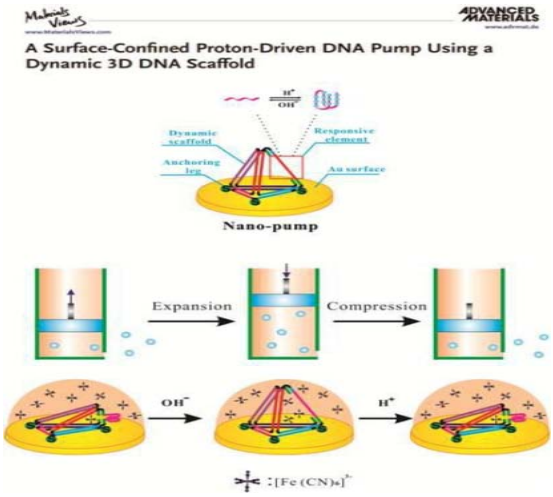

DNA-proton pump

Water pumps are ubiquitous devices in everyday life. It is probably even more intriguing to study water pumps or channels at the nanoscale. Aquaporins are naturally existing proteins that channel water in and out of cells in an organized manner. DNA provides a unique opportunity to mimic natural aquaporins. We have developed a proton-driven DNA nanopump using surface-confined, dynamic 3D DNA nanostructure. This 3D DNA nanostructure-based nanodevice provides several unprecedented advantages. Firstly, compared to inorganic carbon nanotube-based water pumps, our DNA tetrahedron based pump represents a novel biomolecular nanopump, which would be less cytotoxic and highly compatible to living biological systems. Secondly, our dynamic DNA nanodevices are highly tunable in size and shape based on the precise Watson-Crick base pairing rules. Besides, DNA pumps driven by some other stimuli can be readily designed by replacing the proton sensitive i-motif sequence. Thirdly, our dynamic DNA nanodevice is highly functionalizable, through which a wide range of functional element can be conjugated on the nanodevice. Last, this 3D nanostructure can be assembled rapidly and reliably with high yields, readily immobilized onto surfaces with high stability, ordered orientation and well-controlled lateral spacing, which offer a readily available system for surface-confine dfunctional nanodevices[1,2].

DNA computing derives

Oligonucleotide-based technologies for biosensing or bio-regulation produce huge amounts of rich high-dimensional information. There is a consequent need for flexible means to combine diverse pieces of such information to form useful derivative outputs, and to display those immediately. Here we demonstrate this capability in a DNA-based system that takes two input numbers, represented in DNA strands, and returns the result of their multiplication, writing this as a number in a display. Unlike a conventional calculator, this system operates by selecting the result from a library of solutions rather than through logic operations. The multiplicative example demonstrated here illustrates a much more general capability—to generate a unique output for any distinct pair of DNA inputs. The system thereby functions as a lookup table and could be a key component in future, more powerful data-processing systems for diagnostics and sensing[3].

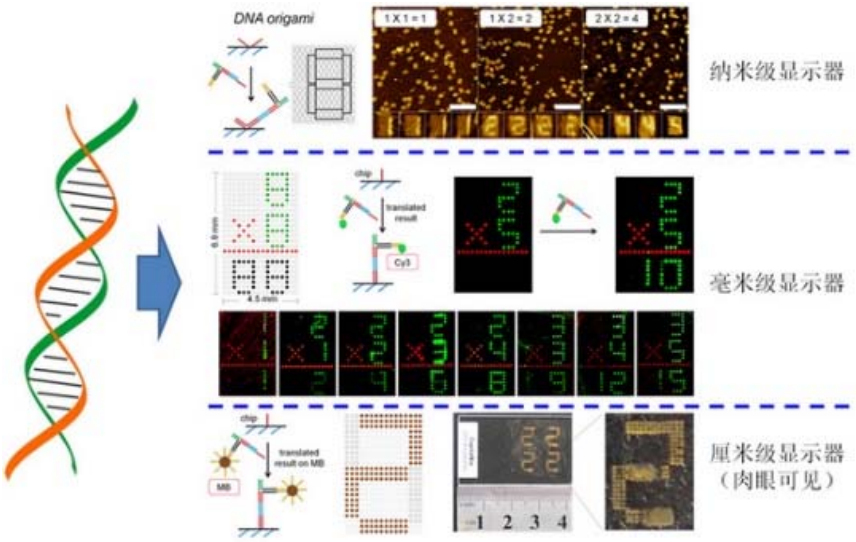

Displaying the results of multiplication reactions

DNA origami-based Supersized Plasmonic nanostructure

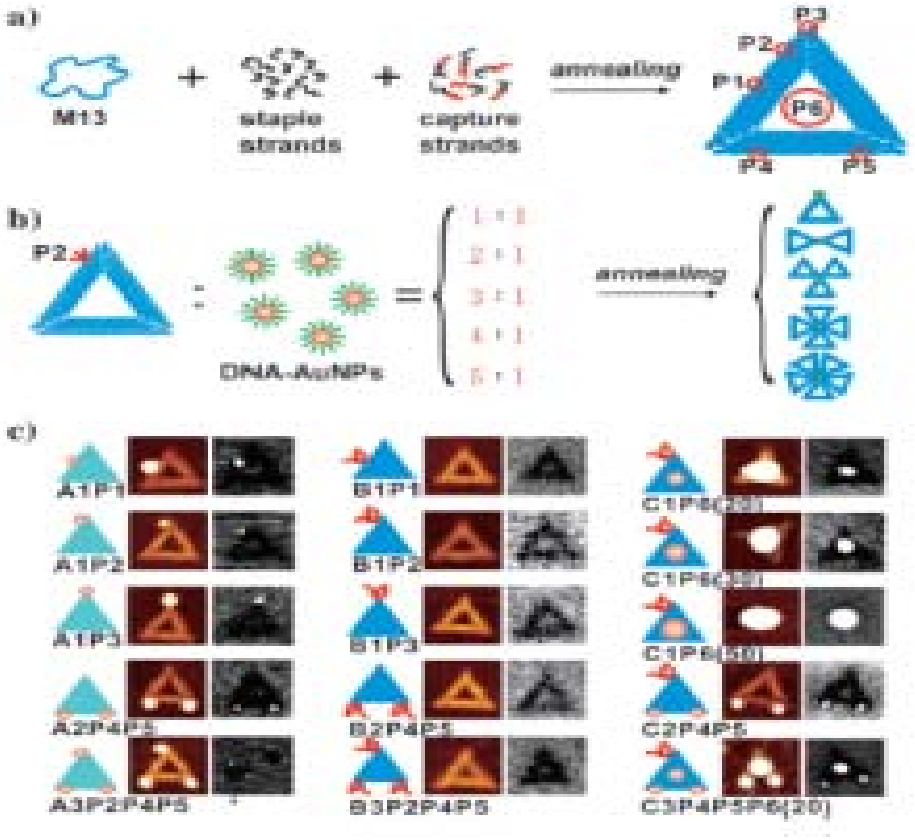

Schematic representation of AuNP-mediated jigsaw-puzzlelikeassembly of super-origami

DNA origami has rapidly emerged as a powerfuland programmable method to con-struct functional nanostructures. We report a jig-saw-puzzle-like assemblystrategy mediated by gold nanoparticles (AuNPs) to breakthe size limitation of DNA origami. We demonstrated that oligonucleotide-functionalized AuNPs function as universaljoint units for the one-pot assembly of parent DNA origami oftriangular shape to form sub-microscale super-origami nanostructures. AuNPs anchored at predefined positions of thesuper-origami exhibited strong interparticle plasmonic coupling. This AuNP-mediated strategy offers new opportu-nitiesto drive macroscopic self-assembly and to fabricatewell-defined nanophotonic materials and devices[4].

Reference

1. Zhu D, Pei H, Yao G, *et al.* A surface-confined proton-driven DNA pump using a dynamic 3D DNA scaffold[J]. Adv Mater, 2016, **28**: 6860.
2. Pacchioni G. Nature Reviews Materials, 2016, DOI: 10.1038/natrevmats.2016.47
3. Liu H, Wang J, Song S, *et al.* A DNA-based system for selecting and displaying the combined result of two input variable[J]. Nature Commun. 2015, **6**: 10089.
4. Yao G B, Li J, Chao J, *et al.* Gold-nanoparticle-mediated jigsaw-puzzle-like assembly of supersized plasmonic DNA origami[J]. Angew Chem Int Ed, 2015, **54**: 2966.

生物传感检测新方法

物理生物学研究室

在 2015−2016 年，我们课题组基于前期生物传感和生物检测的积累，设计和构建了一系列新型生物传感和生物检测新方法。主要研究成果包括以下几个方面：

1　基于酸碱调控的室温 PCR 新方法

PCR 是体外通过酶反应合成、高灵敏扩增目标基因片段的一种方法，是最常用的分子生物学技检测技术之一。常规 PCR 是通过控制溶液温度实现 DNA 分子的可逆变复性，达到复制扩增的目的。这个过程通常需要复杂的控温装置并消耗大量能源。基于 DNA 变复性还可以通过酸碱变性来实现，我组与清华大学化学系刘冬生课题组合作，张一博士和李茜副研究员发现微流控电化学可以有效控制 PCR 反应体系的 pH 值，实现了室温下的酸碱驱动的 IM-PCR 扩增(Ion-Mediated Polymerase Chain Reaction, IM-PCR)[1]。与传统 PCR 技术相比，这一新型的集成化 IM-PCR 技术无需变温过程，所有反应步骤均在室温下进行。这一小型化、低成本、易于集成的 PCR 新技术有望在生物检测、临床诊断及环境监测中发挥作用。

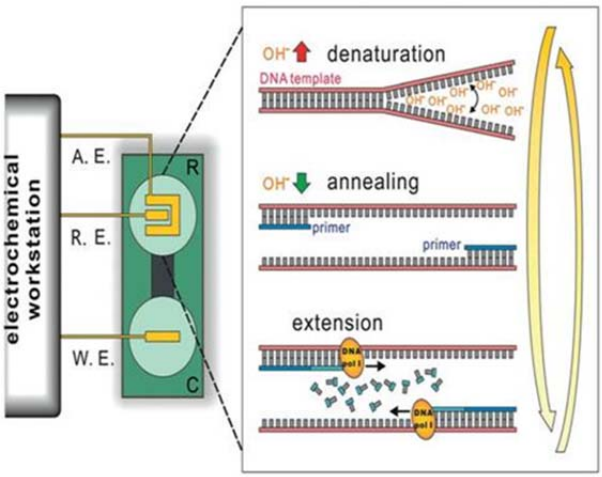

IM-PCR 扩增

2　跨尺度生物传感界面调控

构筑有序、可控的生物传感界面是生物检测研究领域的挑战性问题之一。针对这一问题，我们组对生物分子在界面上的组装过程开展了长期、系统的研究[2]。近期，博士生林美华等充分利用了 DNA 纳米结构精确可调的特点，设计了一系列具有不同尺寸的 DNA 四面体纳米结构，并利用这些结构在金界面的有序组装发展了一种“软光刻”技术[3]。这一新型的跨尺度界面调控技术可以实现在宏观的金界面上构筑纳米尺度可控的框架结构，从而精确调控依托于这些结构上的 DNA 探针之间的距离。他们还系统研究 DNA 分子之间的纳米距离与生物传感性能之间的关系，并提高了界面生物分子识别的热力学和动力学过程，进而显著提升了电化学生物传感器的检测灵敏度和速度。

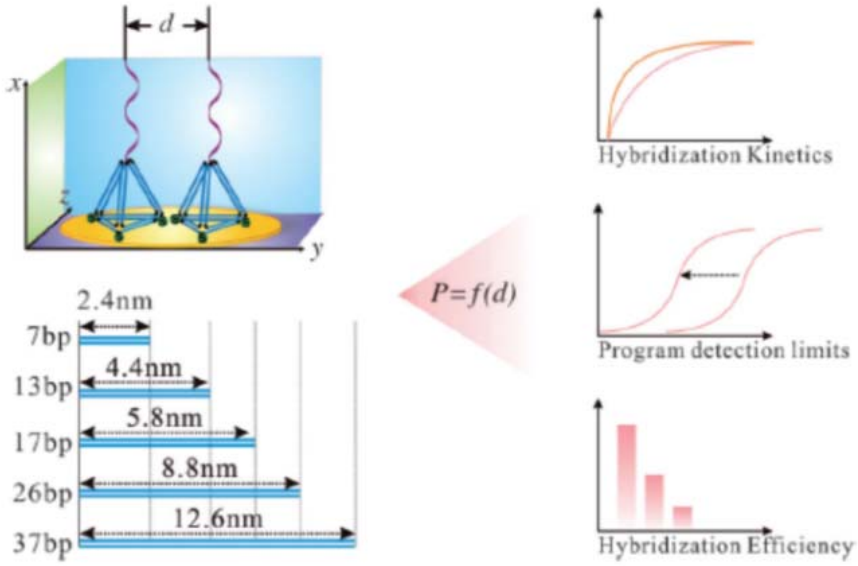

跨尺度生物传感界面

3　多分子水平检测生物传感平台

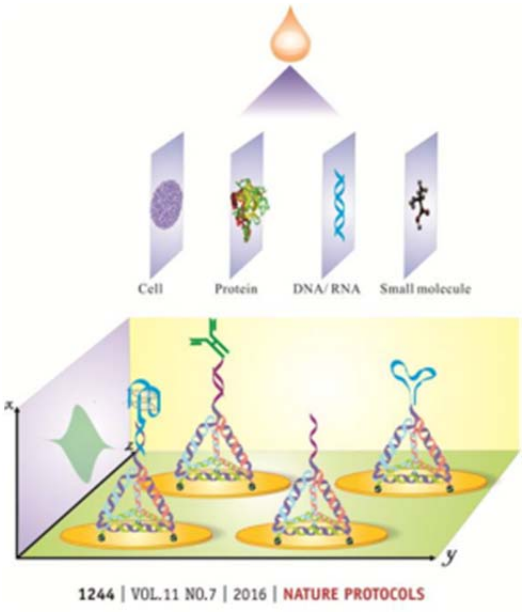

多分子水平检测生物传感平台

课题组基于 DNA 纳米技术发展了精确自组装的 DNA 四面体纳米结构，在国际上率先提出利用三维 DNA 纳米结构进行界面调控的电化学生物传感策略。充分利用 DNA 纳米结构精确可调的特点，在金电极上构筑了纳米尺度精确可控的自组装界，并进一步发展了针对蛋白质、核酸(DNA/RNA)、小分子等不同分子水平靶标的高灵敏检测方法。基于这一精确自组装策略发展的通用生物检测平台为实现多分子水平肿瘤标志物的联合奠定了基础，为实现癌症早期精准检测提供了强有力的工具。左小磊研究员等应邀在《自然-实验方法》撰写了精确自组装电化学传感方面的实验方法论文[4]，系统阐述了精确自组装 DNA 四面体纳米结构的设计、制备、表征及其在电极界面上的组装过程，并建立了多分子水平检测生物靶标的生物传感平台。Nature Protocols 审稿人评价这一工作：“迈出了非常重要的一步，在技术创新与实际应用之间构筑起一道桥梁”。

参考文献

1. Zhang Y, Li Q, Guo L, *et al*. Ion-mediated polymerase chain reactions performed with an electronically driven microfluidic device[J]. Angew Chem In Ed, 2016, **55**: 12450.
2. Pei H, Zuo X L, Zhu D, *et al*. Functional DNA nanostructures for theranostic applications[J], Acc Chem Res, 2014, **47**: 550.
3. Lin M, Wang J, Zhou G, *et al*. Programmable engineering of biosensing interface with tetrahedral DNA nanostructures for ultrasensitive DNA detection[J]. Angew Chem Int Ed, 2015, **54**: 2151.
4. Lin M, Song P, Zhou G, *et al*. Electrochemical detection of nucleic acids, proteins, small molecules and cells using a DNA nanostructure-based universal biosensing platform[J]. Nature Protocols, 2016, **11**: 1244.

New Method of Biosensor

Division of Physical Biologyb

In 2015−2016, we continued our research on design, synthesis of new biosensors and biological detection methods. Some accomplishments were summarized in the following.

1 Ion-mediated PCR (IM-PCR)

The polymerase chain reaction (PCR) is a powerful method for exponentially amplifying very low amounts of target DNA from genetic, clinical, and forensic samples. However, the heating and cooling steps in PCR largely hamper the miniaturization of thermocyclers for on-site detection of pathogens and point-of-care tests. Herein, we devise an ion-mediated PCR (IM-PCR) strategy by exploiting ion-induced DNA denaturation/renaturation cycles. DNA duplexes are effectively denatured in alkaline solutions; whereas, the denatured single-stranded DNA strands readily reform duplexes at neutral pH. By using an integrated microchip that can programmablely control the solution pH simply switching the potential in a range of several hundred millivolts, we can trigger IM-PCR at a constant temperature. Analogously to thermal cycling, 30 cycles of pH-induced denaturation/renaturation were used to amplify protein DNA fragments as confirmed by DNA sequencing. We anticipate that this portable, low-cost, and scalable IM-PCR holds great promise for widespread biological, clinical, and environmental applications.

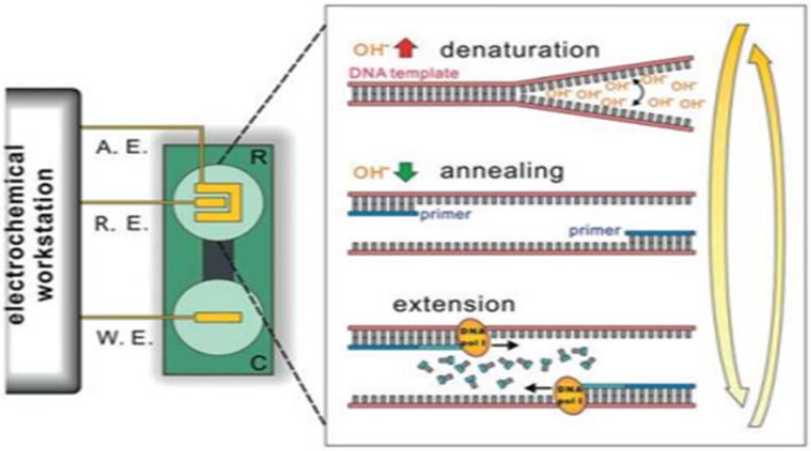

Ion-mediated PCR

2 Programmable Engineering of a Biosensing Interface

Self-assembled DNA nanostructures with precise sizes allow a programmable “soft lithography” approach to engineer the interface of electrochemical DNA sensors. By using millimeter-sized gold electrodes modified with several types of tetrahedral DNA nanostructures (TDNs) of different sizes, both the kinetics and thermodynamics of DNA hybridization were profoundly affected. Because each DNA probe is anchored on an individual TDN, its lateral spacing and interactions are finely tuned by the TDN size. By simply varying the size of the TDNs, the hybridization time was decreased and the hybridization efficiency was increased. More significantly, the detection limit for DNA detection was tuned over four orders of magnitude with differentially nanostructured electrodes, and achieved attomolar sensitivity with polymeric enzyme amplification.

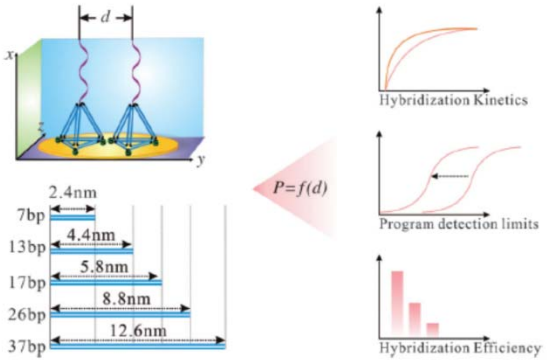

Programmable engineering of a biosensing interface

3 Biosensing platform of multimolecular detection

The dection of single tumor marker is unfit for accurate cancer detection. Fan Chunhai's team devised an accurate self-assembled DNA tetrahedral nanostructures based on DNA nanotechnology. And it's first to raised a new concept to achieve improved probe–target recognition properties by introducing a probe bearing a 3D DNA nanostructure-based chip platform. They has been worked hand in glove for years and built a nanoscale precise controllable self-assembly interface in gold electrode by making full use of the highly precise and programmable self-assembly property of DNA. Then they made further development on protein, nucleic (DNA/RNA) and other small molecules for high sensitive detection. Thus it is highly desirable to develop a single platform for detecting multilevel biomarkers for early-stage diagnosis. Recently, Zuo Xiaolei was invited to review self-assembled of electrochemical sensing in natural - experimental method[1]. They reported a protocol on DNA-nanostructure-based programmable engineering of the biomolecular recognition interface, which provides a universal electrochemical biosensing platform for the ultrasensitive detection of multilevel.Rebiewers of Nature Protocols gave a highly evaluation: It's a big step between technological innovation and practical applications.

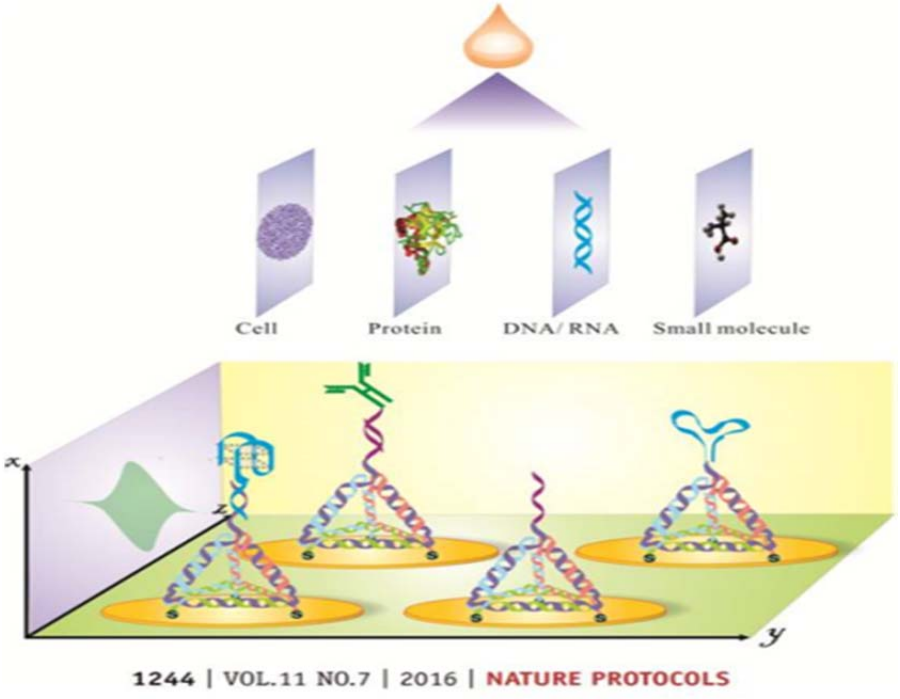

Biosensing platform of multimolecular detection

Reference

1. Zhang Y, Li Q, Guo L, *et al*. Ion-mediated polymerase chain reactions performed with an electronically driven microfluidic device[J]. Angew Chem In Ed, 2016, **55**: 12450.
2. Pei H, Zuo X L, Zhu D, *et al*. Functional DNA nanostructures for theranostic applications[J\. Acc Chem Res, 2014, **47**: 550.
3. Lin M, Wang J, Zhou G, *et al*. Programmable engineering of biosensing interface with tetrahedral DNA nanostructures for ultrasensitive DNA detection[J]. Angew Chem Int Ed, 2015, **54**: 2151.
4. Lin M, Song P, Zhou G, *et al*. Electrochemical detection of nucleic acids, proteins, small molecules and cells using a DNA nanostructure-based universal biosensing platform[J]. Nature Protocols, 2016, **11**: 1244.

纳米气泡研究进展

物理生物学实验室 上海光源软 X 射线组

本课题组依托于物理生物学研究室和上海光源软 X 射线组，主要从事纳米气泡和纳米气层的基本性质、纳米气泡在环境，生物科学领域中的应用研究。2015–2016 年研究主要进展包括：界面纳米气层的物理性质测量、纳米气泡在不同基底的可控生长和界面张力的原位测量等。

界面纳米气层的定量纳米力学性质与成像

界面纳米气层是气体在纳米尺度下聚集的一种形式。无论理论还是实验对它的理解非常有限。该工作利用 PF-QNM 首次对界面纳米气层在纯水和乙醇水溶液中进行定量纳米力学测量。研究发现：纳米气层的硬度随着乙醇浓度的增加而减小，纳米气层在一个临界乙醇浓度以上将不能被观察到，但是当用纯水替换了乙醇溶液之后，纳米气层又重现。定量纳米力学成像模式原子力显微镜的硬度测量提供了一种更加灵敏的方法用以监测界面纳米气层的存在和层数，并且能更灵敏的区分纳米气泡、纳米气层与基底[1]。

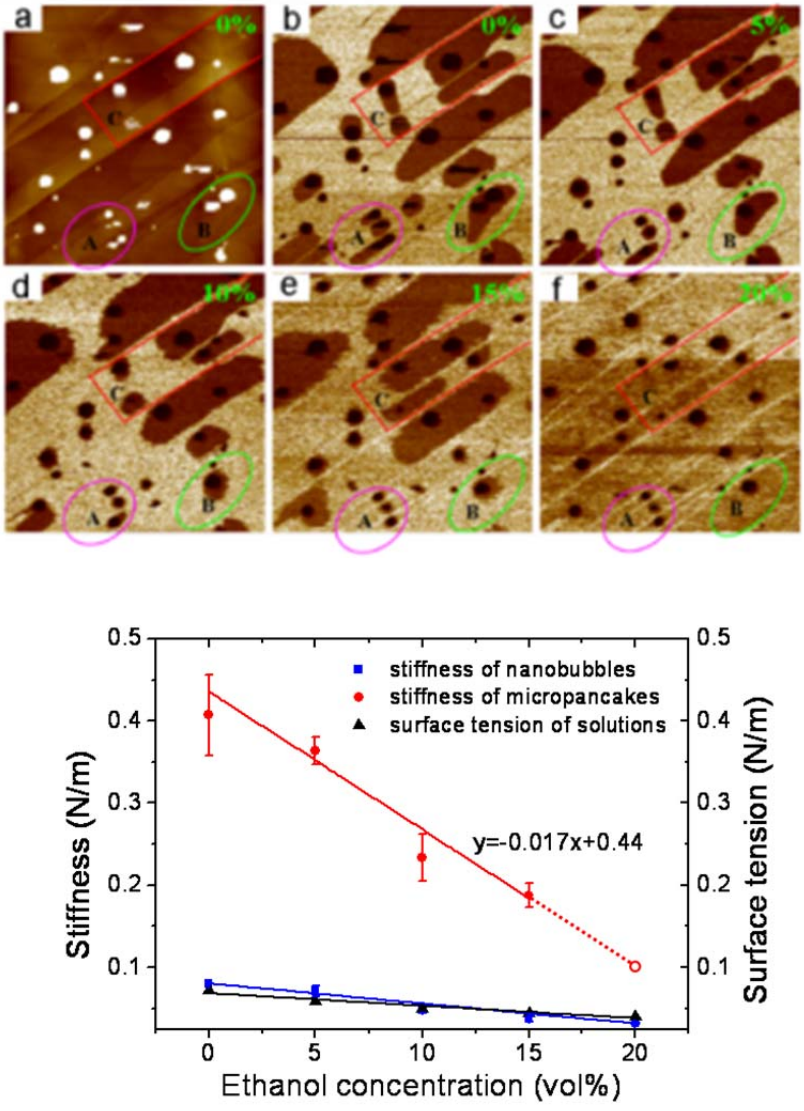

图 1 PF-QNM 得到的纳米气泡和纳米气层复合体的 stiffness 图和纳米气层随不同乙醇浓度 stiffness 的变化情况

纳米气泡在不同疏水基底表面的可控生长

纳米气泡在固体界面上具有超级稳定性和大的接触角等重要性质。普遍认为纳米气泡的接触角与基底、温度以及气体的种类都是密切相关的。本工作比较了纳米气泡在不同疏水性质的基底上生成和生长的界面性质。结果表明：基底的疏水性越强，纳米气泡的液相接触角越大。另外，利用分子动力学模拟，通过改变石墨烯的碳原子的电偶极矩产生疏水性差的表面。结果表明：纳米气泡可以稳定在疏水性表面而不是亲水性的表面。其次，通过修饰适当的电偶极矩产生边缘效应（水墙）并预先放置气体成核点的方法。纳米气泡也被固定在这个封闭区域。这些结果将有助于从理论方面理解纳米气泡的长寿命和纳米气泡在微流体应用[2−3]。

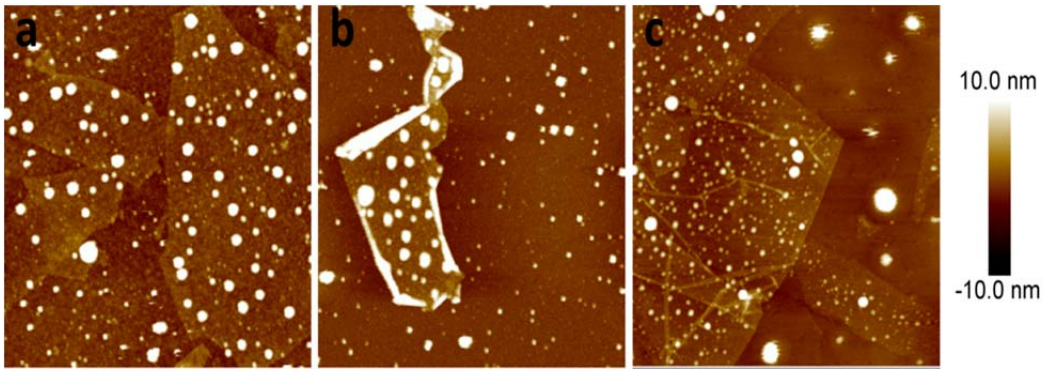

图 2 The PF-QNM images of nanobubbles on substrates of rGO-Si_3N_4 (a), rGO-mica (b) and rGO-HOPG (c). These nanobubbles were produced by ethanol-water exchange. The concentrations of the rGO were 0.2 mg/ml, 0.4 mg/ml and 0.1 mg/ml, respectively. Scan size: 3 μm×3 μm

界面纳米气泡接触角和表面张力的原位测量

表面张力是纳米气泡极为重要的物理参数之一，低的表面张力被认为有助于理解纳米气泡的超大接触角和超长稳定性。因为纳米气泡与探针的相互作用极其复杂，而且在纳米尺度下表面张力的精确测量一直是一个技术难点，因此，理论上和实验上一直都鲜见有对纳米气泡表面张力的定量研究。本研究中，通过系统调控溶液浓度原位定量地研究溶液表面张力对纳米气泡界面特性的影响，我们发现纳米气泡的高度随乙醇浓度的增加而略微增大，而其横向尺寸随溶液乙醇浓度的增加而略微减小；纳米气泡的表面张力约是对应宏观溶液表面张力的一半；纳米气泡的接触角在纯水中和乙醇水溶液中都比对应的宏观接触角大得多；表面张力和接触角都随乙醇浓度的增大而减小。研究结果为用低表面张力解释纳米气泡的超长稳定性和超大接触角提供了定量的实验依据[4]。

另外，课题组系统研究了 AFM 针尖与纳米液滴的作用，发现当针尖与液滴接触之后，三相线被固定在了针尖上了，整个体系的力学响应是线性的。进一步建立了一个模型，解释了纳米液滴的硬度与其大小的关系，这一套方法可以进一步用在研究纳米尺度的浸润问题上[5]。

参考文献

1. Zhao B, Wang X, Song Y, *et al.* Phys Chem Chem Phys, 2015, **17**: 13598−13605.
2. Wang X, Zhao B, Ma W, *et al.* Chem Phys Chem, 2015, **16(5)** : 1003–1007.
3. Ma W, Zhang M, Nie X, *et al.* Chinese Physics Letter, 2015, **32**: 046801.
4. Zhao B, Wang X, Wang S, *et al.* Soft Matter, 2016, **12**(14): 3303−3309.
5. Wang S, Wang X, Zhao B, *et al*, Langmuir, 2016, **32**(43): 11230−11235.

Latest of Nanobubble Research

Laboratory of Physical Biology Soft X-ray Group of SSRF

Based on Laboratory of Physical Biology and Soft X-ray Group of SSRF, this project mainly focuses on the research about the basic properties of nanobubbles and nanolayers and their applications in environmental scicence, biological science, etc. The large progress during the years of 2015 and 2016 mainly included the measurement of interfacial micropancakes, the controllable growth of nanobubbles on different substrates and in situ measurement of interfacial tension of nanobubbles.

Quantitativly measurement of mechanical property of interfacial micropancakes

Interfacial micropancakes are the state of gas aggregation at nanometer scale. The understanding to them is very few from both theoretical and experimental aspects. Here, for the first time the mechanical properties of micropancakes were measured quantitatively in pure water and ethanol solution. It was found that the stiffness of micropancakes decreases with the concentration of ethanol in water and the pancakes would be invisible when ethanol concentration reaches to a critical value. But they will appear after the replacing by pure water. The measurement of stiffess using AFM quantitatively nano mechanical imaging mode provides a sensitive method for detecting the existence and layers of micropancakes, and also distinguish nanobubles, nano gas layers and substrates[1].

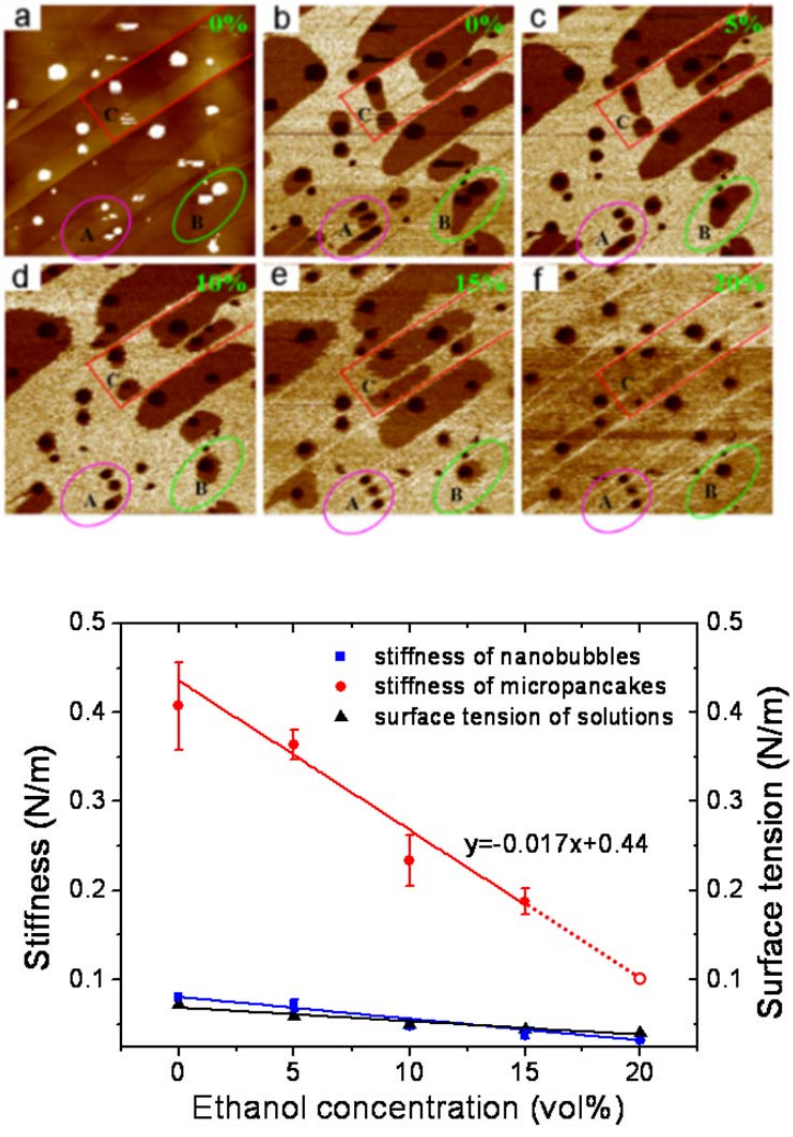

Fig.1 (a) The stiffness images of nanobubbles and micropancakes obtained by PF-QNM. (b) The change of stiffness of micropacke with the concentration of ethanol in water

Controllable growth of nanobubbles at different substrates

Interfacial nanobubbles have super stability and large contact angle on solid surface. It is generally believed that the contact angle of nanobubbles is closely related to the substrate, temperature, and the types of gas. In this work, the generation and growth of nanobubbles at different substrates with varied hydrophobic properties were compared. Results showed the contact angle of nanobubbles become larger and larger with the stronger hydrophobic substrates. In addition, using molecular dynamics simulation, by changing the carbon atoms of graphene electric dipole moment to modifiy the difference of hydrophobic surface. The results showed that nanobubbles can be stable on the hydrophobic surface rather than hydrophilic one. Second, by modifying the appropriate electric dipole moment to produce the edge effect (water wall) and first placed gas nucleation to fix Nanobubbles in the enclosed area.These results will help to understand the long life of nanobubbles from the of theoritical aspects and also used in microfluidic applications[2−3].

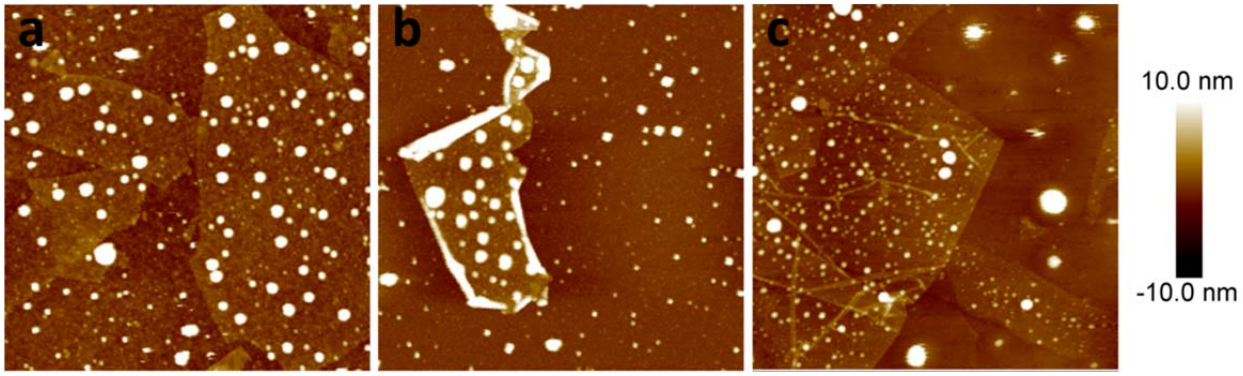

Fig.2 The PF-QNM images of nanobubbles on substrates of rGO-Si_3N_4 (a), rGO-mica (b) and rGO-HOPG (c). These nanobubbles were produced by ethanol-water exchange. The concentrations of the rGO were 0.2 mg/mL, 0.4 mg/ml and 0.1 mg/ml, respectively. Scan size: 3 μm×3 μm

The in situ measurement of contact angle and surface tension of nanobubbles

Surface tension is an important factor of nanobubbles and low surface tension is considered to help to understand the large contact angle and long lifetime of nanobubbles. The interaction between nanobubble and AFM tip is more complicated and also it is difficulty to measure accurately at nanometer scale. Therefore, it is very few report about the measurement of surface tension of nanobubble both theory and experiment. Here, the influence of surface tension on the nanobubble interfacial properties was in situ quantitatively investigated by systematically controlling the solution concentration, it was found that the height of nanobubbles increases slightly, and the lateral sizes slightly decrease with the increase of the concentration of ethanol. The surface tension of the nanometer bubble is about half of the surface tension at the macroscopic scale. The contact angle of the nanometer bubbles is much larger than the corresponding macroscopic contact Angle in pure water and ethanol solution. Both surface tension and contact angle decrease with the increase of ethanol concentration. These results will provide the experimental evidence for understanding the ultra-long stability and large contact angle of nanobubbles by using low surface tension [4].

In addition, this group has also systematically investiged the interaction between AFM tip and nanodroplets. It was found that when the tip contacts with nanodroplet, three-phase line are fixed on the top of tip, the mechanical response of the whole system is linear. A new model is established to explain the relationship between the stiffness and size of the nanoscale droplets, which can be further used in the study of the nano-scale wetting problem[5].

Reference

1. Zhao B, Wang X, Song Y, *et al.* Phys Chem Chem Phys, 2015, **17**: 13598−13605.
2. Wang X, Zhao B, Ma W, *et al.* Chem Phys Chem, 2015, **16(5)** : 1003–1007.
3. Ma W, Zhang M, Nie X, *et al.* Chinese Physics Letter, 2015, **32**: 046801.
4. Zhao B, Wang X, Wang S, *et al.* Soft Matter, 2016, **12(**14**)**: 3303−3309.
5. Wang S, Wang X, Zhao B, *et al,* Langmuir, 2016, **32(**43**)**: 11230−11235.

附录 1

2015–2016 年博士、硕士学位授予一览表

PhD and MD Programs Completed at SINAP IN 2015-2016

2015

No.	学位	姓名	专业	论文题目	研究方向	导师
1	博士	林维豪	核技术及应用	大尺寸反射镜高精度检测方法研究	光学检测	王劼
2	博士	曾友石	核技术及应用	氢及其同位素在熔盐中的渗透与扩散行为研究	熔盐堆中氚的控制	刘卫
3	博士	寿齐烨	粒子物理与原子核物理	相对论重离子碰撞(RHIC)强磁场中的电荷分离和手征磁波的研究	高能核物理	马余刚
4	博士	姜先凯	粒子物理与原子核物理	DNA 分子与纳米材料的相互作用的理论研究	纳米结构中光电子的关联效应及其应用	怀平
5	博士	张志宏	核技术及应用	2 MWt 液态钍基熔盐堆辐射屏蔽的预概念设计	反应堆安全	夏晓彬
6	博士	吴娜	无机化学	基于原子力显微镜的 DNA 折纸上单分子反应的研究	纳米技术	胡钧
7	博士	王超鹏	核技术及应用	C-band 微波脉冲压缩器设计和实验研究	加速器物理与微波技术	赵振堂
8	博士	张志刚	核技术及应用	同步辐射光源增强器高频数字化低电平系统研制	加速器技术及应用	刘建飞
9	博士	吴军	核技术及应用	上海先进质子治疗装置旋转机架优化设计	质子治疗技术与装置	薛松
10	博士	陈直	核技术及应用	硬 X 射线折射透镜的纳米聚焦特性研究	X 射线光学	肖体乔
11	博士	尹聪聪	核技术及应用	钍基熔盐堆 EPICS 控制系统可靠性技术应用研究	信号处理与控制技术	李勇平
12	博士	陈利芳	无机化学	PVDF 抗污染膜的研制及膜技术处理放射性废水的研究	滤膜的改性及应用	陆晓峰
13	博士	吕明	粒子物理与原子核物理	中能重离子碰撞中热密核物质性质的研究	放射性核束物理和重离子物理	马余刚
14	博士	何万兵	粒子物理与原子核物理	奇异结构原子核的巨偶极共振性质研究	放射性核束物理和重离子物理	蔡翔舟
15	博士	刘可	粒子物理与原子核物理	国产 Ni 基合金材料离子辐照与熔盐腐蚀效应研究	核分析技术在材料科学中的应用	李燕
16	博士	周永年	核技术及应用	上海光源基于 EPICS 的 QXAFS 数据采集系统的研究与实现	同步辐射光束线控制与数据获取	李勇平
17	博士	代智涛	粒子物理与原子核物理	中子皮厚度敏感探针研究	放射性核束物理	沈文庆

18	博士	刘应都	粒子物理与原子核物理	11B 原子核的高激发态能级研究	放射性核束物理和重离子物理	马余刚
19	博士	海洋	粒子物理与原子核物理	HDPE、HDPE/C 结构及其辐照效应的 SAXS 研究	材料辐照损伤研究	朱智勇
20	博士	赵亮	粒子物理与原子核物理	纳米受限双亲分子溶液的分子动力学模拟研究	纳米尺度溶液中分子的成核性质	朱智勇
21	博士	宋士雄	核能科学与工程	熔盐冷却球床堆热工水力特性研究	反应堆热工水力	蔡翔舟
22	博士	朱贵凤	核技术及应用	氟盐冷却球床高温堆钍利用研究	反应堆物理	徐洪杰
23	博士	谢思远	无机化学	静电纺丝法制备海水提铀用纳米纤维吸附材料及其性能研究	聚合物纳米复合材料	李景烨
24	博士	江大卫	无机化学	功能 DNA 纳米结构双模态探针的制备与生物性质研究	分子影像与放射性药物	张岚
25	博士	朱丹	无机化学	纳米界面上 DNA 分子反应活性的研究及其在生物传感中的应用	纳米生物学	宋世平
26	博士	刘蒙蒙	无机化学	应用暗场显微镜研究细胞与纳米金相互作用	纳米材料	樊春海
27	博士	赵彬钰	无机化学	固液界面纳米气泡界面特性的先进纳米成像研究	界面纳米科技	胡钧
28	博士	邢淑	无机化学	高阶 DNA 纳米结构的构建及其生物学应用	DNA 纳米材料	樊春海
29	博士	张招红	核技术及应用	上海光源光束线站 TRXEOL 方法的研究和实现	同步辐射光束线站控制	薛松
30	博士	阴慧琴	无机化学	腐蚀产物 CrF3 对 LiF-NaF-KF 熔盐物化性质的影响研究	熔盐物性研究	谢雷东, 王文锋
31	博士	汪德高	无机化学	基于金属氧化物半导体的人工光合作用	太阳能分解水	樊春海
32	博士	张明俊	核技术及应用	铁电体中极化团簇动力学的相干光实验研究	铁电体中极化团簇动力学过程	邰仁忠
33	博士	邱杰	核技术及应用	含 Cr 的镍基合金在熔盐环境中的腐蚀机理研究	高温合金腐蚀研究	徐洪杰
34	博士	许周烽	核技术及应用	Si 对 GH3535 合金热暴露后的组织和力学性能的影响	堆结构材料	周兴泰
35	博士	程宏伟	核技术及应用	Te 导致 GH3535 合金晶间开裂行为的研究	核反应堆结构材料	周兴泰
36	博士	廖浪	核技术及应用	微波微脉冲电子枪的研究与设计	微波微脉冲电子枪的研究与设计	赵明华
37	博士	赵镍	核技术及应用	自组装介孔薄膜与自组装聚电解质薄膜的掠入射 X 射线散射研究	同步辐射掠入射 X 射线散射	王劼

38	博士	林美华	无机化学	四面体 DNA 纳米结构探针设计及其在生物传感中的应用	基于 DNA 纳米技术的生物传感	樊春海
39	博士	欧阳湘元	无机化学	基于 DNA 折纸的纳米材料的构建和应用	DNA 纳米技术	樊春海
40	博士	谭建豪	粒子物理与原子核物理	用于超短束团长度测量的 X 波段行波偏转结构的研究	自由电子激光与加速器物理	赵振堂
41	博士	吴景霞	无机化学	超疏水纺织品的辐射方法制备及其服用性能研究	高分子材料接枝改性	李景烨
42	博士	李林	核技术及应用	软 X 射线自由电子激光 LLRF 控制系统建模及算法研究	低电平控制系统	顾强
43	博士	徐宇列	无机化学	吉米沙星、巴洛沙星、妥舒沙星等氟喹诺酮类药物的光化学性质及其对生物分子的光敏损伤研究	快速反应动力学	王文锋,何建华
44	博士	田佳甲	核技术及应用	基于绝缘芯平面变压器的高压电源研制	加速器技术及应用	李德明
45	博士	田甜	无机化学	针灸和 DNA 四面体载药体系在治疗脑部疾病中的作用研究	纳米生物学	樊春海
46	博士	侯尚国	核技术及应用	基于多种非线性效应的超分辨成像研究	光学超分辨成像	樊春海
47	博士	汪全全	核技术及应用	钍基熔盐堆棒控棒位系统及功率控制系统研究	反应堆控制与测量	李勇平
48	博士	李晓丽	核技术及应用	稀土 Y 对熔盐反应堆结构材料 GH3535 镍合金微观结构和抗高温腐蚀性能的影响	堆用高温合金的抗高温腐蚀性能的研究	余笑寒
49	博士	李建喜	无机化学	LDPE 基核用电缆含磷阻燃体系的制备及性能研究	高分子材料加工与应用	李景烨
50	博士	何永周	核技术及应用	低温永磁波荡器永磁体磁特性及样机磁场研究	波荡器应用磁学	周巧根
51	博士	汪颖	核技术及应用	基于原子力显微镜的单片层氧化石墨烯及其还原态材料的电学和力学性质研究	纳米材料	胡钧
52	硕士	董晓雨	无机化学	钍基熔盐堆氟化物燃料高温水解研究	钍基核燃料水法后处理	张岚
53	硕士	袁超	信号与信息处理	数字化裂变室宽量程中子通量密度测量的研究	中子通量密度测量的研究	李勇平
54	硕士	薛冰	粒子物理与原子核物理	电子关联体系角分辨光电子谱理论研究	电子光谱学	朱志远
55	硕士	陈峰	信号与信息处理	放射性气体气溶胶监测系统数据采集技术与控制软件设计	辐射探测系统开发与研究	夏晓彬
56	硕士	资明	粒子物理与原子核物理	三维空间分辨共聚焦方法及应用研究	同步辐射方法学研究	黄宇营

57	硕士	李万新	高分子化学与物理	纺织品表面辐射接枝金属有机框架化合物的研究	高分子辐射化学	李景烨
58	硕士	皮力	无机化学	用氢同位素估算氚在熔盐堆材料中的渗透	氚科学技术与材料	刘卫
59	硕士	刘少海	核技术及应用	并行冗余协议在反应堆仪控系统控制网络中的应用研究	冗余控制网络的可靠性	陈永忠
60	硕士	孙鹏飞	粒子物理与原子核物理	同步辐射微束荧光 CT 及其稀土元素定量分析研究	同步辐射荧光 CT	肖体乔
61	硕士	张春波	核技术及应用	基于图像分析的同步辐射光束诊断系统研究	光束线技术	何建华
62	硕士	朱亚	核技术及应用	新型纯永磁波荡器 EPU200 磁结构的力学分析和研究	加速器机械	周巧根
63	硕士	魏书华	核技术及应用	板型先进高温堆的可燃毒物优化设计研究	反应堆物理	余笑寒
64	硕士	耿合龙	信号与信息处理	储存环束流轨道联锁及数据后分析系统的关键技术研究	数据采集与信号处理	冷用斌
65	硕士	郁亚男	信号与信息处理	电流型可编程扫描磁铁电源研究	加速器电子学方面，包括特种电源研制和数据采集	李德明
66	硕士	刘哲	核技术及应用	熔盐堆用镍基合金中氦行为的离子束技术研究	核分析技术在材料科学中的应用	李燕
67	硕士	芮小军	信号与信息处理	基于 FPGA 的同步光反馈控制技术的研究	运动控制与探测器信号处理	郑丽芳
68	硕士	朱晓慧	信号与信息处理	医用质子加速器数字化扫描电源技术的研究	信号与信息处理	李瑞
69	硕士	吴清雷	粒子物理与原子核物理	多肽骨架铝环结构与氨基酸环状侧链相互作用的理论研究	量子化学模拟	宋波
70	硕士	杨峻	电磁场与微波技术	1500 MHz 5-cell 超导腔的仿真及优化	核技术及应用	刘建飞
71	硕士	巫邦庭	高分子化学与物理	接枝型聚苯胺基导电织物的制备及其性能研究	高分子辐射化学	李景烨
72	硕士	史万龙	无机化学	萃取色层法在 U-233 提取流程中分析的应用研究	核燃料水法后处理	张岚
73	硕士	陈媚	粒子物理与原子核物理	基于微纳加工的闪烁体表面修饰技术应用探索	闪烁探测材料与微纳光学	邰仁忠
74	硕士	曹寅	核能与核技术工程	涡流二极管的设计优化与实验研究	反应堆热工水力学	陈堃
75	硕士	夏凯	生物工程	Fe3O4 纳米颗粒与蛋白的相互作用及生物学效应研究	纳米材料生物效应研究	樊春海
76	硕士	何健	核能与核技术工程	SAXS Channel-cut 分光晶体加工与检测研究	同步辐射光学元件设计、加工与检测	王劼

77	硕士	林超	核能与核技术工程	硝酸盐自然循环回路运行特性的数值模拟	反应堆热工水力学	陈堃
78	硕士	韩仲康	生物工程	二氧化铈体系表面化学性质及其催化性能的第一性原理研究	理论催化	高嶷
79	硕士	丁祥彬	核能与核技术工程	Hastelloy N 合金和 316L 不锈钢在 LiF-NaF-KF 熔盐中的腐蚀行为研究	高温合金在氟化熔盐中的腐蚀研究	周兴泰
80	硕士	梁传晖	电子与通信工程	X 射线图像降噪和对比度增强算法研究	图像处理	肖体乔
81	硕士	王婷婷	核能与核技术工程	1A GeV Au+Au 碰撞产生 π 介子动力学模拟	粒子物理与原子核物理	马余刚
82	硕士	唐延泽	核能与核技术工程	基于 Aspen HYSYS 软件的熔盐堆实验装置热工瞬态仿真	反应堆热工水力	王纳秀
83	硕士	王飞飞	核能与核技术工程	GPU 技术在反应堆设计中的应用研究	核技术及应用	沈立人
84	硕士	马永朋	核能与核技术工程	基于同步辐射的原子分子康普顿轮廓研究	核技术及应用	杨科
85	硕士	李佳	生物工程	硅油对淀粉样蛋白和多肽积聚的促进作用	生物工程	胡钧
86	硕士	罗承明	电子与通信工程	加速器工具箱的并行优化	信息与微系统控制	姜伯承
87	硕士	田金	核能与核技术工程	10MWt 固态燃料熔盐冷却实验堆(TMSR-SF1)乏燃料贮存系统的临界安全分析	第四代先进核能系统核安全	夏晓彬
88	硕士	麦锡源	核能与核技术工程	核燃料包覆喷动床气固流动特性模拟研究	反应堆物理与工程	朱智勇
89	硕士	赵欢欢	核能与核技术工程	偕胺肟基聚丙烯腈纤维的制备及其对铀酰和竞争离子吸附性能研究	高分子辐射化学	王敏
90	硕士	王国林	电子与通信工程	基于高梯度加速结构高功率测试平台控制和测量的研究	数字和脉冲信号与信息处理	顾强
91	硕士	官龙腾	电子与通信工程	超声流量计数字化网络通信系统设计与实现	电子与通信工程	李勇平
92	硕士	夏冬琴	核能与核技术工程	金属裂变产物在核石墨上的吸附和扩散的理论研究	反应堆材料物理	怀平
93	硕士	雷蕾	电子与通信工程	反应堆控制系统软件配置管理工具研究与开发	反应堆控制系统软件	李勇平
94	硕士	董玉玺	核能与核技术工程	自由电子激光装置中关键支撑系统机械稳定性研究	加速器机械	王莉

No.	学位	姓名	专业	论文题目	研究方向	导师
1	博士	吕彬	核技术及应用	基于T-S模糊模型的强流电子枪建模与控制算法研究	加速器控制	李德明
2	博士	曹玲玲	粒子物理与原子核物理	基于同步辐射技术研究城市生活垃圾焚烧中元素的迁移转化及其对环境的影响	同步辐射技术在环境中的应用	李燕
3	博士	刘健	粒子物理与原子核物理	富含芳香环的碳基材料表面水与离子的吸附和动力学行为的理论研究	核物理与计算物理	方海平
4	博士	王昌英	粒子物理与原子核物理	锕系碳化物和氟化物材料的电子结构和成键特性的理论研究	熔盐堆材料	怀平
5	博士	张庆磊	粒子物理与原子核物理	上海光源插入件效应研究	加速器物理	赵振堂
6	博士	孟虎	无机化学	铀酰离子印迹聚合物的合成与性能研究	铀吸附分离材料	张岚
7	博士	张淼	粒子物理与原子核物理	波荡器动力学积分场效应及其磁场垫补方法的研究	加速器物理	周巧根
8	博士	赵翠兰	核技术及应用	伽玛射线成像探测技术研究	射线成像	李勇平
9	博士	孙国民	核能科学与工程	基于MCNP5和ORIGEN2.1的熔盐堆燃料管理程序开发与应用研究	反应堆物理分析	戴志敏
10	博士	吕晓雯	核技术及应用	2MW液态钍基熔盐实验堆气载放射性流出物辐射环境影响分析	辐射环境影响分析	夏晓彬
11	博士	安振东	粒子物理与原子核物理	氦燃烧中12C(α,γ)16O反应天体物理S因子及其热核反应率的综合研究	核天体物理	马余刚
12	博士	郭盼	粒子物理与原子核物理	羧基终端的烷链自组装单层膜表面纳米水层的理论研究	纳米尺度界面水的结构和性质研究	方海平
13	博士	孔令伟	粒子物理与原子核物理	耦合双粒子在不对称体系中的输运现象研究	内部作用对输运性质的影响	方海平
14	博士	谭海	粒子物理与原子核物理	显微CT三维血管图像定量分析的研究	显微CT三维血管图像定量分析的研究	肖体乔
15	博士	杨昆	核技术及应用	基于修正中子平衡方法的Candle堆特性研究	核反应堆物理	蔡翔舟
16	博士	李麒成	核技术及应用	强流高压加速器束流性能提升的研究	加速器技术及应用	李德明
17	博士	尚明丰	无机化学	同步辐射原位XAFS实验方法表征燃料电池催化剂在工作状态下的结构变化	同步辐射应用技术	黄宇营
18	博士	李怡雯	核技术及应用	同步辐射原位微流设备的研制及在蛋白质研究中的应用	同步辐射技术及应用	王劼
19	博士	马垚	无机化学	静电纺丝法制备胺基纳米纤维材料及其水处理应用研究	高分子材料	李景烨

20	博士	杜林	核技术及应用	环境样品中有机氚(OBT)比活度的测定	氚科学与技术	刘卫
21	博士	王震	粒子物理与原子核物理	高增益自由电子激光微束团的产生与应用研究	加速器物理	赵振堂
22	博士	丁洪利	核技术及应用	固态射频功率源的研究与设计	加速器技术	赵明华
23	博士	沈建磊	无机化学	DNA 介导复杂金属纳米粒子的合成，组装及表面等离子体效应研究	材料合成及表面等离子体光子学效应研究	樊春海
24	博士	陈世兴	无机化学	基于电化学传感器分析基因甲基化及羟甲基化修饰	生物传感器	宋世平
25	博士	彭超	核技术及应用	球床型氟盐冷却高温堆正常运行工况下放射性源项的初步分析	反应堆安全分析	陈堃
26	博士	宋萍	无机化学	纳米生物界面精确调控及在生物传感中的应用	生物传感器	宋世平,樊春海
27	博士	杨勇	核技术及应用	储存环逐束团位置测量关键技术研究	信号与信息处理	冷用斌
28	博士	刘珍宝	核能科学与工程	钍基熔盐堆保护系统定期试验平台开发	反应堆工程与技术	刘桂民
29	博士	孙亚平	核能科学与工程	熔盐堆含氟放射性废物磷酸盐固化方案及固化体性能研究	放射性废物安全	夏晓彬
30	博士	秦为为	无机化学	等离子纳米粒子在可视化成像检测及纳米马达中的应用	纳米金 LSPR 性质的应用	樊春海
31	博士	王少朋	无机化学	DNA 纳米技术在细胞动态控制和细胞动态成像中的应用	纳米材料研究及应用	樊春海
32	博士	王璐	无机化学	纳米材料引发的细胞自噬机制与效应研究	纳米生物学	王丽华,陈楠
33	博士	张学强	无机化学	肌动蛋白在固液界面的组装行为及机械力对组装过程的影响探究	单分子纳米操纵	张益
34	博士	李勇军	核技术及应用	上海光源高热负载前端区的系统设计与研究	同步辐射光学与技术	薛松
35	博士	徐艳	无机化学	HRP 催化的单颗粒检测探针的构建及单分子研究	单分子催化	胡钧,樊春海
36	博士	张瑜	无机化学	免疫调控药物纳米金刚石-CpG 寡脱氧核苷酸复合物的研究	生物	李迪
37	博士	邢晨阳	无机化学	离子液体接枝的聚偏氟乙烯及其结构与性能的研究	高分子材料辐照改性	李景烨
38	博士	吕丽君	核技术及应用	钍基熔盐堆氚吸附与储存用 LaNi4.25Al0.75 和 ZrCo 合金性能改进研究	储氚金属材料	李晓林
39	博士	邓王平	无机化学	电化学生物传感器在 POCT 中的应用研究	纳米生物传感与生物检测	樊春海

40	硕士	武海龙	光学工程	基于激光康普顿散射的伽玛射线源的理论及模拟研究	加速器物理与技术	王东
41	硕士	王晓宁	无机化学	氧化石墨烯及其复合材料的制备与钍、铀吸附性能研究	放射化学分离技术	张岚
42	硕士	胡佳	信号与信息处理	低能电子束固化仪的控制系统设计	加速器的控制	李德明
43	硕士	谢新华	电磁场与微波技术	多 cell 1.5 GHz 超导腔双输入耦合器研究	超导高频技术	刘建飞
44	硕士	李巧	信号与信息处理	同步辐射双能 CT 图像的高精度配准研究	X 射线成像光学	肖体乔
45	硕士	贾昀澎	无机化学	熔盐堆燃料干法处理中裂变产物铯的行为与分离研究	钍铀燃料干法分离技术	李晴暖
46	硕士	郭萍	生物物理学	脯氨酸 endo/exo 构象异构体对 PPII 结构的影响	计算生物学	高嶷
47	硕士	仇婷婷	无机化学	干法尾料水法后处理中氟化物的分析	核燃料水法后处理	周伟
48	硕士	黄佩	生物物理学	人源 FABP4 蛋白和 PABPN1 蛋白的结构与功能研究	生物大分子结构	何建华
49	硕士	戴责已	粒子物理与原子核物理	可批量化生产的行波加速管的设计	加速管设计	赵明华
50	硕士	郑海伟	核能科学与工程	氟盐冷却高温堆系统响应特性研究及应用	核能科学与工程	王纳秀
51	硕士	李秀芳	粒子物理与原子核物理	轻丰中子核的中子皮厚度研究	放射性核束物理	方德清
52	硕士	何欣钟	高分子化学与物理	聚四氟乙烯低温等离子体接枝改性及无钯化学镀铜	高分子材料表面改性	吴国忠
53	硕士	周晓苓	核技术及应用	镍基碳化硅复合材料的辐照性能研究	核材料性能	徐洪杰
54	硕士	李甫梧	生物物理学	基于 DNA 甲基化特异性位点区分癌症种类、以及同种癌症分型并定量检测血液中的循环肿瘤细胞	生物物理学	王丽华
55	硕士	潘亮	高分子化学与物理	DNA 纳米结构和纳米金的生物安全性研究	纳米生物学	李迪
56	硕士	杨亚运	核技术及应用	多元荧光探测器 Soller 狭缝自动对焦方法研究	核技术及应用	黄宇营
57	硕士	潘登	核技术及应用	球床熔盐堆堆芯流动压降与对流换热的等效研究	核反应堆热工水力	余笑寒
58	硕士	李松	信号与信息处理	基于 FPGA 的电子直线加速器低电平系统前馈控制的实现	信号与信息处理	赵明华
59	硕士	朱亚胜	核技术及应用	Ni 基合金焊接件在氟化物熔盐中腐蚀行为及机理研究	合金材料的腐蚀	周兴泰

60	硕士	杨凡	信号与信息处理	上海光源面探测器图像数据获取与处理系统设计	光束线站图像数据的获取与处理	薛松
61	硕士	杨君	信号与信息处理	工业加速器的远程网络监测和控制系统研究及实现	加速器控制	李德明
62	硕士	高韶华	粒子物理与原子核物理	阳离子-π作用对基于碳纳米管的锂离子电池电压的影响	计算化学	方海平
63	硕士	唐兴海	信号与信息处理	低电平上层应用软件的研究	应用软件，控制系统	顾强
64	硕士	张永栋	核技术及应用	TRISO 包覆燃料颗粒结构和失效行为的研究	反应堆燃料研究	朱智勇
65	硕士	刘华秋	粒子物理与原子核物理	蒸汽辅助沉积法制备甲胺铅碘钙钛矿薄膜的微观结构研究	表面科学与材料科学	高兴宇
66	硕士	刘婷	信号与信息处理	高温熔盐超声流量计的信号处理方法与技术研究	信号与信息处理	李勇平
67	硕士	韦贵生	生物物理学	DNA 四面体纳米结构探针设计及 细胞标记成像应用	DNA 纳米生物应用	樊春海
68	硕士	李贺	核能科学与工程	兰州重离子储存环外靶实验终端时间投影室样机的研究	核辐射探测器研制	马余刚
69	硕士	李昌亮	核能与核技术工程	上海光源储存环垂直发射度的研究	加速器物理与束流动力学	张文志
70	硕士	马佳文	核能与核技术工程	碳纳米材料与金属复合结构中空位缺陷产生和作用机制的理论研究	粒子束与纳米结构的相互作用	朱志远
71	硕士	缪亚运	电子与通信工程	质子治疗装置脉冲电源的研制	加速器凸轨磁铁脉冲电源研究	谷鸣
72	硕士	许健	核能与核技术工程	金属镍中氦与位错相互作用的原子尺度模拟	材料的辐照效应	怀平
73	硕士	王晓勋	电子与通信工程	PSD 位置测量系统在波荡器磁场测量中的应用	波荡器技术	周巧根
74	硕士	童新宇	光学工程	高精度光学检测中镜面几何参数的拟合方法研究	X 射线光学技术	王劼
75	硕士	王龙龙	核能与核技术工程	上海光源BL14W1线站TXRF方法的发展及其在水样的应用研究	核技术及应用	黄宇营
76	硕士	张白鑫	核能与核技术工程	基于遗传算法的自由电子激光优化软件的开发	信号与信息处理	刘波
77	硕士	卢兰露	核能与核技术工程	Te 在镍中的晶间脆化微观机理的研究	核技术及应用	姜政
78	硕士	刘树林	核能与核技术工程	W 含量对 Ni-xW-6Cr 合金微观组织和拉伸力学性能的影响研究	高温镍基合金力学性能研究	周兴泰
79	硕士	刘小吉	电子与通信工程	水环境对金钛团簇 TiAu4 的影响	计算材料学	高嶷

80	硕士	陆瑞游	光学工程	多通道 X 射线吸收精细结构谱数据采集系统应用研究	仪器科学与技术	司锐
81	硕士	岳兵兵	生物工程	静电纺丝法制备仿荷叶自清洁热粘性纤维薄膜的研究	仿生材料	李景烨
82	硕士	周振华	核能与核技术工程	2MW 液态钍基熔盐流量分配设计	核反应堆热工水力学	余笑寒
83	硕士	何杰	核能与核技术工程	基于 MCNPX 与 Fluent 的液态钍基熔盐堆物理热工耦合研究	反应堆安全	夏晓彬
84	硕士	苏芝	电子与通信工程	TMSR 热工回路漏热功率监测软件开发	控制系统	刘桂民
85	硕士	胡晓娟	生物工程	铜抗菌作用的生物物理学研究	生物工程	吕军鸿
86	硕士	刘卓	生物工程	DNA 纳米结构及其仿生矿化的生物学效应研究	生物工程	宋世平
87	硕士	席瑞成	电子与通信工程	超导波荡器失超保护器件特性测试及失超动态过程测量研究	超导波荡器失超保护	许皆平
88	硕士	孙皓	电子与通信工程	基于神经网络的上海光源光束线故障预警的方法研究	数学分析	龚培荣

附录 2

2015-2016 年论文发表一览表

Papers Published in 2015-2016

2015

No.	论文名称	期刊名称	期	卷	页	作者
1	High electrocatalytic activity for borohydride oxidation on palladium nanocubes enclosed by {200} facets	JOURNAL OF POWER SOURCES	299		241	Qin, Haiying; Chen, Kaijian; Zhu, Cai
2	A review on the mechanical performance and fatigue behavior of 3-D angle-interlock woven composites	JOURNAL OF THE TEXTILE INSTITUTE	106	12	1306	Wang, Chunxia; Lu, Zhenqian; Jin, Limin
3	Corrosion behavior of ZrC-SiC composite ceramics in LiF-NaF-KF molten salt at high temperatures	CERAMICS INTERNATIONAL	41	10	12996	Wang, Yang; Tang, Zhong-Feng; Fu, Yuan
4	Enhancement of Water Evaporation on Solid Surfaces with Nanoscale Hydrophobic-Hydrophilic Patterns	PHYSICAL REVIEW LETTERS	115	19	195901	Wan, Rongzheng; Wang, Chunlei; Lei, Xiaoling
5	Shape-Dependent Activity of Ceria for Hydrogen Electro-Oxidation in Reduced-Temperature Solid Oxide Fuel Cells	SMALL	11	41	5581	Tong, Xiaofeng; Luo, Ting; Meng, Xie
6	Applications of VUV extra-focus mechanism: high-performance dual-mode monochromator from VUV to soft X-ray	JOURNAL OF SYNCHROTRON RADIATION	22		1353	Xue, Chaofan; Wu, Yanqing; Zou, Ying
7	Structural characterization and low-temperature properties of Ru/C multilayer monochromators with different periodic thicknesses	JOURNAL OF SYNCHROTRON RADIATION	22		1379	Jiang, Hui; He, Yan; He, Yumei
8	Breed-and-burn strategy in a fast reactor with optimized starter fuel	PROGRESS IN NUCLEAR ENERGY	85		11	Huang, Jinfeng; Han, Jianlong; Cai, Xiangzhou
9	Startup and burnup strategy for Th-U/U-Pu fuel cycles in an EM2 reactor	PROGRESS IN NUCLEAR ENERGY	85		764	Ma, Y. W.; Li, X. X.; Cai, X. Z.
10	Analysis of minor actinides transmutation for a Molten Salt Fast Reactor	ANNALS OF NUCLEAR ENERGY	85		597	Yu, Chenggang; Li, Xiaoxiao; Cai, Xiangzhou
11	Real-time observation of graphene layer growth: Coupling of the interlayer spacing with thickness	CARBON	94		775	Zhu, Daming; Gao, Hui; Zhang, Xingmin
12	Mechanical and thermal properties of	CERAMICS	41	9	10949	Gao, Yantao;

	chemical vapor infiltration engineered 2D-woven and 3D-braided carbon silicate composites	INTERNATIONAL				Zhou, Haijun; Liu, Min
13	Water-COOH Composite Structure with Enhanced Hydrophobicity Formed by Water Molecules Embedded into Carboxyl-Terminated Self-Assembled Monolayers	PHYSICAL REVIEW LETTERS	115	18	186101	Guo, Pan; Tu, Yusong; Yang, Jinrong
14	Blockage of Water Flow in Carbon Nanotubes by Ions Due to Interactions between Cations and Aromatic Rings	PHYSICAL REVIEW LETTERS	115	16	164502	Liu, Jian; Shi, Guosheng; Guo, Pan
15	Investigation of finite-size effects in chemical bonding of AuPd nanoalloys	JOURNAL OF CHEMICAL PHYSICS	143	14	144309	Zhu, Beien; Oguz, Ismail Can; Guesmi, Hazar
16	Parameterization of deformed nuclei for Glauber modeling in relativistic heavy ion collisions	PHYSICS LETTERS B	749		215	Shou, Q. Y.; Ma, Y. G.; Sorensen, P.
17	Astrophysical S factor of the C-12(alpha,gamma) O-16 reaction calculated with reduced R-matrix theory	PHYSICAL REVIEW C	92	4	45802	An, Zhen-Dong; Chen, Zhen-Peng; Ma, Yu-Gang
18	Direct Methylation of Amines with Carbon Dioxide and Molecular Hydrogen using Supported Gold Catalysts	CHEMSUSCHEM	8	20	3489	Du, Xian-Long; Tang, Gao; Bao, Hong-Liang
19	Photooxidation of arsenic(III) to arsenic(V) on the surface of kaolinite clay	JOURNAL OF ENVIRONMENTAL SCIENCES-CHINA	36		29	Ding, Wei; Wang, Yajie; Yu, Yingtan
20	Preparation and characterization of surface imprinted polymer for selective sorption of uranium(VI)	JOURNAL OF RADIOANALYTICAL AND NUCLEAR CHEMISTRY	306	1	139	Meng, Hu; Li, Zheng; Ma, Fuyin
21	Temperature-Induced Molecular Rearrangement of an Ionic Liquid Confined in Nanospaces: An in Situ X-ray Absorption Fine Structure Study	JOURNAL OF PHYSICAL CHEMISTRY C	119	39	22724	Jiang, Fangling; Li, Cheng; Fu, Haiying
22	Technical Note: Synchrotron-based high-energy x-ray phase sensitive microtomography for biomedical research	MEDICAL PHYSICS	42	10	5595	Liu, Huiqiang; Wu, Xizeng; Xiao, Tiqiao
23	Thermal and elemental analysis of the combustion chamber deposits in a large-scale two-stroke marine diesel engine	SCIENCE CHINA-TECHNOLOGICAL SCIENCES	58	10	1717	Zhang XuSheng; Zeng XiangMing; Sun XiuCheng
24	Strange quark matter and strangelets in the improved quasiparticle model	EUROPEAN PHYSICAL JOURNAL A	51	10	124	Wu, Chen; Xu, Renli;

25	Radiation-induced oxidation of ultra-high molecular weight polyethylene (UHMWPE) powder by gamma rays and electron beams: A clear dependence of dose rate	RADIATION PHYSICS AND CHEMISTRY	115		88	Wang, Honglong; Xu, Lu; Hu, Jiangtao
26	Immobilization of Ionic Liquids onto the Poly(vinylidene fluoride) by Electron Beam Irradiation	INDUSTRIAL & ENGINEERING CHEMISTRY RESEARCH	54	38	9351	Xing, Chenyang; Wang, Yanyuan; Zhang, Cong
27	Giant negative thermal expansion covering room temperature in nanocrystalline GaNxMn3	APPLIED PHYSICS LETTERS	107	13	131902	Lin, J. C.; Tong, P.; Zhou, X. J.
28	Reversible Regulation of Catalytic Activity of Gold Nanoparticles with DNA Nanomachines	SCIENTIFIC REPORTS	5		14402	Zhou, Peipei; Jia, Sisi; Pan, Dun
29	Hydrogen bond network in the hydration layer of the water confined in nanotubes increasing the dielectric constant parallel along the nanotube axis	JOURNAL OF CHEMICAL PHYSICS	143	11	114708	Qi, Wenpeng; Zhao, Hongwei;
30	Dilute or Concentrated Electrolyte Solutions? Insight from Ionic Liquid/Water Electrolytes	JOURNAL OF PHYSICAL CHEMISTRY LETTERS	6	18	3713	Sha, Maolin; Dong, Huaze; Luo, Fabao
31	Microstructure of atmospheric particles revealed by TXM and a new mode of influenza virus transmission	NUCLEAR INSTRUMENTS & METHODS IN PHYSICS RESEARCH SECTION B-BEAM INTERACTIONS WITH MATERIALS AND ATOMS	359		167	Bao, L. M.; Zhang, G. L.; Lei, Q. T.
32	A novel ultrasensitive electrochemical DNA sensor based on double tetrahedral nanostructures	BIOSENSORS & BIOELECTRONICS	71		434	Zeng, Dongdong; Zhang, Huan; Zhu, Dan
33	Effects of molecular weight distribution (M-d) on the performances of the polyethersulfone (PES) ultrafiltration membranes	JOURNAL OF MEMBRANE SCIENCE	490		220	Shen, Liguo; Li, Liang; Chen, Jianrong
34	Nanostructured Poly(vinylidene fluoride)/Ionic Liquid Composites: Formation of Organic Conductive Nanodomains in Polymer Matrix	JOURNAL OF PHYSICAL CHEMISTRY C	119	36	21155	Xing, Chenyang; You, Jichun; Li, Yongjin
35	Adsorption of Uranyl ions on Amine-functionalization of MIL-101(Cr) Nanoparticles by a Facile Coordination-based Post-synthetic strategy and X-ray Absorption Spectroscopy Studies	SCIENTIFIC REPORTS	5		13514	Zhang, Jian-Yong; Zhang, Na; Zhang, Linjuan

36	Nanoscale Hydrophilicity on Metal Surfaces at Room Temperature: Coupling Lattice Constants and Crystal Faces	JOURNAL OF PHYSICAL CHEMISTRY C	119	35	20409	Xu, Zhen; Gao, Yi; Wang, Chunlei
37	Rapidity dependence of elliptic and triangular flow in proton-nucleus collisions from collective dynamics	PHYSICS LETTERS B	748		301	Bozek, Piotr; Bzdak, Adam; Ma, Guo-Liang
38	Defect stability in thorium monocarbide: An ab initio study	CHINESE PHYSICS B	24	9	97101	Wang Chang-Ying; Han, Han; Kuan, Shao
39	Injection performance evaluation for SSRF storage ring	CHINESE PHYSICS C	39	9	97003	Yang Yong; Leng Yong-Bin; Yan Ying-Bing
40	Novel DNA Polymer for Amplification Pretargeting	ACS MEDICINAL CHEMISTRY LETTERS	6	9	972	Li, Xiao; Huang, Qingqing; Xiao, Jie
41	Strong Local Coordination Structure Effects on Subnanometer PtOx Clusters over CeO2 Nanowires Probed by Low-Temperature CO Oxidation	ACS CATALYSIS	5	9	5164	Ke, Jun; Zhu, Wei; Jiang, Yingying
42	Effect of Milling Time on the Microstructure and Tensile Properties of Ultrafine Grained Ni-SiC Composites at Room Temperature	JOURNAL OF MATERIALS SCIENCE & TECHNOLOGY	31	9	923	Huang, Hefei; Yang, Chao; de los Reyes, Massey
43	High-temperature corrosion behavior of Ni-16Mo-7Cr-4Fe superalloy containing yttrium in molten LiF-NaF-KF salt	JOURNAL OF NUCLEAR MATERIALS	464		342	Li, Xiao-li; He, Shang-ming; Zhou, Xing-tai
44	Study on the Air Core Formation of a Gas-Liquid Separator	JOURNAL OF FLUIDS ENGINEERING-TRANSACTIONS OF THE ASME	137	9	91301	Yin, Junlian; Li, Jingjing; Ma, Yanfei
45	A molecular dynamics study of helium diffusion and clustering in fcc nickel	COMPUTATIONAL MATERIALS SCIENCE	107		54	Wang, Chengbin; Ren, Cuilan; Zhang, Wei
46	Focusing performance of hard X-ray single Kinoform lens	ACTA PHYSICA SINICA	64	16	164104	Chen Zhi; Xu Liang; Chen Rong-Chang
47	Graphene Oxide Transparent Hybrid Film and Its Ultraviolet Shielding Property	ACS APPLIED MATERIALS & INTERFACES	7	32	17558	Xie, Siyuan; Zhao, Jianfeng; Zhang, Bowu
48	A new phase of ThC at high pressure predicted from a first-principles study	PHYSICS LETTERS A	379	26-27	1607	Guo, Yongliang; Qiu, Wujie; Ke, Xuezhi
49	In Situ XAFS Methods for Characterizing Catalyst Structure in Proton Exchange	ACTA PHYSICO-CHIMICA SINICA	31	8	1609	Shang Ming-Feng;

	Membrane Fuel Cell					Duan Pei-Quan; Zhao Tian-Tian
50	A scheme design of collimator for gantry in proton therapy facility	NUCLEAR INSTRUMENTS & METHODS IN PHYSICS RESEARCH SECTION A-ACCELERATORS SPECTROMETERS DETECTORS AND ASSOCIATED EQUIPMENT	791		47	Liu, Ming; Yin, Chongxian; Chu, Kecheng
51	A Near-Infrared-Emissive Alkynyl-Protected Au-24 Nanocluster	ANGEWANDTE CHEMIE-INTERNATIONAL EDITION	54	33	9683	Wan, Xian-Kai; Xu, Wen Wu; Yuan, Shang-Fu
52	Energy dependence of K pi, p pi, and Kp fluctuations in Au plus Au collisions from root s(NN)=7.7 to 200 GeV	PHYSICAL REVIEW C	92	2	21901	Adamczyk, L.; Adkins, J. K.; Agakishiev, G.
53	Investigation of Compton profiles of NO and C2H2	ACTA PHYSICA SINICA	64	15	153302	Ma Yong-Peng; Zhao Xiao-Li; Liu Ya-Wei
54	Universal Fluorescence Biosensor Platform Based on Graphene Quantum Dots and Pyrene-Functionalized Molecular Beacons for Detection of MicroRNAs	ACS APPLIED MATERIALS & INTERFACES	7	30	16152	Zhang, Huan; Wang, Yunsheng; Zhao, Daiwei
55	Isothermal Oxidation Behavior of GH3535 Superalloy at 700 degrees C	RARE METAL MATERIALS AND ENGINEERING	44	8	1953	Fan Jinxin; Lu Yanling; Li Zhijun
56	Study on technetium-99m labeling of graphene oxide nanosheets through click chemistry-Tc-99m labeling of graphene oxide nanosheets	NUCLEAR SCIENCE AND TECHNIQUES	26	4	40301	Jiang Da-wei; Peng Cheng; Sun Yan-Hong
57	Two-mode polarized traveling wave deflecting structure	NUCLEAR SCIENCE AND TECHNIQUES	26	4	40102	Tan Jian-Hao; Gu Qiang; Fang Wen-Cheng
58	Gantry optimization of the Shanghai Advanced Proton Therapy facility	NUCLEAR SCIENCE AND TECHNIQUES	26	4	40201	Wu Jun; Du Han-Wen; Xue Song
59	Interaction of Al-induced peptide backbone ring structure with the sidechains of His, Phe, Trp and Tyr	NUCLEAR SCIENCE AND TECHNIQUES	26	4	40504	Wu Qing-Lei; Song Bo;
60	Latest advances in soft X-ray spectromicroscopy at SSRF	NUCLEAR SCIENCE AND TECHNIQUES	26	4	40101	Zhang Li-Juan; Xu Zi-Jian; Zhang Xiang-Zhi
61	Time structure measurement of the SSRF storage ring using TRXEOL method	NUCLEAR SCIENCE AND TECHNIQUES	26	4	40202	Zhang Zhao-Hong; Jiang Zheng;

						Xue Song
62	Simulation of radiation dose distribution and thermal analysis for the bulk shielding of an optimized molten salt reactor	NUCLEAR SCIENCE AND TECHNIQUES	26	4	40603	Zhang Zhi-Hong; Xia Xiao-Bin; Cai Jun
63	Effects of Si Addition and Long-Term Thermal Exposure on the Tensile Properties of a Ni-Mo-Cr Superalloy	ACTA METALLURGICA SINICA-ENGLISH LETTERS	28	8	951	Xu, Zhou-Feng; Dong, Jia-Sheng; Jiang, Li
64	Time-Resolved XEOL Experiment System on BL14W1 at SSRF	SPECTROSCOPY AND SPECTRAL ANALYSIS	35	8	2324	Zhang Zhao-hong; Jiang Zheng; Xue Song
65	Uranium utilization with thorium blanket in Pebble Bed Fluoride salt-cooled high temperature reactor	PROGRESS IN NUCLEAR ENERGY	83		374	Zhu, Guifeng; Zou, Yang; Xu, Hongjie
66	EPMA and TEM characterization of intergranular tellurium corrosion of Ni-16Mo-7Cr-4Fe superalloy	CORROSION SCIENCE	97		1	Cheng, Hongwei; Leng, Bin; Chen, Kai
67	SAXS investigation of latent track structure in HDPE irradiated with high energy Fe ions	NUCLEAR INSTRUMENTS & METHODS IN PHYSICS RESEARCH SECTION B-BEAM INTERACTIONS WITH MATERIALS AND ATOMS	356		129	Hai, Yang; Huang, Can; Ma, Mingwang
68	Theoretical study of the interaction between metallic fission products and defective graphite	COMPUTATIONAL MATERIALS SCIENCE	106		129	Xia, Dongqin; Ren, Cuilan; Zhang, Wei
69	Local structure of AlSb2Te3 thin film studied by experimental and theoretical methods	JOURNAL OF PHYSICS AND CHEMISTRY OF SOLIDS	83		52	Zhang, Ling; Song, Sannian; Xi, Wei
70	Suppression of microbunching instability via a transverse gradient undulator	NEW JOURNAL OF PHYSICS	17		73028	Feng, Chao; Huang, Dazhang; Deng, Haixiao
71	In Situ X-ray Diffraction Study of Co-Al Nanocomposites as Catalysts for Ammonia Decomposition	JOURNAL OF PHYSICAL CHEMISTRY C	119	30	17102	Gu, Ying-Qiu; Fu, Xin-Pu; Du, Pei-Pei
72	Impeded Mass Transportation Due to Defects in Thermally Driven Nanotube Nanomotor	JOURNAL OF PHYSICAL CHEMISTRY C	119	30	17362	Chen, Jige; Gao, Yi; Wang, Chunlei
73	Ion irradiation induced element-enriched and depleted nanostructures in Zr-Al-Cu-Ni metallic glass	JOURNAL OF APPLIED PHYSICS	118	3	35308	Chen, H. C.; Cao, G. Q.; Liu, R. D.
74	Experimental study of photon correlation spectroscopy for the long-range fluctuation of polarization in ferroelectrics	ACTA PHYSICA SINICA	64	14	147801	Zhang Ming-Jun; Guo Zhi; Tai Ren-Zhong
75	The status of the first infrared beamline at	NUCLEAR INSTRUMENTS	788		116	Ji, Te; Tong,

	Shanghai Synchrotron Radiation Facility	& METHODS IN PHYSICS RESEARCH SECTION A-ACCELERATORS SPECTROMETERS DETECTORS AND ASSOCIATED EQUIPMENT				Yajun; Zhu, Huachun
76	Microstructures and Tensile Properties of Ultrafine-Grained Ni-(1-3.5) wt% SiCNp Composites Prepared by a Powder Metallurgy Route	ACTA METALLURGICA SINICA-ENGLISH LETTERS	28	7	809	Yang, Chao; Huang, He-Fei; de los Reyes, Massey
77	Uniform Doping of Titanium in Hematite Nanorods for Efficient Photoelectrochemical Water Splitting	ACS APPLIED MATERIALS & INTERFACES	7	25	14072	Wang, Degao; Chen, Huaican; Chang, Guoliang
78	Use of square wave voltammeter for online monitoring of O2- concentration in molten fluorides at 600 degrees C	JOURNAL OF ELECTROANALYTICAL CHEMISTRY	748		34	Shen, Miao; Peng, Hao; Ge, Min
79	DNA-based plasmonic nanostructures	MATERIALS TODAY	18	6	326	Chao, Jie; Lin, Yunfeng; Liu, Huajie
80	Observation of Charge Asymmetry Dependence of Pion Elliptic Flow and the Possible Chiral Magnetic Wave in Heavy-Ion Collisions	PHYSICAL REVIEW LETTERS	114	25	252302	Adamczyk, L.; Adkins, J. K.; Agakishiev, G.
81	Unraveling the Atomic Structures of the Au-68(SR)(34) Nanoparticles	JOURNAL OF PHYSICAL CHEMISTRY C	119	25	14224	Xu, Wen Wu; Gao, Yi;
82	Constructing Higher-Order DNA Nanoarchitectures with Highly Purified DNA Nanocages	ACS APPLIED MATERIALS & INTERFACES	7	24	13174	Xing, Shu; Jiang, Dawei; Li, Fan
83	Preparation of a Thermally Insulating Nanocomposite by Blending Ultra-High-Molecular-Weight Polyethylene with Gas-Phase Silica	INDUSTRIAL & ENGINEERING CHEMISTRY RESEARCH	54	23	6093	Li, Jianxi; Zhang, Cong; Chen, Tao
84	Fluorescent In Situ Targeting Probes for Rapid Imaging of Ovarian-Cancer-Specific gamma-Glutamyltranspeptidase	ANGEWANDTE CHEMIE-INTERNATIONAL EDITION	54	25	7349	Wang, Feiyi; Zhu, Ying; Zhou, Li
85	Electrical Switchability and Dry-Wash Durability of Conductive Textiles	SCIENTIFIC REPORTS	5		UNSP 11255	Wu, Bangting; Zhang, Bowu; Wu, Jingxia
86	Beam energy distribution influences on density modulation efficiency in seeded free-electron lasers	PHYSICAL REVIEW SPECIAL TOPICS-ACCELERATORS AND BEAMS	18	6	60701	Wang, Guanglei; Zhang, Weiqing; Wu, Guorong
87	A Nanostructured Architecture for	ADVANCED ENERGY	5	11	1500375	Zhou, Yucun;

	Reduced-Temperature Solid Oxide Fuel Cells	MATERIALS				Wu, Hao; Luo, Ting
88	Optimum complexation of uranyl with amidoxime in aqueous solution under different pH levels: density functional theory calculations	MOLECULAR PHYSICS	113	11	1327	Guo, Xiaojing; Wang, Yaxing; Li, Cheng
89	Dose rate effect on micro-structure and hardness of Hastelloy-N irradiated by Xe ions	JOURNAL OF NUCLEAR SCIENCE AND TECHNOLOGY	52	6	829	Liu, Ke; Lin, Jun; Bao, Liang-man
90	Azimuthal Asymmetry of Pion-Meson Emission around the Projectile and Target Sides in Au plus Au Collision at 1A GeV	CHINESE PHYSICS LETTERS	32	6	62501	Wang Ting-Ting; Lu Ming; Ma Yu-Gang
91	Mechanism of Filling and Feeding of Thin-Walled Structures during Gravity Casting	MATERIALS	8	6	3701	Li, Faguo; Zhang, Jiao; Bian, Fenggang
92	Identification of radiolytic products of [C(4)mim][PF6] under gamma-irradiation	NUCLEAR SCIENCE AND TECHNIQUES	26	3	30302	Ao Yin-Yong; Xu Min; Peng Jing
93	Irradiation and flame retardant effect of poly[bis(phenoxyphosphazene)] and magnesium hydroxide in LDPE composites	NUCLEAR SCIENCE AND TECHNIQUES	26	3	30304	Li Jian-Xi; Zhang Cong; Chen Tao
94	Improving oxidation resistance of Ni-16Mo-7Cr-4Fe nickel-based superalloy by yttrium microalloying	NUCLEAR SCIENCE AND TECHNIQUES	26	3	30201	Li Xiao-Li; He Shang-Ming; Zhou Xing-Tai
95	Parallelizing AT with open multi-processing and MPI	NUCLEAR SCIENCE AND TECHNIQUES	26	3	30104	Luo Cheng-Ming; Tian Shun-Qiang; Wang Kun
96	Small angle X-ray scattering beamline at SSRF	NUCLEAR SCIENCE AND TECHNIQUES	26	3	30101	Tian Feng; Li Xiu-Hong; Wang Yu-Zhu
97	Magnetic flux leakage analysis and compensation of high-frequency planar insulated core transformer	NUCLEAR SCIENCE AND TECHNIQUES	26	3	30105	Tian Jia-Jia; Liu Yong-Hao; Li Rui
98	Synchrotron radiation X-ray fluorescence analysis of Fe, Zn and Cu in mice brain associated with Parkinson's disease	NUCLEAR SCIENCE AND TECHNIQUES	26	3	30506	Tian Tian; Zhang Ji-Chao; Lei Hao-Zhi
99	The control and measurement of high power high-gradient acceleration structures	NUCLEAR SCIENCE AND TECHNIQUES	26	3	30102	Wang Guo-Lin; Zhang Jun-Qiang; Li Lin
100	Supercritical water oxidation of spent	NUCLEAR SCIENCE AND	26	3	30601	Wang Shuai; Qin

	extraction solvent simulants	TECHNIQUES				Qiang; Chen Kun
101	Angle-resolved photoemission spectroscopy in Hubbard model based on cluster perturbation	NUCLEAR SCIENCE AND TECHNIQUES	26	3	30501	Xue Bing; Ren Cui-Lan; Zhang Wei
102	Digital LLRF controller for SSRF booster RF system upgrade	NUCLEAR SCIENCE AND TECHNIQUES	26	3	30106	Zhang Zhi-Gang; Zhao Yu-Bin; Xu Kai
103	The Gibbs-free-energy landscape for the solute association in nanoconfined aqueous solutions	NUCLEAR SCIENCE AND TECHNIQUES	26	3	30504	Zhao Liang; Wang Chun-Lei; Fang Hai-Ping
104	Microstructure of a pyrolytic carbon coating on a nuclear graphite substrate IG-110	NEW CARBON MATERIALS	30	3	275	Feng Shang-lei; Yang Ying-guo; Bai Shuo
105	Kinetic behavior of subsonic solitary wave in graphene nanoribbon	JOURNAL OF STATISTICAL MECHANICS-THEORY AND EXPERIMENT			P06007	Chen, Jige; Qi, Wenpeng; Zhang, Meng
106	Generating intense fully coherent soft x-ray radiation based on a laser-plasma accelerator	OPTICS EXPRESS	23	11	14993	Feng, Chao; Xiang, Dao; Deng, Haixiao
107	Thermodynamic Modeling of KF-CrF3 Binary System	CHEMICAL RESEARCH IN CHINESE UNIVERSITIES	31	3	461	Yin Huiqin; Wang Kun; Xie Leidong
108	A new method to evaluate the sealing reliability of the flanged connections for Molten Salt Reactors	NUCLEAR ENGINEERING AND DESIGN	287		90	Li, Qiming; Tian, Pan; Zhou, Chong
109	Effects of Te on intergranular embrittlement of a Ni-16Mo-7Cr alloy	JOURNAL OF NUCLEAR MATERIALS	461		122	Cheng, Hongwei; Han, Fenfen; Jia, Yanyan
110	Evaluation of soil aggregate microstructure and stability under wetting and drying cycles in two Ultisols using synchrotron-based X-ray micro-computed tomography	SOIL & TILLAGE RESEARCH	149		1	Ma, Renming; Cai, Chongfa; Li, Zhaoxia
111	Design of Cold Mass Supports for a Superconducting Undulator Prototype at SINAP	IEEE TRANSACTIONS ON APPLIED SUPERCONDUCTIVITY	25	3	4101004	Liu, Yiyong; Wang, Jian; Wang, Li
112	Friction Reduction at a Superhydrophilic Surface: Role of Ordered Water	JOURNAL OF PHYSICAL CHEMISTRY C	119	21	11679	Wang, Chunlei; Wen, Binghai; Tu, Yusong
113	Coordination-Mediated Programmable Assembly of Unmodified Oligonucleotides on Plasmonic Silver Nanoparticles	ACS APPLIED MATERIALS & INTERFACES	7	20	11047	Zhu, Dan; Chao, Jie; Pei, Hao
114	Highly efficient extraction separation of uranium(VI) and thorium(IV) from nitric	SEPARATION AND PURIFICATION	146		192	Tan, Mengling; Huang, Chao;

	acid solution with di(1-methyl-heptyl) methyl phosphonate	TECHNOLOGY				Ding, Songdong
115	Umbellate Distortions of the Uranyl Coordination Environment Result in a Stable and Porous Polycatenated Framework That Can Effectively Remove Cesium from Aqueous Solutions	JOURNAL OF THE AMERICAN CHEMICAL SOCIETY	137	19	6144	Wang, Yanlong; Liu, Zhiyong; Li, Yuxiang
116	Improved resolution in fluorescence microscopy with the FRET pairs by time gating	OPTICS EXPRESS	23	10	13121	Hou, Shangguo; Chen, Jianfang; Deng, Suhui
117	Isolation of flow and nonflow correlations by two- and four-particle cumulant measurements of azimuthal harmonics in root s(NN)=200 GeV Au+Au collisions	PHYSICS LETTERS B	745		40	Abdelwahab, N. M.; Adamczyk, L.; Adkins, J. K.
118	Quantitative investigation of the poly-adenine DNA dissociation from the surface of gold nanoparticles	SCIENTIFIC REPORTS	5		10158	Lu, Weiwen; Wang, Lihua; Li, Jiang
119	Possible observables for the chiral electric separation effect in Cu plus Au collisions	PHYSICAL REVIEW C	91	5	54901	Ma, Guo-Liang; Huang, Xu-Guang;
120	Characterization and Cytotoxicity of PM < 0.2, PM0.2-2.5 and PM2.5-10 around MSWI in Shanghai, China	INTERNATIONAL JOURNAL OF ENVIRONMENTAL RESEARCH AND PUBLIC HEALTH	12	5	5076	Cao, Lingling; Zeng, Jianrong; Liu, Ke
121	Fluorine-18 click radiosynthesis and MicroPET/CT evaluation of a small peptide-a potential PET probe for carbonic anhydrase IX	JOURNAL OF NUCLEAR MEDICINE	56	3		Jia, Lina; Jiang, Dawei; Cheng, Dengfeng
122	Stability of dibaryon (Xi(0)Xi(-)) in the quasiparticle model	EPL	110	4	42001	Wu, Chen; Xu, Renli;
123	Electrochemical Sensors Using Two-Dimensional Layered Nanomaterials	ELECTROANALYSIS	27	5	1062	Su, Shao; Chao, Jie; Pan, Dun
124	Weak magnetic field accelerates chromate removal by zero-valent iron	JOURNAL OF ENVIRONMENTAL SCIENCES	31		175	Feng, Pian; Guan, Xiaohong; Sun, Yuankui
125	A Comparative Study on the Self-Assembly of an Amyloid-Like Peptide at Water-Solid Interfaces and in Bulk Solutions	MICROSCOPY RESEARCH AND TECHNIQUE	78	5	375	Du, Qiqige; Dai, Bin; Hou, Jiahua
126	Low-Temperature Growth of Bismuth Thin Films with (111) Facet on Highly Oriented Pyrolytic Graphite	ACS APPLIED MATERIALS & INTERFACES	7	16	8525	Song, Fei; Wells, Justin W.; Jiang, Zheng
127	Reexamination of the neutron-to-proton-ratio puzzle in	PHYSICAL REVIEW C	91	4	47601	Kong, Hai-Yun; Xia, Yin; Xu,

	intermediate-energy heavy-ion collisions					Jun
128	Different mechanism of two-proton emission from proton-rich nuclei Al-23 and Mg-22	PHYSICS LETTERS B	743		306	Ma, Y. G.; Fang, D. Q.; Sun, X. Y.
129	Effect of event selection on jetlike correlation measurement in d plus Au collisions at root s(NN)=200 GeV	PHYSICS LETTERS B	743		333	Adamczyk, L.; Adkins, J. K.; Agakishiev, G.
130	Suppression of Upsilon production in d + Au and Au + Au collisions at root s(NN) = 200 GeV (vol 735, pg 127, 2014)	PHYSICS LETTERS B	743		537	Adamczyk, L.; Adkins, J. K.; Agakishiev, G.
131	DNA-Directed Assembly of Gold Nanohalo for Quantitative Plasmonic Imaging of Single-Particle Catalysis	JOURNAL OF THE AMERICAN CHEMICAL SOCIETY	137	13	4292	Li, Kun; Wang, Kun; Qin, Weiwei
132	Graphene Oxide-Assisted Nucleic Acids Assays Using Conjugated Polyelectrolytes-Based Fluorescent Signal Transduction	ANALYTICAL CHEMISTRY	87	7	3877	Li, Fan; Chao, Jie; Li, Zhenhua
133	A transition between bistable ice when coupling electric field and nanoconfinement	JOURNAL OF CHEMICAL PHYSICS	142	13	134704	Mei, Feng; Zhou, Xiaoyan; Kou, Jianlong
134	Photoelectron spectroscopy and theoretical studies of gaseous uranium hexachlorides in different oxidation states: UCl6q-(q=0-2)	JOURNAL OF CHEMICAL PHYSICS	142	13	134308	Su, Jing; Dau, Phuong D.; Liu, Hong-Tao
135	Squared form factors for the A(1)Pi and B-1 Sigma(+) vibronic bands of carbon monoxide studied by high-resolution inelastic x-ray scattering	PHYSICAL REVIEW A	91	4	42501	Ni, Dong-Dong; Kang, Xu; Yang, Ke
136	Interfacial Nanobubbles on Atomically Flat Substrates with Different Hydrophobicities	CHEMPHYSCHEM	16	5	1003	Wang, Xingya; Zhao, Binyu; Ma, Wangguo
137	New measurement of the excited states in B-11 via elastic resonance scattering of Be-10 + p	PHYSICAL REVIEW C	91	4	44302	Liu, Y. D.; Wang, H. W.; Ma, Y. G.
138	Observation of dual relaxation dynamics of polarization clusters in barium titanate by photon correlation spectroscopy	JAPANESE JOURNAL OF APPLIED PHYSICS	54	4	42401	Zhang, Mingjun; Guo, Zhi; Tai, Renzhong
139	The control system for water-cooled DCMS in SSRF	NUCLEAR SCIENCE AND TECHNIQUES	26	2	20103	Jia Wen-Hong; Ma Shi-Wei; Zheng Li-Fang
140	Reversible addition-fragmentation chain transfer graft polymerization of acrylonitrile onto PE/PET composite fiber initiated by gamma-irradiation	NUCLEAR SCIENCE AND TECHNIQUES	26	2	20301	Ma Yao; Yu Ming; Li Lin-Fan

141	Latest advances of X-ray imaging and biomedical applications beamline at SSRF	NUCLEAR SCIENCE AND TECHNIQUES	26	2	20102	Xie Hong-Lan; Deng Biao; Du Guo-Hao
142	Introduction of the X-ray diffraction beamline of SSRF	NUCLEAR SCIENCE AND TECHNIQUES	26	2	20101	Yang Tie-Ying; Wen Wen; Yin Guang-Zhi
143	Preface for Special Section on International Workshop on Nuclear Dynamics in Heavy-Ion Reactions (IWND 2014)	NUCLEAR SCIENCE AND TECHNIQUES	26	2	CP1	Ma, Yu-Gang; Chen, Lie-Wen; Xu, Hu-Shan
144	PERMEATION OF HYDROGEN IN HASTELLOY C-276 ALLOY AT HIGH TEMPERATURE	FUSION SCIENCE AND TECHNOLOGY	67	3	681	Zhang, Dongxun; Liu, Wei; Qian, Yuan
145	Highly Dispersed Copper Oxide Clusters as Active Species in Copper-Ceria Catalyst for Preferential Oxidation of Carbon Monoxide	ACS CATALYSIS	5	4	2088	Wang, Wei-Wei; Du, Pei-Pei; Zou, Shi-Hui
146	Studies of an LL-type 500 MHz 5-cell superconducting cavity at SINAP	CHINESE PHYSICS C	39	4	47001	Hou Hong-Tao; Ma Zhen-Yu; Mao Dong-Qing
147	Modeling and analysis of SLED	CHINESE PHYSICS C	39	4	47002	Li Lin; Fang Wen-Cheng; Wang Chao-Peng
148	Controllable Nucleation of Nanobubbles at a Modified Graphene Surface	CHINESE PHYSICS LETTERS	32	4	46801	Ma Wang-Guo; Zhang Meng; Nie Xue-Chuan
149	A Study on the Degree of Amidoximation of Polyacrylonitrile Fibers and Its Effect on Their Capacity to Adsorb Uranyl Ions	INDUSTRIAL & ENGINEERING CHEMISTRY RESEARCH	54	12	3101	Zhao, Huanhuan; Liu, Xiyan; Yu, Ming
150	Structural analysis of [Bmim](2)CuCl4 ionic liquids in the presence of water and ethanol by XAFS technique	SCIENCE CHINA-CHEMISTRY	58	4	716	Jiang, Fangling; Li, Cheng; Fu, Haiying
151	Effect of neutron skin thickness on projectile fragmentation	PHYSICAL REVIEW C	91	3	34618	Dai, Z. T.; Fang, D. Q.; Ma, Y. G.
152	Examining the effect of a binding-energy-dependent clusterization algorithm on isospin-sensitive observables in heavy-ion collisions	PHYSICAL REVIEW C	91	3	34612	Kumar, Sanjeev; Ma, Y. G.;
153	Effect of Ar+ ion irradiation on the microstructure of pyrolytic carbon	JOURNAL OF APPLIED PHYSICS	117	11	115101	Feng, Shanglei; Yang, Yingguo; Li, Li
154	Charged-to-neutral correlation at forward rapidity in Au plus Au collisions at root	PHYSICAL REVIEW C	91	3	34905	Adamczyk, L.; Adkins, J. K.;

	s(NN)=200 GeV					Agakishiev, G.
155	Photochemical Reaction Kinetics of Duroquinone in a Mixture of Ionic Liquid [BPy][BF4] and Acetonitrile	ACTA PHYSICO-CHIMICA SINICA	31	3	419	Zhu Guang-Lai; Wang Yu; Zhang Liang-Wei
156	Binding-induced collapse of DNA nano-assembly for naked-eye detection of ATP with plasmonic gold nanoparticles	BIOSENSORS & BIOELECTRONICS	65		171	Wang, Jingjing; Lu, Jianxin; Su, Shao
157	Novel multifunctional nanofibers based on thermoplastic polyurethane and ionic liquid: towards antibacterial, anti-electrostatic and hydrophilic nonwovens by electrospinning	NANOTECHNOLOGY	26	10	105704	Xing, Chenyang; Guan, Jipeng; Chen, Zhouli
158	Tunable assembly of amyloid-forming peptides into nanosheets as a retrovirus carrier	PROCEEDINGS OF THE NATIONAL ACADEMY OF SCIENCES OF THE UNITED STATES OF AMERICA	112	10	2996	Dai, Bin; Li, Dan; Xi, Wenhui
159	Isobaric yield ratio difference and Shannon information entropy	PHYSICS LETTERS B	742		19	Ma, Chun-Wang; Wei, Hui-Ling; Wang, Shan-Shan
160	Pectin/lysozyme bilayers layer-by-layer deposited cellulose nanofibrous mats for antibacterial application	CARBOHYDRATE POLYMERS	117		687	Zhang, Tingting; Zhou, Panghu; Zhan, Yingfei
161	Gold-Nanoparticle-Mediated Jigsaw-Puzzle-like Assembly of Supersized Plasmonic DNA Origami	ANGEWANDTE CHEMIE-INTERNATIONAL EDITION	54	10	2966	Yao, Guangbao; Li, Jiang; Chao, Jie
162	Isospin splitting of nucleon effective mass and shear viscosity of nuclear matter	PHYSICAL REVIEW C	91	3	37601	Xu, Jun;;
163	Fast X-ray micro-tomography for low-Z materials	JOURNAL OF INSTRUMENTATION	10		C03010	Xu, L.; Chen, R.; Du, G.
164	Bimetallic nano-mushrooms with DNA-mediated interior nanogaps for high-efficiency SERS signal amplification	NANO RESEARCH	8	3	731	Shen, Jianlei; Su, Jing; Yan, Juan
165	Analysis of the microbunching instability in a mid-energy electron linac	CHINESE PHYSICS C	39	3	38101	Huang Da-Zhang; Gu Qiang; Wang Zhen
166	Culture Medium-Associated Physicochemical Insights on the Cytotoxicity of Carbon Nanomaterials	CHEMICAL RESEARCH IN TOXICOLOGY	28	3	290	Kong, Huating; Wang, Lihua; Zhu, Ying
167	Compton profile of molecular hydrogen	CHINESE PHYSICS B	24	3	33301	Zhao Xiao-Li; Yang Ke; Xu Long-Quan
168	Stable Alkali Metal Ion Intercalation	NANO LETTERS	15	3	2180	Zhao, Yunlong;

	Compounds as Optimized Metal Oxide Nanowire Cathodes for Lithium Batteries					Han, Chunhua; Yang, Junwei
169	A new extra-focus monochromator designed for high-performance VUV beamlines	JOURNAL OF SYNCHROTRON RADIATION	22		328	Xue, Chaofan; Wu, Yanqing; Zou, Ying
170	Photosensitive damage of lysozyme caused by pazufloxacin and the protective effect of ferulic acid	SCIENCE CHINA-CHEMISTRY	58	3	508	Xu, Yulie; Liu, Yancheng; Li, Haixia
171	A highly sensitive chemiluminescence sensor for detecting mercury (II) ions: a combination of Exonuclease III-aided signal amplification and graphene oxide-assisted background reduction	SCIENCE CHINA-CHEMISTRY	58	3	514	Tian, Yang; Wang, Yue; Xu, Yan
172	Optimization of CeO2 as sintering aid for Tb3Al5O12 Faraday magneto-optical transparent ceramics	JOURNAL OF MATERIALS SCIENCE	50	6	2517	Chen, Chong; Li, Xiaoli; Feng, Yue
173	Investigation of Compton profiles of molecular methane and ethane	JOURNAL OF CHEMICAL PHYSICS	142	8	84301	Zhao, Xiao-Li; Yang, Ke; Xu, Long-Quan
174	Status of the crystallography beamlines at SSRF	EUROPEAN PHYSICAL JOURNAL PLUS	130	2	32	He, Jianhua; Gao, Xingyu;
175	Photoinduced electron transfer between 2-methylanthraquinone and triethylamine in an ionic liquid: Time-resolved EPR and transient absorption spectroscopy study	SPECTROCHIMICA ACTA PART A-MOLECULAR AND BIOMOLECULAR SPECTROSCOPY	137		148	Zhu, Guanglai; Wang, Yu; Fu, Haiying
176	Thermal analysis of the first canted-undulator front-end components at SSRF	NUCLEAR INSTRUMENTS & METHODS IN PHYSICS RESEARCH SECTION A-ACCELERATORS SPECTROMETERS DETECTORS AND ASSOCIATED EQUIPMENT	774		94	Xu, Zhongmin; Feng, Xinkang; Wang, Naxiu
177	Growth and Origami Folding of DNA on Nanoparticles for High-Efficiency Molecular Transport in Cellular Imaging and Drug Delivery	ANGEWANDTE CHEMIE-INTERNATIONAL EDITION	54	8	2431	Yan, Juan; Hu, Chongya; Wang, Ping
178	Three-Dimensional Fe2N@C Microspheres Grown on Reduced Graphite Oxide for Lithium-Ion Batteries and the Li Storage Mechanism	CHEMISTRY-A EUROPEAN JOURNAL	21	8	3249	Yu, Peng; Wang, Lei; Sun, Fanfei
179	Investigating the microstructures of piston carbon deposits in a large-scale marine diesel engine using synchrotron X-ray microtomography	FUEL	142		173	Zhang, Xusheng; Peng, Guanyun; Du, Guohao

180	Nanodiamonds act as Trojan horse for intracellular delivery of metal ions to trigger cytotoxicity	PARTICLE AND FIBRE TOXICOLOGY	12		2	Zhu, Ying; Zhang, Yu; Shi, Guosheng
181	Synthesis and detection the oxidization of Co cores of Co@SiO2 core-shell nanoparticles by in situ XRD and EXAFS	NANOSCALE RESEARCH LETTERS	10		1	Zhang, Kunhao; Zhao, Ziyan; Wu, Zhonghua
182	Unraveling the Role of Hydrogen Peroxide in alpha-Synuclein Aggregation Using an Ultrasensitive Nanoplasmonic Probe	ANALYTICAL CHEMISTRY	87	3	1968	Xu, Yan; Li, Kun; Qin, Weiwei
183	Developments at SSRF in soft X-ray interference lithography	NUCLEAR SCIENCE AND TECHNIQUES	26	1	5	Yang Shu-Min; Wang Lian-Sheng; Zhao Jun
184	The macromolecular crystallography beamline of SSRF	NUCLEAR SCIENCE AND TECHNIQUES	26	1	12	Wang Qi-Sheng; Yu Feng; Huang Sheng
185	Translocation and biotransformation of CuO nanoparticles in rice (Oryza sativa L.) plants	ENVIRONMENTAL POLLUTION	197		99	Peng, Cheng; Duan, Dechao; Xu, Chen
186	Multipacting saturation in parallel plate and micro-pulse electron gun	CHINESE PHYSICS C	39	2	76	Liao Lang; Zhang Meng; Zhao Ming-Hua
187	Single-shot measurement of free-electron laser polarization at SDUV-FEL	CHINESE PHYSICS C	39	2	97	Feng Lie; Deng Hai-Xiao; Zhang Tong
188	Photochemical properties of gemifloxacin: A laser flash photolysis study	JOURNAL OF PHOTOCHEMISTRY AND PHOTOBIOLOGY B-BIOLOGY	143		30	Xu Yulie; Liu Yancheng; Zhao Jianfeng
189	Occurrence of bisphenol A in surface and drinking waters and its physicochemical removal technologies	FRONTIERS OF ENVIRONMENTAL SCIENCE & ENGINEERING	9	1	16	Liang, Liping; Zhang, Jing; Feng, Pian
190	The effect of silicon on precipitation and decomposition behaviors of M6C carbide in a Ni-Mo-Cr superalloy	JOURNAL OF ALLOYS AND COMPOUNDS	620		197	Xu, Zhoufeng; Jiang, Li; Dong, Jiasheng
191	Thermal properties of asymmetric nuclear matter with an improved isospin- and momentum-dependent interaction	PHYSICAL REVIEW C	91	1	14611	Xu, Jun; Chen, Lie-Wen; Li, Bao-An
192	Preparation and characterization of p-type transparent conducting SnO thin films	MATERIALS LETTERS	139		39	Yang, Tieying; Zhao, Jun; Li, Xiaolong
193	Lambda Lambda Correlation Function in Au plus Au Collisions at root s(NN)=200 GeV	PHYSICAL REVIEW LETTERS	114	2	22301	Adamczyk, L.; Adkins, J. K.; Agakishiev, G.

194	Cotranscriptionally Folded RNA Nanostructures Pave the Way to Intracellular Nanofabrication	CHEMBIOCHEM	16	1	39	Li, Jiang; Chao, Jie; Shi, Jiye
195	Tailoring graphene oxide assemblies by pinning on the contact line of a dissolving microdroplet	SOFT MATTER	11	43	8479	Yang, Haijun; Song, Yuting; Downton, Matthew T.
196	Syngas production by high temperature steam/CO2 coelectrolysis using solid oxide electrolysis cells	FARADAY DISCUSSIONS	182		341	Chen, Xinbing; Guan, Chengzhi; Xiao, Guoping
197	Visualizing dopamine released from living cells using a nanoplasmonic probe	NANOSCALE	7	37	15070	Qin, W. W.; Wang, S. P.; Li, J.
198	Geometrical and morphological optimizations of plasmonic nanoarrays for high-performance SERS detection	NANOSCALE	7	37	15487	Li, W. Q.; Wang, G.; Zhang, X. N.
199	Elaborately designed diblock nanoprobes for simultaneous multicolor detection of microRNAs	NANOSCALE	7	38	15822	Wang, Chenguang; Zhang, Huan; Zeng, Dongdong
200	Electrochemical investigation of the stable chromium species in molten FLINAK	RSC ADVANCES	5	94	76689	Peng, Hao; Shen, Miao; Wang, Chenyang
201	Graphene-based nanoprobes for molecular diagnostics	ANALYST	140	19	6439	Chen, Shixing; Li, Fuwu; Fan, Chunhai
202	Transportation and fate of gold nanoparticles in oilseed rape	RSC ADVANCES	5	90	73827	Zhang, Jichao; Pan, Liang; Lv, Min
203	Enhancing the effect of bisulfite on sequestration of selenite by zerovalent iron	RSC ADVANCES	5	93	76032	Li, Jinxiang; Wang, Chao; Qiao, Junlian
204	The Core/Shell Structure of CdSe/ZnS Quantum Dots Characterized by X-Ray Absorption Fine Spectroscopy	JOURNAL OF NANOMATERIALS			764712	Wei, Huijing; Zhou, Jing; Zhang, Linjuan
205	Synthesis and characterization of surface ion-imprinted polymer based on SiO2-coated graphene oxide for selective adsorption of uranium(VI)	RSC ADVANCES	5	83	67662	Meng, Hu; Li, Zheng; Ma, Fuyin
206	Excess titanium dioxide nanoparticles on the cell surface induce cytotoxicity by hindering ion exchange and disrupting exocytosis processes	NANOSCALE	7	30	13105	Wang, Yanli; Yao, Chenjie; Li, Chenchen
207	Application of Carbon Nanomaterials in	CURRENT	21	22	3191	Li, Lanying;

	Gene Delivery for Endogenous RNA Interference In Vitro and In Vivo	PHARMACEUTICAL DESIGN				Wen, Yanli; Xu, Qin
208	Transfer printing of magnetic structures with enhanced performance using a new type of water-soluble sacrificial layer	RSC ADVANCES	5	70	56959	Zhao, Bin; Ji, Gengwu; Gao, Xingyu
209	Production of Kaon and Lambda in Nucleus-Nucleus Collisions at Ultrarelativistic Energy from a Blast-Wave Model	ADVANCES IN HIGH ENERGY PHYSICS			460590	Zhang, S.; Ma, Y. G.; Chen, J. H.
210	Properties of Full Jet in High-Energy Heavy-Ion Collisions from Parton Scatterings	ADVANCES IN HIGH ENERGY PHYSICS			967474	Ma, Guo-Liang; Nie, Mao-Wu;
211	Synthesis of a highly dense and selective imprinted polymer via pre-irradiated surface-initiated graft polymerization	JOURNAL OF MATERIALS CHEMISTRY A	3	25	13237	Meng, Hu; Gao, Qianhong; Li, Zheng
212	Bio-inspired laminated graphite nanosheets/copper composites	RSC ADVANCES	5	63	51342	Wang, P.; Liu, W.; Chen, L.
213	Red emissive organic light-emitting diodes based on codeposited inexpensive Cu-I complexes	JOURNAL OF MATERIALS CHEMISTRY C	3	22	5835	Ni, Tianchi; Liu, Xiaochen; Zhang, Tao
214	Sequestering uranium from UO2(CO3)(3)(4-) in seawater with amine ligands: density functional theory calculations	PHYSICAL CHEMISTRY CHEMICAL PHYSICS	17	22	14662	Guo, Xiaojing; Huang, Liangliang; Li, Cheng
215	3D elemental sensitive imaging by full-field XFCT	ANALYST	140	10	3521	Deng, Biao; Du, Guohao; Zhou, Guangzhao
216	Stiffness and evolution of interfacial micropancakes revealed by AFM quantitative nanomechanical imaging	PHYSICAL CHEMISTRY CHEMICAL PHYSICS	17	20	13598	Zhao, Binyu; Wang, Xingya; Song, Yang
217	Chemical interactions between zirconium and free oxide in molten fluorides	RSC ADVANCES	5	51	40708	Shen, Miao; Peng, Hao; Ge, Min
218	Structural evolution of OBC/carbon nanotube bundle nanocomposites under uniaxial deformation	RSC ADVANCES	5	42	32909	Wu, Siduo; Huang, Guangsu; Wu, Jinrong
219	On the gold-ligand covalency in linear [AuX2](-) complexes	DALTON TRANSACTIONS	44	12	5535	Xiong, Xiao-Gen; Wang, Yi-Lei; Xu, Cong-Qiao
220	BiOBr-BiOI microsphere assembled with atom-thick ultrathin nanosheets and its high photocatalytic activity	RSC ADVANCES	5	31	24777	Guo, Xue-Jing; Zhen, Mengmeng; Liu, Huajie

221	Designing breathable superhydrophobic cotton fabrics	RSC ADVANCES	5	35	27752	Wu, Jingxia; Li, Jingye; Wang, Ziqiang
222	Uniform 2 nm gold nanoparticles supported on iron oxides as active catalysts for CO oxidation reaction: structure-activity relationship	NANOSCALE	7	11	4920	Guo, Yu; Gu, Dong; Jin, Zhao
223	Monodispersed nanoparticles of conjugated polyelectrolyte brush with high charge density for rapid, specific and label-free detection of tumor marker	ANALYST	140	6	1842	Liu, Xingfen; Shi, Lin; Zhang, Zhiyong
224	Towards Automated Quantitative Vasculature Understanding via Ultra High-Resolution Imagery	SIGNAL AND IMAGE ANALYSIS FOR BIOMEDICAL AND LIFE SCIENCES	823		177	Li, Rongxin; Wang, Dadong; Sun, Changming
225	Electrospun nanofibrous adsorbents for uranium extraction from seawater	JOURNAL OF MATERIALS CHEMISTRY A	3	6	2552	Xie, Siyuan; Liu, Xiyan; Zhang, Bowu
226	Clicking DNA to gold nanoparticles: poly-adenine-mediated formation of monovalent DNA-gold nanoparticle conjugates with nearly quantitative yield	NPG ASIA MATERIALS	7		UNSP e159	Yao, Guangbao; Pei, Hao; Li, Jiang
227	Optimization of temperature coefficient and breeding ratio for a graphite-moderated molten salt reactor	NUCLEAR ENGINEERING AND DESIGN	281		114	Zou, C. Y.; Cai, X. Z.; Jiang, D. Z.
228	Terahertz Time-Domain Spectroscopy and Quantitative Analysis of Metal Gluconates	APPLIED SPECTROSCOPY	69	1	52	Li, Shaoxian; Yang, Jingqi; Zhao, Hongwei
229	In situ study of the catalytic mechanism for the oxygen reduction reaction on a polypyrrole modified carbon supported cobalt hydroxide cathode in direct borohydride fuel cells (vol 15, pg 9070, 2013)	PHYSICAL CHEMISTRY CHEMICAL PHYSICS	17	5	3919	Qin, Haiying; Wang, Juan; Liu, Jiabin
230	Analysis of thorium and uranium based nuclear fuel options in Fluoride salt-cooled High-temperature Reactor	PROGRESS IN NUCLEAR ENERGY	78		285	Li, X. X.; Cai, X. Z.; Jiang, D. Z.
231	An Effective Method for Improving the Imaging Spatial Resolution of Terahertz Time Domain Spectroscopy System	SPECTROSCOPY AND SPECTRAL ANALYSIS	35	1	1	Zhang Zeng-yan; Ji Te; Zhu Zhi-yong
232	Preparation of pyrolytic carbon coating on graphite for inhibiting liquid fluoride salt and Xe-135 penetration for molten salt breeder reactor	JOURNAL OF NUCLEAR MATERIALS	456		33	Song, Jinliang; Zhao, Yanling; He, Xiujie

233	A 2D-3D structure transition of gold clusters on CeO2-X(111) surfaces and its influence on CO and O-2 adsorption: a comprehensive DFT plus U investigation	NANOSCALE	7	1	308	Han, Zhong-Kang; Gao, Yi;
234	Effects of rare-earth on the cohesion of Ni Sigma 5 (012) grain boundary from first-principles calculations	COMPUTATIONAL MATERIALS SCIENCE	96		374	Liu, Wenguan; Han, Han; Ren, Cuilan
235	Helium ion irradiation behavior of Ni-1wt.%SiCNPcomposite and the effect of ion flux	Journal of Nuclear Materials	467		848	Zhou, X.L.; Huang, H.F.; Xie, R.
236	Irradiation resistance of MAX phases Ti3SiC2 and Ti3AlC2: Characterization and comparison	Journal of Nuclear Materials	465		640	Huang, Qing; Liu, Renduo; Lei, Guanhong
237	High-temperature stability of Ni-3 wt.% SiCNPcomposite and the effect of milling time	Journal of Nuclear Materials	467		635	Yang, Chao; Huang, Hefei; Zhou, Xiaoling
238	Shanghai Synchrotron Radiation Facility fast obit feedback system	Yuanzineng Kexue Jishu/Atomic Energy Science and Technology	49		615	Yin, Chong-Xian; Zhao, Li-Ying; Jiang, Bo-Cheng
239	Photoelectron spectroscopy and theoretical studies of gaseous uranium hexachlorides in different oxidation states: UCl6q-(q = 0-2)	Journal of Chemical Physics	142	13		Su, Jing; Dau, Phuong D.; Liu, Hong-Tao
240	Intergranular diffusion and embrittlement of a Ni-16Mo-7Cr alloy in Te vapor environment	Journal of Nuclear Materials	467		341	Cheng, Hongwei; Li, Zhijun; Leng, Bin
241	Precision Measurement of the Longitudinal Double-Spin Asymmetry for Inclusive Jet Production in Polarized Proton Collisions at s =200GeV	Physical Review Letters	115	9		Adamczyk, L.; Adkins, J.K.; Agakishiev, G.
242	Research on electron beam center trajectory correction algorithm based on differential evolution CMAC	Yuanzineng Kexue Jishu/Atomic Energy Science and Technology	49		611	Su, Hai-Jun; Li, De-Ming; Wang, Sheng-Li
243	Small angle X-ray scattering measurements of HDPE microstructure evolution with temperature	Gaofenzi Cailiao Kexue Yu Gongcheng/Polymeric Materials Science and Engineering	31	9	117	Hai, Yang; Liu, Yi; Chen, Xiliang
244	Development of 800 kV/30 mA Cockcroft-Walton electron accelerator for radiation application	Yuanzineng Kexue Jishu/Atomic Energy Science and Technology	49		578	Liu, Yong-Hao; Li, Min-Xi; Zhang, Jin-Ling
245	Λ Λ correlation function in Au+Au collisions at sNN =200GeV	Physical Review Letters	114	2		Adamczyk, L.; Adkins, J.K.; Agakishiev, G.

246	Thermal conductivity of high temperature fluoride molten salt determined by laser flash technique	International Journal of Heat and Mass Transfer	90		872	An, Xue-Hui; Cheng, Jin-Hui; Yin, Hui-Qin
247	First-principles calculations of the interaction between hydrogen and 3d alloying atom in nickel	Journal of Nuclear Materials	465		254	Liu, Wenguan; Qian, Yuan; Zhang, Dongxun
248	Real-time tune monitor system on Shanghai Synchrotron Radiation Facility	Qiangjiguang Yu Lizishu/High Power Laser and Particle Beams	27	4		Lai, Longwei; Yan, Yingbing; Chen, Zhichu
249	Research on the contrast enhancement algorithm of synchrotron radiation X-Ray image	Guangxue Xuebao/Acta Optica Sinica	35	3		Liang, Chuanhui; Wang, Yudan; Du, Guohao
250	Isothermal oxidation behavior of GH3535 superalloy at 700	Xiyou Jinshu Cailiao Yu Gongcheng/Rare Metal Materials and Engineering	44	8	1953	Fan, Jinxin; Lu, Yanling; Li, Zhijun
251	Thermodynamic description of the AgCl-CoCl2-InCl3-KCl system	Materials Chemistry and Physics	163		73	Wang, Kun; Fei, Zejie; Wang, Jian
252	Molecular dynamics studies of the structure of pure molten ThF4 and ThF4-LiF-BeF2 melts	Journal of Molecular Liquids	211		747	Dai, Jianxing; Long, Dewu; Huai, Ping
253	Development of global data warehouse for beam diagnostics at SSRF	Yuanzineng Kexue Jishu/Atomic Energy Science and Technology	49	6	1149	Lai, Long-Wei; Leng, Yong-Bin; Yan, Ying-Bing
254	Effects of rare-earth on the cohesion of Ni Σ 5 (012) grain boundary from first-principles calculations	Computational Materials Science	96	PA	374	Liu, Wenguan; Han, Han; Ren, Cuilan
255	Structure, Optical Absorption, and Performance of Organic Solar Cells Improved by Gold Nanoparticles in Buffer Layers	ACS Applied Materials and Interfaces	7	44	24430	Yang, Yingguo; Feng, Shanglei; Li, Meng
256	Synchrotron radiation phase-contrast computed tomography study on self-assembly of polystyrene colloidal crystals via solvent evaporation	Colloid Journal	77	6	795	Fu, Yanan; Xie, Honglan; Deng, Biao
257	Vacuum layout and chamber design for synchrotron ring of Shanghai Proton Therapy Facility	Yuanzineng Kexue Jishu/Atomic Energy Science and Technology	49		529	Tang, Qi-Sheng; Wang, Zhi-Shan; Li, Xue-Jun
258	Vacuum system design for CLS in-vacuum insert devices	Yuanzineng Kexue Jishu/Atomic Energy Science and Technology	49		523	Tang, Qi-Sheng; Hu, Xiao; Li, Xue-Jun
259	Structural analysis of [Bmim]2CuCl4 ionic liquids in the presence of water and ethanol by XAFS technique	Science China Chemistry	58	4	716	Jiang, Fangling; Li, Cheng; Fu, Haiying

260	Use of square wave voltammeter for online monitoring of O2- concentration in molten fluorides at 600 ° c	Journal of Electroanalytical Chemistry	748		34	Shen, Miao; Peng, Hao; Ge, Min
261	Stress analysis and structural integrity evaluation of piping system in TMSR	Hedongli Gongcheng/Nuclear Power Engineering	36	5	152	Gong, Wei; Zhang, Xiaochun; Wang, Xiao
262	On the gold-ligand covalency in linear [AuX2]- complexes	Dalton Transactions	44	12	5535	Xiong, Xiao-Gen; Wang, Yi-Lei; Xu, Cong-Qiao
263	Progress of digital BPM signal processor	Yuanzineng Kexue Jishu/Atomic Energy Science and Technology	49		607	Lai, Long-Wei; Leng, Yong-Bin; Yan, Ying-Bing
264	Effect of γ -ray irradiation on the pre-oxidation of polyacrylonitrile fibers	Gaofenzi Cailiao Kexue Yu Gongcheng/Polymeric Materials Science and Engineering	31	5	51	Liu, Weihua; Wang, Mouhua; Zhang, Wenfa
265	Development of burnup calculation code for pebble-bed high temperature reactor at equilibrium state	Yuanzineng Kexue Jishu/Atomic Energy Science and Technology	49	5	890	Zhu, Gui-Feng; Zou, Yang; Li, Ming-Hai
266	ABB 控制器 CD522 在棒控棒位系统中的应用	核技术	38	9	90404	韩利峰; 汪全全; 邓辉宇
267	纳米金颗粒在靶向放射治疗中的应用	核技术	38	9	90501	刘蒙蒙; 王坤; 陈楠
268	三步法接枝聚合苯胺制备抗静电织物	辐射研究与辐射工艺学报	33	4	40302	巫邦庭; 张伯武; 吴景霞
269	GH3535 合金 700℃恒温氧化行为研究	稀有金属材料与工程	44	8	1953	范金鑫; 陆燕玲; 李志军
270	光子晶体制备方法对同步辐射闪烁体探测器成像分辨率的影响	核技术	38	7	70101	陈媚; 于怀娜; 赵俊
271	螺旋线圈在同步辐射光源冷却系统中的应用	核技术	38	7	70102	金利民; 徐中民; 王纳秀
272	两种~(18)F 标记多肽方法的对比研究	核技术	38	7	70301	江大卫; 孙艳红; 王丽华
273	TMSR 硝酸盐自然循环回路控制系统设计	核技术	38	7	70401	张宁; 郭冰; 韩立欣
274	基于绝缘芯平面变压器的新型高压直流电源的调试及输出特性	核技术	38	7	70402	田佳甲; 刘永好; 张金玲
275	不同 Cr 含量的镍基高温合金在 LiF-NaF-KF 熔盐中的腐蚀行为	核技术	38	7	70601	邱杰; 邹杨; 李志军
276	熔盐冷冻壁形成及控制实验研究	核技术	38	7	70602	周金豪; 孙波; 佘长锋
277	氦离子辐照对镍基合金硬度的影响	核技术	38	7	70605	刘哲; 包良满;

						刘可
278	硅油对淀粉样蛋白和多肽积聚的促进作用	核技术	38	8	80501	李佳；雷豪志；其其格
279	上海质子治疗示范装置旋转机架电机谐响应分析	核技术	38	8	80503	吴军；杜涵文；杜跃斐
280	采用 SCALE 计算氟盐冷却高温堆产氚量的一些问题	核技术	38	8	80601	彭超；朱兴望；张国庆
281	NO 与 C_2H_2 的康普顿轮廓研究	物理学报	64	15	153302	马永朋；闫帅；杨科
282	EPICS 环境下数字超声流量计网络接口设计与应用	核技术	38	8	80401	官龙腾; 尹聪聪; 刘婷
283	RHIC 束流能量扫描实验中正反粒子椭圆流的平均场势效应	原子核物理评论	32	2	146	柯治明；李锋；徐骏
284	纳米颗粒-蛋白相互作用及其生物效应研究	中国科学. 化学	45	7	671	夏凯；孔华庭；李晓霞
285	同步辐射真空紫外圆二色谱技术在 DNA 结构研究中的应用	辐射研究与辐射工艺学报	33	3	30101	周培培; 樊春海; 王丽华
286	抗菌性壳聚糖双胍醋酸盐的辐照辅助制备及其生物毒性	功能高分子学报	28	2	183	谭奕哲; 曾虹燕; 吴国忠
287	应用氩离子抛光-扫描电镜方法研究四川九老洞组页岩微观孔隙特征	岩矿测试	34	3	278	王羽; 金婵; 汪丽华
288	gamma 射线辐照处理对聚丙烯腈纤维预氧化反应的影响	高分子材料科学与工程	31	5	51	刘伟华; 王谋华; 张文发
289	用同步辐射共聚焦 X 射线方法研究古代彩绘样品的层状结构	核技术	38	6	60101	资明；魏向军；于海生
290	一种波荡器段间四极铁支撑平台的机械稳定性	核技术	38	6	60102	董玉玺；高飞；文雍梅
291	1 500 MHz 5-cell 超导腔的仿真优化	核技术	38	6	60103	杨峻；马震宇；王岩
292	具有加速因子的 OSEM 重建算法用于 X 射线荧光 CT 研究	核技术	38	6	60201	孙鹏飞；邓彪；杨群
293	放射性 alpha 气溶胶监测仪数据采集系统的设计	核技术	38	6	60401	陈峰；夏晓彬；张志宏
294	EPICS 环境下的软件规范管理	核技术	38	6	60501	雷蕾；韩利峰；徐海霞
295	轻核 alpha 团簇结构理论和实验研究进展	科学通报	60	17	1557	曹喜光; 马余刚;
296	基于 DCM 的 QXAFS 数据采集与控制	核技术	38	5	50101	周永年; 张招红; 刘平
297	同步辐射光束线束斑形状实时分析技术	核技术	38	5	50102	张春波; 汪启胜; 黄胜
298	EJ339A 俘获门控中子探测器双脉冲特性	核技术	38	5	50403	常乐；马春旺；刘龙祥
299	Fe_3O_4 纳米颗粒-蛋白的相互作用及生	核技术	38	5	50501	夏凯；孔华庭；

	物效应					崔之芬
300	热堆中钍铀转化规律	核技术	38	5	50601	张海青；林俊；曹长青
301	10-MWt 固态钍基熔盐堆乏燃料贮存系统临界安全影响分析	核技术	38	5	50602	田金；夏晓彬；彭超
302	聚乙烯膜表面辐射接枝甲基丙烯酸-4,5-二甲氧基-2-硝基苯甲酯实现光敏化	辐射研究与辐射工艺学报	33	2	20301	李万新; 王自强; 俞初红
303	利用EQMD模型对原子核基态性质的研究	原子核物理评论	32	1	24	王闪闪; 曹喜光; 张同林
304	同步辐射红外谱学显微光束线站的空间分辨率测试	光学学报	35	4	430002	朱化春; 佟亚军; 吉特
305	UF_4 氟化反应及其反应动力学	核化学与放射化学	37	2	71	孙理鑫; 牛永生; 张焕琦
306	TEVA 树脂分离-ICP-MS 测量钍基体中微量铀	核化学与放射化学	37	2	89	史万龙; 马付银; 李峥
307	劳厄弯晶色散特性的光线追迹研究	核技术	38	4	40101	陈灿；许照乾；毛定立
308	基于 PRP 协议的 EPICS 冗余技术	核技术	38	4	40401	刘少海; 陈永忠; 韩利峰
309	TMSR 数字化反应堆保护系统数字信号与逻辑处理功能的 FPGA 实现探讨	核技术	38	4	40404	刘烨；后接；刘珍宝
310	TRISO 颗粒缓冲层包覆喷动床气固流动特性	核技术	38	4	40501	麦锡源；张锋；林俊
311	基于GPU的三维扩散方程在反应堆计算中的应用	核技术	38	4	40502	王飞飞; 王海玲; 俞海英
312	HYSYS 软件应用于熔盐冷却系统瞬态分析的可行性研究	核技术	38	4	40601	唐延泽; 郑海伟; 陈玉爽
313	硝酸盐自然循环回路系统特性分析	核技术	38	4	40602	王凯；蔡创雄；何兆忠
314	反应堆仪控 HA 设备冗余状态监测	核技术	38	4	40603	张宁；郭冰；孙雪静
315	基于 DNA 自组装过程的纳米结构研究	生物技术通报	31	4	120	俞洋；李江；樊春海
316	低放射性废水处理设施升级改造工程	中国给水排水	31	8	85	王帅；秦强；钱正华
317	不同固体慢化剂对花型快谱超临界水冷堆中子学性能的影响分析	核动力工程	36	1	173	于涛；李志峰；谢金森
318	二氟沙星在乙腈溶液中的激光光解研究	辐射研究与辐射工艺学报	33	1	10302	李海霞; 刘艳成; 唐睿智
319	基于 I/Q 解调原理的校准方法及实验	核技术	38	3	30102	张志刚; 赵玉彬; 徐凯
320	上海光源新型波荡器 EPU200 磁结构的机械设计及力学分析	核技术	38	3	30103	朱亚；邓荣兵；周巧根
321	用氢同位素估算氚在熔盐堆结构材料中	核技术	38	3	30602	皮力；刘卫；张

	的渗透					东勋
322	固态钍基熔盐堆中~(14)C 的产生及释放探讨	核技术	38	3	30603	朱兴望；王帅；彭超
323	吡啶离子液体[BPy][BF_4]与乙腈混合体系中杜醌的光化学反应动力学	物理化学学报	31	3	419	朱光来；王玉；张良伟
324	ICP-AES 中多重谱线拟合(MSF)扣除光谱干扰法在 Th、U 测定中的应用	核化学与放射化学	37	1	37	罗艳；丛海霞；赵中奇
325	裂变室输出信号数字化处理的仿真研究	核技术	38	1	10401	袁超；李勇平；黄跃峰
326	基于蒙特卡罗方法的反照中子剂量计刻度	核技术	38	1	10501	张国庆; 李长园; 蔡军
327	板型先进高温堆的可燃毒物装载优化	核技术	38	1	10601	魏书华; 余笑寒; 邹杨
328	涡腔倒角结构对涡流二极管性能影响的数值模拟	核技术	38	1	10602	曹寅；吴燕华；林超
329	不同背压下旋流式气液分离器工作特性	核技术	38	1	10603	李华; 张宁; 钱渊
330	非常规油气储集孔隙多尺度连通性的定量显微 CT 研究	矿物岩石地球化学通报	34	1	86	王玉丹; 任玉琦; 谭海
331	酶聚合体电流信号放大多通道电化学免疫传感体系及蛋白肿瘤标志物检测	电化学	21	1	39	邓王平; 窦艳枝; 苏静
332	EJ301 液体闪烁体探测器的波形甄别和能量刻度	核技术	38	2	20501	常乐；刘应都；杜龙
333	TMSR 核功率控制系统的 PID 设计与仿真	核技术	38	2	20601	汪全全; 尹聪聪; 孙雪静
334	不同温度 FLiNaK 熔盐对 Hastelloy-N 合金腐蚀的影响	核技术	38	2	20602	刘可；徐良；刘哲
335	氢在FLiNaK(LiF-NaF-KF)熔盐中的渗透行为	核技术	38	2	20603	曾友石；杜林；皮力
336	固态熔盐堆全厂断电 ATWS 事故工况下的堆芯安全探讨	核技术	38	2	20604	焦小伟；王凯；何兆忠
337	广角 X 射线散射实验的散射角度修正	中国科学. 物理学, 力学, 天文学	45	1	17001	赵镍；边风刚；王玉柱
338	不同芯材增强材料抗压性能比较的有限元计算	纺织学报	36	1	88	宋孝浜; 王春霞; 金利民

2016

No.	论文名称	期刊名称	期	卷	页	作者
1	Multicolour emission	NATURE PHOTONICS	10	11	695	Feng, Chao; Deng, Haixiao;
2	A single stage EEHG at SXFEL for narrow-bandwidth soft X-ray generation	SCIENCE BULLETIN	61	15	1202	Feng, Chao; Huang, Dazhang; Deng, Haixiao
3	Two-beam based two-stage EEHG-FEL	SCIENCE BULLETIN	61	9	720	Zhao, Zhentang;

	for coherent hard X-ray generation					Feng, Chao; Chen, Jianhui
4	Transverse to longitudinal phase space coupling in an electron beam for suppression of microbunching instability	PHYSICAL REVIEW ACCELERATORS AND BEAMS	19	10	100701	Huang, Dazhang; Feng, Chao; Deng, Haixiao
5	Fully coherent hard X-ray generation by two-stage phase-merging enhanced harmonic generation	CHINESE PHYSICS C	40	9	98101	Wang, Guang-Lei; Zhang, Wei-Qing; Yang, Xue-Ming
6	Beam dynamics of the superconducting wiggler on the SSRF storage ring	CHINESE PHYSICS C	40	3	37001	Zhang, Qing-Lei; Tian, Shun-Qiang; Jiang, Bo-Cheng
7	Seeded FEL Experiments at the SDUV-FEL Test Facility	IEEE TRANSACTIONS ON NUCLEAR SCIENCE	63	2	930	Zhao, Z. T.; Wang, D.;
8	Development of a nonresonant perturbation technique and its application to multicell traveling-wave deflectors	NUCLEAR INSTRUMENTS & METHODS IN PHYSICS RESEARCH SECTION A-ACCELERATORS SPECTROMETERS DETECTORS AND ASSOCIATED EQUIPMENT	835		148	Tan, Jianhao; Tong, Dechun; Gu, Qiang
9	Feasibility study of generating ultra-high harmonic radiation with a single stage echo-enabled harmonic generation scheme	NUCLEAR INSTRUMENTS & METHODS IN PHYSICS RESEARCH SECTION A-ACCELERATORS SPECTROMETERS DETECTORS AND ASSOCIATED EQUIPMENT	834		30	Zhou, Kaishang; Feng, Chao; Wang, Dong
10	Design, fabrication and first beam tests of the C-band RF acceleration unit at SINAP	NUCLEAR INSTRUMENTS & METHODS IN PHYSICS RESEARCH SECTION A-ACCELERATORS SPECTROMETERS DETECTORS AND ASSOCIATED EQUIPMENT	823		91	Fang, Wencheng; Gu, Qiang; Sheng, Xing
11	Wakefield issue and its impact on X-ray photon pulse in the SXFEL test facility	NUCLEAR INSTRUMENTS & METHODS IN PHYSICS RESEARCH SECTION A-ACCELERATORS SPECTROMETERS DETECTORS AND ASSOCIATED EQUIPMENT	822		71	Song, Minghao; Li, Kai; Feng, Chao
12	Study of the output pulse stability of a cascaded high-gain harmonic generation free-electron laser	NUCLEAR INSTRUMENTS & METHODS IN PHYSICS RESEARCH SECTION A-ACCELERATORS	820		1	Wang, Zhen; Feng, Chao; Gu, Qiang

13	Comparative study of coherent multi-color radiation generation in a seeded free-electron laser	SPECTROMETERS DETECTORS AND ASSOCIATED EQUIPMENT NUCLEAR INSTRUMENTS & METHODS IN PHYSICS RESEARCH SECTION A-ACCELERATORS SPECTROMETERS DETECTORS AND ASSOCIATED EQUIPMENT	815		91	Wang, Zhen; Xiang, Dao; Zhao, Zhentang
14	Using a double-frequency RF system to facilitate on-axis beam accumulation in a storage ring	NUCLEAR INSTRUMENTS & METHODS IN PHYSICS RESEARCH SECTION A-ACCELERATORS SPECTROMETERS DETECTORS AND ASSOCIATED EQUIPMENT	814		1	Jiang, B. C.; Zhao, Z. T.; Tian, S. Q.
15	Generation of two-color ultra-short radiation pulses from two electron bunches and a chirped seeded free-electron laser	NUCLEAR INSTRUMENTS & METHODS IN PHYSICS RESEARCH SECTION A-ACCELERATORS SPECTROMETERS DETECTORS AND ASSOCIATED EQUIPMENT	807		79	Feng, Chao; Wang, Zhen; Wang, Xingtao
16	The Truncated Human Telomeric Sequence forms a Hybrid-Type Intramolecular Mixed Parallel/antiparallel G-quadruplex Structure in K+ Solution	CHEMICAL BIOLOGY & DRUG DESIGN	88	1	122	Liu, Yuxia; Cheng, Dengfeng; Ge, Min
17	Deciphering buried air phases on natural and bioinspired superhydrophobic surfaces using synchrotron radiation-based X-ray phase-contrast imaging	NPG ASIA MATERIALS	8		e306	Hu, Zhanhao; Sun, Ming; Lv, Min
18	OSCILLATOR STRENGTHS OF VIBRIONIC EXCITATIONS OF NITROGEN DETERMINED BY THE DIPOLE (gamma, gamma) METHOD	ASTROPHYSICAL JOURNAL	819	2	142	Liu, Ya-Wei; Kang, Xu; Xu, Long-Quan
19	Anisotropic shrinkage of insect air sacs revealed in vivo by X-ray microtomography	SCIENTIFIC REPORTS	6		32380	Xu, Liang; Chen, Rongchang; Du, Guohao
20	Hydration induced material transfer in membranes of osmotic pump tablets measured by synchrotron radiation based FTIR	EUROPEAN JOURNAL OF PHARMACEUTICAL SCIENCES	84		132	Wu, Li; Yin, Xianzhen; Guo, Zhen
21	A robust method for high-precision quantification of the complex three-dimensional vasculatures acquired by X-ray microtomography	JOURNAL OF SYNCHROTRON RADIATION	23		1216	Tan, Hai; Wang, Dadong; Li, Rongxin
22	Synchrotron X-ray tomographic	CERAMICS INTERNATIONAL	42	15	17137	Gao, Yantao;

	characterization of CVI engineered 2D-woven and 3D-braided SiCf/SiC composites					Wang, Yudan; Yang, Xinmei
23	The absolute optical oscillator strengths of the 3p(5)4s and 3p(5)4s ' excitations of argon measured by the dipole (gamma, gamma) method	JOURNAL OF PHYSICS B-ATOMIC MOLECULAR AND OPTICAL PHYSICS	49	6	64010	Xu, Xin; Ni, Dong-Dong; Kang, Xu
24	Full-field x ray nano-imaging system designed and constructed at SSRF	CHINESE OPTICS LETTERS	14	9	93401	Feng, Binggang; Deng, Biao; Ren, Yuqi
25	Microscopic identification of Chinese medicinal materials based on X-ray phase contrast imaging: from qualitative to quantitative	JOURNAL OF INSTRUMENTATION	11		C07001	Xue, Y.; Liang, Z.; Tan, H.
26	Quantitative multi-scale analysis of mineral distributions and fractal pore structures for a heterogeneous Junger Basin shale	JOURNAL OF INSTRUMENTATION	11		C04005	Wang, Y. D.; Liu, K. Y.; Yang, Y. S.
27	Study of Scintillator thickness optimization of lens-coupled X-ray imaging detectors	JOURNAL OF INSTRUMENTATION	11		C03057	Xie, H.; Du, G.; Deng, B.
28	X-ray propagation-based equally sloped tomography for mouse brain	JOURNAL OF X-RAY SCIENCE AND TECHNOLOGY	24	1	79	Ren, Yuqi; Wang, Yudan; Zhou, Guangzhao
29	Investigation of Compton Profile of Molecular Propane	CHINESE PHYSICS LETTERS	33	7	93301	Mei, Xiao-Xun; Zhao, Xiao-Li; Xu, Long-Quan
30	Two-Dimensional Organic-Inorganic Hybrid Perovskite Photonic Films	NANO LETTERS	16	7	4166	Meng, Ke; Gao, Shanshan; Wu, Longlong
31	In situ measurement of contact angles and surface tensions of interfacial nanobubbles in ethanol aqueous solutions	SOFT MATTER	12	14	3303	Zhao, Binyu; Wang, Xingya; Wang, Shuo
32	Facile preparation of bridged silsesquioxane microspheres with interconnected multi-cavities and open holes	RSC ADVANCES	6	26	21571	Wang, Zhen; Qian, Zhenchao; Cao, Yuan
33	Tuning the mechanical properties of cellulose nanofibrils reinforced polyvinyl alcohol composites via altering the cellulose polymorphs	RSC ADVANCES	6	86	83356	Miao, Xiaran; Tian, Feng; Lin, Jinyou
34	Optimization of the design for beamline with fast polarization switching elliptically polarized undulators	JOURNAL OF SYNCHROTRON RADIATION	23		436	Cao, Jiefeng; Wang, Yong; Zou, Ying

35	Development of broadband X-ray interference lithography large area exposure system	REVIEW OF SCIENTIFIC INSTRUMENTS	87	4	43303	Xue, Chaofan; Wu, Yanqing; Zhu, Fangyuan
36	Observation of dual relaxation dynamics of polarization clusters in barium titanate by photon correlation spectroscopy (vol 54, 042401, 2015)	JAPANESE JOURNAL OF APPLIED PHYSICS	55	1	19203	Zhang, Mingjun; Guo, Zhi; Tai, Renzhong
37	DNA REACTION NETWORKS Providing a panoramic view	Nature Chemistry	8	8	738	Wang, Fei; Fan, Chunhai;
38	A Surface-Confined Proton-Driven DNA Pump Using a Dynamic 3D DNA Scaffold	ADVANCED MATERIALS	28	32	6860	Zhu, Dan; Pei, Hao; Yao, Guangbao
39	One-Shot Immunomodulatory Nanodiamond Agents for Cancer Immunotherapy	ADVANCED MATERIALS	28	14	2699	Zhang, Yu; Cui, Zhifen; Kong, Huating
40	Dietary Iron Oxide Nanoparticles Delay Aging and Ameliorate Neurodegeneration in Drosophila	ADVANCED MATERIALS	28	7	1387	Zhang, Yi; Wang, Zhuyao; Li, Xiaojiao
41	Ion-Mediated Polymerase Chain Reactions Performed with an Electronically Driven Microfluidic Device	ANGEWANDTE CHEMIE-INTERNATIONAL EDITION	55	40	12450	Zhang, Yi; Li, Qian; Guo, Linjie
42	Transfer of Two-Dimensional Oligonucleotide Patterns onto Stereocontrolled Plasmonic Nanostructures through DNA-Origami-Based Nanoimprinting Lithography	ANGEWANDTE CHEMIE-INTERNATIONAL EDITION	55	28	8036	Zhang, Yinan; Chao, Jie; Liu, Huajie
43	DNA orientation-specific adhesion and patterning of living mammalian cells on self-assembled DNA monolayers	CHEMICAL SCIENCE	7	4	2722	Wang, Shaopeng; Cai, Xiaoqing; Wang, Lihua
44	Activity modulation and allosteric control of a scaffolded DNAzyme using a dynamic DNA nanostructure	CHEMICAL SCIENCE	7	2	1200	Mao, Xiuhai; Simon, Anna J.; Pei, Hao
45	On-Electrode Synthesis of Shape-Controlled Hierarchical Flower-Like Gold Nanostructures for Efficient Interfacial DNA Assembly and Sensitive Electrochemical Sensing of MicroRNA	SMALL	12	28	3794	Su, Shao; Wu, Yan; Zhu, Dan
46	Silica Nanoparticles Target a Wnt Signal Transducer for Degradation and Impair Embryonic Development in Zebrafish	THERANOSTICS	6	11	1810	Yi, Hongyang; Wang, Zhuyao; Li, Xiaojiao
47	Structural and optical control of DNA-mediated Janus plasmonic	NANOSCALE	8	17	9337	Xu, Lifeng; Wang, Geng;

	nanostructures					Shen, Jianlei
48	Mechanical force-induced polymerization and depolymerization of F-actin at water/solid interfaces	NANOSCALE	8	11	6008	Zhang, Xueqiang; Hu, Xiuyuan; Lei, Haozhi
49	Highly narrow nanogap-containing Au@Au core-shell SERS nanoparticles: size-dependent Raman enhancement and applications in cancer cell imaging	NANOSCALE	8	4	2090	Hu, Chongya; Shen, Jianlei; Yan, Juan
50	Multiple-Armed Tetrahedral DNA Nanostructures for Tumor-Targeting, Dual-Modality in Vivo Imaging	ACS APPLIED MATERIALS & INTERFACES	8	7	4378	Jiang, Dawei; Sun, Yanhong; Li, Jiang
51	Aptamer-initiated on-particle template-independent enzymatic polymerization (aptamer-OTEP) for electrochemical analysis of tumor biomarkers	BIOSENSORS & BIOELECTRONICS	86		536	Wang, Pengjuan; Wan, Ying; Deng, Shengyuan
52	Hybridization chain reaction amplification for highly sensitive fluorescence detection of DNA with dextran coated microarrays	BIOSENSORS & BIOELECTRONICS	81		92	Chao, Jie; Li, Zhenhua; Li, Jing
53	Dynamic Modulation of DNA Hybridization Using Allosteric DNA Tetrahedral Nanostructures	ANALYTICAL CHEMISTRY	88	16	8043	Song, Ping; Li, Min; Shen, Juwen
54	PolyA-Mediated DNA Assembly on Gold Nanoparticles for Thermodynamically Favorable and Rapid Hybridization Analysis	ANALYTICAL CHEMISTRY	88	9	4949	Zhu, Dan; Song, Ping; Shen, Juwen
55	High-Sensitivity and High-Efficiency Detection of DNA Hydroxymethylation in Genomic DNA by Multiplexing Electrochemical Biosensing	ANALYTICAL CHEMISTRY	88	7	3476	Chen, Shixing; Dou, Yanzhi; Zhao, Zhihan
56	Acupuncture promotes mTOR-independent autophagic clearance of aggregation-prone proteins in mouse brain	SCIENTIFIC REPORTS	6		19714	Tian, Tian; Sun, Yanhong; Wu, Huangan
57	Molecular Mechanisms of Ultrafiltration Membrane Fouling in Polymer-Flooding Wastewater Treatment: Role of Ions in Polymeric Fouling	ENVIRONMENTAL SCIENCE & TECHNOLOGY	50	3	1393	Liu, Guicai; Yu, Shuili; Yang, Haijun
58	CO Adsorption-Induced Surface Segregation and Formation of Pd Chains on AuPd(100) Alloy: Density Functional Theory Based Ising Model and Monte Carlo Simulations	JOURNAL OF PHYSICAL CHEMISTRY C	120	1	350	Zhu, Beien; Creuze, Jerome; Mottet, Christine

59	Size-Dependent Stiffness of Nanodroplets: A Quantitative Analysis of the Interaction between an AFM Probe and Nanodroplets	LANGMUIR	32	43	11230	Wang, Shuo; Wang, Xingya; Zhao, Binyu
60	Electrochemical detection of PCR amplicons of Escherichia coli genome based on DNA nanostructural probes and polyHRP enzyme	ANALYST	141	18	5304	Wen, Yanli; Wang, LeLe; Xu, Li
61	Editorial: Translating the advances of biosensors from bench to bedside	BIOTECHNOLOGY JOURNAL	11	6	727	Fan, Chunhai; Tamiya, Eiichi;
62	Thermodynamic description of the AgCl-CoCl2-InCl3-NaCl system	JOURNAL OF ALLOYS AND COMPOUNDS	663		885	Wang, Kun; Robelin, Christian; Wu, Zhu
63	Lab on smartphone with interfaced electrochemical chips for on-site gender verification	JOURNAL OF ELECTROANALYTICAL CHEMISTRY	777		117	Deng, Wangping; Dou, Yanzhi; Song, Ping
64	Direct imaging charge distribution in reduced graphene oxide sheets induced by isolated charges	JOURNAL OF PHYSICS D-APPLIED PHYSICS	49	41	415303	Shen, Yue; Wang, Ying; Zhou, Yuan
65	Critical evaluation and thermodynamic optimization of the (U plus Bi), (U plus Si) and (U plus Sn) binary systems	JOURNAL OF CHEMICAL THERMODYNAMICS	92		158	Wang, Jian; Wang, Kun; Ma, Chunhua
66	Multi-metal element analysis for the identification of foodborne pathogenic bacteria	ANALYTICAL METHODS	8	27	5421	Zhang, Xingxing; Li, Xueling; Wang, Yadi
67	Hetero-assembly of gold nanoparticles on a DNA origami template	SCIENCE CHINA-CHEMISTRY	59	6	730	Chao, Jie; Zhang, Yinan; Zhu, Dan
68	Superresolution imaging of telomeres with continuous wave stimulated emission depletion (STED) microscope	SCIENCE CHINA-CHEMISTRY	59	11	1519	Wang, Shaopeng; Deng, Suhui; Cai, Xiaoqing
69	Quantum dots protect against MPP+-induced neurotoxicity in a cell model of Parkinson's disease through autophagy induction	SCIENCE CHINA-CHEMISTRY	59	11	1486	Wang, Lu; Li, Xiaoming; Han, Yuping
70	Structure stability of TiAu4 nanocluster with water adsorption	PHYSICS LETTERS A	380	22-23	1971	Liu, Xiaoji; Zhu, Beien; Gao, Yi
71	Special Issue of "DNA Nanotechnology"	CHINESE JOURNAL OF CHEMISTRY	34	3	251	Fan, Chunai; Pei, Hao;
72	Strong Hydrophobic Interaction Between Graphene Oxide and Supported Lipid Bilayers Revealed by AFM	MICROSCOPY RESEARCH AND TECHNIQUE	79	8	721	Hu, Xiuyuan; Lei, Haozhi; Zhang, Xueqiang
73	Recent Progresses in Molecule Motors Driven by Enzymatic Reactions	CHINESE JOURNAL OF ANALYTICAL CHEMISTRY	44	7	1133	Qin Wei-Wei; Sun Le-Le; Peng Tian-Huan

74	Biosensors in POCT Application	PROGRESS IN CHEMISTRY	28	9	1341	Deng Wangping; Wang Lihua; Song Shiping
75	Preparation and Biological Applications of DNA Hydrogel	PROGRESS IN CHEMISTRY	28	5	628	Song Ping; Ye Dekai; Song Shiping
76	Synchrotron FTIR spectroscopy reveals molecular changes in Escherichia coli upon Cu2+ exposure	NUCLEAR SCIENCE AND TECHNIQUES	27	3	56	Hu, Xiao-Juan; Liu, Zhi-Xiao; Wang, Ya-Di
77	Shape Evolution of Metal Nanoparticles in Water Vapor Environment	NANO LETTERS	16	4	2628	Zhu, Beien; Xu, Zhen; Wang, Chunlei
78	Anisotropy Enhancement of Thermal Energy Transport in Supported Black Phosphorene	JOURNAL OF PHYSICAL CHEMISTRY LETTERS	7	13	2518	Chen, Jige; Chen, Shunda; Gao, Yi
79	Effect of Water Adsorption on the Photoluminescence of Silicon Quantum Dots	JOURNAL OF PHYSICAL CHEMISTRY LETTERS	7	10	1788	Yang, Jinrong; Fang, Haiping; Gao, Yi
80	Unraveling a generic growth pattern in structure evolution of thiolate-protected gold nanoclusters	NANOSCALE	8	14	7396	Xu, Wen Wu; Li, Yadong; Gao, Yi
81	3D flexible water channel: stretchability of nanoscale water bridge	NANOSCALE	8	10	5676	Chen, Jige; Wang, Chunlei; Wei, Ning
82	Medium-sized Au-40(SR)(24) and Au-52(SR)(32) nanoclusters with distinct gold-kernel structures and spectroscopic features	NANOSCALE	8	3	1299	Xu, Wen Wu; Li, Yadong; Gao, Yi
83	Impact of cation-pi interactions on the cell voltage of carbon nanotube-based Li batteries	NANOSCALE	8	3	1451	Gao, Shaohua; Shi, Guosheng; Fang, Haiping
84	Enhanced Aerogen- Interaction by a Cation- Force	CHEMISTRY-A EUROPEAN JOURNAL	22	8	2586	Miao, Junjian; Song, Bo; Gao, Yi
85	Water Adsorption and Dissociation on Ceria-Supported Single-Atom Catalysts: A First-Principles DFT plus U Investigation	CHEMISTRY-A EUROPEAN JOURNAL	22	6	2092	Han, Zhong-Kang; Gao, Yi;
86	Adsorption of Antibiotics on Graphene and Biochar in Aqueous Solutions Induced by pi-pi Interactions	SCIENTIFIC REPORTS	6		31920	Peng, Bingquan; Chen, Liang; Que, Chenjing
87	Manipulation of a neutral and nonpolar nanoparticle in water using a nonuniform electric field	JOURNAL OF CHEMICAL PHYSICS	144	1	14302	Xu, Zhen; Wang, Chunlei; Sheng, Nan
88	Semiconducting boron carbides with better	JOURNAL OF PHYSICS	49	35	355302	Echeverria,

	charge extraction through the addition of pyridine moieties	D-APPLIED PHYSICS				Elena; Dong, Bin; Peterson, George
89	Conformational flexibility of PPII-helix: A density functional theory study	CHEMICAL PHYSICS LETTERS	651		109	Guo, Ping; Lei, Xiaoling; Gao, Yi
90	A new understanding of inert gas narcosis	CHINESE PHYSICS B	25	1	13602	Zhang, Meng; Gao, Yi; Fang, Haiping
91	Force Drift in Force Mode Dip-Pen Nanolithography	JOURNAL OF NANOSCIENCE AND NANOTECHNOLOGY	16	7	7030	Yang, Haijun; Zhang, Chen; Zhang, Jinjin
92	A new association state of solutes in nanoconfined aqueous solutions	SCIENCE CHINA-PHYSICS MECHANICS & ASTRONOMY	59	11	110511	Tu, YuSong; Zhao, Liang; Fang, HaiPing
93	Effect of solvent on directional drift in Brownian motion of particle/molecule with broken symmetry	SCIENCE CHINA-PHYSICS MECHANICS & ASTRONOMY	59	8	680511	Kong, FanDong; Sheng, Nan; Wan, RongZheng
94	Asymmetric self-diffusion with orientation-dependence of water molecule in finite timescale	SCIENCE CHINA-PHYSICS MECHANICS & ASTRONOMY	59	7	670511	Wei, Xu; Sheng, Nan; Wan, RongZheng
95	Transportation of Two Coupled Particles in an Asymmetric Saw-Tooth Potential	CHINESE PHYSICS LETTERS	33	2	20501	Kong, Ling-Wei; Wan, Rong-Zheng; Fang, Hai-Ping
96	Interfacial water at microscopic level: from quasi-one-dimensional, two-dimensional confined space, to biomolecules surfaces and material surfaces	ACTA PHYSICA SINICA	65	18	186101	Fang Hai-Ping;;
97	In situ synchrotron small- and wide-angle X-ray study on the structural evolution of Kevlar fiber under uniaxial stretching	RSC ADVANCES	6	85	81552	Li, Xiaoyun; Tian, Feng; Zhou, Ping
98	A novel heating area design of temperature-jump microfluidic chip for synchrotron radiation solution X-ray scattering	NUCLEAR SCIENCE AND TECHNIQUES	27	4	92	Li, Yi-Wen; Bian, Feng-Gang; Wang, Jie
99	Development of the bunch-by-bunch beam position acquisition system based on BEEcube	NUCLEAR SCIENCE AND TECHNIQUES	27	2	47	Yang, Yong; Leng, Yong-Bin; Yan, Ying-Bing
100	High Efficiency Pb-In Binary Metal Perovskite Solar Cells	ADVANCED MATERIALS	28	31	6695	Wang, Zhao-Kui; Li, Meng; Yang, Ying-Guo
101	High-Performance Perovskite Solar Cells	ACS APPLIED MATERIALS &	8	23	14503	Feng, Shanglei;

	Engineered by an Ammonia Modified Graphene Oxide Interfacial Layer	INTERFACES				Yang, Yingguo; Li, Meng
102	Facile usage of a MYTHEN 1K with a Huber 5021 diffractometer and angular calibration in operando experiments	JOURNAL OF APPLIED CRYSTALLOGRAPHY	49		1182	Gao, Mei; Gu, Yueliang; Li, Li
103	Automatic crystal centring procedure at the SSRF macromolecular crystallography beamline	JOURNAL OF SYNCHROTRON RADIATION	23		1323	Wang, Zhijun; Pan, Qiangyan; Yang, Lifeng
104	Facile preparation of nitrogen-doped graphene sponge as a highly efficient oil absorption material	MATERIALS LETTERS	178		95	Yang, Wenlong; Gao, Hui; Zhao, Yu
105	Synthesis of Tb4O7 complexed with reduced graphene oxide for Rhodamine-B absorption	MATERIALS RESEARCH BULLETIN	77		111	Gao, Hui; Zhou, Yang; Chen, Keqin
106	A new layered nano hybrid perovskite film with enhanced resistance to moisturee-induced degradation	CHEMICAL PHYSICS LETTERS	658		71	Jiang, Wenlong; Ying, Jifei; Zhou, Wei
107	Shear-Coupled Grain Growth and Texture Development in a Nanocrystalline Ni-Fe Alloy during Cold Rolling	METALLURGICAL AND MATERIALS TRANSACTIONS A-PHYSICAL METALLURGY AND MATERIALS SCIENCE	47A	12	6632	Li, Li; Ungar, Tamas; Toth, Laszlo S.
108	Enhanced Stability of CH3NH3PbI3 Thin Films Deposited on FTZO	CHEMISTRY LETTERS	45	7	819	Jiang, Wenlong; Yang, Tieying; Gao, Yanmin
109	The formation of eutectic phases and hot cracks in one Ni-Mo-Cr superalloy	MATERIALS & DESIGN	93		324	Li, Jiang; Shrestha, Sachin L.; Long, Yan
110	Convective heat transfer characteristics in the turbulent region of molten salt in concentric tube	APPLIED THERMAL ENGINEERING	98		213	Chen, Y. S.; Wang, Y.; Zhang, J. H.
111	Intermediate temperature embrittlement of one new Ni-26W-6Cr based superalloy for molten salt reactors	MATERIALS SCIENCE AND ENGINEERING A-STRUCTURAL MATERIALS PROPERTIES MICROSTRUCTURE AND PROCESSING	668		137	Jiang, Li; Ye, Xiangxi; Cui, Chuanyong
112	Effect of tungsten content on the microstructure and tensile properties of Ni-xW-6Cr alloys	MATERIALS SCIENCE AND ENGINEERING A-STRUCTURAL MATERIALS PROPERTIES MICROSTRUCTURE AND PROCESSING	655		269	Liu, Shulin; Ye, Xiang-Xi; Jiang, Li
113	Effects of post-weld heat treatment on microstructure and mechanical properties of laser welds in GH3535 superalloy	OPTICS AND LASER TECHNOLOGY	81		18	Yu, Kun; Jiang, Zhenguo; Leng, Bin
114	Research Progress on the Indirect	CHEMSUSCHEM	9	4	322	Du, Xian-Long;

	Hydrogenation of Carbon Dioxide to Methanol					Jiang, Zheng; Su, Dang Sheng
115	Determination and evaluation of the thermophysical properties of an alkali carbonate eutectic molten salt	FARADAY DISCUSSIONS	190		327	An, Xuehui; Cheng, Jinhui; Zhang, Peng
116	Corrosion of SiC induced by Hastelloy N alloy and its corrosion products in LiF-NaF-KF molten salt	CORROSION SCIENCE	109		62	Yang, Xinmei; Zhang, Dongsheng; Liu, Min
117	The high-temperature corrosion of Hastelloy N alloy (UNS N10003) in molten fluoride salts analysed by STXM, XAS, XRD, SEM, EPMA, TEM/EDS	CORROSION SCIENCE	106		249	Ye, Xiang-Xi; Ai, Hua; Guo, Zhi
118	A niobium-necked cluster [As3Nb(As3Sn3)](3-) with aromatic Sn-3(2-)	DALTON TRANSACTIONS	45	9	3874	Pan, Fu-Xing; Xu, Cong-Qiao; Li, Lei-Jiao
119	Origin of heterogeneous dynamics in local molecular structures of ionic liquids	SOFT MATTER	12	43	8942	Sha, Maolin; Liu, Yusheng; Dong, Huaze
120	Accurate viscosity measurement of nitrates/nitrites salts for concentrated solar power	SOLAR ENERGY	137		385	Jin, Yuan; Cheng, Jinhui; An, Xuehui
121	Extraction of local coordination structure in a low-concentration uranyl system by XANES	JOURNAL OF SYNCHROTRON RADIATION	23		758	Zhang, Linjuan; Zhou, Jing; Zhang, Jianyong
122	The significant role of covalency in determining the ground state of cobalt phthalocyanines molecule	AIP ADVANCES	6	3	35306	Zhou, Jing; Zhang, Linjuan; Hu, Zhiwei
123	The effect of corrosion product CrF3 on thermo-physical properties of FLiNaK	JOURNAL OF NUCLEAR SCIENCE AND TECHNOLOGY	53	1	61	Yin, Huiqin; Zhang, Peng; An, Xuehui
124	The Magnetic Order in Ion Irradiated Graphite	CHINESE PHYSICS LETTERS	33	4	46101	Li, Li-Juan; Yang, Xin-Mei; Xia, Hui-Hao
125	Magnetic Design and Measurement Results of a CPMU Prototype at SSRF	IEEE TRANSACTIONS ON APPLIED SUPERCONDUCTIVITY	26	4		Zhang, Wei; Wang, Hongfei; He, Yongzhou
126	Research on Magnetic Properties of Nd(Pr)FeB Magnet for Cryogenic Permanent-Magnet Undulator of SSRF	IEEE TRANSACTIONS ON APPLIED SUPERCONDUCTIVITY	26	4	604204	He, Y. Z.; Zhou, Q. G.; Zhang, W.
127	Analyses on the Cooling Performance of the CPMU Magnetic Structure at SSRF	IEEE TRANSACTIONS ON APPLIED SUPERCONDUCTIVITY	26	4	4101305	Wang, Jian; Liu, Yiyong; Wang, Shuhua
128	The Magnetic Performance of an Exotic	IEEE TRANSACTIONS ON	26	4	410170	Zhou, Qiaogen;

	APPLE-Knot Undulator Developed at SSRF	APPLIED SUPERCONDUCTIVITY			4	Qian, Maofei; Wang, Hongfei
129	Application of Magnetic Materials in Synchrotron Radiation and Free Electron Laser	JOURNAL OF INORGANIC MATERIALS	31	10	1031	He Yong-Zhou; Zhou Qiao-Gen;
130	Measurements of Lambda Lambda correlation function in heavy-ion collisions at RHIC	15TH INTERNATIONAL CONFERENCE ON STRANGENESS IN QUARK MATTER (SQM2015)	668		12009	Chen, J. H.;;
131	Beam Energy Dependence of the Third Harmonic of Azimuthal Correlations in Au plus Au Collisions at RHIC	PHYSICAL REVIEW LETTERS	116	11	112302	Adamczyk, L.; Adkins, J. K.; Agakishiev, G.
132	Centrality and Transverse Momentum Dependence of Elliptic Flow of Multistrange Hadrons and phi Meson in Au plus Au Collisions at root S NN=200 GeV	PHYSICAL REVIEW LETTERS	116	6	62301	Adamczyk, L.; Adkins, J. K.; Agakishiev, G.
133	Jet-like correlations with direct-photon and neutral-pion triggers at root S-NN=200 GeV	PHYSICS LETTERS B	760		689	Adamczyk, L.; Adkins, J. K.; Agakishiev, G.
134	Production of multistrange hadrons, light nuclei and hypertriton in central Au plus Au collisions at root S-NN=11.5 and 200 GeV	PHYSICS LETTERS B	754		6	Shah, N.; Ma, Y. G.; Chen, J. H.
135	Multilayer Network Analysis of Nuclear Reactions	SCIENTIFIC REPORTS	6		31882	Zhu, Liang; Ma, Yu-Gang; Chen, Qu
136	NEW ASTROPHYSICAL REACTION RATE FOR THE C-12(alpha, gamma)O-16 REACTION	ASTROPHYSICAL JOURNAL LETTERS	817	1	L5	An, Zhen-Dong; Ma, Yu-Gang; Fan, Gong-Tao
137	Isospin properties of quark matter from a 3-flavor NJL model	PHYSICAL REVIEW D	94	6	65032	Liu, He; Xu, Jun; Chen, Lie-Wen
138	Centrality dependence of identified particle elliptic flow in relativistic heavy ion collisions at root s(NN)=7.7-62.4 GeV	PHYSICAL REVIEW C	93	1	14907	Adamczyk, L.; Adkins, J. K.; Agakishiev, G.
139	Measurement of elliptic flow of light nuclei at root s(NN)=200, 62.4, 39, 27, 19.6, 11.5, and 7.7 GeV at the BNL Relativistic Heavy Ion Collider	PHYSICAL REVIEW C	94	3	34908	Adamczyk, L.; Adkins, J. K.; Agakishiev, G.
140	Beam-energy dependence of charge balance functions from Au plus Au collisions at energies available at the BNL Relativistic Heavy Ion Collider	PHYSICAL REVIEW C	94	2	24909	Adamczyk, L.; Adkins, J. K.; Agakishiev, G.
141	Near-side azimuthal and pseudorapidity	PHYSICAL REVIEW C	94	1	14910	Abelev, B.;

	correlations using neutral strange baryons and mesons in d plus Au, Cu plus Cu, and Au plus Au collisions at root S-NN=200 GeV					Adamczyk, L.; Adkins, J. K.
142	J/psi production at low transverse momentum in p plus p and d plus Au collisions at root s(NN)=200 GeV	PHYSICAL REVIEW C	93	6	64904	Adamczyk, L.; Adkins, J. K.; Agakishiev, G.
143	Analysis techniques for the evaluation of the neutrinoless double-beta decay lifetime in Te-130 with the CUORE-0 detector	PHYSICAL REVIEW C	93	4	45503	Alduino, C.; Alfonso, K.; Artusa, D. R.
144	Probing parton dynamics of QCD matter with Omega and phi production	PHYSICAL REVIEW C	93	2	21903	Adamczyk, L.; Adkins, J. K.; Agakishiev, G.
145	Dipole oscillation modes in light alpha-clustering nuclei	PHYSICAL REVIEW C	94	1	14301	He, W. B.; Ma, Y. G.; Cao, X. G.
146	Predictions for root s(NN)=5.02 TeV Pb + Pb collisions from a multiphase transport model	PHYSICAL REVIEW C	93	5	54911	Ma, Guo-Liang; Lin, Zi-Wei;
147	Understanding transport simulations of heavy-ion collisions at 100A and 400A MeV: Comparison of heavy-ion transport codes under controlled conditions	PHYSICAL REVIEW C	93	4	44609	Xu, Jun; Chen, Lie-Wen; Tsang, ManYee Betty
148	phi-meson production at forward/backward rapidity in high-energy nuclear collisions from a multiphase transport model	PHYSICAL REVIEW C	93	4	44904	Ye, Y. J.; Chen, J. H.; Ma, Y. G.
149	Investigating the scaling of higher-order flows in relativistic heavy-ion collisions	PHYSICAL REVIEW C	93	2	24906	Zhang, Chun-Jian; Xu, Jun;
150	A scaling phenomenon in the difference of Shannon information uncertainty of fragments in heavy-ion collisions	JOURNAL OF PHYSICS G-NUCLEAR AND PARTICLE PHYSICS	43	4	45102	Ma, Chun-Wang; Song, Yi-Dan; Qiao, Chun-Yuan
151	Rapidity bin multiplicity correlations from a multi-phase transport model	EUROPEAN PHYSICAL JOURNAL A	52	3	46	Wang, Mei-Juan; Chen, Gang; Wu, Yuan-Fang
152	Flow in small systems from parton scatterings	NUCLEAR PHYSICS A	956		745	Ma, Guo-Liang; Bzdak, Adam;
153	Spin transport in intermediate-energy heavy-ion collisions as a probe of in-medium spin-orbit interactions	NUCLEAR PHYSICS A	955		41	Xia, Yin; Xu, Jun; Li, Bao-An
154	Nuclear point mass effects in the interaction of energetic ion with carbon nanotubes	APPLIED PHYSICS A-MATERIALS SCIENCE & PROCESSING	122	3	222	Zheng, Li-Ping; Yan, Long; Zhu, Zhi-Yong
155	Neutron time-of-flight spectroscopy	CHINESE PHYSICS C	40	5	56202	Liu, Long-Xiang;

	measurement using a waveform digitizer					Wang, Hong-Wei; Ma, Yu-Gang
156	Interaction Chamber Design for an Energy Continuously Tunable Sub-Mev Laser-Compton Gamma-Ray Source	IEEE TRANSACTIONS ON NUCLEAR SCIENCE	63	2	906	Xu, Hanghua; Fan, Gongtao; Wu, Hailong
157	Low-mass vector meson production at forward rapidity in p plus p and d plus Au collisions at root s(NN)=200 GeV from a multiphase transport model	NUCLEAR SCIENCE AND TECHNIQUES	27	4	87	Xu, Yi-Fei; Ye, Yong-Jin; Chen, Jin-Hui
158	Neutron excess method for performance assessment of thorium-based fuel in a breed-and-burn reactor with various coolants	NUCLEAR SCIENCE AND TECHNIQUES	27	4	99	Yang, Kun; Qin, Wei; Chen, Jin-Gen
159	Determination of the neutron skin thickness from interaction cross section and charge-changing cross section for B, C, N, O, F isotopes	NUCLEAR SCIENCE AND TECHNIQUES	27	3	71	Li, Xiu-Fang; Fang, De-Qing; Ma, Yu-Gang
160	Effect of C-5 position on the photochemical properties and phototoxicity of antofloxacin and levofloxacin: A stable and transient study	JOURNAL OF PHOTOCHEMISTRY AND PHOTOBIOLOGY B-BIOLOGY	155		122	Zhao, Jianfeng; Liu, Yancheng; Jiang, Xingxing
161	Characterization of typical 3D pore networks of Jiulaodong formation shale using nano-transmission X-ray microscopy	FUEL	170		84	Wang, Yu; Pu, Jie; Wang, Lihua
162	High Molecular Weight Polyethylenimine-Functionalized Multiwalled Carbon Nanotubes as Efficient Gene Delivery Vehicles	JOURNAL OF NANOSCIENCE AND NANOTECHNOLOGY	16	7	7210	Ma, Jifei; Li, Yulan; Yu, Bozhang
163	An improved combustion apparatus for the determination of organically bound tritium in environmental samples	APPLIED RADIATION AND ISOTOPES	110		218	Du, Lin; Shan, Jian; Ma, Yu-Hua
164	Occurrence of HTO and NE-OBT in soil in the vicinity of the Qinshan Nuclear Power Plant	NUCLEAR SCIENCE AND TECHNIQUES	27	4	77	Du, Lin; Zhang, Qin; Xia, Zheng-hai
165	Analysis of tritium production in a 2 MW liquid-fueled molten salt experimental reactor and its environmental impact	NUCLEAR SCIENCE AND TECHNIQUES	27	4	78	Lyu, Xiao-Wen; Xia, Xiao-Bin; Zhang, Zhi-Hong
166	3D microstructures of nuclear graphite: IG-110, NBG-18 and NG-CT-10	NUCLEAR SCIENCE AND TECHNIQUES	27	3	66	Jing, Shi-Pei; Zhang, Can; Pu, Jie
167	Properties of phosphate glass waste forms containing fluorides from a molten salt reactor	NUCLEAR SCIENCE AND TECHNIQUES	27	3	63	Sun, Ya-Ping; Xia, Xiao-Bin; Qiao, Yan-Bo

168	The application of EPICS in TMSR radiation protection and access control system	NUCLEAR SCIENCE AND TECHNIQUES	27	2	41	Han, Li-Feng; Chen, Yong-Zhong; Cai, Jun
169	Investigation on hydrogen absorption/desorption properties of as-cast La(1-x)MgxNi4.25Al0.75 (x=0.0, 0.1, 0.2, 0.3) alloys for tritium storage	NUCLEAR SCIENCE AND TECHNIQUES	27	2	32	Lu, Li-Jun; Cheng, Hong-Hui; Han, Xing-Bo
170	Tritium concentration in soybean plants exposed to atmospheric HTO during nighttime and daytime	NUCLEAR SCIENCE AND TECHNIQUES	27	2	39	Shen, Hui-Fang; Liu, Wei;
171	Structures and Hydrogen Storage Properties of La1-xMgxNi4.25Al0.75 (x=0.0, 0.1, 0.2, 0.3) Alloys	RARE METAL MATERIALS AND ENGINEERING	45	1	56	Lu Lijun; Cheng Honghui; Han Xingbo
172	Sodium alginate-functionalized nanodiamonds as sustained chemotherapeutic drug-release vectors	CARBON	97		78	Cui, Zhifen; Zhang, Yu; Zhang, Jichao
173	Electrochemical behavior of Th(IV) and its electrodeposition from ThF4-LiCl-KCl melt	ELECTROCHIMICA ACTA	196		286	Wang, Xianbin; Huang, Wei; Gong, Yu
174	Probing the spontaneous reduction mechanism of platinum ions confined in the nanospace by X-ray absorption fine structure spectroscopy	PHYSICAL CHEMISTRY CHEMICAL PHYSICS	18	28	19259	Jiang, Fangling; Li, Cheng; Fu, Haiying
175	Preparation and characterization of superhydrophobic organic-inorganic hybrid cotton fabrics via gamma-radiation-induced graft polymerization	CARBOHYDRATE POLYMERS	149		308	Gao, Qianhong; Hu, Jiangtao; Li, Rong
176	Crystallization and temperature-dependent structure deflection of C(6)mimBr ionic liquid intercalated in LAPONITE (R)	RSC ADVANCES	6	100	98018	Jiang, Fangling; Li, Cheng; Guo, Xiaojing
177	Functionalized and reusable polyethylene fibres for Au(III) extraction from aqueous solution with high adsorption capacity and selectivity	RSC ADVANCES	6	90	87221	Pang, Li-juan; Li, Rong; Gao, Qian-hong
178	Highly hydrophilic ultra-high molecular weight polyethylene powder and film prepared by radiation grafting of acrylic acid	APPLIED SURFACE SCIENCE	382		162	Wang, Honglong; Xu, Lu; Li, Rong.
179	Extended X-ray Absorption Fine Structure and Density Functional Theory Studies on the Complexation Mechanism of Amidoximate Ligand to Uranyl Carbonate	INDUSTRIAL & ENGINEERING CHEMISTRY RESEARCH	55	15	4224	Zhang, Linjuan; Su, Jing; Yang, Shitong

180	First-principle investigation of the structure and vibrational spectra of the local structures in LiF-BeF2 Molten Salts	JOURNAL OF MOLECULAR LIQUIDS	213		17	Dai, Jianxing; Han, Han; Li, Qingnuan
181	DFT investigations of uranium complexation with amidoxime-, carboxyl- and mixed amidoxime/carboxyl-based host architectures for sequestering uranium from seawater	INORGANICA CHIMICA ACTA	441		117	Guo, Xiaojing; Xiong, Xiao-Gen; Li, Cheng
182	Improving the creep resistance and tensile property of UHMWPE sheet by radiation cross-linking and annealing	RADIATION PHYSICS AND CHEMISTRY	125		41	Wang, Honglong; Xu, Lu; Li, Rong
183	Radiation synthesis of a new amidoximated UHMWPE fibrous adsorbent with high adsorption selectivity for uranium over vanadium in simulated seawater	RADIATION PHYSICS AND CHEMISTRY	122		1	Gao, Qianhong; Hu, Jiangtao; Li, Rong
184	Preparation, characterization and ion-exchange behavior of polyantimonic acid-polyacrylonitrile (PAA-PAN) composite beads for strontium(II)	JOURNAL OF RADIOANALYTICAL AND NUCLEAR CHEMISTRY	308	1	155	Ma, Fuyin; Shi, Wanlong; Meng, Hu
185	Preparation of High Hydrophilic PTFE Powder and Its Dispersion Stability	ACTA POLYMERICA SINICA		9	1247	Li, Hui; Zeng, Hong-yan; Xing, Zhe
186	Influence of Preparation Method on Oxidation Degree of Graphene Oxide and Adsorption for Th (IV) and U(VI)	JOURNAL OF INORGANIC MATERIALS	31	5	454	Wang Xiao-Ning; Meng Hu; Ma Fu-Yin
187	Laser Flash Photolysis Mechanism of Anthraquinone-2-Sodium Sulfonate Pyridine Ionic Liquid/Water Mixed System	CHINESE JOURNAL OF CHEMICAL PHYSICS	29	1	140	Zhu, Guang-lai; Zhang, Liang-wei; Liu, Yan-cheng
188	Variations in surface and electrical properties of polytetrafluoroethylene film after plasma-induced grafting of acrylic acid	NUCLEAR SCIENCE AND TECHNIQUES	27	3	62	Li, Rong; He, Xin-Zhong; Gao, Qian-Hong
189	Thermal performance and cost analysis of a multi-layered solid-PCM thermocline thermal energy storage for CSP tower plants	APPLIED ENERGY	178		784	Zhao, Bing-chen; Cheng, Mao-song; Liu, Chang
190	Development of a MCNP5 and ORIGEN2 based burnup code for molten salt reactor	NUCLEAR SCIENCE AND TECHNIQUES	27	3	65	Sun, Guo-Min; Cheng, Mao-Song;
191	Numerical analysis of the activity of irradiated alloy-N in an FHR	NUCLEAR SCIENCE AND TECHNIQUES	27	2	44	Peng, Chao; Zhu, Xing-Wang; Zhang, Guo-Qing

192	Development of an innovative detection system for pebble bed kinematic studies	NUCLEAR SCIENCE AND TECHNIQUES	27	2	31	Zhao, Ying; Qu, Shi-Xiang; Zhu, Xing-Wang
193	Dancoff factor analysis for pebble bed fluoride salt cooled high temperature reactor	PROGRESS IN NUCLEAR ENERGY	88		332	Qin, Wei; Yang, Kun; Chen, Jingen
194	Benchmarking of Th-232 evaluation by a 14.8 MeV neutron leakage spectra experiment with slab samples	ANNALS OF NUCLEAR ENERGY	96		181	Lin, Zuokang; Nie, Yangbo; Cai, Xiangzhou
195	Development and application of a system analysis code for liquid fueled molten salt reactors based on RELAP5 code	NUCLEAR ENGINEERING AND DESIGN	305		378	Shi, Chengbin; Cheng, Maosong; Liu, Guimin
196	Molecular dynamics study of thermal transport across grain boundaries in silicon carbide nanorod	MATERIALS RESEARCH EXPRESS	3	3	35018	Wang, Hao; Zhang, Wei; Wang, Chengbin
197	Preparation of ultrafine-grain graphite by liquid dispersion technique for inhibiting the liquid fluoride salt infiltration	CARBON	102		208	Lian, Pengfei; Song, Jinliang; Liu, Zhanjun
198	Effect of oxygen on the corrosion of SiC in LiF-NaF-KF molten salt	CORROSION SCIENCE	103		165	Yang, Xinmei; Liu, Min; Gao, Yantao
199	A first-principles study on the defective properties of MAX phase Cr2AlC: the magnetic ordering and strong correlation effect	RSC ADVANCES	6	87	84262	Han, Han; Wickramaratne, Darshana; Huang, Qing
200	High stability of the He atom confined in a U@C-60 fullerene	RSC ADVANCES	6	35	29288	Lei, Yanyu; Wang, Bo; Gao, Yang
201	Structural and electronic phase transitions of ThS2 from first-principles calculations	PHYSICAL REVIEW B	94	13	134104	Guo, Yongliang; Wang, Changying; Qiu, Wujie
202	Effect of long-term thermal exposure on the hot ductility behavior of GH3535 alloy	MATERIALS SCIENCE AND ENGINEERING A-STRUCTURAL MATERIALS PROPERTIES MICROSTRUCTURE AND PROCESSING	673		299	Han, F. F.; Zhou, B. M.; Huang, H. F.
203	The tensile behavior of GH3535 superalloy at elevated temperature	MATERIALS CHEMISTRY AND PHYSICS	182		22	Han, F. F.; Zhou, B. M.; Huang, H. F.
204	Evolution of dislocation loops in He ion irradiated nickel under different temperature	JOURNAL OF APPLIED PHYSICS	120	12	125303	Chen, H. C.; Lui, R. D.; Ren, C. L.
205	Atomistic simulation of the trapping	MODELLING AND	24	8	85004	Gong, Hengfeng;

	capability of He- vacancy defects at Ni Sigma 3(1(1)over-bar2)[110] grain boundary	SIMULATION IN MATERIALS SCIENCE AND ENGINEERING				Wang, Chengbin; Zhang, Wei
206	Effects of exposing temperature on corrosion performance of weld joint of a Ni-Mo-Cr alloy	JOURNAL OF FLUORINE CHEMISTRY	182		69	Zhu, Yasheng; Hou, Juan; Yu, Guojun
207	Helium permeability of different structure pyrolytic carbon coatings on graphite prepared at low temperature and atmosphere pressure	JOURNAL OF NUCLEAR MATERIALS	468		31	Song, Jinliang; Zhao, Yanling; Zhang, Wenting
208	Adsorption and diffusion of fluorine on Cr-doped Ni(111) surface: Fluorine-induced initial corrosion of non-passivated Ni-based alloy	JOURNAL OF NUCLEAR MATERIALS	478		295	Ren, Cui-Lan; Han, Han; Gong, Wen-Bin
209	Development of a pair potential for Ni-He	JOURNAL OF NUCLEAR MATERIALS	472		105	Zhang, Wei; Wang, Chengbin; Gong, Hengfeng
210	Edge effects on the characteristics of uranium diffusion on graphene and graphene nanoribbons	CHINESE PHYSICS B	25	8	86301	Cheng, Cheng; Han, Han; Ren, Cui-Lan
211	The energy and stability of helium-related cluster in nickel: A study of molecular dynamics simulation	NUCLEAR INSTRUMENTS & METHODS IN PHYSICS RESEARCH SECTION B-BEAM INTERACTIONS WITH MATERIALS AND ATOMS	368		75	Gong, Hengfeng; Wang, Chengbin; Zhang, Wei
212	Atomistic Simulations of the Effect of Helium on the Dissociation of Screw Dislocations in Nickel	CHINESE PHYSICS LETTERS	33	2	26102	Xu, Jian; Wang, Cheng-Bin; Zhang, Wei
213	Photo-enhanced oxidizability of tetrazolium salts and its impact on superoxide assaying	CHEMICAL COMMUNICATIONS	52	77	11595	Zhao, Jianfeng; Zhang, Bowu; Li, Jingye
214	Significant Improvement in Thermal and UV Resistances of UHMWPE Fabric through in Situ Formation of Polysiloxane-TiO2 Hybrid Layers	ACS APPLIED MATERIALS & INTERFACES	8	35	23311	Hu, Jiangtao; Gao, Qianhong; Xu, Lu
215	Antisuperbug Cotton Fabric with Excellent Laundering Durability	ACS APPLIED MATERIALS & INTERFACES	8	31	19866	Yu, Ming; Wang, Ziqiang; Lv, Min
216	Graphene oxide: A potential bodyguard protecting proteins from photosensitive damage	CARBON	109		487	Zhao, Jianfeng; Zhang, Bowu; Yu, Chuhong
217	Engineering nano-porous graphene oxide by hydroxyl radicals	CARBON	105		291	Yu, Chuhong; Zhang, Bowu; Yan, Feng
218	Poly(vinylidene fluoride) Nanocomposites	MACROMOLECULES	49	3	1026	Xing, Chenyang;

	with Simultaneous Organic Nanodomains and Inorganic Nanoparticles					Wang, Yanyuan; Huang, Xingyi
219	Covalent immobilization of metal-organic frameworks onto the surface of nylon-a new approach to the functionalization and coloration of textiles	SCIENTIFIC REPORTS	6		22796	Yu, Ming; Li, Wanxin; Wang, Ziqiang
220	Saturation of ion irradiation effects in MAX phase Cr2AlC	ACTA MATERIALIA	110		1	Huang, Qing; Han, Han; Liu, Renduo
221	Electrospun nanofibers with both surface nanopores and internal interpenetrated nanochannels for oil absorption	RSC ADVANCES	6	40	33781	Guan, Jipeng; Li, Jingye; Li, Yongjin
222	Lotus-effect tape: imparting superhydrophobicity to solid materials with an electrospun Janus composite mat	RSC ADVANCES	6	21	17215	Yue, Bingbing; Zhang, Bowu; You, Jichun
223	Synergistic nanofibrous adsorbent for uranium extraction from seawater	RSC ADVANCES	6	85	81995	Zhang, Bowu; Guo, Xiaojing; Xie, Siyuan
224	Electrospun nanofibrous polyethylenimine mat: a potential adsorbent for the removal of chromate and arsenate from drinking water	RSC ADVANCES	6	36	30739	Ma, Yao; Zhang, Bowu; Ma, Hongjuan
225	Mitigation of He embrittlement and swelling in nickel by dispersed SiC nanoparticles	MATERIALS & DESIGN	90		359	Huang, H. F.; Zhang, W.; De Los Reyes, M.
226	Preparation of Amidoximated Ultrahigh Molecular Weight Polyethylene Fiber by Radiation Grafting and Uranium Adsorption Test	INDUSTRIAL & ENGINEERING CHEMISTRY RESEARCH	55	15	4118	Hu, Jiangtao; Ma, Hongjuan; Xing, Zhe
227	Engineering Reduced Graphene Oxide Aerogel Produced by Effective gamma-ray Radiation-Induced Self-Assembly and Its Application for Continuous Oil-Water Separation	INDUSTRIAL & ENGINEERING CHEMISTRY RESEARCH	55	13	3775	He, Yalei; Li, Jihao; Luo, Kou
228	Gamma-ray irradiation-induced reduction and self-assembly of graphene oxide into three-dimensional graphene aerogel	MATERIALS LETTERS	177		76	He, Yalei; Li, Jihao; Li, Linfan
229	Effects of exposing duration on corrosion performance in weld joint of Ni-Mo-Cr alloy in FLiNaK molten salt	JOURNAL OF FLUORINE CHEMISTRY	191		110	Hou, Juan; Yu, Guojun; Zeng, Chaoliu
230	Radiation induced graft polymerization of multi-walled carbon nanotubes for superhydrophobic composite membrane preparation	SCIENCE CHINA-CHEMISTRY	59	3	303	Zhang, Bowu; Xie, Siyuan; Wei, Rongmao

231	Ion irradiation induced disappearance of dislocations in a nickel-based alloy	NUCLEAR INSTRUMENTS & METHODS IN PHYSICS RESEARCH SECTION B-BEAM INTERACTIONS WITH MATERIALS AND ATOMS	377		94	Chen, H. C.; Li, D. H.; Lui, R. D.
232	The Effect of Grain Size and Dislocation Density on the Tensile Properties of Ni-SiCNP Composites During Annealing	JOURNAL OF MATERIALS ENGINEERING AND PERFORMANCE	25	3	726	Yang, Chao; Huang, Hefei; Thorogood, Gordon James
233	Preparation of flexible graphene@SnO2 composite fiber via in situ chemical reduction and self-assembly method	FULLERENES NANOTUBES AND CARBON NANOSTRUCTURES	24	8	531	Luo, Kou; Li, Jihao; He, Yalei
234	Crystallization Behavior of Nanostructured Poly(vinylidene fluoride)/1-Vinyl-3-butylimidazolium Chloride Ionic Liquid Composites	CHEMICAL JOURNAL OF CHINESE UNIVERSITIES-CHINESE	37	4	775	Xing Chenyang; Wang Yanyuan; Li Yongjin
235	Decay of Free Radicals in Polycarbosilane Induced by gamma-Rays Irradiation	CHEMICAL JOURNAL OF CHINESE UNIVERSITIES-CHINESE	37	3	595	Cheng Yong; Li Xiaohu; Liu Weihua
236	The synergy reduction and self-assembly of graphene oxide via gamma-ray irradiation in an ethanediamine aqueous solution	NUCLEAR SCIENCE AND TECHNIQUES	27	3	61	He, Ya-Lei; Li, Ji-Hao; Li, Lin-Fan
237	Preparation of Amidoxime-Based Nylon-66 Fibers for Removing Uranium from Low-Concentration Aqueous Solutions and Simulated Nuclear Industry Effluents	INDUSTRIAL & ENGINEERING CHEMISTRY RESEARCH	55	40	10523	Zhang, Mingxing; Gao, Qianhong; Yang, Chenguang
238	Design and Test of a Short Mockup Magnet for the Superconducting Undulator at the SSRF	PROCEEDINGS OF THE 12TH INTERNATIONAL CONFERENCE ON SYNCHROTRON RADIATION INSTRUMENTATION (SRI2015)	1741		20027	Xu, Jieping; Ding, Yi; Cui, Jian
239	Contributions of distinct gold species to catalytic reactivity for carbon monoxide oxidation	NATURE COMMUNICATIONS	7		13481	Guo, Li-Wen; Du, Pei-Pei; Fu, Xin-Pu
240	Structural Determination of Catalytically Active Subnanometer Iron Oxide Clusters	ACS CATALYSIS	6	5	3072	Yang, Qi; Fu, Xin-Pu; Jia, Chun-Jiang
241	A hierarchical and gradient structured supersorbent comprising three-dimensional interconnected porous fibers for efficient oil spillage cleanup	JOURNAL OF MATERIALS CHEMISTRY A	4	24	9635	Zhao, Yueyue; Miao, Xiaran; Lin, Jinyou
242	Novel donor-acceptor polymers containing	JOURNAL OF MATERIALS	4	26	10212	Wang, Ning;

	o-fluoro-p-alkoxyphenyl-substituted benzo[1,2-b:4,5-b ']dithiophene units for polymer solar cells with power conversion efficiency exceeding 9%	CHEMISTRY A				Chen, Weichao; Shen, Wenfei
243	A General Method for Constructing Two-Dimensional Layered Mesoporous Mono- and Binary-Transition-Metal Nitride/Graphene as an Ultra-Efficient Support to Enhance Its Catalytic Activity and Durability for Electrocatalytic Application	ACS Applied Materials & Interfaces	8	29	18770	Liu, Baocang; Huo, Lili; Si, Rui
244	Iron Oxide with Different Crystal Phases (alpha- and gamma-Fe2O3) in Electroanalysis and Uftrasensitive and Selective Detection of Lead(II): An Advancing Approach Using XPS and EXAFS	ANALYTICAL CHEMISTRY	88	1	906	Li, Shan-Shan; Li, Wen-Juan; Jiang, Tian-Jia
245	Structural Dependence of Platinum Nanostructures on Catalytic Performance in Aromatic Azo Compound Reaction Investigated by X-ray Absorption Fine Structure Spectroscopy	JOURNAL OF PHYSICAL CHEMISTRY C	120	27	14712	Zhang, Duo; Mcleod, John; Hu, Lei
246	Promoted Multimetal Oxide Catalysts for the Generation of Hydrogen via Ammonia Decomposition	JOURNAL OF PHYSICAL CHEMISTRY C	120	14	7685	Yan, Han; Xu, Yue-Jiao; Gu, Ying-Qiu
247	Formation of various crystalline structures in a polypropylene/polycarbonate in situ microfibrillar blend during the melt second flow	PHYSICAL CHEMISTRY CHEMICAL PHYSICS	18	20	14030	Xia, Xiao-Chao; Yang, Wei; He, Shan
248	Local structure study of tellurium corrosion of nickel alloy by X-ray absorption spectroscopy	CORROSION SCIENCE	108		169	Lu, Lanlu; Jia, Yanyan; Ye, Xiang-Xi
249	pH-dependent phosphatization of ZnO nanoparticles and its influence on subsequent lead sorption	ENVIRONMENTAL POLLUTION	208		723	Xu, Huacheng; Li, Lina; Lv, Hua
250	Effect of strongly bound copper species in copper-ceria catalyst for preferential oxidation of carbon monoxide	APPLIED CATALYSIS A-GENERAL	518		87	Du, Pei-Pei; Wang, Wei-Wei; Jia, Chun-Jiang
251	Broadband antireflective double-layer mesoporous silica coating with strong abrasion-resistance for solar cell glass	RSC ADVANCES	6	30	25191	Wang, Jing; Yang, Chunming; Liu, Yi
252	Adsorption mechanism on metal organic frameworks of Cu-BTC, Fe-BTC and ZIF-8 for CO2 capture investigated by	RSC ADVANCES	6	67	62705	Du, Meng; Li, Lina; Li, Mingxing

	X-ray absorption fine structure					
253	Probing the surface microstructure of layer-by-layer self-assembly chitosan/poly(L-glutamic acid) multilayers: A grazing-incidence small-angle X-ray scattering study	MATERIALS SCIENCE & ENGINEERING C-MATERIALS FOR BIOLOGICAL APPLICATIONS	58		352	Zhao, Nie; Yang, Chunming; Wang, Yuzhu
254	Study on structural evolution of polytetrafluoroethylene irradiated by electron beam under stretching using SAXS/WAXS	EUROPEAN POLYMER JOURNAL	83		35	Li, Xiaoyun; Tian, Feng; Tang, Zhongfeng
255	Gold-Iron Oxide Catalyst for CO Oxidation: Effect of Support Structure	CATALYSTS	6	3	37	Cui, Hui-Zhen; Guo, Yu; Wang, Xu
256	Support effect of zinc tin oxide on gold catalyst for CO oxidation reaction	CHINESE JOURNAL OF CATALYSIS	37	10	1702	Li, Wei; Du, Linying; Jia, Chunjiang
257	CO oxidation over Au/ZrLa-doped CeO2 catalysts: Synergistic effect of zirconium and lanthanum	CHINESE JOURNAL OF CATALYSIS	37	8	1331	Yang, Qi; Du, Linying; Wang, Xu
258	In-situ study of precipitates in Al-Zn-Mg-Cu alloys using anomalous small-angle x-ray scattering	CHINESE PHYSICS B	25	6	66101	Yang, Chun-Ming; Bian, Feng-Gang; Xiong, Bai-Qing
259	The development of TXRF method and its application on the study of trace elements in water at SSRF	NUCLEAR INSTRUMENTS & METHODS IN PHYSICS RESEARCH SECTION B-BEAM INTERACTIONS WITH MATERIALS AND ATOMS	375		49	Wang, L. L.; Yu, H. S.; Li, L. N.
260	Performance Improvement of CH3NH3PbI3 Perovskite Solar Cell by CH3SH Doping	NANOMATERIALS AND NANOTECHNOLOGY	6		24	Li, Hong; Yang, Yingguo; Feng, Xiao
261	Synthesis and detection the thermal expansion of CdSe quantum dots from room temperature to 700 degrees C	JOURNAL OF NANO RESEARCH	35		11	Zhao, Ziyan; Zhou, Ying; Bian, Fenggang
262	Data-collection system for high-throughput X-ray absorption fine structure measurements	NUCLEAR SCIENCE AND TECHNIQUES	27	4	82	Lu, Rui-You; Gao, Qian; Gu, Song-Qi
263	The Key Role of Ball Milling Time in the Microstructure and Mechanical Property of Ni-TiCNPComposites	Journal of Materials Engineering and Performance	25	12	5280	Zhou, Xiaoling; Huang, Hefei; Xie, Ruobing
264	Investigation of carbonaceous airborne particles by scanning proton microprobe	Huanjing Kexue/Environmental Science	37	1	1	Bao, Liang-Man; Liu, Jiang-Feng; Lei, Qian-Tao
265	Evolution law of helium bubbles in	Materials	9	10		Gao, Jie; Bao,

	Hastelloy N alloy on post-irradiation annealing conditions					Liangman; Huang, Hefei
266	Decay of free radicals in polycarbosilane induced by γ-rays irradiation	Gaodeng Xuexiao Huaxue Xuebao/Chemical Journal of Chinese Universities	37	3	595	Cheng, Yong; Li, Xiaohu; Liu, Weihua
267	A facile method for preparing 3D graphene/Ag aerogel via gamma-ray irradiation	Fullerenes Nanotubes and Carbon Nanostructures	24	11	720	Luo, Kou; Li, Jihao; Li, Linfan
268	Atomistic simulations of the interactions of helium with dislocations in nickel	Nuclear Materials and Energy	7		12	Xu, Jian; Wang, Chengbin; Zhang, Wei
269	The Effect of Grain Size and Dislocation Density on the Tensile Properties of Ni-SiCNPComposites During Annealing	Journal of Materials Engineering and Performance	25	3	726	Yang, Chao; Huang, Hefei; Thorogood, Gordon James
270	Microstructural Evolution and Mechanical Properties of 2D－SiCf/SiC and Hastelloy N Joints Using 82.5Au－17.5Ni Brazing Filler	Advanced Engineering Materials	18	11	1967	Liu, Min; Yang, Xinmei; Zhou, Haijun
271	Benchmarking of232Th evaluation by a 14.8 MeV neutron leakage spectra experiment with slab samples	Annals of Nuclear Energy	96		181	Lin, Zuokang; Nie, Yangbo; Cai, Xiangzhou
272	Extending and verification of RELAP5 code for liquid fueled molten salt reactor	Hedongli Gongcheng/Nuclear Power Engineering	37	3	16	Shi, Chengbin; Cheng, Maosong; Liu, Guimin
273	Leak frequency analysis of the primary coolant for the molten salt reactor	International Congress on Advances in Nuclear Power Plants, ICAPP 2016	2		779	Yang, Qun; He, Zhaozhong; Shao, Shiwei
274	Design and implementation of T3 periodic test for reactor protection system of TMSR-SF1	Hedongli Gongcheng/Nuclear Power Engineering	37	5	105	Liu, Zhenbao; Hou, Jie; Liu, Guimin
275	Crystallization and temperature-dependent structure deflection of C6mimBr ionic liquid intercalated in LAPONITE®	RSC Advances	6	100	98018	Jiang, Fangling; Li, Cheng; Guo, Xiaojing
276	First-principle investigation of the structure and vibrational spectra of the local structures in LiF-BeF2Molten Salts	Journal of Molecular Liquids	213		17	Dai, Jianxing; Han, Han; Li, Qingnuan
277	Experimental study on the thickness detection of molten salt frozen-wall	Huagong Jinzhan/Chemical Industry and Engineering Progress	35	8	2373	Zhou, Jinhao; Sun, Bo; She, Changfeng
278	Atomistic study of the copper cluster deposition on Si(001) and Si(111) surface	Materials Science Forum	850		287	Gong, Hengfeng; Li, Gongping; Zhang, Shixu
279	Study on cementation formulation of	Yuanzineng Kexue Jishu/Atomic	50	11	1943	Liu, Xue-Yang;

	simulated radioactive fluoride liquid waste	Energy Science and Technology				Qian, Zheng-Hua; Qiao, Yan-Bo
280	Structures and hydrogen storage properties of La1-xMgxNi4.25Al0.75(x=0.0, 0.1, 0.2, 0.3) alloys	Xiyou Jinshu Cailiao Yu Gongcheng/Rare Metal Materials and Engineering	45	1	56	Lü, Lijun; Cheng, Honghui; Han, Xingbo
281	Development of general atca epics device support module based on HPI	Yuanzineng Kexue Jishu/Atomic Energy Science and Technology	50	4	745	Yin, Cong-Cong; Zhang, Ning; Wang, Quan-Quan
282	Measurements of correlation function in heavy-ion collisions at RHIC	Journal of Physics: Conference Series	668	1		Chen, J.H.;;
283	Improve the P-type conductivity of SnO films by Na ion implantation	Materials Science Forum	848		477	Yang, Tie Ying; Zhao, Jun; Li, Xiao Long
284	Structure design and optimization of high heat load absorbers in SSRF front-end	Guangxue Jingmi Gongcheng/Optics and Precision Engineering	24	7	1640	Li, Yong-Jun; Zhang, Min; Xue, Song
285	The application of silicon nanowire field-effect transistor-based biosensors in molecular diagnosis	Kexue Tongbao/Chinese Science Bulletin	61	4-5	442	Lu, Na; Gao, Anran; Dai, Pengfei
286	Research on high accuracy registration of dual energy CT images in synchrotron radiation	Guangxue Xuebao/Acta Optica Sinica	36	4		Li, Qiao; Zhou, Guangzhao; Xiao, Tiqiao
287	Synchrotron radiation X-ray stereo imaging based on capillary beam splitting	Guangxue Xuebao/Acta Optica Sinica	36	8		Wang, Feixiang; Deng, Biao; Wang, Yudan
288	X-ray lasers: Multicolour emission	Nature Photonics	10	11	695	Feng, Chao; Deng, Haixiao;
289	基于 FPGA 的电子直线加速器低电平系统前馈功能的实现	核技术	39	7	70402	李松; 张俊强; 张猛
290	250 MHz 固态功率放大器的设计	核技术	39	6	60401	丁洪利; 赵明华; 肖诚成
291	SDUV-FEL 装置上利用电光频谱解码法测量束团长度实验设计与仿真	核技术	39	4	40102	华连发; 张文艳; 王兴涛
292	可批量化生产的行波加速管的设计	核技术	39	1	10202	戴责已; 钟少鹏; 赵明华
293	基于遗传算法的自由电子激光优化设计	核技术	39	2	20101	张白鑫; 张彤; 陈建辉
294	一种抑制高压加速管电子负载效应的新方法	核技术	39	7	70204	李麒成; 李德明; 何子锋
295	基于毛细管分光的同步辐射 X 射线立体成像	光学学报	36	8	834004	王飞翔; 邓彪; 王玉丹
296	同步辐射双能 CT 图像的高精度配准研	光学学报	36	4	411003	李巧; 周光照;

	究					肖体乔
297	一种基于实时数字图像处理的同步辐射微探针自动化扫描新方法	核技术	39	1	10101	梁东旭; 兰旭颖; 闫帅
298	1.5 GHz 超导加速腔双输入耦合器研究	核技术	39	6	60103	谢新华; 王岩; 马震宇
299	上海光源二期工程的垂直发射度研究	核技术	39	5	50102	李昌亮; 田顺强; 张文志
300	蒙特卡罗模拟人工自旋冰的退磁过程	核技术	39	6	60502	虞丽菊; 孟祥雨; 李俊琴
301	基于微通道板的电离室及其在同步辐射中的应用	核技术	39	5	50101	李俊琴; 邹鹰; 陈振华
302	液体环境单分子免疫球蛋白 G 的原子力显微镜高分辨成像	分析化学	44	8	1215	赵志杰; 张萍; 杨家香
303	纳米金在肿瘤检测及放射治疗中的应用	辐射研究与辐射工艺学报	34	4	40103	韦贵生; 相法伟; 田甜
304	肌动蛋白在不同衬底上的组装	辐射研究与辐射工艺学报	34	4	40701	张学强; 胡修源; 雷豪志
305	云母-石墨烯界面纳米尺度受限水层的湿润-去湿润研究	核技术	39	7	70501	杨硕; 汪颖; 杨海军
306	基于电化学分析法定量检测 MicroRNA 的生物传感器	辐射研究与辐射工艺学报	34	3	30101	李甫梧; 王丽华; 宋世平
307	DNA 纳米结构的生物安全性研究	中国科学. 化学	46	2	188	潘亮; 孔华庭; 孙艳红
308	硅纳米线场效应晶体管生物传感器在肿瘤分子诊断中的应用	科学通报	61	424 65	442	鲁娜; 高安然; 戴鹏飞
309	铜 L-色氨酸配合物的合成与表征	分析测试学报	35	6	734	刘慧; 李少萍; 党亚茹
310	NiMo 合金在水环境中表面偏析现象的理论模拟研究	中国科学. 物理学, 力学, 天文学	46	5		朱倍恩; 刘小吉; 高嶷
311	生物分子表面水的生物功能研究	中国科学. 物理学, 力学, 天文学	46	5		郭盼; 涂育松; 方海平
312	石墨烯和氧化石墨烯对细胞脂膜破坏作用研究?	中国科学. 物理学, 力学, 天文学	46	6	60501	涂育松; 方海平;
313	纳米限阈下的水分子作为载体的信号转换、传导和放大	中国科学. 物理学, 力学, 天文学	46	5		涂育松; 修鹏; 方海平
314	常温下不完全浸润的有序单层水和分子尺度亲水性	中国科学. 物理学, 力学, 天文学	46	5		王春雷; 方海平;
315	上海光源前端高热负载挡光器的结构设计与优化	光学精密工程	24	7	1640	李勇军; 张敏; 薛松
316	MATLAB 神经网络分析上海光源光束线的运行数据	计算机工程与应用	52	16	233	孙皓; 龚培荣;
317	长程面形仪测量数据的拟合方法	核技术	39	8	80102	童新宇; 彭川黔; 何玉梅
318	基于 MATLAB 的上海光源光束线运行	核技术	39	7	70104	孙皓; 龚培荣;

	状态分析与预警					
319	微带传输线束流信号展宽处理设计	强激光与粒子束	28	9		杨勇; 冷用斌; 阎映炳
320	质子治疗中点扫描照射技术的仿真模拟	核技术	39	9	90202	贾亚军; 李永江; 张潇
321	基于 MicroTCA 的自动频率控制系统	核技术	39	7	70102	唐兴海; 刘亚娟; 张俊强
322	15-MeV 电子直线加速器的低电平系统	核技术	39	3	30403	张俊强; 刘亚娟; 钟少鹏
323	阿司匹林及其衍生物与脂肪酸结合蛋白 4 复合物的晶体学研究	核技术	39	8	80101	黄佩; 李敏军; 左刚
324	穿透型金刚石 X 射线位置灵敏探测器及其在同步辐射光束线上的应用	核技术	39	7	70101	崔莹; 汪启胜; 黄胜
325	衬底温度对蒸汽辅助沉积法制备钙钛矿薄膜微观结构的影响	核技术	39	6	60104	刘华秋; 朱大明; 刘星
326	固溶热处理对 GH3535 合金组织和性能的影响	稀有金属材料与工程	45	6	1583	张文竹; 许周烽; 蒋力
327	富锂锰基材料 xLi_2MnO_3・ (1-x)LiMn_(1/3)Ni_(1/3)Co_(1/3)O_2(x = 0.3,0.5,0.7)的电化学和同步辐射研究	电化学	22	3	288	侯孟炎; 鲍洪亮; 王珂
328	原位 XAFS 表征双金属纳米催化剂 PtCo/C 在工作状态下的结构变化	核技术	39	6	60101	尚明丰; 赵天天; 鲍洪亮
329	几种典型熔盐冷却剂的热物性研究	核技术	39	5	50604	金愿; 程进辉; 王坤
330	SSRF 波荡器 EPU148 动力学积分场效应磁场垫补	核技术	39	7	70103	张淼; 周巧根;
331	PSD 位置测量系统在波荡器磁场测量中的应用	核技术	39	5	50103	王晓勋; 王宏飞; 周巧根
332	一种波荡器段间四极铁远程精密调节机构的研制	核技术	39	4	40101	文雍梅; 王莉; 高飞
333	兰州重离子储存环外靶实验终端时间投影室的动量分辨率模拟	核技术	39	7	70401	李贺; 张松; 卢飞
334	活化过硫酸钠/多壁碳纳米管降解氯苯的研究	环境科学与技术	39	7	118	马继飞; 姚剑; 侯惠奇
335	高温下 GH3535 合金中的氢同位素扩散渗透效应分析	核科学与工程	36	2	185	张东勋; 刘卫; 钱渊
336	CR-39 应用于中子探测的化学蚀刻条件优化研究	核技术	39	6	60402	李洋; 夏晓彬; 曹振
337	2 MW 液态钍基熔盐实验堆气载放射性流出物近场扩散的数值模拟	核技术	39	5	50603	吕晓雯; 陈畅其; 夏晓彬
338	2 MW 液态钍基熔盐实验堆主屏蔽温度场分析	核技术	39	4	40601	何杰; 夏晓彬; 蔡军
339	La_(1-x)Mg_xNi_(4.25)Al_(0.75) (x=0.0,	稀有金属材料与工程	45	1	56	Lu Lijun; Cheng

	0.1, 0.2, 0.3)合金的结构与储氢性能					Honghui; Han Xingbo
340	熔盐冷冻壁应用中关键工艺影响因素研究	核技术	39	8	80602	孙波; 周金豪; 佘长锋
341	熔盐冷冻壁厚度测量方法	化工进展	35	8	2373	周金豪; 孙波; 佘长锋
342	制备方法对氧化石墨烯氧化程度及对Th(IV)、U(VI)吸附的影响	无机材料学报	31	5	454	王晓宁; 孟虎; 马付银
343	离子交换法提取大量钍中微量铀	核化学与放射化学	38	3	159	陈姆妹; 李峥; 何淑华
344	吡啶离子液体与水混合体系中蒽醌-2-磺酸钠的激光闪光光解机理	化学物理学报	29	1	140	Guang Laizhu; Zhang Liangwei; Liu Yancheng
345	Thorex 流程钍铀分离工艺单元计算机模拟研究	原子能科学技术	50	2	227	于婷; 李瑞芬; 李峥
346	FLiNaK 熔盐中 CsF 的蒸发与分离	核技术	39	2	20602	贾昀澎; 王子豪; 耿俊霞
347	熔盐自然循环回路热损失功率实验及计算	核技术	39	8	80601	王雷; 蔡创雄; 赵晶
348	小型模块化熔盐快堆燃料管理初步分析	核技术	39	7	70603	孙国民; 程懋松; 戴志敏
349	RELAP5 应用于液态燃料熔盐堆的扩展及验证	核动力工程	37	3	16	施承斌; 程懋松; 刘桂民
350	基于 HPI 的通用 ATCA EPICS 设备支持模块开发	原子能科学技术	50	4	745	尹聪聪; 张宁; 汪全全
351	基于层次分析法选取影响硝酸盐自然循环回路性能的关键参数	核技术	39	4	40603	邵世威; 王凯; 曲世祥
352	球形燃料元件累积旋转角度和角速度问题研究	核技术	39	3	30603	赵颖; 朱兴望; 曲世祥
353	炭/炭复合材料对活化片辐照的影响	核技术	39	2	20601	周雪梅; 孟令杰; 赖伟
354	规则球床堆熔盐流动压降与对流换热 CFD 模拟	核技术	39	8	80604	潘登; 余笑寒; 邹杨
355	基于中子平衡研究增殖燃料实现 CANDLE 模式的最优配置	核技术	39	6	60601	杨昆; 陈金根; 蔡翔舟
356	HYSYS 软件在反应堆系统仿真中的应用探索	核技术	39	6	60602	郑海伟; 鄂彦志; 唐延泽
357	一种液态燃料熔盐堆堆芯流量分配设计	核技术	39	5	50601	周振华; 潘登; 陈玉爽
358	氢化锆慢化熔盐堆钍铀转换性能初步分析	核技术	39	5	50605	吴攀; 蔡翔舟; 余呈刚
359	氟盐冷却球床堆与 HTR-10 和 MSRE 的定量相似性分析	核技术	39	1	10601	杨群; 于世和; 邹杨
360	内嵌金属的多壁碳纳米管辐射损伤研究	核技术	39	6	60503	马佳文; 巩文斌;

						张伟
361	X 射线 CT 技术在 C/C 复合材料研究中的应用	宇航材料工艺	46	1	42	李新涛; 张东生; 冯志海
362	组件型熔盐堆燃料组件的设计研究	核技术	39	9	90602	薛春; 张海青; 朱智勇
363	低温等离子体接枝改性聚四氟乙烯薄膜表面无钯化学镀铜	辐射研究与辐射工艺学报	34	4	40301	何欣钟; 李荣; 高乾宏
364	酶促反应分子马达的研究进展	分析化学	44	7	1133	秦为为; 孙乐乐; 彭天欢
365	含有季铵盐的超高分子量聚乙烯纤维对Au(III)的吸附效应	辐射研究与辐射工艺学报	34	3	30301	李光珍; 高乾宏; 胡江涛
366	具有纳米结构的聚偏氟乙烯/1-乙烯基-3-丁基咪唑氯盐离子液体复合材料的结晶行为	高等学校化学学报	37	4	775	邢晨阳; 王艳媛; 李勇进
367	gamma 射线辐射诱导聚碳硅烷自由基的衰变	高等学校化学学报	37	3	595	程勇; 李小虎; 刘伟华
368	球形燃料元件温度分布对包覆燃料颗粒失效概率的影响	核技术	39	1	10603	张永栋; 林俊; 朱天宝
369	超声波增湿撞击流泡沫捕捉塔处理含铍废气研究	核技术	39	1	10604	凡思军; 吴磊; 刘忠英
370	碳质大气颗粒物的扫描质子微探针分析	环境科学	37	1	1	包良满; 刘江峰; 雷前涛
371	质子治疗装置脉冲电源研制	核技术	39	4	40401	缪亚运; 谷鸣; 陈志豪
372	Au/ZrLa 掺杂 CeO_2 催化剂在 CO 氧化反应中优异的催化活性: 锆镧协同作用	催化学报	37	8	1331	Yang Qi; Du Linying; Wang Xu
373	生物 X 射线小角散射实验站控制和数据采集系统	核技术	39	9	90101	周平; 洪春霞; 王玉柱
374	一种生物 X 射线小角散射光束线站自动换样溶液蠕动装置	核技术	39	1	10102	洪春霞; 周平; 李怡雯

附录 3

2015-2016 年专利授权一览表

Patents in 2015-2016

2015

No.	专利名称	申请号	申请日	授权日	类型	发明人
1	一种 99mTc 配合物、其制备方法、中间体及其应用	201110040441.0	2011/2/18	2015/9/30	发明	沈玉梅 张元庆 许晓平 孙艳红 杨光 崔巍 朱华
2	适用于太赫兹时域光谱测量的液体样品架及其方法	201110040716.0	2011/2/18	2015/9/30	发明	赵红卫 吴胜伟 朱海云 张增艳 李晴暖 刘晓鸿 朱智勇
3	一种纳米金-单宁酸-氧化石墨烯纳米复合材料的制备方法	201110045170.8	2011/2/24	2015/4/8	发明	张玉杰 张小勇 彭程 张欢 胡文兵 黄庆
4	一种改性高分子筛网及其制备方法和应用	201110451402.X	2011/12/27	2015/8/12	发明	李景烨 邓波 于洋 蒋海青 李林繁 虞鸣
5	一种基于荧光共振能量转移的超分辨成像方法	201210288305.8	2012/8/14	2015/11/25	发明	樊春海 黄庆 程亚 陈建芳 邓素辉 梁乐
6	使用波带片将柱面波线光源聚焦为点光斑的方法	201210391151.5	2012/10/15	2015/5/20	发明	毛成文 闫芬 闫帅 李爱国 余笑寒
7	熔盐样品制备装置、制得的熔盐样品及其制备、析晶方法	201210425507.2	2012/10/30	2015/4/8	发明	耿俊霞 张国欣 李晴暖
8	一种二硼化镁超导波荡器	201210488830.4	2012/11/27	2015/4/15	发明	张正臣 许皆平 李炜 崔剑 李明 江勇
9	一种高温介质泵热屏蔽装置	201210510151.2	2012/12/3	2015/4/8	发明	黎忠 傅远 黄建平 张健宇 林良程 毛文玉 王纳秀 王晓李波 陆世瑞
10	一种氨基改性的接枝共聚物、制备方法及其应用	201310020242.2	2013/1/18	2015/8/12	发明	马红娟 李景烨 王敏 姚思德 虞鸣
11	高压型加速器的自动高压锻炼方法及自动高压锻炼系统	201310050635.8	2013/2/7	2015/9/16	发明	苏海军 王胜利 郭洪雷 吕彬
12	一种功能性纳米纺织品及其制备方法	201310074045.9	2013/3/7	2015/5/20	发明	虞鸣 李景烨 王自强 刘汉洲
13	一种贵金属复合材料和贵金属微纳材料及其制备方法	201310096044.4	2013/3/22	2015/4/8	发明	马红娟 李景烨 王敏 姚思德 虞鸣
14	一种血吸虫病电化学传感快速测定试剂盒及其检测方法和制备方法	201310118394.6	2013/4/7	2015/5/20	发明	樊春海 宋世平 邓王平 冯正 胡薇
15	一种溶液样品蠕动实验装置	201310139099.9	2013/4/19	2015/4/8	发明	边风刚 李怡雯 王劼
16	一种用于液氦温区的温度精确测量装置	201310143343.9	2013/4/23	2015/2/25	发明	张正臣 许皆平 李炜 崔剑 李明 江勇
17	一种熔盐堆缓冲盐自然循环冷却系统	201310300734.7	2013/7/17	2015/8/12	发明	陈堃 蔡创雄 赵兆颐 马志善 王纳秀 何兆忠

18	滚球阻尼缓冲器	201310304306.1	2013/7/18	2015/11/25	发明	曹云 周永峰 毛文玉 樊辉青 顾正军
19	胆汁酸类化合物、中间体及其制备方法和应用	201310365746.8	2013/8/20	2015/8/12	发明	张岚 贾丽娜 程登峰 江大卫 石洪成
20	一种法兰连接组件	201310475912.X	2013/10/12	2015/9/16	发明	李启明 王纳秀 王允 张金红 孔祥波 张钦华 林良程
21	一种镨铁硼永磁铁及其制备方法	201310482719.9	2013/10/15	2015/11/25	发明	何永周 吴红平
22	X 射线转换靶	201310521465.7	2013/10/28	2015/5/11	发明	何子锋 杨永金 黄建鸣 李德明 张宇田 朱希恺
23	X 射线转换靶	201310517781.7	2013/10/28	2015/11/25	发明	何子锋 杨永金 黄建鸣 李德明 张宇田 朱希恺
24	一种溶液样品蠕动实验系统	201410038379.5	2014/1/26	2015/12/23	发明	边风刚 李怡雯 洪春霞 王劼
25	用于氟化物熔盐的 Ni/NiF2 参比电极及制作方法	201410158185.9	2014/4/19	2015/5/11	发明	郑海洋 蒋锋 黄卫 田丽芳 佘长锋 龙德武 李晴暖
26	电磁式熔盐蒸发方法	201410339236.8	2014/7/16	2015/9/30	发明	杨洋 窦强 付海英 耿俊霞 王子豪 李晴暖
27	一种料浆浇注制备炭/炭复合材料型材的方法	201410407206.6	2014/8/18	2015/11/25	发明	张东生 夏汇浩 周兴泰 杨新梅 宋金亮
28	一种同步辐射 X 射线显微 CT 成像样品台	201420568921.3	2014/9/29	2015/4/15	实用新型	彭冠云 肖体乔 谢红兰 邓彪 杜国浩 佟亚军 薛艳玲
29	一种压弯装置	201520095012.7	2015/2/10	2015/7/1	实用新型	计展 薛松 祝万钱 王楠 陈家华 吴佳兴
30	一种遮挡杂散 X 光的装置	201520286566.5	2015/5/6	2015/9/16	实用新型	闫帅 杨科 蒋升 张丽丽 王华 梁东旭 兰旭颖
31	一种非弹性 X 射线散射装置	201520286567.X	2015/5/6	2015/5/6	实用新型	闫帅 杨科 张玲 何燕 王娟 何上明 李爱国
32	多功能同步辐射微聚焦样品控制平台	201520341888.5	2015/5/25	2015/9/16	实用新型	闫帅 杨科 蒋晖 郑怡 董朝晖 毛成文 李爱国
33	一种燃料电池阳极原位测试装置	201520384088.1	2015/6/4	2015/11/18	实用新型	王娟 何燕 秦海英 刘嘉斌 李爱国 闫帅 闫芬
34	一种双驱动压辊式压弯装置	201520385313.3	2015/6/4	2015/11/18	实用新型	计展 薛松 祝万钱 王楠 陈家华 吴佳兴
35	一种半电池原位测试装置	201520384947.7	2015/6/4	2015/11/18	实用新型	何燕 王娟 秦海英 刘嘉斌 李爱国 闫帅 闫芬
36	一种具有沟道切割晶体及夹具的组件	201520464300.5	2015/7/1	2015/11/18	实用新型	闫帅 杨科 何燕 王娟 张玲 兰旭颖 李爱国
37	一种用于四晶单色器的晶体组件	201520464296.2	2015/7/1	2015/11/18	实用新型	闫帅 杨科 蒋晖 郑怡 董朝晖 毛成文 李爱国
38	一种四晶单色器	201520464281.6	2015/7/1	2015/11/18	实用新型	闫帅 杨科 蒋升 张丽丽 王华 梁东旭 李爱国

39	一种四晶单色器保护装置	201520503509.8	2015/7/13	2015/11/18	实用新型	闫帅 杨科 蒋晖 毛成文 郑怡 董朝晖 李爱国
40	一种简易四晶单色器	201520503530.8	2015/7/13	2015/12/23	实用新型	闫帅 杨科 蒋升 张丽丽 王华 梁东旭 李爱国
41	蛋白质晶体样品捕获环底座的感应识别装置	201520900604.1	2015/11/12	2015/5/11	实用新型	杨利峰 黄胜 王志军 汪启胜 崔莹 何建华

2016

序号	专利名称	申请号	申请日	授权日	类型	发明人
1	一种稳定双链 DNA 的方法及双链 DNA 稳定剂	201110040726.4	2011/2/18	2016/7/6	发明	雷豪志 米丽娟 张益 陈佳佳 郭守武 胡钧
2	一种高分子接枝的氧化石墨烯及其制备方法	201110088928.6	2011/4/8	2016/5/4	发明	李景烨 黄庆 张伯武 张玉杰 邓波 李林繁 彭程 虞鸣 胡文兵 吕敏
3	电子射线源产生装置及产生低剂量率电子射线的方法	201210348278.9	2012/9/18	2016/1/20	发明	何子锋 朱希恺 翟光延 黄建鸣 李林繁 李景烨 盛康龙 张宇田 李德明 张海荣
4	电子射线源产生装置及产生低剂量率电子射线的方法	201210425491.5	2012/10/30	2016/11/16	发明	李景烨 李林繁 王敏 张阔 沈蓉芳 蒋海青 张聪
5	电子射线源产生装置及产生低剂量率电子射线的方法	201210556558.9	2012/12/19	2016/9/28	发明	何子锋 朱希恺 翟光延 黄建鸣 李林繁 李景烨 盛康龙 张宇田 李德明 张海荣
6	一种碳纳米材料-免疫刺激序列复合物的制备方法及其应用	201310116820.2	2013/4/7	2016/8/24	发明	诸颖 张瑜 崔之芬 孔华庭 孙艳红 黄庆 樊春海
7	一种氟盐冷却高温堆的非能动余热排出系统	201310190388.1	2013/5/21	2016/2/10	发明	陈堃 黎超文 邵世威 蔡创雄 王纳秀 吴燕华 袁晓凤 孙慎德
8	熔盐冷却球床反应堆系统	201310303825.6	2013/7/18	2016/2/3	发明	曹云 周永峰 邹杨 胡瑞荣 刘桂民
9	一种解决水锁效应的方法	201310318008.8	2013/7/25	2016/1/20	发明	方海平 李景烨 狄勤丰 许友生 盛楠 王自强
10	用于 X 射线转换靶的基体及其加工方法	201310517782.1	2013/10/28	2016/2/24	发明	何子锋 杨永金 黄建鸣 李德明 张宇田 朱希恺

11	X 射线转换靶片、靶层板及靶层板的加工方法	201310517785.5	2013/10/28	2016/2/24	发明	何子锋 杨永金 黄建鸣 吴新时 李德明 张宇田 朱希恺
12	一种针对前列腺癌不同类型血清标志物进行同时检测的微流控电化学生物传感系统	201310638230.6	2013/12/2	2016/5/4	发明	樊春海 杨帆 左小磊 黄庆
13	一种用于快速生化分析的集成式的微流控电化学生物传感系统及其使用方法	201310638228.9	2013/12/2	2016/5/11	发明	樊春海 杨帆 左小磊 黄庆
14	一种用于超导波荡器磁体的铁芯	201310676926.8	2013/12/12	2016/5/11	发明	许皆平 张正臣 崔剑 李明 徐俊杰 郁静芳 樊勇 季现凯 江勇
15	一种控制棒驱动机构的落棒系统及方法	201310686852.6	2013/12/13	2016/2/3	发明	赵汉财 刘桂民 周兴泰 余笑寒 黎忠 陈堃 王晓 张东生 周雪梅 梅龙伟 孟令杰
16	用于辐照加速器 X 射线转换靶的支承装置	201310724217.2	2013/12/24	2016/7/6	发明	杨永金 何子锋 黄建鸣 李德明 张宇田
17	测量堆芯模拟装置内的状态参数的无线探测系统及方法	201310727919.6	2013/12/25	2016/5/4	发明	赵颖 陈堃 何兆忠 邵世威
18	用于球床反应堆燃料球的装载装置及装载方法	201410003035.0	2014/1/3	2016/7/6	发明	孙健 曹云
19	用于球床反应堆燃料球的装载装置及装载方法	201410002666.0	2014/1/3	2016/7/6	发明	曹云 孙健 朱琳
20	用于球床反应堆燃料球的卸料装置及卸料方法	201410003111.8	2014/1/3	2016/7/6	发明	曹云 孙健
21	一种纳米银抗菌纺织品及其制备方法	201410003499.1	2014/1/3	2016/1/20	发明	李景烨 虞鸣 刘汉洲 马红娟 李林繁
22	一种石墨烯纤维的制备方法	201410016557.4	2014/1/14	2016/7/6	发明	李景烨 李吉豪 张伯武 谢思远 李林繁 张阔 贾娜
23	一种测量粒子加速器束流位置的方法	201410080631.9	2014/3/6	2016/1/20	发明	赖龙伟 冷用斌 阎映炳 陈之初
24	用于熔盐反应堆的镍基合金及其制备方法	201410116793.3	2014/3/26	2016/1/20	发明	李晓丽 何上明 周兴泰 怀平 李志军 余笑寒
25	束流中心轨道偏移的检测系统和方法以及校正系统和方法	201410163382.X	2014/4/22	2016/10/12	发明	苏海军 王胜利 郭鑫 郭洪雷 吕彬
26	一种交联聚丙烯腈纤维的制备方法	201410190697.3	2014/5/7	2016/5/11	发明	王谋华 吴国忠 刘伟华 张文礼 张文发

27	一种微气泡生成装置及其应用	201410395362.5	2014/8/12	2016/10/12	发明	李华 刘卫 吴胜伟 钱渊 张宁 黄悟真 韩兴博
28	沉积装置及制备圆柱形和圆筒形各向同性热解炭的方法	201410407180.5	2014/8/18	2016/8/24	发明	张东生 夏汇浩 周兴泰 杨新梅 宋金亮
29	一种检测粒子加速器束流异常的自触发方法	201410407159.5	2014/8/18	2016/7/6	发明	赖龙伟 冷用斌 阎映炳
30	有机配体包裹的金纳米颗粒薄膜及其场致电子发射装置	201410406414.4	2014/8/18	2016/8/24	发明	高兴宇 杨迎国 冯尚蕾 王菲 王鹏
31	用于高温熔盐的密封连接装置及其方法	201410456294.9	2014/9/9	2016/8/24	发明	唐忠锋 陆惠菊 傅远 张钦华 谢雷东 黎忠
32	一种石墨烯气凝胶及其制备方法和应用	201410461586.1	2014/9/11	2016/7/6	发明	李景烨 李吉豪 张伯武 李林繁
33	一种同步辐射 X 射线显微 CT 成像样品台	201410513981.X	2014/9/29	2016/8/24	发明	彭冠云 肖体乔 谢红兰 邓彪 杜国浩 佟亚军 薛艳玲
34	去除恒流注入对同步辐射红外光束线站影响的系统及方法	201410654932.8	2014/11/17	2016/5/11	发明	佟亚军 陈敏 吉特 张增艳 朱化春 彭蔚蔚 杜国浩 肖体乔
35	一种有机氚氧化燃烧管以及有机氚氧化燃烧方法	201510119394.7	2015/3/18	2016/8/24	发明	刘卫 杜林 王玲 马玉华 曾友石 皮力 秦来来 王广华 吕丽君
36	一种液态氟化氢溶液的分离装置及其方法	201510305702.5	2015/6/4	2016/11/2	发明	宋昱龙 刘玉侠 张岚
37	一种闭式循环氚浓度监测系统	201510500762.2	2015/8/14	2016/11/16	发明	刘卫 钱楠 王广华 黄豫 钱渊 郭冰 魏永波 张宁 曾友石 邓珂
38	一种基于伪随机函数的窄带噪声频率信号发生装置	201520878515.1	2015/11/6	2016/5/18	实用新型	童金 谷鸣 袁启兵 刘永芳
39	一种用于质子治疗装置慢引出系统的线性扫频信号发生器	201520899568.1	2015/11/12	2016/5/11	实用新型	刘永芳 谷鸣 袁启兵 童金
40	同步辐射 X 光连续衰减装置	201520966274.6	2015/11/27	2016/6/29	实用新型	李冰 黄胜 汪启胜 崔莹 何建华
41	一种窄带频率信号发生器	201520989314.9	2015/12/2	2016/5/11	实用新型	刘永芳 谷鸣 袁启兵 童金 周孝轩 吴勇华
42	膜蛋白自动化脂立方相结晶系统	201521019186.1	2015/12/9	2016/7/6	实用新型	崔莹 孙波 徐琴 郁峰 汪启胜 何建华
43	一种混合型永磁波荡器的磁结构	201521074136.3	2015/12/21	2016/7/6	实用新型	何永周 周巧根
44	一种纯永磁型永磁波荡器的磁结构	201521074119.X	2015/12/21	2016/7/6	实用新型	何永周 周巧根

45	一种用于软 X 射线谱学显微成像的原位磁场系统	201620017001.1	2016/1/8	2016/7/6	实 用新型	孟祥雨 王勇 甄香君 郭智张丽娟 张祥志 于怀娜 曹杰锋 李俊琴 郜仁忠
46	一种长程面形测量装置	201620139408.1	2016/2/24	2016/8/24	实 用新型	彭川黔 何玉梅 王劼
47	一种长程光学表面面形检测系统	201620139375.0	2016/2/24	2016/8/24	实 用新型	彭川黔 何玉梅 王劼
48	一种长程光学表面面形检测仪	201620138629.7	2016/2/24	2016/8/24	实 用新型	彭川黔 何玉梅 王劼
49	一种长程面形测量仪	201620138630.X	2016/2/24	2016/10/12	实 用新型	彭川黔 何玉梅 王劼
50	一种快速温度跃升微流芯片系统	201620155721.4	2016/3/1	2016/8/24	实 用新型	边风刚 李怡雯 洪春霞 王劼
51	一种线形探测器的安装校准装置	201620334588.9	2016/4/20	2016/10/12	实 用新型	高梅 文闻 顾月良 高兴宇
52	一种气体净化装置	201620497103.8	2016/5/26	2016/12/21	实 用新型	李俊琴 邹鹰 刘腾飞 陈振华 王勇 郜仁忠

附录 4

2015-2016 年国际学术会议报告表

Presentations by SINAP Scientists at International Scientific Meetings in 2015-2016

2015

No.	会议全称	报告名称	报告人	报告类别	报告学科领域	时间	地点
1	2015 年 SPIE 光学与光电子学国际会议	Crossed-planar undulators technique for free-electron laser polarization switching	邓海啸	分会报告	光学	2015-04-12	捷克共和国
2	2015 年 SPIE 光学与光电子学国际会议	Applications of the transverse gradient undulators on high-gain FELs in China	刘波	分会报告	光学	2015-04-12	捷克共和国
3	2015 年 SPIE 光学与光电子学国际会议	Status of operational and planned FEL facilities	王东	分会报告	光学	2015-04-12	捷克共和国
4	IPAC15 会议	Electron Beam Heating for Suppression of Microbunching Instability via a Transverse Gradient Undulator	黄大章	分组报告	束流物理与加速器技术	2015-05-02	美国
5	第三届国际能源转换与储存化学研讨会	Recent Research for Energy Conversion Based on Nuclear Energy in TMSR	王建强	分会报告	催化化学	2015-01-16	德国
6	第三届国际能源转换与储存化学研讨会	Copper-Based Catalysts for the Efficient Hydrogenolysis of Alkyl Formate to Methano	姜政	分组报告	催化化学	2015-01-16	德国
7	第三届国际能源转换与储存化学研讨会	Copper-Based Catalysts for the Efficient Hydrogenolysis of Alkyl Formate to Methano	杜贤龙	分会报告	催化化学	2015-01-16	德国

8	第 249 届美国化学学会会议	Adsorption Behavior of Uranium from Seawater on Amidoxime-based UHMWPE Prepared by Radiation Induced Graft Polymerization	马红娟	分会报告	核技术在工、农业和医学中的应用	2015-03-21	美国
9	第九届计算物理学国际会议	Asymmetrical Free Diffusion with Orientation-dependence of molecules in Finite Timescales	方海平	大会报告	理论计算机科学	2015-01-06	新加坡
10	“重离子碰撞中的手征、涡旋和磁场”国际会议	Final state effects on initial chiral phenomena	马国亮	大会报告	核物理	2015-01-19	美国
11	第 249 届美国化学学会会议	Nanofiber Absorbents for Uranium Extraction from Seawater	李景烨	分会报告	核技术在工、农业和医学中的应用	2015-03-21	美国
12	第 249 届美国化学学会会议	Synthesis and Properties of Amidoxime-based Fibrous Adsorbents for Extraction Uranium from Seawater by Radiation-induced Graft Polymerization	吴国忠	分会报告	核技术在工、农业和医学中的应用	2015-03-21	美国
13	第 249 届美国化学学会会议	Application of Synchrotron Radiation technique in Extraction Uranium from Seawater	张林娟	分会报告	核技术在工、农业和医学中的应用	2015-03-21	美国
14	“美国能源部-中国科学院 X 射线光学与探测器国际会议”	The development of nano-probe imaging at SSRF	李爱国	大会报告	同步辐射技术及其应用	2015-01-13	美国
15	“美国能源部-中国科学院 X 射线光学与探测器国际会议”	Present status and future development of optical metrology at SSRF	王劼	大会报告	同步辐射技术及其应用	2015-01-13	美国

16	“美国能源部-中国科学院 X 射线光学与探测器国际会议”	The development of X-ray optics and detector at SSRF	肖体乔	大会报告	同步辐射技术及其应用	2015-01-13	美国
17	美国能源部-中国科学院 X 射线光学与探测器国际会议	Transient thermal analysis for XBPM at SSRF	徐中民	大会报告	同步辐射技术及其应用	2015-01-13	美国
18	美国能源部-中国科学院 X 射线光学与探测器国际会议	The development of XBPM at SSRF	龚培荣	大会报告	同步辐射技术及其应用	2015-01-13	美国
19	美国能源部-中国科学院 X 射线光学与探测器国际会议	The software for X-ray imaging processing at SSRF	陈荣昌	大会报告	同步辐射技术及其应用	2015-01-13	美国
20	ACS 全国第 249 次会议暨展览会	Physical and Biochemical Insights on DNA Structures in Artificial and Living Systems	黄庆	分会报告	无机材料化学	2015-03-21	美国
21	第四届 ANSTO-SINAP 年度工作会议	Progress of TMSR materials	周兴泰	大会报告	核技术及其应用	2015-02-08	澳大利亚
22	第四届 ANSTO-SINAP 年度工作会议	Reactor physics of TMSR	余笑寒	大会报告	核技术及其应用	2015-02-08	澳大利亚
23	第四届 ANSTO-SINAP 年度工作会议	Current Status of Shanghai Synchrotron Radiation Facility	肖体乔	大会报告	核技术及其应用	2015-02-08	澳大利亚
24	第四届 ANSTO-SINAP 年度工作会议	Overview of Thorium based Molten Salts Reactor (TMSR)	徐洪杰	大会报告	核技术及其应用	2015-02-08	澳大利亚
25	第三届熔盐堆发展的国际会议	Status of TMSR Project in China	徐洪杰	大会报告	核放射化学	2015-01-28	韩国
26	第三届熔盐堆发展的国际会议	Th-U fuel cycle and pyroprocess	李晴暖	大会报告	核放射化学	2015-01-28	韩国

27	第三届熔盐堆发展的国际会议	TMSR Reactor physics and technologies	刘桂民	大会报告	核放射化学	2015-01-28	韩国
28	第 11 届 Keele 铝会议	Aluminum-induced Formation of Ring Structures	宋波	大会报告	高分子理论计算与模拟	2015-02-27	法国
29	第四届 ANSTO-SINAP 年度工作会议	Progress of TMSR reactor physics	邹杨	分会报告	反应堆物理与技术	2015-02-08	澳大利亚
30	第四届 ANSTO-SINAP 年度工作会议	Progress of TMSR reactor thermohydraulics	王纳秀	分会报告	反应堆物理与技术	2015-02-08	澳大利亚
31	第四届 ANSTO-SINAP 年度工作会议	Making the TMSR walk-away safe	陈堃	分会报告	反应堆物理与技术	2015-02-08	澳大利亚
32	2015 年美国物理学会春季年会	Water-A New Player of the Solid Surface	高嶷	分会报告	计算模拟方法与应用	2015-03-02	美国
33	M&C+SNA+MC 2015 国际会议	氟盐冷却高温堆堆芯热工水力程序的 GPU 并行计算方法研究	鄂彦志	分会报告	核裂变、核聚变、核衰变	2015-04-18	美国
34	同位旋、核结构、核反应及对称能国际研讨会(ISTRO）	中能重离子碰撞中的自旋轨道耦合	徐骏	大会报告	核物理	2015-05-01	斯洛伐克共和国
35	聚焦显微国际会议	Improved resolution in STED microscopy using the Fluorescence transfer pairs as fluorescent probes	邓素辉	分组报告	光学在生命科学中的应用	2015-03-29	德国
36	2015 年同步辐射仪器国际会议	A Novel Optical Design for a Micro-focusing Beamline	何建华	分会报告	同步辐射技术及其应用	2015-07-05	美国
37	2015 年同步辐射仪器国际会议	VUV extra-focus principle and its application to high performance grating monochromators	吴衍青	分会报告	同步辐射技术及其应用	2015-07-05	美国

38	第十一届固体和液体中物质扩散国际会议	Asymmetrical self-Diffusion with Orientation-Dependence of Molecules on Finite Timescale	盛楠	分会报告	理论计算机科学	2015-06-21	德国
39	“未来的研究设施-挑战与机遇”国际研讨会	Current status and Future Development of Light Sources in China	赵振堂	大会报告	同步辐射技术及其应用	2015-07-07	意大利
40	“未来的研究设施-挑战与机遇”国际研讨会	Catalysis research with advanced X-ray techniques in SSRF: Present and future challenge	王建强	大会报告	同步辐射技术及其应用	2015-07-07	意大利
41	第 15 届辐射研究国际会议 (ICRR 2015)	Radiation induced graft polymerization to prepare better performance lithium-ion secondary battery separator	李林繁	分组报告	辐射化学	2015-05-24	日本
42	第 15 届辐射研究国际会议 (ICRR 2015)	Amidoxime-based fibers adsorbent for recovery of uranium from seawater	许璐	分组报告	辐射化学	2015-05-24	日本
43	第 15 届辐射研究国际会议 (ICRR 2015)	Modification and functionalization of UHMWPE fiber by radiation-induced graft polymerization	邢哲	分组报告	辐射化学	2015-05-24	日本
44	第 15 届辐射研究国际会议 (ICRR 2015)	Radiation degradation of chitosan and its application as an animal feed additive	吴国忠	大会报告	辐射化学	2015-05-24	日本
45	2015 年度国际核-核碰撞大会	antihypertriton and 3H lifetime puzzle	马余刚	大会报告	核物理	2015-06-19	意大利
46	短期输运模型讨论会	输运模型现状及比较	徐骏	大会报告	核物理	2015-07-03	波兰
47	第 7 届高能重离子碰撞中的硬和电磁探针国际会议	“AMPT model studies on reconstructed jets in Pb+Pb collisions at 2.76 TeV”	马国亮	分会报告	核物理	2015-06-28	加拿大

48	美国机械工程师学会 2015 压力容器与管道会议	The Effects of Thermal Ageing on Microstructural and Mechanical Properties of GH3535 alloy Welded Joint	陈双建	分会报告	焊接结构、工艺与装备	2015-07-18	美国
49	2015ASTM 碳和石墨小组委员会议	Tensile strength measurement for small graphite samples	曾广礼	分会报告	分析力学	2015-06-21	美国
50	ASME2015 压力容器与管道国际会议	Stress Analysis and Optimum Design of the Heat Transport System at Molten Salt Reactor	张小春	分会报告	结构力学与结构优化	2015-07-18	美国
51	中国－以色列国际纳米技术研讨会	Nanodiamond Applications in Biomedicine	樊春海	分会报告	生物无机化学	2015-07-03	以色列
52	2015 国际奇异夸克物质大会	RHIC STAR 国际实验组在 Lambda 超子相互作用研究上的最新进展	陈金辉	大会报告	核物理	2015-07-05	俄罗斯
53	戈登研究会议及国际轨道角动量大会	X-rays carrying OAM at SINAP	陈建辉	分组报告	束流物理与加速器技术	2015-07-25	美国
54	国际辐射研究大会 ICRR2015	Radiation Safety System for a Particle Therapy Facility	夏晓彬	大会报告	辐射剂量学和辐射防护	2015-05-25	日本
55	FRIB-中国核与强子物理研讨会、核化学 Gorden 会议及 RHIC-STAR 合作组大会	介绍 12C-16O 的 Cluster 结构和巨偶极共振的关系	马余刚	大会报告	核物理	2015-05-27	美国
56	第三次国际电化学研讨会	Biosensing strategies based on nanoprobes and nano-interface	宋世平	大会报告	生物电分析化学	2015-05-24	南非
57	第六届国际加速器会议	Consideration on the Future Major Upgrades of the SSRF Storage Ring	赵振堂	分组报告	束流物理与加速器技术	2015-05-02	美国

58	2015 年加速器可靠性研讨会	Reliability and Performance Introduction of SSRF Magnet Power Supply System	李瑞	分组报告	束流物理与加速器技术	2015-04-25	美国
59	2015 年度对称能国际会议	中能重离子碰撞自旋动力学研究	徐骏	分会报告	核物理	2015-06-28	波兰
60	同位旋、核结构、核反应及对称能国际研讨会(ISTROS)	重离子碰撞的的集体流与约化粘滞系数	马余刚	大会报告	核物理	2015-04-30	斯洛伐克共和国
61	由英国皇家化学协会法拉第论坛组织的高温电解会议	利用固体氧化物电解池进行高温共电解制备合成气	陈新冰	分会报告	反应堆物理与技术	2015-07-11	英国
62	第四届 ANSTO-SINAP 年度工作会议	Progress of TMSR reactor thermohydraulics	王纳秀	大会报告	核技术及其应用	2015-05-02	澳大利亚
63	第四届 ANSTO-SINAP 年度工作会议	Progress of TMSR reactor physics	邹杨	大会报告	核技术及其应用	2015-05-02	澳大利亚
64	第四届 ANSTO-SINAP 年度工作会议	Making the TMSR walk-away safe	陈堃	大会报告	核技术及其应用	2015-05-02	澳大利亚
65	第四届 ANSTO-SINAP 年度工作会议	Th-U cycle of TMSR	蔡翔舟	大会报告	核技术及其应用	2015-05-02	澳大利亚
66	第四届 ANSTO-SINAP 年度工作会议	Overview of Thorium based Molten Salts Reactor (TMSR)	徐洪杰	大会报告	核技术及其应用	2015-05-02	澳大利亚
67	第四届 ANSTO-SINAP 年度工作会议	Current Status of Shanghai Synchrotron Radiation Facility	肖体乔	大会报告	核技术及其应用	2015-05-02	澳大利亚
68	第四届 ANSTO-SINAP 年度工作会议	Progress of TMSR materials	周兴泰	大会报告	核技术及其应用	2015-05-02	澳大利亚

69	第四届ANSTO-SINAP 年度工作会议	Reactor physics of TMSR	余笑寒	大会报告	核技术及其应用	2015-05-02	澳大利亚
70	EIPBN2015 国际会议	The introduction of SSRF XIL beamline station(BL08U1B)	吴衍青	分组报告	同步辐射技术及其应用	2015-05-25	美国
71	钍熔盐国际论坛研讨会，并访问福井大学	Progress of TMSR in China	徐洪杰	大会报告	反应堆物理与技术	2015-04-22	日本
72	2015 年度先进核电站国际大会	sustainability of thorium-uranium in pebble bed fluoride salt-cooled high temperature reactor	朱贵凤	分会报告	反应堆物理与技术	2015-05-02	法国
73	关于生物材料在医疗领域的应用重点项目专题讨论会	Designing nanomaterials for biosensors	樊春海	分会报告	生物无机化学	2015-04-19	香港
74	第四次生物传感技术国际研讨会	DNA Nanostructure-Based Universal Multiplex Sensing Platform	宋世平	大会报告	生物电分析化学	2015-05-09	葡萄牙
75	2015 年度国际核-核碰撞大会	Mechanism of two-proton emission from 23Al and 22Mg	方德清	分会报告	核物理	2015-06-19	意大利
76	核化学 Gordon 研究会议	Mechanism of two-proton emission from 23Al and 22Mg	方德清	分组报告	核物理	2015-05-30	美国
77	第 76 届日本应用物理学会秋季会议	Highly-Ordered Self-Assembled Nanostructures based on DNA	樊春海	分会报告	生物无机化学	2015-09-13	日本
78	第 24 届国际磁铁技术会议	Mechanical Design of a Superconducting Undulator Coil at SSRF	丁祎	分组报告	束流物理与加速器技术	2015-10-17	韩国
79	第 24 届国际磁铁技术会议	Research on magnetic properties of Nd(Pr)FeB magnet for cryogenic permanent magnet undulator of SSRF	何永周	分组报告	束流物理与加速器技术	2015-10-17	韩国

80	第 24 届国际磁铁技术会议	A Multi-function Experimental Apparatus at Low Temperature for CPMU and SCU Development at SSRF	王莉	分会报告	束流物理与加速器技术	2015-10-17	韩国
81	第 24 届国际磁铁技术会议	The Magnetic Performance of an Exotic APPLE-Knot Undulator Developed at SSRF	周巧根	分组报告	束流物理与加速器技术	2015-10-17	韩国
82	第 24 届国际磁铁技术会议	Magnetic measurement of cryogenic permanent magnet undulator at SSRF	张伟	分组报告	束流物理与加速器技术	2015-10-17	韩国
83	2015 年界面水研讨会	Unexpected Hydrophobicity due to Surface Morphology	王春雷	分会报告	计算模拟方法与应用	2015-10-04	意大利
84	熔盐堆技术会议和 MSRE 启动 50 周年纪念会	TMSR Project Overview	徐洪杰	大会报告	反应堆物理与技术	2015-10-13	美国
85	第八届同步辐射医学应用会议（MASR-2015）	The dynamic x-ray micro-tomography with monochromatic beam	陈荣昌	分组报告	同步辐射技术及其应用	2015-10-04	法国
86	第八届同步辐射医学应用会议（MASR-2015）	Investigation on the relationship between morphology and active ingredient of Chinese medicinal materials based on X-ray quantitative micro-tomography	薛艳玲	分组报告	同步辐射技术及其应用	2015-10-04	法国
87	第八届同步辐射医学应用会议（MASR-2015）	X-ray biomedical imaging and its applications at SSRF	肖体乔	大会报告	同步辐射技术及其应用	2015-10-04	法国

88	第八届同步辐射医学应用会议（MASR-2015）	X-ray fluorescence computed tomography at SSRF	邓彪	分组报告	同步辐射技术及其应用	2015-10-04	法国
89	2015 年度国际束流测量会议	Accelerators in Asia	赵振堂	大会报告	束流物理与加速器技术	2015-09-12	澳大利亚
90	“熔盐冷却的聚变堆、裂变堆中氚控制及捕获”研讨会	Calculation of tritium distribution in TMSR-SF1 in SINAP	刘文冠	分会报告	反应堆物理与技术	2015-10-25	美国
91	“熔盐冷却的聚变堆、裂变堆中氚控制及捕获”研讨会	Tritium control technology of TMSR in SINAP	刘卫	分会报告	反应堆物理与技术	2015-10-25	美国
92	“熔盐冷却的聚变堆、裂变堆中氚控制及捕获”研讨会	Diffusion characterization of hydrogen isotopes in Hastelloy N alloy and molten salt reactor	张东勋	分会报告	反应堆物理与技术	2015-10-25	美国
93	2015 年亚洲反应堆物理会议	Burnup Calculation of Pebble Bed Fluoride Salt-cooled High Temperature Reactor by Monte Carlo Neutron Transport Calculation Methods	戴叶	分会报告	反应堆物理与技术	2015-09-16	韩国
94	2015 年亚洲反应堆物理会议	Helium Production Analysis of Nickel-based Alloy in Molten Salt Reactor	周波	分会报告	反应堆物理与技术	2015-09-16	韩国
95	2015 年度国际自由电子激光会议	Coherent hard X-ray production by cascading stages of Phase-merging Enhanced Harmonic Generation	邓海啸	分组报告	自由电子激光原理和技术	2015-08-23	韩国
96	2015 年度国际自由电子激光会议	Status of Shanghai X-ray Free Electron Laser	刘波	大会报告	自由电子激光原理和技术	2015-08-23	韩国

97	2015 年度国际自由电子激光会议	Generating Intense Fully Coherent Soft X-Ray Radiation Based on a Laser-Plasma Accelerator	冯超	大会报告	自由电子激光原理和技术	2015-08-23	韩国
98	2015 年国际自由电子激光会议	Progress of the Synchronization System Development for the Shanghai Soft X-ray Free-Electron Laser Test Facility	张文艳	分组报告	自由电子激光原理和技术	2015-08-23	韩国
99	2015 年国际自由电子激光会议	Development of a 2.856GHz RF-laser synchronization device at the SDUV-FEL	刘晓庆	分组报告	自由电子激光原理和技术	2015-08-23	韩国
100	2015 年国际自由电子激光会议	Progress of the Synchronization System Development for the Shanghai Soft X-ray Free-Electron Laser Test Facility	王东	分组报告	自由电子激光原理和技术	2015-08-23	韩国
101	X 射线及中子光栅相衬成像会议	X-ray tube based compact micro-CT system at SSRF	肖体乔	分组报告	光学成像、图像分析与处理	2015-09-07	美国
102	X 射线及中子光栅相衬成像会议	X-ray tube based compact micro-CT system at SSRF	陈荣昌	分组报告	光学成像、图像分析与处理	2015-09-07	美国
103	第 24 届国际标准化组织表面化学分析技术委员会全体会议	同步辐射全反射 X 射线荧光测定水中杂质方法研究	黄宇营	大会报告	同步辐射技术及其应用	2015-10-13	美国
104	IBIC 国际会议	Bunch-by-Bunch Study of the Transient State of Injection at the SSRF	陈之初	分组报告	束流传输和测量技术	2015-09-12	澳大利亚
105	IBIC 国际会议	INTERFEROMETER DATA ANALYZING USING PCA METHOD AT SSRF	冷用斌	分组报告	束流传输和测量技术	2015-09-12	澳大利亚

106	第 23 界国际 X 射线光学与微分析会议	PDF method development at SSRF	林鹤	分组报告	同步辐射技术及其应用	2015-09-13	美国
107	ICALEPCS 2015 国际会议	Parameter Tracking and Fault Diagnosis based on NoSQL Database at SSRF	阎映炳	分组报告	束流物理与加速器技术	2015-10-17	澳大利亚
108	第十五届加速器和大型实验物理控制系统国际会议	Femtosecond Timing System development in SSRF	戴晓磊	分会报告	束流物理与加速器技术	2015-10-16	澳大利亚
109	韩国科学院科学与技术研究院&基础科学学院光电纳米结构研讨会	Nanodiamond pplications in Biomedicine。	樊春海	大会报告	生物无机化学	2015-08-12	韩国
110	第 16 届核反应堆热工水力国际会议	A Specialized Thermal-hydraulic Code with Porous Media Model and SIMPLEC Algorithm for PB-FHRs	鄂彦志	分会报告	核技术及其应用	2015-08-29	美国
111	第 12 届超核与奇异粒子物理大会	Lifetime Measurementof Hypertriton at STAR	徐亦飞	分会报告	核物理	2015-09-06	日本
112	NURETH-16 国际会议	Analysis on UCRW-ATWS in TMSR-SF1	徐博	分会报告	反应堆物理与技术	2015-08-29	美国
113	NURETH-16 国际会议	NUMERICAL PREDICTION OF TURBULENT CONVECTIVE HEAT TRANSFER WITH MOLTEN SALT IN CIRCILAR PIPE	陈玉爽	分会报告	反应堆物理与技术	2015-08-29	美国
114	NURETH-16 国际会议	Loss of Coolant Flow Accident Analysis for Fluoride Salt Cooled High Temperature Reactor	傅瑶	分组报告	反应堆物理与技术	2015-08-29	美国
115	Global2015 国际会议	Recovery Uranium and Thorium from Molten Salts by	龙德武	分会报告	核化学与核燃料化学	2015-09-20	法国

		Electrochemical Techniques					
116	第 25 届夸克物质国际会议	__HEAVY FLAVOR TRIGGERED AZIMUTHAL CORRELATIONS IN P+P AND AU+AU COLLISIONS FROM STAR_	李薇	分会报告	核物理	2015-09-26	日本
117	第 25 届夸克物质国际会议	Flow in small systems from parton scatterings	马国亮	分会报告	核物理	2015-09-26	日本
118	第 25 届夸克物质国际会议	Azimuthal anisotropies of reconstructed jets in Pb + Pb collisions at √sNN = 2.76 TeV in a multiphase transport model	聂茂武	分组报告	核物理	2015-09-26	日本
119	第 25 届夸克物质国际会议	Energy dependence of HBT correlation from the blast-wave model	张松	分会报告	核物理	2015-09-26	日本
120	“未来的研究设施-挑战与机遇”国际研讨会	Catalysis research with advanced X-ray techniques in SSRF: Present and future challenge	王建强	大会报告	同步辐射技术及其应用	2015-07-07	意大利
121	“未来的研究设施-挑战与机遇”国际研讨会	Current status and Future Development of Light Sources in China	赵振堂	大会报告	同步辐射技术及其应用	2015-07-07	意大利
122	第十三届 Tihany 辐射化学国际会议	RADIATION INDUCED GRAFT POLYMERIZATION OF GLYCIDYL METHACRYLATE ONTO UHMWPE FABRIC AND ITS MODIFICATION TOWARD ORGANIC-INORG	王谋华	分组报告	辐射化学	2015-08-28	匈牙利

		ANIC HYBRID MATERIALS					
123	第十三届 Tihany 辐射化学国际会议	PREPARATION OF ADSROBENTS CONTAINING DIFFERENT SURFACE ZETA POTENTIAL VIA RADIATION GRAFTING METHOD FOR URANIUM EXTRACTION FROM SEA WATER	虞鸣	分组报告	辐射化学	2015-08-28	匈牙利
124	第四届 CAS-DOE 能源科学合作协调委员会会议	中科院上海应物所与美国能源部的合作情况介绍	戴志敏	大会报告	核技术及其应用	2015-07-29	美国
125	第十届国际表面、涂层与纳米材料会议	WATER-INDUCED BIMETALLIC ALLOY SURFACE SEGREGATION	朱倍恩	分会报告	高分子理论计算与模拟	2015-09-12	英国
126	“可持续发展材料科学与技术国际会议”	X-ray Spectra Study of Surface Recombination in Quantum Dots Sensitized Solar Cells and Their Reduction	陈振华	分会报告	半导体光伏材料与太阳电池	2015-07-14	法国
127	第 5 届人体数值模型辐射国际研讨会（CP2015）	Development of a Male Adult Human Head Phantom Based on Polygon Mesh Surfaces	夏晓彬	大会报告	辐射剂量学和辐射防护	2015-07-19	韩国
128	第十六届国际 X 射线吸收精细结构谱学会	Interface structures of perodic multilayers studied	魏向军	分组报告	同步辐射技术及其应用	2015-08-22	德国

	议及其卫星会议	by standing wave XAFS					
129	第十六届国际X射线吸收精细结构谱学会议及其卫星会议	Quick-scanning system update at SSRF XAFS experimental station	顾颂琦	分会报告	同步辐射技术及其应用	2015-08-22	德国
130	第十六届国际X射线吸收精细结构谱学会议及其卫星会议	Potential Applications on Environmental Science by Medium Energy XAFS Technique Proposed in SSRF Phase-II Beamlines Project	李丽娜	分组报告	同步辐射技术及其应用	2015-08-22	德国
131	第十六届国际X射线吸收精细结构谱学会议及其卫星会议	XAFS technique application and development on catalysts at SSRF	黄宇营	大会报告	同步辐射技术及其应用	2015-08-22	德国
132	第十六届国际核石墨专家会议	TMSR 核石墨进展	夏汇浩	大会报告	核技术及其应用	2015-09-12	英国
133	第 12 届同步辐射仪器国际会议	Research and Development of a Model Superconducting Undulator in SSRF	许皆平	分组报告	光源、光学器件和光学系统中的物理问题	2015-07-05	美国
134	第十六届 X 射线吸收精细结构谱学国际会议	High OER activity in nanosized Li2Co2O4 originated from {001} facet containing intermediate-spin state Co3+ ions	周靖	分组报告	同步辐射技术及其应用	2015-08-21	德国
135	第十六届 X 射线吸收精细结构谱学国际会议	A high-resolution Johann-type hard x-ray spectrometer at SSRF	李炯	分组报告	同步辐射技术及其应用	2015-08-21	德国
136	第十六届 X 射线吸收精细结构谱学国际会议	Beamline Station for Energy Materials Study (E-line)	姜政	分组报告	同步辐射技术及其应用	2015-08-21	德国

137	第十六届 X 射线吸收精细结构谱学国际会议	Exact analytic of spatial locak structure of uranyl ion in solution based MS/XAS technology	张林娟	分组报告	同步辐射技术及其应用	2015-08-21	德国
138	ASTM 人造碳和石墨生产的 DO2.F 小组会议	Numerical analyses of tensile test for irradiated small graphite sample	曾广礼	大会报告	应用数学方法	2015-12-06	美国
139	2015 泛太国际化学会议	Synchrotron Radiation infrared 3D microspcetroscopy using iterated algorithm	陈敏	分会报告	束线光学技术和实验方法	2015-12-14	美国
140	日本表面科学学会与真空学会 2015 联合会议	Progress and Future of the Shanghai Synchrotron Radiation Facility	殷立新	分会报告	束流物理与加速器技术	2015-11-30	日本
141	第 9 届中日核物理研讨会	Two-proton emission from proton-rich nuclei-22Mg and 23Al	方德清	大会报告	核物理	2015-11-07	日本
142	ASME 管道及分析方法小组委员会议	Analytical Solutions and Structural Evaluation Method for TMSR Piping Components at Elevated Temperature	张小春	分会报告	结构力学与结构优化	2015-11-01	美国
143	多粒子动力学国际研讨会	The Study of Two Anti-proton Interaction via Correlation Measurement at STAR	张正桥	分会报告	核物理	2015-10-03	德国
144	环太平洋地区化学会议	Synchrotron-based X-ray microscopic studies for bioeffects of nanomaterials	诸颖	分会报告	生物无机化学	2015-12-14	美国
145	第三届中日核燃料循环学术研讨会	Dissolution properties of fluoride in hydrogen fluoride and its	李峥	分会报告	核化学与核燃料化学	2015-12-01	日本

		application in TMSR fuel reprocessing.					
146	第三届中日核燃料循环学术研讨会	An improvement study on the closed chamber distillation system for recovery of carrier fluoride molten salts.	付海英	分会报告	核化学与核燃料化学	2015-12-01	日本
147	第三届中日核燃料循环学术研讨会	Study on Fluoride Volatility in Fluoride Salts at TMSR.	窦强	分会报告	核化学与核燃料化学	2015-12-01	日本
148	2015 年太平洋区域国际化学会议	Probing the dipole-bound excited state of cold anions by temperature controlled electrospray ionization combined with photoelectron imaging	刘洪涛	分会报告	物理无机化学	2015-12-15	美国
149	第九届亚太同步辐射研究论坛（AOFSRR）暨澳大利亚光源 2015 年用户年会	In Operando Structure-property Studies of Advanced Nano Materials for Lithium Batteries	文闻	分会报告	同步辐射技术及其应用	2015-11-23	澳大利亚
150	第九届亚太同步辐射研究论坛（AOFSRR）暨澳大利亚光源 2015 年用户年会	Small angle X-ray scattering beamline development at SSRF	曾建荣	分组报告	同步辐射技术及其应用	2015-11-23	澳大利亚
151	第 24 届国际磁体技术会议 MT24	Analyses on the cooling performance of the CPMU magnetic structure at the SSRF	王健	分会报告	束流物理与加速器技术	2015-10-17	韩国
152	2015 国际加速器会议网站联席会议	ICAP2015 Conference Report	韩欣	分组报告	核技术及其应用	2015-11-16	意大利

153	2015 太平洋化学:受限液体动力学的最新进展研讨会	Ordered nonwetting water，water-surface composition structure，evaporation and heat transfer on the surfaces studied using molecular dynamics simulations	方海平	大会报告	高分子理论计算与模拟	2015-12-14	美国
154	ASME 石墨和组件设计小组会议	UMAT for TMSR graphite component	曾广礼	大会报告	分析力学	2015-10-30	美国
155	夸克物质 2015 国际会议	Proton-proton correlation function in heavy ion collision	方德清	分会报告	核物理	2015-09-26	日本
156	2015 环太平洋国际化学会议	Electrospun nanofiber absorbents for uranium extraction from seawater	李景烨	分组报告	合成化学	2015-12-15	美国
157	2015 环太平洋国际化学会议	Fabrication of few-layer graphene sheets using a serious linear diamino alkanes	李吉豪	分组报告	合成化学	2015-12-15	美国
158	第 36 届中美高能物理合作委员会议	2014-2015 年度上海应用物理所与美方的合作情况介绍	赵振堂	大会报告	中高能核物理	2015-11-02	美国
159	重离子物理前沿研讨会	轻核结团结构和巨偶极共振	马余刚	大会报告	中高能核物理	2015/8/14	中国
160	重离子物理前沿研讨会	上海激光伽马源进展	王宏伟	大会报告	中高能核物理	2015/8/14	中国
161	重离子物理前沿研讨会	Hypernuclear physics from the STAR	陈金辉	大会报告	中高能核物理	2015/8/14	中国
162	重离子物理前沿研讨会	Flow mechanism in small collisions at LHC	马国亮	大会报告	中高能核物理	2015/8/14	中国
163	重离子物理前沿研讨会	从反应总截面到双质子关联(info)	方德清	大会报告	中高能核物理	2015/8/14	中国
164	重离子物理前沿研讨会	中能重离子碰撞中的自旋动力学	徐骏	大会报告	中高能核物理	2015/8/14	中国
165	重离子物理前沿研讨会	17Ne 的破裂反应研究	卢飞	大会报告	中高能核物理	2015/8/14	中国

166	2015 年 RHIC-STAR 实验国际合作组年会	Heavy Flavor Triggered Azimuthal Correlations in p+p at 500	马龙	墙报	核物理	2015/9/25	中国
167	第十二届国际计算加速器物理大会	Python-Based High-Level Applications Development for Shanghai	张彤	大会报告	加速器物理	2015/10/12	中国
168	第十二届国际计算加速器物理大会	Soft X-Ray Free-Electron Laser Parallel Optimization of Accelerator Toolbox by OpenMP and MPI	王坤	大会报告	加速器物理	2015/10/12	中国
169	多尺度多维度同步辐射成像会议	Exploring the Nano-world by means of Synchrotron radiation x-rays	邰仁忠	大会邀请报告	同步辐射技术及其应用	2015/11/3	中国
170	多尺度多维度同步辐射成像会议	SSRF X-ray imaging beamline and its X-ray fluorescence tomography	邓彪	大会报告	同步辐射技术及其应用	2015/11/3	中国
171	多尺度多维度同步辐射成像会议	Microscopic identification of Chinese medicinal materials based on X-ray imaging:from structure to function	薛艳玲	大会报告	同步辐射技术及其应用	2015/11/3	中国
172	第七届高频低电平国际学术研讨会	LLRF Activities at SSRF	赵玉斌	大会报告	加速器物理	2015/11/1	中国
173	第七届高频低电平国际学术研讨会	Overview of Accelerator Projects in China	冷用斌	大会报告	加速器物理	2015/11/1	中国
174	2015 年核结团及核核关联相关前沿问题国际研讨会	Determining for the first time forces between anti-protons using their correlation functions taken at RHIC/STAR	马余刚	大会报告	中高能核物理	2015/12/14	中国

175	2016 年核结团及核核关联相关前沿问题国际研讨会	Proton-proton correlations in nuclear reactions	方德清	大会报告	中高能核物理	2015/12/14	中国
176	2017 年核结团及核核关联相关前沿问题国际研讨会	Spin-isospin dynamics in nuclear reactions	徐骏	大会报告	中高能核物理	2015/12/14	中国

2016

No.	会议全称	报告名称	报告人	报告类别	报告学科领域	时间	地点
1	美国矿物、金属和材料协会 2016 年国际大会	Mitigation of He Embrittlement and Swelling in Nickel by Dispersed SiC Nanoparticles	黄鹤飞	分会报告	新型金属结构材料	2016-02-13	美国
2	第 2 届“重离子碰撞中的手征、涡旋和磁场”国际会议	Isobar collision simulations using AMPT model	马国亮	大会报告	核物理	2016-02-22	美国
3	第 2 届“重离子碰撞中的手征、涡旋和磁场”国际会议	The status of exotic particle study in RHIC-STAR experiment	陈金辉	大会报告	核物理	2016-02-22	美国
4	CLIC 研讨会	Progress in C and X-band technology	方文程	大会报告	束流物理与加速器技术	2016-01-17	瑞士
5	2016 年度低能反质子物理国际会议	“Anti-matter production in relativistic heavy ion collisions"	马余刚	大会报告	核物理	2016-03-05	日本
6	ACS 全国第 251 次会议暨展览会	DNA nanotechnology-based electrochemical platform for biosensing of nucleic acids and protein and bioimaging	樊春海	大会报告	生物无机化学	2016-03-12	美国
7	第二届文物艺术品研究及新技术创新国际会议	The stratified structure of ancient paintings in Forbidden City studied by Synchrotron radiation micro X-ray methods	魏向军	大会报告	同步辐射技术及其应用	2016-03-20	比利时
8	材料学会 2016 年度春季会议	Defect Stability in Thorium Monocarbides: An Ab Initio Study	程诚	分会报告	核技术及其应用	2016-03-27	美国

9	2016 年高能核反应中奇异粒子研究会议	Study Hyperon-Hyperon via proton and Omega correlation in Heavy Ion Collisions at RHIC	NEHA SHAH	大会报告	核物理	2016-03-22	日本
10	2016 年高能核反应中奇异粒子研究会议并作大会报告	Recent progress on Exotic particle search at RHIC	陈金辉	大会报告	核物理	2016-03-22	日本
11	美国光纤通讯展览会及研讨会	Storage ring based FEL for EUV lithography	冯超	分会报告	光学	2016-03-19	美国
12	第十五届国际 IUPAC 会议-高温材料化学	Stability of Protective Oxide Films in Molten Salt Reactor (MSR) Environment-Solubility Measurement of Oxides in Molten Fluorides	申淼	分会报告	太阳能利用中的工程热物理问题	2016-03-28	法国
13	第十一届氟科学与工程国际大会	The Sorption of Hydrogen Isotope on Graphite in Molten Salt Reactor	钱渊	墙报	核技术及其应用	2016-04-16	美国
14	第七届国际粒子加速器会议	Beam Instability Research of High Gradient X-band Accelerating Structure at SINAP	黄晓霞	墙报	束流物理与加速器技术	2016-05-07	韩国
15	第七届国际粒子加速器会议	Proposal of polarization control for soft x-ray free electron laser using RF undulator afterburner 和 Longitudinal wakefields calculation in the undulator section of SXFEL user facility	宋明豪	墙报	束流物理与加速器技术	2016-05-07	韩国
16	第七届国际粒子加速器会议	Bunch Length Measurement at Bunch by Bunch in Harmonics Method at Shanghai SSRF Storage Ring	段立武	墙报	束流物理与加速器技术	2016-05-07	韩国
17	第七届国际粒子加速器会议	Implementation of SINAP Timing System	赵斌清	墙报	束流物理与加速器技术	2016-05-07	韩国

		in Shanghai Proton Therapy					
18	访问伯克利实验室，IRP-FHR 工作组会议及 2016 年核电站进展国际会议（2016ICAPP）	Study on performance of vortex diode in a Fluoride salt cooled High-Temperature Reactor	徐洪杰	大会报告	核技术及其应用	2016-04-12	美国
19	访问伯克利实验室，IRP-FHR 工作组会议及 2016 年核电站进展国际会议（2016ICAPP）	Design and Construction of a High-Temperature Molten Salt Natural Circulation Test Loop	陈堃	大会报告	核技术及其应用	2016-04-12	美国
20	生物传感 2016 年学术年会	Plasmonic Nanoparticles in Biosensing, Bioimaging and Single-Particle Catalysis	李迪	墙报	生物化学	2016-05-24	瑞典
21	访问加州大学伯克利分校热工水力实验室，FHR Benchmark Workshop 与 ICAPP 2016 会议	The Control Technology of Tritium in TMSR	王广华	分会报告	反应堆物理与技术	2016-04-12	美国
22	第 14 届国际流体性质和相平衡会议	DFT investigations of uranium complexation with amidoxime,carboxyl-and mixed amidoxime/carboxyl-based host architechtures for sequestering uranium from seawater	郭晓静	墙报	化工流体力学和传递性质	2016-05-20	葡萄牙
23	2016 生物传感 Gordon 研究会议	3-Dimensional DNA Probes Decorated Biosensing Interface	左小磊	大会报告	生物化学	2016-06-26	美国
24	第七届国际粒子加速器会议	A New Fast RF Trip Diagnostic System in SSRF	赵申杰	墙报	束流物理与加速器技术	2016-05-07	韩国
25	第七届国际粒子加速器会议	《 The soft-x-ray self-seeding system	张开庆	墙报	束流物理与加速器技术	2016-05-07	韩国

		scheme design for SXFEL user facillity》《 The soft-x-ray self-seeding system scheme design for SXFEL user facillity》					
26	第七届国际粒子加速器会议	Optimization of the Field Integrals of Two Small Gap IDs for CLS	钱茂飞	墙报	束流物理与加速器技术	2016-05-07	韩国
27	第 14 届国际辐射防护大会	Individual Monitoring for External Exposure of Users at Synchrotron Radiation Facilitates and New Solutions	夏晓彬	墙报	辐射剂量学和辐射防护	2016-05-07	南非
28	第六届国际胶体会议	Self-assembly of Polystyrene Colloidal Crystals by Floatage Deposition Method with Mixed Solvent	付亚楠	墙报	胶体与界面化学	2016-06-18	德国
29	2016 年 Gordon 研讨会—超越石墨烯的二维电子学会议	A spontaneous assymmetry in a symmetric molecule	宋波	墙报	量子计算中的凝聚态物理问题	2016-06-04	美国
30	第 55 届粒子治疗合作组织国际会议并进行质子治疗系统方面的交流	GPU Accelerated Optimization of Multiple Slice Scanning Paths in Particle Cancer Therapy	蒲越虎	分会报告	核技术及其应用	2016-05-25	捷克共和国,意大利
31	第 55 届粒子治疗合作组织国际会议	GPU Accelerated Optimization of Multiple Slice Scanning Paths in Particle Cancer Therapy	吴超	墙报	核技术及其应用	2016-05-21	捷克共和国
32	第 55 届粒子治疗合作组织国际会议	GPU Accelerated Optimization of Multiple Slice Scanning Paths in Particle Cancer Therapy	贾亚军	墙报	核技术及其应用	2016-05-21	捷克共和国
33	第七届国际粒子加速器会议	A New Digital Direct Feedback Loop for SSRF	夏洋洋	墙报	束流物理与加速器技术	2016-05-07	韩国
34	第七届国际粒子加速器会议	Shanghai Soft X-ray FEL	王东	大会报告	自由电子激光原理和技术	2016-05-08	韩国
35	中美海水提铀	Uranium Extraction	吴国忠	大会报告	有机高分子功能	2016-07-18	美国

	信息交流会议及海水提铀国际会议	from Seawater Research Activities in Chinese Academy of Sciences			材料		
36	第二十六届国际统计物理学术交流会议	Spontaneous Directional Motion of Shaped Nanoparticle before the Onset of Diffusive Brownian Motion	盛楠	分会报告	量子计算中的凝聚态物理问题	2016-07-17	法国
37	ASME 2016 压力容器与管道会议	Research and Development of structure alloy for molten salts reactor in China	李志军	分会报告	极端条件下使用的金属材料	2016-07-16	加拿大
38	ASME 2016 压力容器与管道会议	Evaluation of repair welding influence on GH3535 superalloy microstructure and mechanical properties	黎超文	分会报告	极端条件下使用的金属材料	2016-07-16	加拿大
39	EPICS 2016 年合作交流会议	CSS 的本地化及其多样化应用	韩利峰	大会报告	监测和诊断及控制	2016-05-22	瑞典
40	2016 丹佛 X 射线国际会议并访问 BNL-NSLSII 新光源	1，Three Crystals Spectrometer for Highenergy Resolution Fluorescence Detected X-Ray Absorption Spectroscopy and X-Ray Emission Spectroscopy at SSRF 2，Recent experience in developing industrial research program and the crystal spectrometer for high energy resolution fluorescence detected X-ray absorption spectroscopy and X-ray emission spectroscopy at Shanghai Synchrotron Radiation Facility	黄宇营	分会报告	同步辐射技术及其应用	2016-07-26	美国
41	2016 丹佛 X 射线国际会议并访问	The Development of TXRF Method and its Application on the	魏向军	墙报	同步辐射技术及其应用	2016-07-26	美国

	BNL-NSLSII 新光源	Study of Trace Elements in Water at SSRF					
42	第 14 届国际表面 X 射线和中子散射大会	kinoform lens optimized for various X-ray energy range and its application at SSRF	林鹤	分会报告	同步辐射技术及其应用	2016-07-09	美国
43	奇异夸克物质 2016 国际会议组织委员会	HEAVY FLAVOR TRIGGERED AZIMUTHAL CORRELATIONS IN P+P AND AU+AU COLLISIONS FROM STAR	李薇	分会报告	核物理	2016-06-26	美国
44	2016 年度 X 射线显微国际会议	RECENT PROGRESS ON SSRF PHASE-II BEAMLINES	邰仁忠	大会报告	光学成像、图像分析与处理	2016-08-14	英国
45	2016 年度 X 射线显微国际会议	Potential Applications on Environmental Science by Medium Energy Micro-probe Technique Proposed in SSRF Phase-II Beamlines Project	李丽娜	墙报	光学成像、图像分析与处理	2016-08-14	英国
46	2016 年度 X 射线显微国际会议	LOW-DOSE, HIGH-RESOLUTION AND HIGH-EFFICIENCY PTYCHOGRAPHY AT STXM STATION OF SSRF	许子健	分会报告	光学成像、图像分析与处理	2016-08-14	英国
47	2016 年度 X 射线显微国际会议	Medium energy beamline in SSRF	王连升	墙报	光学成像、图像分析与处理	2016-08-14	英国
48	2016 年度 X 射线显微国际会议	AGGREGATION OF GAS AT MICROSCOPIC SCALE INVESTIGATED BY SYNCHROTRON RADIATION TECHNIQUE	张立娟	分会报告	光学成像、图像分析与处理	2016-08-14	英国
49	BLTP/JINR-SKLTP/CAS 核物	有关反物质相互作用报告	马余刚	大会报告	核物理	2016-06-27	俄罗斯

	理联合会议						
50	第 19 届国际超晶材料、纳米材料与纳米器件会议	Shape Evolution of Metal Nanoparticles in Water Vapor Environments	朱倍恩	分会报告	基础物理学	2016-07-24	香港
51	第 252 届美国化学会学术年会	Preparation of breathable cotton fabric with superhydrophobic performance	虞鸣	分会报告	辐射化学	2016-08-19	美国
52	第 252 届美国化学会学术年会	Electrospun nanofibrous polymeric adsorbents for water purification	张伯武	分会报告	辐射化学	2016-08-19	美国
53	美国材料与试验协会 DO2F 委员会会议	Impregnation of graphite with molten salt	曾广礼	大会报告	分析力学	2016-06-26	美国
54	第二十六届国际统计物理学术交流会议	Enhancement of water evaporation on solid surfaces with nanoscale hydrophobic-hydrophilic patterns	万荣正	墙报	量子计算中的凝聚态物理问题	2016-07-17	法国
55	美国 2016 年度应用超导学大会	Development of a Model Superconducting Undulator at the SSRF	许皆平	分会报告	光源、光学器件和光学系统中的物理问题	2016-09-03	美国
56	美国 2016 年度应用超导学大会	Quench Protection for a Model Superconducting Undulator at the SSRF	丁祎	墙报	光源、光学器件和光学系统中的物理问题	2016-09-03	美国
57	国际核工业展并出席第 22 届四代堆论坛熔盐堆系统执委会会议	Thorium Molten Salt Reactor Energy System (TMSR) Program Update	陈堃	大会报告	核技术及其应用	2016-06-27	法国
58	2016 年国际直线加速器会议	上海软 X 射线 FEL 装置中束流去调频研究	赵明华	墙报	束流物理与加速器技术	2016-09-24	美国
59	2016 年国际直线加速器会议	上海光源直线加速器能量反馈系统	汪宝亮	墙报	束流物理与加速器技术	2016-09-24	美国
60	第 4 届中泰高能物理、天体物理双边会议	有关 RHIC 上的反物质轻核和反物质相互作用	马余刚	大会报告	核物理	2016-07-03	泰国
61	2016年度X 射线显微国际会议	Full-field X-ray nano-CT at SSRF	邓彪	分会报告	同步辐射技术及其应用	2016-08-14	英国
62	2016年度X 射线显微国际会议	COATED YAG:Ce SCINTILLATOR FOR EFFICIENCY	杜国浩	墙报	同步辐射技术及其应用	2016-08-14	英国

		IMPROVEMENT IN INDIRECT X-RAY DETECTOR					
63	2016年度X 射线显微国际会议	Flat beam based X-ray diffraction micro-CT for grain analysis in polycrystalline materials	肖体乔	墙报	同步辐射技术及其应用	2016-08-14	英国
64	2016年度X 射线显微国际会议	Calcium oxalate cluster crystals investigation of wild ginseng via quantitative X-ray micro-tomography	薛艳玲	分会报告	同步辐射技术及其应用	2016-08-14	英国
65	2016 年核燃料循环评估研讨会议	Research Progress of TMSR Th-U Fuel Cycle	徐洪杰	大会报告	反应堆物理与技术	2016-07-13	美国
66	2016 年核燃料循环评估研讨会议	Safety Analysis of TMSR fuel cycle	陈堃	大会报告	反应堆物理与技术	2016-07-13	美国
67	第十六届有序分子膜国际会议	Designer DNA Architectures for Bionanotechnology	樊春海	分会报告	生物无机化学	2016-07-24	芬兰
68	第三届熔盐堆安全评估研讨会	Thorium Molten Salt Reactor Energy System (TMSR) Program and its Safety Research Update	陈堃	大会报告	核技术及其应用	2016-06-26	法国
69	纳米科学 2016 国际会议暨第十一届纳米科学和分子纳米技术国际会议	A new stitching Soft X-ray interference lithography technique	吴衍青	分会报告	纳米效应与纳米技术	2016-10-19	意大利
70	纳米科学 2016 国际会议暨第十一届纳米科学和分子纳米技术国际会议	The introduction of SSRF beamline station (BL08U1B)	赵俊	墙报	纳米效应与纳米技术	2016-10-19	意大利
71	国际光学工程及应用会议	X-ray microtomography at Shanghai Synchrotron Radiation Facility	肖体乔	大会报告	光学成像、图像分析与处理	2016-08-28	美国
72	第 26 届国际核物理会议	Final State Effects On Chiral Magnetic Effects In Relativistic Heavy-ion Collisions	马国亮	大会报告	核物理	2016-09-10	澳大利亚

73	钍资源利用研讨会	Progress of Thorium Molten Salt Reactor in China	徐洪杰	大会报告	反应堆物理与技术	2016-07-19	奥地利
74	第二十届国际真空大会	A DIFFERENTIAL PUMPING SYSTEM FOR THE GAS ATTENUATOR OF SXFEL	刘俊男	墙报	真空电子学	2016-08-21	韩国
75	第二十届国际真空大会	RESEARCH OF THE ACOUSTIC DELAY LINE IN THE VACUUM SYSTEM OF SSRF BEAMLINES	陈明	墙报	真空电子学	2016-08-21	韩国
76	第 11 届国际表面、涂层与纳米材料会议	Prediction of the active shape evaluation of metal nanoparticles under reaction conditions	朱倍恩	分会报告	量子计算中的凝聚态物理问题	2016-09-05	葡萄牙
77	2016 年国际束流测量仪器大会	CBPM system for DCLS	冷用斌	分会报告	束流物理与加速器技术	2016-09-10	西班牙
78	2016 年国际束流测量仪器大会	Batch application of digital BPM processors at SINAP	赖龙伟	分会报告	束流物理与加速器技术	2016-09-10	西班牙
79	2016 年国际束流测量仪器大会	Stable transmission of RF signals and timing events with accuracy at femtoseconds	刘鸣	墙报	束流物理与加速器技术	2016-09-10	西班牙
80	2016 年国际直线加速器会议并赴阿贡国家实验室进行学术交流	Applying Transverse Gradient Undulators to Suppression of Microbunching Instability	黄大章	墙报	束流物理与加速器技术	2016-09-21	美国
81	2016 年国际束流仪器仪表会议	Development of Electro-Optical Based Bunch Arrival-Time Monitor at SINAP	刘波	墙报	自由电子激光原理和技术	2016-09-10	西班牙
82	2016 年国际束流仪器仪表会议	Time Resolution Enhancement of RF Deflector With Transverse Gradient Undulator	邓海啸	墙报	自由电子激光原理和技术	2016-09-10	西班牙
83	第 17 届国际核	1）Effect of porosity on	曾广礼	大会报告	分析力学	2016-09-03	奥地利

	石墨专家会议	graphite by using a multi-scale mothed 2）A tensile strength test for small graphite samples 3）A material model for graphite components in molten salt reactor 4）Dynamic analysis of graphite components in molten salt reactor 5）Safety analysis of graphite core in molten salt test reactor					
84	第 22 届太阳能和化学储能国际会议	Determination of Thermal Physical Properties of Alkali Fluoride/ Carbonate Eutectic Molten Salt	安学会	分会报告	物理无机化学	2016-10-10	阿拉伯联合酋长国
85	美国机械工程师协会 BPV 委员会会议	4 point bending experiment for HHA-3217	曾广礼	大会报告	分析力学	2016-08-20	美国
86	2016 同步辐射装置设备与仪器机械工程设计大会	Progress of FEL Project in SINAP	殷立新	大会报告	束流物理与加速器技术	2016-09-09	西班牙
87	2016 同步辐射装置设备与仪器机械工程设计大会	Ground vibration monitoring for SXFEL construction	邓荣兵	墙报	束流物理与加速器技术	2016-09-09	西班牙
88	2016 同步辐射装置设备与仪器机械工程设计大会	Dynamic Performance of a Support System for BBA in FEL Projects”	高飞	墙报	束流物理与加速器技术	2016-09-09	西班牙
89	2016 同步辐射装置设备与仪器机械工程设计大会	The cooling system for the cryogenic permanent magnet undulator prototype at SSRF	刘以勇	分会报告	束流物理与加速器技术	2016-09-09	西班牙
90	2016 同步辐射装置设备与仪器机械工程设计大会	A high heat load front-end for the superconducting wiggler beamline at SSRF	李勇军	分会报告	束流物理与加速器技术	2016-09-09	西班牙

91	2016 同步辐射装置设备与仪器机械工程设计大会	Design of a leave spring bender for double Laue crystal monochromator at SSRF	秦宏亮	墙报	束流物理与加速器技术	2016-09-09	西班牙
92	第二届先进低发射度储存环技术会议并访问 SAES 公司	Overview of Insertion devices at Shanghai Synchrotron Radiation Facility	王宏飞	大会报告	束流物理与加速器技术	2016-09-13	意大利
93	第 17 届国际核石墨专家会议	The microstructure of nuclear graphite and its interaction with molten sal	贺周同	大会报告	离子束与物质相互作用和辐照损伤	2016-09-03	奥地利
94	第六届国际核燃料干法技术研讨会	Study on fluoride volatility in fluoride salts at TMSR	窦强	分会报告	核放射化学	2016-09-21	韩国
95	第六届国际核燃料干法技术研讨会	Electrochemical extraction of U and Th fromTMSR fuel salt.	黄卫	分会报告	核放射化学	2016-09-21	韩国
96	第六届国际核燃料干法技术研讨会	Development of a low pressure distillation process for fluoride molten salts treatment	付海英	分会报告	核放射化学	2016-09-21	韩国
97	第三届锕系光谱学先进技术国际会议	Probing the Electronic Structures of Thorium Oxides Using Anion Photoelectron Velocity Map Imaging	刘洪涛	大会报告	光谱与波谱学	2016-11-06	美国
98	第三届锕系光谱学先进技术国际会议	Coordination Structure of Uranium Complexes in disordered Systems using X-ray Absorption Fine Structure Spectroscopy	张林娟	大会报告	光谱与波谱学	2016-11-06	美国
99	2016 年美国化学工程师协会年会	One-Pot Granulation of Graphene Oxide Aerogels with Hierarchical Porous Three-Dimensional Structures	杨海军	分会报告	胶体与界面化学	2016-11-10	美国
100	第 14 届亚洲辐射固化国际会议	Functional Fabrics by Radiation Induced Graft Polymerization Methods	李景烨	分会报告	核技术及其应用	2016-10-23	日本
101	第 14 届亚洲辐射固化国际会	Graphene aerogel produced by effective	李吉豪	分会报告	核技术及其应用	2016-10-23	日本

	议	radiation induced self-assembly and its application for oil-water separation					
102	“能源转化与存储”中丹双边研讨会	Hybrid Energy Research in TMSR	王建强	大会报告	应用无机化学	2016-09-30	丹麦
103	第25届国际标准化组织表面化学分析技术委员会全体会议和第七届国际实用表面分析研讨会	The development of TXRF method and its application on the study of trace elements in water at SSRF	黄宇营	墙报	同步辐射技术及其应用	2016-10-12	韩国
104	熔盐堆技术研讨会并访问加州大学伯克利分校，进行熔盐堆技术交流和讨论	SINAP loop operations – summary of experience to date	徐洪杰	大会报告	核技术及其应用	2016-10-03	美国
105	2016年国际直线加速器会议	Linac-based Free Electron Laser in China	赵振堂	大会报告	束流物理与加速器技术	2016-09-24	美国
106	第四届生物扫描探针显微镜学国际研讨会	Klenow Fragment (KF) Activity Observed with Atomic Force Microscopy	李宾	墙报	细胞、亚细胞、生物大分子力学	2016-10-02	日本
107	第11届亚洲同步辐射医学成像会议	Latest advances at SSRF X-ray imaging and biomedical application beamline	邓彪	大会报告	同步辐射技术及其应用	2016-10-07	韩国
108	第11届亚洲同步辐射医学成像会议	Study on biomedical materials for bone tissue regeneration by synchrotron radiation-based X-ray Imaging	郭瀚	墙报	同步辐射技术及其应用	2016-10-07	韩国
109	2016 年 SLAC 国家实验室用户会议	Inchoate Study of Sample Delivery System for SXFEL	孙波	分会报告	同步辐射光源原理和技术	2016-10-04	美国
110	2016年度低温与同位素分离进展会议并访问罗马尼亚低温与同位素技	Study on properties of ZrCo0.8M0.2(M=Co 、Cu、Cr、Mn、Al) alloys for hydrogen storage	韩兴博	分会报告	核技术及其应用	2016-10-16	罗马尼亚

	术研究所						
111	第十一届国际热工水力、运行和安全国际会议	Experimental research on forced convective heat transfer of molten salts in circular tubes	陈玉爽	分会报告	传热过程及设备	2016-10-09	韩国
112	美国核学会2016年冬季会议	benchmark study of infinite lattice of pebble fuel within Flibe coolant for TMSR-SF1 Design	冀锐敏	分会报告	反应堆物理与技术	2016-11-05	美国
113	第四届国际核材料会议	In Situ Investigation of Load Allocation in Ni-Mo-Cr Alloy With High Energy X-Ray	谢若冰	分会报告	核化学与核燃料化学	2016-11-06	法国
114	第四届国际核材料会议	Hydrothermal treatment to make crack-free ThO2 microspheres using external gelation process	林俊	分会报告	核化学与核燃料化学	2016-11-06	法国
115	第四届国际核材料会议	Grazing incident X-ray diffraction study of the synergy effect of irradiation and corrosion in Ni based alloy	于存	分会报告	核化学与核燃料化学	2016-11-06	法国
116	访问韩国基础科学研究中心并核输运与对称能研讨会	核物质对称能及输运模型	徐骏	大会报告	核物理	2016-11-21	韩国
117	2016年核光子学国际会议	Gamma-ray Source Activities at Shanghai Synchrotron Radiation Facility	陈建辉	大会报告	束流物理与加速器技术	2016-10-15	美国
118	国际熔盐堆技术研讨会	Thorium Molten Salt Reactor(TMSR) Development in China	戴志敏	大会报告	反应堆物理与技术	2016-10-30	奥地利
119	1)第五届奇异性核物理国际学校;2)中子星核物质国际研讨会及第8届亚洲核物理协会研讨会	Strangeness Physics at RHIC	马余刚	大会报告	核物理	2016-11-17	日本
120	2016年高分子	Biomass-based and	吴国忠	大会报告	高分子光化学与	2016-11-06	印度尼西亚

	科学技术创新国际会议	Biodegradble Polymer			辐射化学		
121	2016 年国际对撞机研讨会	Development of x-band technology at SINAP	谭建豪	分会报告	束流物理与加速器技术	2016-12-04	日本
122	第十届海峡两岸生物学启发的理论科学问题研讨会	不对称分子是“活”的	盛楠	大会报告	生物化学	2016/6/19	上海
123	第十届海峡两岸生物学启发的理论科学问题研讨会	Asymmetry induces Q-band split in the electronic excitations of magnesium porphyrin: Implications for high-efficiency light harvesting	宋波	大会报告	生物化学	2016/6/19	上海
124	第 5 届国际核反应动力学研讨会-IWND2016	Equations of motion of test particles for solving the spin-dependent Boltzmann-Vlasov equation	夏银	大会报告	核物理	2016/5/15	河南
125	第 5 届国际核反应动力学研讨会-IWND2016	Understanding transport simulations of heavy-ion collisions at intermediate energies	徐骏	大会报告	核物理	2016/5/15	河南
126	第 5 届国际核反应动力学研讨会-IWND2016	Probing α clustering configurations via collective flows in 16O+16O/12C+12C collisions at Fermi energy	何万兵	大会报告	核物理	2016/5/15	河南
127	第 5 届国际核反应动力学研讨会-IWND2016	Measurement on interaction between antiprotons at RHIC	马余刚	大会报告	核物理	2016/5/15	河南
128	第 5 届国际核反应动力学研讨会-IWND2016	Measurement of D-meson triggered correlation in p+p collisions at 500GeV	马龙	大会报告	核物理	2016/5/15	河南
129	第 5 届国际核反应动力学研讨会-IWND2016	Investigating the scaling of higher-order flows in relativistic heavy-ion collision	张春健	大会报告	核物理	2016/5/15	河南
130	激光核物理国	Shanghai Laser Electron	范功涛	大会报告	核物理	2016/6/22	上海

	际研讨会-IWPNP2016	Gamma Source					
131	激光核物理国际研讨会-IWPNP2016	A bright gamma ray source at SXFEL complex	陈建辉	大会报告	核物理	2016/6/22	上海
132	第十届亚太同步辐射论坛-AOFSRR2016	Shanghai XFEL Projects	赵振堂	大会报告	束流物理与加速器技术	2016/11/2	上海
133	第十届亚太同步辐射论坛-AOFSRR2016	SSRF Phase-II Beamlines Project	邰仁忠	大会报告	同步辐射技术及其应用	2016/11/2	上海
134	第十届亚太同步辐射论坛-AOFSRR2016	Structure-Activity Relationship in Nano-Catalysis: X-ray Absorption Fine Structure Application at SSRF	司锐	分会报告	同步辐射技术及其应用	2016/11/2	上海
135	第十届亚太同步辐射论坛-AOFSRR2016	Tackling Rapid Reaction Kinetics at Mineral/Water Interface Using Quick-Scanning X-ray Absorption Fine Structure Spectroscopy	李炜	分会报告	同步辐射技术及其应用	2016/11/2	上海
136	第十届亚太同步辐射论坛-AOFSRR2016	Phase Transitions of ThC and ThC2 under High Pressure Revealed by Micro X-Ray Diffraction	谢若冰	分会报告	同步辐射技术及其应用	2016/11/2	上海
137	第十届亚太同步辐射论坛-AOFSRR2016	XAFS Characterization of Industrial Catalysts: Cu-ZnOx/SiO2 Catalyst for Ester Hydrogenolysis	王建强	分会报告	同步辐射技术及其应用	2016/11/2	上海
138	第十届亚太同步辐射论坛-AOFSRR2016	Application of Synchrotron Radiation Technique in Nuclear Energy Material and Chemistry Research	王建强	大会报告	同步辐射技术及其应用	2016/11/2	上海
139	第十届亚太同步辐射论坛-AOFSRR2016	Soft X-ray Spectromicroscopy at SSRF and Their Significant Applications	张立娟	墙报	同步辐射技术及其应用	2016/11/2	上海
140	第十届亚太同步辐射论坛	Soft X-ray Interference Lithography Beamline	吴衍清	墙报	同步辐射技术及其应用	2016/11/2	上海

	-AOFSRR2016						
141	第十届亚太同步辐射论坛-AOFSRR2016	Experimental Techniques and Results: Dreamline at Shanghai Synchrotron Radiation Facility	邹鹰	墙报	同步辐射技术及其应用	2016/11/2	上海
142	第十届亚太同步辐射论坛-AOFSRR2016	X-ray Imaging and Biomedical Applications Beamline at SSRF	谢红兰	墙报	同步辐射技术及其应用	2016/11/2	上海
143	第十届亚太同步辐射论坛-AOFSRR2016	The Latest Developing Situation of XAFS Beamline at SSRF	马静远	墙报	同步辐射技术及其应用	2016/11/2	上海
144	第十届亚太同步辐射论坛-AOFSRR2016	BL14B1 Diffraction Beamline of the Shanghai Synchrotron Radiation Facility (SSRF)	文闻	墙报	同步辐射技术及其应用	2016/11/2	上海
145	第十届亚太同步辐射论坛-AOFSRR2016	A Multitechnique Hard X-ray Micro-Focusing Beamline (BL15U1) at the Shanghai Synchrotron Radiation Facility	张丽丽	墙报	同步辐射技术及其应用	2016/11/2	上海
146	第十届亚太同步辐射论坛-AOFSRR2016	Development of Methodologies and Application Highlight at Small Angle X-ray Scattering Beamline at SSRF	边风刚	墙报	同步辐射技术及其应用	2016/11/2	上海
147	第十届亚太同步辐射论坛-AOFSRR2016	The Macromolecular Crystallography Beamline (BL17U1) of SSRF	郁峰	墙报	同步辐射技术及其应用	2016/11/2	上海
148	全球华人物理和天文学会第九届加速器学校-OCPA9	Mechanics and Survey	殷立新	大会报告	束流物理与加速器技术	2016/7/25	上海
149	全球华人物理和天文学会第九届加速器学校-OCPA9	Cryogenics System	王莉	大会报告	束流物理与加速器技术	2016/7/25	上海
150	全球华人物理和天文学会第	Radiation Protection	夏晓彬	大会报告	辐射安全	2016/7/25	上海

	九届加速器学校-OCPA9						
151	第一届碳基水输运材料研讨会-CarbonWater17	Carbon-based materials for energy storage	王勇	大会报告	同步辐射技术及其应用	2016/11/4	上海
152	第一届碳基水输运材料研讨会-CarbonWater17	Ion effect on the carbon based nanotube and membrane	方海平	大会报告	水科学	2016/11/4	上海
153	第一届碳基水输运材料研讨会-CarbonWater17	Small Angle X ray Scattering beamlines at Shanghai Synchrotron Radiation Facility	边风刚	大会报告	同步辐射技术及其应用	2016/11/4	上海
154	第二届 X 射线光学与探测器 BES-CAS 研讨会	Optical metrology at SSRF: from laboratory to at wavelength	王劼	大会报告	同步辐射技术及其应用	2016/11/15	浙江
155	第二届 X 射线光学与探测器 BES-CAS 研讨会	Dynamic bending K-B system and phase compensation technique for X-ray nanoprobe at SSRF	李爱国	大会报告	同步辐射技术及其应用	2016/11/15	浙江
156	第二届 X 射线光学与探测器 BES-CAS 研讨会	Full field X-ray nanoscope under developing at SSRF	邓彪	大会报告	同步辐射技术及其应用	2016/11/15	浙江
157	第二届 X 射线光学与探测器 BES-CAS 研讨会	High heat load optics for high energy X-ray beamline at SSRF	杨科	大会报告	同步辐射技术及其应用	2016/11/15	浙江
158	第二届 X 射线光学与探测器 BES-CAS 研讨会	Finite element analysis of optics for SSRF Phase-II project	徐中民	大会报告	同步辐射技术及其应用	2016/11/15	浙江
159	第二届 X 射线光学与探测器 BES-CAS 研讨会	Crystal polychromator design for energy-dispersive XAS at SSRF	魏向军	大会报告	同步辐射技术及其应用	2016/11/15	浙江